CALIFORNIA COOPERATIVE OCEANIC FISHERIES INVESTIGATIONS

Reports

VOLUME 57
JANUARY 1 TO DECEMBER 31, 2016

Cooperating Agencies:

CALIFORNIA DEPARTMENT OF FISH AND WILDLIFE
UNIVERSITY OF CALIFORNIA, SCRIPPS INSTITUTION OF OCEANOGRAPHY
NATIONAL OCEANIC AND ATMOSPHERIC ADMINISTRATION, NATIONAL MARINE FISHERIES SERVICE

CALCOFI COORDINATOR John N. Heine
EDITOR John N. Heine

Printed and distributed December 2016, La Jolla, California
ISSN 0575-3317

CONTENTS

REPORTS AND REVIEWS

STATE OF THE CALIFORNIA CURRENT 2015–16: COMPARISONS WITH THE 1997–98 EL NIÑO

SAM MCCLATCHIE
NOAA Fisheries
Southwest Fisheries Science Center
8901 La Jolla Shores Drive
La Jolla, CA 92037-1509

RALF GOERICKE
Scripps Institution of Oceanography
University of California, San Diego
La Jolla, CA 92024

ANDREW LEISING
Environmental Research Division
National Marine Fisheries Service
99 Pacific St., Suite 255A
Monterey, CA 93940-7200

TOBY D. AUTH
Pacific States Marine Fisheries Commission
Hatfield Marine Science Center
2030 Marine Science Drive
Newport, OR 97365

ERIC BJORKSTEDT[1] AND
ROXANNE R. ROBERTSON[2]
[1]Southwest Fisheries Science Center
National Marine Fisheries Service
NOAA
Santa Cruz, CA 95064
[2]CIMEC
Humboldt State University

RICHARD D. BRODEUR[1],
XIUNING DU[2], ELIZABETH A. DALY[2],
AND CHERYL A. MORGAN[2]
[1]NOAA-Fisheries
Northwest Fisheries Science Center
Hatfield Marine Science Center
Newport, OR 97365
[2]Cooperative Institute for
Marine Resources Studies
Oregon State University
2030 Marine Science Drive
Newport, OR 97365

FRANCISCO P. CHAVEZ
Monterey Bay Aquarium Research Institute
Moss Landing, CA 95039

AMANDA J. DEBICH AND
JOHN HILDEBRAND
Marine Physical Laboratory
Scripps Institution of Oceanography
University of California, San Diego
La Jolla, CA 92024

JOHN FIELD AND KEITH SAKUMA
Southwest Fisheries Science Center
National Marine Fisheries Service
NOAA
Santa Cruz, CA 95064

MICHAEL G. JACOX[1, 2]
Institute of Marine Sciences
University of California, Santa Cruz
Santa Cruz, CA 95064
[2]Southwest Fisheries Science Center
NOAA
Monterey, CA 93940

MATI KAHRU
Scripps Institution of Oceanography
University of California, San Diego
La Jolla, CA 92024

RAPHAEL KUDELA[1] AND
CLARISSA ANDERSON[2, 3]
[1]Ocean Sciences Department
University of California, Santa Cruz
Santa Cruz, CA 95064
[2]Institute of Marine Sciences
University of California, Santa Cruz
Santa Cruz, CA 95064
[3]Southern California Coastal
Ocean Observing System
Scripps Institution of Oceanography
University of California, San Diego
San Diego, CA 92037

JOHN LARGIER
Bodega Marine Laboratory
University of California, Davis
P.O. Box 247
Bodega Bay, CA 94923

BERTHA E. LAVANIEGOS[1],
JOSE GOMEZ-VALDES[1], AND
S. PATRICIA A. JIMÉNEZ-ROSENBERG[2]
[1]Oceanology Division
Centro de Investigación Científica y
Educación Superior de Ensenada
Carretera Ensenada-Tijuana No. 3918
Zona Playitas, C.P. 22860, Ensenada
Baja California, Mexico
[2]Department of Plankton and Marine Ecology
Instituto Politécnico Nacional
CICIMAR
Av. IPN s/n, Col. Playa Palo de Sta. Rita
C.P. 23096, La Paz
BCS, Mexico

RYAN MCCABE
Joint Institute for the Study
of the Atmosphere and Ocean
University of Washington
Seattle, WA 98195

SHARON R. MELIN
National Marine Fisheries Service
Alaska Fisheries Science Center
Marine Mammal Laboratory
NOAA
7600 Sand Point Way N. E.
Seattle, WA 98115

MARK D. OHMAN AND LINSEY M. SALA
Scripps Institution of Oceanography
University of California, San Diego
La Jolla, CA 92093

BILL PETERSON AND JENNIFER FISHER
NOAA-Fisheries
Northwest Fisheries Science Center
Hatfield Marine Science Center
Newport, OR 97365

ISAAC D. SCHROEDER,
STEVEN J. BOGRAD, AND
ELLIOTT L. HAZEN
Environmental Research Division
National Marine Fisheries Service
99 Pacific St., Suite 255A
Monterey, CA 93940-7200

STEPHANIE R. SCHNEIDER AND
RICHARD T. GOLIGHTLY
Department of Wildlife
Humboldt State University
1 Harpst St.
Arcata, CA 95521

ROBERT M. SURYAN[1],
AMANDA J. GLADICS[1],
STEPHANIE LOREDO[1], AND
JESSICA M. PORQUEZ[2]
[1]Department of Fisheries and Wildlife
[2]College of Earth, Ocean, and
Atmospheric Sciences
Oregon State University
Hatfield Marine Science Center
Newport, OR 97365

ANDREW R. THOMPSON,
EDWARD D. WEBER, AND
WILLIAM WATSON
NOAA
Southwest Fisheries Science Center
8901 La Jolla Shores Drive
La Jolla, CA 92037-1509

VERA TRAINER
Northwest Fisheries Science Center
National Marine Fisheries Service
National Oceanic and
Atmospheric Administration
Seattle, WA 98112

PETE WARZYBOK, RUSSELL BRADLEY,
AND JAIME JAHNCKE
Point Blue Conservation Science
3820 Cypress Drive, Suite 11
Petaluma, CA 94954

ABSTRACT

Warm conditions in the North Pacific in 2014–15 were a result of the continuation of the North Pacific marine heat wave, a large area of exceptionally high SST anomalies that originated in the Gulf of Alaska in late 2013. The North Pacific heat wave interacted with an El Niño developing in the equatorial Pacific in 2015. Weekly periods of exceptionally high temperature anomalies (>2°C) occurred until the start of the El Niño (winter of 2015), when SSTs were still high but not as high as those due to the marine heat wave. During the 2015–16 El Niño, the depth of the 26.0 kg m^{-3} isopycnal ($d_{26.0}$) was considerably shallower than during the 1982–83 and 1997–98 events. The area affected by the marine heat wave and the 2015–16 El Niño in the mixed layer was comparable to the 1997–98 El Niño, but lasted longer. Water column stratification in the upper 100 m during 2015–16 was as strong as the most extreme values during the 1997–98 El Niño. This stratification was primarily driven by the warming of the upper 100 m. Despite notable perturbations, the effects of the 2015–16 El Niño on hydrographic properties in the CalCOFI domain were not as strong as those observed during the 1997–98 El Niño.

Warm ocean conditions, stratification, nutrient suppression, and silicic acid stress likely favored initiation of a toxic *Pseudo-nitzschia* bloom in fall 2014. Very low zooplankton displacement volumes were associated with anomalously warm and saline surface waters off Baja California. In contrast, during the 1997–98 El Niño, zooplankton volume was near average. Off California, pelagic red crab (*Pleuroncodes planipes*) adults were abundant in the water column and frequently washed up on beaches of southern California from January 2015 into 2016, and central California by September 2015. Glider measurements of integrated transport up to June 2015 did not detect anomalous northward advection. As expected, HF radar indicated northward surface currents along the central California coast in fall and winter 2015–16. Northward advection appeared to be much stronger during the 1997–98 El Niño. Throughout 2015–16, the zooplankton community on the Oregon shelf was dominated by lipid-poor tropical and sub-tropical copepods and gelatinous zooplankton, indicating poor feeding conditions for small fishes that are prey for juvenile salmon. The presence of rarely encountered species increased copepod species richness during 2015–16 to levels higher than the 1998 El Niño. We infer that the unusual copepod vagrants of 2015–16 originated from an offshore and southwesterly source; an important difference from the southerly origin of vagrants during the 1997–98 El Niño.

The very warm conditions caused sardine spawning to shift from central California to Oregon. Mesopelagic fish assemblage off southern California exhibited higher abundances of species with southern affinities, and lower abundances of species with northern affinities. Forage fish (Pacific herring, northern anchovy, and Pacific sardine) were much less abundant in 2015–16 compared to previous years. In contrast, catches of salmon were close to average off northern California. Catches of young-of-the-year rockfishes were high off central California, but low off both northern and southern California. Seabirds at Southeast Farallon Island in 2015 exhibited reduced breeding populations, reduced breeding success, lower chick growth rates, and lower fledging weights. Common murres were negatively affected in central and northern California, but seabird responses were species-specific. It is clear from the results presented here that the warm anomaly effects on the ecosystem were complicated, regionally specific, and that we do not fully understand them yet.

Online supplementary material: http://calcofi.org/ccpublications/state-of-the-california-current-live-supplement.html

INTRODUCTION

Over the last three years the California Current System (CCS) has been profoundly affected by the North Pacific marine heat wave of 2014–15 (DiLorenzo and Mantua 2016), formerly known as the "blob" (Bond et al. 2015), and the El Niño of 2015–16. A consequence of this forcing has been an unusually long period of strong warm anomalies in the CCS from 2014 until mid 2016. There are many precedents for anomalously warm years in the California Current System. Some of them (for example 1940–41, 1982–83, 1997–98, and 2005) are well studied. In this introduction to the 2015–16 warm year, we draw comparisons not only between the 2015–16 event and the 1997–98 El Niño, but also between the recent conditions and previous warm anomalies in the California Current System. Important questions that will guide us are: What caused the anomalous warming of 2015–16 in the California Current System? To what degree was the warming caused by the 2015–16 El Niño? And did the current El Niño have an effect on the California Current System as large as that of the 1997–98 El Niño?

Atmospheric Teleconnections (Local Forcing) And Oceanic Coastally Trapped Waves (Remote Forcing)

DiLorenzo and Mantua (2016) consider that "there is good evidence that [North Pacific] atmospheric teleconnections of tropical origin played a key role in the winter 2013/14 sea-level pressure anomalies." The patterns in sea surface temperature (SST) anomalies are mirrored in the sea level pressure anomalies. The peak anomalies shifted from the central Gulf of Alaska to the coastal

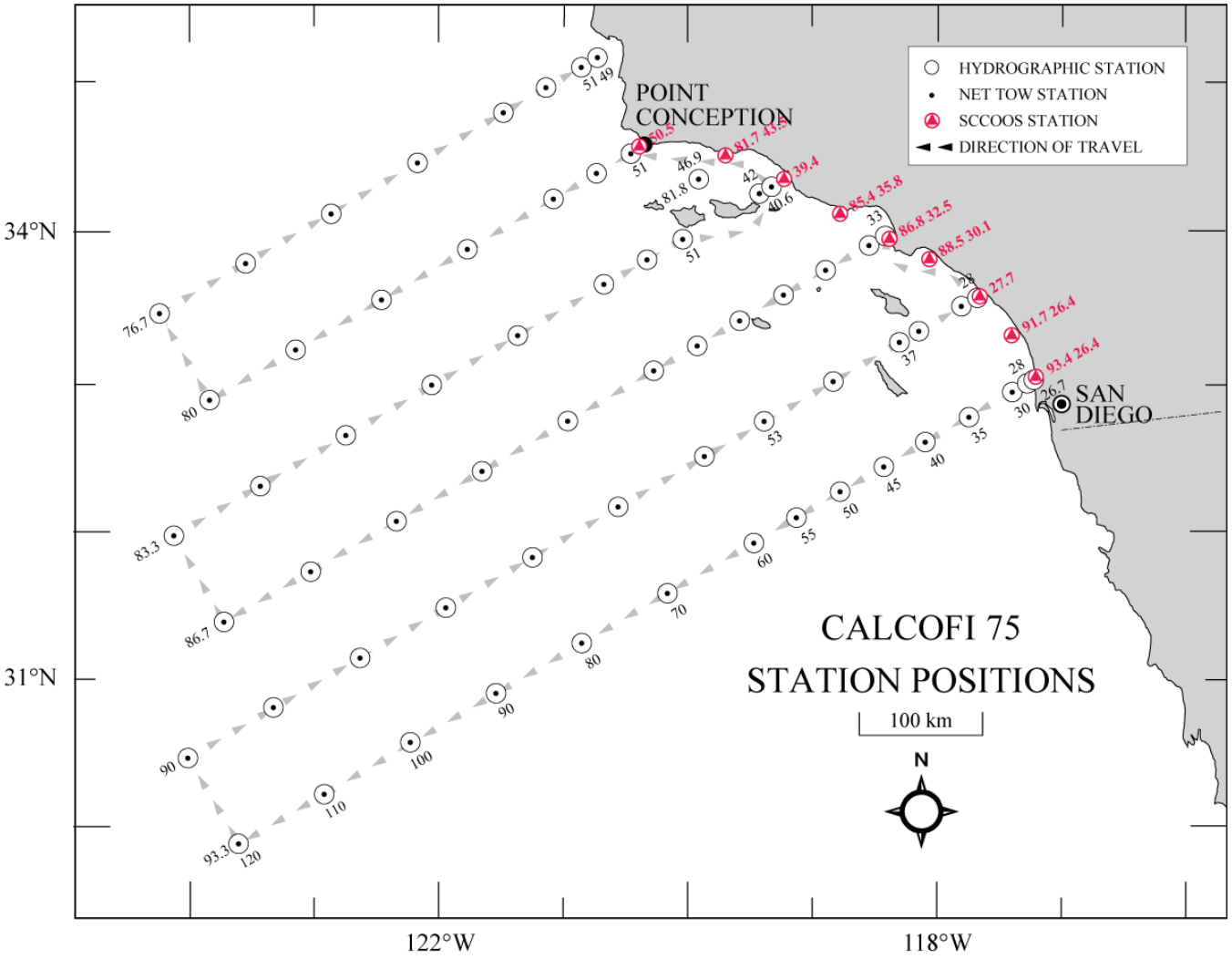

Figure 1. Map of the 75 station CalCOFI station pattern, including 66 core stations and 9 inshore SCCOOS stations.

areas of the Gulf of Alaska and the US West Coast in 2015 (DiLorenzo and Mantua 2016). This shift reflected a transition in the spatial pattern of SST anomalies from an NPGO-like pattern to a PDO-like pattern. Multiyear warm events, depending on the definition of a warm event, occurred in historical times in 1957–58, 1962–63, 1991–92 and 2014–15 (DiLorenzo and Mantua 2016).

As the spatial transition from NPGO to PDO-like patterns was occurring in the North Pacific, an El Niño developed in the tropics (DiLorenzo and Mantua 2016). The subtropical Pacific is connected to the central equatorial Pacific by positive thermodynamic feedback between the oceans and the atmosphere[1], where positive temperature anomalies can reduce the winds, and favor the development of El Niño. Once El Niño feedbacks arise along the equator, "the rearrangement of tropical convection excites atmospheric Rossby waves… which in the case of an eastern Pacific El Niño…injects variance into the Aleutian low in the next boreal fall/winter season" (DiLorenzo and Mantua 2016). In short, the North Pacific warming affected the development of the El Niño, and teleconnections of tropical origin fed back to the variance of the North Pacific, which was manifested in the spatial pattern of sea level pressure anomalies. DiLorenzo and Mantua (2016) estimated that tropical teleconnections accounted for about 50% or ~1.5°C of the peak SST anomalies in the index of their PDO-like pattern in January to March 2015, contributing significantly to making the North Pacific warming an extreme event, which they refer to as a "marine heat wave." Without the tropical teleconnections, the anomalous warming would have fallen within the normal range of variability of SST in the northeast Pacific (DiLorenzo and Mantua 2016).

While the role of atmospheric teleconnections and local forcing on the 2014–16 anomalous warming seems reasonably well understood, the importance of remote

[1]The winds-evaporation-SST (WES) feedback.

forcing remains an open question. There is currently little evidence of coastally trapped waves, connected to remote forcing, along the US West Coast in 2015–16. Downwelling phases of equatorial Kelvin waves were observed propagating eastward across the Pacific in October–November 2015 and January–February 2016 (NOAA Climate Prediction Center/NCEP 29 August, 2016 web page, accessed Sept. 1, 2016). Whether these equatorial waves generated northward propagating coastally trapped waves along the US West Coast, with potential effects on the California Current System, does not appear to have been determined at the time of writing. Until further evidence is accumulated, it is difficult to apportion relative importance of local forcing (via atmospheric pathways) versus remote forcing (propagating along oceanic pathways) on the 2015–16 warm event.

Northward Transport

Among other effects, strong El Niños generally cause changes in the spatial pattern and volume transport of the California Current System. The temporal evolution of volume transport between the surface and 500 m depth across CalCOFI line 90 between nearshore station 30 (11 km of the shelf) and offshore station 120 (683 km from the coast) (fig. 1) reflects the net flow of the equatorward California Current and the poleward flows of the deeper California Undercurrent and shallower Inshore Countercurrent[2,3], (Lynn and Bograd 2002). Anomalous flows can be detected by comparison with the climatological seasonal mean flows (Lynn and Bograd 2002; Zaba and Rudnick 2016).

The 1997–98 El Niño was a case where transport from the south brought unusual fish into the southern California region, probably both by advection of larvae and by adult fish swimming in water masses with favorable conditions (Lea and Rosenblatt 2000). Although occurrences of unusual animals were also a feature of the 2015–16 anomalous warming (see sections below), the observed transport derived from glider data off southern California from 2014 up to June 2015 was not anomalous when averaged over a horizontal distance of 200 km[4] (Zaba and Rudnick 2016).

In contrast to what has so far been reported for the 2015–16 warming, there was clear evidence of anomalous poleward flows during the 1997–98 El Niño. Lynn and Bograd (2002) reported anomalous poleward flows integrated over 0–500 m from November 1997 to February 1998, due to strengthening and broadening of both the Inshore Countercurrent and the California Undercurrent (Lynn and Bograd 2002). Flows between 200–500 m were similar except that there was an earlier poleward flux in July 1997 equaling that observed in November 1997, so there were two poleward transport pulses at depth during the 1997 El Niño (see Lynn and Bograd 2002, their fig. 9). After February 1998 the poleward flows weakened and equatorward flow strengthened. By April 1998 the dominant flow was again toward the equator in a revived California Current that moved progressively offshore at the speed of a propagating Rossby wave (Lynn and Bograd 2002).

The northward extension of animals that are weak swimmers, such as adult red crabs (*Pleuroncodes planipes*) suggests that advective transport from the south occurred in 2015–16, as it did in 1997–98. HF-radar data show that northward-directed surface currents developed off central California in the fall and winter of 2015–16—in addition to the usual poleward surface currents observed in the Southern California Bight during summer (see section below). Beach strandings of red crabs in southern California were reported from January to October 2015. This suggests that the crabs either swam there in water with favorable conditions, or that they were carried there by advection. Further analysis of the glider and HF-radar current velocity data may resolve the issue of how slow swimming red crabs, which are usually found in more tropical southern waters, arrived off southern California.

DESCRIPTIVE PHYSICAL OCEANOGRAPHY

El Niño/Southern Oscillation (ENSO) is a dominant mode of interannual variability in the equatorial Pacific, causing physical and ecological impacts throughout the Pacific basin and California Current System. The Oceanic Niño Index (ONI; http://www.cpc.ncep.noaa.gov/data/indices/), a three-month running mean of sea-surface temperature anomalies averaged over the NINO3.4 region of 5°S–5°N and 120°W–170°W, is used by NOAA as a diagnostic to gauge the state of ENSO. ONI values exceeding the 0.5°C threshold that signifies an El Niño event were observed from April 2015 through May 2016 (Supplement fig. S1). The ONI dropped below the 0.5°C threshold during June 2016. NOAA's Climate Prediction Center (http://www.cpc.ncep.noaa.gov) issued a report in September 2016 stating that El Niño neutral conditions were reached by June 2016 and forecasted a 55%–60% probability of ENSO-neutral conditions by the fall and winter of 2016–17.

Warm conditions in the North Pacific were a result of the continuation of the marine heat wave, a large area of exceptionally high SST anomalies that originated in the Gulf of Alaska in late 2013 (Bond et al. 2015). By the middle of 2014, high SST anomalies were also observed

[2]Other studies (e.g., Zaba and Rudnick 2016) integrate flows over different horizontal intervals.

[3]Note that the Inshore Countercurrent is a surface manifestation of the California Undercurrent and Todd et al. (2011) considered that there is little physical justification for separate names because there is no depth related discontinuity in the transport.

[4]Data of Zaba and Rudnick (2016) only extends to June 2015.

in the CCS and as far south as Baja California (Leising et al. 2015). The Pacific Decadal Oscillation (PDO) index describes the temporal evolution of the dominant spatial pattern of SST anomalies over the North Pacific (Mantua et al. 1997). The PDO values during December 2014 until March 2015 were all higher than 2, which were some of the highest values in the time series (Supplement fig. S1), following a period of consistent negative values from June 2010 through 2013. These high winter PDO values indicate the presence of the marine heat wave since they precede the onset of the 2015 El Niño event, and modulated the regional expression of the El Niño event on the California Current (Jacox et al. 2016). The PDO value of April 2016 was the highest since the 1997–98 El Niño event.

The North Pacific Gyre Oscillation (NPGO) is a low-frequency signal of sea-surface height, indicating variations in the circulation of the North Pacific Subtropical Gyre and Alaskan Gyre, which in turn relate to the source waters for the California Current (Di Lorenzo et al. 2008). Positive values of the NPGO are linked with increased equatorward flow in the California Current, along with increased surface salinities, nutrients, and chlorophyll *a* values. Negative NPGO values are associated with decreases of these variables, inferring less subarctic source waters and generally lower productivity. Negative values of the NPGO occurred from mid-2013 to May 2016, except for a couple of very small positive values in 2014 and at the start of 2016 (Supplement fig. S1).

North Pacific Climate Patterns

A basin-scale examination of sea surface temperatures (SST) and surface wind vectors allows for the interpretation of the spatial evolution of climate patterns and wind forcing over the North Pacific related to trends in the basin-scale and upwelling indices (Supplement fig. S2, S3). Negative SST anomalies in the region of the Subarctic Frontal Zone were evident in the summer of 2015, winter 2016, and spring 2016 (Supplement fig. S3); these negative anomalies first arose in the summer of 2014 (Leising et al. 2015). The SST anomaly pattern during these months with negative SST anomalies in the west and central North Pacific and positive SST anomalies along the west coast of North America and equatorial Pacific resemble the warm phase of the PDO (Mantua et al. 1997). Enhanced westerly wind anomalies, especially in the western Pacific, coincided with these negative SST anomalies. Positive SST anomalies associated with the El Niño were high across the eastern equatorial Pacific from July 2015 to February 2016. During this time, the usual easterly winds along the equator slackened or changed direction as seen by arrows pointing north/south in the region near South America and arrows pointing eastward in the east (fig. S3). The positive SST anomalies first started to subside in the Niño 1+2 region, a coastal region of South America near the equator, in February 2016 and by May 2016 negative SST anomalies extended along the equator from 130° to 80°W and stronger easterly winds extended from 170° to 160°W. Along the coast of North America, high positive SST anomalies due to the marine heat wave started to diminish by December 2015, with values dropping by 1°C from high values experienced in the early part of 2015. Positive SST anomalies remained along the coast in late winter and early spring of 2016, with SST anomalies ranging from 0.5° to 1.5°C. Alongshore winds in the Gulf of Alaska were associated with anomalously cyclonic winds forced by low atmospheric pressure during February 2016. This cyclonic wind pattern switched to an anticyclonic pattern by May 2016 due to a strong North Pacific High (Supplement fig. S3).

Upwelling in the California Current

Monthly means of daily upwelling index (Bakun 1973; Schwing et al. 1996) show the strongest upwelling occurring between 36°–45°N (Supplement fig. S2). Upwelling in these latitudes was unusually strong during the spring and summer of 2014 and for the majority of the year in 2015 (Supplement fig. S2, bottom). El Niño causes the North Pacific atmospheric pressure system to weaken and decrease in size (Schroeder et al. 2013), and as a result, winds that promote upwelling slacken (Schwing et al. 2002). During the winter of 2015–16 downwelling was anomalously strong for latitudes north of 36°N.

The Cumulative Upwelling Index (CUI) is the cumulative sum of the daily UI starting January 1 and ending on December 31, and is used here to compare the 1997–98 El Niño to the current event. Cumulative upwelling during the first two months of 1997 and 2015 was average to slightly greater than average for all latitudes (Supplement fig. S4). By November, downwelling winds associated with El Niño caused the CUI to decline, which is most evident for locations 39° to 48°N. Strong downwelling continued into 1998 and 2016 for all latitudes north of 33°N. The CUI values for 1998 were some of the lowest for all years of the record (since 1967) due to extreme negative upwelling indices, i.e., downwelling in January 1998. In conclusion, upwelling associated with the two El Niño events proceeded similarly, but upwelling during the winter for the 1997–98 event was much weaker than 2015–16.

The date when CUI values increased above their seasonal minimum can be used as an index of the "spring transition." Periods of strong upwelling can occur before the spring transition and these winter upwelling events can precondition the ecosystem for increased production in the spring (Black et al. 2010). The preconditioning index (pCUI) is defined as the cumulative sum of only

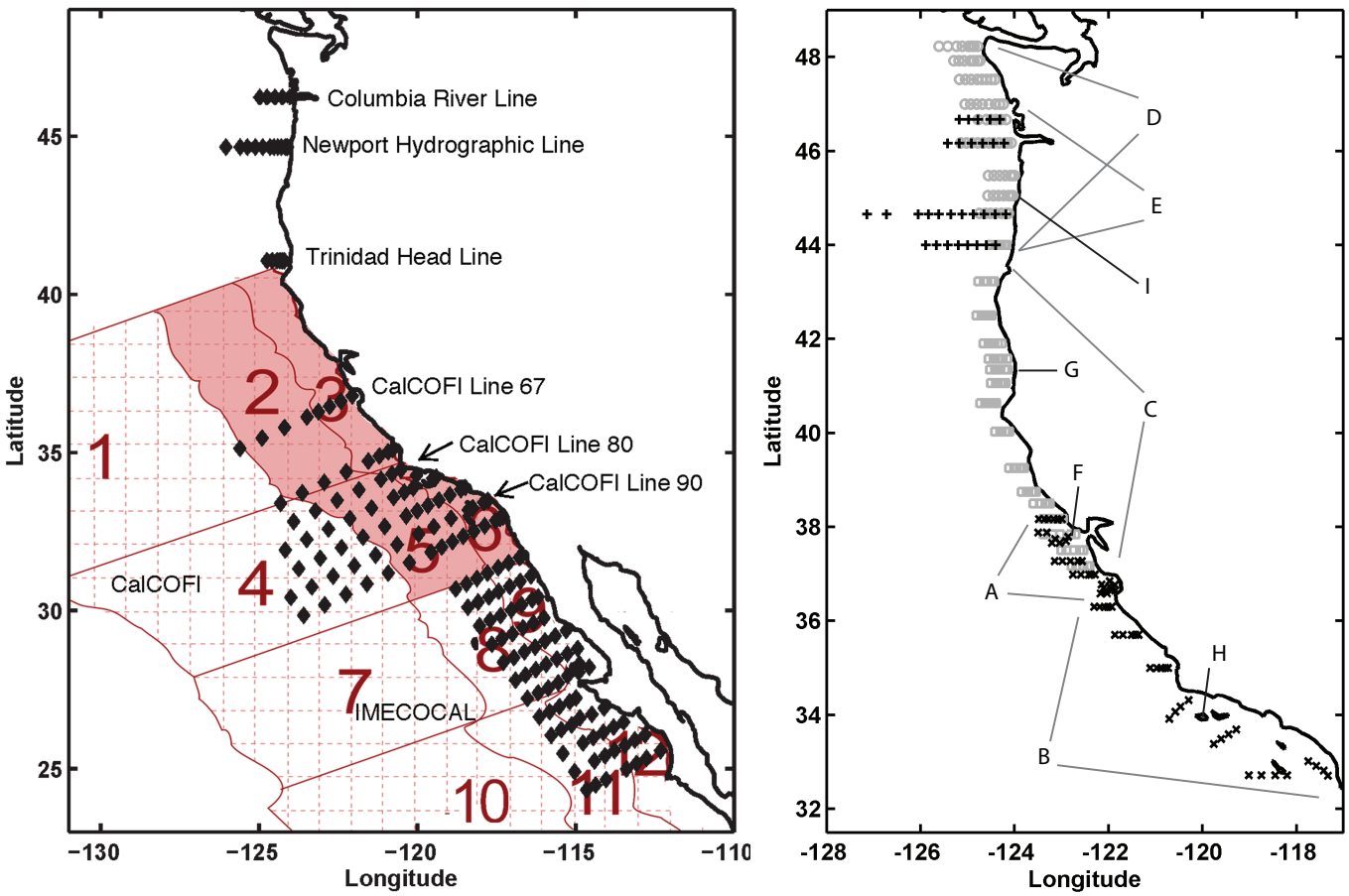

Figure 2. Station maps for surveys that were conducted multiple times per year during different seasons to provide year-round observations in the California Current System. The CalCOFI survey (including CalCOFI Line 67) was occupied quarterly; the winter and spring CalCOFI survey grid usually extends just north of San Francisco. The IMECOCAL survey is conducted quarterly or semiannually. The Newport Hydrographic Line was occupied biweekly. The Trinidad Head Line was occupied at biweekly to monthly intervals. Red overlay and numbers denotes areas for SST and chlorophyll *a* analysis. Right: Location of annual or seasonal surveys, including locations of studies on higher trophic levels, from which data was included in this report. Different symbols are used to help differentiate the extent of overlapping surveys. A. SWFSC Fisheries Ecology Division (FED) midwater trawl survey core region (May–June) B. SWFSC FED midwater trawl survey south region (May–June). C. SWFSC FED salmon survey (June and September) (gray squares). D. NWFSC salmon survey (May, June, and September). E. NOAA/BPA pelagic rope trawl survey (May through September). F. Southeast Farallon Island. G. Castle Rock. H. San Miguel Island. I. Yaquina Head Outstanding Natural Area.

the positive values of the UI from January 1 to the end of February (Schroeder et al. 2013). The pCUI values for 2016 were very low, indicating very few days of upwelling, and the values were very similar to the pCUI values during 1998 (not shown).

Coastal Sea Surface Temperature

Daily SSTs as measured by National Data Buoy Center (NDBC) buoys along the West Coast have mostly been above long-term averages since the summer of 2014 (Supplement fig. S5). Weekly periods of exceptionally high temperature anomalies (greater than 2°C) occurred at all buoy locations from the fall of 2014 to the fall of 2015. By December 2015 SSTs were still high, but not as high as those during the previous year. The meridional winds during the warm SST period were not unusually weak in magnitude or overly downwelling favorable (+ values). The decrease in SST values seen in the central CCS during the spring of 2015 corresponded with an extended period of upwelling favorable winds (– values). Long episodes of downwelling favoring winds occurred during January and March of 2016 at all locations.

Sea Surface Temperature and Chlorophyll Anomalies off California from Remote Sensing

To analyze temporal trends of remotely sensed SST and surface chlorophyll *a*, the southern CCS region has been divided into 10 areas (fig. 2). For this analysis data from areas 2, 3, 5, and 6 were used. Significant SST and chlorophyll *a* anomalies[5] were present before

[5]The effects of the 2015–16 El Niño on the California Current System (CCS) were evaluated using satellite-detected SST and surface chlorophyll *a* concentration, using the same methods that Kahru and Mitchell (2000) applied to the major 1997–98 El Niño. SST data were derived from the version 2.0 daily datasets of optimally interpolated global blended AVHRR temperatures (Reynolds et al. 2007; https://podaac.jpl.nasa.gov/dataset/AVHRR_OI-NCEI-L4-GLOB-v2.0). Chlorophyll *a* data were derived from the merged multisensor regionally optimized dataset for the CCS (Kahru et al. 2012, 2015; http://spg.ucsd.edu/Satellite_Data/CC4km/CC4km.htm). Anomalies were calculated relative to the long-term (1981–2016) mean monthly values.

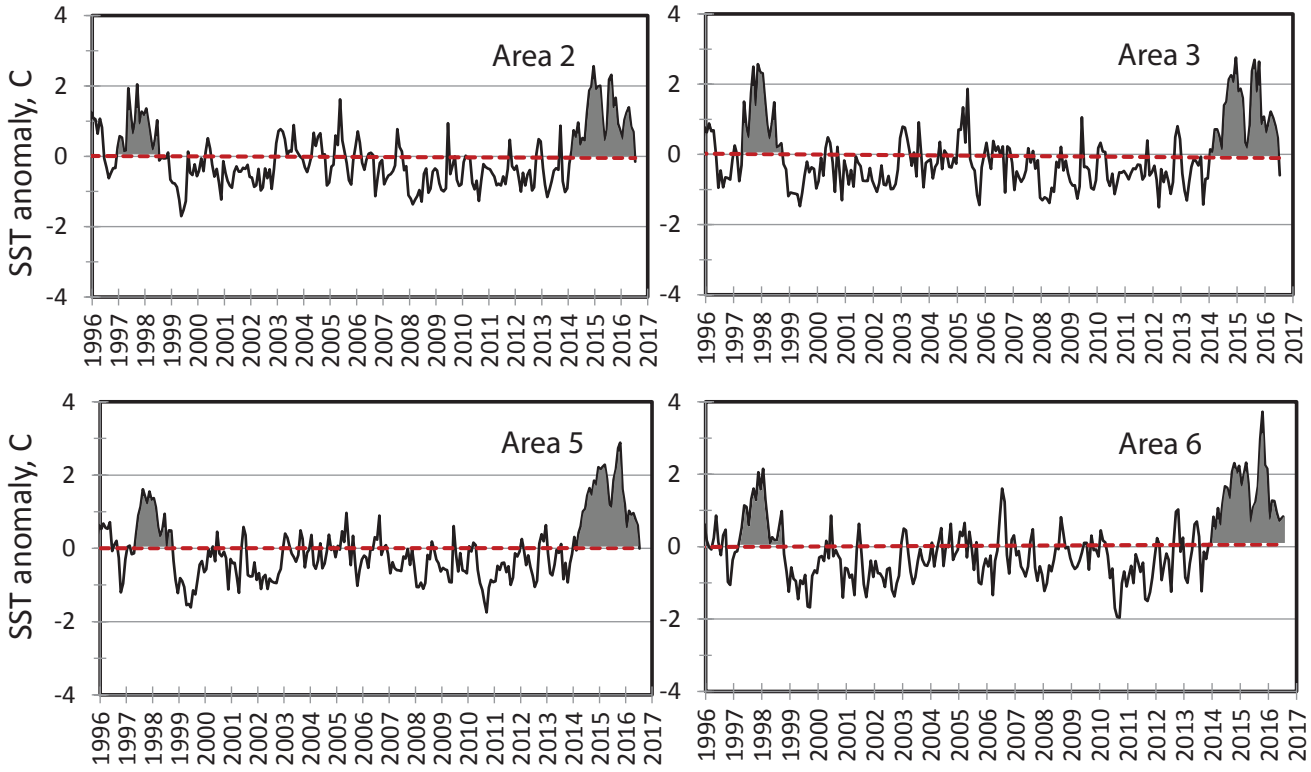

Figure 3. Anomalies of monthly mean sea-surface temperature in coastal and transitional areas of central and southern California (see map in fig. 2). Anomalies were calculated relative to monthly means of Sept. 1981–July 2016. The shaded areas correspond to the anomalies of 1997–98 and 2014–16, respectively. Anomalies were calculated relative to the long-term (1981–2016) mean monthly values.

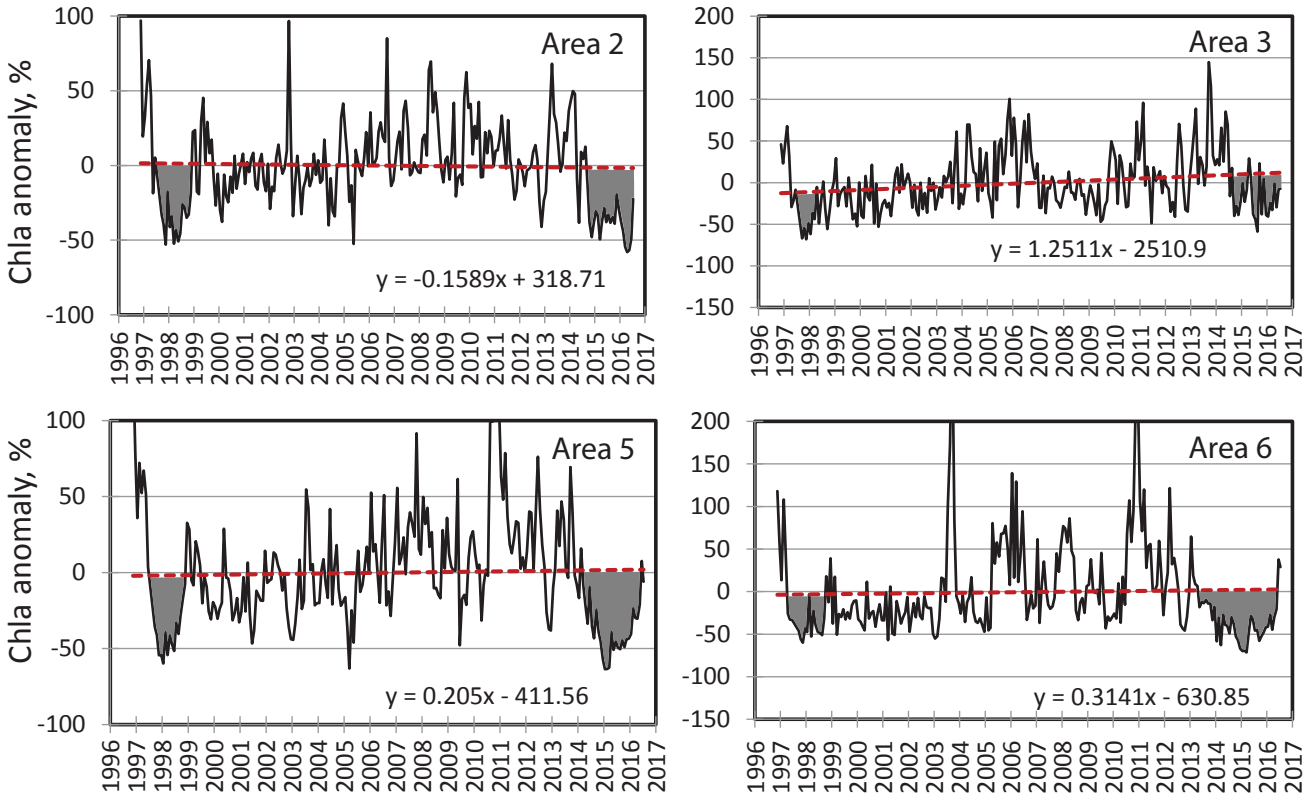

Figure 4. Anomalies in monthly mean surface chlorophyll *a* concentration in coastal and transitional areas of central and southern California (see fig. 2a). Anomalies were calculated relative to monthly means of Nov. 1996–July 2016. The red dashed line and the linear equation shows the mean linear trend. The shaded areas correspond to the anomalies of 1997–98 and 2014–16, respectively.

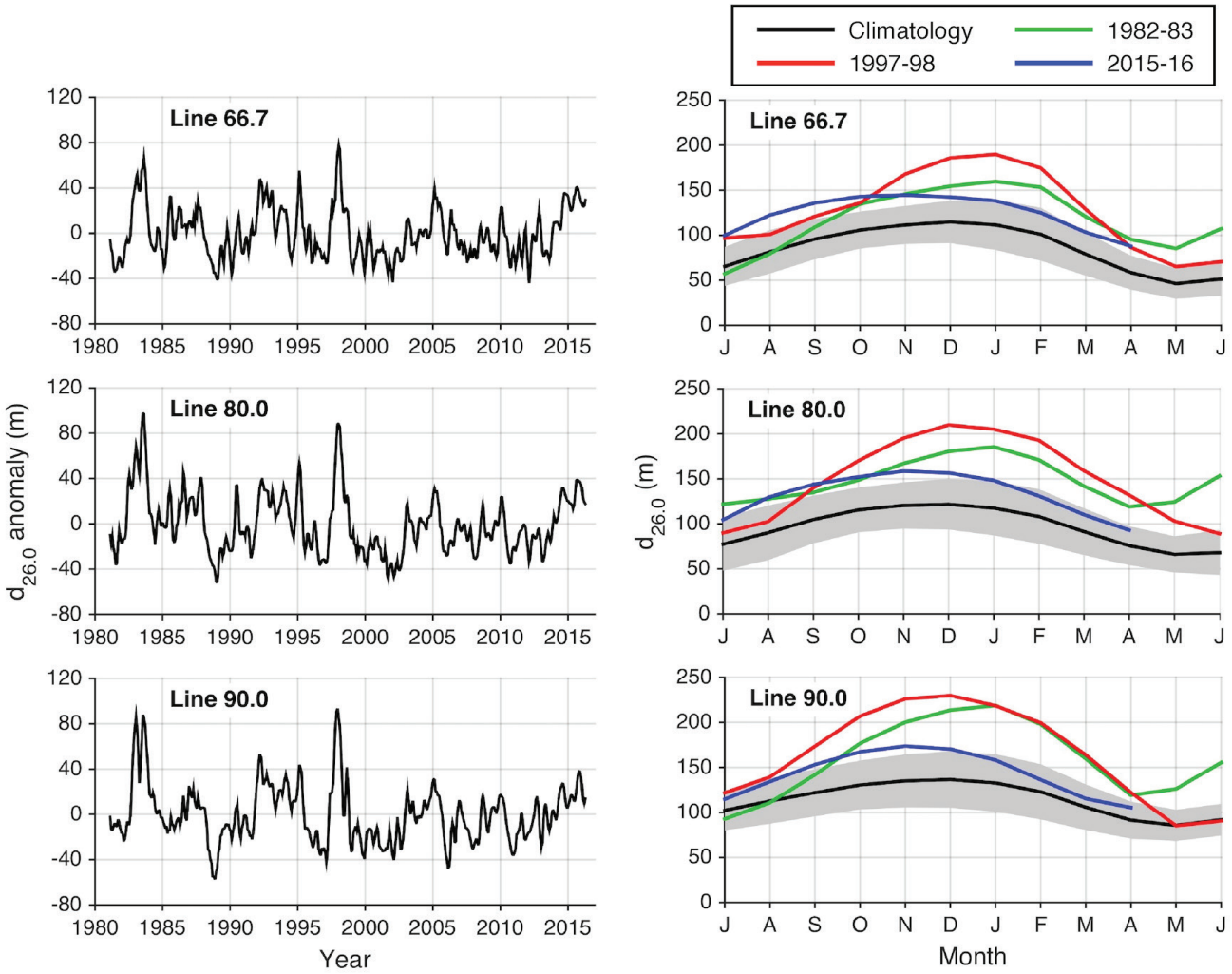

Figure 5. Time series of 26.0 kg m^{-3} isopycnal depth ($d_{26.0}$), averaged within 50 km of shore on CalCOFI lines 66.7, 80, and 90. (Left) $d_{26.0}$ anomalies from 1981 to April 2016, computed relative to a 1981–2015 climatology. (Right) 12-month (July–June) progression of $d_{26.0}$ for the three strongest El Niños of recent decades. Gray shading marks one standard deviation of the interannual variability about the climatology (black line). All time series are smoothed with a three-month running mean. Adapted from Jacox et al. (2016).

as well as during the 2015–16 warming. SST anomalies exceeded 2.5°C, which is comparable to or higher than those observed during the 1997–98 El Niño when SST anomalies reached about 2.0°C (2.5°C off central California coastal region) (fig. 3). Corresponding negative chlorophyll anomalies of about 50% were comparable to those of the 1997–98 El Niño (fig. 4). The strongest SST anomalies during 2014–16 occurred in two events separated by a weakening in the middle of 2015[6]. The anomalies began prior to the El Niño proper and were part of the multiyear North Pacific heat wave. This contrasts with the short-lived 1997–98 anomaly.

The spatial distribution of the chlorophyll *a* anomalies was evaluated using principal component analysis. The first principal component (PC1, not shown) was associated with a negative anomaly along the central California coast where upwelling is common. During El Niño events PC1 is weaker as it is associated with reduced upwelling and lower than normal chlorophyll *a* off central California. According to this measure, the 2015–16 chlorophyll *a* anomaly was weaker than the 1997–98 El Niño.

Vertical Structure of the Marine Heat Wave off California

The impact of recent climate anomalies on the subsurface structure of the CCS is highlighted by temporal variability in the depth of the 26.0 kg m^{-3} isopycnal ($d_{26.0}$). Figure 5 shows time series of $d_{26.0}$ in the nearshore region (<50 km from the coast) of CalCOFI lines 66.7, 80, and 90. These time series were obtained by combining a data assimilative regional ocean model with sustained underwater glider observations (see Jacox et al. 2016). The past year produced positive (deep) $d_{26.0}$

[6]The developing El Niño of early 2014 that was aborted by easterly wind burst in June 2014 is beyond the scope of this manuscript.

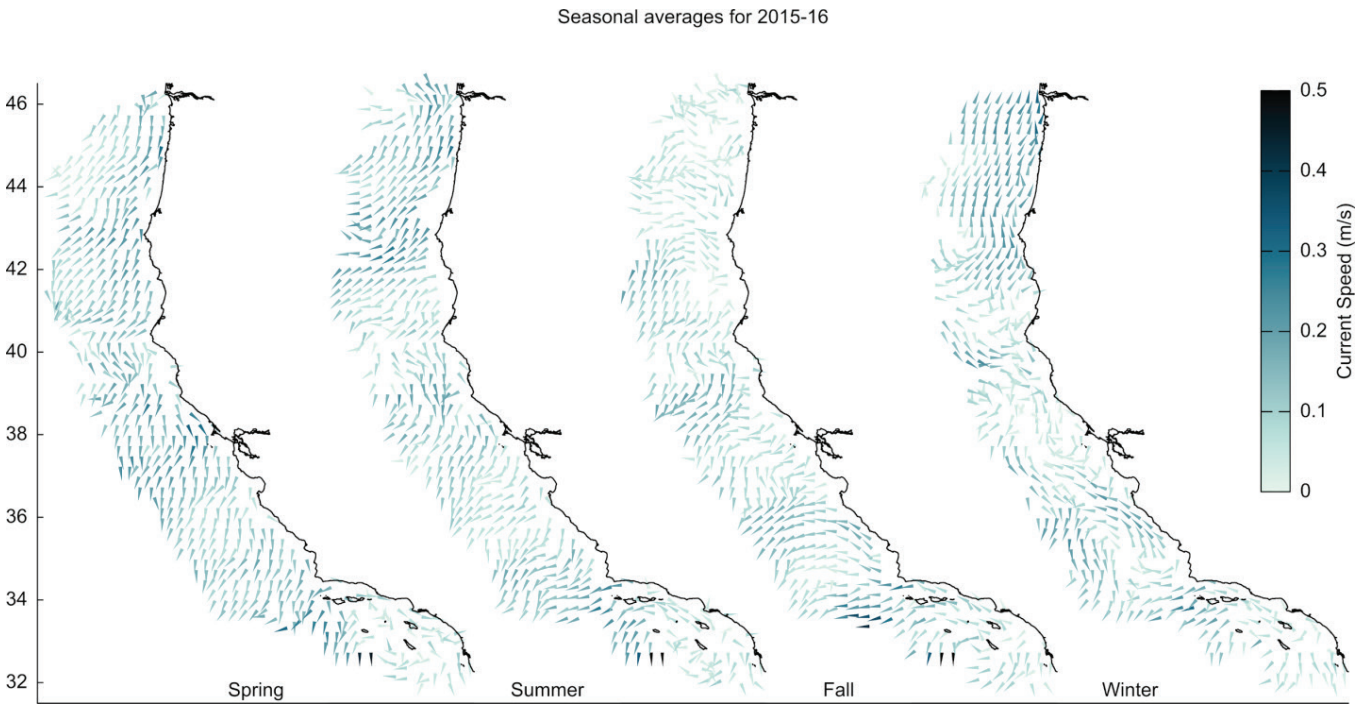

Figure 6. Maps of seasonal mean surface currents observed in the CCS with HF radar. From left to right, the panels present data for spring (March–May 2015), summer (June–August 2015), fall (September–November 2015), and winter (December–February 2016). Current speed is indicated by depth of shading and direction given by orientation of arrow extending from observation location. Currents are displayed with spatial resolution of 0.25°.

anomalies, a condition associated with limited nutrient availability and suppressed productivity. However, during the 2015–16 warming, $d_{26.0}$ was considerably shallower than during the 1982–83 and 1997–98 events, and also showcased a much different temporal evolution. The past strong El Niño events were characterized by $d_{26.0}$ increasing rapidly beginning in summer, reaching peak anomalies in winter (November to February), and then decreasing again into the spring. In contrast, 2015–16 saw $d_{26.0}$ anomalies that were already positive due to anomalous warming that began in 2014 (Zaba and Rudnick 2016), and those anomalies remained nearly constant throughout the latter half of 2015 rather than growing as would be expected during a strong El Niño. These data suggest that observed anomalies in 2015–16 were still associated with warm anomalies present for several years, with El Niño's contribution being relatively minor when compared to past strong El Niños. In the first half of 2016, $d_{26.0}$ has gradually shoaled, approaching climatological values and suggesting the decline of both El Niño and the preexisting warm anomalies.

Surface Coastal Jets Associated with 2015–16 El Niño

During 2015–16, surface currents[7] between Point Conception (34°N) and the Columbia River (46°N) were predominantly southward through spring and summer (fig. 6). During fall, as in most years, a strong mean northward flow was seen between Point Conception (34°N) and Point Sur (36.3°N). In addition, a northward flow associated with El Niño conditions was present in winter (fig. 6). This flow was weaker, farther offshore and less coherent between 37° and 41°N (San Francisco to Trinidad Head). As is usual in the winter, a coherent northward flow was observed north of the Oregon-California border (42°N), but the flow was stronger in 2015–16 than in other years.

In the Southern California Bight, the usual southward flow was observed south of San Diego (33°N) in all seasons. A poleward (westward) flow was observed between Point Vicente and Point Conception (33.8°–34.5°N) in summer, fall, and winter linking to the westward flow jetting offshore from Point Conception. Offshore jets were also observed in spring and summer southwest of major headlands as in past years (Cape Blanco 43°N, Cape Mendocino 40°N and Point Arena 39°N). In the fall, the Mendocino and Arena features appear as one, and the Blanco feature had dissipated. Meanwhile, a well-defined jet was observed off Point Sur (36.3°N) in fall associated with northward flow. In winter the northward flow continued past Point Sur.

[7]These data on surface currents were obtained from high-frequency (HF) radar, with vectors calculated hourly at 6 km resolution using optimal interpolation (Kim et. al. 2008; Terrill et. al. 2006). Real-time displays can be viewed at www.sccoos.org/data/hfrnet/ and www.cencoos.org/sections/conditions/Google_currents/ as well as at websites maintained by the institutions that contributed the data reported here (listed in Acknowledgments).

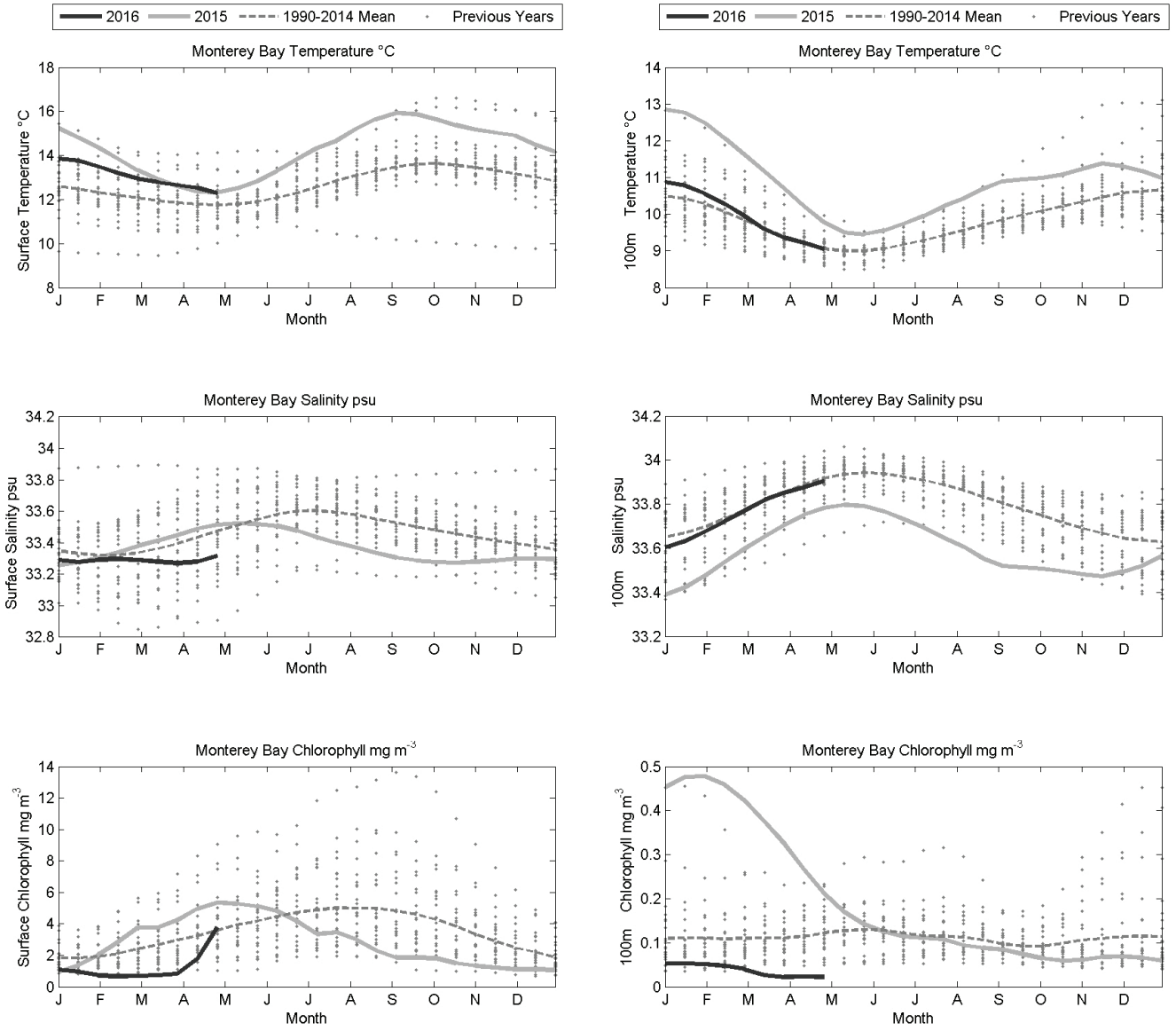

Figure 7. Temperature (top panels), salinity (middle panels) and chlorophyll *a* concentration (bottom panels) at the surface (left-hand column) and at 100 m (right hand column) observed at the M1 mooring in Monterey Bay, CA.

Warm Temperatures, Low Salinities, and Low Chlorophyll Production in Monterey Bay

Surface temperatures at the M1 mooring in Monterey Bay were only slightly above the climatological average, i.e., normal, during the spring of 2015 but began to increase in the Bay with the advent of the El Niño, declining to slightly above normal during the late spring of 2016 (fig. 7). Temperatures at 100 m were above normal during 2015, approaching normal values in the spring of 2016 (fig. 7).

Surface salinities were near the climatological average during this time period, except for the summer-fall of 2015 when extremely fresh waters were observed (fig. 7). Fresher than normal waters had been observed at 100 m throughout 2015, returning to normal values early in 2016. It is thus likely that the fresh surface waters observed during the fall of 2015 were driven by the freshening of the subsurface waters throughout 2015.

Chlorophyll *a* at the surface and at 100 m was unusually low throughout the summer and fall of 2015 and the winter and spring of 2016, only rising to average values in May 2016 (fig. 7). This may have been driven by strong stratification of the surface waters, preventing large fluxes of nitrate into this layer.

Contrasting Effects of the North Pacific Marine Heat Wave and El Niño off Southern California

This report of oceanographic observations off Southern California is based on data collected on four

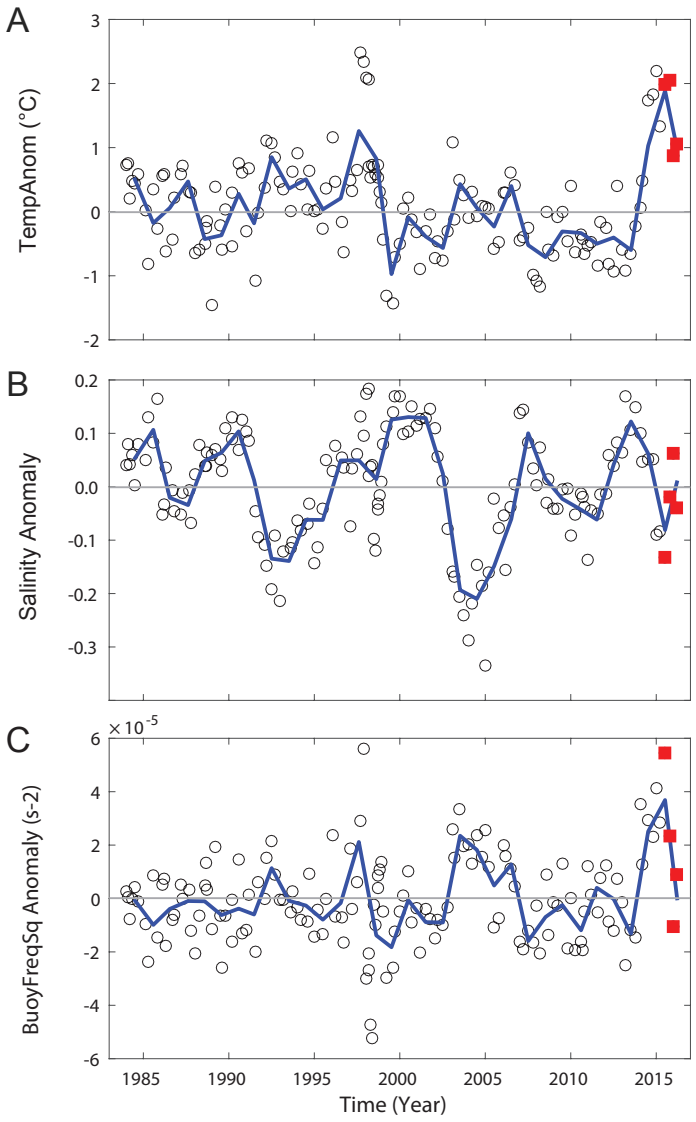

Figure 8. Cruise averages of property anomalies for the mixed layer (ML) of the CalCOFI 66 station standard grid (Figure 1) for 1984 to the spring of 2016. A: ML temperature, B: ML salinity. C: buoyancy frequency squared (N^2) in the upper 100 m. Data from individual CalCOFI cruises are plotted as open circles; data from the four most recent cruises, 201507 to 201604, are plotted as solid red symbols. Blue solid lines represent annual averages, gray horizontal lines the climatological mean, which is zero in the case of anomalies. Anomalies are based on the 1984 to 2012 time period.

CalCOFI cruises in July and November of 2015 and January and April of 2016[8].

Average mixed layer[9] (ML) temperatures during the summer and fall of 2015 in the CalCOFI domain were as high as those observed during 2014 and early 2015 (fig. 8A), likely reflecting the effects of the marine heat wave during the first half of the year and the effects of the El Niño during the second half of the year. ML temperature anomalies cooled by ~1°C during the first half of 2016, consistent with fading of the 2015–16 warming.

The area affected by the marine heat wave and the 2015–16 El Niño in the mixed layer was comparable to the 1997–98 El Niño, but the event lasted longer (fig. 9A). However, as reported previously (Leising et al. 2015), the effects of the marine heat wave on temperatures at depth were small, on the order of 0.5°C, increasing to as much as 1.5°C during the 2015–16 El Niño (fig. 9B, 100 m). This effect was particularly pronounced in the Southern California Bight compared to offshore waters, as was the case during the 1997–98 El Niño, although the effects in 2015–16 were weaker than in 1997–98 (fig. 8B). Such changes in water column properties and depth of the thermocline are thought to be

[8]Each cruise covers 66 stations off southern California (fig. 1), i.e., the CalCOFI domain, a region that encompasses the southern California Current, the Southern California Bight (SCB), the coastal upwelling region at and north of Pt. Conception and the edge of the North Pacific Gyre. At each station a CTD cast and various net tows are carried out. Up to 20 depths are sampled at each station between the surface and, bottom depth permitting, 515 m. Results are presented as time series of averages over all 66 stations (the CalCOFI domain) covered during a cruise or as anomalies of such values with respect to the 1984–2012 time period. When appropriate averages from selected regions are used, i.e., these are based on a subset of the 66 standard CalCOFI stations. The buoyancy frequency was calculated for all depths and averaged for the upper 100 m of the water column. The nitracline depth is defined as the depth where concentrations of nitrate reach values of 1 µM, calculated from measurements at discrete depths using linear interpolation. Methods used to collect samples and analyses carried out on these samples are described in detail at CalCOFI.org/methods.

[9]Mixed layer depth was defined as the depth where density of the water is 0.02 kg m^{-3} larger than density at 10 m depth.

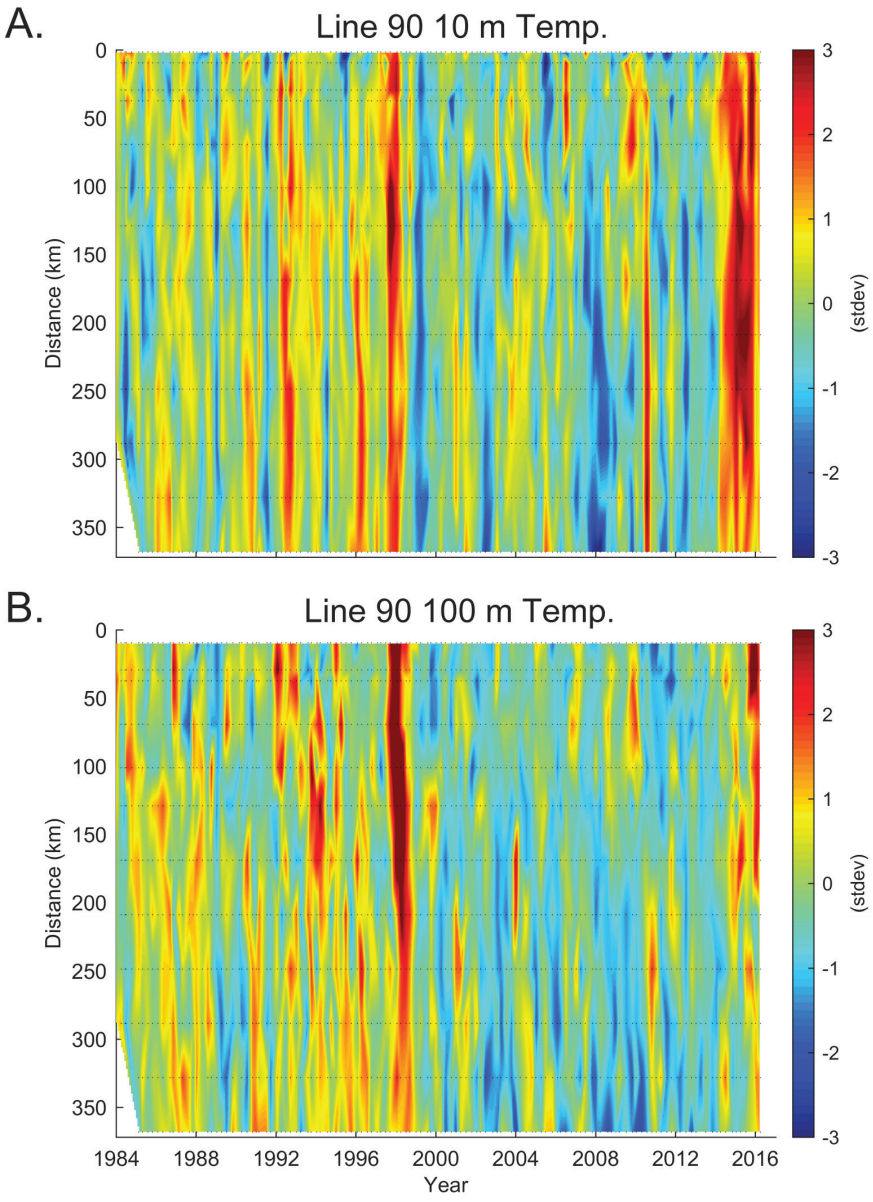

Figure 9. Standardized temperature anomalies for CalCOFI line 90 plotted against time and distance from shore for a depth of 10 m (A) and 100 m (B). Plotted data are deviations from expected values in terms of standard deviations in order to illustrate the strength of the relative changes at different depths.

driven by poleward propagating coastally trapped waves and the northward advection of warm saline water masses (Chelton and Davis 1982; Lynn and Bograd 1992). However, very little warming was observed during the 2015–16 El Niño along Line 80 at depth, in contrast to the 1997–98 El Niño (Supplement fig. S6). These observations suggest that the effects of the 2015–16 El Niño on hydrographic properties in the CalCOFI domain were not as strong as those observed during the 1997–98 El Niño.

Water column stratification in the upper 100 m (fig. 8C) during the 2015–16 marine heat wave was as strong as the most extreme values observed during the 1997–98 El Niño. However, this stratification was primarily driven by the warming of the upper 100 m. Water column stratification was strongest during the marine heat wave, decreasing as the El Niño took hold of the region. The upper ocean was unusually fresh during 2015 in most regions off southern California (Supplement fig. S7), suggesting a strengthening of the California Current.

The depth of the σ_t 26.4 isopycnal (fig. 10), which is usually found at a depth of about 200 m, increased by ~25 m during the 2015–16 marine heat wave and remained there during 2015–16. A similar change in this isopycnal depth was observed during 1997–98 El Niño.

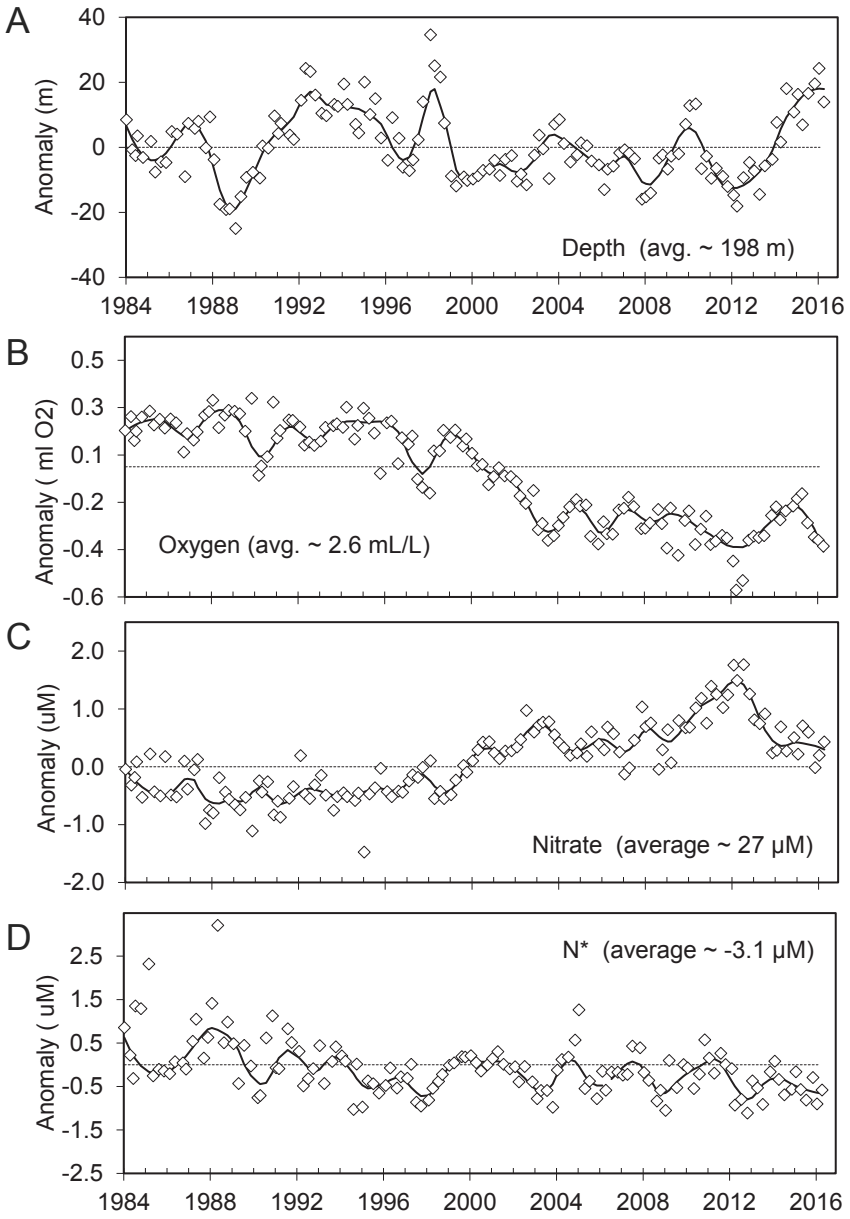

Figure 10. Anomalies of hydrographic properties at the σ_t 26.4 isopycnal (open diamonds) averaged over the standard CalCOFI stations. Shown are anomalies of isopycnal depth, oxygen, nitrate, and N*. The solid line represents a loess fit to the data; average values for the properties are listed.

Changes of spiciness at this isopycnal during 2015–16 suggest that the advection of warm saline waters into the region was likely driven by the El Niño. However, other properties at the isopycnal, such as oxygen, nitrate, and N*, a biogeochemical indicator that reflects the deficit of nitrate in a system relative to concentrations of phosphate (Gruber and Sarmiento 1997), (fig. 10B–D) were not affected by either the marine heat wave or by the El Niño.

Mixed-layer concentrations of chlorophyll *a* have been extremely low over the last three years, similar to those observed during the 1997–98 El Niño (fig. 11A). These low chlorophyll concentrations were likely caused by the low availability of inorganic nutrients such as nitrate (fig. 11B). Mixed-layer nitrate concentrations are controlled by the depth of the nitracline and by stratification. Nitracline depths, compared to the previous 15 years, have been unusually deep over the last two years (fig. 11C), and, as stated above, stratification in the upper 100 m has been unusually strong (fig. 8C). The response of chlorophyll *a* to environmental forcing during the marine heat wave and the 2015–16 El Niño differed significantly between regions within the CalCOFI domain. For example, in 2014 chlorophyll *a* concentrations in the

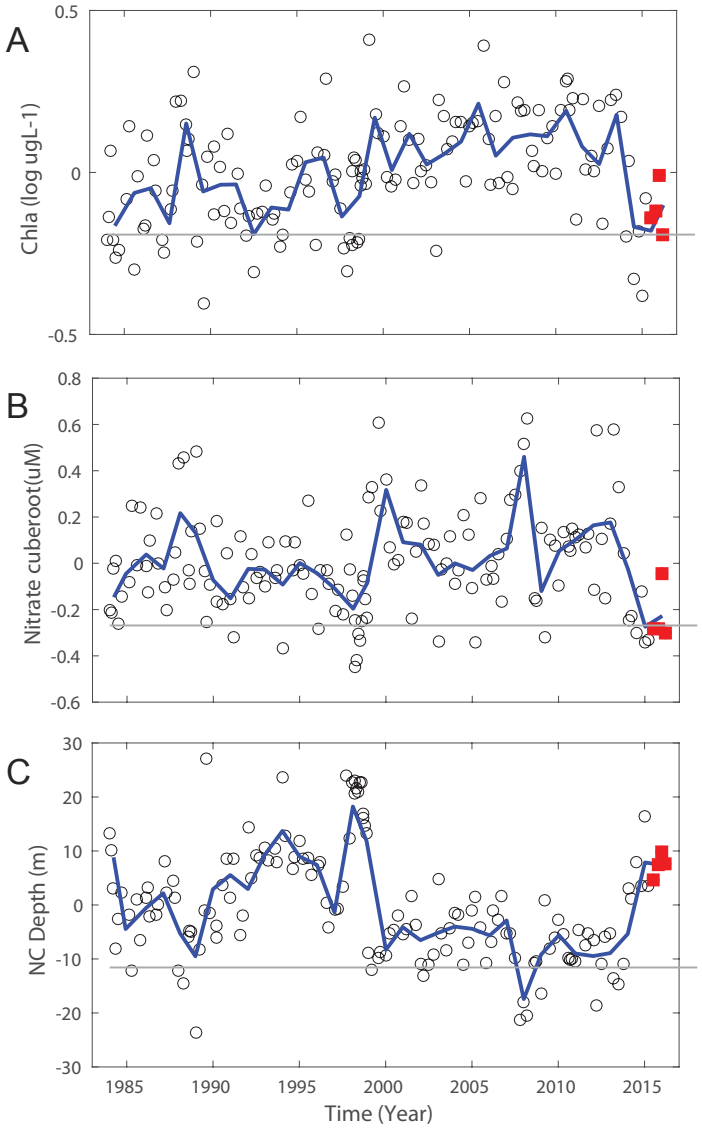

Figure 11. Cruise averages of property anomalies for a depth of 10 m for the CalCOFI standard grid. A: the log10 of chlorophyll *a*, B: the cube root of nitrate, and C: nitracline depth. Data are derived and plotted as described for Figure 8.

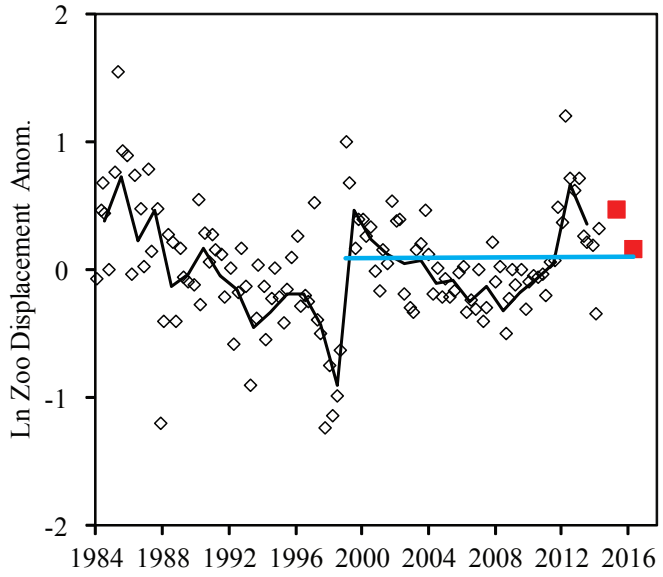

Figure 12. Cruise averages of the anomalies of the log of zooplankton displacement value relative to the 1984 to 2014 time period. Symbols used are as described in Figure 8. The blue lines are linear regressions on data for the time periods 1984 to 1998 and 1999 to the present.

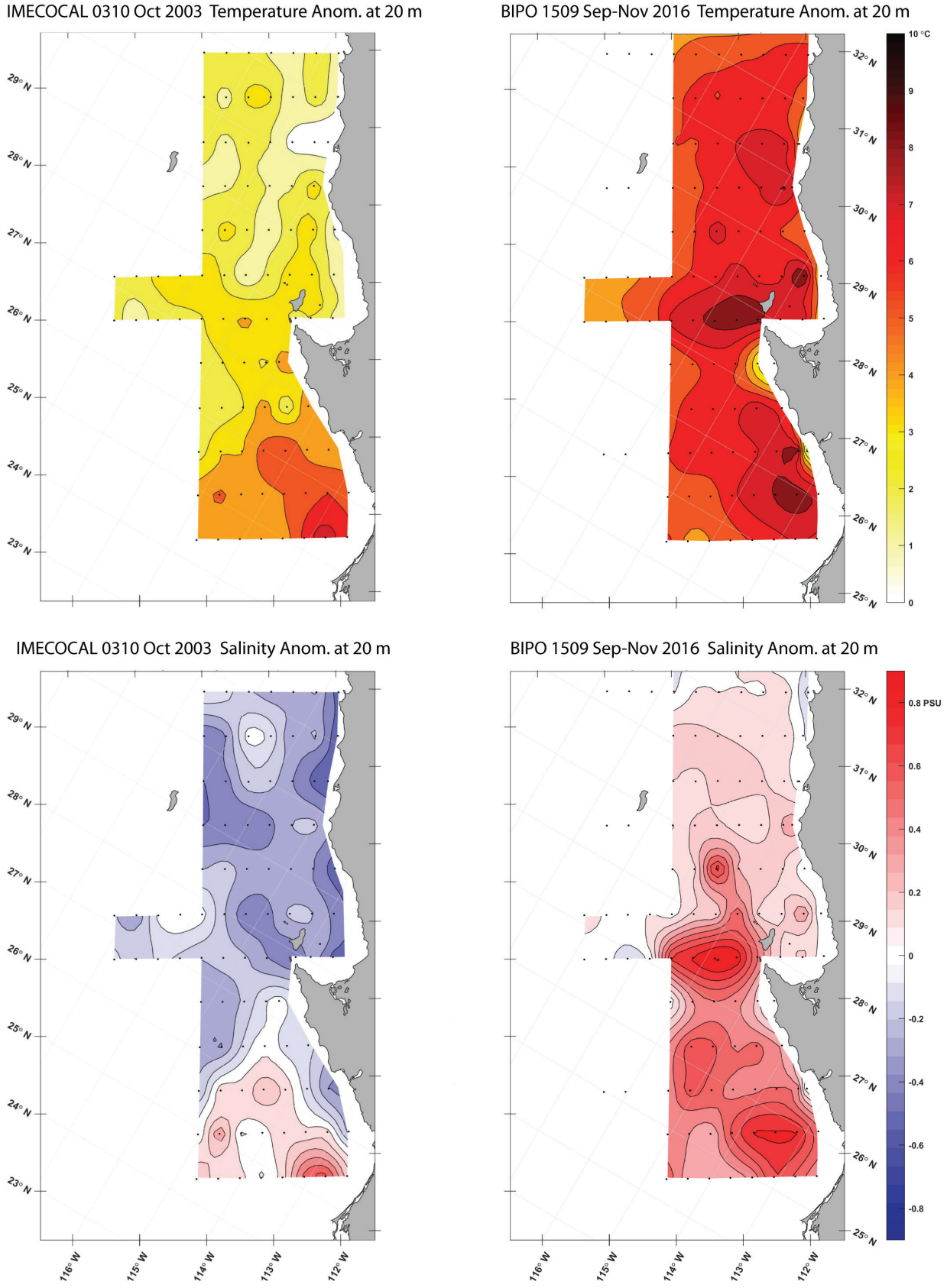

Figure 13. Temperature and salinity anomalies at 20 m depth during October 2003 (IMECOCAL cruise 0310) and September–November 2015 (BIPO cruise 1509).

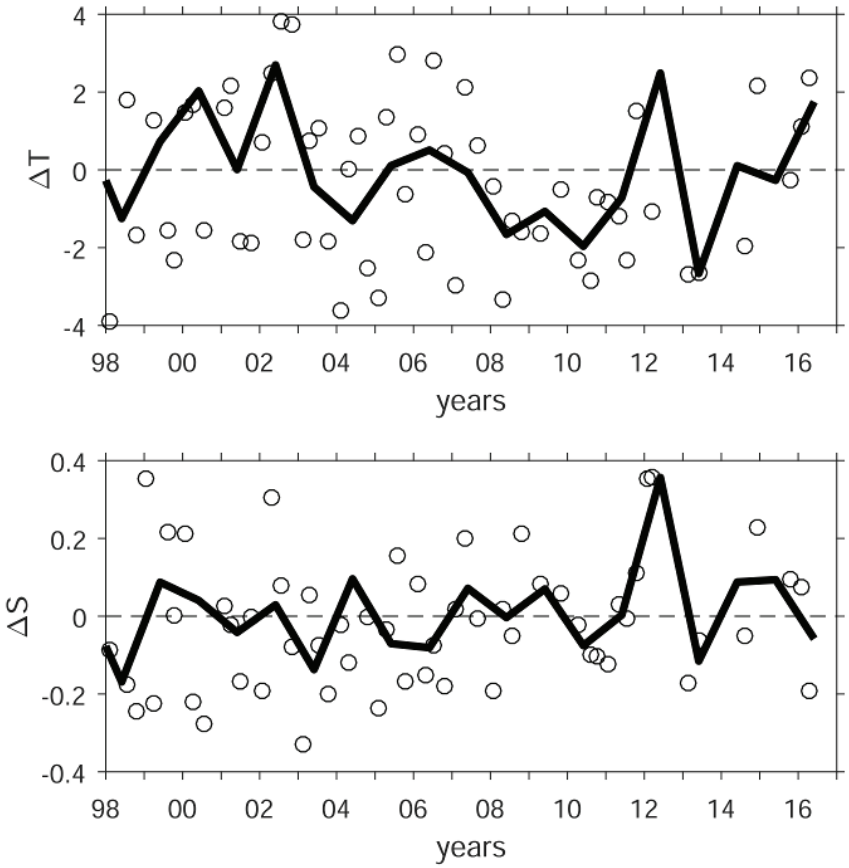

Figure 14. Mixed layer temperature and salinity anomalies in the IMECOCAL region for the period 1998–2016 (white circles) and the mean of each year (thick line).

northern coastal region were significantly below long-term averages, but were similar to these in 2015 (Supplement fig. S8). For the southern coastal area of the CalCOFI domain the opposite holds true. These regional differences are associated with interannual differences in upwelling between 2014 and 2015 (Supplement fig. S2, S4). Upwelling primarily affects the central California coast rather than the southern coastal area, which is sheltered from alongshore winds. In the southern offshore areas that are affected by the North Pacific Central Gyre, chlorophyll *a* maxima were significantly deeper during 2015, and this change was driven by differences in stratification; the temperature–nitrate relationship (data not shown) has been stable in recent years. In contrast to chlorophyll *a*, zooplankton displacement volumes for the spring seasons of 2015 and 2016 were similar to the long-term average observed over the last 15 years, indicating that zooplankton volume did not respond to the marine heat wave and the El Niño (fig. 12).

High Temperatures and High Chlorophyll Production off Baja California

Conditions off Baja California during the 2015–16 El Niño are compared here with those during October 2003[10]. The comparison with the 2003 El Niño was made because there were limited data from the Baja region during the 1997 El Niño. In October 2003, the highest SST anomalies (~6°C) were found south of Punta Eugenia and the lowest anomalies (~2°C) farther north (fig. 13). During the autumn of 2015, temperature anomalies at 20 m depth were also stronger off southern Baja and Punta Eugenia (fig. 13), but conditions were as much as 4°C warmer over the whole region (fig. 13). During the 2015–16 surveys the mean seasonal tempera-

[10]Three IMECOCAL cruises were conducted during 2015–16 aboard the oceanographic vessel *Alpha Helix*. From September 1–5, 2015 coverage was restricted to lines 100–110 off northern Baja California. During 2016, coverage was expanded to Punta Eugenia (lines 100–117) during January 21–28 and April 12–20. The third cruise was carried out during September–November 2015, as part of the INAPESCA program using the vessel *BIPO*. This cruise covered a wide area off Baja California but in the present study, we only used the data from the IMECOCAL region. CTD casts and zooplankton tows were deployed at each station of the IMECOCAL grid. Zooplankton were collected with a bongo net (0.7 m diameter, 0.5 mm mesh) towed obliquely between the surface and 210 m depth.

The mixed layer anomalies were obtained as follows. First, the long-term mean mixed layer temperature or salinity was calculated using each cast in the 1998–2016 IMECOCAL data set. Second, seasonal averages were calculated from each survey. Mixed layer anomalies for each survey were obtained by subtracting the long-term mean from the seasonal means derived from individual cruises. Temperature anomalies were computed as the difference between particular survey's temperatures and the mean temperatures from the IMECOCAL data set (1997–2016).

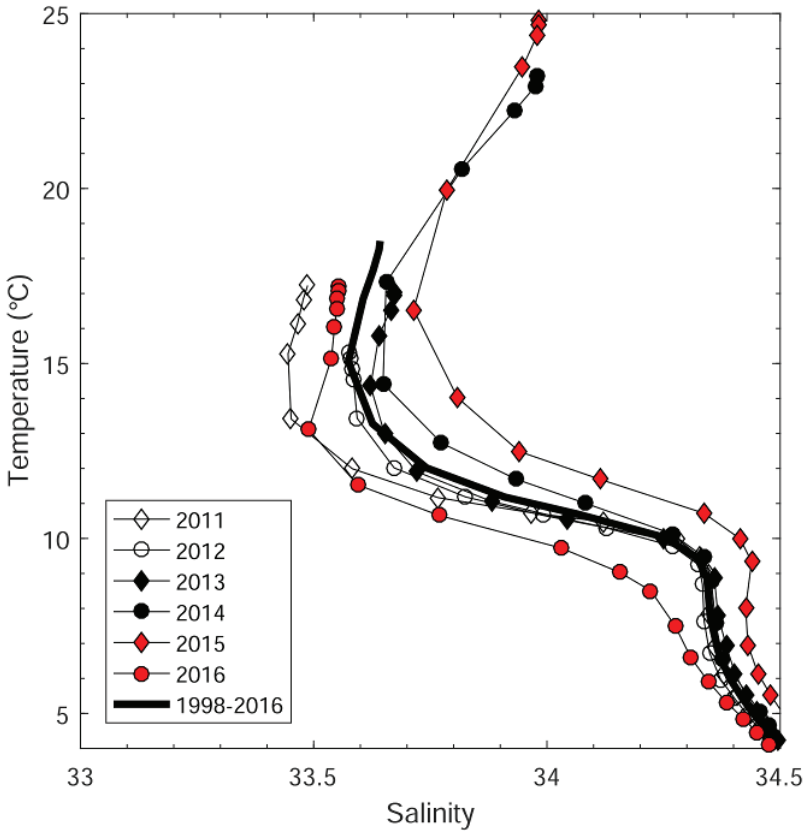

Figure 15. Annual temperature-salinity plots in the IMECOCAL region for 2011–16 compared to the long-term 1998–2016 mean.

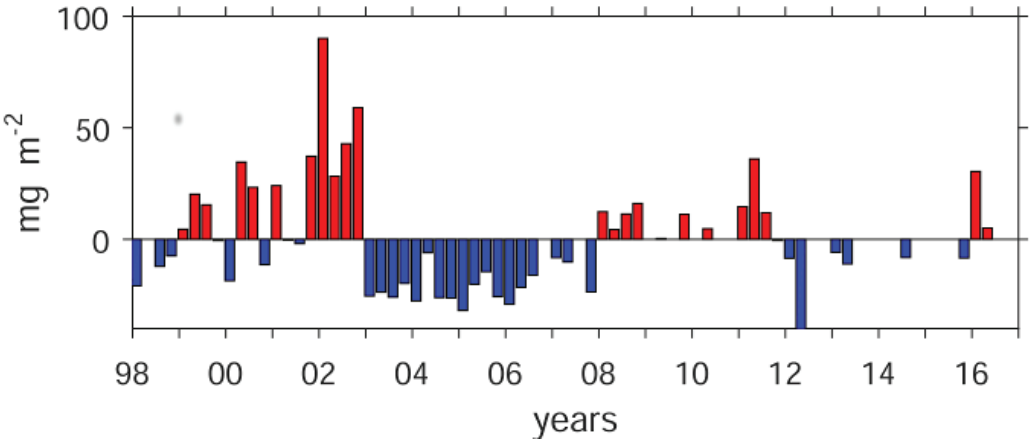

Figure 16. Depth-integrated (0–100 m) chlorophyll *a* anomalies in the IMECOCAL region. Note that chlorophyll concentrations in fall of 2015 only contain data from northern Baja California (30˚-32˚N), and are not directly comparable with the rest of the time series.

ture anomaly was of the order of +2˚C and the salinity anomaly was variable (fig. 14). Temperature-salinity plots for the IMECOCAL region clearly show the presence of anomalously warm, more saline water in 2014, increasing in 2015, before decreasing again in 2016 (fig. 15).

Salinity anomalies at 20 m depth in October 2003 tended to be negative north of Punta Eugenia and nearshore, but positive south of Punta Eugenia, except near shore (fig. 13). In contrast, during autumn 2015, salinity anomalies were positive over the entire region (fig. 13), and the salinity and temperature anomalies (fig. 13) were positively correlated. No evidence of upwelling was seen during either the autumn of 2003 or 2015.

A strong positive chlorophyll anomaly was observed during January 2016 in the IMECOCAL region (fig. 16). This positive chlorophyll anomaly during the peak of the 2015–16 El Niño contrasts with the negative chlorophyll anomaly observed in January 1998 during

the peak of the 1997–98 El Niño. By April 2016 chlorophyll had almost returned to the long-term mean concentration. We note that both chlorophyll and salinity anomalies off Baja were positive in 2015 at the same time that these anomalies were negative off southern and central California.

SUMMARY: DESCRIPTIVE PHYSICAL OCEANOGRAPHY

Warm conditions in the North Pacific, from 2014 to mid-2015, were a result of the continuation of the marine heat wave, a large area of exceptionally high SST anomalies that originated in the Gulf of Alaska in late 2013. Along the coast of North America, high positive SST anomalies due to the marine heat wave started to diminish by December 2015. Positive SST anomalies associated with the El Niño were high across the eastern equatorial Pacific from July 2015 to February 2016. Negative SST anomalies first arose in the summer of 2014 in the region of the Subarctic Frontal Zone. These negative SST anomalies persisted into May 2015. Enhanced westerly wind anomalies in the northwestern Pacific coincided with these negative SST anomalies. Westerly wind bursts are an important driver of the Kelvin waves that propagate across the Pacific, initiating El Niño conditions at the eastern boundary. The Oceanic Nino Index reached the highest positive values since the 1997–98 El Niño during the fall of 2015 and winter of 2015–16.

Positive SST anomalies remained along the coast until late winter and early spring of 2016, with SST anomalies ranging from 0.5° to 1.5°C. Daily SST as measured by NDBC buoys along the West Coast remained above the long-term average since the summer of 2014. Weekly periods of exceptionally high temperature anomalies (greater than 2°C) were observed until the fall of 2015. During the winter and spring of 2015–16, SSTs were still high but not as high as those observed previously. The decrease in SST values seen in the central CCS during the spring of 2015 corresponded with an extended period of upwelling favorable winds. Upwelling associated with the 1997–98 and 2015–16 warming events proceeded similarly, but upwelling during the winter for the 1997–98 event was much weaker than 2015–16.

The impact of recent climate anomalies on the subsurface structure of the CCS was highlighted by temporal variability in the depth of the 26.0 kg m^{-3} isopycnal ($d_{26.0}$). During the 2015–16 warming, $d_{26.0}$ was considerably shallower than during the 1982–83 and 1997–98 events, and also showcased a much different temporal evolution. The past strong El Niño events were characterized by $d_{26.0}$ increasing rapidly beginning in summer, reaching peak anomalies in winter (November to February), and then decreasing again into the spring. In contrast, 2015–16 saw $d_{26.0}$ anomalies that were already positive due to anomalous warming of the North Pacific that began in 2014. In the first half of 2016, $d_{26.0}$ gradually shoaled, as is often the case, approaching climatological values and suggesting the decline of both El Niño and the preexisting warm anomalies.

Mixed layer temperature anomalies off southern California in 2014–16 were significantly higher than those observed during the previous 15 years, and did not begin to cool until the first half of 2016. The area affected by the marine heat wave and the 2015–16 El Niño in the mixed layer was comparable to the 1997–98 El Niño, but the event lasted longer. Water column stratification in the upper 100 m during the 2015–16 marine heat wave was as strong as the most extreme values observed during the 1997–98 El Niño. However, this stratification was primarily driven by the warming of the upper 100 m. The upper ocean was unusually fresh during 2015 in most regions off southern California, suggesting a strengthening of the California Current. We note that this contrasted with higher than normal salinity off Baja California in 2015. Nitracline depths, compared to the previous 15 years, have been unusually deep over the last two years and stratification in the upper 100 m was unusually strong. Despite these notable perturbations, the effects of the 2015–16 El Niño on hydrographic properties in the CalCOFI domain were not as strong as those observed during the 1997–98 El Niño.

UNPRECEDENTED HARMFUL ALGAL BLOOM OF 2015–16

Off central California temperature anomalies exceeding 7°–8°C were observed at shore stations such as the Santa Cruz Municipal Wharf during the marine heat wave. Nutrient data from the Santa Cruz Municipal Wharf (SCMW) in Monterey Bay suggest that associated changes in the mixed layer led to dramatically suppressed nutrient concentrations. Silicic acid, nitrate (fig. 17A), and $Si(OH)_4$:NO_3 were low despite normal upwelling index values throughout the time period (fig. S2). This likely provided perfect conditions for the particularly toxic species, *Pseudo-nitzschia* australis, to bloom in 2015 since it appears to be a good competitor in post-upwelling scenarios where nutrients (particularly Si) are in limiting supply (Sommer 1994; Marchetti et al. 2004; Anderson et al. 2006; 2008). This historic bloom was truly unprecedented given its long duration from mid-April to September (fig. 17B) and its geographic extent along the entire US West Coast—occurring nearly simultaneously from Santa Barbara, CA, to Kodiak, AK—in direct association with the marine heat wave's expansion throughout the North Pacific from 2014 to 2015. This massive bloom led to record-breaking levels of domoic acid

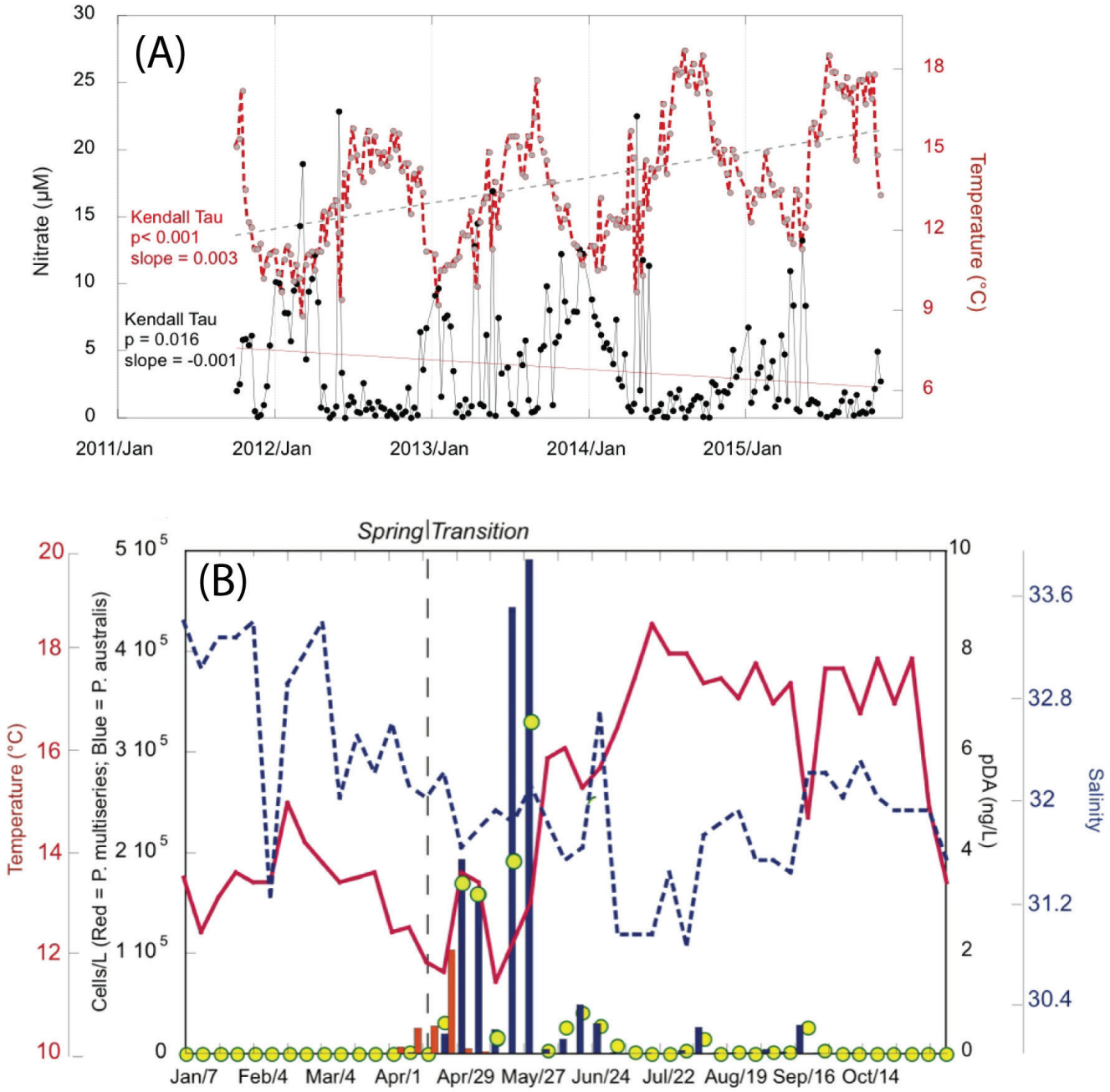

Figure 17. Physical, chemical, and biological properties in the CCS during 2015. (A) SST and nitrate (2011–16) at the Santa Cruz Municipal Wharf (SCMW) in northern Monterey Bay; (B) SCMW records of SST, salinity, *Pseudo-nitzschia* cell counts, and particulate DA in spring to summer 2015 (Kudela, unpublished data).

(DA) in the water column (fig. 18, observations) and extensive food web effects, such as record closures of several economically important fisheries, including the highly lucrative Dungeness crab fishery. Toxin levels hit new highs in dissolved and particulate DA, anchovy, Dungeness and rock crab, and pelicans. DA toxin was found in the fillets of several species of commercially harvested fish (McCabe et al., submitted), and toxin was routinely detected in Monterey Bay Aquarium tanks as well as in the captive sea lion tanks at Moss Landing Marine Laboratory, where one sea lion exhibited symptoms of DA exposure (Kudela et al., unpublished data).

The California Harmful Algae Risk Mapping (C-HARM) System publishes daily nowcasts and 3-day forecasts of *Pseudo-nitzschia* bloom and domoic acid event likelihoods for coastal California on the Central and Northern California Ocean Observing System (CeNCOOS) data portal. C-HARM captured the bloom dynamics at the Santa Cruz Municipal Wharf (SCMW) with 61% and 73% accuracy for

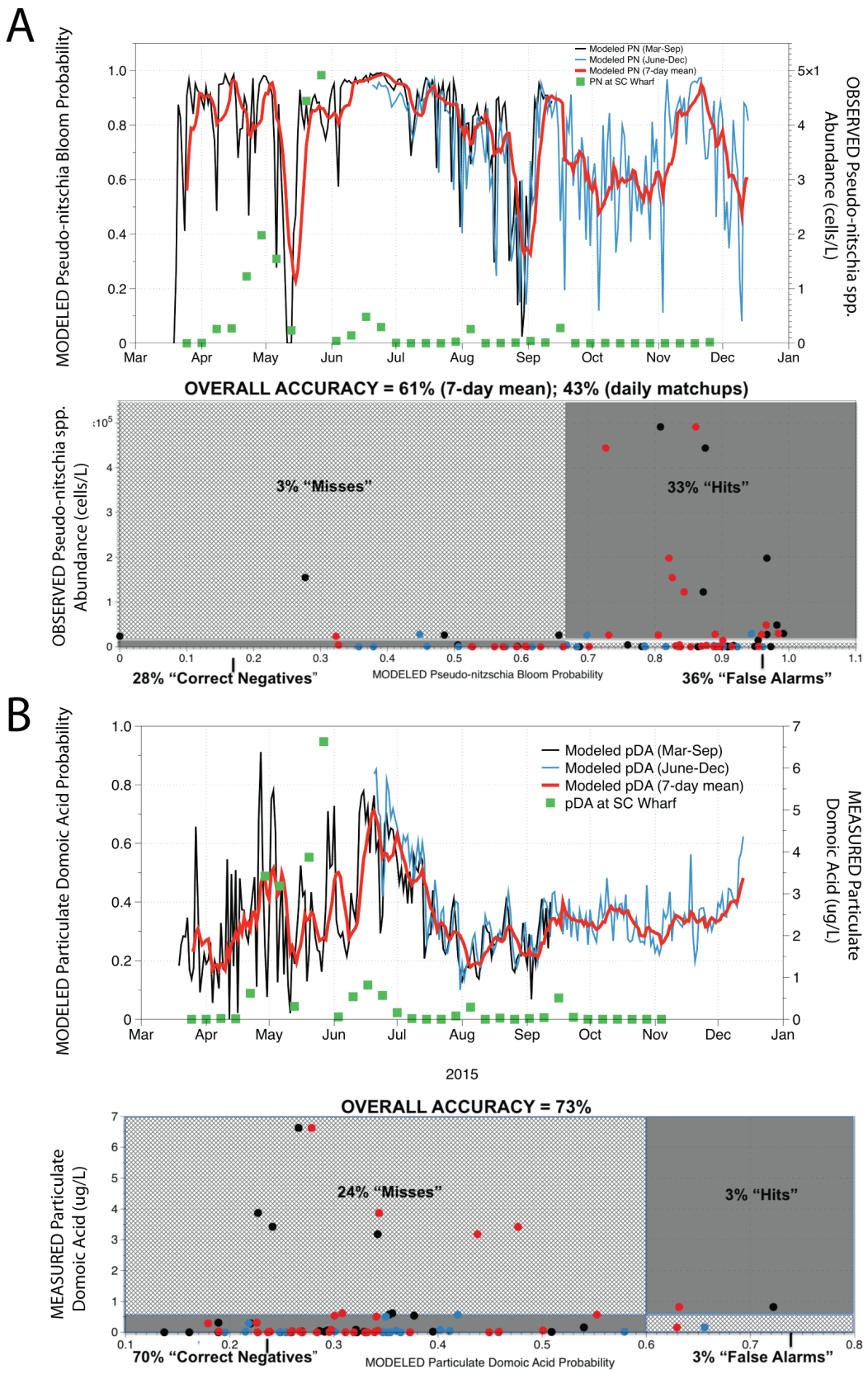

Figure 18. Contingency plots showing the performance of the California HAB model at the Santa Cruz Wharf in 2015. Top = accuracy of *Pseudo-nitzschia* bloom predictions; Bottom = accuracy of the particulate domoic acid (pDA) predictions.

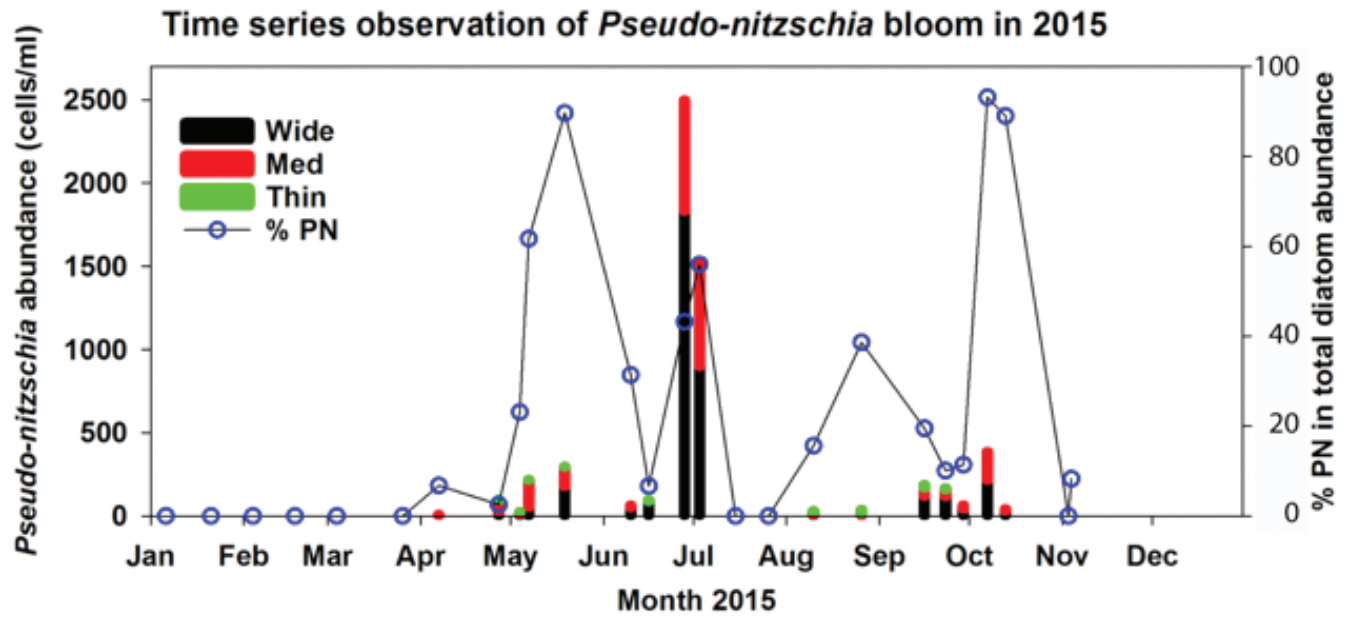

Figure 19. The bloom initiation and development observed at the nearshore station NH5. Bars stacked by the three sized *Pseudo-nitzschia* groups indicate cell abundances (left *y*-axis). Circles connected by dotted lines represent proportions of *Pseudo-nitzschia* (blue circles, right *y*-axis) in the total diatom abundance.

Pseudo-nitzschia and domoic acid, respectively (fig. 18). Interestingly, the abundance of *Pseudo-nitzschia* was not unusually high into the summer at the SCMW (fig. 17B) and total domoic acid levels exceeded 2015 results in both 2014 and 2016. As a result, the 3 km model overpredicted the severity of the bloom at the SCMW, but accurately predicted the high toxin levels exhibited immediately offshore.

In contrast to the central California results, the model successfully identified a new toxic "hot spot" off northern California. Observations from the Southwest Fisheries Science Center's Trinidad Head Line identified maximum total DA concentrations in excess of 15,000 ng/L. Visual inspection of zooplankton samples indicated high concentrations of *Pseudo-nitzschia* from spring through early fall of 2015, coincident with elevated DA concentrations during this period. Record concentrations of DA were observed in razor clams from Humboldt County (340 ppm DA in late 2015), and the waters off Humboldt County were the last to see the crab fishery opened for harvest; both of these observations further attest to the intensity and duration of the HAB off northern California.

The Toxic and Persistent *Pseudo-Nitzchia* Bloom off the Oregon Coast in 2015

The *Pseudo-nitzschia* bloom that developed off Oregon in 2015 led to the closures of razor clam harvest for nearly a year and delayed the opening of the Dungeness crab fishery for only 6 weeks. Oceanographic conditions preceding, during, and following this bloom were tracked from biweekly to monthly field observations of temperature, salinity, nutrients, and *Pseudo-nitzschia* abundance off Newport, Oregon (44.6°N) (Du et al., submitted).

Pseudo-nitzschia cells were first detected in late March nearshore and increased slightly prior to the spring transition in mid-April (fig. 19). After the spring transition, *Pseudo-nitzschia* abundance increased to 105 cells/L in late April but contributed only a low percentage (2.5%) of the total diatom abundance. Following the episodic strong upwelling events in early May, *Pseudo-nitzschia* abundance continued to increase. By late May, the first *Pseudo-nitzschia* bloom peaked at Newport along with a dramatic increase of *Pseudo-nitzschia* percentage from 23% to 90% of total diatoms, indicating the formation of a monospecific bloom. Following this bloom peak, domoic acid concentration in razor clams (Oregon Department of Agriculture) reached its highest level in early June at Newport. The bloom began to decay in mid-June, as inferred from the declines of both the abundance and proportion of *Pseudo-nitzschia*. A second bloom peak was observed in late June and cell abundance remained high in early July with a higher magnitude (106 cells/L) than the first peak. The percentages of *Pseudo-nitzschia* cells were about half of total diatom abundance. However, there was no report of increasing DA in clams even though *Pseudo-nitzschia* abundances were the highest during this time. *Pseudo-nitzschia* cells were absent in mid-late July but recurred following a resurgence of stronger upwelling in early August. A bloom did not form until the end of August albeit with a low magnitude. The bloom continued in

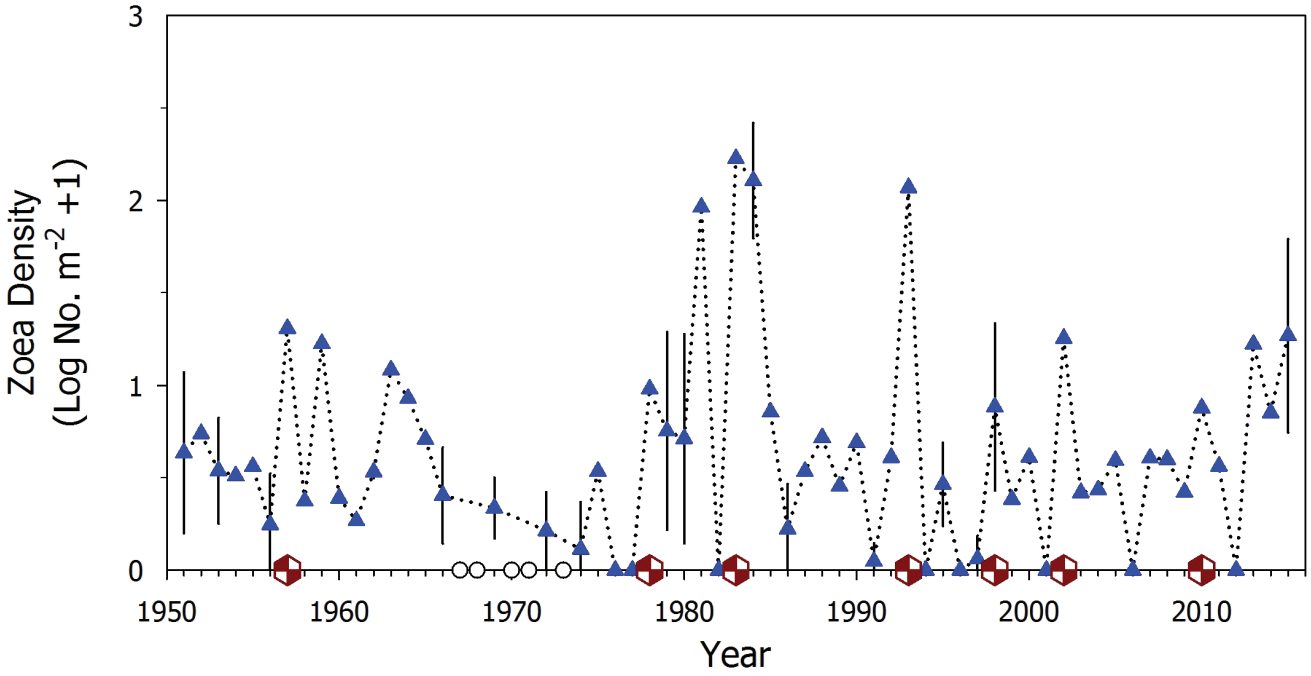

Figure 20. Time series of *Pleuroncodes planipes* total zoeae in nighttime CalCOFI net samples from springtime cruises off southern California, for the region indicated in Figure 21. Density (Log No. m^{-2} +1) of *Pleuroncodes planipes zoeae.* Error bars indicate 95% C.L. when individual samples were enumerated; otherwise pooled samples were enumerated (cf. Lavaniegos and Ohman 2007). Open circles on abscissa indicate years when no CalCOFI spring sampling was conducted. Red semaphores indicate years in which the effects of El Niño were evident in Californian waters. From the SIO Pelagic Invertebrate Collection.

September through early October and then decayed completely shortly after the end of the upwelling season. From July until the end of 2015, DA in clams maintained at a constant level near Newport.

Triggers of the Toxic Bloom

Macronutrient conditions likely played a critical role in triggering the toxic bloom off Oregon. Silicic acid limitation stress is one of the recognized toxin-induction factors. Silicic acid concentrations were <0.3 μM, nitrate concentrations <0.4 μM and Si:N ratios ranged from 0.04 to 0.8 in March and early April. Nutrient stress preceding the toxic bloom was related to two oceanographic events: from September 2014 through 2015 by the marine heat wave, leading to a highly stratified water column and deepening of nutricline, and the drawdown of available nitrate and silicic acid during an intense winter phytoplankton bloom in February and early March 2015. Replenishment of nutrients to the upper water column from upwelling events after the spring transition promoted and sustained the *Pseudo-nitzschia* bloom. For example, at no time in May and June did concentrations of NO_3 fall below 3 μM or SiO_4 below 5 μM. The ratios of Si:N ranged between 1.6–2.3.

The strength of upwelling and associated onshore-offshore Ekman transport regulated the availability of toxic *Pseudo-nitzschia* cells to razor clam beds to some extent and likely contributed to the differences of toxin accumulation in razor clams. Upwelling was intermittent during mid- and late May and toxic *Pseudo-nitzschia* cells were retained very nearshore. The continuous exposure to the toxic cells likely led to the sharp increase of DA level in clams. In contrast, upwelling in June was strongest in 2015. The resultant stronger offshore transport kept most of the toxic *Pseudo-nitzschia* cells away from the nearshore zone and thus reduced the toxic effects.

SUMMARY: UNPRECEDENTED HARMFUL ALGAL BLOOM

Warm ocean conditions and associated stratification combined with nutrient suppression and silicic acid stress likely favored initiation of the *Pseudo-nitzschia* toxic bloom in fall 2014. The winter/spring phytoplankton bloom of February and early March 2015, and higher nutrient concentrations following the spring transition to upwelling, favored explosive growth of the bloom. Local-scale forcing from coastal upwelling driving richer nutrient conditions and cross-shelf transport provided the ultimate explanation for the development of the *Pseudo-nitzschia* bloom and toxic effects.

CHANGES IN THE DISTRIBUTION AND ABUNDANCE OF ZOOPLANKTON

Red Crabs off Southern California

Pleuroncodes planipes (red or tuna crab) is a micronektonic crustacean well adapted to a pelagic life during the larval phase and in the first adult year. During nor-

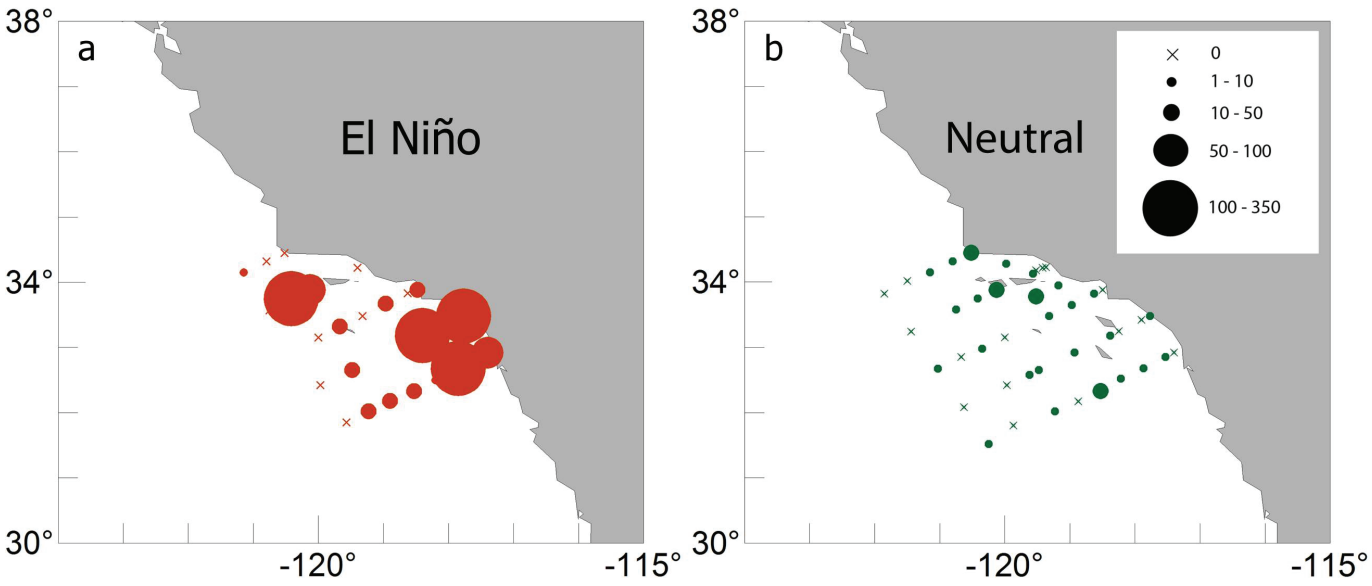

Figure 21. Density of *Pleuroncodes planipes* total zoeae (No. m^{-2}) in nighttime CalCOFI net samples from springtime cruises off southern California, during (a) El Niño-influenced years, and (b) El Niño-neutral years. Only years in which individual stations were analyzed ("unpooled samples," cf. Lavaniegos and Ohman 2007; Niño: cruises 1979, 1984, 1998; Neutral: 1951, 1953, 1956, 1966, 1972, 1974, 1979, 1980, 1986, 1991, 1995, 1997) are included. "X" indicates no specimens found. From the SIO Pelagic Invertebrate Collection.

mal years it forms dense aggregations off southern Baja California and in the offshore region of the Mexican tropical Pacific, but during El Niño years it is often found off southern and central California (Boyd 1967; Gómez-Gutiérrez and Robinson 2006; Longhurst 1967). It's eaten by large predators including yellowfin tuna, skipjack tuna, and many other fishes, birds, turtles, pinnipeds, and whales.

The first observation of an adult *Pleuroncodes planipes* in plankton samples off southern California in 2014 appears to have been on 29 July 2014 off San Diego's Nine Mile Bank (M.D. Ohman, pers. obs.). The first reports in 2015 were from fishers who found pelagic red crabs in the stomach contents of California yellowtail (*Seriola lalandi*) on 1 Jan. 2015 ~8 km west of Mission Bay, San Diego (L. Sala, pers. obs.). Beach strandings of adult *Pleuroncodes planipes* were subsequently widely reported in southern and central California during 2015, beginning on San Clemente Island in January and progressing intermittently northward to San Miguel Island by June, eventually reaching Pacific Grove by October. The northernmost location appears to have been an adult collected in a Tucker trawl off Cordell Bank in September 2015 (J. Jahncke, pers. comm.). Adults were common in the water column at Nine Mile Bank in June 2015 (to densities of 5–15 individuals m^{-2} visible at the sea surface, usually at night, M.D. Ohman, pers. obs.). Many accounts of occurrence at sea and beach strandings of adults were subsequently reported during the El Niño of 2015–16.

Turning to larval stages sampled in the plankton by CalCOFI, a multidecadal springtime time series shows that zoea stages of *P. planipes* have been present in the southern California region in spring in nearly all years in the last 6½ decades (fig. 20). Of a total of 60 spring surveys enumerated, in only 8 years (1976, 1977, 1982, 1994, 1996, 2001, 2006, 2012) were no zoeae detected. However, densities are typically very low, averaging 3.3 zoeae m^{-2} (untransformed range: 0–163 m^{-2}; note log scale in fig. 20) across the time series. Average density increases during and/or immediately after El Niño years (e.g., 1957–58, 1977–78, 1983–84, 1992–93, 1998, 2009–10; red semaphores in fig. 20) but also during warm water years that are not linked to El Niño. The major El Niño of 1957–59 showed moderately high densities of *P. planipes* zoeae, despite the widespread occurrence of adults in CalCOFI samples (Longhurst 1967).

The historical (i.e., prior to 2015) spatial distribution of zoea stages of *P. planipes* in springtime reveals that during El Niño years, zoea larvae are typically most abundant nearshore in the Southern California Bight and in the vicinity of the Channel Islands (fig. 21a). Densities decrease in offshore waters. This spatial distribution is consistent with an influx of larvae in coastal waters originating to the south, possibly followed by offshore transport in the Southern California Eddy. In contrast, during El Niño-neutral springs, densities of zoea larvae are nearly an order of magnitude lower in abundance ($p < 0.01$, Mann-Whitney U) and show less tendency to be elevated near the coast (fig. 21b).

In spring 2015 *P. planipes* total zoeae showed a generally coastal distribution, with some zoeae extending to station 86.7 60 (fig. 22f), although few nighttime samples were available from cruise 1504NH to resolve distributions close to shore or in proximity to the Channel

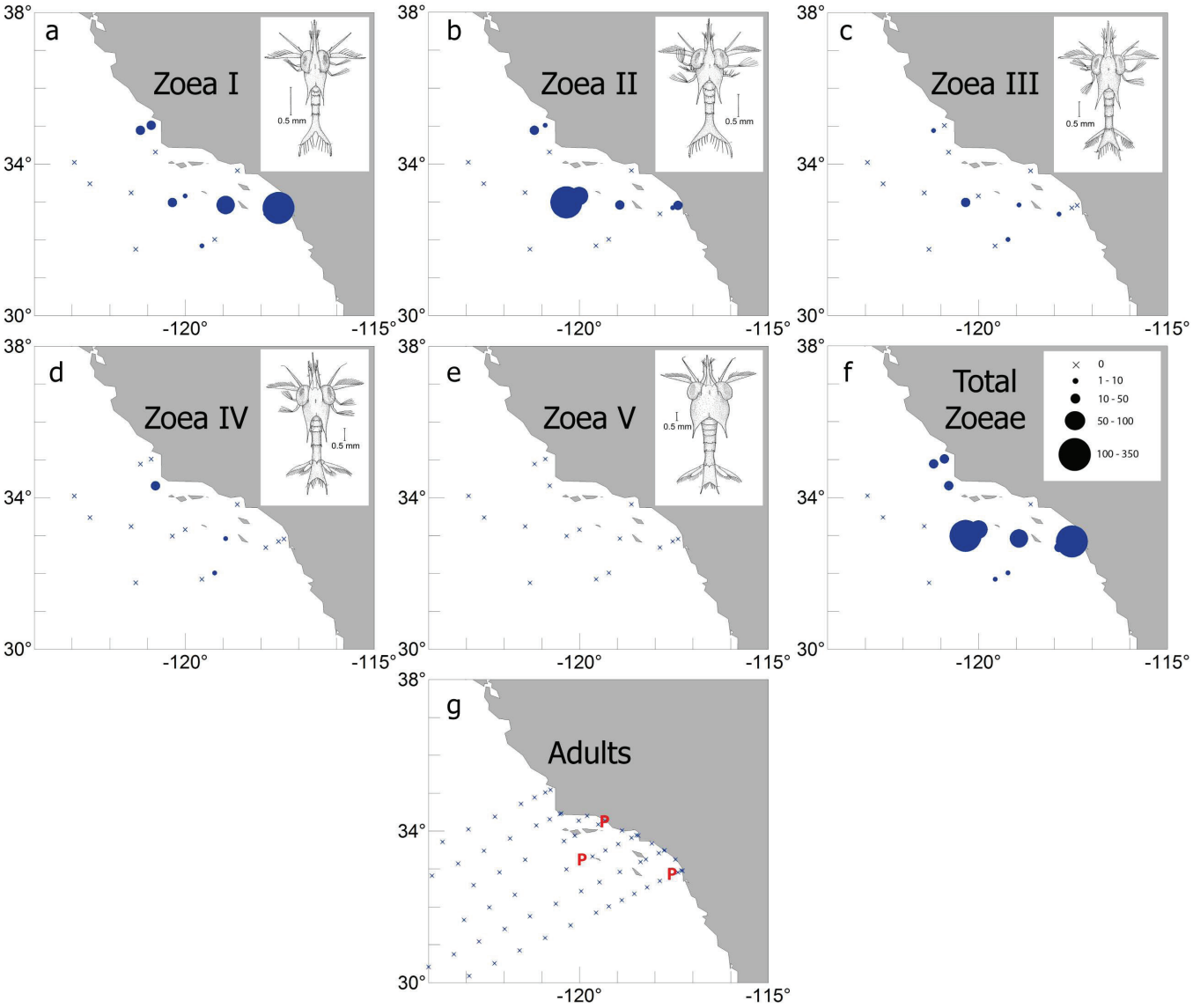

Figure 22. Occurrence of *Pleuroncodes planipes* in CalCOFI bongo net samples on cruise 1504NH (April 2015). Panels (a)–(f) indicate density (No. m^{-2}) of zoea stages I–V and the sum of all zoea stages, respectively, enumerated only from nighttime samples. Panel (g) indicates the presence ("P") of adults enumerated from both day and night samples, although all three positive records occurred at night. "X" indicates no specimens found. Illustrations of zoeae reproduced from Boyd (1960). From the SIO Pelagic Invertebrate Collection.

Islands. Analysis of the spatial distribution of the five zoea stages of *P. planipes* treated separately shows that stages I and II were the most abundant, with markedly lower abundances of zoea stages III and IV, and no stage Vs detected (fig. 22a–e). Adults were found in net samples at only three locations, all toward the southeastern part of the sampling pattern (fig. 22g).

It is highly unlikely that the proliferation of larval and adult *P. planipes* in southern California in spring 2015, when beach strandings of adults were common, can be attributed to in situ population growth alone without preceding advection from more southern waters. The adults found at sea and on beaches were in size classes typical of 2-year old *P. planipes* (Boyd 1962, 1967), suggesting that a very protracted period of favorable conditions in situ would have been necessary to lead to such abundances. However, in April 2015 larval stages were dominated by zoea I and II, with few zoea IV and no zoea stage V detected, suggesting inhospitable conditions for larval survival and population growth. It is more likely that adults had been advected into the region from the southeast in northward coastal flows, followed by advection offshore and relatively high mortality of later zoea stages. While Zaba and Rudnick (2016) concluded that there was no evidence of anomalous northward advection in this region in 2014–15, they averaged glider-derived velocity data over the nearshore 200 km. In contrast, coastally located moorings in southern

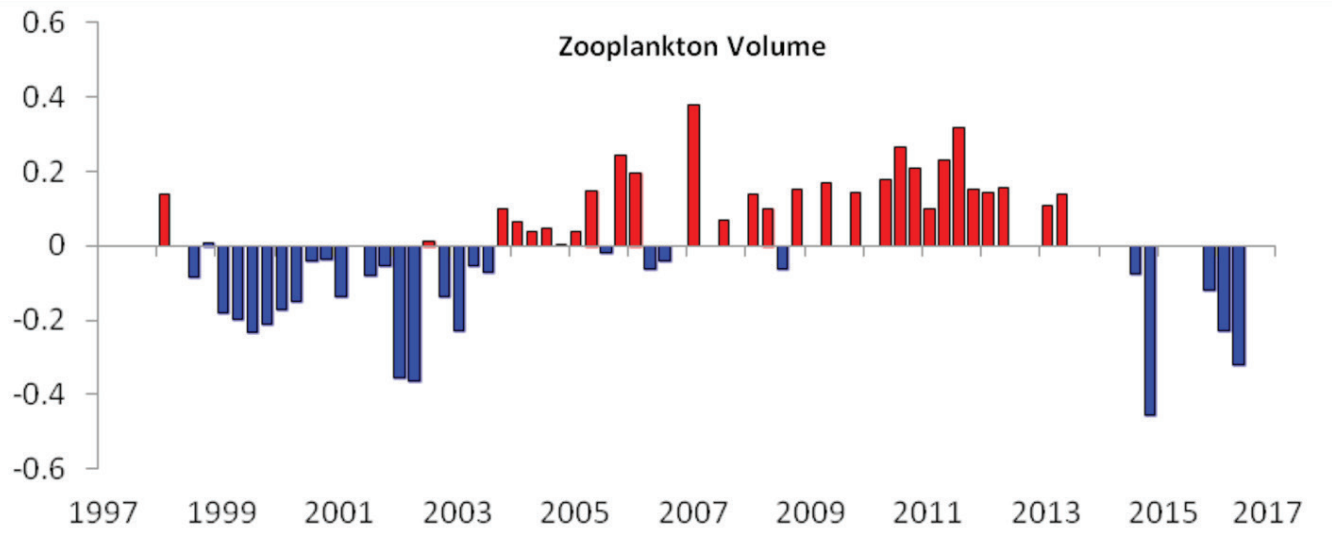

Figure 23. Zooplankton biomass anomalies (Log µl m^{-3}) off Baja California from January 1998 to January 2016.

California indicate anomalously large northward flows at two locations close to the continental shelf (U. Send, pers. comm.). Furthermore, mean advection close to the coast is typically northward, especially in fall–winter (the Inshore Countercurrent, Lynn and Simpson 1987). Satellite altimetry averaged across 200 km from the coast suggests anomalous northward flows off Baja California from April–Nov 2014, resuming weakly northward in Feb–March 2015 (P.T. Strub, pers. comm.), indicating a southern source for *P. planipes* during this event.

Expansion of Tropical Species off Baja California

The high positive temperature anomalies recorded off Baja California in 2015–16 were associated with extremely low zooplankton displacement volumes (fig. 23). Note that low zooplankton volumes were observed in 2014 before the onset of the 2015–16 El Niño, ending a period (2004–13) of positive zooplankton volume anomalies. Despite high SST during the El Niños of both 1997–98 and 2015–16, the response of zooplankton volume was quite different, reflecting the unique character of each El Niño. Low zooplankton volume in fall 2015 and January 2016 (fig. 23) was caused by low abundance of gelatinous plankton, copepods, and euphausiids. It is possible that lower grazing pressure contributed to higher chlorophyll in 2016 (fig. 16). In contrast, during the 1997–98 El Niño, zooplankton volume was close to the average, with abundant copepods, euphausiids, and salps at some stations.

During autumn 2015, tropical species such as *Pleuroncodes planipes* (red crabs) expanded into the northern IMECOCAL region and extended their distribution offshore south of Punta Eugenia (fig. 24). During a typical autumn such as October 2003, adult red crabs were observed only over the southern shelf (fig. 24). The expanded distribution during fall 2015 resembled that seen during the 1958–59 El Niño (Longhurst 1967), when the entire Baja California region and parts of southern California were occupied by adult red crabs. In contrast, during 1955–57, before the 1958–59 El Niño, red crabs remained south of Punta Eugenia (28°N). Interestingly, red crabs were absent on the shelf during autumn 2015 (fig. 24) although in the prior seasons (spring–summer of 2015), and subsequently in spring 2016, red crabs washed up on the beaches of Baja California and California (Durán 2016).

Vinciguerria lucetia is the most abundant mesopelagic fish species all year round off Baja California (Jiménez-Rosenberg et al. 2007, 2010). *V. lucetia* and *Triphoturus mexicanus* increased in abundance during the 2015–16 El Niño. The mean abundance of *V. lucetia* during October 2003 was 172 larvae/10 m^2; in contrast during September 2015 mean abundance increased by a factor of five (938 larvae/10 m^2). The highest abundances during October 2003 were concentrated in oceanic waters (fig. 24), while the high abundances of *V. lucetia* larvae during September 2015 included the shelf stations (fig. 24). Similar to the 2015–16 El Niño, a notable increase in the abundances of *V. lucetia* larvae was also observed during the 1997–98 El Niño (Jiménez-Rosenberg et al. 2007, 2010). There was also a notable shift northwards in the distribution of *V. lucetia* larvae in 2015 relative to 2003 (fig. 24).

Persistence of a Low-Lipid, Diverse, Warm Water Copepod Assemblage off Oregon

The warm water that intruded onto the Oregon shelf in Sept 2014, the coastal expression of the marine heat wave, remained throughout 2014–15 and continued

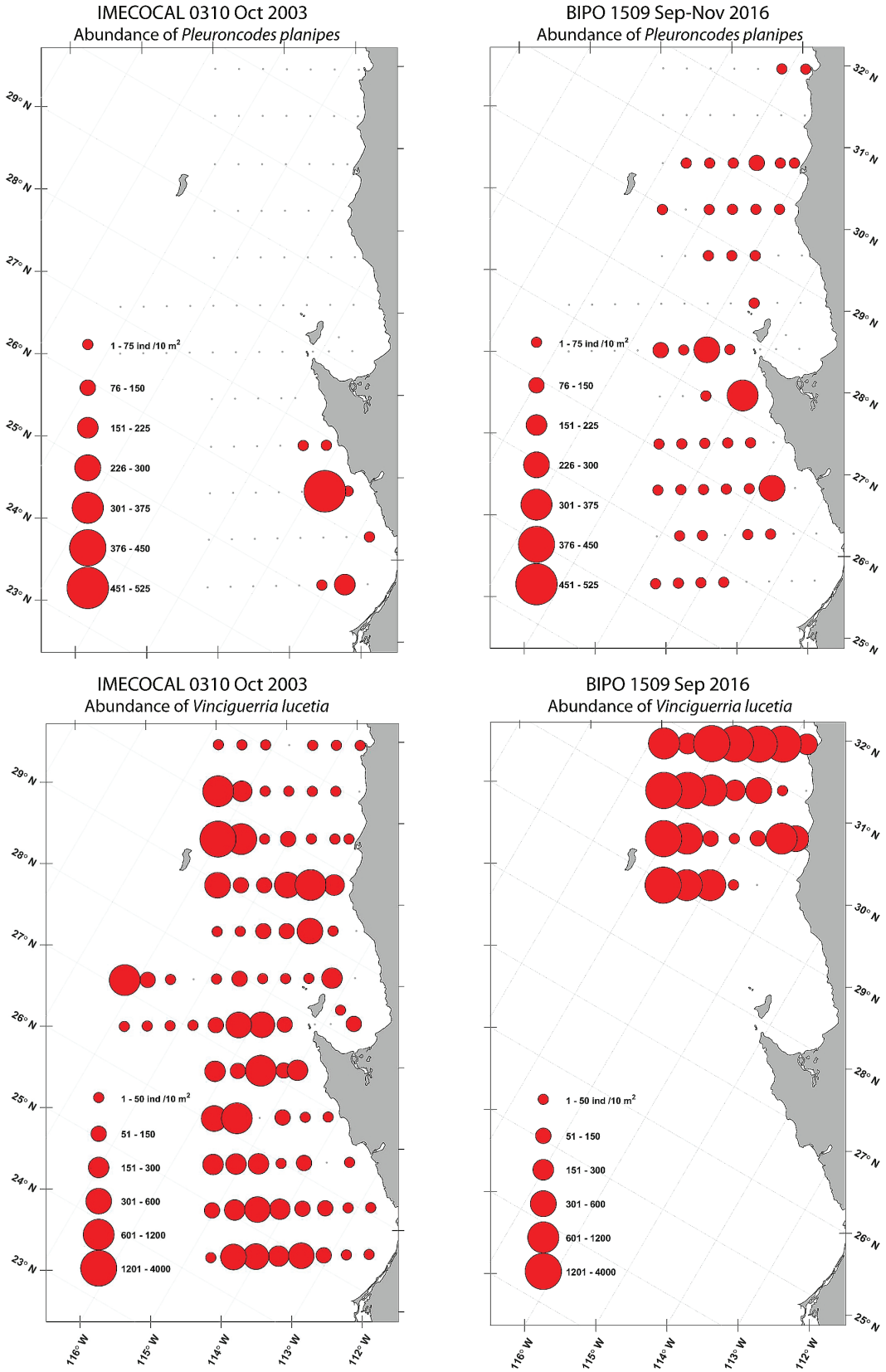

Figure 24. Distribution of adult galatheid crab (*Pleuroncodes planipes*) and larval Panama lightfish (*Vinciguerria lucetia*) during October 2003 (IMECOCAL cruise 0310) and September–November 2015 (BIPO cruise 1509).

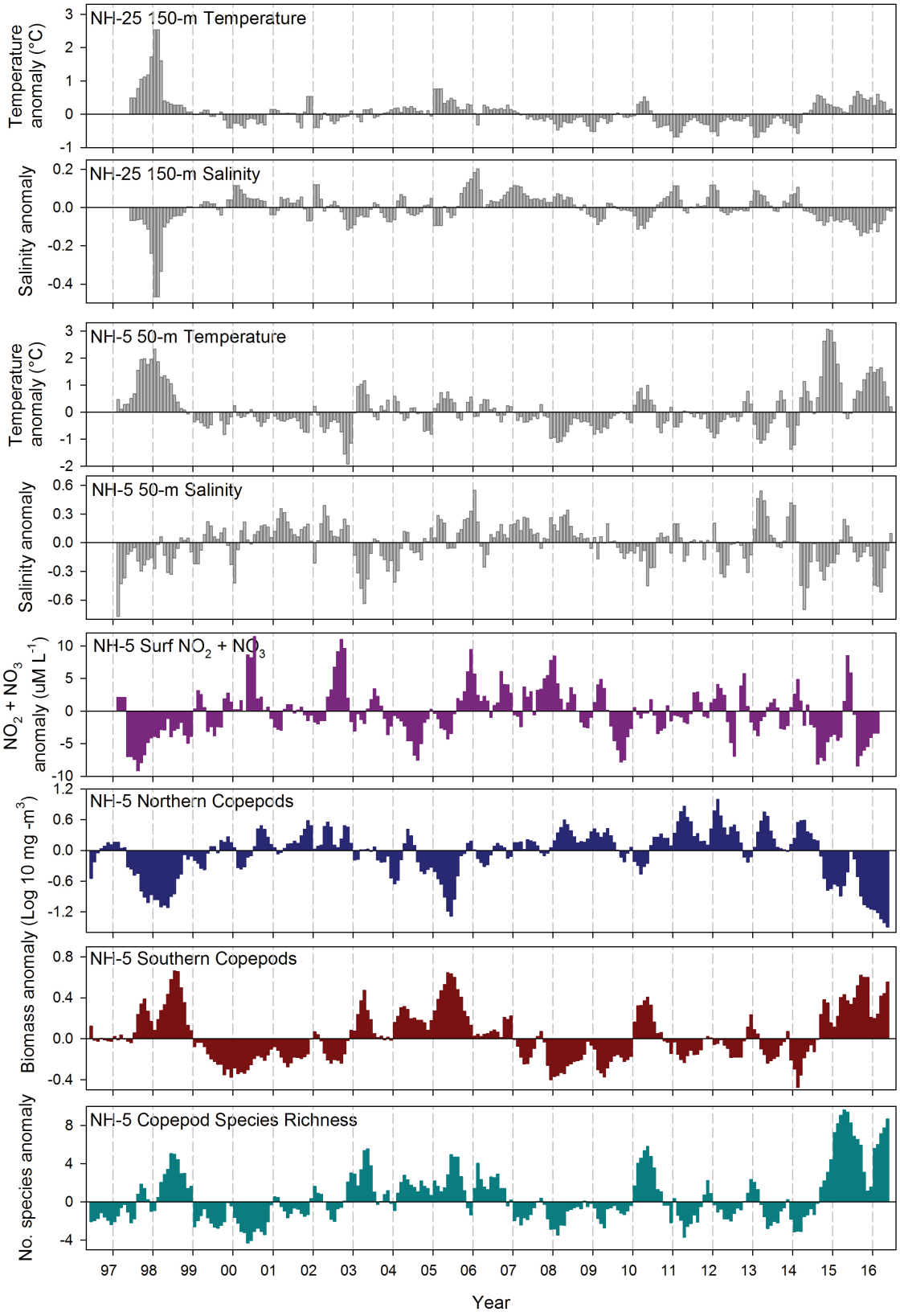

Figure 25. Time series plots of local physical and biological anomalies (monthly climatology removed) from 1997–present at NH-25 (Latitude: 44.6517 N Longitude: 124.65 W; top two panels) NH-5 (Latitude: 44.6517 N Longitude: 124.1770 W; lower six panels) along the Newport Hydrographic Line. Temperature and salinity from 150 m and 50 at NH-25 and NH-5 respectively, NO_2 + NO_3 from the surface, and copepod biomass and species richness anomalies are integrated over the upper 60 m. All data were smoothed with a 3-month running mean to remove high frequency variability.

into 2016, affecting local hydrography and pelagic communities. Despite the unusual ocean conditions during 2015 on the Newport Hydrographic Line (see fig. 2), the duration of the upwelling season (13 April–5 October) was similar to its long-term average. Cumulative upwelling over the season was the highest in the past 20 years (fig. S4, latitude 45°N). Despite strong inferred cumulative upwelling, temperatures at 50 m at the shelf station (NH-5) and 150 m at the slope station (NH25) remained warmer than average (fig. 25), surface nitrate was anomalously low (fig. 25) and chlorophyll (not shown) was lower than average throughout most of 2015. In May and June 2015, during the strongest upwelling period, shelf waters at both 50 and 150 m cooled, salinity increased, and nitrate increased greatly (fig. 25). However, positive temperature anomalies and lower than average nitrate and chlorophyll returned quickly in July and persisted into 2016. Dissolved oxygen at depth on the Oregon shelf remained average or higher than average throughout both 2015 and 2016 (not shown).

During this time period, the zooplankton community was dominated by lipid-poor tropical and subtropical copepods and gelatinous zooplankton. This generally indicates poor feeding conditions for small fishes which are prey for juvenile salmon. With the exception of June and July 2015, following strong upwelling, the biomass of lipid-rich northern or "cold water" copepods was the lowest observed in the 20-year time series (fig. 25). The biomass of southern ("warm water") copepods fluctuated greatly but was generally higher than average throughout 2015 and 2016 (fig. 25). We also observed 17 copepod species with Transition Zone and North Pacific Gyre affinities that have rarely been observed off Newport since sampling began in 1969. The presence of these species greatly increased copepod species richness which exceeded the number of species observed during the strong El Niño in 1998 (fig. 25). In 2015 and in 2016, the usual seasonal shift from a winter copepod community to a summer community, which is associated with strengthening of the Davidson Current in winter and its disappearance in spring, did not happen (data not shown). This seasonal transition in the copepod community also did not occur during the 1997–98 El Niño or during the anomalously warm year of 2005. Euphausiid biomass during 2016 was also among the lowest in 20 years (data not shown).

Despite a strong El Niño signal at the equator during much of 2015 and into 2016, we did not encounter the copepod or euphausiid species that have occurred off Oregon during other El Niño events. Copepods are good indicators of large-scale transport. We know that the unusual copepod species observed off Oregon in 2015–16 have Transition Zone and North Pacific Gyre affinities. Thus it is unlikely that these copepods have southerly coastal origins, as is usual during El Niño events. It is also unlikely that they were transported north by the California Undercurrent because the T-S properties at 150 m during this time period were unusually warm and fresh, rather than warm and more saline (fig. 25). The biogeographic affinities of the copepods in anomalously warm, fresh water suggest offshore intrusion Central Pacific water and mixing with subarctic Pacific water of the California Current. This suggests that the unusual copepod vagrants of 2015–16 originated from an offshore and southwesterly source.

Shelf waters off Oregon in mid-2016 remain warm, northern copepod biomass is the lowest, and copepod species richness remains the highest in the 20-year time series (fig. 25). We know from past warm events such as the 1997–98 El Niño, that the return to a lipid-rich copepod community following warm ocean conditions is strongly dependent on the magnitude and the duration of the event (Fisher et al. 2015). The Oregon shelf has been in an anomalously warm state since September 2014 (22 months as of this writing), far exceeding the duration of the 1997–98 El Niño that lasted 13 months. The copepod community recovered after 17 months following the 1997–98 El Niño (Peterson et al. 2002). Given that the PDO is still in a positive (warm) phase, and that a change in the copepod community lags the PDO by 2–6 months, we expect that we will not see a transition to a northern copepod community for at least a year to come.

Copepods and Krill Respond to Warm Conditions off Trinidad Head, Northern California

Coastal waters off northern California (Trinidad Head Line, station TH02, fig. 2) cooled during the first half of 2015 (fig. 26a) in response to mild winter upwelling events, reinforced by average upwelling during the spring and above-average upwelling during the summer of 2015 (Supplement fig. S4, latitude 41°N). Near-bottom temperatures returned to slightly warmer than average conditions during the summer and into the fall as upwelling weakened (fig. 26a and b).

Elevated phytoplankton concentrations developed over the inner to middle shelf in spring and persisted throughout the summer of 2015 (fig. 26c). The toxic species *Pseudo-nitzschia* was common, producing elevated concentrations of domoic acid (DA) (fig. 26d; see previous discussion of HAB). Shelf waters warmed during winter 2016, driven by persistent southerly winds, and remained relatively warm into spring 2016. Early observations of the phytoplankton bloom in spring 2016 indicated that *Pseudo-nitzschia* was again abundant.

Throughout much of 2015 and early 2016, the copepod community was dominated by warm-water species while the biomass of northern species was lower than usual (fig. 26e, f). Copepod community structure in this area reflects changes in water temperature. Copepod spe-

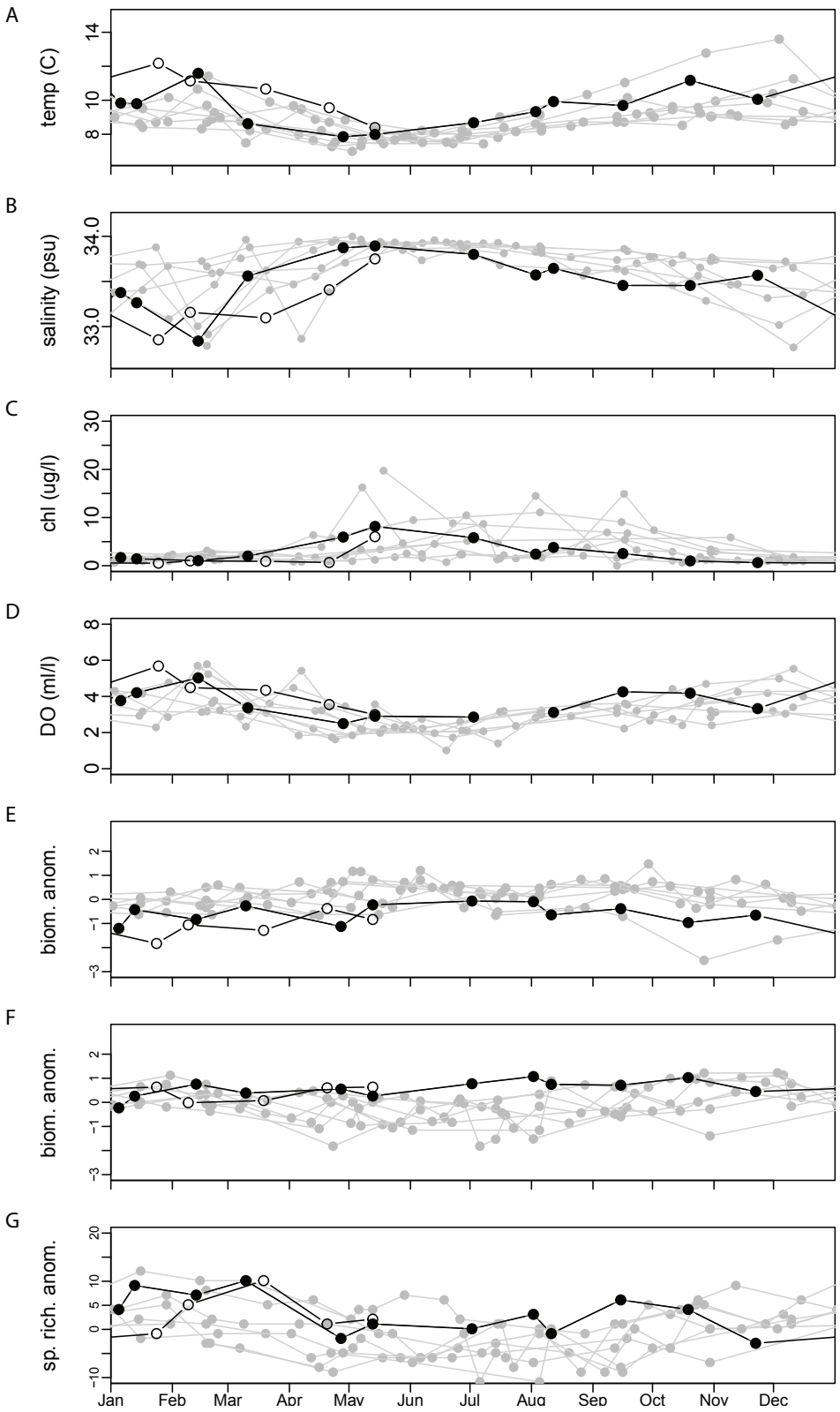

Figure 26. Hydrographic and ecosystem indicators at midshelf along the Trinidad Head Line (station TH02; 41 03.5'N, 124 16'W, 75 m depth). Panels from top to bottom show (A) near-bottom (68 m) temperature, (B) near-bottom (68 m) salinity, (C) mean chlorophyll *a* concentration over the upper 30 meters of the water column, (D) near-bottom (68 m) dissolved oxygen concentrations, (E) biomass anomalies for northern copepod species (ln g C m^{-3}), (F) biomass anomalies for southern copepod species (ln g C m^{-3}), and (G) species richness anomalies (N). All assemblages are defined following Hooff and Peterson (2006), and all anomalies are calculated using means from the full time series (2006–16). For all plots, gray symbols indicate historical observations (2006–14), filled circles indicate observations during 2015, and unfilled symbols indicate observations in 2016.

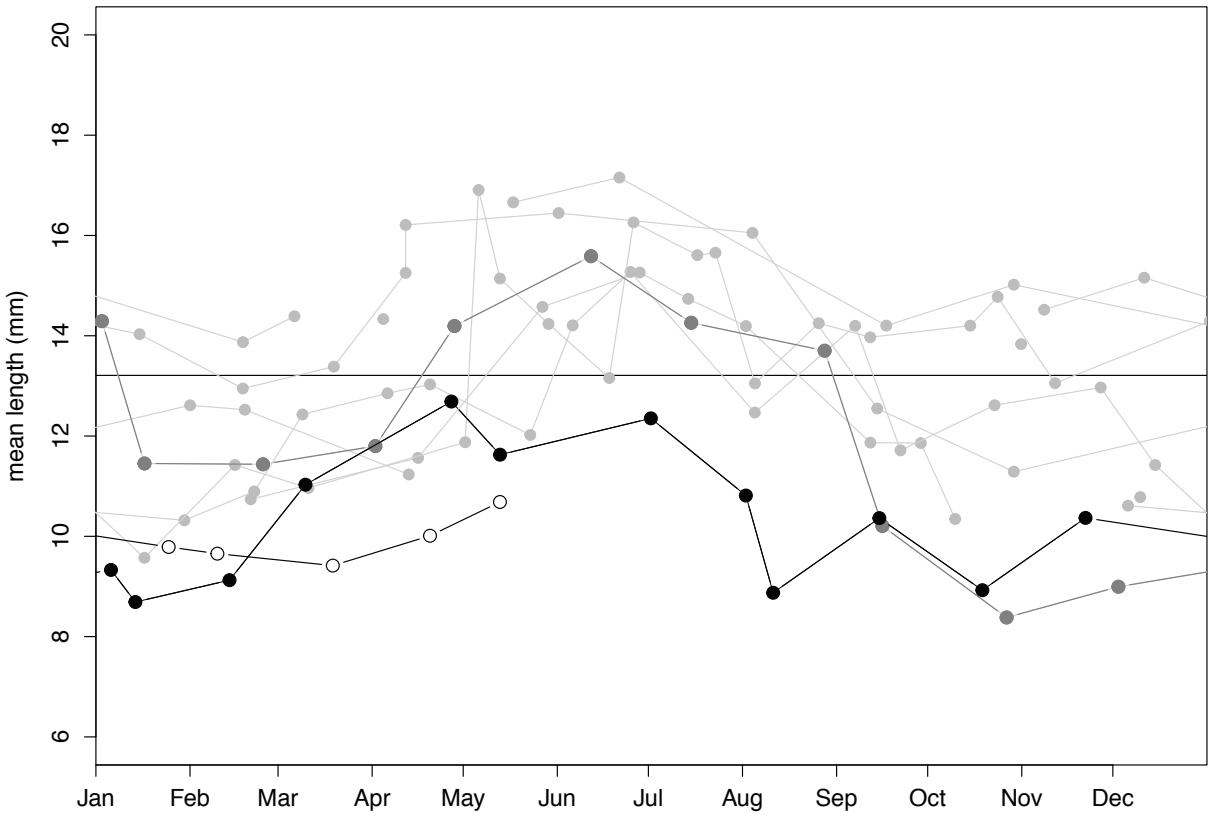

Figure 27. Mean rostral-dorsal length of adult *Euphausia pacifica* (males and females combined) captured along the Trinidad Head Line. Light gray symbols indicate observations from late 2006 through 2013. Dark gray symbols indicate observations for 2014, black symbols, for 2015, and open symbols for early 2016.

cies richness was high throughout much of 2015 when the marine heat wave was evident over the shelf. Richness peaked again in early 2016 (fig. 26g) associated with increased poleward transport. These diverse, warm-water copepod assemblages included several southern and offshore species not reported from this area prior to 2014.

Among the euphausiids, the abundance of *Thysanoessa spinifera* declined while both the subtropical *Euphausia recurva* and the warm water-associated *Nyctiphanes simplex* increased throughout 2015 and early 2016. *N. simplex* was the most abundant adult euphausiid observed in January 2016 in a region normally dominated by *E. pacifica* and *T. spinifera* (data not shown). In addition to their low abundance, adult *E. pacifica* were small relative to sizes observed prior to summer 2014 (fig. 27). Mean size of *E. pacifica* remained small through early 2016, and growth during spring and summer months was slower than normal.

Changes in Gelatinous Zooplankton off Oregon

The numerically dominant large jellyfish[11] off Oregon and Washington is cool-water associated scyphozoan species *Chrysaora fuscescens*. In June 2015, *Chrysaora* abundance was the second lowest of the time-series (fig. 28). These jellyfish were only found at 25% (11/44) of the stations sampled the following year, in June 2016, mostly nearshore, north of the Columbia River (fig. 2b). Although the time series is relatively short (18 years), and does not extend across the 1997–98 El Niño years, the data do show a notable decline in *Chrysaora* in other warm years (2003, 2005, and 2010) similar to that observed in 2015 and 2016 (fig. 28).

The more offshore taxa of hydromedusae, *Aequorea* spp. (Suchman et al. 2012), shows a less convincing relationship between abundance and warm years compared to *Chrysaora* (fig. 28). One plausible explanation for this may be that abundance of offshore species is more related to intrusion of offshore waters rather than to temperature. As described elsewhere in this paper, advective forcing differs between anomalously warm years, and this would affect the distribution of offshore species. The offshore hydroid, *Velella velella*, which lives in the pleuston, occurred in much lower abundances in June 2016 than in 2015, suggesting less onshore intrusion of offshore water in June 2016 than in the previous "warm blob" year.

Southern species such as the large scyphozoans *Phacellophora camchatica* and *Aurelia aurita* and the colonial

[11]Large gelatinous zooplankton taxa have been quantified from pelagic surface trawls off Oregon and Washington every June since 1999 (see Suchman et al. 2012 for collection methods).

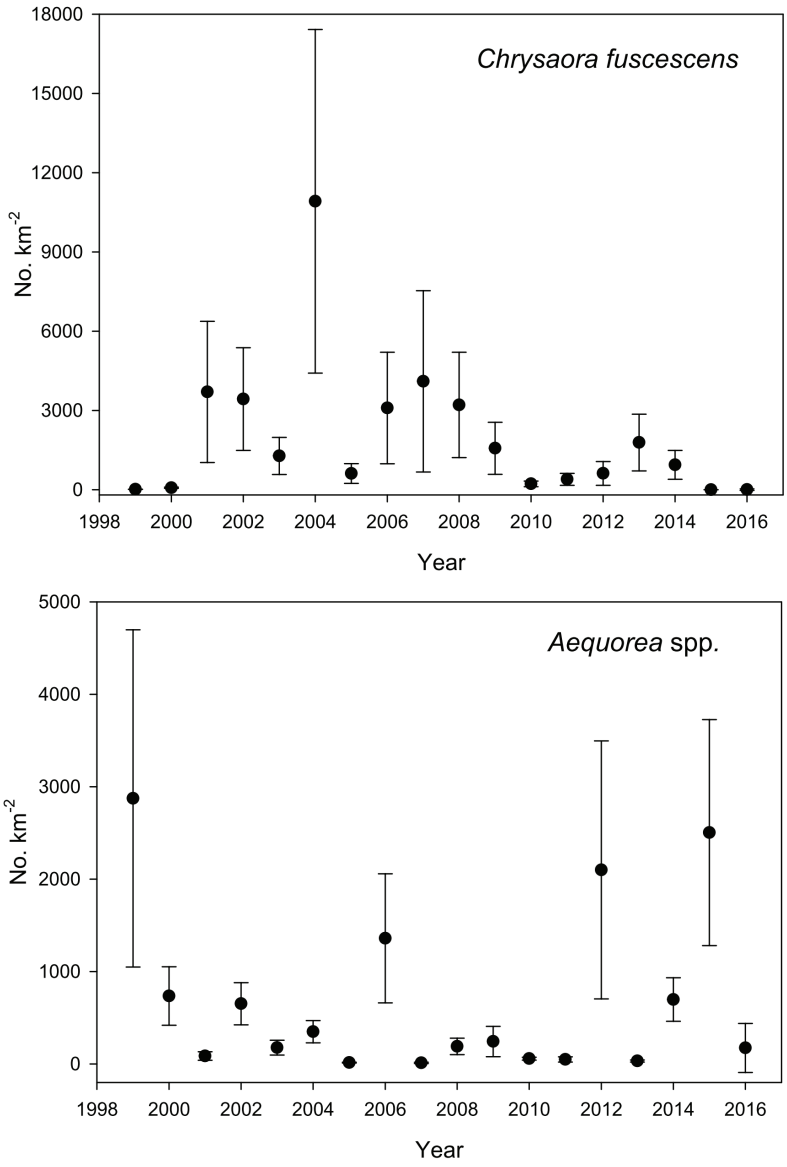

Figure 28. The abundance of the large jellyfish *Chrysaora fuscescens* and the hydromedusae, *Aequorea* spp. off Oregon and Washington during June.

salps (*Salpa* and *Thetys*) were found in higher abundances during the June 2016 cruise and the June NOAA Pre-recruit survey (data not shown) conducted during the warm ocean conditions of 2016, suggesting increased northward transport due to the El Niño event.

The combined data support the idea that offshore intrusion during the anomalous North Pacific warming of 2015 increased the occurrence of the offshore *Aequorea* spp., but that as the 2015–16 El Niño developed, advection from more southern sources increased the occurrences of southern gelatinous species.

SUMMARY: CHANGES IN THE DISTRIBUTION AND ABUNDANCE OF ZOOPLANKTON

The anomalies of temperature and salinity at 20 m depth in the IMECOCAL region off Baja California were higher during 2015–16 El Niño than during the 2003 year. The distribution of near-surface temperature and salinity during the 2015–16 El Niño suggests that warm, more saline waters typically found south of Punta Eugenia, extended to the north during the 2015–16 El Niño. Anomalously warm and saline surface waters off Baja California were associated with very low zooplankton displacement volumes in 2015–16. In contrast, during the 1997–98 El Niño, zooplankton volume was close the average, with abundant copepods, euphausiids, and salps at some stations. Tropical species such as red crab and the mesopelagic fishes *V. lucetia* and *T. mexicanus* increased in abundance and extended their range northwards in 2015–16, a phenomenon also seen during the 1997–98 El Niño.

Off California, pelagic red crab (*Pleuroncodes planipes*) adults were abundant in the water column and frequently washed up on beaches of southern California in winter

and spring 2015. They were reported in central California by September–October 2015. Zoea larval stages are found in southern California waters in most springtimes of the CalCOFI time series, although typically at very low abundances. However, during springs of historical El Niño years, zoea abundances increased dramatically, with a coastal distribution suggestive of northward transport from Baja California in the Inshore Countercurrent. In spring 2015, the presence of only adults and the youngest zoea stages, together with their coastal distribution, is suggestive of advective transport from Baja California waters.

Despite strong cumulative upwelling, temperatures at 50 m on the Oregon shelf remained warmer than average, surface nitrate was anomalously low, and chlorophyll was lower than average throughout most of 2015. Throughout 2015 and 2016, the zooplankton community was dominated by lipid-poor tropical and subtropical copepods and gelatinous zooplankton. This generally indicates poor feeding conditions for small fishes that in turn are prey for juvenile salmon. The biomass of southern copepods fluctuated greatly but was generally higher than average throughout 2015 and 2016. Seventeen copepod species with Transition Zone and North Pacific Gyre affinities that have rarely been collected off Newport, Oregon, were also observed. The presence of these species greatly increased copepod species richness which exceeded the number of species observed during the strong El Niño in 1998. Despite a strong El Niño signal at the equator during much of 2015 and into 2016, copepod or euphausiid species that have occurred off Oregon during other El Niño events were not encountered. Temperature-salinity properties at 150 m during 2015 indicated unusually warm and fresh waters, consistent with water properties of the upper 80–100 m over the slope. The conditions off Newport, Oregon, appear to have been influenced by intrusion of offshore waters. This suggests that the unusual copepods vagrants of 2015–16 originated from an offshore and southwesterly source, which is an important difference from the southerly origin of vagrants during the 1997–98 El Niño.

Coastal waters cooled off Trinidad Head in northern California due to winter upwelling events, reinforced by more sustained upwelling in spring and summer. A bloom of toxic *Pseudo-nitzschia* developed, producing high levels of domoic acid. Similar to the Oregon shelf, the copepod assemblage was dominated by a more diverse, warm water assemblage in 2015. Krill species common off northern California were diminished in size and abundance as subtropical and warm water species became more abundant. For a brief period near the end of the anomalously warm period, the dominant krill species was *Nyctiphanes simplex* rather than *Euphausia pacifica*.

The large cool water associated jellyfish (*Chrysaora fuscescens*) showed reduced abundance in warm years (2003, 2005, 2010, 2014, and 2015) off Oregon. In contrast, an offshore species (*Aequorea* spp.) showed a less convincing relationship between abundance and warm years, compared to *Chrysaora*. We speculate that intrusion of offshore waters during the anomalous North Pacific warming of 2015 increased the occurrence of the offshore *Aequorea* spp., but that as the 2015–16 El Niño developed, advection from more southern sources increased the occurrences of southern gelatinous species.

CHANGES IN THE DISTRIBUTION AND ABUNDANCE OF FISH

Changes in Ichthyoplankton Assemblages Associated with Anomalous Warming

Coastal pelagic fish egg abundance has declined off central and southern California in the last 16 years (2000–16) (Supplement fig. S9, fig. 29). Sardine, anchovy, and jack mackerel eggs were found at very low concentrations in the spring of 2016 consistent with this decadal-scale trend[12].

Jack mackerel eggs were an order of magnitude more abundant than sardine off southern California in spring 2016, but were less abundant than in spring 2015. The distribution of jack mackerel eggs in 2016 extended farther offshore than in 2015 (fig. 29). Offshore spawning of mackerel, which is commonly regarded as being typical, nevertheless occurred at low densities in spring 2016 (fig. S9, fig. 29). Anchovy eggs were an order of magnitude more abundant in spring 2016 compared to 2015, but the increase was spatially restricted to small areas off Ventura, California, and Newport, Oregon (Supplement fig. S9, fig. 29). We see no evidence in the distribution of anchovy eggs of a coast-wide recovery of anchovy abundance. The spawning distribution of sardine eggs was centered even further north in 2016 (43°–44.5°N, off Oregon) than in spring 2015 (41°–43°N, California-Oregon border). Sardine eggs are rarely found north of San Francisco in spring, meaning that the spring spawning distribution was again much farther north than usual. Sardine egg densities off Oregon in spring 2016 were <3 eggs m^{-3} (compared to <1.5 eggs m^{-3} in spring 2015), which was extremely low compared to spring 2000–13 (fig. 29).

Conditions off central and southern California were unusually warm in spring 2016 (see elsewhere in this report). Sardine spawning, centered off Oregon in a band about 50–60 nm from shore as well as nearshore, occurred in surface water temperatures of 12°–13°C (Supplement fig. S9, fig. 29). Mackerel eggs were found in water with surface temperatures of 14°–18°C,

[12]Ichthyoplankton sampling methods used by CalCOFI were summarized in McClatchie (2014).

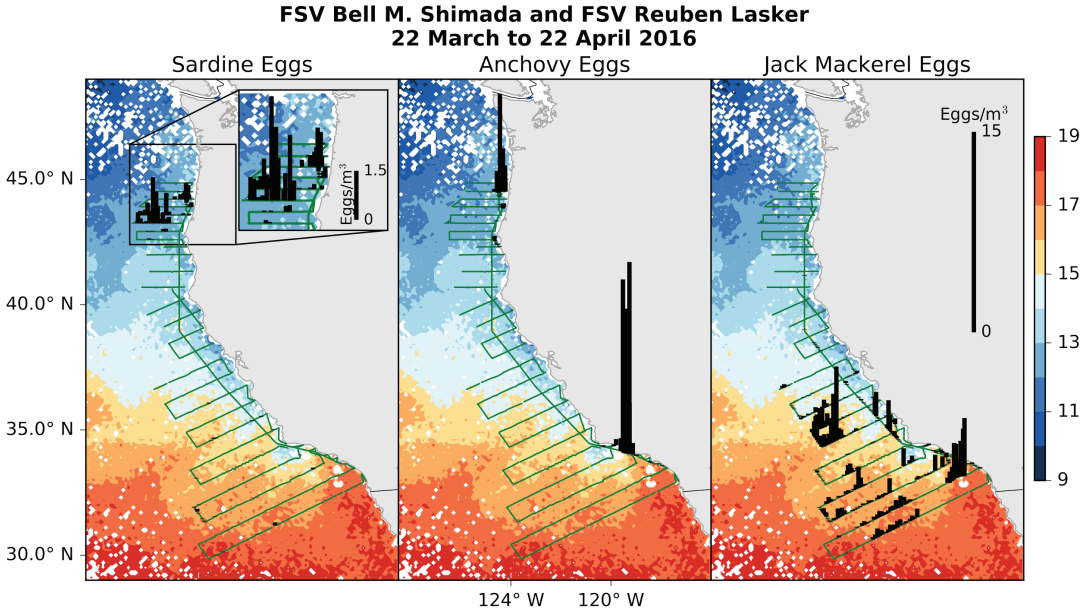

Figure 29. Density of eggs of sardine, anchovy, and jack mackerel collected with the continuous underway fish egg sampler (CUFES) during the spring 2016 CalCOFI and coastal pelagic fish cruises overlaid on satellite sea surface temperatures (°C).

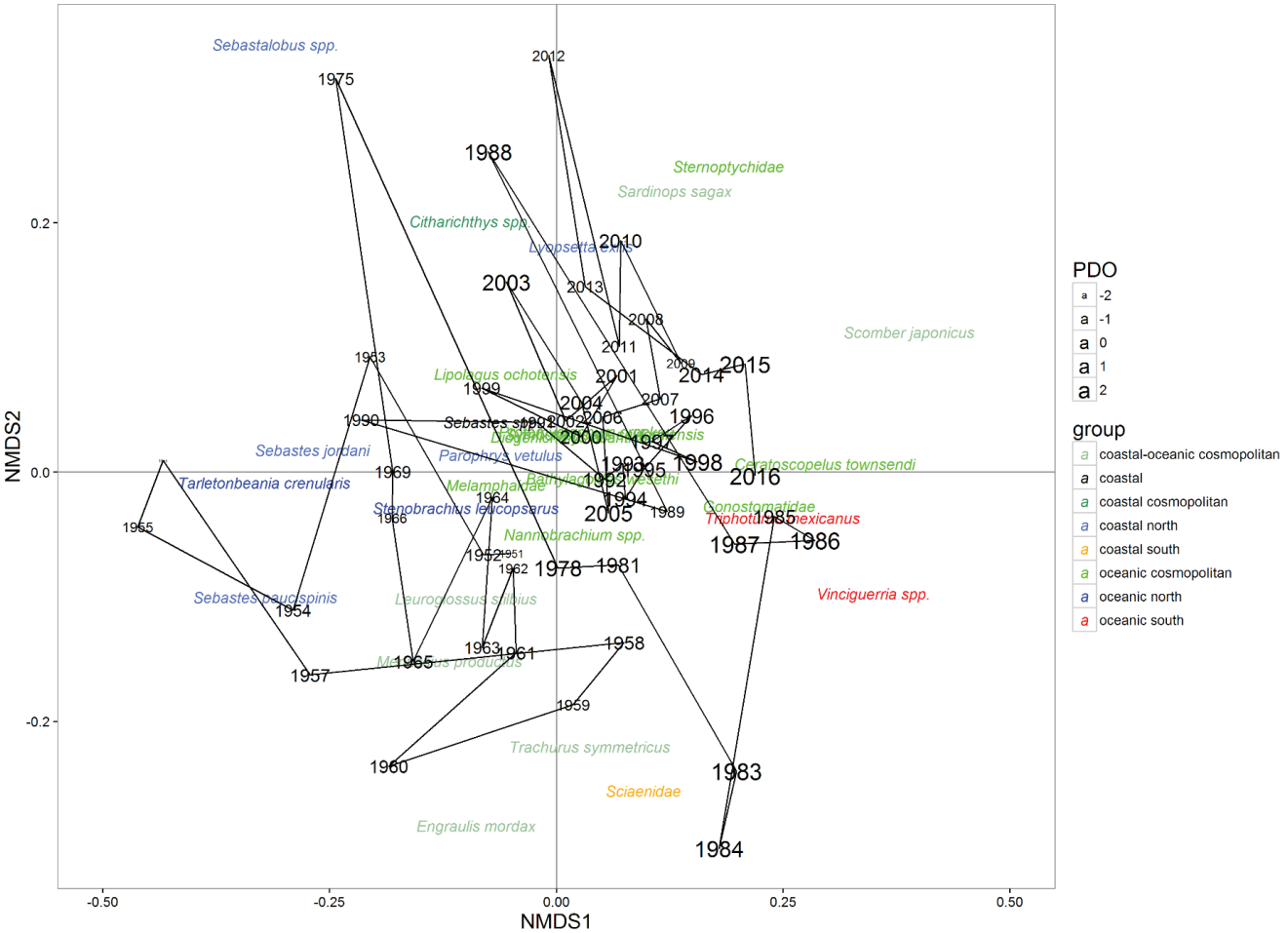

Figure 30. Nonmetric multidimentional scaling plot of the ichthyoplankton assemblage. The nMDS analysis utilized square-root transformed delta mean abundances for each year. Only taxa whose mean sums across the time series were at least 50 are included. Species are color coded based on their habitat (coastal, coastal-oceanic, and oceanic) and biogeographic range relative to the CalCOFI region (cosmopolitan, northern, and southern). Font size of the years is scaled by the PDO value in March of that year. Taxa that were not consistently identified to the species level since 1951 were grouped to either genus or family. The stress value for the analysis is 0.20.

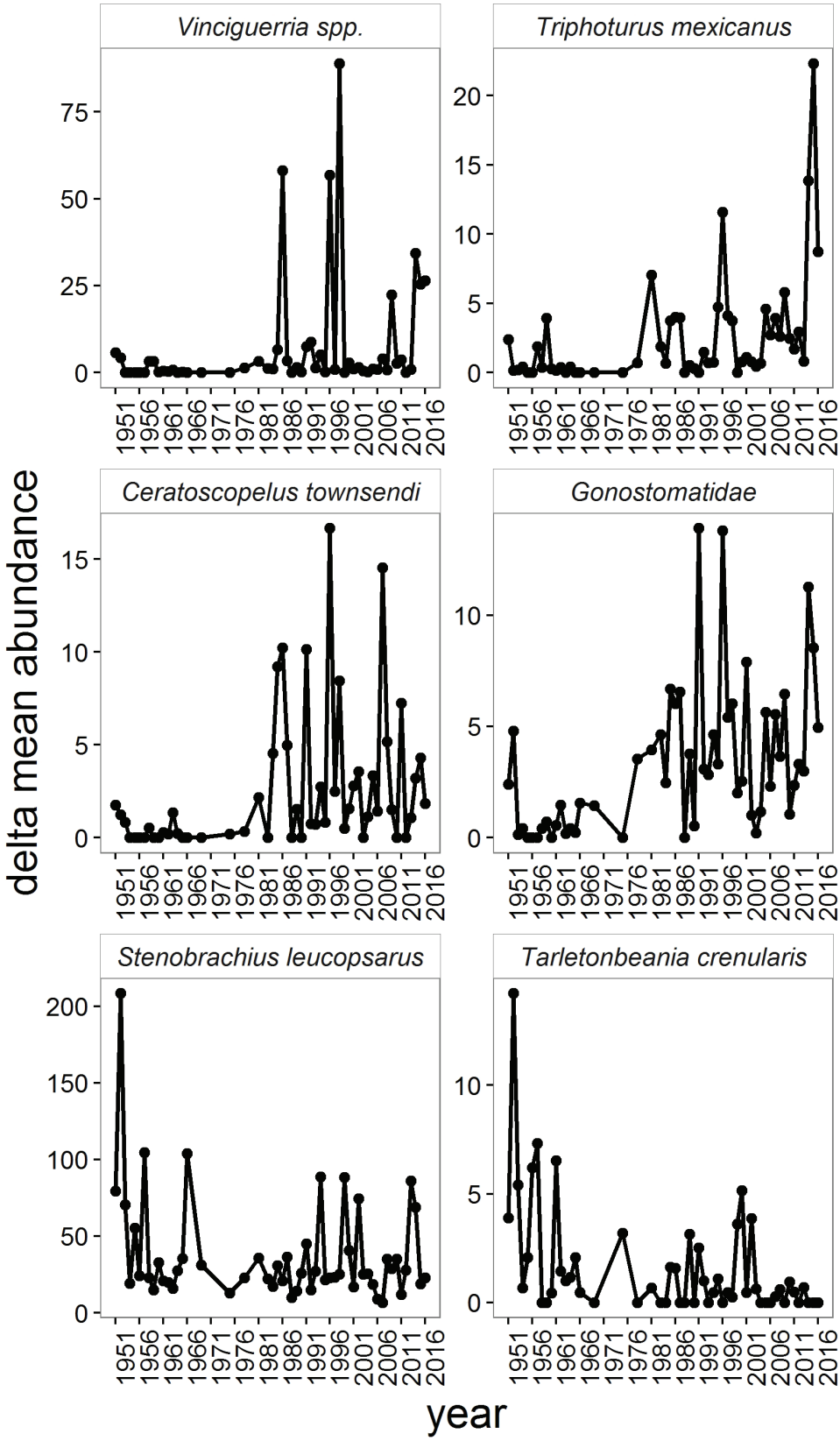

Figure 31. Delta-mean abundances of common mesopelagic taxa that drive the nMDS analysis. Delta mean was used rather than simple averaging because it is better suited for data with many zero values. *Vinciguerria* spp., *Triphoturus mexicanus*, *Ceratoscopelus townsendi*, and Gonostomatidae have southerly biogeographic ranges while *Stenobrachius leucopsarus* and *Tarletonbeania crenularis* are have northerly ranges. Note that southern taxa have high nMDS1 scores and the northern taxa low nMDS1 values.

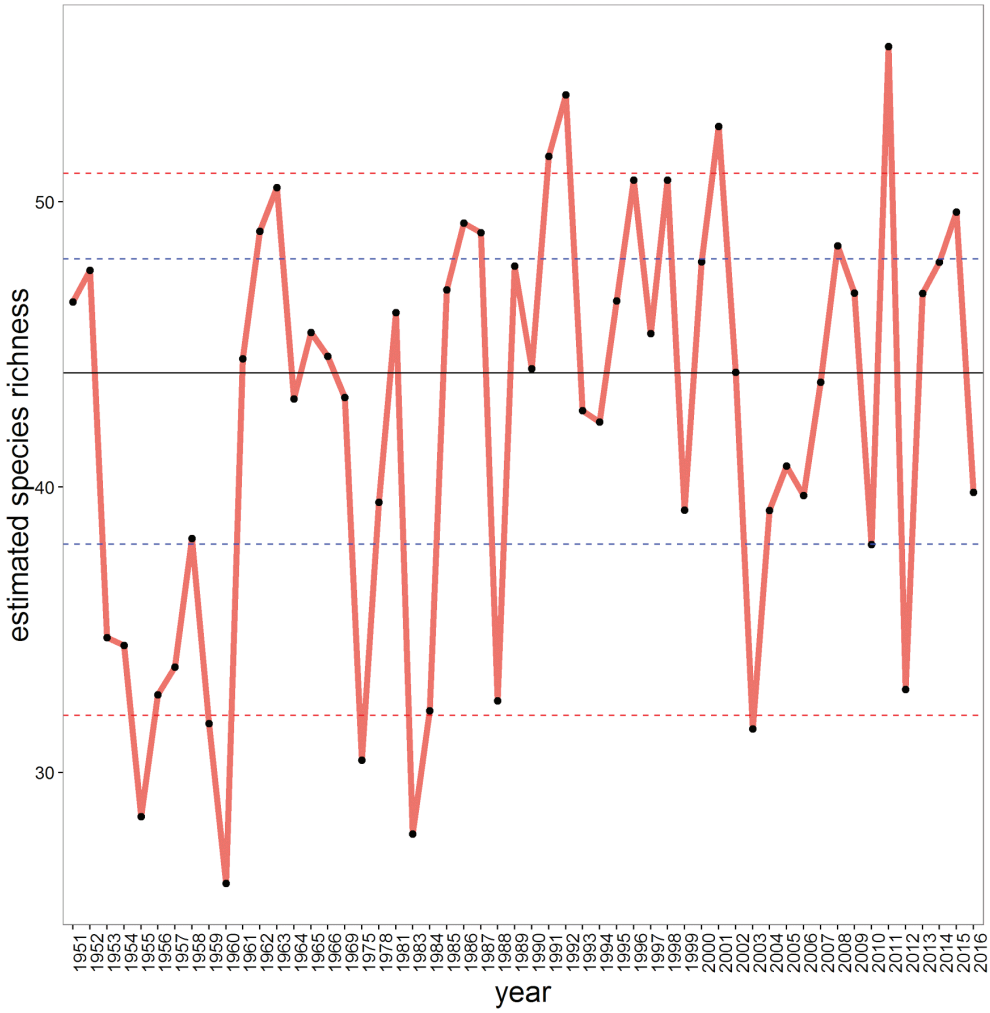

Figure 32. Estimated species richness based on a bootstrap species accumulation curve. The solid, black horizontal line depicts the long-term median, the dashed blue lines the 25th and 75th quantiles, and the dashed red the 5th and 95th quantiles.

and anchovy spawned in temperatures ranging from 12°–17°C. Both mackerel and anchovy spawned in a wider range of temperatures than sardine.

The ichthyoplankton assemblage in 2014–16 (based on spring samples from lines 80 and 90) was similar to previous years when there was either an El Niño or anomalously warm waters (fig. 30). Under these oceanographic conditions the assemblage tends to have high abundances of mesopelagic species with southerly or cosmopolitan biogeographic ranges such as *Ceratoscopelus townsendi*, Gonostomatidae (mostly in the genus *Cyclothone*, predominantly *C. signata*), *Triphoturus mexicanus*, and *Vinciguerria* spp. (mostly *V. lucetia*) and low abundances of midwater species with northern biogeographic affinities such as *Stenobrachius leucopsarus* and *Tarletonbeania crenularis* (fig. 31).

Species richness was down in 2016 relative to 2014 and 2015 but still between the 25th and 50th percentile of the long-term median (fig. 32). The 2016 drop in species richness was due in part to the complete lack of a few species that are typically common such as *Bathylagus pacificus*, *Citharichthys* spp. (mostly *C. sordidus* and *C. stigmaeus*), and *Sebastes paucispinis*.

Ichthyoplankton composition and relative concentrations of dominant taxa off Newport, Oregon, in June–July 2015 was similar to the previous seven years (fig. 33)[13]. Mean larval concentration for all species combined was the third highest in the nine-year time-series.

[13]Oregon ichthyoplankton samples were collected from 3–4 stations representing coastal (<100 m in depth), shelf (100–1000 m), and offshore (>1000 m) regions along both the Newport Hydrographic (NH; 44.65°N, 124.35°–125.12°W) and Columbia River (CR; 46.16°N, 124.22°–125.18°W) lines off the coast of Oregon during June–July in 2007–15 (for complete sampling methods, see Auth [2011] cited in the main paper). In addition, post-larval (i.e., juvenile and adult) fish were collected using a modified Cobb midwater trawl (MWT) with a 26 m headrope and a 9.5 mm codend liner fished for 15 min at a headrope depth of 30 m and ship speed of ~2 kt. MWT collections were made at 4–6 evenly-spaced, cross-shelf stations representing coastal, shelf, and offshore regions along nine half-degree latitudinal transects between 42.0° and 46.0°N latitude in the northern California Current region during June–July in 2011–16 (although no sampling was conducted in 2012). Sampled volume was assumed to be uniform for all hauls. All fish collected were counted and identified to the lowest taxonomic level possible onboard, although prerecruit rockfish were frozen and taken back to the lab for identification using precise meristic and pigmentation metrics.

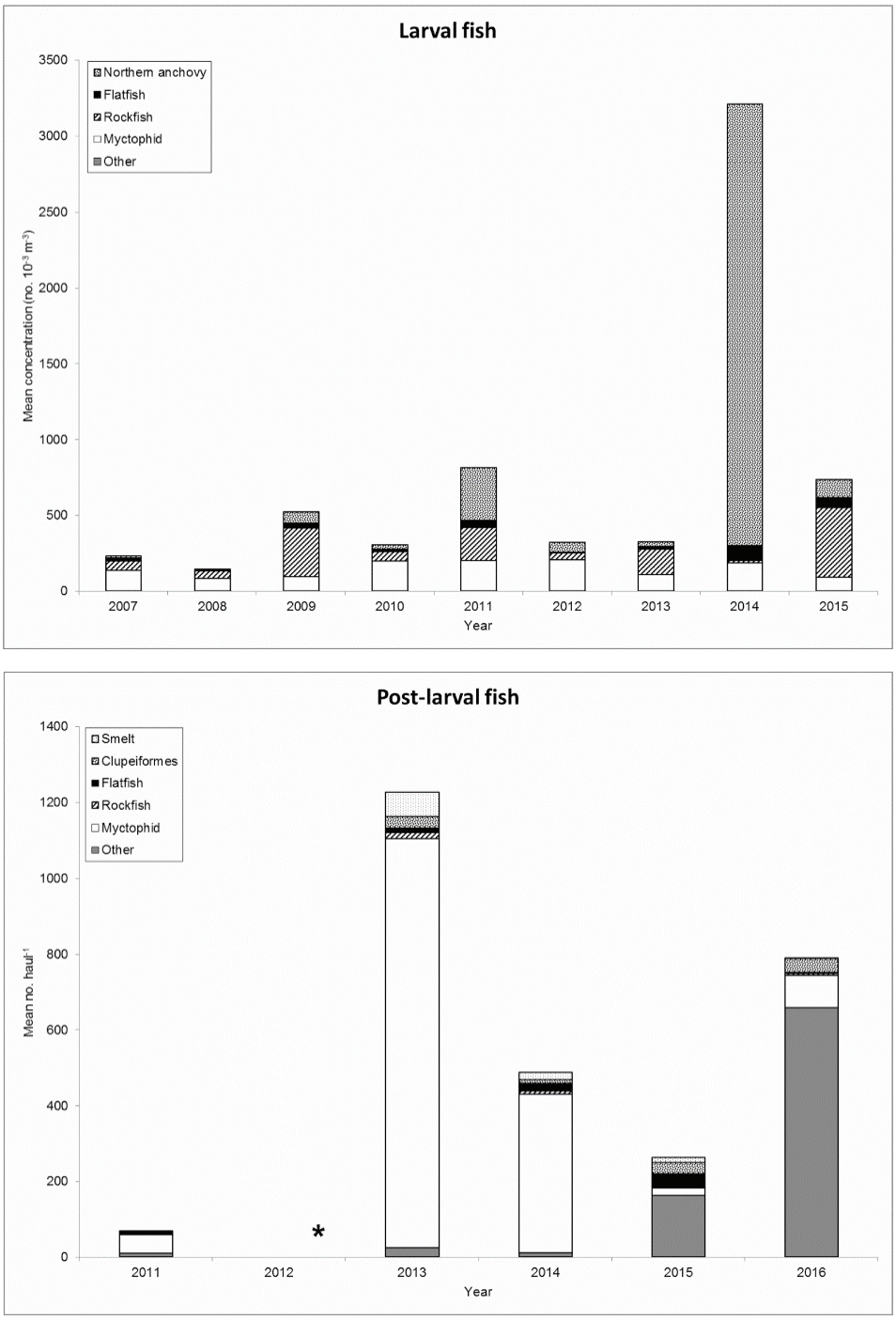

Figure 33. (Upper) Mean concentrations (no. 10^{-3} m^{-3}) of the dominant larval fish taxa collected during June–July in 2007–15 along the Newport Hydrographic (NH; 44.65°N, 124.35°–125.12°W) and Columbia River (CR; 46.16°N, 124.22°–125.18°W) lines off the coast of Oregon. (Lower) Mean catches (no. $haul^{-1}$) of the dominant post-larval fish taxa collected during June–July in 2011–16 along nine half-degree latitudinal transects between 42.0° and 46.0°N latitude in the northern California Current region. * = no samples were collected in 2012.

Larval rockfish in 2015 were found in the highest concentration of the time-series, while flatfish concentration was second only to that of 2014. Similar to flatfish, but even more exaggerated, northern anchovy were also present in unusually high concentrations in 2014, declining again in 2015 (fig. 33).

The post-larval fish assemblage in 2016 differed from the assemblage structure found in the same area and season in 2011–15, primarily due to the dominance of Pacific hake, (*Merluccius productus*). Post-larval hake comprised 82% of the total mean abundance of all post-larval fish (fig. 33). At the other extreme, the abundances

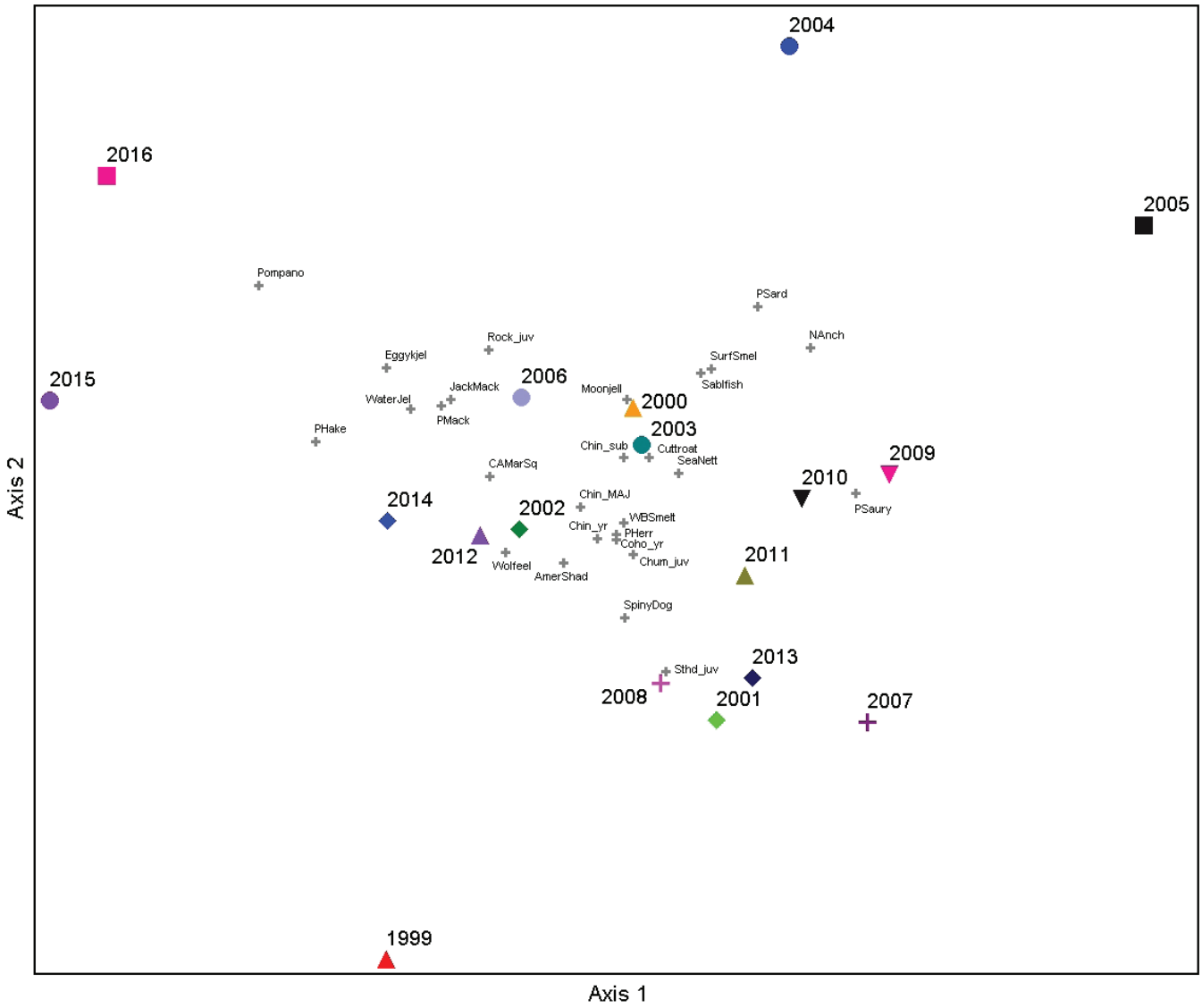

Figure 34. NMS ordination of northern California Current pelagic assemblages. The NMS ordination explained 87.0% of the total variability in the first two dimensions.

of flatfish and smelt in 2016 were the lowest of the five-year time series. Myctophids were another group showing strong interannual variability. It is notable that post-larval myctophids were numerically dominant prior to the anomalous warming of 2014–16, but that hake dominated the assemblage during the anomalous warming. This may be because the dominant myctophid taxa off Oregon are cool water-associated species.

Northern California Current Nekton and Fish

The June fish and invertebrate assemblage[14] in the northern California Current during 2016 was unusual and dominated by species that normally occur in warmer ocean waters to the south of the study area. An NMS ordination clearly showed that the 2015 and 2016 assemblages were outliers, distinct not only from the 1999 La Niña assemblages, but also from the assemblage sampled during the 2005 warm event in the northern California Current (fig. 34).

[14]Pelagic fish and invertebrate catch data were collected by the NWFSC NOAA/Bonneville Power Administration surveys using surface trawls on standard stations along transects between northern Washington and Newport, OR, in June from 1999 to 2016 (fig. 2b). All tows were made during the day at predetermined locations along transects extending off the coast to the shelf break (Brodeur et al. 2005). We restricted the data set to stations that were sampled consistently over the sampling time period (>9 y). Large sharks, ocean sunfish (*Mola mola*), and adult salmonids were removed from the dataset as a Marine mammal excluder device that has been used in the trawl since June 2014, has been shown to exclude these taxa from the catch. Numbers of individuals were recorded for each species caught in each haul and were standardized by the horizontal distance sampled by the towed net as CPUE (number/km towed). A log(x+1) transformation was applied to the species at each station and then averaged by year for each species. The species data matrix included the 27 most abundant species captured over the 18 years sampled years (27 species x 18 years). A nonmetric multidimensional scaling (NMS) ordination was used to describe the similarity of each year's community in species space.

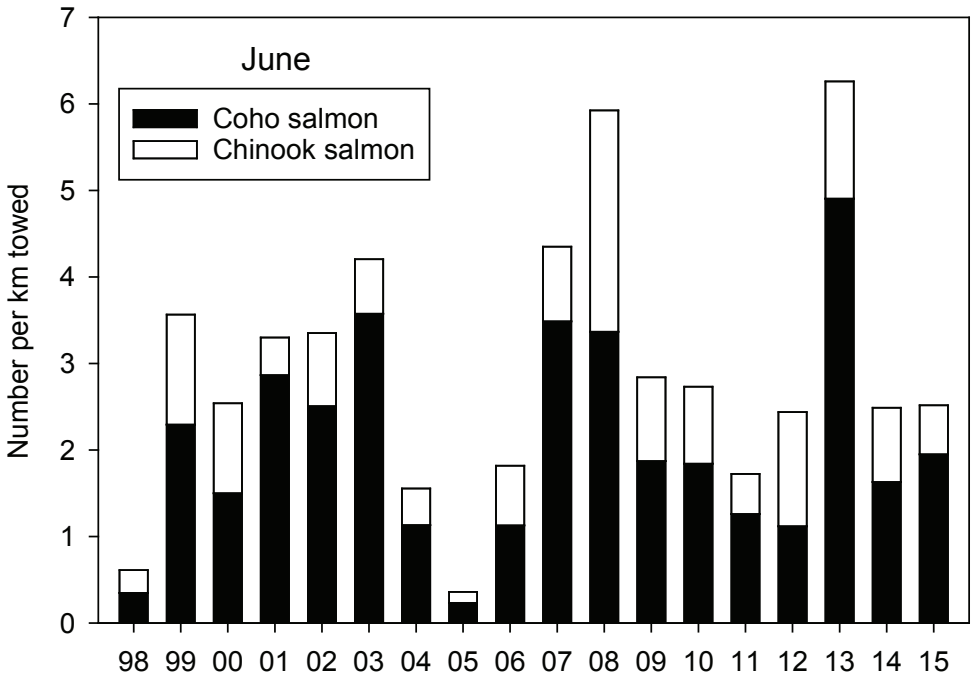

Figure 35. Catches of juvenile coho (black bars) and Chinook (white bars) salmon off the coast of Oregon and Washington in June from 1998–present.

The fish and invertebrate community in 2016 was more similar to 2015 than to any of the previous years (fig. 34). Taxa indicative of 2016 included Pacific pompano (*Peprilus simillimus*), California market squid (*Doryteuthis opalescens*), water jellyfish (*Aequorea* sp.), egg yolk jellyfish (*Phacellophora camtschatica*), age-0 Pacific hake (*Merluccius productus*), Pacific chub mackerel (*Scomber japonicus*), and jack mackerel (*Trachurus symmetricus*). Age-0 rockfishes (*Sebastes* spp.) were also extremely abundant in 2016, especially off the Washington coast. However, it should be noted that age-0 rockfish are not well quantified by the sampling gear. Forage fish species typically found in these surveys, such as Pacific herring (*Clupea pallasii*), northern anchovy (*Engraulis mordax*), and Pacific sardines (*Sardinops sagax*) were much less abundant in 2015 and 2016 than in previous years.

Catches of yearling salmon off Washington and Oregon in June may be a good indicator of early ocean survival of yearling Chinook (*Oncorhynchus tshawytscha*) and coho salmon (*O. kisutch*). The abundance of yearling Chinook salmon during June surveys has a significant and positive relationship to spring Chinook jack counts at the Bonneville Dam the following spring, as does the abundance of yearling coho salmon to subsequent coho smolt to adult survival (Morgan et al. 2016). Catch per unit effort (CPUE, number per km trawled) of yearling Chinook and coho salmon during the June 2016 survey was about average compared to the 18 previous June surveys 1998–2015 (fig. 35). Catches of yearling Chinook salmon in June 2016 were eleventh of the 19 years of sampling, and catches of yearling coho salmon were ranked 13 out of the 18 years.

Shifts in Forage and Gelatinous Plankton off Central and Southern California

Very high catches[15] of young-of-the-year (YOY) rockfish (fig. 36) were collected off central California (fig. 2b) in summer 2016, as was the case in 2015. In contrast, catches of YOY rockfish in the north central region were lower than previous years and catches in the south region were very low. Catches of YOY anchovy,

[15]The Fisheries Ecology Division of the SWFSC has conducted a late spring midwater trawl survey for pelagic juvenile (young-of-the-year, YOY) rockfish (*Sebastes* spp.) and other groundfish off central California (approximately 36 to 38°N) since 1983, and has enumerated most other epipelagic micronekton encountered in this survey since 1990 (Ralston et al. 2015; Sakuma et al. in prep). The survey expanded the spatial coverage to include waters from the US/Mexico border north to Cape Mendocino in 2004 (fig. 2b). The results here include time series of anomalies of some of the key species or groups of interest in this region since 1990 (core area) or 2004 (expanded survey area), and an update of a principal component analysis (PCA) of the pelagic micronekton community in the core area developed by Ralston et al. (2015), all of which have also been reported in earlier SoCC reports. The data for the 2016 survey are preliminary, corresponding oceanographic information (CTD casts, continuous data on surface conditions and productivity, and acoustic data) and seabird and marine mammal abundance data are also collected but not reported here. Catches are shown as standardized anomalies from the mean of the log transformed catch rates.

In addition to the six species shown in Figure 36, an additional 14 species and groups were included in the analysis of the forage assemblage within the core (1990–2015) area developed by Ralston et al. (2015), and are subsequently represented in the PCA of this assemblage (fig. 38). The results of the PCA for the core area (fig. 38, 1990–2016) were comparable to those originally reported by Ralston et al. (2015) and Leising et al. (2015), with a greater fraction of the total variance explained by the first two principal components (due to the smaller number of time series included).

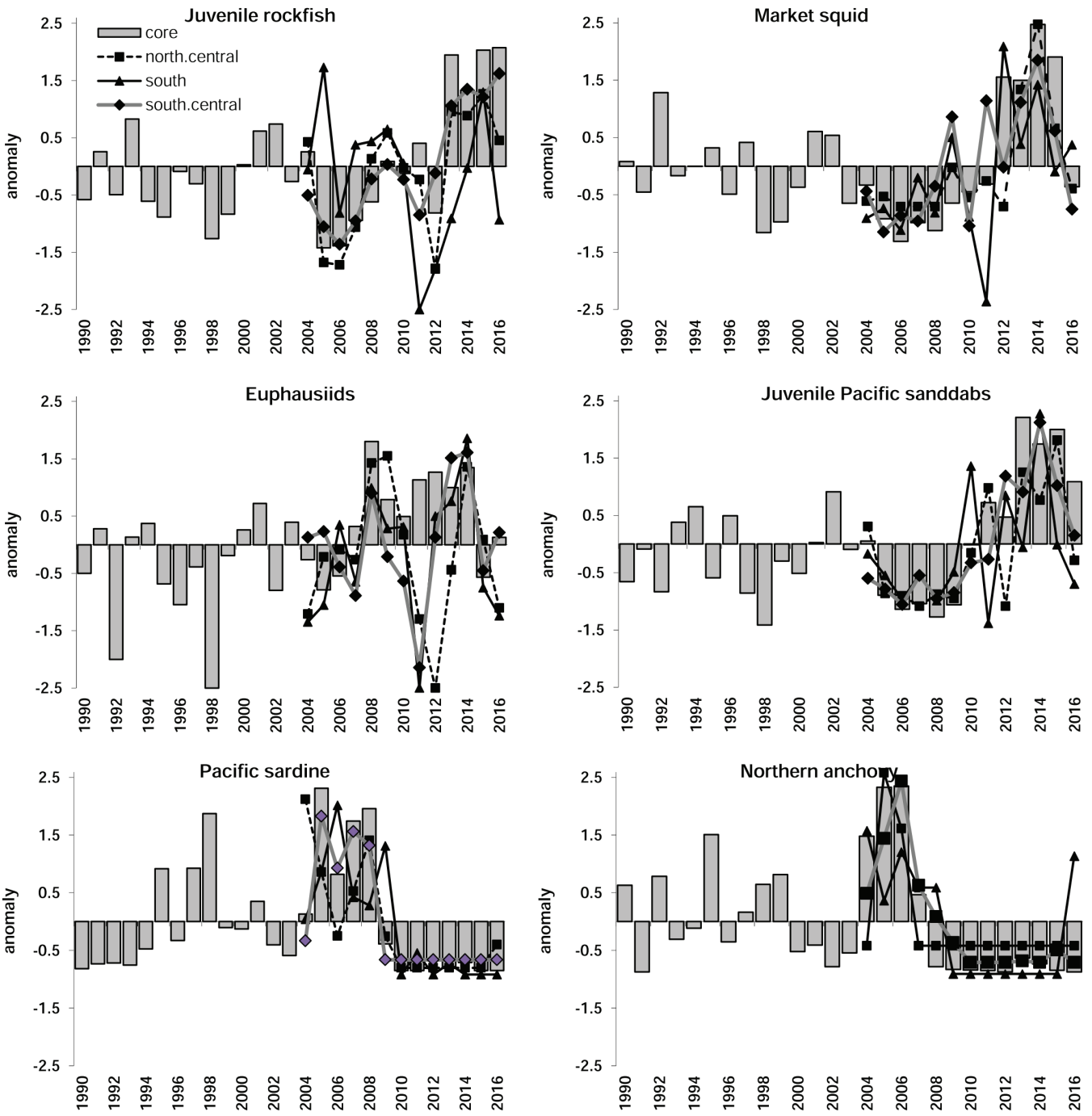

Figure 36. Long-term standardized anomalies of several of the most frequently encountered pelagic forage species from rockfish recruitment survey in the core (central California) region (1990–2014) and the southern, south-central and north-central survey areas (2004–15). Forage groups are YOY rockfish, market squid (*Doryteuthis opalescens*), krill (primarily *Euphausia pacifica* and *Thysanoessa spinifera*), YOY Pacific sanddab (*Citharichthys sordidus*), Pacific sardine (*Sardinops sagax*) and young-of-the-year Northern anchovy (*Engraulis mordax*).

which are enumerated separately from age 1+ anchovy, were the highest ever observed in the Southern California Bight, while in other regions of the California Current their numbers in summer 2016 were reduced compared to 2015 (unpublished data). *Thetys vagina* and *Pyrosoma* spp. were caught in large numbers, but other salps (i.e., non-*Thetys* salps) were less abundant compared to the past several years (fig. 37). As in summer 2015 (Leising et al. 2015), high numbers of pelagic red crabs (*Pleuroncodes planipes*) and California lizardfish were captured in summer 2016. These species are typically associated with warm water.

The abundance of both krill and market squid declined in summer 2016 in most areas relative to

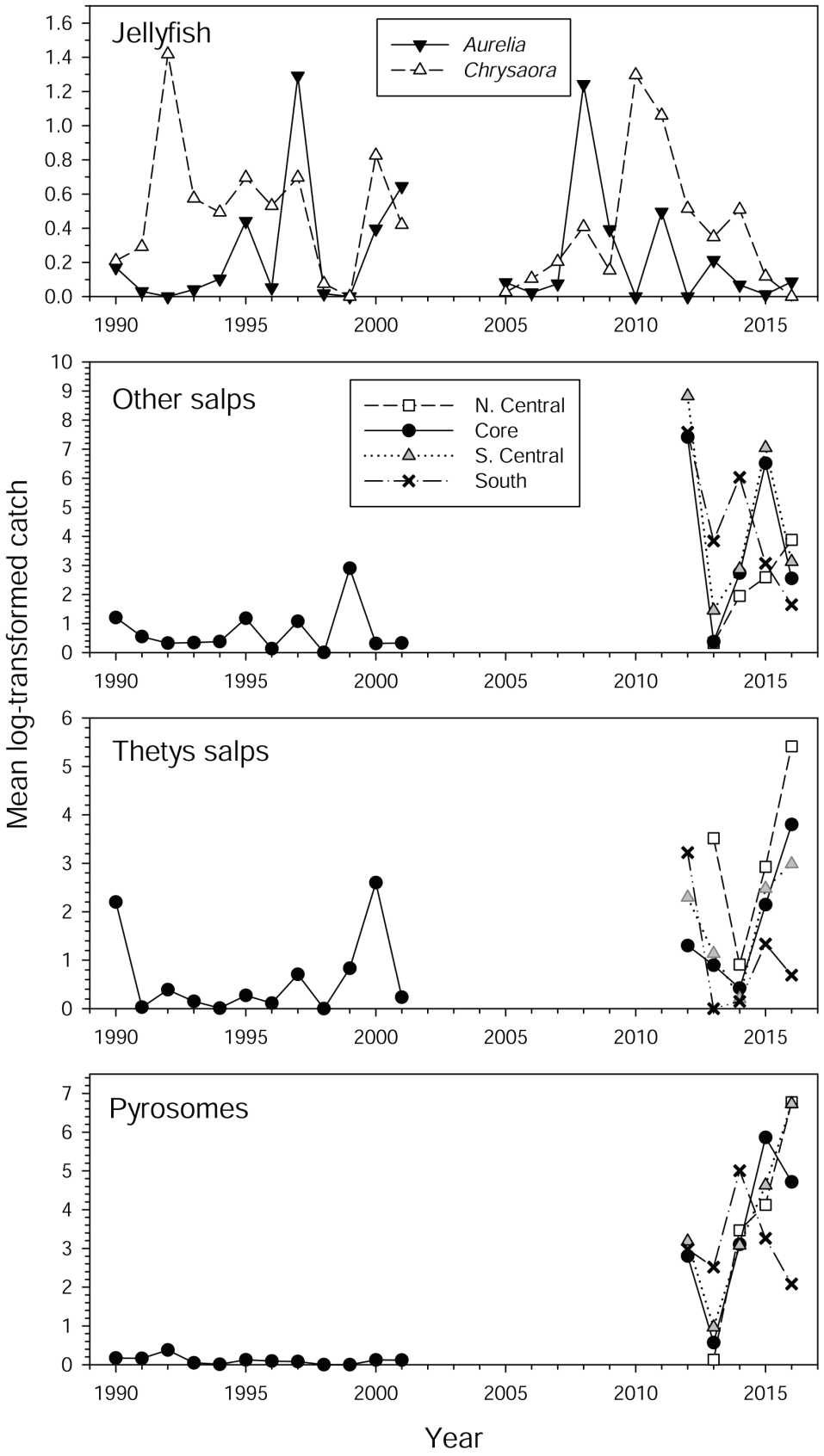

Figure 37. Standardized catches of jellyfish (*Aurelia* and *Chrysaora* spp.) and pelagic tunicates in the core and expanded survey areas.

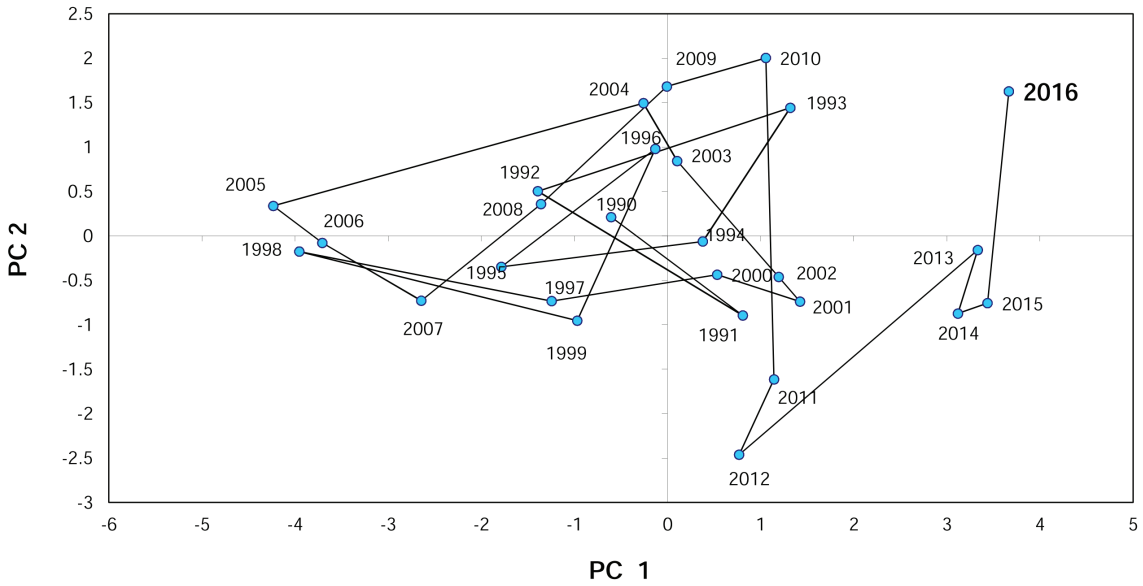

Figure 38. Principal component scores plotted in a phase graph for the nine key taxonomic groups of forage species sampled in the central California core area in the 1990–2016 period.

2015, with abundance close to or below average levels, and catches of juvenile Pacific sanddabs also declined to lower levels relative to previous years (fig. 36). The abundance of adult Pacific sardine and northern anchovy remained very low for most regions as well. Both of these species have rarely been encountered in most of the times and regions monitored since 2009, with the exception of adult anchovy in the Southern California Bight in 2016. This suggests that the biomass may be too low to be meaningfully indexed by the survey, or that a substantial fraction of the biomass is primarily located in nearshore or offshore habitats not sampled by the survey. Catches of scyphozoan jellyfish (primarily *Aurelia* spp. and *Chrysaora* spp.) continued to be unusually low in 2016 (fig. 37). Many of the more rare and unusual species that were encountered in summer 2015 (discussed in Leising et al. 2015 and Sakuma et al., in review) were not observed in the 2016 summer survey.

As in past analyses, there were sharp differences in principal component (PC) loadings between coastal pelagic (Pacific sardine, northern anchovy) and mesopelagic species (myctophids) relative to most of the YOY groundfish, krill and cephalopods. The two leading PCs for the assemblage are shown in a phase plot (fig. 38). The dramatic (and apparently ongoing) separation of the 2013 through 2016 period is apparent from these years being extremely orthogonal to the low productivity years of 1998, 2005, and 2006. Such shifts in the forage base have important implications for seabirds, marine mammals, salmon, and adult groundfish that forage primarily, or exclusively, on one or another component of the forage assemblage.

SUMMARY: CHANGES IN THE DISTRIBUTION AND ABUNDANCE OF FISH

The very warm conditions were not associated with a large spawning of sardine, but were associated with a northern shift of the sardine spawning area from central California to Oregon. Anchovy larvae were very abundant off Newport, Oregon, in 2014, but not subsequently. The ichthyoplankton assemblages off southern California and Oregon were similar to those seen in other anomalously warm or El Niño years. The mesopelagic fish assemblage off southern California exhibited higher abundances of species with southern affinities, and lower abundances of species with northern affinities. The increase in abundance and northward shift of southern species off southern California was similar to what was observed for mesopelagic fish species and red crabs off the Baja Peninsula. Off Oregon, post-larval fishes exhibited shifting dominance from myctophids prior to and at the beginning of the anomalous warming to hake becoming numerically dominant during the warming.

Fish and nekton assemblages in 2015 and 2016 were different from assemblages present during the 1997–99 El Niño/La Niña and the 2005 warm event. Forage fish such as Pacific herring, northern anchovy, and Pacific sardine were much less abundant in 2015–16 compared to previous years. In contrast, catches of salmon were close to average off northern California. Catches of young-of-the-year rockfishes were high off central California, but low off both northern and southern California. High numbers of warm water species like red crabs and lizardfish were captured in 2016, but many rare species encountered in summer 2015 were absent in 2016.

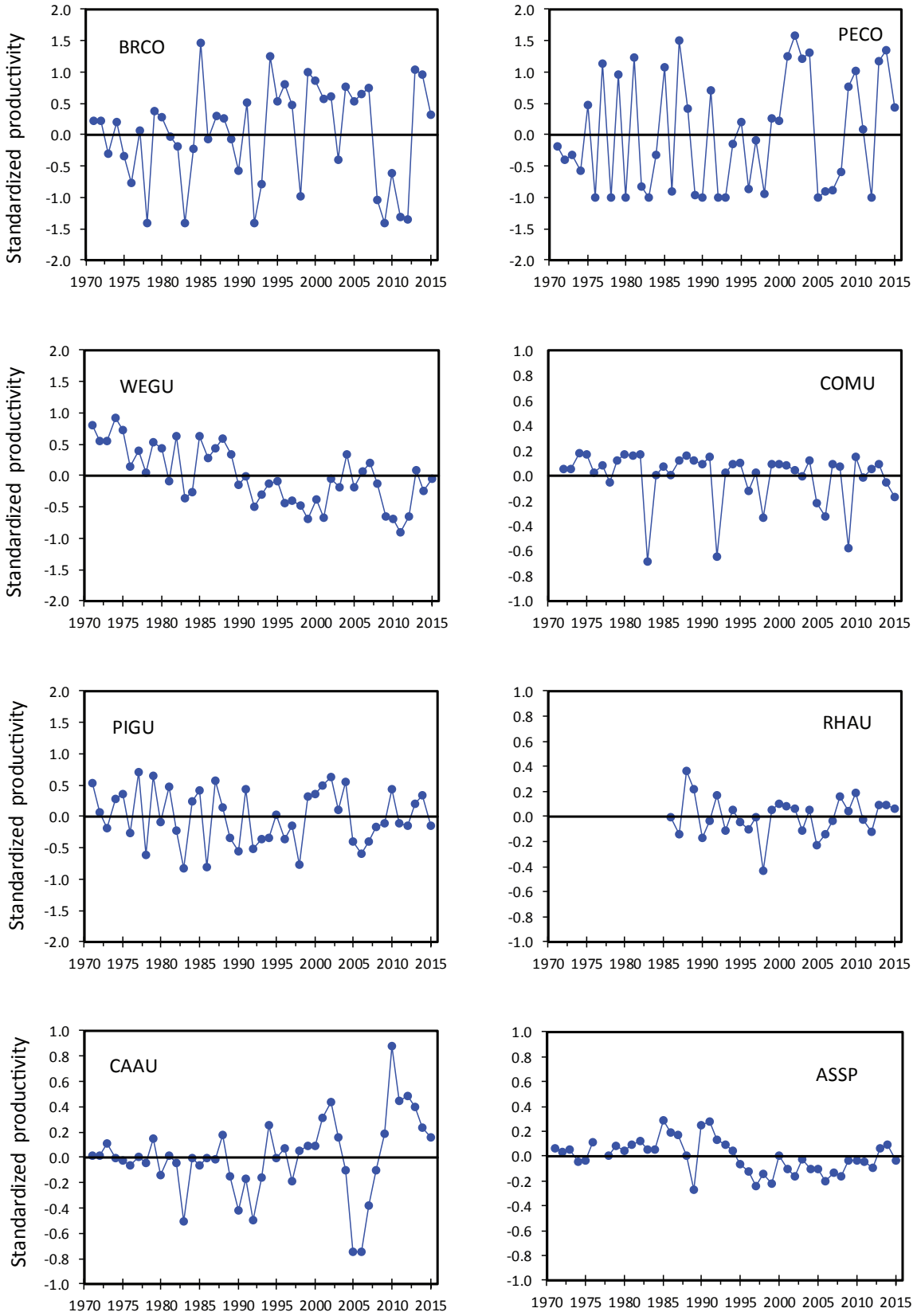

Figure 39. Standardized productivity anomalies (annual productivity minus 1971–2015 mean productivity) for 8 species of seabirds on Southeast Farallon Island. The species are: BRCO – Brandt's cormorant, PECO – pelagic cormorant, WEGU – western gull, COMU – common murre, PIGU – pigeon guillemot, RHAU – rhinoceros auklet, CAAU – Cassin's auklet, ASSP – ashy storm-petrel.

Similarly to northern California, numbers of adult sardine and anchovy were very low in summer 2016, and the survey may not provide reliable estimates at such low abundances. Multivariate analyses suggest that there may have been a shift in the composition of the forage base since 2013, and this has important implications for predators feeding exclusively on one or another component of the forage base.

SEABIRD BREEDING, PHENOLOGY, AND DIET

Reduced Seabird Breeding Populations and Breeding Success off Central California

During 2015, seabird breeding populations at Southeast Farallon Island (fig. 2a) decreased relative to 2014 for all species (data not shown) except tufted puffin (*Fratercula cirrhata*). Tufted puffins continued to increase, establishing a new high count. The upward trend for puffins contrasted with other species. The number of breeding western gulls was the lowest observed during 45 years of monitoring. Breeding populations of pigeon guillemots (*Cepphus columba*), pelagic cormorants (*Phalacrocorax peligacus*), Brandt's cormorants (*Phalacrocorax penicillatus*), and Cassin's auklets (*Ptychoramphus aleuticus*) also exhibited significant declines relative to 2014, although all except Brandt's cormorants were above long-term means. Double-crested cormorants (*Phalacrocorax auritus*) had their lowest breeding populations since 1974.

Standardized productivity (fig. 39) was lower for most species in 2015 when compared to 2014, but remained near or above long-term mean values. Chicks generally took longer to grow and fledged at lower weights than in the past few seasons. Common murres (*Uria aalge*) and pigeon guillemots were the only species below the long-term mean breeding success, while western gulls were the only species to have higher success relative to 2014. Black oystercatchers (*Haematopus bachmani*) had the lowest productivity and population ever observed for this colony, due primarily to disturbance caused by sea lions. In both 2014 and 2015, Cassin's auklets failed to produce any successful second broods resulting in their lowest productivity in six years. However, a high success rate for first broods ultimately resulted in a productive season.

A shift in chick diets from rockfish to anchovies was observed. Juvenile rockfish (*Sebastes* spp.), was still important in chick diets at Southeast Farallon Island colonies comprising 51% of the common murre chick diet and 29% of the rhinoceros auklet (*Cerorhinca monocerata*) chick diet, but rockfish were much less prominent in the diet compared to the previous two years. Anchovies returned as a major prey item for the first time since 2008 (Warzybok et al. 2015). Northern anchovy comprised 33% of common murre chick diet and 62% of rhinoceros auklet chick diet in 2015.

The Gulf of the Farallones was characterized by very warm sea-surface temperatures (SST) throughout most of the 2015 breeding season. Mean seasonal SST measured at the island in 2015 was the warmest since 1992 and joins 1992, 1998, and 2014 as the only years in which the seasonal mean was greater than 13°C (Warzybok et al. 2015). While April and May were close to the long-term average temperatures, mean monthly values for both July and August were the highest ever recorded at the Farallones. It appears that early breeding birds, in particular Cassin's auklets, fared better than later breeding species, which appear to have been affected by changed prey availability in late summer.

Warm water brought unusual bird species into the region. These included the first island records for wedge-rumped storm-petrel (*Oceanodroma tethys*) and kelp gull (*Larus dominicanus*), as well as record numbers of brown boobies (*Sula leucogaster*).

Breeding Success, Nesting Phenology, and Diet of Common Murres and Brandt's Cormorants Nesting in Far Northern California

Castle Rock National Wildlife Refuge (hereafter Castle Rock) is the most populous single-island seabird breeding colony in California (Carter et al. 1992). This island is located off the coast of Crescent City, just south of Point St. George, in the northern California Current System (fig. 2b). Here we describe the reproductive performance of common murre and Brandt's cormorants. For common murre, we also document prey composition delivered to chicks between 2007 and 2015[16].

Common murre are the most abundant surface-nesting seabird at Castle Rock and their reproductive success, nesting phenology, and chick diet have been studied since 2007. The percent of nesting pairs that successfully fledged young in 2015 was based on 87 nest sites that were monitored every other day for the entire breeding season. During 2015, fledging was 10% lower than the long-term average for this colony (63% of nests fledged young) (fig. 40A). Hatching was also 4% lower than the long-term average. The cause of depressed hatching success at Castle Rock in 2015 is not known, although hatching success at this colony is commonly influenced by egg dislodgment, egg abandonment, and inclement weather (e.g., rain) during incubation. In 2015 we infer that inadequate prey reduced the ability of murres to raise chicks to fledging age at Castle Rock because (1) chicks were observed dead at their nest site and (2) alternate sources of chick mortality (e.g., colony disturbance, predation of chicks) were not observed. Although murres do not respond directly to upwelling,

[16]To facilitate long-term monitoring of seabirds nesting at this colony, a remotely-controlled video monitoring system was installed in 2006.

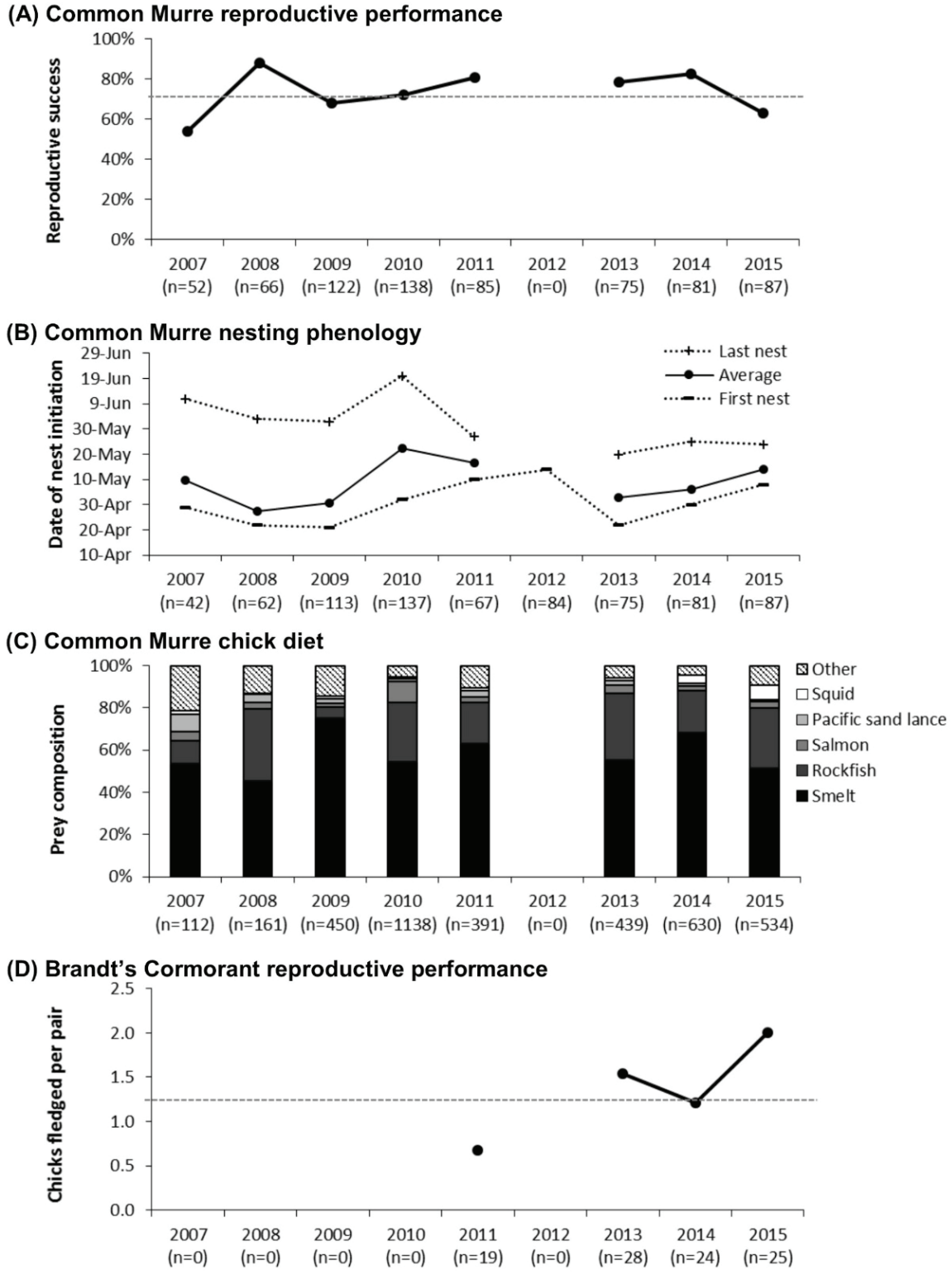

Figure 40. Reproductive performance, phenology, and chick diet of seabirds nesting at Castle Rock National Wildlife Refuge, Del Norte County, CA, between 2007 and 2015. (**A**) Percent of common murre nesting pairs that successfully fledged young. The dashed line represents the long-term (2007–15) average in reproductive success for first-clutches at this colony and the sample size (n) represents the total number of nesting pairs observed per year. (**B**) First, average, and last dates for nests initiated by common murre where the sample size (n) represents the total number of nests observed each year where nest initiation dates were accurate to ±3.5 days. (**C**) Composition of prey delivered to chicks by common murre where the sample size (n) represents the total number of prey identified each year. (**D**) Chicks fledged per each Brandt's cormorant nesting pair. The dashed line represents the long-term (2011–15) average in reproductive success for first-clutches at this colony and sample size (n) represents the total number of nesting pairs observed per year. For all subplots, data from 2012 is missing due to early failure of the video monitoring system.

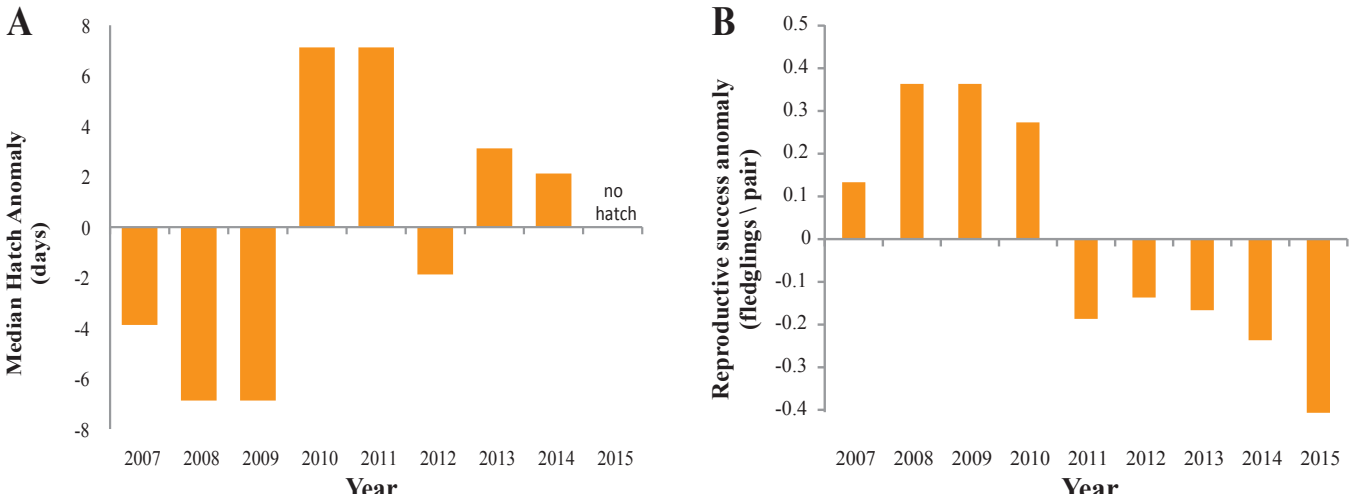

Figure 41. Anomalies of median chick hatch date and reproductive success for common murres nesting at Yaquina Head, Oregon, 2007–15. 2015 was the first year that all pairs in our reproductive plots failed to produce chicks.

increased availability of food associated with upwelling improves the body condition of egg-laying females and thereby influences the timing of nesting (Perrins 1970; Reed et al. 2006; Schroeder et al. 2009). In 2015, average nest initiation date was 5 days later (14 May) than the long-term average observed at this colony (fig. 40B), suggesting female body condition was suboptimal for early breeding.

In 2015, 16 prey types were identified[17]. All prey types had been observed in previous years with the exception of one octopus observed in 2015. Prey composition in 2015 was generally similar to other years, with smelt (Osmeridae) being the predominant prey fed to chicks and rockfish (*Sebastes* sp.) being the second-most common prey (fig. 40C). Market squid (*Doryteuthis opalescens*) were 4.2 times more frequent in murre chick diets than the long-term average and were the third most common prey type fed to chicks in 2015. Unusually in 2015, murres fed their chicks many subadult (as opposed to young-of-the-year) rockfish.

Brandt's cormorants are the second-most abundant surface-nesting seabird at Castle Rock and their reproductive success has been studied since 2011. The reproductive success of Brandt's cormorants, measured as the number of fledglings produced per pair, was determined by monitoring 26 nests every three days throughout the entire breeding season. In 2015, in contrast to the murres, cormorant breeding pairs produced 2.0 chicks on average which was 47% more than the long-term average at this colony and 29% greater than the year with the most successful reproduction (2013; fig. 40D). This illustrates an important species-specific difference between the reduced breeding success of murres and increased breeding success of cormorants during the anomalously warm conditions.

[17]Prey composition was monitored using 2-hour diet surveys conducted 6 days per week during the murre chick-rearing period (approximately 62 hours surveyed in 2015).

Reproductive Failures of Most Seabirds at Yaquina Head, Oregon: Bottom-Up Impacts Under Top-Down Control

Common murres (*Uria aalge*) and pelagic cormorants (*Phalocrocorax pelagicus*) at Yaquina Head (fig. 2b) experienced complete reproductive failure in 2015. Murre eggs were laid, but none were incubated long enough to hatch chicks. This was the first time that no murre chicks were produced in 14 years of data collection, maintaining a 5-yr run (2011–15) of low reproductive success that is less than half the success for the first four years of the study (2007–10, fig. 41). Murre reproductive success during the 1998 El Niño (Gladics et al. 2015), and 2010, 2014, and 2015 were the lowest on record. Pelagic cormorants had the lowest brood size and reproductive success in 2015 for our 8-year record (only 2011 was similarly low; fig. 42B). In contrast, Brandt's cormorants (*P. penicillatus*) had the highest reproductive success and second-highest brood size during our 8 year record (fig. 42A). Median hatch date for cormorants was over a week later than the mean (fig. 43).

Since 2011 much of the reproductive loss for murres has been due to egg and chick predators (Horton 2014). In 2015, however, the disturbance by primarily bald eagles (*Haliaeetus leucocephalus*) was so intense early in the breeding season that no eggs were incubated long enough to hatch chicks. Persistent eagle disturbance early in the season is also in part responsible for the later laying and hatching dates of murres and cormorants.

The three main forage fish species fed to murre chicks are smelt (Osmeridae), Pacific herring or sardine

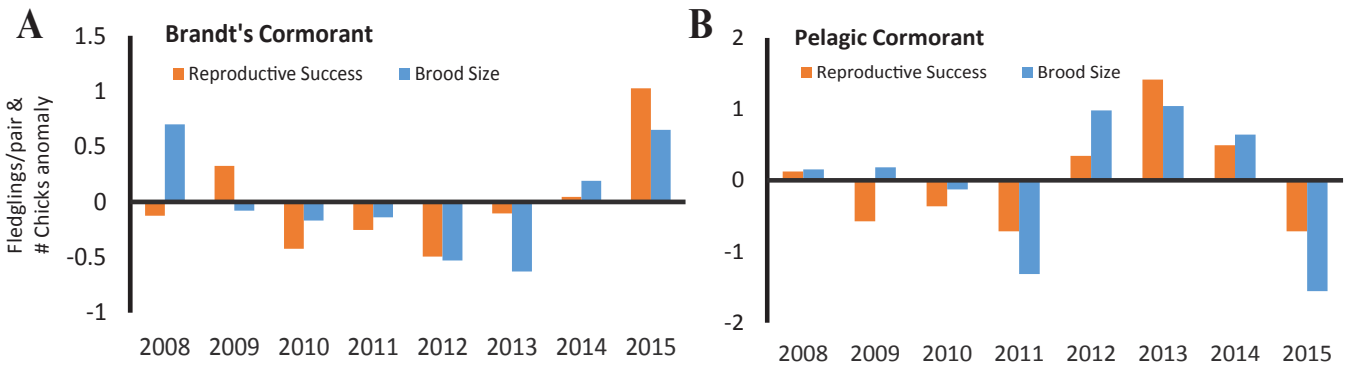

Figure 42. Anomalies of reproductive success and brood size for cormorants nesting at Yaquina Head, Oregon, 2007–15. Brandt's cormorants had an above average year for chick production, but pelagic cormorants, like murres, had a complete reproductive failure.

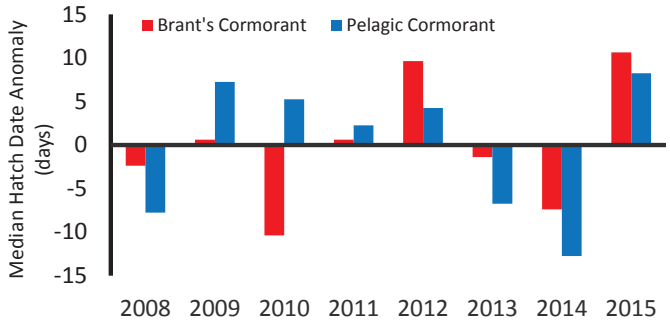

Figure 43. Anomalies of median hatch dates for Brandt's and pelagic cormorants at Yaquina Head, Oregon, 2007–15. Both species experienced one of the latest hatch dates recorded.

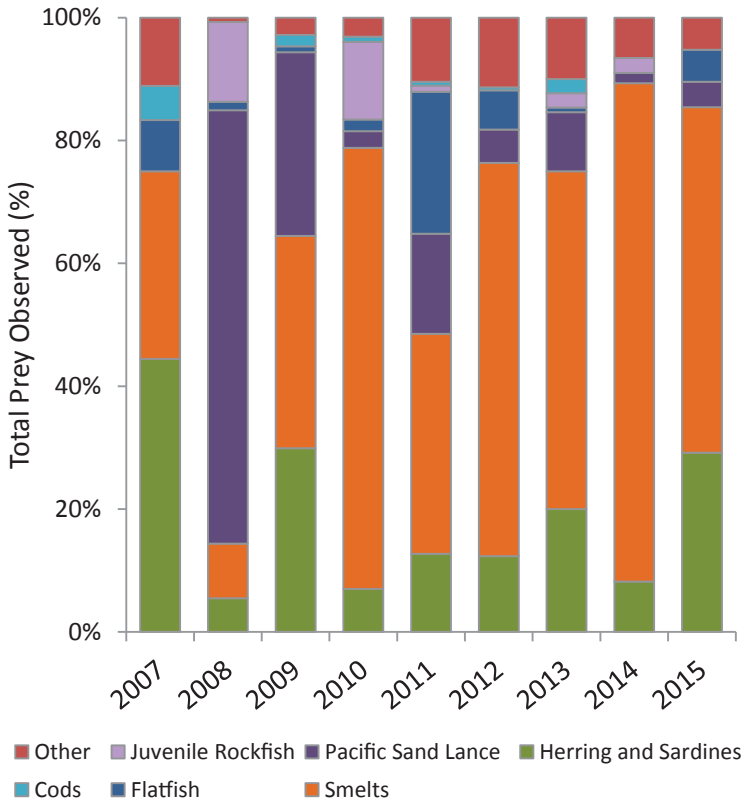

Figure 44. Prey fed to common murres chicks (% occurrence) at Yaquina Head, Oregon, 2007–15.

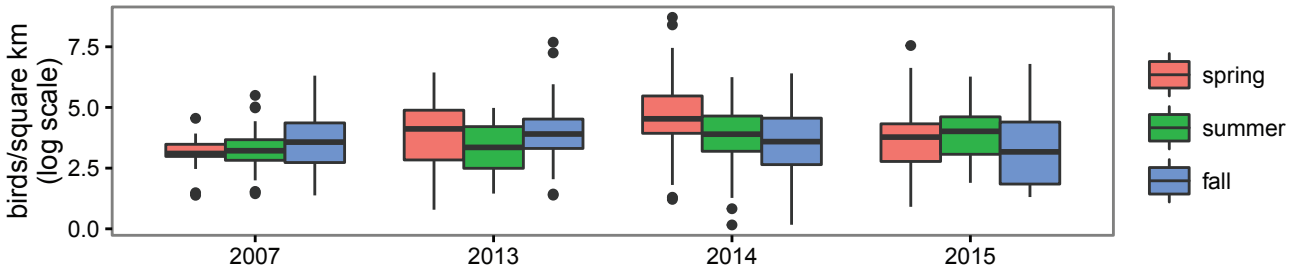

Figure 45. Boxplots of overall seabird density from vessel-based surveys off Newport, Oregon, including along the Newport Hydrographic Line and adjacent nearshore waters.

(Clupeidae), and Pacific sand lance (*Ammodytes hexapterus*). The relative proportion of the three species can be similar or one species may be numerically dominant in a given year. Smelt was the main prey item in 2015, continuing a trend of smelt-dominated diets for 4 of the past 5 years (fig. 44). In 2015, however, there was an increase in Clupeids (herring/sardine) compared to recent years. Pacific sand lance continues to be minimal in diets since 2010. The dominance of smelt and lack of herring and sand lance is notably different than diets during the 1998 El Niño (Gladics et al. 2015). Sand lance are generally more prominent in murre diets during cold water years (Gladics et al. 2014, 2015), as highlighted by their prevalence in 2008 (fig. 44). Clupeids, primarily Pacific herring (*Clupea pallasii*), are generally associated with warmer water and positive PDO (Gladics et al. 2015), although their occurrence in recent warm water years has been lower than expected.

Vessel-based seabird surveys off Newport, Oregon, indicated reduced seabird densities in spring 2015 relative to 2014 (especially for common murre, Brandt's and pelagic cormorants), but average or above average densities in nearshore waters during summer 2015 (fig. 45).

SUMMARY: SEABIRD BREEDING, PHENOLOGY, AND DIET

Seabirds at Southeast Farallon Island in 2015 exhibited reduced breeding populations, reduced breeding success, lower chick growth rates, and lower fledging weights. Chick diets shifted from a high proportion of rockfish to more anchovies compared with the previous two years. Coincident with reduced breeding and the dietary shift, the temperatures in the Gulf of Farallones were anomalously warm. Unusual bird species were observed in the region during these anomalously warm conditions. Common murre reproductive success was lower than average in northern California, similar to observations from central California during 2015, and a complete reproductive failure in central Oregon. Reduced prey availability was likely the cause as chick mortality resulted primarily from starvation, with the added pressure of increasing bald eagle predation in central Oregon. Murre chick diets were similar to other warm years, with anchovies dominating in the central and smelt dominating in the northern California Current, with another year of notable lack of sand lance off central Oregon. Fewer rockfish were consumed by murres in central California and an older age class was consumed in northern California. An increase in California market squid that began in 2014 continued in 2015 potentially indicating northward shift in these squid populations due to the prevalence of warm sea-surface temperatures across the CCS in 2015. Unlike murres and Pelagic cormorants, Brandt's cormorants were more successful in 2015 than previously observed indicating that seabird response to conditions in the CCS are species specific.

FEW PUPS AND LOW GROWTH AT SAN MIGUEL SEA LION ROOKERIES

California sea lions (*Zalophus californianus*) are permanent residents of the CCS, breeding in the California Channel Islands and feeding throughout the CCS in coastal and offshore habitats. They are also sensitive to changes in the CCS on different temporal and spatial scales and so provide a good indicator species for the status of the CCS at the upper trophic level (Melin et al. 2012). Two indices are particularly sensitive to prey availability, pup production, and pup growth during the period of maternal nutritional dependence. Pup production is a result of successful pregnancies and is an indicator of prey availability to and nutritional status of adult females from October to the following June. Pup growth from birth to 7 months of age is an index of the transfer of energy from the mother to the pup through lactation between June and the following February, which is related to prey availability to adult females during that time.

After a 12% increase in pup births at San Miguel Island in 2014, pup births declined 26% in 2015 and were 16% lower than the long-term average between 1997 and 2015 (fig. 46). Pup condition and pup growth for the 2015 cohort was the lowest observed over the time series. The average weights of three-month-old pups were 27% and 30% lower than the long-term average for female and male pups, respectively (fig. 47). Pup growth rates from three to seven months of age were 79% below average

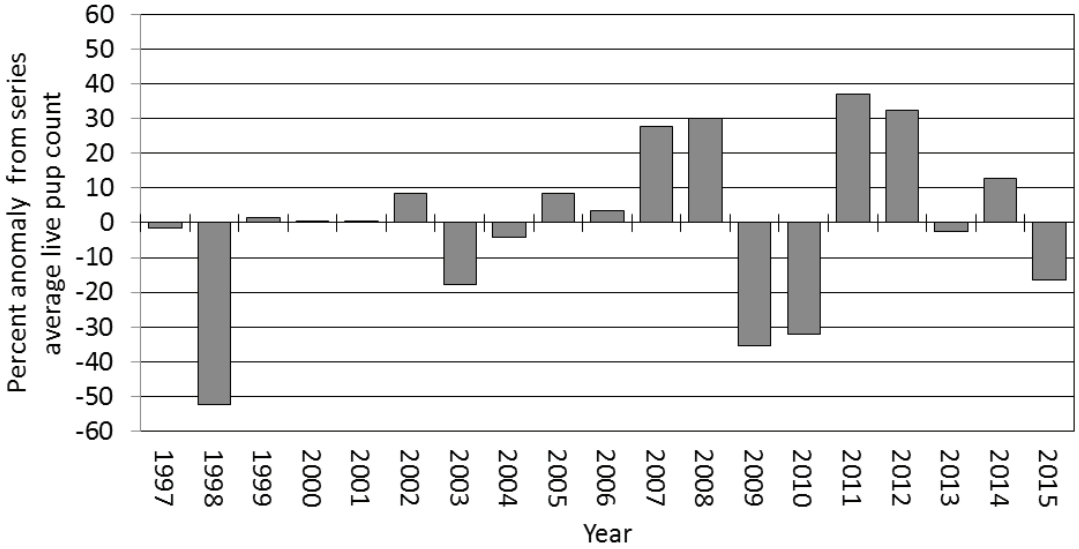

Figure 46. The percent anomaly of live California sea lion pup counts at San Miguel Island, California, based on a long-term average of live pup counts between 1997-2015 in late July when surviving pups were about 6 weeks old.

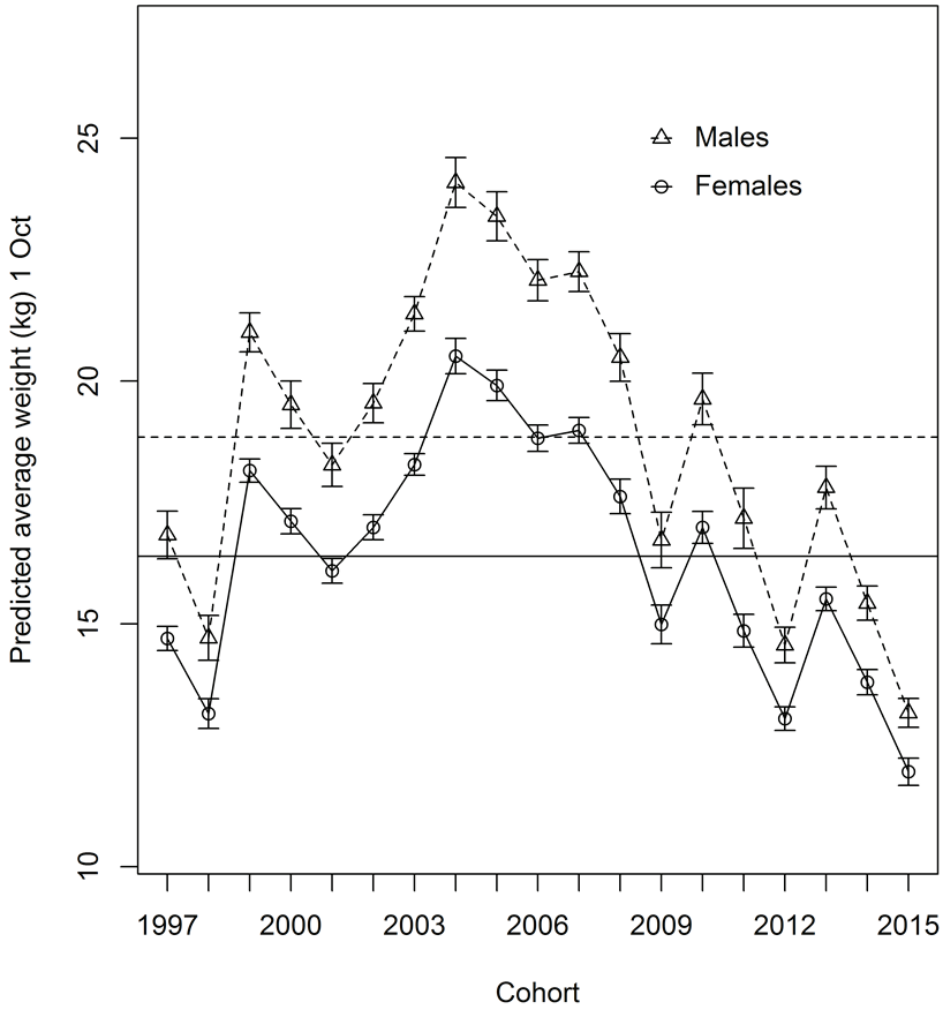

Figure 47. Predicted average weights of 3-month-old female (open circle) and male (open triangle) California sea lion pups at San Miguel Island, California, 1997–2015 and long-term average between 1997 and 2015 for females (solid line) and males (dashed line). Error bars are ± 1 standard error.

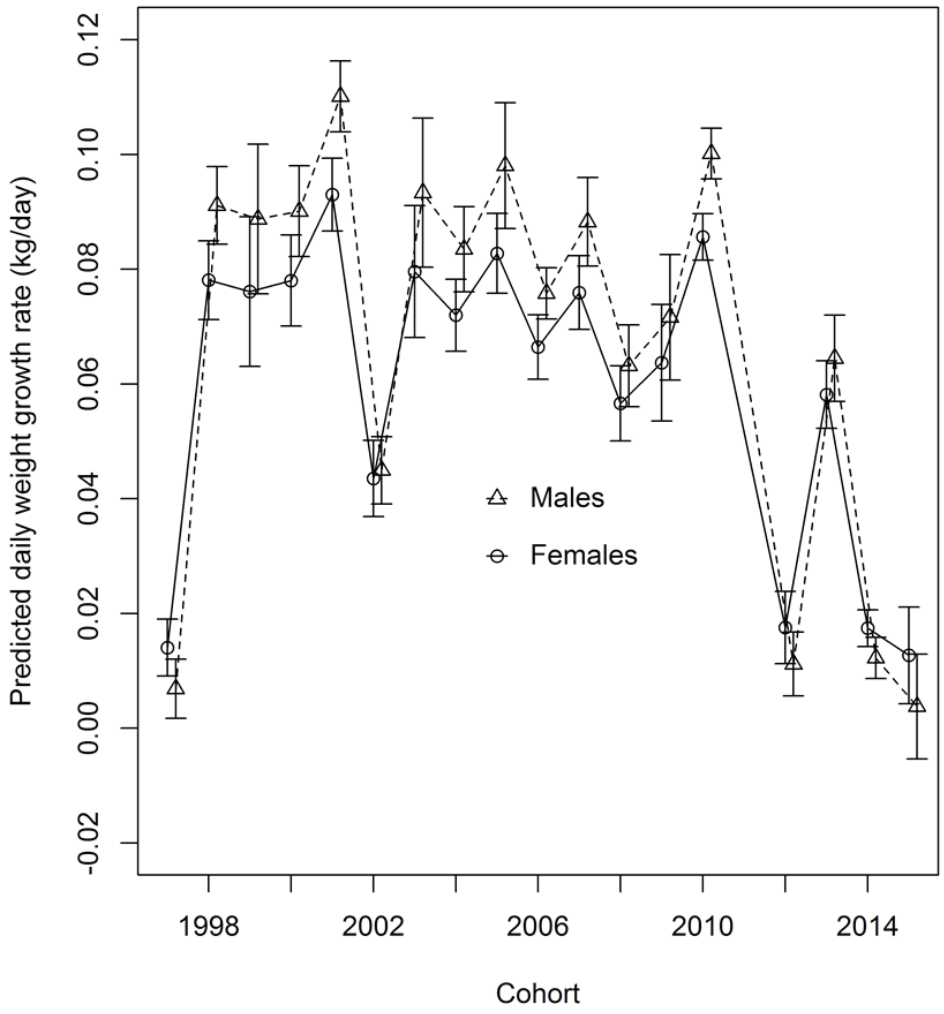

Figure 48. Predicted average daily growth rate of female (open circle) and male (open triangle) California sea lion pups between 3 and 7 months old at San Miguel Island, California, 1997–2015, and long-term average between 1997 and 2015 for females (solid line) and males (dashed line). Error bars are ± 1 standard error.

for female pups and 94% lower than average for male pups in 2015, indicating that male pups had almost no growth over the four month period (fig. 48).

Since 2009, the California sea lion population has experienced low pup survival, low pup births or both (Melin et al. 2010, 2012; Leising et al. 2014). An unusual mortality event (UME) was declared for California sea lions in southern California in response to unusually high numbers of young pups from the 2012, 2014, and 2015 cohorts stranding along the coast between January and April and poor condition of pups at San Miguel Island and other rookeries during the winter (Wells et al. 2013; Leising et al. 2014). Since 2013, fisheries surveys during the springs each year indicated that several of the primary fish prey of California sea lions that typically are associated with years of normal or better pup condition (Melin et al. 2012), including Pacific sardine (*Sardinops sagax*), northern anchovy (*Engraulis mordax*), and Pacific hake (*Merluccius productus*), were not abundant along the central California coast in the foraging range of nursing females (Wells et al. 2012, 2013, 2014; Leising et al. 2014, 2015). Analysis of scat contents of California sea lion females during these periods indicated increased consumption of rockfish (*Sebastes* spp.) and market squid (*Doryteuthis opalescens*) (Melin et al., in review). Thus, the composition of the prey community available to nursing females during the UME period was quite different from previous years when pups were in better condition (Melin et al. 2012; McClatchie et al. 2016). The combination of the residual effects of the marine heat wave and the El Niño conditions during the fall and spring of 2014–15 continued to influence the availability of prey to nursing females. Consequently, nursing females were not able to provide enough energy for their pups to grow, pups weaned too early or weaned in poor condition, and large numbers of pups stranded along the California coast contributed to the continuation of the UME in 2015. We anticipate low numbers of births,

poor condition and survival of pups, and elevated strandings along the coast to continue until the composition and abundance of the prey community increases and provides sufficient food for nursing females to support pregnancies and the energetic demands of pup growth from birth to weaning.

LOWER NUMBERS OF BALEEN WHALES AND DOLPHINS BUT CLOSER INSHORE

Marine mammal surveys were only initiated as part of the CalCOFI cruises in 2004 so it is not possible to compare distribution and abundance between the 2015–16 and the 1997–98 El Niños. This contribution focuses on the spatial distribution patterns of cetaceans off southern California and their seasonal variability in the last 5 years (2012–16) derived from visual monitoring using standard line-transect survey protocols. Methods are described in detail in Campbell et al. (2015).

The spatial distribution of several species of baleen whales differed both seasonally and interannually (fig. 49). During winter and spring, most baleen whale sightings occurred within ~370 km of the shoreline. During summer and fall, baleen whales were sighted primarily along the continental slope and in offshore waters. The exception was the fall 2015 cruise when baleen whales were mainly seen in the coastal areas of Southern California Bight. However, minke whales (*Balaenoptera acutorostrata*) and gray whale (*Eschrichtius robustus*) sightings were restricted to the continental shelf. Sightings of baleen whales in fall 2015 were significantly fewer than usual. The timing and the reduced number of sightings of baleen whales during fall 2015 coincided with anomalously warm conditions, but was prior to the winter peak of the 2015–16 El Niño.

Among the toothed (Odontocete) whales, short-beaked common dolphins (*Delphinus delphis*) were detected more frequently offshore in contrast to long-beaked common dolphins (*D. capensis*) that were more commonly seen inshore (fig. 50). During summer and fall 2015, short-beaked common dolphins extended their distribution inshore. There were fewer sightings of odontocetes during fall 2015, as was also the case for baleen whales.

Both baleen whales and odontocetes were sighted less frequently during anomalous warming off southern California prior to the peak of the 2015–16 El Niño. Baleen whales and short-beaked common dolphins normally occur offshore (e.g., over the continental slope), but in fall 2015 baleen whales (except minke and gray whales) and short-beaked common dolphins extended their distribution inshore.

OVERALL SUMMARY

Warm conditions in the North Pacific in 2014–15 were a result of the continuation of the marine heat wave, a large area of exceptionally high SST anomalies that originated in the Gulf of Alaska in late 2013. The North Pacific heat wave conditions interacted with an El Niño developing in the equatorial Pacific in 2015. Along the coast of North America, high positive SST anomalies due to the marine heat wave and the El Niño started to diminish by December 2015. The ONI reached the highest positive values since the 1997–98 El Niño during the fall of 2015 and winter of 2015–16.

Positive SST anomalies remained along the coast in late winter and early spring of 2016, with SST anomalies ranging from 0.5° to 1.5°C. Weekly periods of exceptionally high temperature anomalies (greater than 2°C) occurred until the start of the 2015–16 El Niño (winter of 2015), when SSTs were still high but not as high as those due to the marine heat wave. The decrease in SST values seen in the central CCS during the spring of 2015 corresponded with an extended period of upwelling favorable winds.

PDO values during December 2014 until March 2015 were all higher than 2, which are some of the highest values in the time series. These high winter PDO values can be attributed to the marine heat wave since they preceded the onset of the 2015 El Niño event, and modulated the regional expression of the El Niño event on the California Current (Jacox et al. 2016). High PDO values persisted during the El Niño event and reached their highest value in the past 15 years in May 2016.

During the 2015–16 warming, the depth of the 26.0 kg m^{-3} isopycnal ($d_{26.0}$) was considerably shallower than during the 1982–83 and 1997–98 events, and also showcased a much different temporal evolution. The past strong El Niño events were characterized by $d_{26.0}$ increasing rapidly beginning in summer, reaching peak anomalies in winter (November to February), and then decreasing again into the spring. In contrast, 2015–16 saw $d_{26.0}$ anomalies that were already positive due to anomalous warming of the North Pacific that began in 2014. In the first half of 2016, $d_{26.0}$ gradually shoaled, as is often the case, approaching climatological values and suggesting the decline of both El Niño and the pre-existing warm anomalies.

Mixed layer temperatures off southern California in 2014–15 were significantly higher than those observed during the previous 15 years, and did not begin to cool until the first half of 2016. The area affected by the marine heat wave and the 2015–16 El Niño in the mixed layer was comparable to the 1997–98 El Niño, but lasted longer. Water column stratification in the upper 100 m during the 2015–16 marine heat wave was as strong as the most extreme values observed during the 1997–98 El Niño. However, this stratification was primarily driven by the warming of the upper 100 m. The upper ocean was unusually fresh during 2015 in most regions off

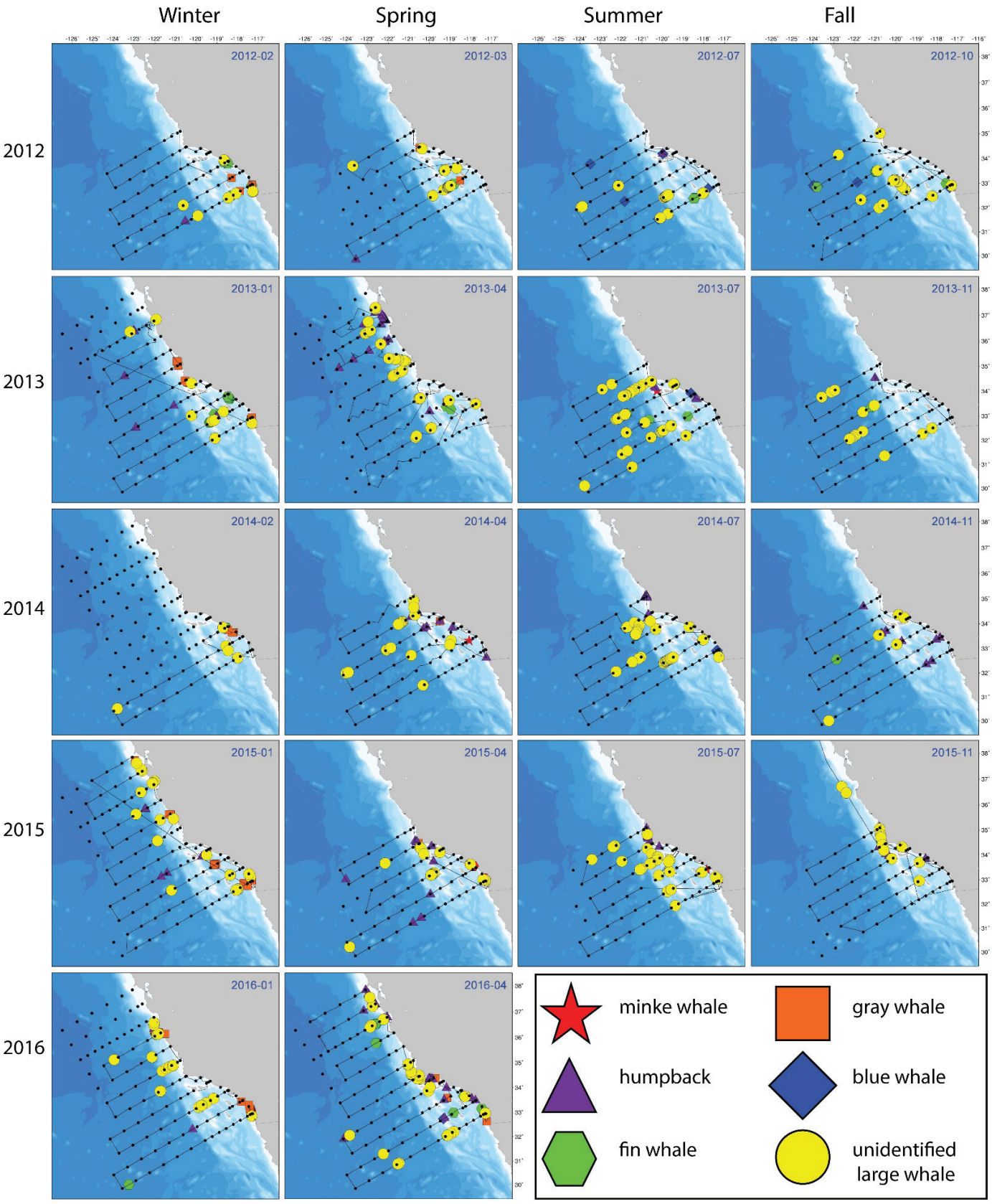

Figure 49. On-effort baleen whale sightings during CalCOFI cruises 2012–16. CalCOFI stations are represented by black dots and the ship's trackline is represented as a solid black line between stations.

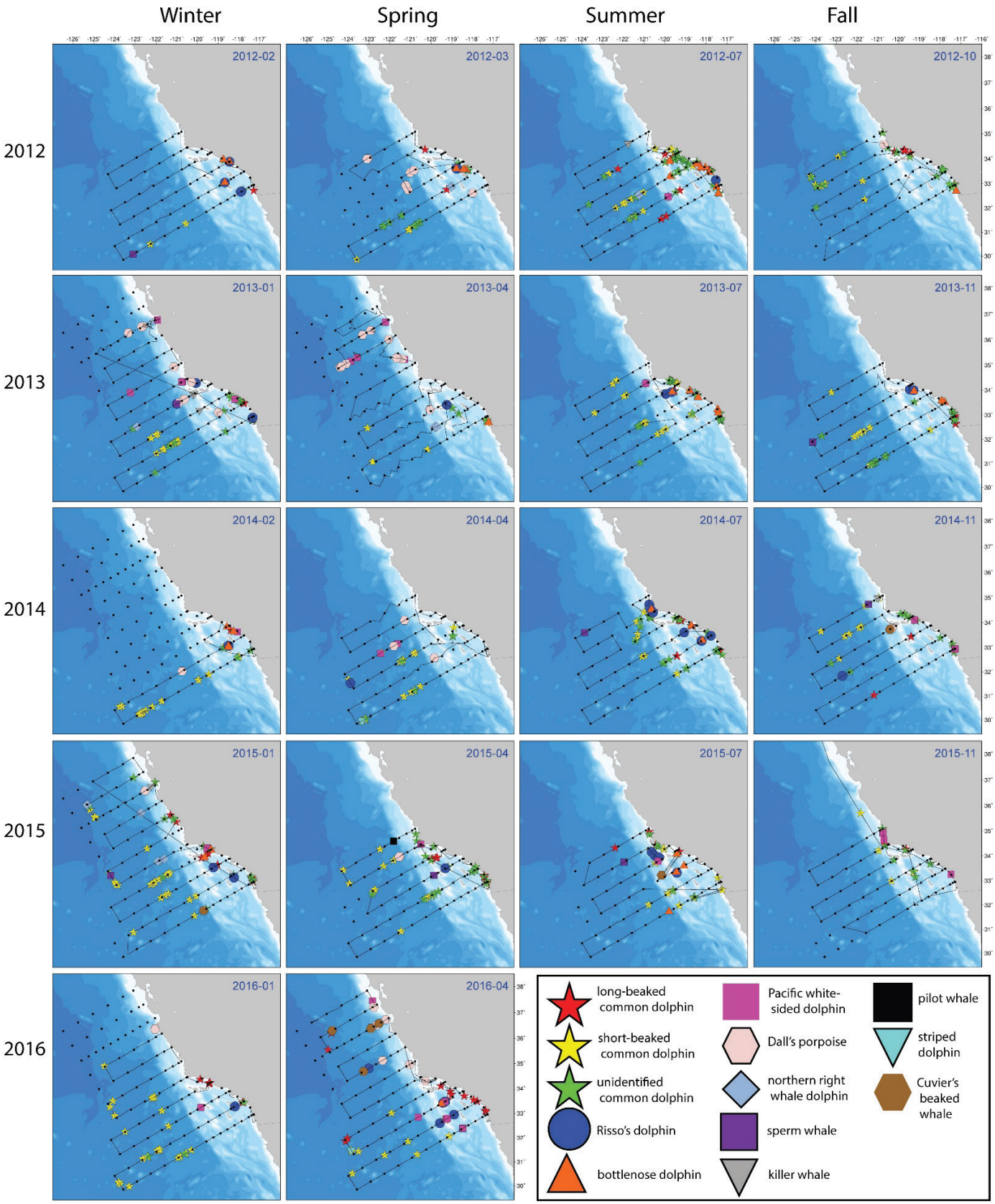

Figure 50. On-effort odontocete sightings during CalCOFI cruises 2012–16. CalCOFI stations are represented by black dots and the ship's trackline is represented as a solid black line between stations.

TABLE 1
List of CCS environmental indices, their current status, trend, implication, and figure reference (e.g., S1 = Supplement Figure S1; http://calcofi.org/ccpublications/state-of-the-california-current-live-supplement.html

Index	Current State	Trend	Implication	Figure
PDO	Positive	Increasing	Warm, low productivity	S1
NPGO	Negative	Increasing	Low to moderate productivity	S1
ENSO (ONI)	Positive	Increasing	El Niño	S1
Upwelling Anomaly	Positive, but delayed	NA	Moderately productive between 36°–42°N	S2
Cumulative Upwelling	Low north of 39°N	NA	Late spring transition north of 39°N	S4
SST Anomaly	Positive	Increasing	Warm surface waters	S3, S5
Wind Anomaly	Anticyclonic	Increasing anticyclonic	Upwelling favorable	S3
Isopycnal Depth, CalCOFI	Deeper than average	Deepening	Increased upper water column temperatures	S6
Oxygen, CalCOFI	Negative anomaly	Decreasing	Change in deep source waters	S6
Nitrate, CalCOFI	Slight positive anomaly	Neutral	Change in stratification	S6
Temperature-Salinity, CalCOFI	Warm and fresh in surface	NA	Change in surface transport	S7
Chlorophyll *a* Profiles, CalCOFI	Negative anomaly	Decreasing	Decreased productivity	S8
Temperature Anomaly, CalCOFI line 80	Positive at 10 m	Increasing	Warm surface layer	S9
Small Pelagic Fish Egg Abundance, CalCOFI	Low for all three species	Decreasing on decadal scales	Associated with reduced spawning stock biomass	S10

southern California, suggesting a strengthening of the California Current. We note that this contrasted with higher than normal salinity off Baja California in 2015. Nitracline depths, compared to the previous 15 years, have been unusually deep over the last two years and stratification in the upper 100 m was unusually strong. Despite these notable perturbations, the effects of the 2015–16 El Niño on hydrographic properties in the CalCOFI domain were not as strong as those observed during the 1997–98 El Niño. These results are summarized as a list of environmental indices in Table 1.

Warm ocean conditions and associated stratification combined with nutrient suppression and silicic acid stress likely favored initiation of the *Pseudo-nitzschia* toxic bloom in fall 2014. The winter/spring phytoplankton bloom of February and early March 2015, with higher nutrient concentrations following the spring transition to upwelling, favored explosive growth of the diatom. Local-scale forcing from coastal upwelling driving richer nutrient conditions and cross-shelf transport provided the ultimate explanation for the development of the *Pseudo-nitzschia* bloom and toxic effects.

The distribution of near-surface temperature and salinity during the 2015–16 El Niño suggests that warm, more saline waters, typically found south of Punta Eugenia, extended to the north during the 2015–16 El Niño. Anomalously warm and saline surface waters off Baja California were associated with very low zooplankton displacement volumes in 2015–16. In contrast, during the 1997–98 El Niño, zooplankton volume was close to the average with abundant copepods, euphausiids, and salps at some stations. Tropical species such as red crab, and the mesopelagic fishes *Vinciguerria lucetia* and *Triphoturus mexicanus* increased in abundance and extended their range northwards in 2015–16, a phenomenon also seen during the 1997–98 El Niño.

Off California, pelagic red crab (*Pleuroncodes planipes*) adults were abundant in the water column and frequently washed up on beaches of southern California in winter and spring 2015–16. They were reported off central California by September–October 2015. In spring 2015, the presence of only adults and the youngest zoea stages, together with their coastal distribution, is suggestive of advective transport from Baja California waters. Glider measurements of integrated transport up to June 2015 did not detect anomalous northward advection. As expected, HF radar indicated northward surface currents along the central California coast in fall and winter 2015–16.

Throughout 2015 and 2016, the zooplankton community on the Oregon shelf was dominated by lipid-poor tropical and subtropical copepods and gelatinous zooplankton. This generally indicates poor feeding conditions for small fishes, which in turn are prey for juvenile salmon. The biomass of southern copepods fluctuated greatly but was generally higher than average throughout 2015 and 2016. The presence of rarely encountered species greatly increased copepod species richness which exceeded the number of species observed during the strong El Niño in 1998. The conditions off Newport, Oregon, appear to have been influenced by intrusion of offshore waters. It is likely that the unusual copepods vagrants of 2015–16 originated from an offshore and southwesterly source, which is an important difference from the southerly origin of vagrants during the 1997–98 El Niño.

Coastal waters cooled off Trinidad Head in northern California, due to winter upwelling events, reinforced by more sustained upwelling in spring and summer. A bloom of toxic *Pseudo-nitzschia* developed, producing high levels of domoic acid. Similar to the Oregon shelf, the copepod assemblage was dominated by a more

diverse, warm water assemblage in 2015. The large cool water associated jellyfish (*Chrysaora fuscescens*) showed reduced abundance off Oregon in 2015, similar to previous warm years (2003, 2005, 2010, 2014).

The very warm conditions were not associated with a large spawning of sardine, but were associated with a northern shift of the sardine spawning area from central California to Oregon. Anchovy larvae were very abundant off Newport, Oregon, in 2014, but not during 2015 or 2016. The ichthyoplankton assemblages off southern California and Oregon were similar to those seen in other anomalously warm or El Niño years. The mesopelagic fish assemblage off southern California exhibited higher abundances of species with southern affinities, and lower abundances of species with northern affinities. The increase in abundance and northward shift of southern species off southern California was similar to what was observed for mesopelagic fish species and red crabs off the Baja Peninsula.

In contrast to the ichthyoplankton, fish, and nekton assemblages in 2015 and 2016 off northern California were different from assemblages present during the 1997–99 El Niño/La Niña and the 2005 warm event. Forage fish such as Pacific herring, northern anchovy, and Pacific sardine were much less abundant in 2015–16 compared to previous years. In contrast, catches of salmon were close to average off northern California. Catches of young-of-the-year rockfishes were high off central California, but low off both northern and southern California. High numbers of warm-water species like red crabs and lizardfish were captured in 2016, but many rare species encountered in summer 2015 were absent in 2016. Similarly to northern California, numbers of adult sardine and anchovy were very low in summer 2016. Multivariate analyses suggest that there may have been a shift in the composition of the forage base since 2013, and this has important implications for predators feeding exclusively on one or another component of the forage base.

Seabirds at Southeast Farallon Island in 2015 exhibited reduced breeding populations, reduced breeding success, lower chick growth rates, and lower fledging weights. Chick diets shifted from a high proportion of rockfish to more anchovies compared with the previous two years. Unusual bird species were observed in the region during the anomalously warm conditions. Common murre reproductive success was lower than average in northern California, similar to observations from central California during 2015, and a complete reproductive failure occurred off central Oregon. Reduced prey availability was likely the cause as chick mortality resulted primarily from starvation, with the added pressure of increasing bald eagle predation in central Oregon. Unlike murres and pelagic cormorants, Brandt's cormorants were more successful in 2015 than previously observed indicating that seabird response to conditions in the CCS is species specific.

After an increase in sea lion pup births at San Miguel Island in 2014, births declined in 2015 and were 16% lower than the long-term average between 1997 and 2015. Pup condition and pup growth for the 2015 cohort was the lowest observed over the time series. The composition of the prey community available to nursing females during 2012, 2014, and 2015 was quite different from previous years when pups were in better condition. The combination of the residual effects of the warm pool of water off the West Coast and the El Niño conditions during the fall and spring of 2014–15 continued to influence the availability of prey to nursing females. Consequently, nursing females were not able to provide enough energy for their pups to grow, pups weaned too early or weaned in poor condition, and large numbers of pups stranded along the California coast.

Both baleen and odontocete whales occurred in lower numbers coincident with anomalous warming off southern California prior to the peak of the 2015–16 El Niño. Baleen whales and short-beaked common dolphins normally occur offshore (e.g., over the continental slope), but in fall 2015 baleen whales (except minke and gray whales) and short-beaked common dolphins extended their distribution inshore.

We note some curious inconsistencies in the recent observations of the California Current System during the anomalous warm conditions. These issues will require more in-depth analyses to resolve than we can present here. Low near-surface salinity off southern California may suggest strengthening of the California Current during the warm anomaly, in contrast to the 1997–98 El Niño when the California Current weakened. Strong stratification off southern California reduced nutrient availability in surface waters and phytoplankton. In contrast, winter preconditioning and upwelling off central California fueled a massive toxic algal bloom. The arrival of weak-swimming red crabs off southern California from the south prior to fall and winter 2015–16 did not appear to be consistent with a lack anomalous northward flow, suggesting either that the crabs are better swimmers than we know, or there were streams of undetected transport from the south. Ichthyoplankton assemblages did not show much difference between warm events off southern California or Oregon, yet there appears to have been a shift in the forage base. This suggests differential survival to recruitment in the recent warm conditions. Finally, seabirds at the Farallones ate more anchovies than rockfishes, yet anchovies are at historically low levels and young-of-the-year rockfishes have been more abundant than normal on the central California coast.

It is clear from the results presented here that the warm anomaly on the ecosystem were complicated, regionally specific, and that we do not fully understand them yet. By highlighting some of the paradoxes in the data collected to date we hope to stimulate further research. Are red crabs in fact good swimmers, or were localized currents transporting these tropical animals northward? Did the warm conditions cause differential survival among fish species, driving a shift in the composition of the forage assemblage? And did the seabirds manage to exploit dense patches of anchovy that represent a spatially restricted refuge of a reduced population? If so, why did their chicks starve? Many questions remain to be answered concerning the ecosystem effects of the marine heat wave and the 2015–16 El Niño.

In closing, we summarize some important differences between our preliminary observations of current conditions and the 1997–98 El Niño event. Warming during the 1997–98 El Niño rapidly deepened over the 1997–98 winter, beginning the previous summer, and ending in the following spring. In contrast, the 2014–16 warming was shallower, began with the North Pacific heat wave in 2014, and did not revert to climatological values until summer of 2016. The recent warm anomaly was both shallower and lasted longer than the 1997–98 El Niño event. Stratification in 2015–16 was primarily driven by the warming of the upper 100 m. The area affected by the marine heat wave and the 2015–16 El Niño was comparable to the 1997–98 El Niño, but lasted longer. Despite unusually deep nutriclines and stratification as strong as the 1997–98 El Niño off southern California, the effects of recent conditions on regional hydrography were not as strong as those observed during the 1997–98 El Niño.

Somewhat surprisingly, zooplankton displacement volumes were much lower off Baja California than during the 1997–98 El Niño, although both periods exhibited increased abundances of red crabs, as well as Panama lightfish (*Vinciguerria lucetia*) and another warm-water associated mesopelagic fish, *Triphoturus mexicanus*. In the northern California Current System off Oregon the species composition of copepods indicated influence of offshore waters, which differs from the more southerly influence detected during the 1997–98 El Niño. The number of copepod species observed off Oregon during the recent warming was higher than during the 1997–98 El Niño. Fish and nekton assemblages were also different in the two periods, perhaps most notably in the very low abundance of forage fishes off Oregon. Finally, there were some indications that the California Current may have strengthened during the 2015–16 warm anomaly, whereas the current weakened during the 1997–98 El Niño. Despite these tantalizing preliminary observations, more analyses are needed before we can make definitive statements about the differences and similarities between the 2015–16 warm anomaly and the 1997–98 El Niño.

ACKNOWLEDGMENTS

This report would have been impossible without the dedicated work of the numerous ship crews and the technician groups that collected the data at sea, often under adverse conditions.

SWFSC and SIO wish to acknowledge the dedication of the NOAA CalCOFI group (comprising fisheries oceanography, ship operations, and the ichthyoplankton lab), and the SIO CalCOFI group and numerous volunteers. Major funding for CalCOFI is provided by NOAA Fisheries. Salaries for S. McClatchie and A. Leising are funded by the NOAA Fisheries and the Environment (FATE) program.

IMECOCAL thank the captain and crew of the R/V *Alpha Helix* of CICESE. Martin de la Cruz provided chlorophyll data and Luis E. Miranda computing assistance.

HF-radar data are available thanks to the initial investment of the state of California in establishing the array in California and to the National Science Foundation for establishing elements of the array in Oregon and California. NOAA-IOOS and participating universities (listed at http://cordc.ucsd.edu/projects/mapping/) provide ongoing funds/support for operation and management.

R. DeLong, J. Harris, H. Huber, J. Laake, A. Orr and many field assistants participated in the data collection and summaries for the sea lion study. Funding was provided by the National Marine Fisheries Service. Research was conducted under NMFS Permit 16087 issued to the Marine Mammal Laboratory, Alaska Fisheries Science Center.

The study of red crabs off southern California is a contribution from the California Current Ecosystem Long-Term Ecological Research site, supported by the US NSF, and from the SIO Pelagic Invertebrate Collection. Inset illustrations within Figure 18 from Boyd, C.M. 1960. *Biol. Bull.* 118:17–30. Reprinted with permission from the Marine Biological Laboratory, Woods Hole, MA.

We are grateful to Paul Fiedler for his internal NOAA review of the manuscript. We also thank three anonymous reviewers who improved the manuscript.

LITERATURE CITED

Anderson, C. R., D. A. Siegel, M. A. Brzezinski, and N. Guillocheau. 2008. Controls on temporal patterns in phytoplankton community structure in the Santa Barbara Channel, California. Journal of Geophysical Research 113: C04038, doi:10.1029/2007JC004321.

Anderson, C. R., M. A. Brzezinski, L. Washburn, and R. Kudela. 2006. Circulation and environmental conditions during a toxigenic *Pseudo-nitzschia australis* bloom in the Santa Barbara Channel, California. Marine Ecology Progress Series 327: 119–133.

Auth, T. D. 2011. Analysis of the spring–fall epipelagic ichthyoplankton community in the northern California Current in 2004–09 and its relation to environmental factors. California Cooperative Oceanic Fisheries Investigations Reports 52: 148–167.

Bakun, A. 1973. Coastal upwelling indices,West Coast of North America, 1946–71, NOAA Tech. Rep., NMFS SSRF-671, 114 pp.

Black, B. A., I. D. Schroeder, W. J. Sydeman, S. J. Bograd, and P. W. Lawson. 2010. Wintertime ocean conditions synchronize rockfish growth and seabird reproduction in the central California Current ecosystem. Canadian Journal of Fisheries and Aquatic Sciences 67: 1149–1158.

Bond, N. A., M. F. Cronin, H. Freeland, and N. Mantua. 2015. Causes and impacts of the 2014 warm anomaly in the NE Pacific, Geophysical Research Letters, 42: 3414–3420, doi:10.1002/2015GL063306.

Boyd, C. M. 1960. The larval stages of *Pleuroncodes planipes* Stimpson (Crustacea, Decapoda, Galatheidae). Biological Bulletin 118: 17–30.

Boyd, C. M. 1962. The biology of a marine decapod crustacean, *Pleuroncodes planipes* Stimpson, 1860. PhD thesis. University of California, San Diego. 123 p.

Boyd, C. M. 1967. The benthic and pelagic habitats of red crab *Pleuroncodes planipes*. Pacific Science 21: 394–403.

Brodeur, R. D., J. P. Fisher, R. L. Emmett, C. A. Morgan, and E. Casillas. 2005. Species composition and community structure of pelagic nekton off Oregon and Washington under variable oceanographic conditions. Marine Ecology Progress Series 298: 41–57.

Campbell, G. S., L.Thomas, K. Whitaker, A. B. Douglas, J. Calambokidis, and J. A. Hildebrand. 2015. Inter-annual and seasonal trends in cetacean distribution, density and abundance off southern California. *Deep Sea Research Part II: Topical Studies in Oceanography*, 112, pp.143–157.

Carter, H. R., U. W. Wilson, R. W. Lowe, M. S. Rodway, D. A. Manuwal, and J. L. Yee. 2001. Population trends of the common murre (*Uria aalge californica*). Pages 33–132 in Biology and conservation of the common murre in California, Oregon, Washington, and British Columbia,Volume 1: Natural history and population trends (D. A. Manuwal, H. R. Carter, T. S. Zimmerman, and D. L. Orthmeyer, Eds.), United States Geological Survey, Information and Technology Report USGS/BRD/ITR-2000-0012, Washington, D.C. Fish and Wildlife Service, Northern Prairie Wildlife Research Center, Dixon, CA.

Chavez, F. P., C. A. Collins, A. Huyer, and D. L. Mackas. 2002. El Niño along the west coast of North America. Progress in Oceanography 54: 1–5.

Di Lorenzo, E., N. Schneider, K. M. Cobb, P. J. S. Franks, K. Chhak, A. J. Miller, J. C. McWilliams, S. J. Bograd, H. Arango, E. Curchitser, T. M. Powell, and P. Rivière. 2008. North Pacific Gyre Oscillation links ocean climate and ecosystem change. Geophysical Research Letters 35, doi:10.1029/2007GL032838.

Di Lorenzo, E., and N. Mantua. 2016. Multi-year persistence of the 2014/15 North Pacific marine heat wave. Nature Climate Change, doi:10.1038/NCLIMATE3082.

Du, X., W. Peterson, J. Fisher, M. Hunter, and J. Peterson. Initiation and development of a toxic and persistent *Pseudo-nitzschia* bloom off the Oregon coast in spring/summer 2015. PLOS One. Submitted June 2015.

Durán, M. J. 2016. Red crabs wash out at La Jolla beaches. The San Diego Union Tribune (http://www.lajollalight.com/news/2016/jun/08/red-crabs/).

Fisher, J. L., W. T. Peterson, and R. R. Rykaczewski. 2015. The impact of El Niño events on the pelagic food chain in the northern California Current. Global Change Biology 21: 4401–4414, doi:10.1111/gcb.13054.

Gómez-Gutierrez, J., and C. Robinson. 2006. Tidal current transport of epibenthic swarms of the euphausiid *Nyctiphanes simplex* in a shallow, subtropical bay on Baja California peninsula, México. Marine Ecology Progress Series 320: 215–231.

Gladics, A. J., R. M. Suryan, R. D. Brodeur, L. M. Segui, and L. Z. Filliger. 2014. Constancy and change in marine predator diets across a shift in oceanographic conditions in the Northern California Current. Marine Biology 161: 837–851.

Gladics, A. J., R. M. Suryan, J. K. Parrish, C. A. Horton, E. A. Daly, and W. T. Peterson. 2015. Environmental drivers and reproductive consequences of variation in the diet of a marine predator. Journal of Marine Systems 146: 72–81.

Gruber, N., and J. L. Sarmiento. 1997. Global patterns of marine nitrogen fixation and denitrification. Global Biogeochemical Cycles 11: 235–266.

Hayward, T. L. 2000. El Niño 1997–98 in the coastal waters of Southern California: A timeline of events. California Cooperative Oceanic Fisheries Investigations Reports 41: 98–116.

Horton, C. A. 2014. Top-down influences of Bald Eagles on Common Murre populations in Oregon. MS thesis, Oregon State University.

Jacox, M. G., E. L. Hazen, K. D. Zaba, D. L. Rudnick, C. A. Edwards, A. M. Moore, and S. J. Bograd. 2016. Impacts of the 2015–16 El Niño on the California Current System: Early assessment and comparison to past events. Geophysical Research Letters 43: 1–9. doi:10.1002/2016GL069716.

Jiménez-Rosenberg, S. P. A., R. J. Saldierna-Martínez, G. Aceves-Medina, and V. M. Cota-Gómez. 2007. Fish larvae in Bahía Sebastián Vizcaíno and the adjacent oceanic region, Baja California, México. Checklist 3: 204–223.

Jiménez-Rosenberg, S. P. A., R. J. Saldierna-Martínez, G. Aceves-Medina, A. Hinojosa-Medina, R. Funes-Rodríguez, M. Hernández-Rivas, and R. Avendaño-Ibarra. 2010. Fish larvae off the northwestern coast of the Baja California Peninsula, Mexico. Checklist 6: 334–349.

Kahru, M., and B. G. Mitchell. 2000. Influence of the 1997–98 El Niño on the surface chlorophyll in the California Current. Geophysical Research Letters 27: 2937–2940.

Kahru, M., R. M. Kudela, M. Manzano-Sarabia, and B. G. Mitchell. 2012. Trends in the surface chlorophyll of the California Current: Merging data from multiple ocean color satellites. Deep-Sea Research II 77: 89–98. http://dx.doi.org/10.1016/j.dsr2.2012.04.007.

Kahru, M., Z. Lee, R. M. Kudela, M. Manzano-Sarabia, and B. G. Mitchell. 2015. Multi-satellite time series of inherent optical properties in the California Current. Deep-Sea Research II 112: 91–106, http://dx.doi.org/10.1016/j.dsr2.2013.07.023.

Lavaniegos, B. E., and M. D. Ohman. 2007. Coherence of long-term variations of zooplankton in two sectors of the California Current System. Progress in Oceanography 75: 42–69

Lea, R., and R. Rosenblatt. 2000. Observations on fishes associated with the 1997–98 El Niño off California. California Cooperative Oceanic Fisheries Investigations Reports 41: 117–129.

Leising, A. W., et al. 2014. State of the California Current 2013–14: El Niño looming. California Cooperative Ocean and Fisheries Investigations Reports 55:31–87.

Leising, A. W., I. D. Schroeder, S. J. Bograd, J. Abell, R. Durazo, G. Gaxiola-Castro, E. P. Bjorkstedt, J. Field, K. Sakuma, R. R. Robertson, R. Goericke, W. T. Peterson, R. D. Brodeur, C. Barceló, T. D. Auth, E. A. Daly, R. M. Suryan, A. J. Gladics, J. M. Porquez, S. McCatchie, E. D. Weber, W. Watson, J. A. Santora, W. J. Sydeman, S. R. Melin, F. P. Chavez, R. T. Golightly, S. R. Schneider, J. Fisher, C. Morgan, R. Bradley, and P. Waryzbok. State of the California Current 2014–15: impacts of the warm-water "blob." California Cooperative Oceanic Fisheries Investigations Reports 56, 31–68. 2015.

Longhurst, A. R. 1967. The pelagic phase of *Pleuroncodes planipes* Stimpson (Crustacea, Galatheidae) in the California Current. California Cooperative Oceanic Fisheries Investigations Reports 11: 142–154.

Lynn, R. J., and J. J. Simpson. 1987. The California Current System: The seasonal variability of its physical characteristics. Journal of Geophysical Research 92: 12947–12966.

Lynn, R. J., and S. J. Bograd. 2002. Dynamic Evolution of the 1997–1999 El Niño-La Niña cycle in the southern California Current system. Progress in Oceanography 54: 59–75.

Marchetti, A., V. L. Trainer, and P. J. Harrison. 2004. Environmental conditions and phytoplankton dynamics associated with *Pseudo-nitzschia* abundance and domoic acid in the Juan de Fuca eddy. Marine Ecology Progress Series 281: 1–12.

McCabe, R. M., B. M. Hickey, R. M. Kudela, K. A. Lefebvre, N. G. Adams, B. D. Bill, F. M. D. Gulland, R. E. Thomson, W. P. Cochlan, and V. L. Trainer, 2016. An unprecedented coastwide algal bloom linked to anomalous ocean conditions. Submitted to Geophysical Research Letters.

McClatchie, S. 2014. Regional fisheries oceanography of the California Current System: the CalCOFI program. Springer. 235pp. ISBN 978-94-007-7222-9.

McClatchie, S., J. Field, A. R. Thompson, T. Gerrodetter, M. Lowry, P. C. Fiedler, W. Watson, K. M. Nieto, and R. D. Vetter. 2016. Food limitation of sea lion pups and the decine of forage off central and southern California. Open Science, 3, p.150628.

Melin, S. R., A. J. Orr, J. D. Harris, J. L. Laake, and R. L. DeLong. 2012. California sea lions: An indicator for integrated ecosystem assessment of the California Current System. California Cooperative Ocean and Fisheries Investigations Reports 53:140–152.

Morgan, C. A., B. R. Beckman, R. D. Brodeur, B. J. Burke, K. C. Jacobson, J. A. Miller, W. T. Peterson, D. M. Van Doornik, L. A. Weitkamp, J. E. Zamon, A. M. Baptista, E. A. Daly, E. M. Phillips, and K. L. Fresh. 2016.

Ocean Survival of Salmonids RME, 1/1/2015–12/31/2015, Annual Report, 1998-014-00. 65pp. Available at: https://pisces.bpa.gov/release/documents/DocumentViewer.aspx?doc=P149018.

Ohman, M., and E. Venrick. 2003. CalCOFI in a changing ocean. Oceanography 16: 76–85.

Perrins, C. M. 1970. The timing of birds' breeding seasons. Ibis 112: 242–255.

Peterson, W. T., J. A. Keister, and L. R. Feinberg. 2002. The effects of the 1997–99 El Niño/La Niña event on hydrography and zooplankton off the central Oregon coast. Progress in Oceanography 54: 381–398.

Ralston, S., J. C. Field, and K. S. Sakuma. 2015. Long-term variation in a central California pelagic forage assemblage. Journal of Marine Systems 146: 26–37.

Reed, T. E., S. Waneless, M. P. Harris, M. Frederiksen, L. E. B. Kruuk, and E. J. A. Cunningham. 2006. Responding to environmental change: plastic responses vary little in a synchronous breeder. Proceedings of the Royal Society of London B 273: 2713–2719.

Reynolds, R. W., T. M. Smith, C. Liu, D. B. Chelton, K. S. Casey, and M. G. Schlax. 2007. Daily high-resolution blended analyses for sea surface temperature. J. Climate 20: 5473–5496.

Ryan, H. F., and M. Noble. Sea level response to ENSO along the central California coast: how the 1997–98 event compares with the historical record. Progress in Oceanography 54: 149–169.

Sakuma, K. M., J. C. Field, B. B. Marinovic, C. N. Carrion, N. J. Mantua, and S. Ralston. In review. Epipelagic micronekton assemblage patterns in the California Current with observations on the influence of "the blob" on pelagic forage in 2015. California Cooperative Oceanic Fisheries Investigations Reports.

Schroeder, I. D., W. J. Sydeman, N. Sarkar, S. A. Thompson, S. J. Bograd, F. B. Schwing. 2009. Winter pre-conditioning of seabird phenology in the California Current. Marine Ecology Progress Series 393: 211–233.

Schroeder, I. D, B. A. Black, W. J. Sydeman, S. J. Bograd, E. L. Hazen, J. A. Santora, and B. K. Wells. 2013. The North Pacific High and wintertime pre-conditioning of California Current productivity. Geophysical Research Letters 40: 541–546.

Schwing, F. B., M. O'Farrell, J. M. Steger, and K. Baltz. 1996. Coastal upwelling indices, West Coast of North America, 1946–95, NOAA Tech. Memo., NOAA-TM-NMFS-SWFSC-231, 144 pp.

Schwing, F. B., T. Murphree, and P. M. Green. 2002. The Northern Oscillation Index (NOI): a new climate index for the northeast Pacific. Progress In Oceanography 53: 115–139.

Simpson, J. 1992. Response of the Southern California current system to the mid-latitude north Pacific coastal warming events of 1982–83 and 1940–41. Fisheries Oceanography 1(1): 57–79.

Sommer, U. 1994. Are marine diatoms favoured by high Si:N ratios? Marine Ecology Progress Series 115: 309–315.

Suchman, C. L., R. D. Brodeur, E. A. Daly, and R. L. Emmett. 2012. Large medusae in surface waters of the Northern California Current: variability in relation to environmental conditions. Hydrobiologia.690: 113–125.

Todd, R. E., D. Rudnick, M. Mazloff, R. Davis, and B. Cornuelle. 2011. Poleward flows in the southern California Current System: glider observation and numerical simulation. Journal of Geophysical Research 116, C02026, doi:10.1029/2010JC006536.

Warzybok, P. M., R. Berger, and R. W. Bradley. 2015. Population size and reproductive performance of seabirds on Southeast Farallon Island. 2015. Unpublished report to the U.S. Fish and Wildlife Service. Point Blue Conservation Science, Petaluma, California. Point Blue Conservation Science Contribution Number 2055.

Wells, B. K., et al. 2013. State of the California Current 2012–13: No Such Thing as an" Average" Year. California Cooperative Ocean and Fisheries Investigations Reports 54:37–71.

Wolter, K., and M. S. Timlin. 2011. El Niño/Southern Oscillation behavior since 1871 as diagnosed in an extended multivariate ENSO index (MEI. ext). International Journal of Climatology 31: 1074–1087.

Zaba, K. D., and D. L. Rudnick. 2016. The 2014–15 warming anomaly in the Southern California Current System observed by underwater gliders. Geophysical Research Letters 43: 1241–1248, doi 10.1002/2015gl067550.

SCIENTIFIC CONTRIBUTIONS

GOPHER ROCKFISH (*SEBASTES CARNATUS*) LIFE HISTORY IN SOUTH-CENTRAL CALIFORNIA

NATASHA L. MEYERS-CHERRY, ROYDEN NAKAMURA,
BENJAMIN I. RUTTENBERG, AND DEAN E. WENDT

Center for Coastal and Marine Sciences
Biological Sciences Department
California Polytechnic State University
1 Grand Avenue
San Luis Obispo, CA 93407-0401
ph: 503-231-2178
fax: 503-872-2737
natasha.meyers-cherry@noaa.gov
nakamura@calpoly.edu
bruttenb@calpoly.edu
dwendt@calpoly.edu

ABSTRACT

Understanding intraspecific variability of life history characteristics is necessary to determine local fisheries management strategies. Gopher rockfish, *Sebastes carnatus*, comprise 50% of the estimated shallow nearshore recreational rockfish catch in California, yet insufficient local data exist regarding life history traits of this species. We defined growth parameters and size and age at reproductive maturity for gopher rockfish in south-central California. The growth parameter values of fish from this study are similar to previously published research from California; however, results from this study also indicate that these fish reach reproductive maturity at a larger size and an older age when compared to gopher rockfish sampled throughout central California between 1977–82. Furthermore, results from this study show that the size and longevity of gopher rockfish has increased after the establishment of two south-central California marine protected areas.

INTRODUCTION

It is well understood that natural and anthropogenic factors affect the physiological condition of individuals and hence the populations they compose. Naturally occurring environmental factors may influence life history traits in fishes (Ruttenberg et al. 2005; Hamilton et al. 2007; Caselle et al. 2011). Furthermore, anthropogenic factors like fishing can also alter these characteristics (Rijnsdorp 1993; Law 2000; Conover 2007). Understanding regional variation in life history characteristics due to multiple environmental influences among geographically distinct locations can improve fisheries management strategies.

Life history growth parameters (L_∞, T_{max}, and K) and size (age) at reproductive maturity can be used as indicators to predict species and population-level vulnerability (Adams 1980; Roff 1984; Reynolds et al. 2005) and to determine localized management strategies (Caselle et al. 2011) in the form of harvest restrictions for economically valuable species. Allowable harvest rates should be calculated based on life history data from local populations so that biological reference points (BRP) for stock biomass, growth, maturity, recruitment, and mortality are regionally accurate and target reference points (TRP) can be set for local populations that aptly promote the long-term sustainable exploitation of stocks. This information is especially valuable for long-lived, slow-growing species that may be vulnerable to overharvesting (Adams 1980). Identifying regional variability of growth parameters as well as size and age at sexual maturity allows management strategies to account for intraspecific differences among local populations.

Moreover, understanding life history traits is relevant to fisheries management because of the reproductive implications of having larger (older) fishes in populations. "The Big Old Fat Fecund Female Fish" (BOFFFF) hypothesis states that larger fish are more fecund and may produce higher quality offspring than smaller individuals in certain species (Berkeley et al. 2004a; Palumbi 2004; O'Farrell and Botsford 2005). Therefore, allowing fishes to reach larger sizes and older ages amplifies their reproductive output. For this reason, preserving larger and older fishes is essential to the stability and future productivity of fisheries systems (Hixon et al. 2013). Marine protected areas (MPAs) are a form of spatial management, in which specific areas of the ocean are protected from various types of human disturbance (Kelleher and Kenchington 1992; Gubbay 1995; Gaines et al. 2010), and may allow fishes to maximize reproductive output (Berkeley et al. 2004b). Point Buchon and Piedras Blancas State Marine Reserves are two large, previously "data-poor" MPAs, established in 2007 along the south-central coast of California as part of the statewide network of MPAs in California, USA. Ideally, these MPAs should allow fishes to attain maximum sizes and ages within their boundaries.

Rockfishes belong to the genus *Sebastes* and are an economically valuable group of fishes that primarily

exist in the Northeast Pacific (Love et al. 2002). They are long-lived, slow growing, late maturing, and have small home ranges (Love et al. 2002). Several rockfish management strategies have been implemented (Leaman 1991; Parker et al. 2000; Love et al. 2002) as fishing has reduced populations (Karpov et al. 1995; Love et al. 1998; Mason 1998).

For this study, we chose gopher rockfish, *Sebastes carnatus* (Jordan and Gilbert 1880) to ascertain regional fisheries variability in populations. Gopher rockfish range from Oregon to Baja California (Love 2011) and are a shallow-water species often targeted by recreational anglers (Chen et al. 2012). They comprise 50% of the estimated shallow nearshore recreational rockfishes catch in California (Key et al. 2005). California recreational groundfish regulations maintain a daily bag limit of ten rockfishes per angler; however, there are no length restrictions on gopher rockfish (California Department of Fish and Wildlife 2014a). Commercial anglers also target gopher rockfish in California and there is a 25.4 cm minimum size limit (unless obtained in trawl nets or landed dead) as well as regional monthly quotas allocated to these fishers (California Department of Fish and Wildlife 2014b). Despite the popularity of gopher rockfish, limited data exists concerning life history characteristics of this species. The first and only stock assessment for gopher rockfish in 2005 by Key et al. (California Department of Fish and Wildlife and the National Marine Fisheries Service) assumed analogous life history information for all populations of gopher rockfish north of Point Conception (in "northern" California). By making this assumption, some populations may be at risk of overexploitation while others may be underutilized. Defining regional life history characteristics allows management of local populations at a more appropriate ecological scale.

We aimed to define growth parameter values and size and age at reproductive maturity of gopher rockfish in south-central California for comparison with broader geographic regions and time periods. We compared life history data from fish between MPAs and adjacent fishable waters, the study areas Point Buchon and Piedras Blancas, and growth data between two time frames. With this knowledge, resource managers can more accurately manage regional stocks.

METHODS

Experimental methods

Sampling protocols We collected gopher rockfish opportunistically during the California Collaborative Fisheries Research Program (CCFRP) field seasons from mid-July through mid-September of 2012 and 2013. Among the areas surveyed by CCFRP, we collected data from the Point Buchon and Piedras Blancas MPAs as well as adjacent reference sites (REFs) in south-central California (fig. 1). We utilized standardized hook and line fishing with baited and unbaited shrimp flies (hooks) and jigs (weighted lures) to obtain fish (Wendt and Starr 2009). In 2012, we collected fish mid-September through mid-November in Point Buchon due to an extended sampling season. We collected additional fish in 2013 from mid-September to mid-November on scuba diving surveys in the Point Buchon MPA/REF sites. We also collected fish from licensed recreational anglers on commercial passenger fishing vessel (CPFV) trips. We recorded individual total length to the nearest whole centimeter and total weight to the nearest gram.

Ageing: otolith analysis To estimate the age of fish, we removed sagittal otoliths from sacrificed fish. We weighed otoliths and then stored them dry in labeled envelopes. We also utilized additional otoliths that were collected from a previous study (Loury 2011) between the years 2007–09.

We aged otoliths using the break-and-burn technique (Chilton and Beamish 1982). For consistent processing, we chose the right otolith from the pair (if available). We snapped otoliths in half along their center (lengthwise) by placing them sulcus side up between the thumb and forefinger of both hands and carefully applying pressure until fragmented. Then, we toasted the broken surface of the postrostrom half of the otolith (when available) next to a direct flame using fine tip forceps until it turned dark brown in color. Caution was taken to burn both sides of the otolith. After cooling on the table, we embedded the unbroken end of the postrostum in adhesive putty and mounted it on a slide. Then, we brushed vegetable oil onto the broken surface to enhance growth rings and placed it under a dissecting microscope to count visible annuli. We counted a pair of prominent translucent (now browned) and opaque zones as one year of growth in the fish (Lea et al. 1999). We read otoliths twice with at least a week between each reading by a single reader without knowledge of fish size or location and year collected. If there was disagreement in years (a difference of a year or greater), we read samples a third time as per established protocol (D. Pearson, National Marine Fisheries Service, Santa Cruz, California, personal communication 2012).

Assigning maturity stage We removed and weighed gonads to the nearest 0.001 g. We assigned macroscopic and histological maturity stages for ovaries and testes based on previously published parameters (Echeverria 1987; Chilton 2007; and TenBrink and Spencer 2013). Macroscopically, we determined ovaries to be immature if they appeared thin, threadlike, small, translucent, round in shape, and yellow-pink in color. The presence of individual eggs,

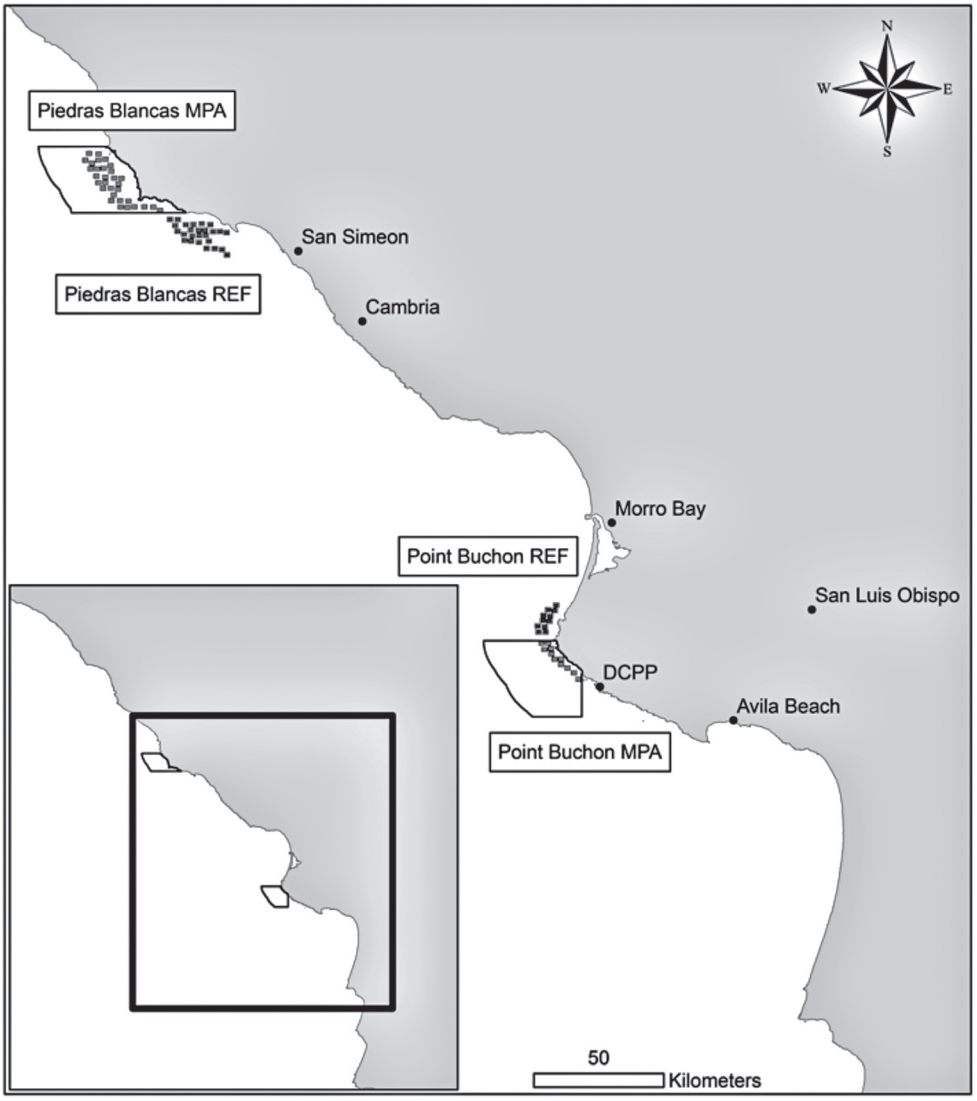

Figure 1. Map of south-central California, USA including Point Buchon and Piedras Blancas State Marine Reserves (MPAs) and adjacent reference sites (REFs). MPAs were designed to include shallow rocky reef environments that provide habitats to many nearshore species, including gopher rockfish. Square marks indicate cells monitored by CCFRP in the MPA and REF sites.

eyed larvae, or black blotches indicated mature ovaries. We determined testes to be macroscopically immature if they appeared thin, threadlike, small, translucent, and slightly triangular in shape. Mature testes were large, firm, triangular in shape, and white in color.

We microscopically staged gonadal tissues to increase accuracy of methods for fishes that were not within their reproductive seasons, but were developmentally mature (Echeverria 1987). After initial staging, we preserved organs in 10% formalin and sent them to be histologically processed by the Central Coast Pathology Lab. One to two gram ovarian and testicular cross sections were embedded in paraffin, thin-sectioned to 4 μm using a rotary microtome, mounted on slides, stained with hematoxilyn and eosin, and read under a compound microscope. We assessed ovary maturity status by defining the most advanced oocyte stage present. We determined ovaries to be immature if ooginal nests and unyolked oocytes were present. Occasionally, initial yolk accumulation in oocytes with very small yolk globules would also indicate immaturity. The presence of tertiary yolk globules and initial oil vesicles, embryonic "eyed larvae," post-ovulatory follicles, atretic oocytes, or residual larvae all signified that ovaries were mature. We designated testes as immature with the presence of germ cells, undifferentiated gonocytes, early to intermediate stages of lumen development, or primary to secondary spermatogonia. The existence of developed lumina filled with spermatozoa, sperm ducts filled with spermatozoa, and clustered organizations of spermatocysts indicated mature testes.

ANALYSES

We used size and age data from years 2007–09 and 2012–13 in the following analyses. We utilized nonlinear regression models to fit size (total length) at a specific age (years) using the von Bertalanffy growth equation: $L_t = L_\infty\ (1 - e^{-K(t - t_0)})$ where L_t is the length of an individual at age t, L_∞ is the theoretical maximum length (asymptotic) if individuals were able to grow indefinitely, K is the growth coefficient that is proportional to rate at which L_∞ is reached, t_0 is the theoretical age at $L = 0$ (often negative or zero), and t represents the age of an individual (von Bertalanffy 1934). Since no information existed for the sex of fish collected from years 2007–09, we combined sexes for all analyses. For all models, we fixed t_0 at the value –0.5 because data for smaller and younger classes was limited, and to compare growth data to data from Lea et al. (1999). We related the model parameters K and L_∞ across area, site, and over time by calculating z-scores from means and SE (standard error) to obtain p-values using two-tailed t tests with 95% confidence intervals. The estimated maximum life span of individuals is represented by T_{max}, and we calculated this by finding the mean of the upper 25% of individuals in a given population, based on highest annuli readings (Beverton 1992). We used two-sample t tests with 95% confidence intervals to compare two means, and we made comparisons to see if area, site, or time period was associated with (T_{max}). We used Bonferroni corrections when making multiple comparisons.

We modeled size (age) at maturity using a logistic regression to fit sigmoid curves utilizing the expression

$$P = Pr\ (Maturity \mid x_1) = \left(\frac{e(b_0 + b_1 x_1)}{1 + e(b_0 + b_1 x_1)} \right).$$

P is the probability an individual is mature at length or age (x_1), and the constants b_0 and b_1 are parameters estimated after fitting the curve. Predicted size (age) at 50% maturity, size (age) at which 50% of fish attain sexual maturity, was estimated with the equation $L\ (or A)_{50} = -b_0/b_1$ using previously estimated constants. We used 95% confidence intervals to see if area or site was associated with maturity.

We completed statistics using JMP Pro 11 (SAS Institute Inc., Cary, NC). We confirmed normal distributions using Shapiro-Wilk test for goodness of fit. Parameters for models are listed as mean ± SE in text and figures, and were reported using 95% confidence intervals.

RESULTS

Growth parameter estimates

When data from all areas (Point Buchon and Piedras Blancas), sites (MPA and REF), and time periods (2007–09 and 2012–13) were combined for gopher rockfish in south-central California, the growth parameter L_∞ (maximum length) was found to be 34.80 ± 0.57; K (growth coefficient) was 0.18 ± 0.01; and T_{max} (maximum age) was 9.58 years ±0.16.

The estimated growth parameters for fish from the Point Buchon MPA sampled between the years 2012–13 showed increased L_∞ ($p = 0.01$) and increased T_{max} ($p < 0.0001$) when compared to individuals sampled in 2007–09 (table 1; fig. 2). Increases in L_∞ ($p = 0.01$) and T_{max} ($p = 0.001$) were also seen over time from fish sampled in the Point Buchon REF site in 2012–13 when compared to fish sampled in 2007–09. The parameter T_{max} was significantly higher in the Point Buchon MPA compared to the REF site ($p < 0.0001$) in 2012–13 (table 1). Temporal differences in growth parameters were found when data from the Point Buchon MPA and REF sites were combined in years 2007–09, and then compared to years 2012–13 (table 1; fig. 2). Individuals from both sites in years 2012–13 had significantly higher L_∞ ($p = 0.002$) and T_{max} ($p < 0.0001$) than individuals from 2007–09.

Temporal differences were also observed in Piedras Blancas when the MPA and REF sites were combined. There was an increase in L_∞ ($p = 0.038$) (table 1; fig. 2) and T_{max} ($p < 0.0001$) (table 1) when years 2008–09 were compared to years 2012–13. Increased T_{max} ($p = 0.0003$) was observed over time from fish sampled in the Piedras

TABLE 1

L_∞, K, and T_{max} estimated for gopher rockfish, *Sebastes carnatus*, in all areas (Point Buchon: PB and Piedras Blancas: BL), sites (MPA: M and REF: R), and years. Estimates given in mean ± standard error (*SE*).

Area	Site	Years	Mean L_∞(*length*) ± *SE*	Mean K ± *SE*	Mean T_{max} (years) ± *SE*	*N*
BL	M	08–09	31.06 ± 1.22	0.24 ± 0.02	8.07 ± 0.23	61
BL	R	08–09	33.05 ± 1.25	0.22 ± 0.02	8.80 ± 0.23	60
BL	M	12–13	34.86 ± 1.88	0.18 ± 0.02	9.92 ± 0.25	46
BL	R	12–13	37.19 ± 1.95	0.17 ± 0.02	10.10 ± 0.28	40
PB	M	07–09	31.81 ± 0.72	0.25 ± 0.01	8.84 ± 0.34	76
PB	R	07–09	29.16 ± 0.87	0.35 ± 0.04	8.07 ± 0.38	61
PB	M	12–13	34.38 ± 0.83	0.22 ± 0.01	12.40 ± 0.38	59
PB	R	12–13	35.43 ± 2.11	0.20 ± 0.03	10.10 ± 0.46	49

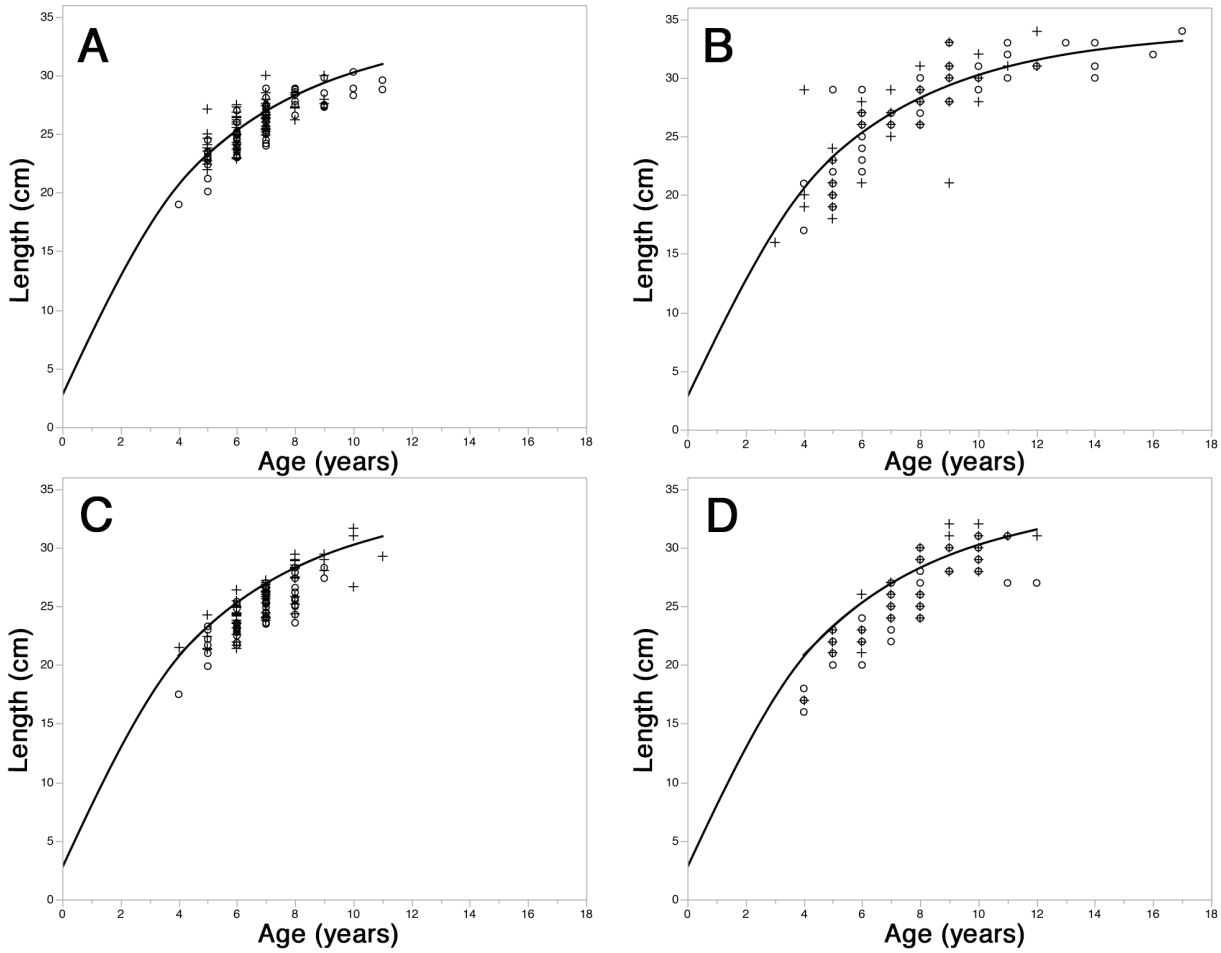

Figure 2. Von Bertalanffy growth curves for gopher rockfish sampled in south-central California. Circles represent data points from the MPA site, and plus symbols represent data points from the REF site. The value for t_0 was fixed at –0.5 (Lea et al. 1999) because data for younger and smaller and younger classes was limited, and to compare growth data to data from Lea et al. (1999). (**a**) Growth curve representing individuals from Point Buchon collected for Loury's 2011 study during the 2007–09 field seasons (n = 136) (Loury 2011). The mean L_∞ value was 31.27 cm ± 0.60, and the mean K value was 0.27 ± 0.01. (**b**) Growth curve representing individuals from Point Buchon during the 2012–13 field seasons (n=108). The mean L_∞ value was 34.65 cm ± 0.88, and the mean K value was 0.21 ± 0.01. (**c**) Growth curve representing individuals from Piedras Blancas collected for Loury's 2011 study during the 2008–09 field seasons (n = 121). The mean L_∞ value was 32.50 cm ± 0.95, and the mean K value was 0.22 ± 0.02. (**d**) Growth curve representing individuals from Piedras Blancas during the 2012–13 field seasons (n = 86). The mean L_∞ value was 35.96 cm ± 1.37, and the mean K value was 0.18 ± 0.01

Blancas REF site in 2012–13 when compared to fish in 2007–09. In addition, T_{max} increased ($p < 0.0001$) for fish from the Piedras Blancas MPA in 2008–09 compared to years 2012–13 (table 1).

Growth coefficient (K) was similar in all areas, sites, and years (table 1). No other significant differences were observed in von Bertalanffy growth parameters between areas, sites, or over time ($p > 0.05$).

Maturity

Size at 50% maturity (L_{50}) for individuals from all areas and sites was 23.61 cm with an approximate 95% confidence interval from 23.04 to 24.15 cm (n = 194; $R^2 = 0.74$; $p < 0.0001$). Age at 50% maturity (A_{50}), for individuals from all areas and sites, was 6.01 years with an approximate 95% confidence interval from 5.72 to 6.29 years (n = 194; $R^2 = 0.60$; $p < 0.0001$). We found no significant differences after comparing 95% confidence intervals for mean size (age) at reproductive maturity between areas or sites. The youngest and smallest mature female was four years old and measured 22 cm. The youngest and smallest mature male was six years old and measured 23 cm. The mean age/length of immature females and males was 5.21 years/20.76 cm and 5.25 years/21.58 cm, respectively. The mean age/length of mature females and males was 8.71 years/28.79 cm and 8.39 years/27.77 cm, correspondingly.

DISCUSSION

Growth parameter estimates

Locally defined growth parameter values from our study were comparable to a study by Lea et al. in 1999. This study examined life history traits of nearshore rock-

fishes, including gopher rockfish, in central California during the 1980s. The majority of samples were collected near Monterey; however, the study region spanned from Monterey Bay to Morro Bay. The K (0.23) and L_∞ (34.10) values from Lea's study are comparable to the K and L_∞ values from this study.

Overall, our results indicate a general pattern that the maximum size and age of gopher rockfish increased after the establishment of MPAs, likely caused by anthropogenic and natural factors, in addition to possible errors in sampling. According to the BOFFFF hypothesis (Berkeley et al. 2004a; Palumbi 2004; O'Farrell and Botsford 2005) these larger and older gopher rockfish after MPA implementation could potentially be more fecund and producing higher quality offspring than pre-MPA individuals. Past fishing has altered growth in Atlantic salmon (Ricker 1981), Atlantic cod (Swain et al. 2007), plaice (Rijnsdorp 1993), grayling (Haugen and Vøllestad 2001), and Atlantic silverside (Conover and Munch 2002). Furthermore, size-selective harvest from fishing can cause size (age)-truncations in populations where the oldest and largest individuals are being preferentially removed (Rochet 1998). Relatively recent pre-MPA data from the south-central coast region show that the fishing effort of recreational anglers on commercial passenger fishing vessels (CPFV) was not as intense in the Piedras Blancas area when compared to the Point Buchon area prior to the implementation of MPAs (Ivens-Duran 2014). Past fishing effort around Point Buchon may have preferentially selected larger and older individuals from the population. With the elimination of fishing in the Point Buchon MPA, it appears that gopher rockfish were able to reach older ages and larger sizes. It has also been shown that a regional shift in CPFV fishing effort away from the Piedras Blancas area occurred with the implementation of MPAs in 2007 (Ivens-Duran 2014). It may be that a significant decrease in fishing effort in the area allowed for fish to reach larger sizes and older ages in the Piedras Blancas area as a whole. However, a pulse of gopher rockfish recruitment leading to a tight concentration of fishes in certain year classes could also explain these results. Furthermore, closely spaced annuli near otolith margins, as counted by prevailing methods, have not yet been validated by other methods to provide accurate age estimates. Thus, it is possible that sampling error also may have influenced these results. Results from this study suggest past fishing pressure and the implementation of MPAs may have influenced the longevity and size of gopher rockfish in both Piedras Blancas and Point Buchon, although additional environmental factors and possible errors in sampling may have also affected growth parameters.

Maturity

The size and age at maturity values from this study contrast with those from Echeverria (1987). Echeverria studied reproductive aspects of rockfishes from July 1977–July 1982 in northern and central California (between Port San Luis and Crescent City). Gopher rockfish (sexes combined) age and size at 50% maturity were calculated as 4 years and 17 cm, respectively (Echeverria 1987). Because our data showed gopher rockfish matured two years later and at over five centimeters larger, this suggests either a change in maturity over time or between regions, due to environmental conditions or potential sampling error. Because our sampling design limited our collection of smaller and younger fishes, it would be beneficial to repeat this study targeting those size and age classes. This may have influenced our results and future studies should aim to increase collections to a broader size and age range. Although we cannot identify the primary driver of these differences, future management should apply this regional knowledge if these results are repeated in future studies.

Area, site, and sex were not associated with changes in age or size at maturity, suggesting that past fishing pressure and the subsequent elimination of fishing pressure have not elicited plastic responses in fishes sampled.

Conclusions

A continuation of this research would verify if these patterns are temporally stable, and elucidate the long-term effects of eliminating fishing on gopher rockfish life history characteristics. While it will be challenging to determine if potential life history changes are due to plastic or adaptive responses, determining the lasting effects of MPA implementation on these parameters merits further investigation. Moreover, additional environmental information should be monitored to determine influence on life history traits. A next step would be to expand the collection of life history information on gopher rockfish to include the full geographic range of this species. Comparing our data among broader geographic scales and over a longer time frame may provide insight into more suitable management strategies.

ACKNOWLEDGEMENTS

Research was supported by California Sea Grant, the David and Lucile Packard Foundation, the Resources Legacy Fund Foundation, the California Coastal Conservancy, and the California Ocean Protection Council. We would like to thank the captains and deckhands associated with Patriot Sportfishing and Virg's Landing, as well as the dedicated volunteer anglers who contributed to this project. Thank you to Erin Loury for donating otoliths from her previous studies, and to Meisha Key for providing us those samples. We'd also

like to thank Don Pearson at NMFS, Santa Cruz, and Katherine Schmidt at Moss Landing Marine Laboratories for their experience ageing rockfish. In addition, thanks to Matthew Preston, Grant Waltz, Lisa Needles, Carolyn Ewers, Morgan Ivens-Duran, Melissa Daugherty, Lenora Brewer, Cate Webster, Heather Price, Eric Anderson, Paul Carvalho, Lesley Stein, Nate Hall, Lindsay Faye, Kristen Byron, Megan Wilson, Brian Zelenke, Cal Poly Scientific divers, and the faculty, staff, and students of the Biological Sciences Department for their contributions.

LITERATURE CITED

Adams, P. B. 1980. Life history patterns in marine fishes and their consequences for fisheries management. Fishery Bulletin. 78:1–12.

Berkeley, S. A., C. Chapman, and S. M. Sogard. 2004a. Maternal age as a determinant of larval growth and survival in a marine fish, *Sebastes melanops.* Ecology. 85(5):1258–1264.

Berkeley, S. A., M. A. Hixon, R. J. Larson, and M. S. Love. 2004b. Fisheries sustainability via protection of age structure and spatial distribution of fish populations. Fisheries. 29(8):23–32.

Beverton, R. J. H. 1992. Patterns of reproductive strategy parameters in some marine teleost fishes. Journal of Fish Biology. 41(sB):137–160.

Bolger, T., and P. L. Connolly. 1989. The selection of suitable indices for the measurement and analysis of fish condition. Journal of Fish Biology. 34(2):171–182.

California Department of Fish and Wildlife. 2014a. Summary of 2014 Recreational Groundfish Regulations. http://www.dfg.ca.gov/marine/bfregs2014.asp#central. [accessed 5 June 2014].

California Department of Fish and Wildlife. 2014b. California Fishing Regulations: Commercial Fishing Digest. https://nrm.dfg.ca.gov/FileHandler.ashx?DocumentID=88056&inline=true. [accessed 5 June 2014].

Caselle, J. E., S. L. Hamilton, D. M. Schroeder, M. S. Love, J. D. Standish, J. A. Rosales-Casian, and O. Sosa-Nishizaki. 2011. Geographic variation in density, demography, and life history traits of a harvested, sex-changing, temperate reef fish. Canadian Journal of Fisheries and Aquatic Sciences. 68(2): 288–303.

Chen, C., L. Weiss, R. Barger, T. Hesselgrave, C. Steinback, J. Bonkoski, K. Sheeran, N. Lyman, J. Bloeser, and D. Aseltine-Neilson. 2012. Assessing Spatial and Socioeconomic Change in the California Central Coast Commercial and CPFV Fisheries. Report to the MPA Monitoring Enterprise, California Ocean Science Trust.

Chilton, E. 2007. Maturity of female Northern Rockfish *Sebastes polyspinis* in the central Gulf of Alaska. Alaska Fishery Research Bulletin. 12:264–269.

Conover, D. O., and S. B. Munch. 2002. Sustaining fisheries yields over evolutionary time scales. Science. 297(5578):94–96.

Conover, D. O. 2007. Fisheries: nets versus nature. Nature. 450(7167): 179–180.

Echeverria, T. W. 1987. Thirty-four species of California rockfishes: Maturity and seasonality of reproduction. Fishery Bulletin. 85(2):229–250.

Gaines, S. D., C. White, M. H. Carr, and S. R. Palumbi. 2010. Designing marine reserve networks for both conservation and fisheries management. PNAS. 107(43):18286–18293.

Gubbay S. 1995. Marine protected areas. Conservation Biology. 5:1–14.

Hamilton, S. L., J. E. Caselle, J. D. Standish, D. M. Schroeder, M. S. Love, J. A. Rosales-Casian, and O. Sosa-Nishizaki. 2007. Size-selective harvesting alters life histories of a temperate sex- changing fish. Ecol. Appl. 17(8):2268–2280.

Haugen T. O., and L. A. Vøllestad. 2001. A century of life-history evolution in grayling. Microevolution Rate, Pattern, Process: Springer Netherlands. 8:475–491.

Hixon, M. A., D. W. Johnson, and S. M. Sogard. 2013. BOFFFFs: on the importance of conserving old-growth age structure in fishery populations. ICES Journal of Marine Science: Journal du Conseil. fst200.

Ivens-Duran, M. 2014. A spatial analysis of changes in recreational fishing pressure on the central coast of California subsequent to MPA implementation. M.Sc. thesis, Department of Biological Sciences, California Polytechnic State University, San Luis Obispo, California.

Jordan, D.S., and C. H. Gilbert. 1880. Description of seven new species of sebastoid fishes, from the coast of California. Proc. U.S. Natl. Mus. 3:287–298.

Karpov, K. A., D. P. Albin, and W. H. Van Buskirk. 1995. The marine recreational fishery in northern and central California. California Department of Fish and Game, Fish Bulletin. 176:195.

Kelleher, G., and R. Kenchington. 1992. Guidelines for Establishing Marine Protected Areas. In: A Marine Conservation and Development Report, IUCN. Gland, Switzerland, vii+ pp 79.

Key, M., A. D MacCall, T. Bishop, and B. Leos. 2005. Stock assessment of the gopher rockfish (*Sebastes carnatus*). California Department of Fish and Game.

Law, R. 2000. Fishing, selection, and phenotypic evolution. ICES Journal of Marine Science: Journal du Conseil. 57(3):659–668.

Lea, R. N., R. D. McAllister, and D. A. VenTresca. 1999. Biological Aspects of Nearshore Rockfishes of the Genus *Sebastes* from Central California With Notes On Ecologically Related Sport Fishes. Fish Bulletin. 177.

Leaman, B. M. 1991. Reproductive styles and life history variables relative to exploitation and management of *Sebastes* stocks. Environmental Biology of Fishes. 30:253–271.

Lee, S. M., I. G. Jeon, and J. Y. Lee. 2002. Effects of digestible protein and lipid levels in practical diets on growth, protein utilization and body composition of juvenile rockfish (*Sebastes schlegeli*). Aquaculture. 211(1):227–239.

Loury, E. K. 2011. Diet of the Gopher Rockfish (*Sebastes carnatus*) Inside and Outside of Marine Protected Areas in Central California. M.Sc. theses: Paper 4060, Moss Landing Marine Laboratory.

Love, M. S., J. E. Caselle, and W. H. Van Buskirk. 1998. A severe decline in the commercial passenger fishing vessel rockfish (*Sebastes* spp.) catch in the Southern California Bight, 1980–96. Calif. Coop. Ocean. Fish. Investig. Rep. 39:180–195.

Love, M. S., M. Yoklavich, and L. Thorsteinson. 2002. The rockfishes of the Northeast Pacific. University of California Press, Berkley. 405.

Love, M. S. 2011. Certainly More Than You Want to Know About the Fishes of the Pacific Coast. Really Big Press. Santa Barbara, California.

Mason, J. E. 1998. Declining rockfish lengths in the Monterey Bay, California, recreational fishery, 195994. Marine Fisheries Review. 60(3):15–28.

Matthews, K. R. 1986. Movement of two nearshore territorial rockfishes previously reported as non-movers and implications to management. California Department of Fish and Game. 72:103–109.

O'Farrell, M. R., and Botsford L. W. 2005. Estimation of change in lifetime egg production from length frequency data. Canadian Journal of Fisheries and Aquatic Sciences. 62(7):1626–1639.

Palumbi, S. R. 2004. Fisheries science: Why mothers matter. Nature. 430(7000):621–622.

Parker, S. J., S. A. Berkeley, J. T. Golden, D. R. Gunderson, J. Heifetz, M. A. Hixon, R. Larson, B. M. Leaman, M. S. Love, J. A. Musick, V. M. O'Connell, S. Ralston, H. J. Weeks, and M. M. Yoklavich. 2000. Management of Pacific rockfish. Fisheries. 25(3):2230.

Rätz, H. J. and J. Lloret. 2003. Variation in fish condition between Atlantic cod (*Gadus morhua*) stocks, the effect on their productivity and management implications. Fisheries Research. 60(2):369–380.

Reynolds, J. D., N. K. Dulvy, N. B. Goodwin, and J. A. Hutchings. 2005. Biology of extinction risk in marine fishes. Proceedings of the Royal Society B: Biological Sciences. 272(1579):2337–2344.

Ricker, W. E. 1981. Changes in the average size and average age of Pacific salmon. Canadian Journal of Fisheries and Aquatic Sciences. 38(12): 1636–1656.

Rijnsdorp, A. D. 1993. Fisheries as a large-scale experiment on life-history evolution: disentangling phenotypic and genetic effects in changes in maturation and reproduction of North Sea plaice, Pleuronectes platessa L. Oecologia. 96(3):391–401.

Roff, D. A. 1984. The evolution of life history parameters in teleosts. Canadian Journal of Fisheries and Aquatic Sciences. 41:898–1000.

Ruttenberg, B. I., A. J. Haupt, A. I. Chiriboga, and R. R. Warner. 2005. Patterns, causes and consequences of regional variation in the ecology and life history of a reef fish. Oecologia. 145(3):394–403.

Swain, D. P., A. F. Sinclair, J. M. Hanson. 2007. Evolutionary response to size-selective mortality in an exploited fish population. Proceedings of the Royal Society B: Biological Sciences. 274(1613):1015–1022.

TenBrink, T. T., and P. D. Spencer. 2013. Reproductive Biology of Pacific Ocean Perch and Northern Rockfish in the Aleutian Islands. North American Journal of Fisheries Management. 33(2):373–383.

von Bertalanffy, L. 1934. Untersuchungen fiber die Gesetzlichkeit des Wachstums. I. Allgemeine Grundlagen der Theorie mathematische und physiologische Gesetzlichkeiten des Wachstums bei Wassertieren. Roux Arch. Entwicklungsmech. 131:613–652.

Walsh, S. M., S. L. Hamilton, B. I. Ruttenberg, M. K. Donovan, and S. A. Sandin. 2012. Fishing top predators indirectly affects condition and reproduction in a reef-fish community. Journal of Fish Biology. 80(3):519–537.

Wendt, D. E., and R. M. Starr. 2009. Collaborative Research: An Effective Way to Collect Data for Stock Assessments and Evaluate Marine Protected Areas in California. Marine and Coastal Fisheries: Dynamics, Management, and Ecosystem Science. 1:315–324.

SEASONAL AND ONTOGENETIC MOVEMENTS OF LINGCOD (*OPHIODON ELONGATUS*) IN CENTRAL CALIFORNIA, WITH IMPLICATIONS FOR MARINE PROTECTED AREA MANAGEMENT

ASHLEY GREENLEY
FishWise
PO Box 233
Santa Cruz, CA 95061
ph: (831) 427-1707
a.greenley@fishwise.org

KRISTEN GREEN
Alaska Department of Fish and Game
304 Lake St. Rm. 103
Sitka, AK 99835
ph: (907) 747-2683
kristen.green@alaska.gov

RICHARD M. STARR
California Sea Grant
Moss Landing Marine Laboratories
8272 Moss Landing Road
Moss Landing, CA 95039
ph: (831) 771-4442
starr@mlml.calstate.edu

ABSTRACT

Movements of lingcod implanted with acoustic transmitters were monitored for a year in central California. Half of the tagged lingcod remained within 5 km of coastline for at least 50% of days in the year, and 30% of lingcod were detected for >80% of the study days. Lingcod demonstrated distinct patterns in residency that were correlated to sex, fish length, and season. Residence times of females decreased with total length; female lingcod >90% maturity were present during the fall spawning season and briefly during the spring. Size-specific movements were less pronounced for males, but daily detections of males declined in spring, at the end of the winter nest-guarding season. The majority of lingcod detections were constrained to a limited area, however a few lingcod exhibited movements up to several kilometers. These results indicate that marine reserves can serve to both protect lingcod and also provide fisheries benefits via spillover.

INTRODUCTION

In recent years, ecosystem-based management approaches such as the use of marine protected areas (MPAs) have augmented traditional fishery management strategies that set harvest guidelines based on fishing mortality rates over large geographic distances (Lester et al. 2009). Meta analyses of field studies have shown that on average, MPAs yield positive results with respect to an increase in biomass, density, species richness, and size of individual organisms protected (e.g., Lester et al. 2009). The magnitude of changes in response variables, however, varies greatly and is dependent upon management parameters (MPA size and protection level, enforcement, and time since MPA was established), environmental conditions (habitat characteristics, oceanographic regimes), species' life histories, and ecological factors (Molloy et al. 2009). For managers, an equally important response variable to measure is the degree to which MPAs result in fisheries benefits via adult "spillover" from reserve boundaries. To determine the latter, it is essential to understand movement patterns of species, how they vary in relation to oceanographic seasons and life stages, and the likelihood to which species movements may extend beyond reserve boundaries (Kramer and Chapman 1999).

Lingcod (*Ophiodon elongatus*) are targeted by commercial and recreational fisheries throughout their range from Alaska to Baja California, Mexico. In 1999, the Pacific Fisheries Management Council officially declared lingcod stocks along the US West Coast to be overfished (Jagielo et al. 2000), prompting a rebuilding phase that included stringent harvest restrictions. Aided by strong recruitment events from 2000–02 and again in 2006, lingcod populations rapidly recovered, first in Oregon and Washington (Jagielo 2005), and later in California (Hamel et al. 2009).

As lingcod populations increased in California, a parallel increase in lingcod abundances in MPAs have been recorded relative to adjacent fished areas (Caselle et al. 2015; Starr et al. 2015). This indicates that lingcod are benefiting from MPA protection, but also leads to questions as to whether lingcod are moving beyond MPA boundaries and thus contributing to increased catches outside of MPAs. Existing movement information for lingcod in California is primarily based on recapture information from external tagging studies (Miller and Geibel 1973; Lea et al. 1999), however these data provide limited movement information and may not capture the nuances of certain life-history attributes of lingcod, such as seasonal migrations and reproductive behaviors.

We designed a project to determine the amount of time that tagged lingcod of different sizes and sexes remained within a continuous stretch of coastline in central California, an area that is now largely encompassed by two separate MPAs. Our primary goal for this study was to determine if lingcod in central California are highly residential, and therefore more likely to remain within an MPA boundary, or if lingcod are characterized by intermediate spatial scales of movements that would allow for partial protection via MPAs while offering some potential for adult spillover to adjacent fishing grounds. We were also interested in determining if movement patterns and residency differed by sex and size class of lingcod, to better understand how MPAs might be best designed to protect critical life stages. Specifically, we hypothesized that female lingcod would

be less residential than males in the nearshore areas we monitored, due to sex-related differences in depth distributions (Jagielo 1990; Gordon 1994). Lingcod migrate to deeper waters at the onset of maturity (Miller and Geibel 1973; Gordon 1994), and thus we hypothesized that smaller lingcod tagged in Carmel Bay would occupy shallower depths than their larger conspecifics. Based on a hypothesis proposed by Matthews (1992), we also examined if smaller, possibly immature lingcod were less site-specific than larger fish. Finally, we hypothesized that movements of all sizes and sexes of lingcod would be stimulated by environmental factors, i.e., that increased upwelling and subsequent food availability would lead to an expansion of movements related to foraging. In short, our study contained three main objectives: 1) determine the residence time of lingcod tagged with acoustic transmitters in the nearshore environment in Carmel Bay for one year; 2) compare movements among sexes and size classes of lingcod; and 3) determine if movements varied with season and or environmental conditions.

MATERIALS AND METHODS

Study Site

Carmel Bay is located on the southwestern side of the Monterey Peninsula in central California coast, near 36°32'N, 121°57'W. Our study site in Carmel Bay was located north of the Carmel Canyon head, from Carmel Point to approximately 1 km northwest of Pescadero Point (fig. 1). The nearshore environment in Carmel Bay is characterized by the seasonal presence of giant kelp (*Macrocystis pyrifera*) and seafloor habitat comprised of contiguous high-relief granite outcrops, patchy areas of low-relief bedrock, and sand bottom. Four separate MPAs are located within or in close proximity of Carmel Bay, however only the Carmel Bay State Marine Conservation Area (SMCA) and the Carmel Pinnacles State Marine Reserve (SMR) were encompassed within the study area.

Fishing and Tagging

We tagged 30 lingcod with acoustic transmitters during two time periods: 8/18/2005–9/8/2005 and 8/21/2006–10/7/2006. Lingcod were caught by hook and line and implanted with sterilized acoustic transmitters (Vemco V13P-1H-S256) using standard surgical techniques for fishes (e.g., Lowe et al. 2009). Each transmitter was programmed to send a signal with a unique identification code along with fish depth at a random interval between 90–270 seconds. Transmitter battery life was estimated to be one year, although some tags were detected for >700 days. For external identification, a t-bar anchor tag was implanted into the dorsal musculature of each fish. Similar procedures have been successful in other lingcod tagging studies (Starr et al. 2004; Lowe et al. 2009; Tolimieri et al. 2009; Bishop et al. 2010).

Two large male lingcod tagged in 2005 were never detected after release and were excluded from the analyses. Another fish (tag #66, male, 62 cm TL) was caught by a spear fisherman after 246 days at liberty, within 500 m of its original tagging location. Residence time for this fish was calculated for the percentage of days detected until the day it was caught (% days at liberty). A second confirmed fishing mortality was tag #71 (female, 94 cm TL), caught by an angler in August 2008, after 702 days at liberty and 371 days since its last detection within the array. The angler reported catching this large female within close proximity (<300 m) to the original tagging location. No adjustments were made to the residence time analysis for tag #71 as this fish was captured after the study had concluded.

Of the 30 fish we tagged, 17 were male and 10 were female lingcod. The sex of three lingcod tagged in 2005 was unidentified and these fish were excluded from sex-specific analyses. For both sexes, we targeted fish in two size classes: fish between the lengths of 50%–90% maturity (five females, eight males, three with unknown gender), and fish at lengths ≥90% percent maturity (five females, nine males). We based our estimates of lengths at 50% maturity (males 47 cm TL; females 57 cm TL) and 90% maturity (males 61 cm TL; females 67 cm TL) on calculations by Silberberg et al. (2001) and Laidig et al. (1997) for lingcod in central California. From age-length relationships, we estimated that the lingcod tagged in this study were between 3–12 years of age.

Receiver Array

We monitored lingcod movements using an array of 30 acoustic receivers (Vemco, Inc. VR-2, 69 kHz) moored parallel to the coastline in Carmel Bay in depths ranging from 7–40 m (fig. 1, fig. 2). Along with a time and date stamp for each signal received, the receivers recorded transmitter IDs and depths of tagged fish swimming within the receiver's detection range. Most of the receivers were deployed 5 m from the seafloor except in areas greater than 30 m depth, where the receivers were elevated 10–15 m from the seafloor to limit SCUBA diving depths during retrieval. Receivers were collected, serviced, and redeployed every six months.

Acoustic Range Testing and Validation

Detection ranges of VR-2 receivers are affected by sea state, biological and anthropogenic noise, bottom topography, and submerged vegetation (Simpfendorfer et al. 2002). We estimated receiver detection ranges by analyzing signal transmissions from V13 transmitters suspended 1 m off the seafloor for 15 minutes, at 50 m increments away from moored receivers. We

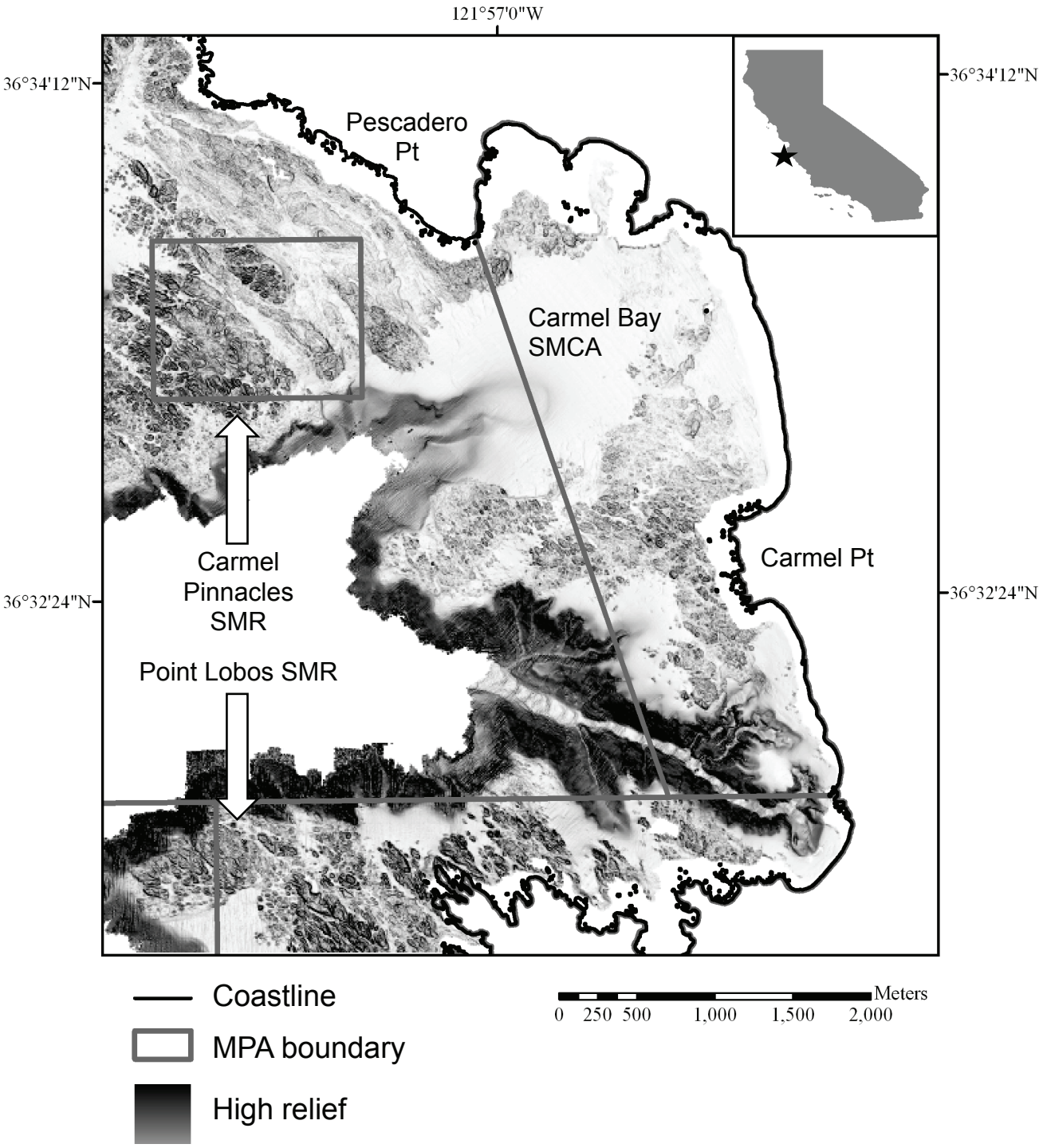

Figure 1. Multibeam bathymetry imagery of Carmel Bay with marine protected area (MPA) boundaries. SMR denotes State Marine Reserve and SMCA denotes State Marine Conservation Area (data courtesy of the Seafloor Mapping Lab of California State University Monterey Bay).

repeated range testing in winter and in late summer, when seasonal densities of giant kelp (*Macrocystis pyrifera*) were low and high, respectively. Our range testing results indicated that the mean number of detections/hr decreased with distance from a receiver; the mean of detections/hr were lower in late summer compared to winter, presumably due to higher seasonal kelp densities in late summer. For this study, we used a conservative estimate of 150 m radii for detection ranges, which was consistent with other reported VR2 receiver ranges in California kelp beds (Topping et al. 2006).

To examine how signal transmissions varied over time,

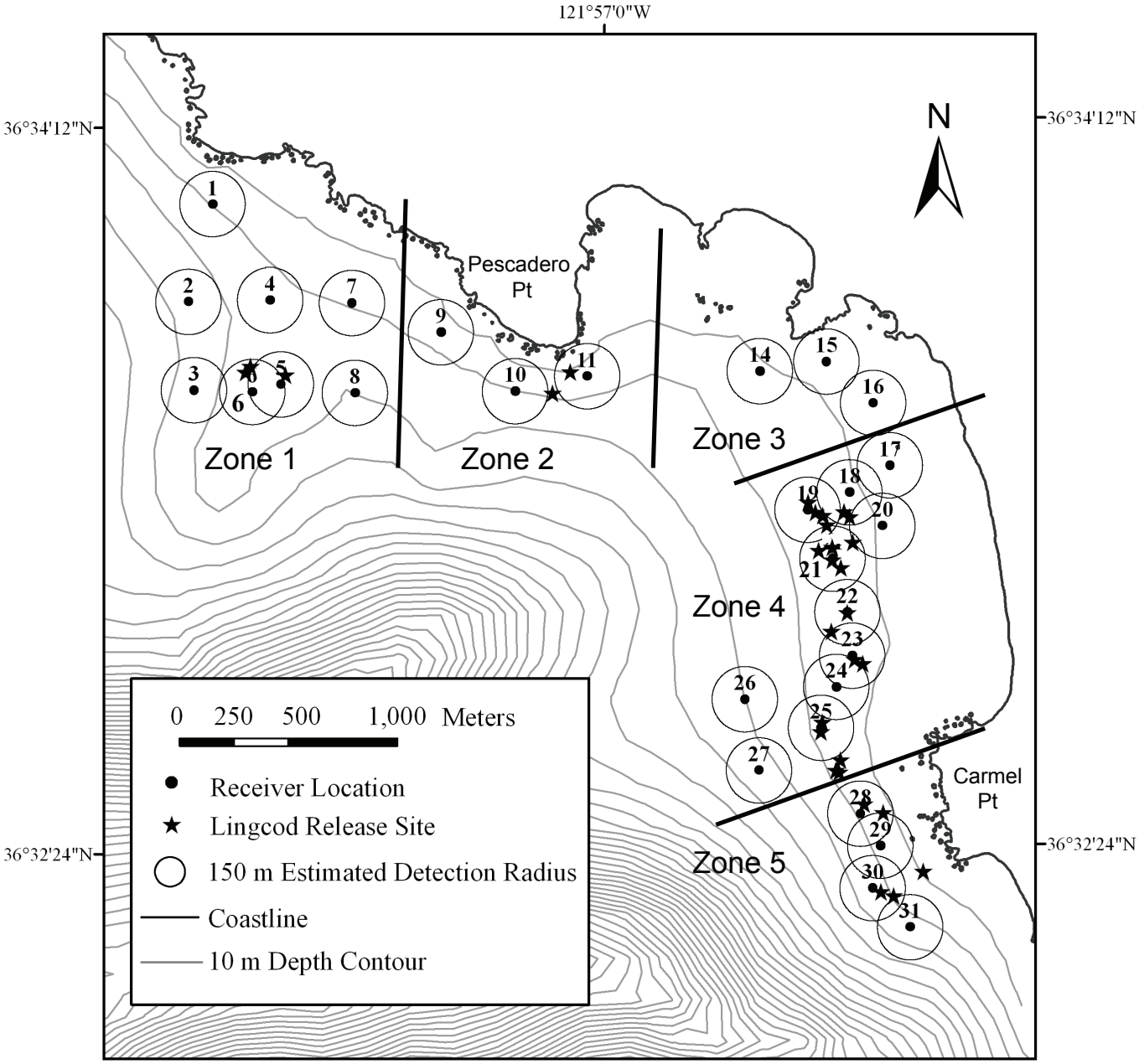

Figure 2. Configuration of VR2 receiver array with estimated 150 m detection ranges and zone delineation. Small black circles indicate receiver locations and stars are release locations of tagged lingcod.

we deployed a V13 "reference" transmitter 1 m off the seafloor and recorded and analyzed its detections over seven months. We placed the reference transmitter 140 m equidistant from two receivers, i.e., within our estimated detection range for the VR2 receivers. The total number of daily detections recorded for the stationary reference transmitter was highly variable, ranging from 7–401 detections/day, and averaging 178.2 ± 101.9 detections per day. At a daily and hourly scale, however, signals from the stationary reference transmitter were detected for 100% of the 212 days deployed and for 92% of all possible hour-bins. Due to the variability in individual transmissions, we analyzed residence times in this study by grouping signals into hour-bins and 24-hr periods (see Data Analysis, next page).

To validate the detection capabilities of the VR2 array and to account for the possibility of detection failure from acoustic shadows, we surveyed a 500 m^2 grid near receivers 18–21 (fig. 2) with a Vemco VR100 directional hydrophone that was mounted on a small boat. We conducted 30-minute VR100 surveys on four separate days and nights, for a total of eight surveys. We then

compared signals of tagged fish recorded by the VR100 with those recorded by VR2 receivers 18–21 for a 24-hr period. Over the eight days we conducted surveys, the VR100 confirmed the presence of five lingcod within the range of receivers 18–21 that would have otherwise gone undetected by those receivers for 24 hrs.

Data Analysis

Residency is a term frequently used to evaluate the tendency of a species to stay in one place. We defined and analyzed residence times as the percentage of days an individual was detected within our study area in relation to total days at liberty (% days, from date of tagging until the last date of detection), as a percentage of hour-bins with detections in relation to total possible hour-bins during time at liberty (% hour), and as a percentage of days detected relative to one year from the tagging date (% year). Due to the possibility of false signals from electronic noise, a fish was only considered present when two or more detections were recorded within a 24-hour period (e.g., Starr et al. 2000). Lingcod were considered to have departed from the array if ≤1 signal was received from the tagged fish during a 24-hour period. For each day a fish was determined to be present in the array, all recorded signals were grouped into one hour time bins relative to the time of signal transmissions (Starr et al. 2002; Green and Starr 2011; Green et al. 2014). For example, signals detected between 14:00:00 hour and 14:59:59 hour were assigned to hour-bin 14.

We used a two-way ANOVA to determine if residence time (% days) was related to total length or sex of tagged lingcod. We performed a separate regression analysis for each sex to test if residence times (% yr) were related to fish length. We analyzed seasonal patterns in residency by calculating the average monthly proportion of days lingcod were detected for each sex and size class. Also, we used a generalized linear model (GLM) to identify differences in proportion of days detected within combinations of sex and size classes. An average monthly depth of each fish was calculated and sexes and size classes were pooled to generate a group mean. Mean monthly depth distributions were compared among sex and size classes using a two-sample KS test. For the depth comparisons, we used lingcod tagged in 2006 and one large female tagged in 2005 (the other 2005 fish either did not have sex assigned or the tags malfunctioned).

Spatial patterns of activity were quantified by tallying the number of days and the number of hour-bins for which a fish was detected at each receiver. Movements over time were examined by dividing the study area into zones of approximately equal size (fig. 2). Zones were numbered north to south, and an average of the zone numbers was used to identify the primary zone that a fish occupied during a week (e.g., Starr et al. 2002). Every hour-bin containing detections from a tagged fish was assigned a zone based on the location of the receivers where the fish was detected for that hour. The hourly zone values were averaged for each week and compared among other weeks using a two-sample KS test for each individual fish. To avoid potential bias caused from the tagging process, the weekly zone average for the second week after release date was selected as the expected value for the KS test. At a finer spatial and temporal scale, we calculated the percentage of time that each lingcod was detected on a particular receiver within the array by summing the total number of hour-bins recorded on a receiver and dividing by the total overall number of hour-bins with detections. We compared the percentages of hour-bins recorded on one primary receiver among sexes and size classes of tagged lingcod using an ANOVA.

Lingcod movements in relation to physical conditions in the environment were examined using cross correlation analyses to compare acoustic data with atmospheric pressure, wind, upwelling indices, wave height, water temperatures, tides, and time of day. Cross correlation analysis addresses autocorrelation of data by fitting a model to time trends and then correlating residuals using lag times in multiples of one day. Temperatures throughout the receiver array were monitored using Onset StowAway TidbiT temperature loggers deployed on receiver mooring lines and positioned at shallow (12–16 m) and deep (27–34 m) depth intervals. Oceanographic and atmospheric data were acquired from the historical data archives of the National Oceanic Atmospheric and Administration (NOAA). Wave height, wind speed, and barometric pressure were recorded from Monterey Buoy 46042, (http://www.ndbc.noaa.gov). Tidal height was recorded from Monterey tide station 9413450, (http://tidesonline.nos.noaa.gov/). Day lengths were derived from the historical archives of the US Naval Observatory from Carmel, California (http://aa.usno.navy.mil/data/). Daily and monthly upwelling indices, expressed as $m^3\ s^{-1}$ 100 m^{-1} of coastline at 122°W, 36°N, were obtained from NOAA Fisheries Pacific Fisheries Environmental Laboratory (PFEL) (www.pfeg.noaa.gov/products/PFEL).

Diel movements were analyzed by calculating the proportion of hour-bins in which a fish was recorded during the day (and night) in relation to the total possible number of day (and night) hour-bins throughout the fish's time at liberty. To account for changing day length throughout the year, the number of possible day and night hour-bins was calculated for each day based on time of sunrise and sunset. Crepuscular movements were excluded from this analysis by eliminating detections within ±1 hour of sunrise and sunset.

TABLE 1

Summary of 30 lingcod tagged in Carmel Bay. Class refers to fish at lengths >90% maturity and between 50%–90% maturity. Residency was calculated as the percentage of days (% d) recorded in relation to total days at liberty (lib), the percentage of hour-bins containing signals in relation to total possible hour-bins during time at liberty (% hr), and the percentage of days relative to one year from the tagging date (% yr).

Tag ID	TL (cm)	Sex	Class	Date Released (mm/dd/yy)	Time at lib (d)	Residency (% d)	Residency (% hr)	Residency (% yr)
37	66	M	>90	08/18/05	–	–	–	–
66	62	M	>90	09/13/06	246	40.2	21.4	27.4
68	62.5	M	>90	10/07/06	210	3.8	0.6	2.2
72	64	M	>90	09/22/06	321	16.8	2.8	14.8
77	63	M	>90	10/07/06	327	9.2	1.0	8.5
79	61	M	>90	09/01/06	371	79.0	39.6	80.5
117	61	M	>90	08/29/06	360	92.2	42.6	91.2
119	63	M	>90	09/11/06	376	79.0	28.6	81.6
4049	66	M	>90	09/06/05	–	–	–	–
63	53	M	50–90	09/22/06	263	67.7	38.5	48.8
64	53	M	50–90	09/04/06	376	43.9	6.7	45.5
65	53	M	50–90	09/12/06	373	67.8	19.1	69.3
70	54	M	50–90	09/23/06	367	99.7	64.1	100
74	46	M	50–90	09/28/06	362	34.8	6.0	34.5
75	57	M	50–90	09/29/06	344	5.8	0.5	5.5
116	53	M	50–90	08/21/06	311	44.7	8.1	38.4
174	59	M	50–90	08/24/06	211	95.7	54.3	55.6
36	87	F	>90	08/18/05	92	8.7	0.5	2.2
69	72	F	>90	09/16/06	281	12.5	3.7	9.9
71	94	F	>90	09/23/06	323	25.4	4.0	22.5
73	85	F	>90	09/27/06	195	23.6	5.9	12.6
173	82	F	>90	09/07/05	325	49.8	9.0	44.4
38	51	F	50–90	09/05/06	385	94.0	50.4	99.5
39	54	F	50–90	09/14/06	75	29.3	4.9	6.0
67	62	F	50–90	08/30/06	391	70.3	15.7	75.6
76	57	F	50–90	09/29/06	361	100	62.4	99.5
118	63	F	50–90	08/29/06	327	68.8	16.9	61.9
172	59	?	50–90	09/07/05	364	100	56.7	100
225	58	?	50–90	09/08/05	747	49.3	10.7	47.7
226	58	?	50–90	09/08/05	747	99.2	47.6	100

RESULTS

Fishing

We identified the sex for 27 of the 30 lingcod we tagged (table 1). Of the lingcod with known sex, the mean length of the 10 females we tagged (70.7 cm ± 4.9 SE) was significantly greater than that for the 17 males tagged (58.6 cm ± 1.2 SE) ($t = 2.941$, $p = 0.007$). There was no significant difference in length between sexes for lingcod grouped in the smaller size class ($t = 1.584$, $p = 1.42$), but females were significantly larger than males for lingcod grouped in the larger size class ($t = 7.611$, $p < 0.001$).

Receiver Array

Between August 2005 and September 2007, three receivers broke free from their moorings but were found on Carmel Beach, and six receivers were permanently lost. The three receivers recovered on the beach were quickly redeployed so that <2 weeks of data were missing from these locations, whereas the other six receivers were replaced after several months. Four of the six locations with missing receivers were in areas with few to no recorded detections for lingcod (receiver locations 12, 18, 20, and 23). Receivers at locations 5 and 6 on the Carmel Pinnacles were missing from November and December 2006, respectively, until June 2007. The loss of data at these locations likely resulted in an underestimate of residency times for two fish (tags #73 and #74). However, tags #73 and #74 were detected on receivers adjacent to the lost receivers throughout the year, indicating the fish were near or within the study area.

Residence Times & Depth Distribution

Tagged lingcod in Carmel Bay were detected an average of 50% of days in a year, and 30% of the lingcod we tagged were detected, on average, for over 80% of days in a year (table 1). A relatively even number of tagged lingcod were detected for <20, 40, 60, 80, and 100% of their days at liberty (fig. 3). Small lingcod were detected significantly more often than large lingcod (% days) (ANOVA: $F = 11.121$; $p = 0.004$), but there was no significant difference in percentage of days detected by sex (ANOVA: $F = 0.491$, $p = 0.494$). There was no significant interaction between sex and size class ($F = 1.619$, $p = 0.221$). A regression analysis revealed that the size-

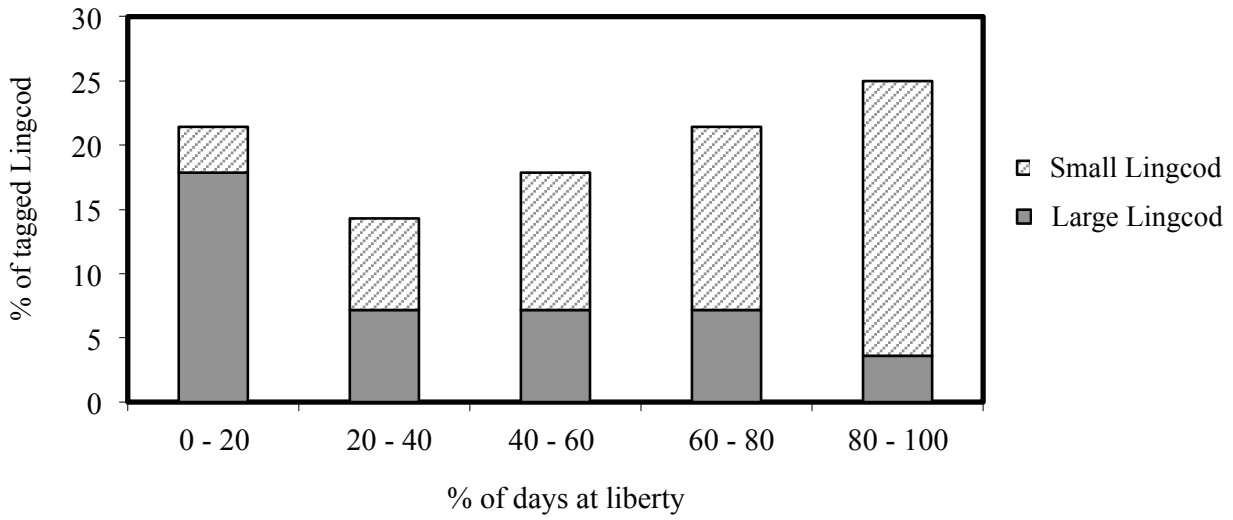

Figure 3. Percentage of days at liberty recorded in the array for 28 tagged lingcod. Two lingcod were excluded from the analysis due to tag failure.

related pattern in residence times was driven by females, for which the percentage of days at liberty (% days) spent in the array was significantly dependent on total length ($r^2 = 0.483$, $p = 0.008$), but not for males ($r^2 = 0.016$, $p = 0.650$). A GLM analysis confirmed that large females were detected significantly fewer days in the study area than other sizes and sexes of lingcod (GLM, $df = 4$, $p < 0.05$).

Six lingcod (20% of the tagged fish) were detected for less than 20% of the possible days at liberty. Despite the low overall percentage of days detected, two of the six fish were detected sporadically for a few days at a time throughout the year, indicating that the fish were probably near the array but just outside of detection. Three lingcod with low overall residence times, tags #69, #75, and #77, were detected sporadically for several months before leaving the array, only to be detected once again after absences of several months (fig. 4). Lingcod tag #36 departed the study area permanently after 91 days at liberty.

Mean monthly depths of large male lingcod ranged from 15.5–20.1 m (fig. 5) and were fairly consistent throughout the year for males and females in the small size classes. Large females occupied a greater depth range (7.0–17.5 m) over time, with the deepest monthly average depths occurring from February to April. The mean monthly depth distribution for large females was significantly different than for combined males and small females (two sample KS, $p = 0.001$), yet it should be noted that female #73 drove the observed depth pattern for large females. This lingcod was detected in deeper areas within the array during the winter while the other large females were primarily absent.

Seasonal Patterns in Residency

Seasonal patterns of residency within the array were notably distinct for large female lingcod, compared to males and small females (fig. 6). Residence times for large females were greatest during the fall and increased again in the spring. Of the five large females tagged, lingcod #173 was detected consistently for a year on the same two receivers whereas residency for the other four females decreased after October or November (fig. 4). Of these four females, #36 was never detected again, whereas #69 was detected seven months later in a different part of the array, approximately 2 km away. The other two large females, #71 and #73, went mostly undetected throughout the winter from November until mid-March, with the exception of a few detections in January and February. Both of these fish were detected again in mid-March, and lingcod #73 was detected on the Carmel Pinnacles for approximately one month before leaving permanently. Fish #73 primarily occupied the pinnacles, an area where receivers were lost, and therefore residency may have been higher than we were able to measure. Lingcod #71 was regularly detected near Pescadero Point through July 2007; in August 2008 it was recaptured near the same area by a recreational fisherman, 371 days after its last detection.

Patterns in residency over time were similar for both size classes of males and small females (fig. 4, fig. 6). For males, presence over time could be characterized by three patterns: 1) male lingcod consistently occupied the study area throughout the year, except for a brief period of absence (≤2 weeks) in late March/April ($n = 8$ fish), 2) male lingcod were not detected in the array ($n = 1$) or were detected only sporadically ($n = 2$) after April; and 3) male lingcod exhibited low overall residence times (detected on <10% of possible days) but were detected intermittently throughout the year of monitoring ($n = 4$). Three of the four male lingcod with low overall residence times (pattern 3) were males in the large size class. Small female lingcod exhibited the

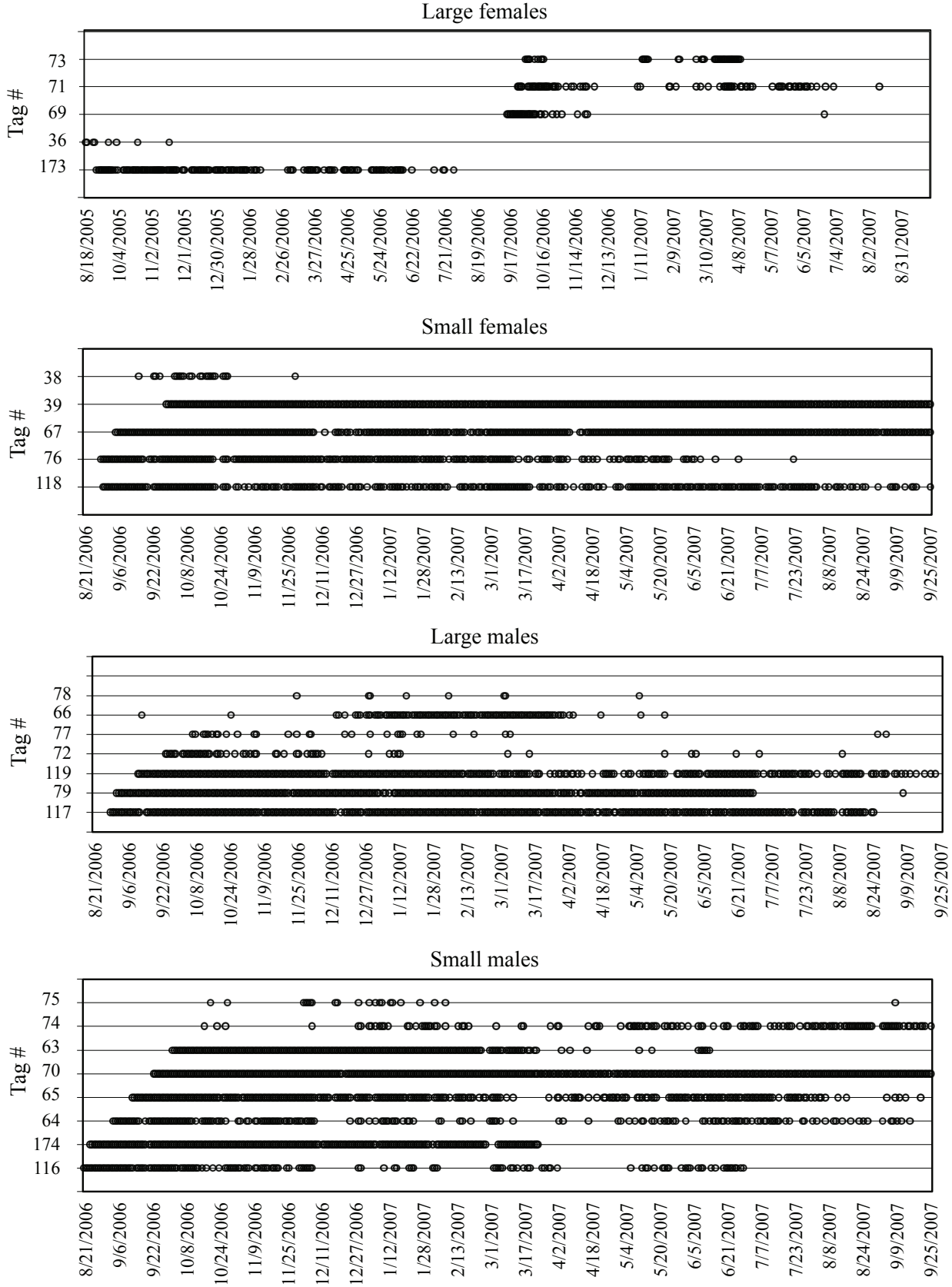

Figure 4. Residency over time for each sex and size class of tagged lingcod. Black circles represent a day for which a lingcod was detected within the study area (with a minimum of two detections per 24 hour period).

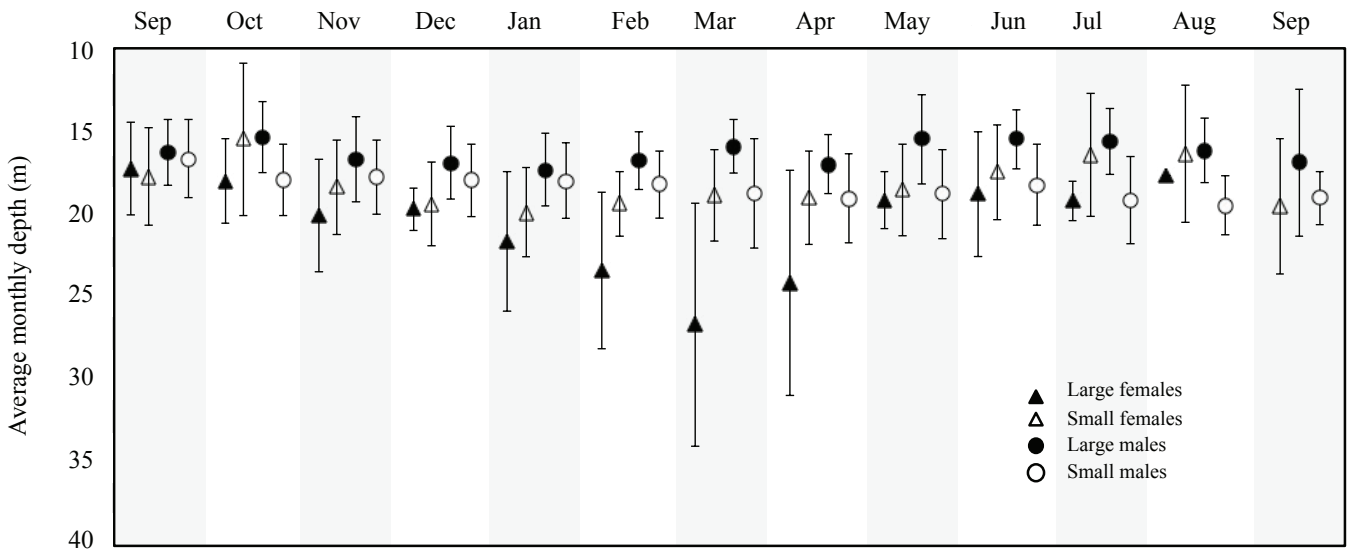

Figure 5. Mean monthly depth distributions (± SD) of tagged lingcod, separated by sex and size class, pooled by month.

highest residency of tagged lingcod. Similar to males, residency decreased in April when two of the tagged small females were absent for several days. Two other small females were detected consistently throughout the year and one was only detected for approximately one month after tagging in September 2006.

Spatial Patterns in Movements

Tagged lingcod exhibited limited movement within the array, and the majority (82%) of tagged lingcod rarely left their primary zone of occupancy during their time at liberty. Two-sample KS tests comparing the expected zone value derived from week two with the observed weekly zone values were only significant for five lingcod (18%) (tag #39, $p = 0.049$; tag #71, $p = 0.000$; tag #72, $p = 0.008$; tag #77, $p = 0.023$; tag #79, $p = 0.000$). At a finer spatial scale, 12 lingcod (42% of males and females in both size classes) were detected on one primary receiver for greater than 90% of hour-bins with detections; of these fish, six lingcod were detected on one receiver for >97% of hour-bins (Appendices A–D). For all lingcod combined, 76.8% (± 3.7 SE) of all hour-bins with detections were recorded on 1 receiver, and 14.1% (±2.5 SE) of all hour-bins were recorded on two adjacent receivers. Percentages of hour-bins with signals recorded for a given lingcod on one primary receiver were not significantly different among the four groups of tagged lingcod: small males, small females, large males, large females (ANOVA: $F = 0.696$; $p = 0.565$).

Although the majority of lingcod movement patterns were constrained to one or two adjacent receivers, some longer distance forays were captured within the 5 km of coastline we monitored (fig. 7). For example, lingcod #74 (male, 46 cm TL) was tagged and released on the Pinnacles (receivers #2–8), where it was detected for 95% of the total hour-bins containing recorded signals. On seven separate occasions, #74 was detected approximately 2.5 km away on receivers #14, 15, and 21 (fig. 7). The time that signals were recorded between distant receivers ranged from 13 minutes (from receiver #3 to #14) to 17 hours (from receiver #14 to #6). Lingcod #77 (male, 63 cm) also displayed an interesting pattern of residency at two separate locations within the array (fig. 7). This fish was detected intermittently on receiver #19 near Carmel Beach for two months before departing in early December. Sixteen days later, it was detected 1.3 km away on receiver #10 near Pescadero Point, where it was again recorded intermittently until March 6. After an absence of five months from the array, this lingcod was detected again on the original receiver (#19) in late August. Lingcod #174 (male, 59 cm) displayed highly directional movement from receiver #25 near Carmel Point through to the southern extension of the array near Carmel Canyon (fig. 7). During this trip, #174 swam in a southerly direction past five receivers (#27–31) before going undetected for 52 hours. The fish then utilized a similar route for the return trip back to its primary receiver, where it remained for the rest of its days at liberty. The overall distance from primary receiver location #25 to the last receiver of detection was approximately 1 km, with the lingcod swimming at an estimate rate of 0.72 km/hour on the trip out and 0.46 km/hour on the way back.

Physical Parameters

Water temperatures were coldest from March to July 2007, when mean monthly temperatures fell below the average annual temperature recorded during our study.

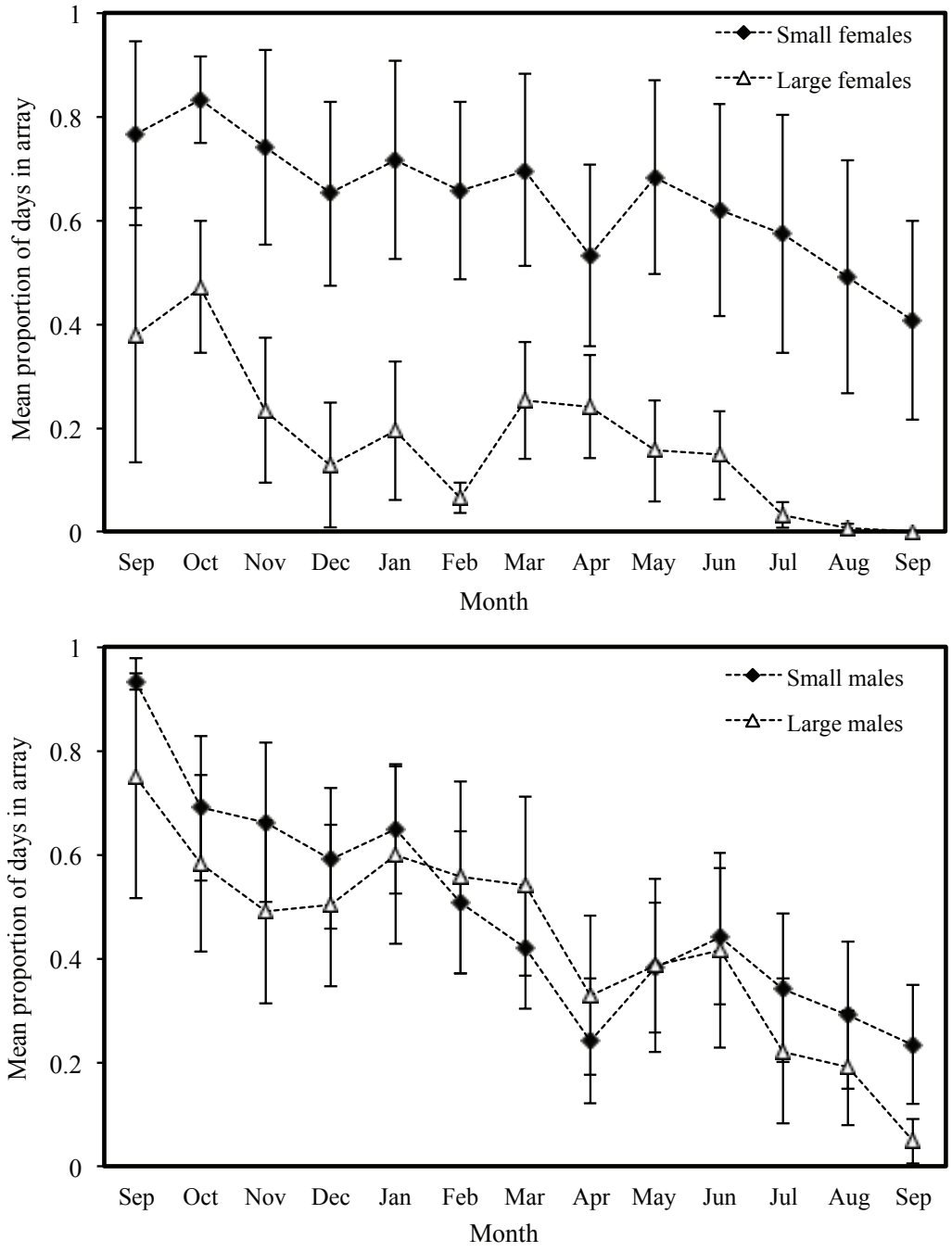

Figure 6. Mean monthly proportion of days (± SE) detected in the array for tagged female (top) and male (bottom) lingcod.

The cold water coincided with strong upwelling conditions. Cross correlation analyses indicated significant relationships between the number of lingcod detected in the array and environmental variables associated with upwelling conditions, such as wind speed, water temperature, and upwelling indices (table 2). The number of lingcod detected in the array increased as wind and the upwelling index increased and water temperatures decreased. Also, more lingcod were detected as the wave energy increased. Lag times for these significant relationships were all 2 days after the onset of upwelling.

Tagged lingcod that were detected in the array for >10% of possible hour-bins did not show a diel pattern in detection, i.e., day and night presence in the array was similar. For example, for the subset of fish we analyzed, the mean proportion of possible hour-bins in which signals were recorded during the day (0.39) was comparable with that for the night (0.42). Twelve lingcod were

TABLE 2

Lag in days, correlation coefficients (r), and p values associated with cross correlations among selected environmental variables and the number of tagged lingcod detected during the time period from 10 November 2005 to 27 September 2007.

Variable	Lag time (d)	Correlation	p
Upwelling index	2	0.279	<0.001
Atmospheric pressure	1	0.240	<0.001
Wind speed	2	0.133	0.018
Wave height (squared)	2	0.258	<0.001
Sea surface temperature	1	–0.180	0.001
Temperature at 14 m deep	1	–0.137	0.014
Temperature at 31 m deep	1	–0.224	<0.001
Temperature difference 14–31 m deep	1	0.130	0.019

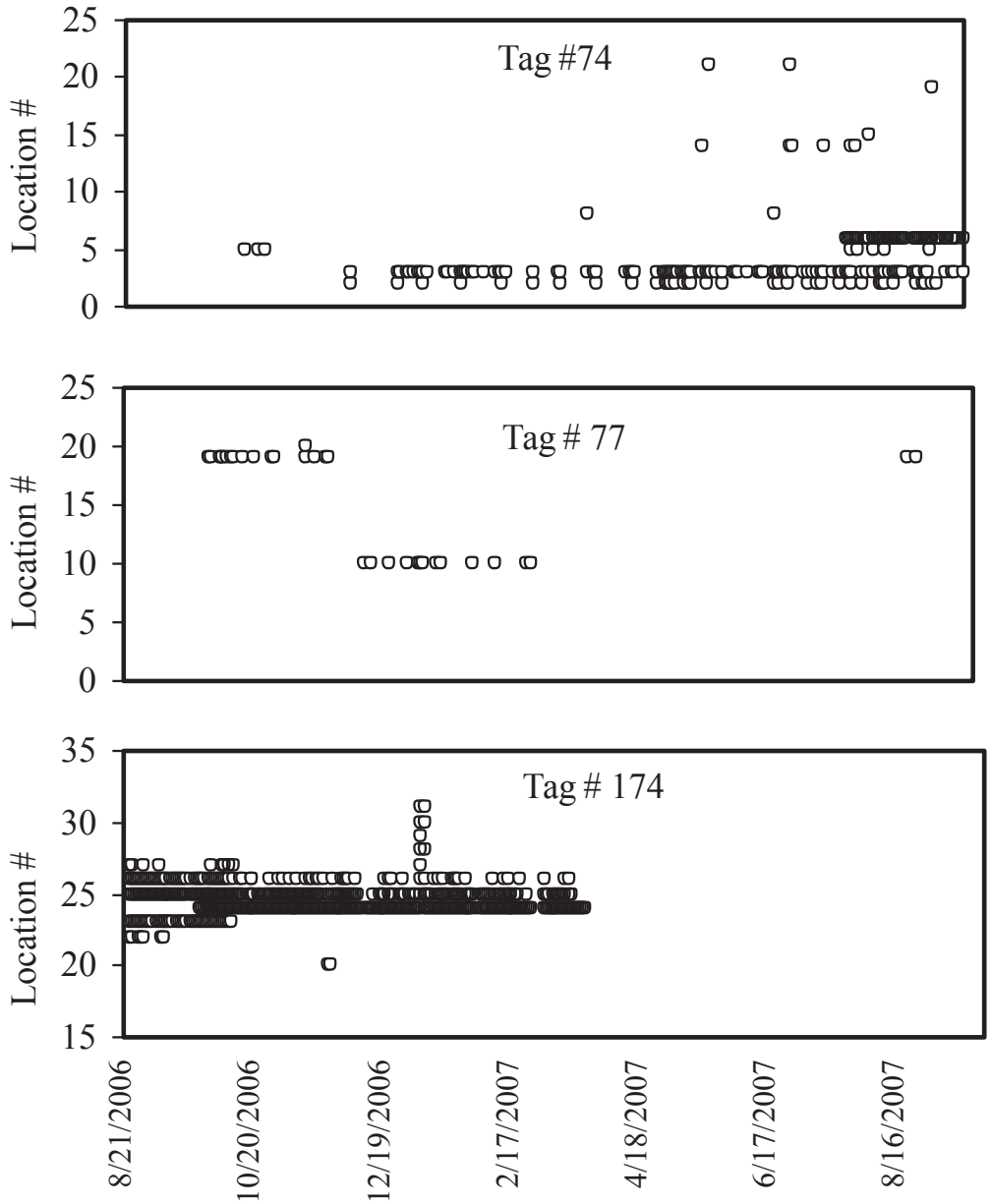

Figure 7. Spatial utilization patterns for tagged lingcod demonstrating movements >1 km. Each circle represents a day in which a receiver detected a tagged fish.

detected for less than <10% of possible hour-bins. Of these fish, ten were primarily recorded during daylight hours and two were detected more during the night.

DISCUSSION

Lingcod Movements and MPA Management

MPAs are often designed with two seemingly contradicting purposes: to protect marine organisms from fishing and to benefit fisheries via spillover of adults beyond reserve boundaries. From the movement patterns we observed, it appears that lingcod are suited to serve both MPA purposes. Over the course of a year, tagged lingcod demonstrated relatively high residency. On average, half of the lingcod we tagged remained within the 5 km area we monitored for at least 50% of days in a year, and 30% of lingcod were detected for over 80% of days in a year. These patterns in residency indicate that lingcod, over the course of a year, are likely to remain within the boundaries of a typical California MPA (~5 km long x 3 km wide), as evident by the higher densities and larger sizes of lingcod found in MPAs than nearby reference areas (Starr et al. 2015).

Our estimates of residence times should be considered conservative; we know from our validation surveys with the VR 100 receiver that some tagged fish were present but went undetected by the stationary VR-2 receivers for a 24 hour period. Given that lingcod are demersal fish that sometimes occupy cracks and crevices, these false absences were likely caused by acoustic shadows. We conducted VR100 surveys over eight days, of which fish with false absences went undetected by the VR-2 receivers for one or two days at the most. This indicates that our estimates of residency were affected over short time scales of a few days, while longer-term absences were likely caused by true departures from the monitored area.

In general, lingcod movements in Carmel Bay were highly constrained, with the majority of lingcod detections recorded at one or two adjacent receiver locations (Appendix A–D). This pattern in spatial utilization did not differ among sexes and size classes of lingcod, and thus we found no evidence that smaller, presumably immature, lingcod were no more or less site-specific than larger fish, at least at the spatial scales we measured. Our observations of restricted movements for lingcod in Carmel Bay are consistent with acoustic tagging studies conducted at finer spatial scales, whereby lingcod also exhibited relatively confined home ranges of 2000–3000 m^2 (Tolimieri et al. 2009) and 21,000 m^2 (Beaudreau and Essington 2011).

Of the larger scale movements we captured, lingcod demonstrated the capacity to travel multiple kilometers in under an hour, as well as the ability to home back to the same receiver location within our study area. Previous displacement experiments on lingcod have shown their ability to home (Matthews 1992) and to travel relatively large distances over short periods of time (Anthony et al. 2012). Two lingcod tagged in our study would, on occasion, leave their primary receiver location and move 1–2 km to another set of receivers. The duration of time between these multiple centers of activity varied by fish, but the general patterns in movements are analogous to the use of multiple core areas described by Tolimieri et al. (2009). The ability of lingcod to travel multiple kilometers, either during a foray or due to an occasional shift in a core area of activity, could result in fishery benefits should the movements span across MPA boundaries.

The residential behavior of lingcod, combined with their ability to travel multiple kilometers, helps explain why previous tag and recapture studies either documented limited lingcod movement or more widespread migratory behavior (Mathews and LaRiviere 1986; Smith et al. 1990; Jagielo 1995). In the present study, 20% of the lingcod we tagged were detected for <20% of days at liberty, and the majority of those fish permanently left the 5 km of coastline in the study area. Although we don't know how far these fish moved, tag and recapture studies conducted over multiple years have reported similar percentages of lingcod emigration, with 20% of tagged lingcod exhibiting movements >8.1 km, and in some cases, as great as 50 km (Hart 1943; Jagielo 1990; Lea et al. 1997). Of importance to MPA managers is that the mean monthly percentage of days tagged lingcod were detected in Carmel Bay declined with time. This indicates that lingcod may exhibit a slow but constant rate of dispersion out a specific MPA with time.

Movements Related to Lingcod Size and Sex

Lingcod tagged in Carmel Bay demonstrated distinct patterns in residency and depth distributions based on sex, size class, and reproductive season. Lingcod are known to migrate to deeper waters at the onset of maturity (Jagielo 1999; Miller and Geibel 1973), and the patterns we observed for females in this study captured this ontogenetic separation. In the relatively shallow (7–40 m) depths we monitored, large female lingcod were present during fall spawning months but exhibited lower overall residence times and occupied deeper depths, compared to males and small females, for the rest of the year. Similarly, Starr et al. (2005) documented that adult lingcod segregate by sex for much of the year in Alaska. In the present study, it appears that this difference in sexual segregation occurs after the onset of maturity, as the small female lingcod tagged in Carmel Bay occupied similar depths and receiver locations as the males. Unlike females, male lingcod did not demon-

strate a size-related difference in depth distributions or residence times, although this could be attributed to the relatively small size range of males tagged in this study.

Movements Related to Season and Physical Factors

The notable presence of large females in the receiver array during the fall directly coincides with their seasonal migration to shallow waters for reproduction (Miller and Geibel 1973). Four of the five large females tagged in this study were detected for several months on a receiver, went undetected for several months, and then were ultimately detected again on the same receivers throughout the year. The largest female we tagged (#71) was recaptured by a fisherman within 300 m of its original tagging location after 702 d at liberty. While we can only speculate on their movements outside of the array, the eventual return of these large females to the study area suggests these fish are not dispersing great distances outside of the reproductive season.

Similar to females, large male lingcod occupy deeper waters than their smaller counterparts for the majority of the year, but migrate to shallower waters to spawn and guard nests in fall and winter months (Cass et al. 1990, Jagielo 1995). Although not statistically significant, three of the four male lingcod exhibiting low overall residence times in this study were categorized in the larger size class and thus may have primarily resided in deeper waters beyond the areas we monitored. Male lingcod only feed opportunistically while guarding nests (Beaudreau & Essington 2007), then disperse in the spring (Low & Beamish 1978; Jagielo 1995; Starr et al. 2005; Bishop et al. 2010). In our study, there was an observed decrease in the mean monthly percentage of days that male lingcod were detected in April, which directly coincided with the end of nest guarding season and the start of spring upwelling conditions. However, the cross correlation analyses revealed an increase in daily detections of tagged lingcod during upwelling. We believe that these results, while seemingly contradictory, support the idea that lingcod in Carmel Bay are more actively foraging in the spring. Because the fish are more active, greater movement rates during spring upwelling conditions increased the likelihood of lingcod being detected by the receivers, even though monthly residency dropped as lingcod expanded their movements beyond the area we monitored. Starr et al. (2005) reported a similar springtime expansion of horizontal and vertical activity spaces for lingcod tagged in Alaska.

Interestingly, six of the seven male lingcod exhibiting low residence times in the spring were detected later in the year in the same area within the array. Thus, whereas male lingcod in Carmel Bay may be more active in the spring, they may not be dispersing far from their winter grounds. King and Withler (2005) used genetic sampling to show that individual male lingcod will return to specific nesting sites over multiple winter spawning seasons. Our results indicate that at least some male lingcod remain in the same general area throughout the rest of the year as well.

The number of lingcod detected was positively correlated with increased atmospheric pressure, wind speed, and upwelling indices and with decreased water temperatures, which are all associated with spring upwelling conditions. As stated earlier, we believe the increased number of detections is related to increased foraging activity, which is caused by an increased in the productivity of coastal waters caused by upwelling and the associated settlement of many juvenile fishes (Caselle et al. 2010). Also, the number of lingcod detected was positively correlated with wave energy. We believe this is related to lingcod coming off the bottom to avoid effects of the increased surge on the seafloor that is associated with wave orbitals.

CONCLUSIONS

Our observations of lingcod movements in Carmel Bay indicate that MPAs can be an effective management tool for conserving lingcod and for providing fishing benefits via adult spillover. Our study documented relatively restricted movements and long residence times for lingcod and supports other studies showing that this species can benefit from spatial closures to fishing (Starr et al. 2004, 2015). Although MPAs may provide a refuge from exploitation, our study reinforced conclusions of other research that suggests lingcod are also capable of moving multiple kilometers while foraging or during seasonal transitions (Jagielo 1990; Starr et al. 2004; Bishop et al. 2010). To this end, fishing grounds adjacent to MPAs are likely to be enhanced when these larger scale movements extend past a reserve boundary. In terms of conservation and fisheries benefits, MPA managers should expect that MPAs the size of California marine reserves (~15 km^2) will protect lingcod for long periods of time in a year, while supplementing fisheries outside the MPAs as a small subset of the lingcod in the MPA move out from time to time.

ACKNOWLEDGMENTS

We would like to thank John "J. D." Douglas, from MLML Marine Operations, and Diana Steller, from the MLML Research Diving Program, for supporting the many field logistics associated with this project. We thank two anonymous reviewers for providing suggested changes to the manuscript. Funding for this project was graciously provided by the UC Sea Grant Extension Program, the Dr. Earl H. Myers and Ethel M.

Myers Marine Biology Trust, the David and Lucile Packard Foundation, the PADI Foundation, and Otter Bay Wetsuits. The Seafloor Mapping Lab at California State University of Monterey Bay provided the multibeam imagery of Carmel Bay. Tagging procedures were conducted under SJSU IACUC permit #814.

LITERATURE CITED

Anthony, K. M., M. S. Love, and C. G. Lowe. 2012. Translocation, homing behavior and habitat use of groundfishes associated with oil platforms in the East Santa Barbara Channel, California. Bull. S. Calif. Acad. Sci., 111(2), pp. 101–118.

Beaudreau, A. H., and T. E. Essington. 2007. Spatial, temporal, and ontogenetic patterns of predation on rockfishes by lingcod. Trans. Am. Fish. Soc. 136:1438–1452.

Beaudreau, A. H., and T. E. Essington. 2011. Use of pelagic prey subsidies by demersal predators in rocky reefs: insight from movement patterns of lingcod. Mar. Biol. 158.2: 471–483.

Bishop, M. A., B. F. Reynolds, and S. P. Powers. 2010. An in Situ, individual-based approach to quantify connectivity of marine fish: ontogenetic movements and residency of lingcod. PLoS ONE 5:12: e14267.

Caselle, J. E., J. R. Wilson, M.H. Carr, D.P. Malone, and D. E. Wendt. 2010. Can we predict interannual and regional variation in delivery of pelagic juveniles to nearshore populations of rockfishes (genus sebastes) using simple proxies of ocean conditions? CalCOFI Rep 51:91–105.

Caselle, J. E., A. Rassweiler, S. L. Hamilton, and R. R. Warner. 2015. Recovery trajectories of kelp forest animals are rapid yet spatially variable across a network of temperate marine protected areas. Sci. Rep. 5: 14102.

Cass, A. J., R. J. Beamish, and G. A. McFarlane. 1990. Lingcod (*Ophiodon elongatus*). Can. Spec. Pub. Fish. Aquat. Sci. 109:1–44.

Gordon, D. A. 1994. Lingcod fishery and fishery monitoring in southeast Alaska. Alaska Fish Res Bull 1:140–152.

Green, K. M., and R. M. Starr. 2011. Movements of small adult black rockfish: implications for the design of MPAs. Mar Ecol Prog Ser. 436:219–230.

Green, K. M., A. P. Greenley, and R. M. Starr. 2014. Movements of blue rockfish (*Sebastes mystinus*) off central California with comparisons to similar species. PLoS ONE 9:6: e98976.

Hamel, O. S., S. A. Sethi, and T. F. Wadsworth. 2009. Status and future prospects for lingcod in waters off Washington, Oregon, and California as assessed in 2009. Status of the Pacific coast groundfish fishery through 2009. Stock Assessments and Fishery Evaluation. Pacific Fishery Management Council, Portland, OR.

Jagielo, T. H. 1990. Movement of tagged lingcod (*Ophiodon elongatus)* at Neah Bay, Washington. Fish. Bull. 88:815–820.

Jagielo, T. H. 1995. Abundance and survival of lingcod at Cape Flattery, Washington. Trans. Am. Fish. Soc. 124:170–183.

Jagielo, T. H. 1999. Movement, mortality, and size selectivity of sport- and trawl-caught lingcod off Washington. Trans. Am. Fish. Soc. 128:31–48.

Jagielo, T. H., D. Wilson-Vandenberg, J. Sneva, S. Rosenfeld, and F. Wallace. 2000. Assessment of lingcod (*Ophiodon elongatus*) for the Pacific Fishery Management Council in 2000. Pacific Fishery Management Council, Portland, OR.

Jagielo, T. H., and F. R. Wallace. 2005. Assessment of lingcod (*Ophiodon elongatus*) for the Pacific Fishery Management Council. Pacific Fishery Management Council, Portland, OR.

King, J. R., and R. E. Withler. 2005. Male nest site fidelity and female serial polyandry in lingcod (*Ophiodon elongatus*, Hexagrammidae). Mol. Ecol. 14:653–660.

Kramer, D. L., and M. R. Chapman. 1999. Implications of fish home range size and relocation for marine reserve function. Environ. Biol. Fish. 55:65–79.

Laidig, T. E., P. B. Adams, K. R. Silberberg, and H. E. Fish. 1997. Conversions between total, fork, and standard lengths for lingcod, *Ophiodon elongatus*. Calif. Dep. Fish. Game, Fish Bull. 83(3):128–129.

Lea, R. N., R. D. McAllister, and D. A. Van Tresca. 1999. Biological aspects of nearshore rockfishes of the genus *Sebastes* from central California. Calif. Dep. Fish. Game, Fish Bull. 177:1–109.

Lester, S. E., B. S. Halpern, K. Grorud-Colvert, J. Lubchenco, B. Ruttenberg, S. D. Gaines, S. Airamé, and R. R. Warner. 2009. Biological effects within no-take marine reserves: a global synthesis. Mar Ecol Prog Ser 384:33–46.

Low, C. J., and R. J. Beamish. 1978. A study of the nesting behavior of lingcod (*Ophiodon elongatus*) in the strait of Georgia, British Columbia. Can. Fish. Mar. Serv. Tech. Rep. 843.

Lowe, C. G., K. M. Anthony, E. T. Jarvis, L. F. Bellquist, and M. S. Love. 2009. Site fidelity and movement patterns of groundfish associated with offshore petroleum platforms in the Santa Barbara Channel. Marine and Coastal Fisheries: Dynamics, Management, and Ecosystem Science. 1:71–89.

Mathews, S. B., and M. LaRiviere. 1987. Movement of tagged lingcod, *Ophiodon elongatus*, in the Pacific Northwest. Fish. Bull, 85:153–159.

Matthews, K. R. 1992. A telemetric study of the home ranges and homing routes of lingcod, *Ophiodon elongatus,* on shallow rocky reefs off Vancouver Island, British Columbia. Fish. Bull. 90:784–790.

Miller, D. J., and J. J. Geibel. 1973. Summary of blue rockfish and lingcod life histories; a reef ecology study; and giant kelp, *Macrocystis pyrifera,* experiments in Monterey Bay, California. Calif. Dept. Fish and Game, Fish. Bull. 158.

Molloy P. P., I. B. McLean, and I. M. Coté. 2009. Effects of marine reserve age on fish populations: a global meta-analysis. J. Appl. Ecol. 46:743–751.

Silberberg, K. R., T. E. Laidig, P. B. Adams, and D. Albin. 2001. Analysis of maturity in lingcod, *Ophiodon elongatus*. Calif. Fish. Game 87:139–152.

Simpfendorfer, C. A., M. R. Heupel, and R. E Hueter. 2002. Estimation of short-term centers of activity from an array of omnidirectional hydrophones and its use in studying animal movements. Can. J. Fish. and Aquat. Sci, 59(1), pp. 23–32.

Smith, B. D., G. A. McFarlane, and A. J. Cass 1990. Movements and mortality of tagged male and female lingcod in the Strait of Georgia, British Columbia. Trans. Am. Fish. Soc. 119:813–824.

Starr, R. M., J. N. Heine, and K. A. Johnson. 2000. Techniques for tagging and tracking deepwater rockfishes. North Am. J. Fish. Manage. 20:597–609.

Starr, R. M., J. N. Heine, J. M. Felton, and G. M. Cailliet. 2002. Movements of bocaccio (*Sebastes paucispinis*) and greenspotted (*S. chlorostictus*) rockfishes in a Monterey submarine canyon: implications for the design of marine reserves. Fish. Bull. 100:324–337.

Starr, R. M., V. O'Connell, and S. Ralston. 2004. Movements of lingcod (*Ophiodon elongatus*) in southeast Alaska: potential for increased conservation and yield from marine reserves. Can. J. Fish. Aquat. Sci. 61:1083–1094.

Starr, R. M., V. O'Connell, S. Ralston, and L. Breaker. 2005. Use of acoustic tags to estimate natural mortality, spillover, and movements of lingcod (*Ophiodon elongatus*) in a marine reserve. Mar. Technol. Soc. J. 39:19–30.

Starr, R. M., D. E. Wendt, C. L. Barnes, C. I. Marks, D. Malone, G. Waltz, K. T. Schmidt, J. Chiu, A. L. Launer, N. C. Hall, and N. Yochum. 2015. Variation in responses of fishes across multiple reserves within a network of marine protected areas in temperate waters. PLoS ONE 10: e0118502.

Tolimieri, N., K. Andrews, G. Williams, S. Katz, and P. S. Levin. 2009. Home range size and patterns of space use by lingcod, copper rockfish and quillback rockfish in relation to diel and tidal cycles. Mar Ecol Prog Ser, 380, pp. 229–243.

Topping, D. T., C. G. Lowe, and J. E. Caselle. 2006. Site fidelity and seasonal movement patterns of adult California sheephead *Semicossyphus pulcher* (Labridae): an acoustic monitoring study. Mar. Ecol. Prog. Ser. 326:257–267.

APPENDIX A

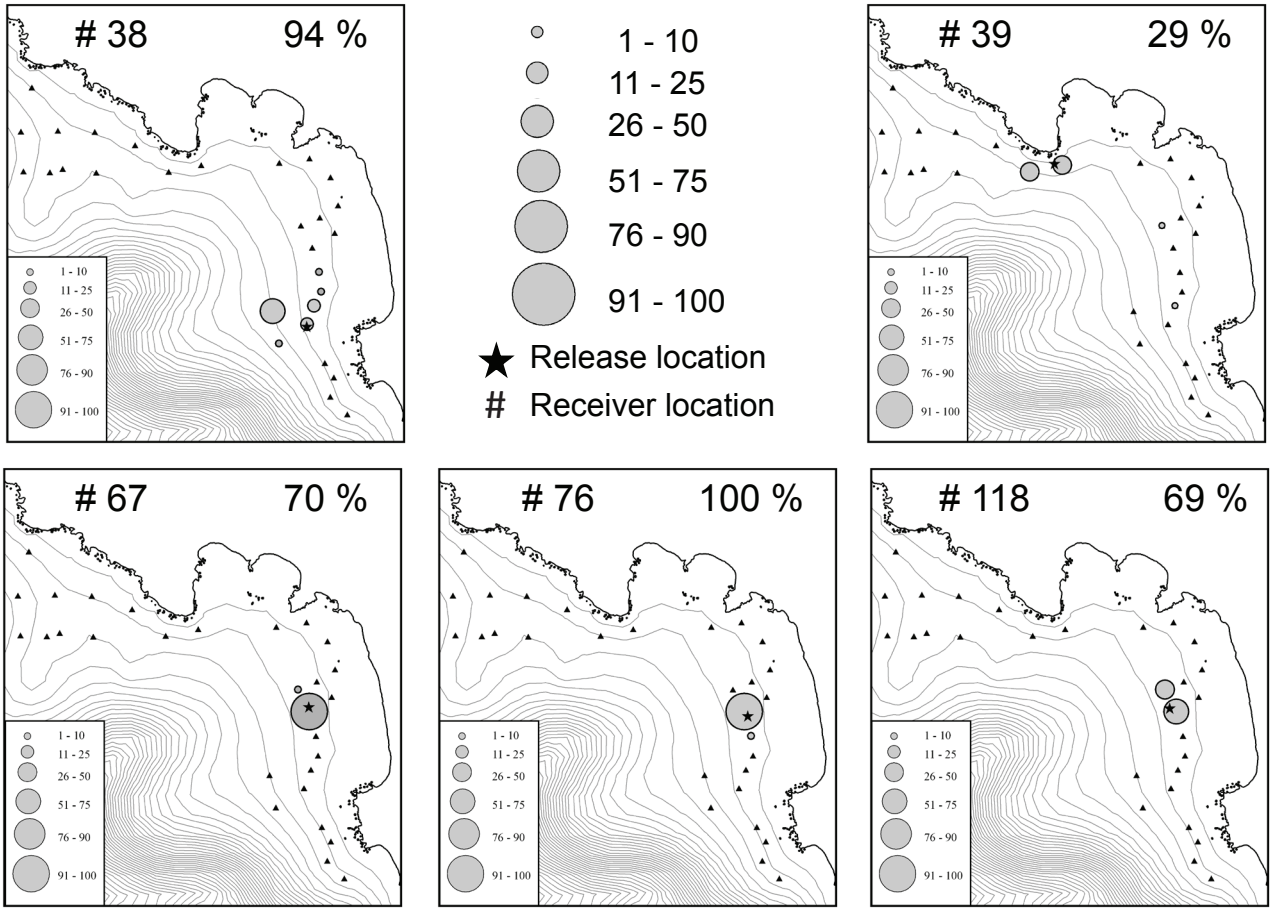

Appendix A. Proportion of hour bins with recorded signals relative to receiver locations for small female lingcod. Numbers at the top of each map correspond to the tag number of the lingcod (left) and the percentage of days at liberty detected in the array (right).

APPENDIX B

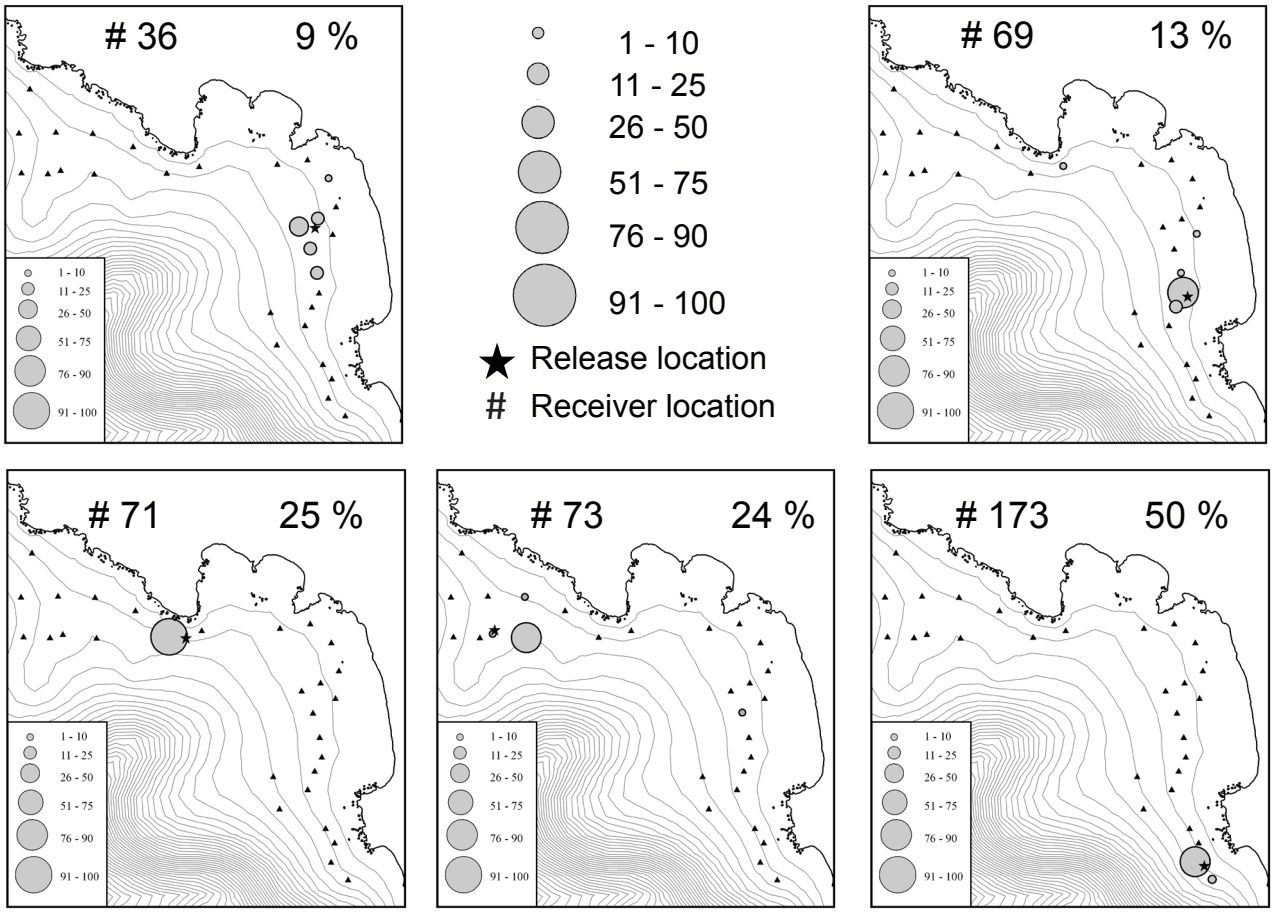

Appendix B. Proportion of hour bins with recorded signals relative to receiver locations for large female lingcod. Numbers at the top of each map correspond to the tag number of the lingcod (left) and the percentage of days at liberty detected in the array (right).

APPENDIX C

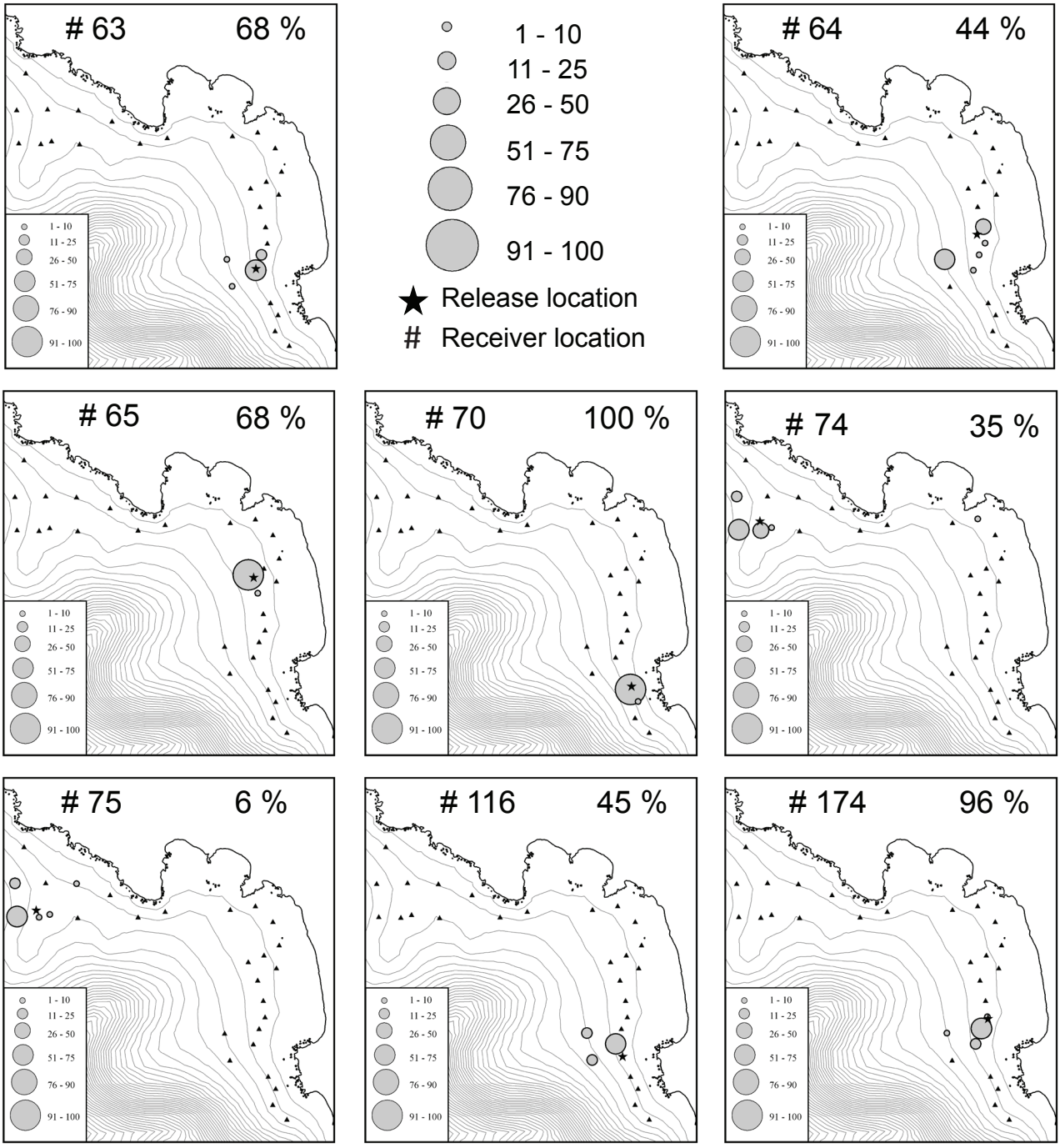

Appendix C. Proportion of hour bins with recorded signals relative to receiver locations for small male lingcod. Numbers at the top of each map correspond to the tag number of the lingcod (left) and the percentage of days at liberty detected in the array (right).

APPENDIX D

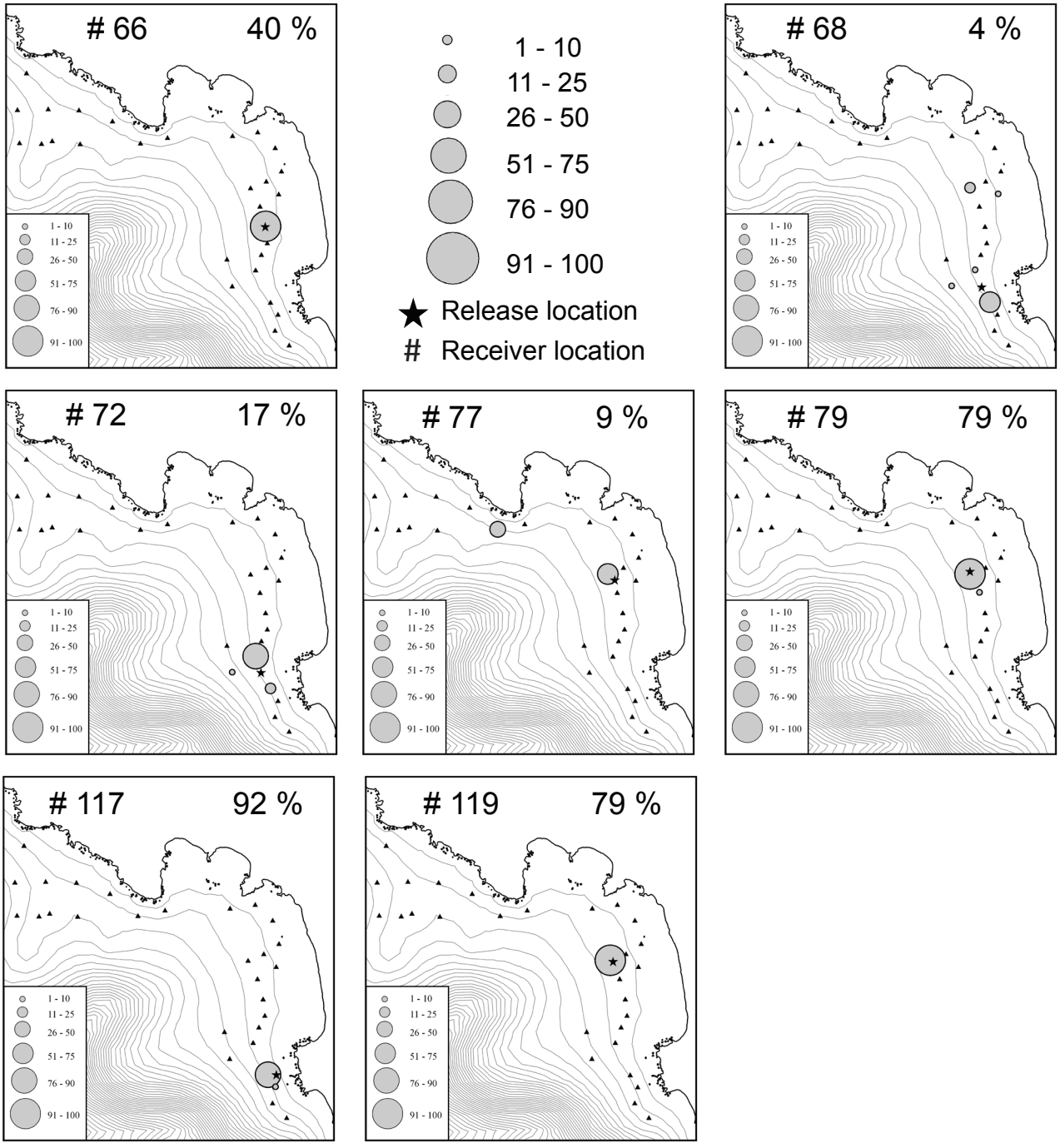

Appendix D. Proportion of hour bins with recorded signals relative to receiver locations for large male lingcod. Numbers at the top of each map correspond to the tag number of the lingcod (left) and the percentage of days at liberty detected in the array (right).

BIOGEOGRAPHY OF THE TRAWL-CAUGHT FISHES OF CALIFORNIA AND AN EXAMINATION OF THE POINT CONCEPTION FAUNAL BREAK

JOHN S. STEPHENS, JR.
DANIEL J. PONDELLA, II
Vantuna Research Group
Occidental College
1600 Campus Road
Los Angeles, CA 90041
Pondella@oxy.edu

JOHN STEINBECK
JAY CARROLL
Tenera Environmental Inc.
141 Suburban Rd., Suite A2
San Luis Obispo, CA 93401

MILTON LOVE
Marine Science Institute
University of California, Santa Barbara
Santa Barbara, CA 93106

ABSTRACT

We analyzed fish data from 2332 trawls collected from depths between 55 and 1280 m off the coast of California. For the 732 species known from California, including 283 species (~39% of the California ichthyofauna) in this study, very few were contained by the faunal break at Point Conception, with 21% limited from the south and only 4% from the north. The South Central Coast generally had a stronger relationship with Monterey Region rather than the Southern California Bight. There was discrete variation of species assemblages among previously defined continental shelf and slope zones and within these zones biogeographic patterns were based upon latitude. However, the overall biogeographic pattern was not determined by Point Conception for all soft bottom habitats. Biogeographic breaks based upon latitude were less evident at depth, especially below 500 m.

INTRODUCTION

Faunal breaks and biogeographic provinces are defined by some geographic or environmental feature or features that serve to limit movement across boundaries. For the nearshore environment in the eastern Pacific, they were originally determined and described based upon the distribution of reef fishes, with the discontinuity of reef habitat coupled with physical oceanographic processes supporting unique communities (Hubbs 1960; Hastings 2000; Horn et al. 2006). During regime shifts, organisms move latitudinally along the coast (i.e., Hubbs 1948; Radovich 1961). Thus, understanding these biogeographic provinces, the organisms contained within them and the processes that maintain them, is insightful for determining changes during various regime shift and climate change scenarios. Point Conception has long been considered such a barrier, as it separates the southern, warm-temperate shelf fauna from the cool-temperate region to the north (Garth 1955; Hubbs 1948; Horn and Allen 1978; Allen and Smith 1988; Horn et al. 2006). The thermal discrepancy across this barrier is based on geographic and latitudinal phenomena that are present during normal conditions (Hickey 1993). The offshore displacement of the cool south-flowing California Current occurs at Point Conception where the California coastline turns to the east to form the Southern California Bight and the cool California Current continues southward, largely to the west of the California Channel Islands. Point Conception also marks the northern extension of the warmer Southern California Counter Current, formed as a north-flowing eddy at around 31°N latitude (Maloney and Chan 1974). The resultant effect can be a relatively sharp temperature change, which marks one of the more recognized biogeographic boundaries for coastal fishes and separates the warm-temperate San Diegan region and the cool-temperate Oregonian region (Horn et al. 2006).

Faunal zones for coastal fishes are generally defined by latitudinal range limits (Horn et al. 2006). The problem with published range limits for species is that they often reflect unusual events and thus extend much further than the region that the species can successfully inhabit. Here, we examine this factor by using a unique data set from bottom trawls collected annually by the National Marine Fisheries Service from 2003 to 2010 in the coastal waters of California between the depths of 55 and 1280 m (Keller et al. 2012). We describe the differences in species composition across this boundary on the continental slope as well as the continental shelf. We include three regional sampling areas to examine the characteristics of the Point Conception faunal break: the Southern California Bight (SCB), here limited to the waters between the Mexican border and Point Conception; the South Central Coast (SCC) region, between Point Conception and Lopez Point, California; and the Monterey region (MONT), Lopez Point to Point Mendocino (fig. 1). Here, we examine the patterns of species composition relative to these biogeographic boundaries and discuss the validity of Point Conception as a biogeographic barrier for these communities.

MATERIALS AND METHODS

Standardized otter trawls were conducted from 2003 to 2010 (Keller et al. 2012). We categorized these data into three regions based on latitude: SCB (32°–34.4°N); SCC (34.5°–35.9°N), and MONT (36°–40.5°N) (fig. 1). The West Coast Groundfish Slope/Shelf Bottom Trawl Survey design started out using the 5 latitudinal INPFC

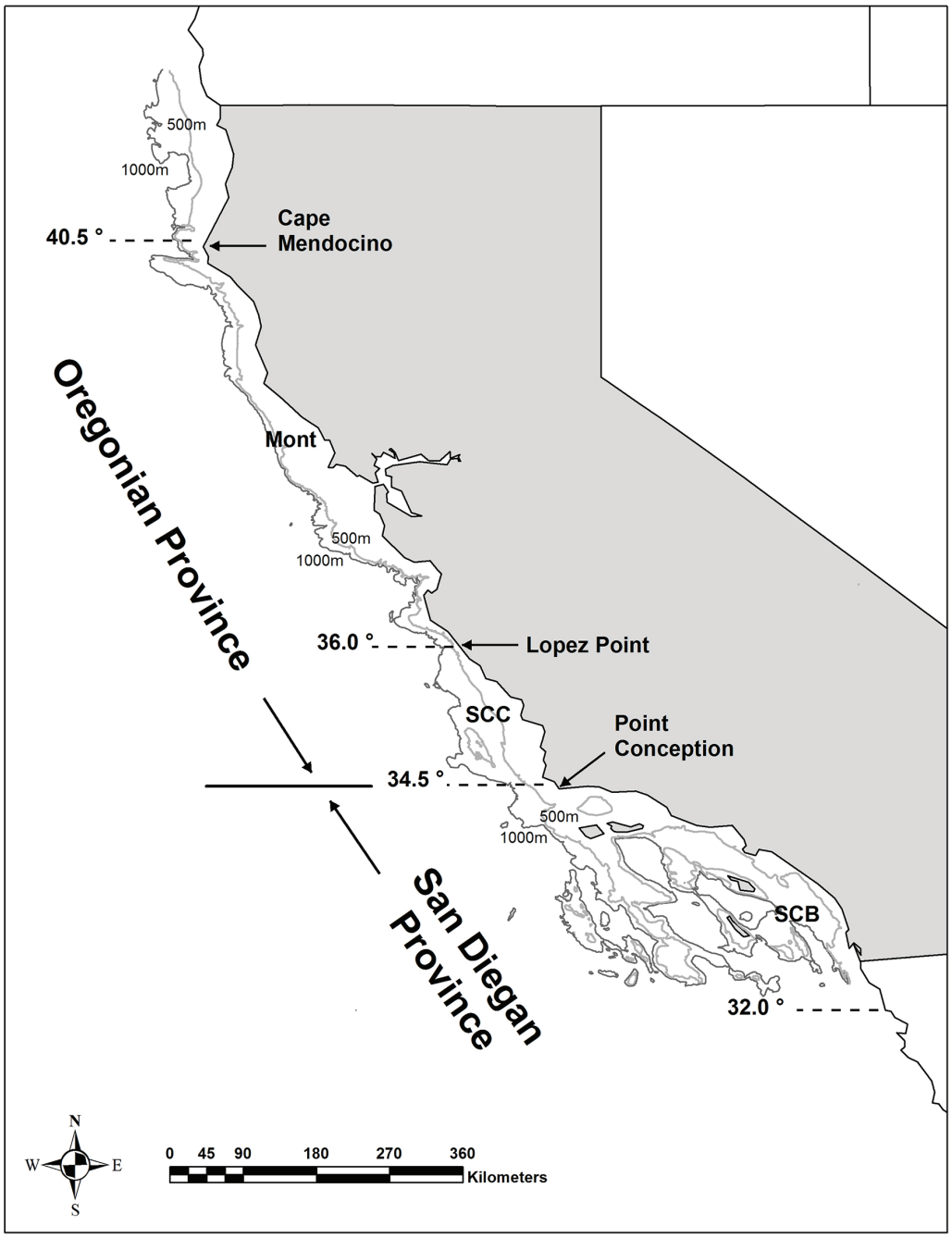

Figure 1. California biogeographic regions and latitudinal points used in the trawl analyses. MONT = Monterey Region, SCC = South Central Coast, SCB = Southern California Bight.

strata in 2003, but changed to a single coastal division at 34°30'N (Point Conception) beginning in 2004. Because this trawl program used the INPFC limits for the Conception region that rounds Point Conception and extends north to Lopez Point, we designated the area between Point Conception and Lopez Point as the South Central Coast. Numerical fish density was calculated by dividing the estimated number of fishes captured by the area (ha) swept by each trawl (Miller and Schiff 2012). All fishes taken were included in the overall catch data and summaries, but only fishes identified to species were included in the assemblage analyses. We did not exclude epi- or mesopelagic species. Rank-order data systems were used to characterize differences between regions based upon abundance (top 10, 15, and 20 species), index of community importance (ICI), and species value (Bond et al. 1999). For each criterion, the rank order was calculated and numbered. These rank

orders were then summed for each species, re-ranked and compared using Kendall's tau rank association statistic. Rank order models were created for each biogeographic region by using each region as the primary ranking in each analysis.

Multivariate analyses were used to identify differences in the fish assemblages across regions and depth ranges and to identify the taxa contributing to the patterns. The data from 283 species were first screened for species that were recorded from less than five trawls or had a total catch across all trawls of less than 10 individuals. The data from these specesies were not analyzed as these less abundant species could influence the analysis, which was intended to focus on major faunal seperations. The remaining 190 taxa (67%) were summarized by categorizing each trawl by latitude and depth. There were 16 latitude categories, encompassing 0.5° of latitude between 32.5° and 40.0°N. The area furthest to the south in latitude 32.0° was not included because it was only sampled from 2007 to 2010 resulting in a total of only 25 trawls. To provide a clean separation at Point Conception the category for latitude 34.0° only included trawls through latitude 34.449°, while the category for latitude 34.5° included trawls from latitude 34.450° through latitude 34.999°. The trawls were also categorized into the three regions described above with four latitude categories in the SCB (32.5–34.0), three latitude categories in the SCC (34.5–35.5), and nine latitude categories in the MONT region (36.0–40.0). The data sets were also assigned to four depth classes based on the depths of the trawls. The classes were <200 m, 201–500 m, 501–1000 m, and >1000 m, which corresponded to the shelf, upper slope, slope, and deep water habitats from Allen and Pondella (2006). The data on the estimated number per hectare for each species for all of the trawls within each half latitude and depth category were averaged resulting in 59 sample groups. There were only 59 and not 64 categories because no trawling was conducted at depths deeper than 200 m for the 37.5° latitude category and deeper than 1000 m for the 38.0° and 38.5° latitude categories.

The summarized biomass data from the 59 sample groups were analyzed using PRIMER VERSION 6.1.12 (© 2009 PRIMER-E Ltd.). The data were transformed as $\sqrt{(x_{ij})}$, then used to calculate Bray-Curtis measures of similarity. Some of the analyses were done on all 59 samples, while other analyses only analyzed the data within each of the four depth categories. The Bray-Curtis similarities among samples were analyzed using nonmetric multidimensional scaling (MDS) and run on the entire data set as well as subsets of the data representing the samples within each of the five depth categories. The ANOSIM routine was used to determine if statistically significant differences observed in the MDS could be detected among groups of samples categorized by depth class and region (Clarke and Gorley 2006). When significant differences among depth groups were detected, the SIMPER routine was used to determine the relative contribution of individual taxa to the average dissimilarity within and among groups that could have contributed to the significant difference detected. The same approach was used for determining the contribution of each taxon to the average dissimilarity (D_{jk}) between groups. The samples were also separated by latitude and separate MDS analyses of the samples within each depth class were used to summarize the relationships among samples within each group. The RELATE routine was used to test if the rank order of samples by latitude for each depth class was significantly correlated with rank order of sample similarities using a Spearman rank correlation with the probabilities of the computed values compared against correlations based on 3,000 random permutations of the sample orders (Clarke and Gorley 2006). A significant value indicated a consistent pattern of change in species composition with latitude.

RESULTS

From 2003 to 2010, 2332 trawls (SCB = 897, SCC = 529, MONT = 906) sampled 4,223 ha (SCB = 1,598, SCC = 987, MONT = 1.638) at depths from 56 to 1269 m (table 1) and included 283 species (38.7%) of the 732 species known to occur within the trawled depths from the Mexican border to Cape Mendocino, 232 of the 669 known from the SCB (34.7%), 182 of 528 from the SCC (34.5%), and 211 of 538 from the MONT (39.2%) (Love et al. 2005; Horn et al. 2006; and Appendix 1). Of the total 732 species known to occur across the sampled regions, 549 species (75%) were known to cross the barrier at Point Conception with the crossing to the south less restrictive. For the 283 species, 155 were not taken north of the SCB (77 stopped by or before reaching the barrier) and 28 species of the SCC and MONT were not taken south of the barrier (the SCB). There were differences in sampling effort for each region (table 1) due to the size of the regions with MONT spanning the largest latitudinal distance (4.5°). After the first two years, the sampling effort was relatively consistent among the regions across years (table 1). The average number of trawls and area sampled over the eight years were similar for the SCB and MONT, which were both consistently higher than the sampling effort in the SCC region. The mean depth was relatively deep for six of the eight years (excluding 2003 and 2004) for the SCB, relatively shallow for MONT, and intermediate for the SCB. The top species collected therefore would reflect this difference and not necessarily a temporal change. Only the SCB has mean depths that do not vary significantly by year.

TABLE 1
Summary of trawl data by biogeographic region and year. Depths are in meters.

Region	Year	N	Area (ha)	Mean ha/trawl	Trawl Depths (m)			Total No. Taxa	Density (Fish/ha)	Biomass (kg/ha)
					Mean	Max.	Min.			
SCB	2003	72	139.3	1.94	436.9	1209	59	124	300.0	36.4
	2004	83	160.8	1.94	468.4	1206	58	130	636.7	57.6
	2005	117	214.7	1.84	485.0	1230	60	158	791.1	64.8
	2006	125	226.8	1.81	483.2	1246	61	158	516.6	49.6
	2007	124	218.8	1.76	462.8	1224	59	152	494.2	54.1
	2008	119	199.3	1.68	448.9	1184	61	147	440.7	47.6
	2009	123	201.3	1.64	423.4	1196	62	153	514.4	51.3
	2010	134	236.8	1.77	464.3	1242	61	161	610.8	56.3
	Total	**897**	**1597.8**							
	Mean	**112**	**199.7**	**1.80**	**459.1**	**1217**	**60**	**148**	**538.1**	**52.2**
SCC	2003	41	76.3	1.86	367.3	1159	56	100	563.6	113.2
	2004	46	92.9	2.02	453.3	1039	57	95	570.3	104.9
	2005	63	124.3	1.97	528.2	1154	61	105	632.3	105.6
	2006	58	110.1	1.90	587.6	1269	63	119	425.7	96.9
	2007	79	152.0	1.92	585.6	1241	68	109	423.8	105.9
	2008	75	133.0	1.77	516.2	1206	59	102	450.3	108.1
	2009	87	151.1	1.74	521.4	1184	66	117	562.9	138.2
	2010	80	147.0	1.84	547.6	1256	59	117	506.3	100.5
	Total	**529**	**986.7**							
	Mean	**66**	**123.3**	**1.88**	**513.4**	**1189**	**61**	**108**	**516.9**	**109.2**
MONT	2003	96	191.3	1.99	395.2	1240	59	133	1168.5	307.8
	2004	91	171.7	1.89	308.3	1145	62	132	1083.6	284.6
	2005	105	186.4	1.77	266.7	1208	60	122	1086.0	249.2
	2006	127	242.1	1.91	392.8	1240	59	133	637.3	167.5
	2007	100	169.5	1.70	365.0	1237	64	132	533.7	153.8
	2008	140	248.6	1.78	383.4	1200	60	137	608.1	137.3
	2009	119	201.5	1.69	381.9	1244	60	134	595.9	134.0
	2010	128	227.0	1.77	354.1	1222	57	131	518.8	109.0
	Total	**906**	**1638.1**							
	Mean	**113**	**204.8**	**1.81**	**355.9**	**1217**	**60**	**132**	**779.0**	**192.9**

*2003 was the first year of the current survey design. The survey extent increased from the previous slope-only survey design to include the entire shelf, the survey design itself was new, and a completely new data collection system was launched. In addition, in 2004 the survey team executed two surveys, the next iteration of the slope/shelf survey and the 2004 iteration of the triennial shelf survey. Since the survey team did not have the resources to execute them both at previous levels, both efforts were scaled down to schedules that could be met by the survey crew. Consequently, fewer tows were executed by the slope/shelf survey in 2003 and 2004 and the level of species identification expertise was likely lower than that accumulated in later survey years.

There were 21 previously unreported range extensions in this data set (table 2). Forty-eight species were taken only from north of Point Conception (SCC and MONT), while 37 were only taken to the south (SCB). Only 15 of the 182 species caught in the SCC were not taken to the north or south. When evaluating differences based on depth restricted analyses, the following number of unique species were recorded by depth for the MONT and SCB regions: 31 and 36 species, respectively from sampling done in <200 m; 15 and 21 species, respectively from 200 to 500 m; 6 and 20 species, respectively from 500 to 1000 m; and 9 and 10 species, respectively from >1000 m. Ten of these depth-unique species show some evidence of latitudinal submergence by a shift to deeper water to the south: *Eptatretus stouti*, *Argyropelecus affinis*, and *Tactostoma macropus* from the shelf to 200 to 500 m; *Albatrossia pectoralis, Careproctus cypseluris, Careproctus gilberti, Paraliparis dactylosus*, and *Symbolophorus californiensis* from 200–500 m to depths of 500 to 1000 m; and *Dicrolene filamentosa* from 500 to 1000 m to >1000 m.

For the SCB, fish density (fish/ha) fluctuated from 300 (2003) to 791.1 (2005). For MONT, the density was high, 1168.5 fish/ha, in 2003 and decreasing to 518.8 fish/ha by 2010. Only *Parmaturus xaniurus* exhibited a strong increase in MONT while a large group of species decreased (*Albatrossia pectoralis*, *Alosa sapidissima*, *Antimora microlepis, Argentina sialis, Citharichthys sordidus*, *Coryphaenoides acrolepis*, *Cymatogaster aggregata*, E*ngraulis mordax*, *Genyonemus lineatus*, *Glyptocephalus zachirus*, *Hydrolagus colliei*, *Lycodapus pacificus*, *Microgadus proximus*, *Microstomus pacificus*, *Peprilus simillimus*, *Raja rhina*, *Raja inornata*, *Sebastolobus altivelis*, *Sebastes goodei*, *Zalembius rosaceous*, and *Zaniolepis latipinnis*). Fluctuating fish density in the SCC was also observed. There were notable decreases in *Citharichthys sordidus*, *Sebastes goodei*, *Zaniolepis latipinnis*, and *Sebastes saxicola*. *Bothrocara brunneum* appeared to have increased. The MONT region usually

TABLE 2
Summary of range extensions. These new records should be viewed with caution as, with the exception of *Paraliparis pectoralis*, no voucher specimens appear to exist.

Species	Latitude	Longitude	Haul ID#	Previous Range (Love et al. 2005)
Bajacalifornia burragei	40.01382569	–124.6504954	803018107	north to southern California (ca 34°N)
Bathyagonus nigripinnis	34.58354301	–120.8804930	1003008194	central California (36°46'N)
Bathyraja aleutica	36.22119179	–122.2063941	703008139	south to Cape Mendocino (N border of Monterey region)
Borostomias panamensis	36.19269648	–122.2185127	1003008132	Chile to Point Conception (34°26'N)
Careproctus colletti	35.61484980	–121.7713301	803010132	northern California (38°42'N)
Careproctus cypselurus	33.36436250	–120.0692875	603008157	central Calif. (34°44'N)
Careproctus gilberti	33.74998625	–120.2019863	1003010186	off Morro Bay (35°10'N)
Caulophryne jordani	36.08399248	–121.9417120	1003017134	north to southern California (ca 34°N)
Clinocottus acuticeps	33.41295591	–117.6828199	803010189	off Big Sur River (36°16'N)
Coryphaenoides cinereus	35.502447655	–121.0987997	703008156	Monterey Bay (ca 36°44'N)
Dasycottus setiger	37.79513550	–122.8823967	303010115	Aleutian chain south to WA
Elassodiscus caudatus	34.67268167	–121.1444792	1003018150	central California (36°54'N)
Elassodiscus tremebundus	33.35561367	–117.8534293	703017187	Japan to Aleutian Islands
Enophrys bison	33.29758333	–118.3936708	703010175	Monterey Bay (ca 36°44'N)
Hippoglossoides elassodon	32.92147324	–117.2941441	503008199	Monterey (ca 36°35'N)
Oneirodes thompsoni	32.44645325	–118.5887397	803010180	northern California (41°20'N, 144°10'W)
Paraliparis dactylosus	32.64158399	–118.4368472	703017178	"central California"
Paraliparis pectoralis	32.43177857	–118.4049071	903008173	Monterey (36°44'N, 122°18'W)
Rhinoliparis attenuatus	32.80213030	–119.9753069	803018167	Monterey Bay (ca 36°44'N)
Stomias atriventer	36.38721489	–122.0663930	503017142	"central California" in Moser 1996, but clearly to at least Cape Mendocino
Thaleichthys pacificus	33.96905327	–118.6554909	303010152	Point Conception (34°26'N)

had the highest fish and biomass density, especially from 2003–05 with a general decrease from 2003 to 2010 (fig. 2). Biomass did not decrease radically by year in the SCC or SCB, but there was a decrease in biomass to the south. While the shallowest depths had the lowest biomass in MONT and the SCC, this was not the case in the SCB. Though the SCB has the lowest numerical and biomass density, it had the highest species richness.

There was marked interannual variation of some individual species densities by region (fig. 3). *Porichthys notatus*, other than a decrease in catch in the MONT from 2003 to 2004, exhibited no regional separation, and its density was relatively constant throughout the study. A representative species from SCB, *Nezumia liolepis*, was relatively absent in MONT, with generally low densities in SCC with a slight decline over time in SCB. Another characteristic SCB species, *Zalembius rosaceus*, was observed at low densities in SCC and MONT and high densities in SCB. The density shift contrasted with *Lycenchelys crotalinus*, a characteristic species of MONT, which had its highest densities in the north, intermediate densities in SCC, and lowest densities in SCB. *Merluccius productus*, another characteristic MONT taxon, had relatively high catches in MONT and lower but similar densities at SCC and SCB. *Bothrocara brunneum*, a characteristic taxon of SCC, had a similar pattern with higher densities in the SCC, especially in 2009 and relatively low densities for the remainder of the study. *Glyptocephalus zachirus*, which was a characteristic species of SCC + MONT, had density values in those two regions that were higher than those in SCB and that showed an apparent declining trend over time. Finally, *Lycodapus pacificus* densities increased and overlapped in SCC and SCB and were relatively low in MONT, and could be considered a characteristic species of both SCC and SCB.

Using the rank order of abundance, the only significant correlation detected was a negative relationship for SCC and MONT rankings for the top ten species (table 3) ($K\tau = -0.598$, $p = 0.019$). No significant correlations were detected for the other rank order tests based upon abundance. In the depth restricted analyses using the same model based upon abundance, no significant correlations were detected between regions for the trawls in the two shallowest depth groups. A significant correlation was detected for the 500–1000 m depth group between SCC and MONT using the MONT model ($K\tau = 0.347$, $p = 0.032$). For the deepest trawls (>1000 m), a significant correlation was detected between SCB and MONT in SCC model ($K\tau = 0.654$, $p < 0.001$) and SCB and SCC in the MONT model ($K\tau = 0.364$, $p = 0.025$).

In the ICI analysis of the trawls on the shelf (<200 m), a significant negative correlation was detected between SCC and MONT regions for the MONT model ($K\tau = -0.343$, $p = 0.029$), and a positive correlation between SCB and MONT for the SCB model ($K\tau = 0.364$, $p = 0.025$). For the trawls in the 200–500 m depth groups, a significant correlation was detected between SCC and MONT in the SCB model ($K\tau = 0.417$, $p = 0.01$). No significant correlations were detected for the data for the

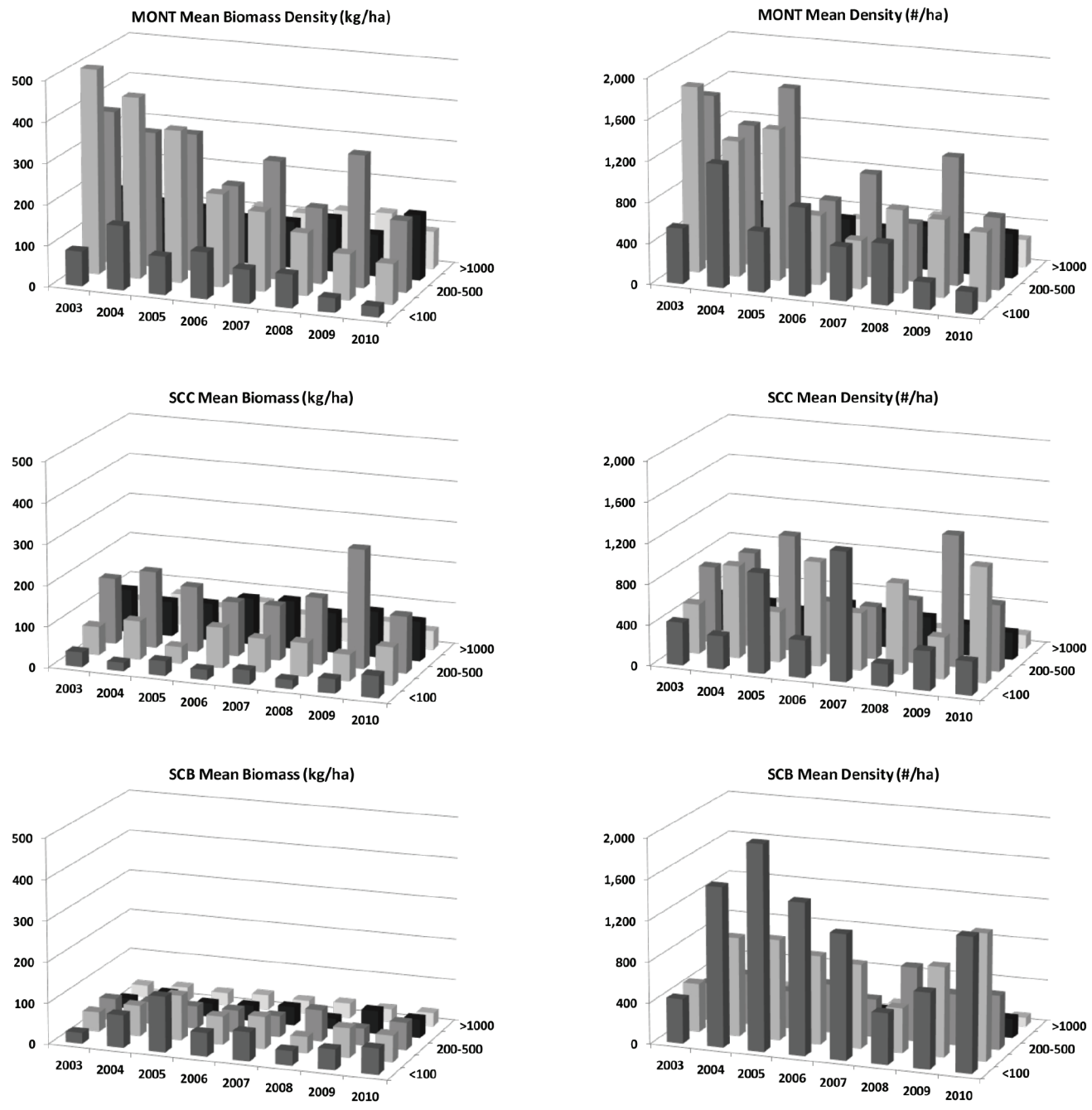

Figure 2. Mean biomass densities (kg/ha) and numerical (#/ha) densities of trawl caught fishes in three California biogeographic regions: MONT = Monterey, SCC = South Central California, SCB = Southern California Bight by depth zone (m).

500 to 1000 m depth group, while >1000 m, significant correlations were detected between SCC and MONT for all the models (MONT, $K\tau = 0.584$, $p < 0.001$; SCC, $K\tau = 0.831$, $p < 0.001$; SCB, $K\tau = 0.883$, $p < 0.001$).

For the species value analyses of the trawls from the shelf depths (<200 m), the only correlations detected were a positive one between MONT and SCC ($K\tau = 0.597$, $p < 0.001$) and negative between MONT and SCB ($K\tau = 0.416$, $p = 0.01$) using the SCB model. No significant correlations were detected for the 200–500 m depth, while for the deeper two depth groups, a significant correlation was detected between MONT and the SCC using the SCB based model ($K\tau = 0.315$, $p = 0.05$) and the SCC model ($K\tau = 0.503$, $p = 0.002$). Similarly, at >1000 m for the SCB and MONT regions, a significant correlation was detected using the SCB

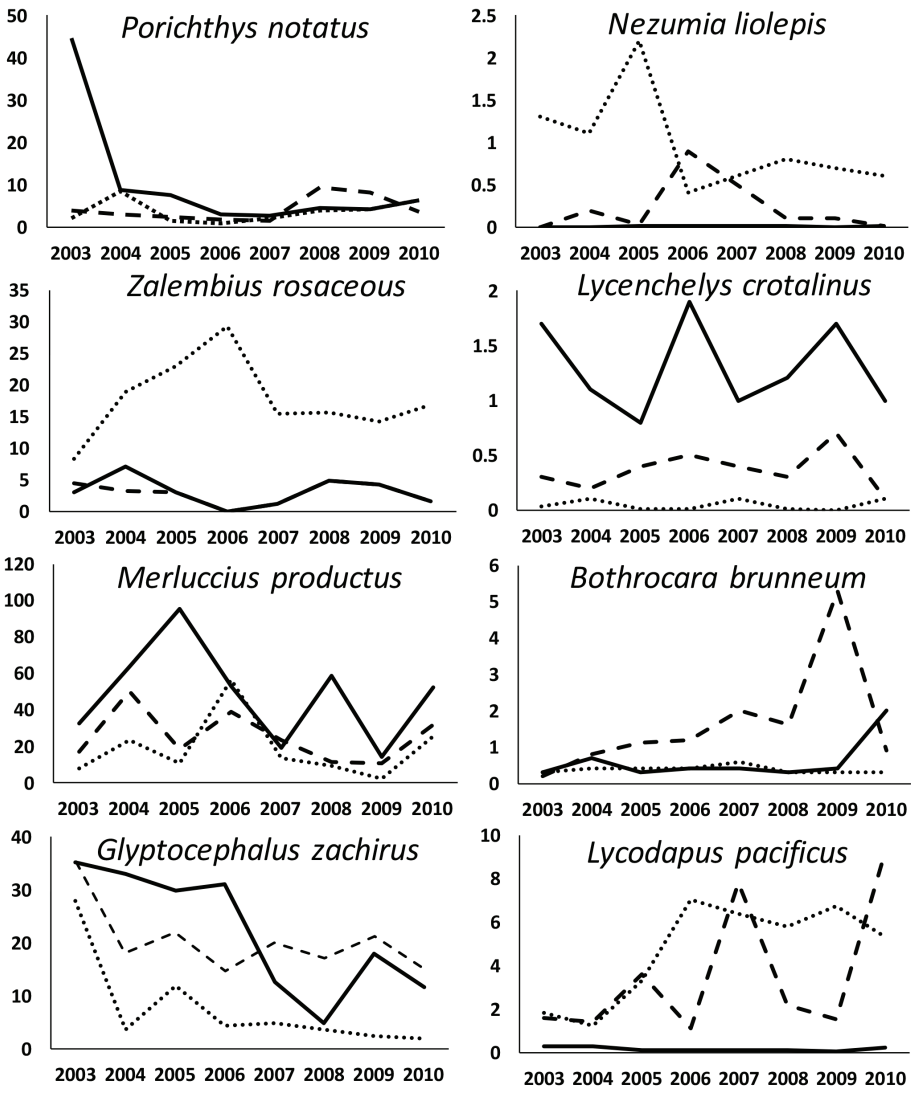

Figure 3. Annual mean density (#/ha) for representative species of biogeographic groupings: Unaligned *Porichthys notatus*; SCB *Nezumia liolepis* and *Zalembius rosaceous*; MONT *Lycenchelys crotalinus* and *Merluccius productus*; SCC *Bothrocara brunneum*; SCC + MONT *Glyptocephalus zachirus*; and, SCC + SCB *Lycodapus pacificus*. Solid line = MONT, hatched line = SCC and dotted line – SCB.

TABLE 3

Summary of the correlations from rank orders by abundance, index of community importance (ICI), species value (p levels: * = 0.5, ** ≤0.01, * ≤0.001).**

	55–200 m			200–500 m			500–1000 m			>1000 m		
	MONT vs SCC	SCC vs SCB	MONT vs SCB	MONT vs SCC	SCC vs SCB	MONT vs SCB	MONT vs SCC	SCC vs SCB	MONT vs SCB	MONT vs SCC	SCC vs SCB	MONT vs SCB
Abundance												
MONT	NS	NS	NS	NS	NS	NS	*	NS	NS	NS	*	NS
SCC	NS	NS	NS	NS	NS	NS	NS	NS	NS	NS	NS	***
SCB	NS	NS	NS	NS	NS	NS	NS	NS	NS	NS	NS	NS
ICI												
MONT	NS–	NS	NS–	NS	NS	NS	NS	NS	NS	***	NS	NS
SCC	NS–	NS–	NS–	NS	NS	NS	NS	NS	NS	***	NS	NS
SCB	NS	*	NS	*	NS	NS	NS	NS	NS	***	NS	NS
Species Value												
MONT	NS	NS–	NS	NS	NS	NS	NS	NS–	NS	**	NS	NS
SCC	NS	NS	NS	NS	NS	NS	**	NS	NS	**	NS	NS
SCB	***	NS	*	NS	NS–	NS–	**	NS	NS	NS	NS	***

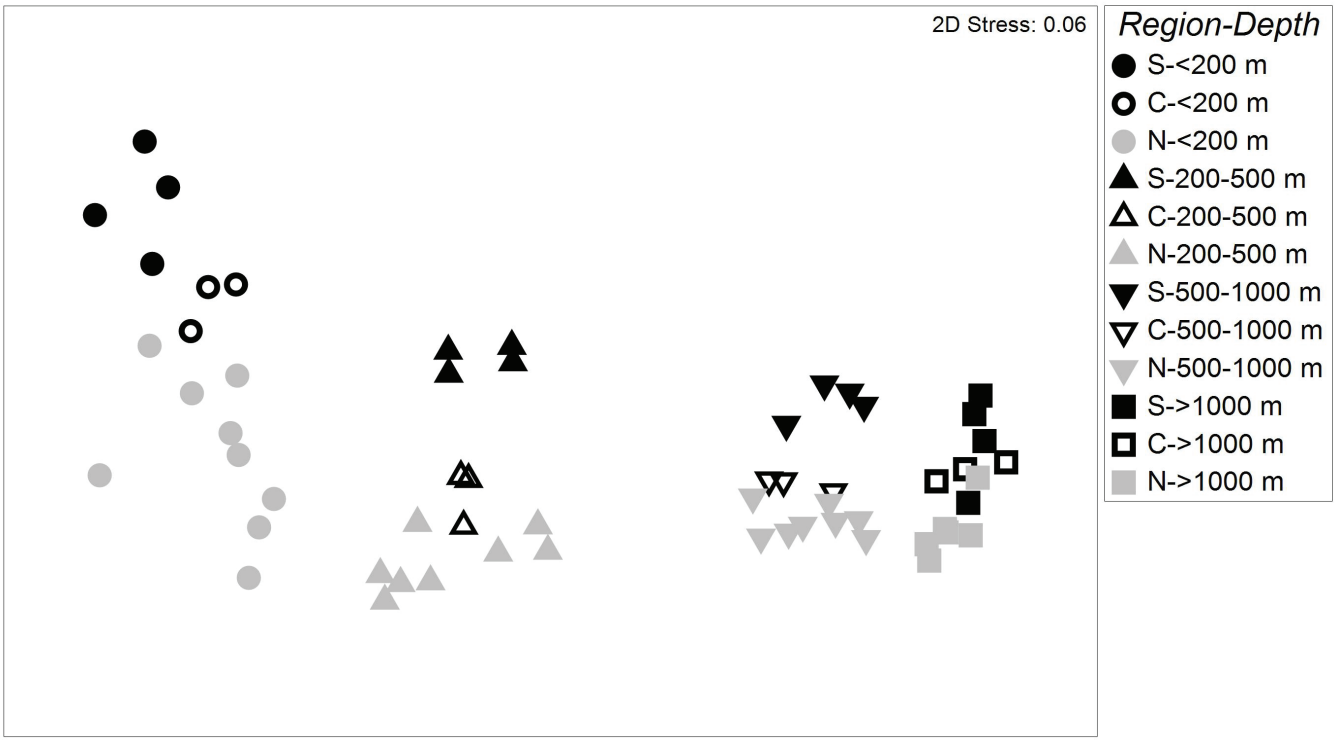

Figure 4. Multidimensional scaling analysis of Bray-Curtis dissimilarity matrix of square root transformed counts per hectare for 190 taxonomic groups from samples averaged into 59 groups representing the samples within four depths (samples from <200 m, 200–500 m, 500–1000 m, and >1000 m) within each half-latitude. The samples within the half-latitude classes are labeled by geographic region (S = half-latitude classes south of Point Conception, C = half-latitude classes from central California from Point Conception north to Lopez Point, and N = half-latitude classes from northern California north of Lopez Point). 2D stress = 0.6.

TABLE 4

SIMPER analysis showing taxa contributing to the similarity among samples within depth groups. The taxa were ranked by their percent contribution. The 15 taxa with the highest percentage contributions were listed as well as the number contributing up to 90% of the similarity within each group. The average similarity for the samples within each group is also presented.

Rank	<200 m Average = 54.2	%	200–500 m Average = 61.2	%	500–1000 m Average = 71.4	%	>1000 m Average = 72.3	%
1	*Citharichthys sordidus*	10.71	*Sebastes diploproa*	14.71	*Sebastolobus altivelis*	26.77	*Sebastolobus altivelis*	25.32
2	*Sebastes goodei*	17.39	*Microstomus pacificus*	25.35	*Microstomus pacificus*	38.77	*Coryphaenoides acrolepis*	37.79
3	*Sebastes saxicola*	23.97	*Sebastes saxicola*	34.27	*Alepocephalus tenebrosus*	45.71	*Alepocephalus tenebrosus*	47.92
4	*Merluccius productus*	30.19	*Glyptocephalus zachirus*	41.47	*Sebastolobus alascanus*	51.38	*Antimora microlepis*	54.43
5	*Sebastes jordani*	36.29	*Merluccius productus*	48.02	*Apristurus brunneus*	57.01	*Microstomus pacificus*	59.39
6	*Parophrys vetulus*	41.39	*Sebastes jordani*	52.46	*Anoplopoma fimbria*	61.43	*Sebastolobus alascanus*	63.98
7	*Sebastes semicinctus*	45.38	*Sebastolobus alascanus*	56.47	*Bothrocara brunneum*	63.84	Bathylagidae	68.52
8	*Zalembius rosaceus*	48.97	*Lyopsetta exilis*	60.26	*Coryphaenoides acrolepis*	66.21	*Albatrossia pectoralis*	72.64
9	*Squalus suckleyi*	52.28	*Lycodes cortezianus*	63.81	*Merluccius productus*	68.50	*Anoplopoma fimbria*	76.58
10	*Hydrolagus colliei*	55.53	*Raja rhina*	66.85	*Embassichthys bathybius*	70.58	*Embassichthys bathybius*	79.86
11	*Glyptocephalus zachirus*	58.12	*Sebastes aurora*	69.83	*Antimora microlepis*	72.49	*Bothrocara brunneum*	82.77
12	*Porichthys notatus*	60.66	*Hydrolagus colliei*	72.63	*Careproctus melanurus*	74.24	*Bathyraja trachura*	85.17
13	*Eopsetta jordani*	63.16	*Sebastolobus altivelis*	75.19	*Raja rhina*	75.94	*Apristurus brunneus*	86.85
14	*Sebastes elongatus*	65.45	*Anoplopoma fimbria*	77.54	*Lycenchelys crotalinus*	77.60	*Lampanyctus* spp.	88.07
15	*Lyopsetta exilis*	67.66	*Squalus suckleyi*	79.48	*Bathylagidae*	79.16	Myxinidae	89.18
	19 others		8 others		10 others		1 other	

model ($K\tau = -0.551$, $p < 0.001$) and between the SCC and MONT using the other two models (SCC, $K\tau = 0.449$, $p = 0.006$; MONT, $K\tau = 0.492$, $p = 0.002$). Thus, the rank correlation for these two depth groups generally unites the SCC region with the MONT region to the north but at the deepest depth it also correlates with the SCB region. At the deepest depth grouping, all three models are based almost completely on the same species.

In the MDS analysis there was a clear and significant separation among the four depth categories (ANOSIM; Global $R = 0.884$; $p \leq 0.01$; fig. 4). While the horizontal axis showed a separation among depth groups,

TABLE 5

SIMPER analysis showing taxa contributing to the average dissimilarity between the following adjoining depth groups: a) <200 m and 200–500 m, b) 200–500 m and 500–1000 m, and c) 500–1000 m and >1000 m. The taxa are ranked by their percentage contribution with the 10 taxa with the highest percentage contributions listed as well as the number contributing up to 90% of the total within each group. The average abundances for each group are based on the square root transformed data used in the analysis. The average dissimilarities between each pair of depth groups are also presented.

a) Average Dissimilarity = 65.9	Abundance			
Taxa	<200 m	200–500 m	% Contribution	Cumulative %
Sebastes diploproa	1.10	13.43	7.82	7.82
Citharichthys sordidus	10.55	1.19	5.84	13.66
Sebastes jordani	6.82	8.63	5.11	18.77
Sebastes semicinctus	7.98	0.62	4.64	23.41
Microstomus pacificus	2.57	9.47	4.47	27.88
Sebastes goodei	6.96	3.17	3.56	31.45
Sebastes saxicola	6.25	8.82	2.95	34.39
Zalembius rosaceus	4.34	0.07	2.68	37.07
Glyptocephalus zachirus	2.77	6.71	2.64	39.71
Merluccius productus	6.69	5.29	2.57	42.28
52 others				

b) Average Dissimilarity = 69.6	Abundance			
Taxa	200–500 m	500–1000 m	% Contribution	Cumulative %
Sebastes diploproa	13.43	0.09	10.89	10.89
Sebastolobus altivelis	2.73	13.62	9.09	19.98
Sebastes saxicola	8.82	0.00	7.15	27.12
Sebastes jordani	8.63	0.00	6.72	33.85
Glyptocephalus zachirus	6.71	1.31	4.44	38.28
Microstomus pacificus	9.47	7.33	3.62	41.90
Merluccius productus	5.29	1.35	3.33	45.23
Lyopsetta exilis	3.68	0.08	3.02	48.25
Alepocephalus tenebrosus	0.08	3.56	2.92	51.16
Hydrolagus colliei	3.12	0.19	2.44	53.61
42 others				

c) Average Dissimilarity = 41.8	Abundance			
Taxa	500–1000 m	>1000 m	% Contribution	Cumulative %
Microstomus pacificus	7.33	2.74	10.37	10.37
Coryphaenoides acrolepis	1.66	6.20	10.10	20.47
Sebastolobus altivelis	13.62	10.79	9.67	30.15
Apristurus brunneus	2.88	0.84	4.48	34.62
Antimora microlepis	1.09	2.64	3.41	38.03
Albatrossia pectoralis	0.67	2.00	2.92	40.96
Merluccius productus	1.35	0.02	2.89	43.85
Glyptocephalus zachirus	1.31	0.00	2.72	46.57
Parmaturus xaniurus	1.12	0.03	2.42	48.99
Bathylagidae	0.92	1.98	2.42	51.41
40 others				

the vertical axis showed a gradient based on geographic region and latitudinal variation within each depth category. The shallowest depth group (samples <200 m) had the greatest variation among samples and separation among geographic regions (S = SCB, C = SCC, and N = MONT). In the SIMPER analysis (fig. 4), differences were reflected in the variation among the samples within each depth category. The average similarity among samples within groups was highest for the >1000 m depth group (72.3%), while only 54.2% for the <200 m depth group (table 4). Taxa groups with the largest contribution to the similarities among groups varied by depth group, with the number of taxa contributing to the similarity within groups being highest for the <200 m depth group. These disparities likely contributed to the higher variability and lower average similarity among the samples within this depth group and contrasts with the lower variability, higher average similarity, and fewer number of taxa for the deepest >1000 m depth category.

The SIMPER analysis was also used to determine the taxa responsible for the dissimilarities between adjoining depth groups, for example between the <200 m and 200 to 500 m depth groups (table 5). The largest dissimilarity was calculated between the 200 to 500 m and the 500 to 1000 m depth groups (average dissimilarity = 69.6). This was reflected in the average abundances for those two

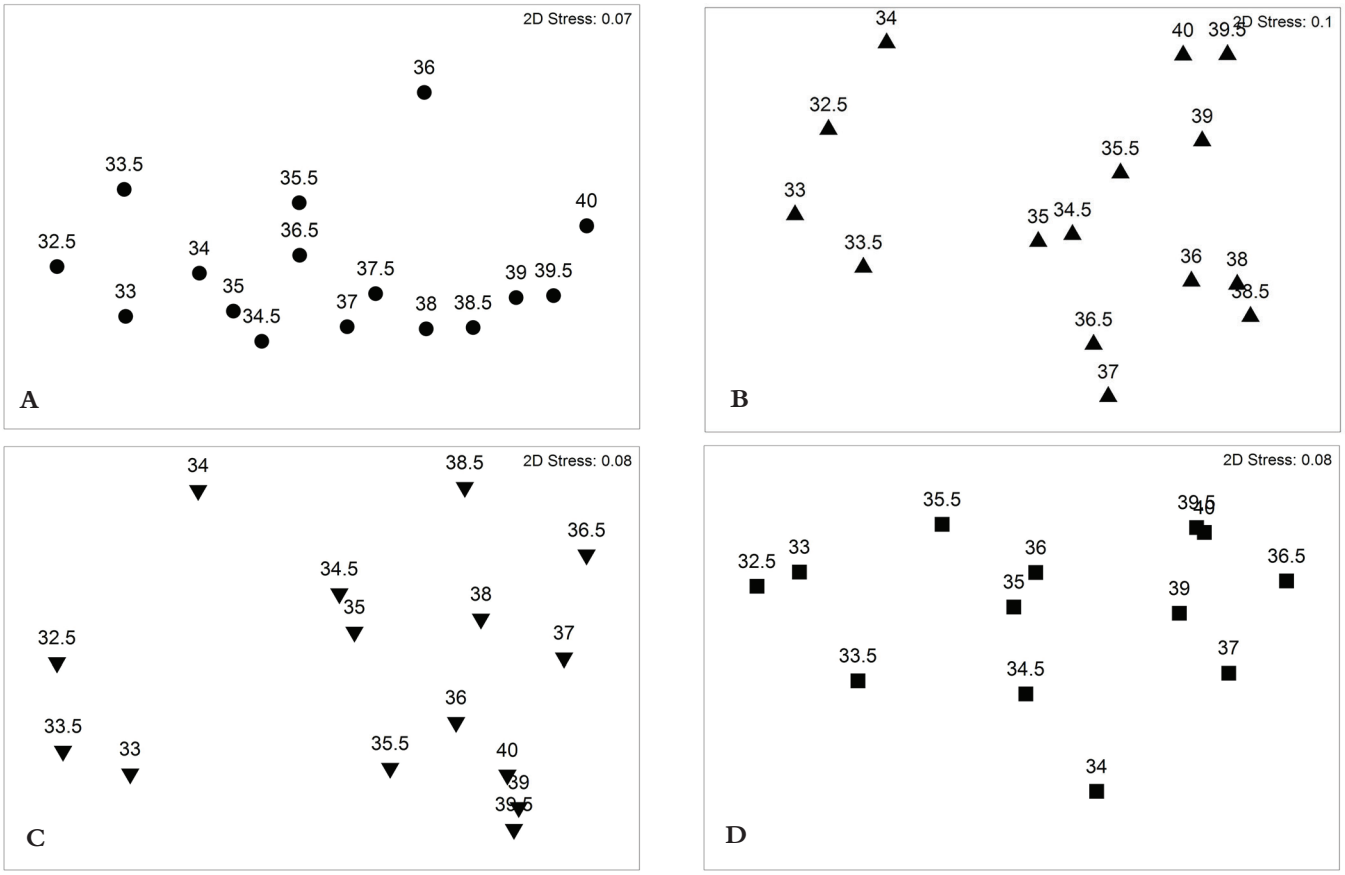

Figure 5. Multidimensional scaling analysis of Bray-Curtis dissimilarity matrix of square root transformed counts per hectare for 190 taxonomic groups from samples averaged into 59 groups representing the samples within four depths (samples from <200 m, 200–500 m, 500–1000 m, and >1000 m) within each half-latitude. The half-latitude groups are labeled in the MDS results for the four depths along with the 2D stress values for the MDS and the PRIMER RELATE analysis test statistic and p-value: a) samples from <200 m (n = 16; 2D stress = 0.07; ρ = 0.84, p <0.01), b) samples from 200–500 m (n = 15; 2D stress = 0.1; ρ = 0.70, p <0.01), c) samples from 500–1000 m (n = 15; 2D stress = 0.08; ρ = 0.67, p <0.01), and d) samples from >1000 m (n = 13; 2D stress = 0.08; ρ = 0.67, p <0.01).

groups that show a distinct shift in the fauna between the two depths that was less distinct for the other two group comparisons (table 5b). For example, the results for the three rockfishes, which were very abundant in the trawls at depths between 200 to 500 m, but almost totally replaced by *Sebastalobus alascanus* in the 500 to 1000 m trawls. These four taxa contribute almost 34% to the total difference between the two depth groups.

The geographic variation shown in the MDS analysis (fig. 4) was analyzed in more detail for each depth group. The samples included in the MDS analyses for each depth group were categorized by their geographic location within each half degree of latitude (fig. 5). All four depth ranges had a statistically significant latitudinal gradient, but the shallowest depth group (<200 m) had the strongest relationship between the rank order based on Bray-Curtis distances among samples and rank order based on latitude. The test statistic for the RELATE procedure for the other three depth groups were similar in value and showed more grouping of samples than shown in the <200 m depth group.

Although all four depth categories had a significant trend consistent with latitudinal variation, the pattern was different for the four groups. The RELATE test value was higher and the pattern of latitudinal variation strongest for the <200 m depth, but no clear break at Point Conception was detected between latitude groups 34.0 and 34.5 (fig. 5a). The break at Point Conception was strongest in the data for the 200 to 500 m depth (fig. 5b), but also apparent in the data from the 500–1000 m depth (fig. 5c). The break at Point Conception was not present in the data from the >1000 m depth category (fig. 5d), which also has the lowest RELATE test value. The results from the MDS for the deepest depth category appear to form three groups with the latitudinal groups around Point Conception more similar to the other data from the SCC.

In the SIMPER analysis for the three geographic regions for the four depth groups, the ten taxa responsible for the greatest degree of similarity within the regional groupings were very similar for all of the depth groups except for the shallowest group (<200 m)

TABLE 6

PRIMER SIMPER analysis showing taxa contributing to the similarity among samples within the south (SCB), central (SCC), and north (MONT) geographic regions for the a) <200 m depth class, b) 200–500 m, c) 500–1000 m, and d) >1000 m depth classes. The 10 taxa with the highest percentage contributions per group are ranked as cumulative percentages, including the number of additional taxa contributing up to 90% of the similarity within each group. The average similarity for the samples within each group for each depth class is also presented.

	SCB		SCC		MONT	
50–200 m						
	Avg. = 68.2		**Avg. = 69.3**		**Avg. = 60.9**	
1	*Sebastes semicinctus*	13.88	*Citharichthys sordidus*	11.43	*Sebastes goodei*	10.71
2	*Citharichthys sordidus*	24.24	*Sebastes jordani*	18.58	*Citharichthys sordidus*	18.83
3	*Zalembius rosaceus*	32.06	*Merluccius productus*	24.79	*Merluccius productus*	26.61
4	*Peprilus simillimus*	39.79	*Sebastes semicinctus*	30.58	*Sebastes saxicola*	33.70
5	*Sebastes jordani*	44.47	*Sebastes saxicola*	36.20	*Parophrys vetulus*	39.66
6	*Genyonemus lineatus*	47.91	*Zalembius rosaceus*	41.16	*Squalus suckleyi*	45.59
7	*Sebastes saxicola*	51.06	*Peprilus simillimus*	45.62	*Sebastes jordani*	50.03
8	*Hydrolagus colliei*	53.69	*Sebastes goodei*	50.03	*Eopsetta jordani*	54.30
9	*Parophrys vetulus*	56.30	*Porichthys notatus*	54.30	*Glyptocephalus zachirus*	58.48
10	*Zaniolepis latipinnis*	58.64	*Parophrys vetulus*	57.64	*Microstomus pacificus*	62.06
	29 other taxa		20 other taxa		19 other taxa	
200–500 m						
	Avg. = 68.1		**Avg. = 78.0**		**Avg. = 66.2**	
1	*Sebastes diploproa*	11.19	*Sebastes diploproa*	18.51	*Microstomus pacificus*	13.99
2	*Sebastes jordani*	21.83	*Microstomus pacificus*	27.04	*Sebastes diploproa*	27.16
3	*Lyopsetta exilis*	28.50	*Sebastes saxicola*	35.02	*Sebastes saxicola*	38.51
4	*Merluccius productus*	35.14	*Merluccius productus*	42.16	*Glyptocephalus zachirus*	46.89
5	*Microstomus pacificus*	41.33	*Glyptocephalus zachirus*	47.73	*Merluccius productus*	51.98
6	*Sebastes saxicola*	46.48	*Sebastes aurora*	51.77	*Sebastolobus alascanus*	55.70
7	*Glyptocephalus zachirus*	51.45	*Parmaturus xaniurus*	55.64	*Lycodes cortezianus*	59.42
8	*Sebastolobus alascanus*	55.73	*Sebastes jordani*	59.46	*Raja rhina*	62.66
9	*Sebastolobus altivelis*	59.87	*Raja rhina*	63.25	*Hydrolagus colliei*	65.77
10	*Citharichthys sordidus*	63.32	*Anoplopoma fimbria*	66.24	*Squalus suckleyi*	68.80
	20 other taxa		11 other taxa		11 other taxa	
500–1000 m						
	Avg. = 74.1		**Avg. = 82.1**		**Avg. = 77.5**	
1	*Sebastolobus altivelis*	25.18	*Sebastolobus altivelis*	23.34	*Sebastolobus altivelis*	26.70
2	*Microstomus pacificus*	33.05	*Microstomus pacificus*	34.32	*Microstomus pacificus*	41.51
3	*Sebastolobus alascanus*	40.68	*Sebastolobus alascanus*	39.92	*Alepocephalus tenebrosus*	48.19
4	*Alepocephalus tenebrosus*	47.48	*Alepocephalus tenebrosus*	45.42	*Apristurus brunneus*	53.84
5	*Apristurus brunneus*	52.18	*Apristurus brunneus*	50.41	*Anoplopoma fimbria*	58.31
6	*Nezumia stelgidolepis*	56.00	*Anoplopoma fimbria*	55.15	*Sebastolobus alascanus*	62.58
7	*Anoplopoma fimbria*	59.39	*Parmaturus xaniurus*	59.15	*Coryphaenoides acrolepis*	65.88
8	*Nezumia liolepis*	62.74	*Sebastes aurora*	61.74	*Embassichthys bathybius*	69.07
9	*Merluccius productus*	65.52	*Raja rhina*	64.30	*Lycenchelys crotalinus*	72.06
10	*Bothrocara brunneum*	67.95	*Coryphaenoides acrolepis*	66.64	*Antimora microlepis*	74.32
	19 other taxa		17 other taxa		10 other taxa	
>1000 m						
	Avg. = 73.2		**Avg. = 79.2**		**Avg. = 78.6**	
1	*Sebastolobus altivelis*	25.74	*Sebastolobus altivelis*	22.17	*Sebastolobus altivelis*	26.78
2	*Alepocephalus tenebrosus*	39.52	*Coryphaenoides acrolepis*	36.24	*Coryphaenoides acrolepis*	43.58
3	*Antimora microlepis*	45.97	*Alepocephalus tenebrosus*	47.11	*Alepocephalus tenebrosus*	50.26
4	*Coryphaenoides acrolepis*	52.20	*Antimora microlepis*	53.83	*Antimora microlepis*	56.30
5	*Microstomus pacificus*	56.94	Bathylagidae	58.78	*Albatrossia pectoralis*	61.44
6	*Sebastolobus alascanus*	61.56	*Albatrossia pectoralis*	63.30	*Microstomus pacificus*	66.42
7	Bathylagidae	65.57	*Sebastolobus alascanus*	67.44	*Sebastolobus alascanus*	70.60
8	*Bathyraja trachura*	69.29	*Anoplopoma fimbria*	71.49	*Embassichthys bathybius*	74.73
9	*Anoplopoma fimbria*	72.94	*Microstomus pacificus*	75.30	*Anoplopoma fimbria*	78.83
10	*Bothrocara brunneum*	76.31	*Bothrocara brunneum*	78.43	Bathylagidae	82.91
	7 other taxa		8 other taxa		4 other taxa	

(table 6). While fishes such as *Citharichthys sordidus* were important in defining the similarity among the samples for all three geographic groups at the <200 m depth, other fishes such as *Genyonemus lineatus* and *Hydrolagus colliei* only occurred in the top ten for the SCB group (table 6). A clear shift was seen in the importance of some of the fishes moving from south to north, such as *Sebastes saxicola*. The number of taxa contributing to the similarity within geographic groups also decreased from south to north for all of the depth groups except for the deepest, >1000 m group. These results, especially for the shallowest <200 m samples reflected the strong gradient seen in the MDS results (figs. 4 and 5). The SIMPER analysis for the geographic regions within each depth class (fig. 5) was consistent with the differences observed in each of the separated depths.

DISCUSSION

In this study, little effect of the Point Conception barrier was shown in the occurrence of taxa in each biogeographic area (Appendix I). Declines in fish density were largely limited to the cooler MONT region, which could have been negatively affected by temperature or other environmental changes that might not have adversely affected the warm temperate species of the SCB, and/or perhaps greater fishing pressure. These presence/absence data were important as this approach is the usual method for documenting faunal breaks. These data showed that most of the identified species were not abundant in their region of occurrence and probably of limited importance to the assemblage in each region. Further, only 16 of the 85 fishes that these data show did cross the barrier were listed in the literature as limited by the barrier, suggesting that their absence in either region was a result of limited sampling. Better information can be derived from the regional abundance data for species not entirely delimited by the regional barrier. Many California fish species were not captured in this trawl program (at least 451 of the 732 species) and some of these may actually be relatively common but patchy enough in distribution to be missed by this level of sampling intensity.

Using nine models for each ranking and depth, we found correlations in only 15 of the 108 comparisons (4 depths, nine models, and 3 rankings) of rank orders between regions by depth (table 3). Thus, 83% of the rank order comparisons imply a distinct separation between regions, providing strong support for the effectiveness of the Point Conception barrier. Only six positive correlations were found between rankings at shelf depths (17%), one for 200 to 500 m (3%), seven for 500–1000 m (19%) and nine for >1000 m (25%). We must note that the probabilities presented were not adjusted for multiple comparisons. If this adjustment was made, there would be, at most, 7 significant correlations (table 3). With the exception of the upper slope, which shows the strongest regional separation, correlations become more common as the depth increases, suggesting a less effective barrier with depth, but fewer species occupy these depths, which could affect this outcome. The number of correlations varies little between models: ten for the MONT model, seven for the SCC model, and eight for the SCB model. The system used to calculate rank orders also varied in number of positive correlations, four using abundance, five using the index of community importance, and eight using species value. The models rarely agreed on the regional correlations. The regional separation based on rank order was greatest at the 200 to 500 m depth, but this depth also had the greatest differences among the top ten species for the different ranking systems. Only one significant correlation was detected at the 200–500 m depth, while at the deeper two depth categories, a significant correlation was detected between MONT and the SCC in the SCB based model and in the SCC model suggesting mixing in this cooler water of the two northern regions but not south of Point Conception. For the ICI, the significant correlations were between the coolest region, MONT, and the SCC (all models, >1000 m), between the MONT and SCC (SCB model, 200 to 500 m) and SCC and SCB (SCB model, <200 m).

At the <200 m and 200–500 m depths, only 7 correlations were detected between regions, supporting the effectiveness of the regional barriers. A significant correlation was detected at the 500–1000 m depth between the SCC and MONT using the MONT model indicating that in the cooler, deeper waters some mixing is occurring. At the deepest sampling depths (>1000 m), a significant correlation was detected between the SCB and MONT in the SCC model and the SCB and SCC in the MONT model, also indicating greater mixing between the regions at depth. Using the rank order of abundance, we detected a significant correlation for the comparison of the SCC and MONT rankings for the top ten species. No significant correlations were detected for the other eight tests. This lack of correlation suggested that a barrier is in place, and perhaps that the SCC and MONT regions were most closely allied.

Rank-order analysis of the data also separated the regions, but the relationships were not highly correlated among the three rank order systems (density, density and fidelity, density, and fidelity and mean weight), used in the study. When not evaluated by depth, none of the comparisons showed a positive correlation between regions. The other rank order comparisons separated the species of each region by depths: 50 to 200 m, 200 to 500 m, 500 to 1000 m, and greater than 1000 m. In this case, there were 108 tests of correlation, and only 14%

of the rank orders showed a positive correlation, the remaining 86% showed no significance or a negative correlation, both supporting regional separation. The two depths below 500 m had a higher number of correlations (11) while those above 500 m had only 4. Interestingly, the upper slope (200 to 500 m) had only 1 correlation. Based upon these rank-order analyses, the regions were basically distinct though less so with depth.

The results of the multivariate analysis also support the Point Conception barrier. The MDS shows the faunal assemblages in the four depth categories were distinct and clearly represented the largest conponent of the variation among the sample groups (fig. 4). Within each of the depth groups there was a strong latitudinal gradient (figs. 4 and 5). The strongest relationship was detected in the shallowest depth, which did not show a break between the latitudinal groups south (34.0) and north (34.5) of Point Conception. This difference may be due to greater variation in water temperatures in the surface waters that cause some mixing of species across the barrier because the results showed a clear separation between the latitudinal groups north and south of Point Conception for the upper slope and 500 to 1000 m depth groups. The latitiudinal groups in the SCB were distinct for all the depth categories except for the greater than 1000 m depths, where the latitudinal relationship was also less apparent.

The species identified as important to the similarity of the samples within each region for each depth support the latitudinal change in assemblage (table 6). For example, *S. semicinctus*, *Zalembius rosaceus*, and *Peprilus simillimus* are all identified as important contributing species to the SCB at depths <200 m. All three of these species dropped off in abundances in the two regions to the north. They were replaced by species such as *S. goodei* that increased in abundance from the SCB to MONT. In contrast, a species such as *C. sordidus* was in approximately equal abundance in all three regions at this depth and was an important contributor to the assemblage in all three regions. These results help explain the gradual latitudinal change seen for the samples collected at <200 m.

The separation between the SCB and the other regions for the 200 to 500 m, and 500 to 1000 m depths (figs. 5b and 5c) was also explained by the changes in species assemblages across the regions. The five species with the largest contributions to the similarity among the samples within the groups were almost identical for SCB and MONT (tables 6b and 6c). These species account for approximately 50% or greater of the similarity within the groups. A different suite of species was associated with the SCB for the 200 to 500 m depth (table 6b). At the 500 to 1000 m depth the top five species were similar across all three regions (table 6c), but other species associated with the SCB, such as *Nezumia stelgidolepis* and *N. liolepis* showed steep declines in abundance between the SCB and SCC, while species such as *Sebastolobus altevelis* and *Microstomus pacificus* showed sharp increases between the two regions. The separation of SCC from the other two regions was likely due to the reduced differences in abundance between the SCC and MONT relative to the changes between the SCB and SCC in these, and other, species.

One of the problems in drawing too strong of a conclusion regarding the Point Conception barrier using these data is the absence of any sampling in shallow water less than 50 m in depth, which was emphasized in earlier studies. Our study did not include sampling of fishes in shallow water habitats such as nearshore reefs, kelp beds, and tide pools. C. Klepado (Scripps Institution of Oceanography) provided us with a list of 74 species taken by University of California collectors in tide pools within the SCB and SCC regions (1950 to 2001). Of these, only 26 (35%) were recorded in our study. Similarly, shallow water species from soft substrate were rare. Love et al. (1986) presented data on shallow trawls at three sites in the SCB: San Onofre, Redondo Beach, and Ormond Beach (maximum depth 18.3 m). At the shallowest depth (6.1 m), 46% of the recorded species were not present in these data, while at 12 m and at 18.3 m, 43.8% and 35.4%, respectively, were not recorded. Similarly, Miller and Shiff (2012), in their analyses of the four SCB trawl surveys since 1994, list 89 species; 39 (43.8%) of these were not taken in this study in the SCB. These SCCWRP data were taken using small 7.6 m head-rope shrimp trawls that are fished primarily in waters between 5 and 200 m. These data included fewer species than in our study, and also many smaller fishes from shallower depths (Allen 2006).

CONCLUSIONS

While the NOAA-NMFS study was designed to evaluate fishery resources, it also provides unique insights into the patterns of variation in the the soft-bottom fish assemblages on our coast. Generally, shallow-water assemblages exhibited greater regional preferences than the deep outer shelf and slope assemblages, where the variation in temperature and habitat at depths is not as evident as it is in shallower environs. It would be interesting to be able to correlate annual changes in species to changes in site oceanographic conditions, but this would require a similar sampling effort among years and regions and that was not the goal of the program.

ACKNOWLEDGEMENTS

The unique data set used in this study was created by NOAA/NMFS. Alphabetically, K. L. Bosely, M. J. Bradburn, J. C. Buchanan, E. L. Fruh, O. S. Hamel, B. H. Horness, D. J. Kamikawa, A. A. Keller, V. H. Simon,

T. J. Stewart, V. J. Tuttle, and R. Wallace were the scientific contributors to the database. For vessels and their crews carried out the trawling: FV *Ms. Julie*, FV *Captain Jack*, FV *Excaliber*, and FV *Blue Horizon*. Beth Horness (NOAA) made the trawl data available to us.

LITERATURE CITED

Allen, M. J. 2006. Continental shelf and upper slope. *In* The ecology of marine fishes: California and adjacent waters. L. G. Allen, D. J. Pondella II, and M. H. Horn, eds., Univ. Calif. Press., Los Angeles, CA. pp 167–202.

Allen, M. J., and G. B. Smith. 1988. Atlas and Zoogeography of Common Fishes in the Bering Sea and Northeastern Pacific. NOAA Tech. Rept. NMFS 66, Seattle, WA.

Bond, A. B., J. S. Stephens Jr., D. J. Pondella II, M. J. Allen, and M. Helvey. 1999. A method for estimating marine habitat values based on fish guilds, with comparisons between sites in the southern California bight. Bull. Mar. Sci 64(2):219–242.

Clarke, K., and R. Gorley. 2006. PRIMER v5: user manual/tutorial. Plymouth, UK: PRIMER-E. 190 pp.

Hastings, P. A. 2000. Biogeography of the Tropical Eastern Pacific: distribution and phylogeny of chaenopsid fishes. Zoological Journal of the Linnean Society 128:319–335.

Hickey, B. M. 1993. Physical Oceanography. *In* The Ecology of the Southern California Bight, Dailey, M. D, D. J. Reish, and J. D. Anderson, eds. Univ. California Press, Berkeley, pp 19–70.

Horn, M. H., and L. G. Allen. 1978. Numbers of species and faunal resemblance of marine fishes in California bays and estuaries. Bull. So. Calif. Acad. Sci. 75:159–170.

Horn, M. H., L. G. Allen, and R. N. Lea. 2006. Biogeography. *In* The ecology of marine fishes: California and adjacent waters. L. G. Allen, D. J. Pondella II, and M. H. Horn, eds., Univ. Calif. Press., Los Angeles, CA. pp 3–25.

Hubbs, C. L. 1948. Changes in the fish fauna of North America correlated with changes in ocean temperature. J. Mar. Res. 7(3):459–482.

Hubbs, C. L. 1960. The marine vertebrates of the outer coast. Syst. Zoo. 9:134–147.

Hyde, J. E., A, Kimbrell, E. Burdick, A. Lynn, and D. Vetter. 2008. Cryptic speciation in the vermilion rockfish (*Sebastes miniatus*) and the role of bathymetry in the speciation process. Mol. Biol. 17:1122–1136.

Keller, A. A., J. R. Wallace, B. H. Horness, O. S. Hamel, and I. J. Stewart. 2012. Variations in eastern North Pacific demersal fish biomass based on the U.S. west coast groundfish bottom trawl survey (2003–10). Fish. Bull. 110:205–222.

Love, M. S., C. W. Mecklenburg, T. A, Mecklenburg, and L. K. Thorsteinson. 2005. Resource Inventory of Marine and Estuarine Fishes of the West Coast and Alaska: a checklist of north Pacific and Arctic Ocean species from Baja California to the Alaska-Yukon Border. U. S. Dept. of Interior, U. S. Geological Survey, Biological Resources Division, Seattle, OCS Study MMS 2005–030 and USGS/NBII 2005=001.

Love, M. S., J. S. Stephens Jr., P. A. Morris, M. M. Singer, M. Sandu, and T. Sciarrotta. 1986. Inshore soft substrata fishes in the southern California bight: an overview. CalCOFI Rep. 27:84–104.

Maloney, N. J., and K. M. Chan. 1974. Physical Oceanography. *In* A summary of knowledge of the Southern California coastal zone and offshore Areas, Dailey, M. D., B. Hill, and N. Lansing, eds. Bureau of Land Management, Dept. Interior. 23 pp.

Miller, E. F., and K. Schiff. 2012. Descriptive trends in southern California bight demersal fish assemblages since 1994. CalCOFI Rep. 53:107–131.

Moser, H. G., R. L. Charter, W. Watson, D. A. Ambrose, J. L. Butler, S. R. Charter and E. M. Sandknop. 2000. Abundance and distribution of rockfish (*Sebastes*) larvae in the southern California bight in relation to environmental conditions and fishery exploitation. CalCOFI Rep. 41:132–147.

Moser, H. G. 1996. The early stages of fishes in the California Current region. CalCOFI Atlas No. 33. 1505 pp.

Radovich, J. 1961. Relationships of some marine organisms of the northeast Pacific to water temperatures, particularly during 1957 through 1959. Calif. Dept Fish and Game, Fish Bull. 112:1–62.

APPENDIX I

Presence (1) versus absence (0) by biogeographic region.

	SCB	SCC	MONT
CEPHALASPIDOMORPHI			
Petromyzontiformes			
Lampetra tridentata	1	1	1
MYXINI			
Myxiniformes			
Eptatretus deani	1	1	1
Eptatretus stoutii	1	1	1
Myxine circifrons	1	1	1
CHONDRICHTHYES			
Chimaeriformes			
Harriotta raleighana	1	0	0
Hydrolagus colliei	1	1	1
Hexanchiformes			
Clamydoselachus anguineus	1	1	0
Hexanchus griseus	1	1	1
Notorynchus cepedianus	1	1	1
Squaliformes			
Centroscyllium nigrum	1	1	0
Echinorhinus cookei	1	1	1
Somniosus pacificus	1	1	1
Squalus suckleyi	1	1	1
Squatiniformes			
Squatina californica	1	1	1
Heterodontiformes			
Heterodontus francisci	1	1	1
Orectolobiformes			
Rhincodon typus	1	1	1
Lamniformes			
Alopias pelagicus	1	0	0
Alopias superciliosus	1	0	0
Alopias vulpinus	1	1	1
Cetorhinus maximus	1	1	1
Carcharodon carcharias	1	1	1
Isurus oxyrinchus	1	1	1
Lamna ditropis	1	1	1
Megachasma pelagios	1	1	0
Mitsukurina owstoni	1	0	0
Odontaspis ferox	1	1	0
Carchariniformes			
Apristurus brunneus	1	1	1
Apristurus kampae	1	1	1
Cephaloscyllium ventriosum	1	1	1
Parmaturus xaniurus	1	1	1
Galeorhinus galeus	1	1	1
Mustelus henlei	1	1	1
Mustelus californicus	1	1	1
Triakis semifasciata	1	1	1
Carcharhinus brachyurus	1	0	0
Carcharhinus longimanus	1	0	0
Carcharhinus obscurus	1	0	0
Prionace glauca	1	1	1
Sphyrna lewini	1	0	0
Sphyrna tiburo	1	0	0
Sphyrna zygaena	1	1	1
Torpediniformes			
Torpedo californica	1	1	1
Rajiformes			
Bathyraja abyssicola	1	1	1
Bathyraja aleutica	0	0	1
Bathyraja interrupta	1	1	1
Bathyraja kincaidii	1	1	1
Bathyraja spinosissima	1	1	1
Bathyraja trachura	1	1	1
Raja binoculata	1	1	1
Raja inornata	1	1	1
Raja rhina	1	1	1
Raja stellulata	1	1	1
Platyrhinoidis triseriata	1	1	1
Rhinobatos productus	1	1	1
Zapteryx exasperata	1	1	0
Gymnura marmorata	1	0	0
Myliobatiformes			
Myliobatis californica	1	1	1
Pteroplatytrygon violacea	1	1	1
Urobatis halleri	1	1	1
Dasyatis dipterura	1	1	0
ACTINOPTERYGII			
Acipenseriformes			
Acipenser medirostris	1	1	1
Acipenser transmontanus	1	1	1
Albuliformes			
Albula sp. A	1	1	1
Notacanthus chemnitzii	1	1	1
Elopiformes			
Elops affinis	1	0	0
Anguilliformes			
Gymnothorax mordax	1	0	0
Muraena argus	1	0	0
Gnathophis cinctus	1	0	0
Myrophis vafer	1	0	0
Derichthys serpentinus	1	0	0
Facciolella equatorialis	1	0	0
Ophichthus triserialis	1	1	1
Ophichthus zophochir	1	1	1
Avocettina bowersii	1	1	1
Avocettina infans	1	1	1
Nemichthys larseni	1	1	1
Nemichthys scolopaceus	1	1	1
Serrivomer sector	1	1	1
Serrivomer jesperseni	1	1	1
Serrivomer samoensis	1	0	0
Venefica tentaculata	1	1	1
Saccopharyngiformes			
Cyema atrum	1	1	1
Saccopharynx lavenbergi	1	1	1
Eurypharynx pelecanoides	1	1	1
Clupeiformes			
Alosa sapidissima	1	1	1
Anchoa compressa	1	1	0
Anchoa delicatissima	1	0	0
Cetengraulis mysticetus	1	0	0
Clupea pallasii	1	1	1
Dorosoma petenense	1	1	1
Engraulis mordax	1	1	1
Etrumeus teres	1	1	1
Harengula thrissina	1	0	0
Opisthonema libertate	1	0	0
Opisthonema medirastre	1	0	0
Sardinops sagax	1	1	1
Siluriformes			
Bagre panamensis	1	0	0
Argentiniformes			
Alepocephalus tenebrosus	1	1	1
Argentina sialis	1	1	1
Bajacalifornia burragei	1	0	0
Bathylagoides wesethi	1	1	1
Bathylagus pacificus	1	1	1
Bathylychnops exilis	1	1	1
Conocara salmoneum	1	0	0
Dolichopteryx longipes	1	0	0
Holtbyrnia latifrons	1	1	1
Leptochilichthys agassizi	1	1	1
Leuroglossus stilbius	1	1	1
Macropinna microstoma	1	1	1

APPENDIX I, Continued
Presence (1) versus absence (0) by biogeographic region.

	SCB	SCC	MONT
Maulisia argipalla	1	1	1
Maulisia mauli	1	1	?
Mentodus eubranchus	1	1	1
Mirorictus taningi	1	1	?
Nansenia candida	1	1	1
Nansenia crassa	1	1	?
Narcetes stomias	1	1	1
Pseudobathylagus milleri	1	1	1
Sagamichthys abei	1	1	1
Talismania bifurcata	1	1	1
Salmoniformes			
Allosmerus elongatus	1	1	1
Hypomesus pretiosus	1	1	1
Spirinchus starksi	1	1	1
Spirinchus thaleichthys	1	1	1
Thaleichthys pacificus	0	1	1
Oncorhynchus clarki	0	0	1
Oncorhynchus gorbuscha	1	1	1
Oncorhynchus keta	1	1	1
Oncorhynchus kisutch	1	1	1
Oncorhynchus mykiss	1	1	1
Oncorhynchus tshawytscha	1	1	1
Stomiiformes			
Cyclothone acclinidens	1	1	1
Cyclothone alba	1	1	1
Cyclothone pallida	1	1	1
Cyclothone pseudopallida	1	1	1
Cyclothone signata	1	1	1
Diplophos proximus	1	0	0
Diplophos taenia	1	1	1
Gonostoma atlanticum	1	1	1
Argyropelecus affinis	1	1	1
Argyropelecus hemigymnus	1	1	1
Argyropelecus lychnus	1	0	0
Argyropelecus sladeni	1	1	1
Aristostomias scintillans	1	1	1
Bathophilus brevis	1	0	0
Bathophilus flemingi	1	1	1
Borostomias panamensis	1	1	1
Chauliodus macouni	1	1	1
Ichthyococcus elongatus	1	1	1
Ichthyococcus irregularis	1	1	1
Idiacanthus antrostomus	1	1	1
Idiacanthus fasciola	1	1	1
Malacosteus niger	1	1	1
Neonesthes capensis	1	1	1
Opostomias mitsuii	0	1	1
Photonectes margarita	1	1	1
Sternoptyx diaphana	1	1	1
Vinciguerria nimbaria	1	0	1
Vinciguerria poweriae	1	1	0
Woodsia nonsuchae	1	0	0
Alepisaurus ferox	1	1	1
Anotopterus nikparini	1	1	1
Arctozenus risso	1	1	1
Benthalbella dentata	1	1	1
Lestidiops pacificus	1	1	1
Lestidiops ringens	1	1	1
Lestidium nudum	1	1	1
Magnisudis atlantica	1	1	1
Scopelosaurus harryi	1	1	1
Stomias atriventer	1	1	1
Tactostoma macropus	1	1	1
Synodus lucioceps	1	1	1
Myctophiformes			
Bolinichthys pyrsobolus	1	0	0
Ceratoscopelus townsendi	1	1	1
Diaphus theta	1	1	1
Diogenichthys laternatus	1	0	0
Diogenichthys atlanticus	1	1	1
Electrona risso	1	1	1
Hygophum reinhardti	1	0	0
Lampadena urophaos	1	1	1
Lampanyctus jordani	1	1	1
Lampanyctus steinbecki	1	1	1
Loweina rara	1	1	1
Myctophum nitidulum	1	1	0
Nannobrachium bristori	1	1	1
Nannobrachium ritteri	1	1	1
Nannobrachium valdiviae	1	1	1
Notoscopelus resplendens	1	1	0
Protomyctophum crockeri	1	1	1
Scopelengys tristis	1	1	1
Stenobrachius leucopsarus	1	1	1
Stenobrachius nannochir	0	0	1
Symbolophorus californiensis	1	1	1
Taaningichthys bathyphilus	1	1	1
Taaningichthys paurolychnus	1	0	0
Tarletonbeania crenularis	1	1	1
Triphoturus mexicanus	1	1	1
Triphoturus nigrescens	1	1	1
Lampridiformes			
Desmodema lorum	1	1	?
Lampris guttata	1	1	1
Stylephorus chordatus	1	1	1
Trachipterus altivelis	1	1	1
Trachipterus fukuzakii	1	1	?
Zu cristatus	1	0	0
Ophidiiformes			
Brosmophycis marginata	1	1	1
Cataetyx rubrirostris	1	1	1
Chilara taylori	1	1	1
Dicrolene filamentosa	1	0	1
Lamprogrammus niger	0	1	1
Ophidion scrippsae	1	1	1
Sciadonus pedicellaris	1	1	1
Spectrunculus grandis	1	1	1
Gadiformes			
Albatrossia pectoralis	1	1	1
Antimora microlepis	1	1	1
Caelorinchus scaphopsis	1	1	1
Coryphaenoides acrolepis	1	1	1
Coryphaenoides cinereus	0	0	1
Coryphaenoides filifer	1	1	1
Coryphaenoides leptolepis	1	1	1
Gadus macrocephalus	1	1	1
Halargyreus johnsonii	0	0	1
Malacocephalus laevis	1	1	1
Melanonus zugmayeri	1	1	1
Merluccius productus	1	1	1
Merluccius angustimanus	1	0	0
Microgadus proximus	1	1	1
Nezumia liolepis	1	1	1
Nezumia stelgidolepis	1	1	1
Physiculus rastrelliger	1	1	1
Theragra chalcogramma	0	0	1
Batrachoidiformes			
Porichthys myriaster	1	0	0
Porichthys notatus	1	1	1
Lophiiformes			
Antennarius avalonis	1	0	0
Caulophryne jordani	1	0	0
Caulophryne polynema	1	0	0
Chaenophryne draco	1	1	1

APPENDIX I, Continued
Presence (1) versus absence (0) by biogeographic region.

	SCB	SCC	MONT
Chaenophryne longiceps	1	1	1
Chaenophryne melanorhabdus	1	1	1
Cryptopsaras couesii	1	1	1
Dolopichthys longicornis	1	1	1
Dolopichthys pullatus	1	0	0
Gigantactis gargantua	1	0	0
Gigantactis macronema	1	0	0
Gigantactis microdontis	1	0	0
Gigantactis savagei	1	0	0
Gigantactis vanhoeffeni	1	1	1
Himantolophus nigricornis	1	1	1
Himantolophus sagamius	1	1	1
Linophryne coronata	1	0	0
Linophryne racemifera	1	0	0
Lophiodes caulinaris	1	1	0
Lophiodes spilurus	1	1	1
Melanocetus johnsonii	1	1	1
Oneirodes acanthias	1	1	1
Oneirodes basili	1	0	0
Oneirodes eschrichtii	1	0	0
Oneirodes thompsoni	0	0	1
Zalieutes elater	1	1	1
Mugiliformes			
Mugil cephalus	1	1	1
Atheriniformes			
Atherinops affinis	1	1	1
Atherinopsis californiensis	1	1	1
Leuresthes tenuis	1	1	1
Beloniformes			
Cheilopogon heterurus	1	0	0
Cheilopogon pinnatibarbatus	1	1	1
Fodiator acutus	1	0	0
Euleptorhamphus viridis	1	0	0
Hyporhamphus naos	1	0	0
Hyporhamphus rosae	1	0	0
Cololabis saira	1	1	1
Strongylura exilis	1	1	1
Cyprinodontiformes			
Fundulus parvipinnis	1	1	0
Stephanoberyciformes			
Barbourisia rufa	1	1	1
Cetichthys parini	1	1	0
Cetostoma regani	1	1	1
Ditropichthys storeri	1	1	1
Eutaeniophorus festivus	1	1	1
Melamphaes acanthomus	1	0	0
Melamphaes longivelis	1	0	0
Melamphaes lugubris	1	1	1
Melamphaes parvus	1	1	1
Poromitra crassiceps	1	1	1
Poromitra megalops	1	0	0
Poromitra oscitans	1	1	?
Rondeletia loricata	1	1	1
Scopeloberyx robustus	1	1	1
Scopelogadus mizolepis	1	1	1
Beryciformes			
Anoplogaster cornuta	1	1	1
Zeiformes			
Zenopsis nebulosa	0	1	1
Gasterosteiformes			
Aulorhynchus flavidus	1	1	1
Cosmocampus arctus	1	1	1
Gasterosteus aculeatus	1	1	1
Hippocampus ingens	1	0	0
Macroramphosus scolopax	1	0	0
Syngnathus auliscus	1	0	0
Syngnathus californiensis	1	1	1
Syngnathus euchrous	1	0	0
Syngnathus exilis	1	1	1
Syngnathus leptorhynchus	1	1	1
Scorpaeniformes			
Scorpaena guttata	1	1	1
Scorpaena mystes	1	0	0
Scorpaenodes xyris	1	0	0
Sebastolobus alascanus	1	1	1
Sebastolobus altivelis	1	1	1
Sebastes aleutianus	1	1	1
Sebastes alutus	0	0	1
Sebastes atrovirens	1	1	1
Sebastes auriculatus	1	1	1
Sebastes aurora	1	1	1
Sebastes babcocki	1	1	1
Sebastes borealis	0	1	1
Sebastes brevispinis	1	1	1
Sebastes carnatus	1	1	1
Sebastes caurinus	1	1	1
Sebastes chlorostictus	1	1	1
Sebastes chrysomelas	1	1	1
Sebastes constellatus	1	1	1
Sebastes crameri	1	1	1
Sebastes crocotulus	1	1	1
Sebastes dalli	1	1	1
Sebastes diploproa	1	1	1
Sebastes elongatus	1	1	1
Sebastes emphaeus	0	0	1
Sebastes ensifer	1	1	1
Sebastes entomelas	1	1	1
Sebastes eos	1	1	1
Sebastes flavidus	1	1	1
Sebastes gilli	1	1	1
Sebastes goodei	1	1	1
Sebastes helvomaculatus	1	1	1
Sebastes hopkinsi	1	1	1
Sebastes jordani	1	1	1
Sebastes lentiginosus	1	0	0
Sebastes levis	1	1	1
Sebastes macdonaldi	1	1	0
Sebastes maliger	1	1	1
Sebastes melanops	1	1	1
Sebastes melanosema	1	1	1
Sebastes melanostomus	1	1	1
Sebastes miniatus	1	1	1
Sebastes mystinus	1	1	1
Sebastes nebulosus	1	1	1
Sebastes nigrocinctus	1	1	1
Sebastes ovalis	1	1	1
Sebastes paucispinis	1	1	1
Sebastes phillipsi	1	1	1
Sebastes pinniger	1	1	1
Sebastes proriger	1	1	1
Sebastes rastrelliger	1	1	1
Sebastes rosaceous	1	1	1
Sebastes rosenblatti	1	1	1
Sebastes ruberrimus	1	1	1
Sebastes rubrivinctus	1	1	1
Sebastes rufinanus	1	0	0
Sebastes rufus	1	1	1
Sebastes saxicola	1	1	1
Sebastes semicinctus	1	1	1
Sebastes serranoides	1	1	1
Sebastes serriceps	1	1	1
Sebastes simulator	1	1	1
Sebastes umbrosus	1	1	1
Sebastes wilsoni	1	1	1

APPENDIX I, Continued
Presence (1) versus absence (0) by biogeographic region.

	SCB	SCC	MONT
Sebastes zacentrus	1	1	1
Bellator xenisma	1	?	?
Prionotus stephanophrys	1	1	1
Anoplopoma fimbria	1	1	1
Erilepis zonifer	0	0	1
Hexagrammos decagrammus	1	1	1
Hexagrammos lagocephalus	0	1	1
Ophiodon elongatus	1	1	1
Oxylebius pictus	1	1	1
Pleurogrammus monopterygius	1	1	1
Zaniolepis frenata	1	1	1
Zaniolepis latipinnis	1	1	1
Rhamphocottus richardsonii	1	1	1
Artedius corallinus	1	1	1
Artedius fenestralis	0	1	1
Artedius harringtoni	1	1	1
Artedius lateralis	1	1	1
Artedius notospilotus	1	1	1
Ascelichthys rhodorus	0	1	1
Chitonotus pugetensis	1	1	1
Clinocottus acuticeps	0	0	1
Clinocottus analis	1	1	1
Clinocottus embryum	1	1	1
Clinocottus globiceps	1	1	1
Clinocottus recalvus	0	0	1
Cottus aleuticus	0	1	1
Cottus asper	1	1	1
Enophrys bison	0	0	1
Enophrys taurina	1	1	1
Hemilepidotus hemilepidotus	0	0	1
Hemilepidotus spinosus	1	1	1
Icelinus burchami	1	1	1
Icelinus cavifrons	1	1	1
Icelinus filamentosus	1	1	1
Icelinus fimbriatus	1	1	1
Icelinus limbaughi	1	0	0
Icelinus oculatus	1	0	0
Icelinus quadriseriatus	1	1	1
Icelinus tenuis	1	1	1
Jordania zonope	0	1	1
Leiocottus hirundo	1	0	1
Leptocottus armatus	1	1	1
Oligocottus maculosus	1	1	1
Oligocottus rimensis	1	1	1
Oligocottus rubellio	1	1	1
Oligocottus snyderi	1	1	1
Orthonopias triacis	1	1	1
Paricelinus hopliticus	1	1	1
Radulinus asprellus	1	1	1
Radulinus boleoides	1	1	1
Radulinus taylori	0	0	1
Radulinus vinculus	1	1	0
Ruscarius creaseri	1	1	1
Scorpaenichthys marmoratus	1	1	1
Synchirus gilli	1	1	1
Zesticelus profundorum	1	1	1
Blepsias cirrhosus	0	1	1
Nautichthys oculofasciatus	1	1	1
Dasycottus setiger	0	0	1
Psychrolutes phrictus	1	1	1
Agonomalus mozinoi	0	1	1
Agonopsis sterletus	1	1	1
Agonopsis vulsa	1	1	1
Anoplagonus inermis	0	0	1
Bathyagonus alascanus	0	0	1
Bathyagonus infraspinatus	0	0	1
Bathyagonus nigripinnis	0	0	1
Bathyagonus pentacanthus	1	1	1
Bathyagonus swanii	0	1	1
Chesnonia verrucosa	0	0	1
Odontopyxis trispinosa	1	1	1
Pallasina barbata	0	0	1
Podothecus accipenserinus	0	0	1
Stellerina xyosterna	1	1	1
Xeneretmus latifrons	1	1	1
Xeneretmus leiops	1	1	1
Xeneretmus ritteri	1	0	0
Xeneretmus triacanthus	1	1	1
Careproctus colletti	0	0	1
Careproctus cypselurus	0	1	1
Careproctus gilberti	0	1	1
Careproctus melanurus	1	1	1
Careproctus ovigerus	1	1	1
Elassodiscus caudatus	0	0	1
Elassodiscus tremebundus	0	0	1
Liparis florae	1	1	1
Liparis fucensis	0	1	1
Liparis mucosus	1	1	1
Liparis pulchellus	0	0	1
Nectoliparis pelagicus	1	1	1
Paraliparis albescens	0	0	1
Paraliparis cephalus	0	0	1
Paraliparis dactylosus	0	1	1
Paraliparis deani	0	0	1
Paraliparis nassarum	1	0	0
Paraliparis pectoralis	0	0	1
Paraliparis rosaceous	1	1	1
Paraliparis ulochir	1	?	1
Psednos cathetostomus	1	0	0
Rhinoliparis attenuatus	0	0	1
Rhinoliparis barbulifer	1	?	?
Perciformes			
Morone saxatilis	1	1	1
Howella brodiei	1	1	1
Stereolepis gigas	1	1	1
Mycteroperca jordani	1	0	0
Mycteroperca xenarcha	1	1	1
Epinephelus analogus	1	0	0
Epinephelus niphobles	1	1	0
Hemanthias signifer	1	0	0
Paralabrax clathratus	1	1	1
Paralabrax maculatofasciatus	1	1	1
Paralabrax nebulifer	1	1	1
Serranus aequidens	1	0	0
Pristigenys serrula	1	1	1
Apogon atricaudus	1	0	0
Apogon guadalupensis	1	0	0
Caulolatilus affinis	1	0	0
Caulolatilus princeps	1	1	1
Nematistius pectoralis	1	0	0
Echeneis naucrates	1	0	0
Phtheirichthys lineatus	1	0	0
Remora australis	1	1	1
Remora brachyptera	1	0	0
Remora osteochir	1	0	0
Remora remora	1	1	1
Remorina albescens	1	1	1
Coryphaena hippurus	1	1	1
Caranx caballus	1	1	1
Caranx sexfasciatus	1	0	0
Caranx vinctus	1	0	0
Chloroscombrus orqueta	1	0	0
Decapterus muroadsi	1	1	1
Naucrates ductor	1	1	1

APPENDIX I, Continued
Presence (1) versus absence (0) by biogeographic region.

	SCB	SCC	MONT
Selene brevoortii	1	0	0
Selene peruviana	1	0	0
Seriola lalandi	1	1	1
Seriola rivoliana	1	0	0
Trachinotus paitensis	1	0	0
Trachinotus rhodopus	1	0	0
Trachurus symmetricus	1	1	1
Uraspis helvola	1	0	0
Brama orcini	1	0	0
Pteraclis aesticola	1	1	1
Taractes asper	1	1	1
Taractichthys steindachneri	1	0	0
Caristius macropus	1	1	1
Lutjanus argentiventris	1	0	0
Lutjanus colorado	1	1	0
Lutjanus novemfasciatus	1	1	0
Lobotes pacificus	1	0	0
Anisotremus davidsoni	1	1	1
Conodon serrifer	1	0	0
Haemulon flaviguttatum	1	0	0
Microlepidotus inornatus	1	0	0
Xenistius californiensis	1	1	1
Calamus brachysomus	1	0	0
Polydactylus approximans	1	1	1
Polydactylus opercularis	1	0	0
Atractoscion nobilis	1	1	1
Cheilotrema saturnum	1	0	0
Cynoscion parvipinnis	1	0	0
Genyonemus lineatus	1	1	1
Menticirrhus undulatus	1	0	0
Roncador stearnsi	1	0	0
Seriphus politus	1	1	1
Umbrina roncador	1	0	0
Pseudupeneus grandisquamis	1	0	0
Chaetodon humeralis	1	0	0
Prognathodes falcifer	1	0	0
Girella nigricans	1	1	1
Hermosilla azurea	1	1	1
Kyphosus analogus	1	0	0
Medialuna californiensis	1	1	1
Sectator ocyurus	1	0	0
Amphistichus argenteus	1	1	1
Amphistichus koelzi	1	1	1
Amphistichus rhodoterus	0	1	1
Brachyistius frenata	1	1	1
Cymatogaster aggregata	1	1	1
Embiotoca jacksoni	1	1	1
Embiotoca lateralis	1	1	1
Hyperprosopon anale	1	1	1
Hyperprosopon argenteum	1	1	1
Hyperprosopon ellipticum	1	1	1
Hypsurus caryi	1	1	1
Micrometrus aurora	1	1	1
Micrometrus minimus	1	1	1
Phanerodon atripes	1	1	1
Phanerodon furcatus	1	1	1
Rhacochilus toxotes	1	1	1
Rhacochilus vacca	1	1	1
Zalembius rosaceus	1	1	1
Abudefduf troschelii	1	0	0
Azurina hirundo	1	0	0
Chromis alta	1	0	0
Chromis punctipinnis	1	1	1
Hypsypops rubicundus	1	1	1
Halichoeres semicinctus	1	1	0
Oxyjulis californica	1	1	1
Semicossyphus pulcher	1	1	1
Nicholsina denticulata	1	0	0
Rathbunella alleni	1	1	1
Rathbunella hypoplecta	1	0	0
Ronquilus jordani	1	1	1
Bothrocara brunneum	1	1	1
Bothrocara molle	1	1	1
Derepodichthys alepidotus	1	1	1
Eucryphycus californicus	1	1	1
Lycenchelys callista	1	?	1
Lycenchelys camchatica	1	1	1
Lycenchelys crotalinus	1	1	1
Lycodapus dermatinus	1	?	1
Lycodapus endemoscotus	1	1	1
Lycodapus fierasfer	1	1	1
Lycodapus mandibularis	1	1	1
Lycodes brevipes	1	1	1
Lycodes cortezianus	1	1	1
Lycodes diapterus	1	1	1
Lycodes pacificus	1	1	1
Lyconema barbatum	1	1	1
Melanostigma pammelas	1	1	1
Taranetzella lyoderma	1	1	1
Anoplarchus insignis	0	0	1
Anoplarchus purpurescens	1	1	1
Cebidichthys violaceus	1	1	1
Chirolophis decoratus	1	1	1
Chirolophis nugator	1	1	1
Ernogrammus walkeri	1	1	1
Esselenichthys carli	1	1	1
Esselenichthys laurae	1	1	1
Kasatkia seigeli	0	1	1
Lumpenopsis clitella	1	0	0
Lumpenus sagitta	0	0	1
Phytichthys chirus	1	1	1
Plagiogrammus hopkinsi	1	1	1
Plectobranchus evides	1	1	1
Poroclinus rothrocki	1	1	1
Xiphister atropurpureus	1	1	1
Xiphister mucosus	1	1	1
Cryptacanthodes aleutensis	0	0	1
Cryptacanthodes giganteus	0	0	1
Apodichthys flavidus	1	1	1
Apodichthys fucorum	1	1	1
Apodichthys sanctaerosae	1	1	1
Pholis clemensi	0	0	1
Pholis schultzi	0	1	1
Anarrhichthys ocellatus	1	1	1
Zaprora silenus	1	1	1
Scytalina cerdale	0	1	1
Trichodon trichodon	0	0	1
Ammodytes hexapterus	1	1	1
Kathetostoma averruncus	1	1	0
Chiasmodon niger	1	1	1
Dysalotus oligoscolus	1	0	0
Kali indica	1	1	1
Kali normani	1	0	0
Alloclinus holderi	1	0	0
Cryptotrema corallinum	1	0	0
Paraclinus integripinnis	1	0	0
Gibbonsia elegans	1	1	0
Gibbonsia metzi	1	1	1
Gibbonsia montereyensis	1	1	1
Heterostichus rostratus	1	1	1
Chaenopsis alepidota	1	0	0
Neoclinus blanchardi	1	1	1
Neoclinus stephensae	1	1	1
Neoclinus uninotatus	1	1	1

APPENDIX I, Continued
Presence (1) versus absence (0) by biogeographic region.

	SCB	SCC	MONT
Hypsoblennius gentilis	1	1	1
Hypsoblennius gilberti	1	1	0
Hypsoblennius jenkinsi	1	1	0
Plagiotremus azaleus	1	0	0
Icosteus aenigmaticus	1	1	1
Gobiesox eugrammus	1	0	0
Gobiesox maeandricus	1	1	1
Gobiesox papillifer	1	0	0
Gobiesox rhessodon	1	1	0
Rimicola cabrilloi	1	0	0
Rimicola dimorpha	1	0	0
Rimicola eigenmanni	1	0	0
Rimicola muscarum	1	1	1
Synchiropus atrilabiatus	1	0	0
Dormitator latifrons	1	0	0
Acanthogobius flavimanus	1	1	1
Clevelandia ios	1	1	1
Ctenogobius sagitta	1	0	0
Eucyclogobius newberryi	1	1	1
Gillichthys mirabilis	1	1	1
Ilypnus gilberti	1	1	1
Lepidogobius lepidus	1	1	1
Lethops connectens	1	1	1
Lythrypnus dalli	1	1	0
Lythrypnus zebra	1	1	1
Quietula y-cauda	1	1	0
Rhinogobiops nicholsii	1	1	1
Tridentiger trigonocephalus	1	0	1
Typhlogobius californiensis	1	1	0
Chaetodipterus zonatus	1	0	0
Luvarus imperialis	1	1	1
Sphyraena argenteum	1	1	1
Sphyraena ensis	1	0	0
Diplospinus multistriatus	1	1	0
Lepidocybium flavobrunneum	1	1	1
Ruvettus pretiosus	1	1	1
Aphanopus intermedius	1	1	1
Assurger anzac	1	0	0
Lepidopus fitchi	1	1	1
Benthodesmus pacificus	0	0	1
Trichiurus nitens	1	0	0
Auxis rochei	1	0	0
Auxis thazard	1	0	0
Euthynnus affinis	1	0	0
Euthynnus lineatus	1	1	0
Katsuwonus pelamis	1	1	1
Sarda chilensis	1	1	1
Scomber japonicus	1	1	1
Scomberomorus concolor	1	1	1
Scomberomorus sierra	1	0	0
Thunnus alalunga	1	1	1
Thunnus albacares	1	1	0
Thunnus obesus	1	1	1
Thunnus orientalis	1	1	1
Xiphias gladius	1	1	1
Istiophorus platypterus	1	0	0
Makaira indica	1	0	0
Makaira nigricans	1	0	0
Tetrapturus angustirostris	1	0	0
Tetrapturus audax	1	0	0
Icichthys lockingtoni	1	1	1
Cubiceps baxteri	1	0	0
Cubiceps capensis	1	0	0
Cubiceps paradoxus	1	0	0
Psenes Pellucidus	1	0	0
Tetragonurus cuvieri	1	1	1
Peprilus simillimus	1	1	1
Pleuronectiformes			
Atheresthes stomias	1	1	1
Citharichthys sordidus	1	1	1
Citharichthys stigmaeus	1	1	1
Citharichthys xanthostigma	1	1	1
Embassichthys bathybius	1	1	1
Engyophrys sanctilaurentii	1	0	0
Eopsetta jordani	1	1	1
Glyptocephalus zachirus	1	1	1
Hippoglossina stomata	1	1	1
Hippoglossoides elassodon	0	0	1
Hippoglossus stenolepis	1	1	1
Isopsetta isolepis	1	1	1
Lepidopsetta bilineata	1	1	1
Lyopsetta exilis	1	1	1
Microstomus pacificus	1	1	1
Paralichthys californicus	1	1	1
Parophrys vetulus	1	1	1
Platichthys stellatus	1	1	1
Pleuronichthys coenosus	1	1	1
Pleuronichthys decurrens	1	1	1
Pleuronichthys guttulata	1	1	1
Pleuronichthys ritteri	1	1	1
Pleuronichthys verticalis	1	1	1
Psettichthys melanostictus	1	1	1
Reinhardtius hippoglossoides	0	1	1
Xystreurys liolepis	1	1	1
Symphurus atricauda	1	1	1
Tetraodontiformes			
Balistes polylepis	1	1	1
Chilomycterus reticulatus	1	0	0
Diodon holocanthus	1	0	0
Diodon hystrix	1	0	0
Lagocephalus lagocephalus	1	1	1
Lactoria diaphana	1	1	1
Mola mola	1	1	1
Ranzania laevis	0	1	1
Sphoeroides annulatus	1	0	0
Sphoeroides lobatus	1	0	0
Xanthichthys mento	1	0	0
Regional Total	**669**	**527**	**538**
Grand Total			**732**

STABILITY OF TRACE ELEMENTS IN OTOLITHS OF JUVENILE PACIFIC SARDINE *SARDINOPS SAGAX*

BARBARA J. JAVOR
Ocean Associates Inc., under contract to
Southwest Fisheries Science Center
National Oceanographic and Atmospheric Administration
8901 La Jolla Shores Drive
La Jolla, CA 92037
ph: +1-858-546-5679
fax: +1-858-546-5652
barbara.javor@noaa.gov

EMMANIS DORVAL
Ocean Associates Inc., under contract to
Southwest Fisheries Science Center
National Oceanographic and Atmospheric Administration
8901 La Jolla Shores Drive
La Jolla, CA 92037

ABSTRACT

We evaluated trace element analysis of otoliths of juvenile Pacific sardine *Sardinops sagax* by inductively coupled plasma mass spectrometry as a potential method to identify regional stocks. Otolith treatment experiments determined the stability of trace elements. Hydrogen peroxide treatment slightly affected Mn, Sr, and Ba, but it removed 35%–43% of Mg and 51% of P. Growth experiments identified ontogenetic and temperature factors that influenced trace element composition. Otolith weight was a major determinant of composition. Mn, Sr, and Ba each had unique ontogenetic and temperature responses. Mg/Ca and P/Ca ratios covaried and decreased with growth at 16°–19°C but increased with growth at 21°C. The decrease in Mg/Ca and P/Ca ratios with age was nonconservative, i.e., the total mass of initially deposited Mg and P decreased as the otoliths grew. The results contradict the assumption that all deposited trace elements are permanently incorporated in otoliths in living fish.

INTRODUCTION

Pacific sardine

Pacific sardine *Sardinops sagax* (Jenyns 1842) occur along approximately 5000 km of coastal waters of North America between Canada and the Baja California peninsula into the Gulf of California, Mexico. Integrated assessment of the fisheries in Canada, the United States (USA), and Mexico requires identification of regional stocks of mature and immature sardine along with knowledge of their spawning habits and migration patterns. It is believed that three North American stocks exist with synchronous, seasonal, north-south migration patterns (Félix-Uraga et al. 2004, 2005) although little genetic structure has been detected (Hedgecock et al. 1989; Grant and Bowen 1998; Pereyra et al. 2004; García-Rodríguez et al. 2011).

Methods that have had some success in identifying regional stocks and migrations include egg, larval, and adult surveys (Lo et al. 2005, 2010, 2011); vertebral counts and tags (Smith 2005); temperature at catch (Félix-Uraga et al. 2004, 2005); analysis of spawning habitats (Reiss et al. 2008; Demer et al. 2012); fish and otolith aging and morphometric analysis (Javor et al. 2011; Javor 2013; Vergara-Solana et al. 2013); and otolith stable isotope measurements (Valle and Herzka 2008; Dorval et al. 2011; Javor and Dorval 2014).

Differences in spawning and feeding regions and changes in seasonal temperature and salinity could offer further evidence of stock structure if they are reflected in trace element composition of otoliths. Sardine spawn at 12°–14°C off southern and central California in the spring with a peak around April (Lo et al. 2005; Reiss et al. 2008). However, the temperature range of sardine habitats is broad, from less than 10°C in the Pacific Northwest (Emmett et al. 2005) to over 25°C in their southern range in the Gulf of California (Mitchell et al. 2002; Félix-Uraga et al. 2004, 2005). Because mature sardine cross regions during migrations, trace elements incorporated into adult otoliths might not give clear signals of stock identity. Juveniles that are incapable of long-distance swimming are believed to remain within or near the water masses where they were spawned. They might provide relatively distinct regional chemical signatures in their otoliths.

Chemistry of biogenic calcium carbonate

Fish otoliths are biogenic calcium carbonate (aragonite) bodies that form in sacculus endolymph fluid secreted from blood plasma. Unlike biogenic calcium carbonate produced by bivalves and corals, otoliths remain internal within the growing fish. Endolymph is an extracellular fluid with gradients and diurnal fluctuations in dissolved ions, proteins, and pH that influence otolith growth (Edeyer et al. 2000; Payan et al. 2002, 2004; Borelli et al. 2003; Takagi et al. 2005; Guibbolini et al. 2006).

Some trace elements typically detected in otoliths may have important functions in animal metabolism (e.g., Mg and P roles in ATP and nucleic acid metabolism) while others have no known biological functions (e.g., Ba). Some trace elements associate with growing otoliths, clam shells, and corals without forming true

crystalline mineral structures in calcium carbonate. The associations may be strong (e.g., ionic bonds) or weak (e.g., adsorption), or chelation with organic ligands. For example, Mg is believed to be largely associated with the organic matrix in bivalves and corals (Watanabe et al. 2001; Takesue et al. 2008; Foster et al. 2008; Jacob et al. 2008; Schöne et al. 2010; Yoshimura et al. 2014; Poulain et al. 2015), while P (as phosphate) is associated either with small domains of hydroxylapatite or amorphous phosphate-carbonate microstructures in newly formed bivalve shells (Xu and Zhang 2014) and corals (Mason et al. 2011; Zhang et al. 2011). The stability of the associations between calcium carbonate and trace elements in biogenic aragonite depends on multiple factors including charge, ionic radii, steric criteria, competing ions, concentration, rate of formation, and the physical structure of the calcium carbonate crystals (Stipp 1998; Watson 2004; Gaetani and Cohen 2006; Gabitov et al. 2006, 2008).

The pioneering work of Campana (1983) showed ^{45}Ca incorporated into salmon otoliths did not resorb within two days after ^{45}Ca exposure. No studies have shown unequivocal calcium loss from otoliths, although an investigation using fluorescent staining techniques demonstrated Ca^{2+} can translocate in otoliths after initial deposition (Beier et al. 2004). It is generally accepted that "any elements or compounds accreted onto its growing surface are permanently retained" in an otolith and serve as permanent natural tags (Campana 1999). However until recently (Veinott et al. 2014), experimental investigations have not been conducted to demonstrate all trace elements are as stable as calcium during otolith growth.

Numerous studies have used otolith trace element chemistry to identify fish stocks. Investigations have addressed factors that influence elemental partitioning into otoliths such as temperature, salinity (Fowler et al. 1995; Hoff and Fuiman 1993; Elsdon and Gillanders 2002; Bath Martin and Wuenschel 2006), age, and ontogeny (Begg et al. 1998; Rooker et al. 2001; Brophy et al. 2003; Ruttenberg et al. 2005). Research has also focused on post-mortem processing and contamination that could alter trace element concentrations (Milton and Chenery 1998; Proctor and Thresher 1998; Rooker et al. 2001; Brophy et al. 2003; Swan et al. 2006). In general, instability of trace elements in otoliths has been treated as a problem to avoid rather than addressing it as a natural factor in vivo.

This investigation

In order to interpret otolith trace element composition in surveys to identify and differentiate regional populations of immature Pacific sardine, we conducted several experiments to determine factors that affected trace element incorporation. We captured juvenile sardine off San Diego, California, USA (32.7°N) to use to track otolith composition under controlled conditions: otolith treatment experiments to measure trace element stability using protocols similar to published methods for bivalves and corals (experiment 1); culture at ambient temperature to determine ontogenetic effects (experiments 2 and 3); and culture at different temperatures to evaluate thermal effects (experiment 4).

We postulated four hypotheses to explain possible outcomes of the growth experiments. The hypotheses compare the ratios of trace elements to calcium (TE/Ca) vs. otolith weight in whole otoliths at the beginning of the experiment (time-0, "core") with those at the end of the experiment (fig. 1, H1–H4). For the purpose of depicting the hypotheses, all time-0 otoliths are shown as lightly stippled figures whereas the color intensity at the end of the experiments represents higher (darker) or lower (no color) element ratios. H1 predicts TE/Ca ratios at the end of the experiment will be the same as the time-0 otoliths. H2 predicts TE/Ca ratios will increase with growth. H3 predicts TE/Ca ratios will decrease with growth with the most extreme case being no deposition of a trace element in the new aragonite. The H3 curve in Figure 1 represents the minimum TE/Ca ratios expected in the whole otoliths, i.e., a dilution curve of core trace elements. H4 is similar to H3 but it also predicts loss of trace elements from the core during the experimental growth period. The trajectory of the H4 curve will be lower than the dilution curve predicted by H3. In light of the results, we discuss the possibility that some elements that associate with noncrystalline matrices at the time of initial otolith formation might be subject to in vivo loss during subsequent growth.

MATERIAL AND METHODS

Juvenile sardine for both the otolith treatment experiment (experiment 1) and growth experiments (experiments 2, 3, 4) were captured in waters off San Diego, California (USA) in the surf zone by beach seine or just offshore by a live bait seiner (Everingham Bros.). It was not possible to capture the same size fish for all the experiments.

Otolith treatment, experiment 1

Experiment 1 tested the effects of otolith treatment methods on weight change and trace element composition. Using both sagittal otoliths from each fish, one otolith was randomly selected and assigned to a specific treatment method, whereas the opposite otolith was used as the control (treated similarly in purified MilliQ™ water, MQ-H_2O, to account for aqueous leaching). The combined effects of time, chemical solution, and temperature were tested in five experimental treatments (table 1) including two time periods in unbuffered 30%

TABLE 1
Summary of factors and experimental treatments for otolith analysis in experiment 1. All samples were analyzed at SIO except treatment F (UCSB).

		Treatment					
Factor	Control	A	B	C	D	E	F
Time	16 h	30 sec	2 h	2 h	2 h	16 h	24 h
Solution	MQ-H_2O	HNO_3	SDS	Pro K	H_2O_2	H_2O_2	H_2O_2
Temperature	Ambient	Ambient	37°C	55°C	Ambient	Ambient	Ambient

TABLE 2
Experimental details of *S. sagax* culture experiments 2, 3, and 4. Growth parameters reported as averages ± S.D.

Experiment	Age at Time-0	Duration of expt	*n*, Time-0	*n*, End	SL (mm)	Fish wt (g)	Otolith wt (mg)
2	6 mo	8 mo					
Time-0			10		69.3 ± 4.2	2.8 ± 0.5	0.338 ± 0.027
End				32	105.2 ± 20.9	17.8 ± 10.9	0.832 ± 0.206
Range					71.0 – 138.0	3.9 – 39.2	0.496 – 1.197
3	~10 mo	5 mo					
Time-0			10		118.5 ± 14.5	13.2 ± 5.1	0.840 ± 0.155
Tank 1				10	147.2 ± 7.6	46.4 ± 9.0	1.037 ± 0.123
Tank 2				10	155.8 ± 10.6	61.8 ± 14.4	1.120 ± 0.115
4	~8 mo	11 mo					
Time-0			10		118.0 ± 8.7	14.9 ± 2.9	0.695 ± 0.055
13°C				10	158.9 ± 11.7	55.9 ± 10.7	1.135 ± 0.143
17°C				10	167.6 ± 10.9	64.7 ± 12.6	1.404 ± 0.130
21°C				12	156.0 ± 10.2	52.7 ± 8.7	1.348 ± 0.141

hydrogen peroxide (J.T. Baker Ultrex II Ultrapure). Watanabe et al. (2001), Krause-Nehring et al. (2011), and Holcomb et al. (2015) used unbuffered 30% H_2O_2 in their treatment protocols with bivalves and corals, and we followed suit. Watanabe et al. (2001) found little difference in the results between buffered and unbuffered H_2O_2 in their experiments. We tested 30 sec exposure to 0.1% nitric acid. We also tested two solutions to solubilize proteins: 2% sodium dodecyl sulfate (SDS; Gibco-BRL UltraPURE) dissolved in MQ-H_2O, and proteinase K (ProK, USB Corp.) dissolved in 100 mM Tris-HCl, pH 8.0, to a working concentration of 1 mg ml^{-1}. For weight change measurements after these treatments, an additional set of control otoliths was evaluated in which both left and right otoliths were soaked in MQ-H_2O for 2 h. For the control and treatments A–E, the average initial weight of the otoliths (± standard deviation, S.D.) was 0.720 ± 0.090 mg. The sardine were approximately one year old.

Except for the acid treatment that was performed on glass microscope slides, each otolith was treated in a small volume of the test solution in a 0.5 ml microfuge tube by periodically tumbling it gently with a pipette or by flicking the tube. After each treatment, the otoliths were washed with a pipette by gentle tumbling with at least four changes of MQ-H_2O. After drying they were reweighed. A follow-up assay was conducted to verify repeatability of the overnight treatment with H_2O_2. The experimental otoliths were treated for 24 h with unbuffered 30% H_2O_2 from a freshly opened bottle (treatment F, table 1). The juveniles in treatment F were captured in the same seine haul as those used for growth experiment 2 described below and in Table 2. Phosphorus was measured in treatment F, but not in treatments A through E.

Growth experiments 2, 3, and 4

Wild-caught juveniles were maintained in tanks at our facility on a 12 h light/12 h dark cycle. They were fed a commercial pellet diet, Bio-diet brood formulation (Bio-Oregon), *ad libitum* in temperature-regulated, circular (1.83 m diameter, 1600 L) or elliptical (1.5 x 3.0 m diameter, 3200 L) tanks with an approximate daily turnover of ten seawater volumes. Seawater was obtained from the Scripps Institution of Oceanography pier where little variation in salinity has been noted. Surface seawater salinity measured quarterly during 1990–2012 from three nearshore sampling stations within 27 km of the pier averaged 33.470 ± 0.168 (S.D., n = 279)

(www.calcofi.org, accessed 30 January 2014). Average monthly sea surface temperature at the site of collection ranges between 13.9° and 20.0°C, with an annual average of 16.6°C (www.nodc.noaa.gov/dsdt/cwtg/spac.html, accessed 12 February 2015). Fish that died during the experiments were removed but not enumerated. All the growth experiments were conducted between 2004 and 2006.

Table 2 lists experimental details for the growth experiments. The experiments were designed to evaluate whether any of the four hypotheses, H1–H4, described the outcomes of the trace element ratios in otoliths between the time-0 fish and the fish at the end of the experimental growth period. Ten fish were randomly selected at time-0. To determine ontogenetic effects on otolith trace elements, experiment 2 used juveniles from a single school that were raised in one tank for eight months at ambient temperature (16° to 19°C for most of the period). At time-0 the average age based on counts of daily otolith increments was six months (Takahashi and Checkley 2008). Experiment 3 further examined ontogenetic effects, this time with fish from a single seine haul maintained for five months in duplicate tanks. The age at time-0 was estimated to be about ten months based on a presumed April birthday.

In experiment 4, which assessed thermal effects on trace element deposition in otoliths, juveniles were cultured in duplicate tanks at 13°, 17°, or 21°C. Wild immature sardine near San Diego experience this temperature range during the course of a year (Javor and Dorval 2014). Experimental details are described in Dorval et al. (2011). Based on previous data, we converted fork length to standard length by subtracting 3 mm.

Otolith preparation

Growth experiments 2, 3, and 4 used primarily left otoliths for analysis. No difference in trace element composition was noted between left and right otoliths in preliminary measurements. After initially cleaning in MQ-H_2O, otoliths were dried, weighed on a Cahn C-33 microbalance (0.005 mg accuracy), and stored in plastic microfuge tubes.

All glass and plastic implements were cleaned in 10% nitric acid. Otoliths were further prepared in a Class 100 clean room. Sardine otoliths are fragile and often break during the sonication step of standard cleaning protocols. We developed a procedure that avoided breaking the otoliths while minimizing dissolution during cleaning: 30 min in 2% SDS, at least four MQ-H_2O washes, 3–5 min in unbuffered 30% H_2O_2, and four final MQ-H_2O washes. Each otolith was checked under a microscope after the washing steps, and further cleaned with glass probes if necessary. Most otoliths did not require additional cleaning after the washing protocols.

Inductively coupled plasma mass spectrometry (ICPMS)

For treatment experiment 1 and growth experiments 2 and 3, otoliths were dissolved in 2% HNO_3 (Fisher Optima) with 2 ppb In for trace element analysis by solution-based ICPMS on a Finnegan MAT Element 2 instrument. Due to unavoidable circumstances, different spectrometers were used during the course of the study. The instruments were at Scripps Institution of Oceanography (SIO, La Jolla, California), University of California Santa Barbara (UCSB), Old Dominion University (ODU, Norfolk, Virginia), or Woods Hole Oceanographic Institute (WHOI; Woods Hole, Massachusetts). Given the documented variations in trace element measurements determined in different laboratories and with different instruments (Campana et al. 1997), we tried to minimize any biases that the different spectrometers might have introduced (described below).

Analysis of whole otoliths by solution-based ICPMS allowed us to calculate mass balances and relative gain or loss of trace elements in treatment experiment 1 and at the beginning and end of growth experiments 2 and 3. In experiment 1, otolith samples from treatments A through E plus the control set were analyzed in a single run at SIO, whereas treatment F was analyzed at UCSB. Because we were interested in measuring percent gain or loss in each treatment, bias in elemental concentration measurement due to laboratory-specific spectrometer procedures would not have had any significant effects on our results. For experiment 2, analysis was conducted in a single run at ODU so the results were internally consistent. For experiment 3, analysis at SIO was conducted in a single run.

Solution samples were randomized in sets of eight samples in blocks between a blank (to determine minimum detection limits and baseline) and a repeating standard (to determine drift). The detection limits were similar for the different spectrometers. Average detection limits were: ^{24}Mg, 0.01 ppb; ^{31}P, 0.22 ppb; ^{48}Ca, 0.01 ppm; ^{55}Mn, <0.01 ppb; ^{88}Sr, 0.01 ppb; and ^{137}Ba, <0.01 ppb (determined at ODU). Standards for solution-based ICPMS were prepared by diluting a stock mixture in 2% HNO_3 (Fisher Optima) with similar element ratios as determined in preliminary analyses of sardine otoliths: 200 ppm Ca, 30 ppb Mg, 300 ppb P, 2 ppb Mn, 300 ppb Sr, 8 ppb Ba, and 2 ppb In as internal standard. Conversion of gravimetric units to molar ratios of the standards yielded the following ratios: Mg/Ca, 0.247 mmol mol^{-1}; P/Ca, 1.935 mmol mol^{-1}; Sr/Ca, 0.685 mmol mol^{-1}; Mn/Ca, 7.280 μmol mol^{-1}; and Ba/Ca, 11.660 μmol mol^{-1}. All elements except P were prepared from certified trace element standards obtained from High Purity Standards, CPI International, or Spex CertiPrep. The phosphorus stock

solution was prepared from reagent grade sodium phosphate (Fisher Scientific).

For experiment 4 in which temperature was the tested variable, laser ablation ICPMS (LA-ICPMS) of the distal edges of whole otoliths was conducted at WHOI using a UP 213 (New Wave Research) laser ablation sampler to monitor changes between time-0 fish and experimental fish. We did not compare measured trace element concentrations by the two analytical methods (solution vs. laser ablation) because we did not intercalibrate the two methods. Rather, we evaluated the results between the beginning and the end of each temperature treatment to assess trends in trace element ratios. LA-ICPMS employed two solid standards: Canadian National Research Council FEBS-1, a certified otolith reference material from the red snapper *Lutjanus campechanus*; and a second otolith material prepared from the red emperor *Lutjanus sebae* (Yoshinaga et al. 2000). Neither standard quantified phosphorus, which is reported as the ratio of counts per second (cps) of P/Ca after subtracting the blank values. For intact otoliths sampled by laser ablation, mean RSD(%) were: Mg, 6.16%; Ca, 5.27%; Sr, 2.85%; and Ba, 3.68%. RSD values for P and Mn were not provided by WHOI.

Inductively coupled plasma-optical emission spectrometry

The elemental composition of seawater is generally conservative, and surface seawater near SIO pier showed little variation in salinity over 23 years (noted above). To corroborate those findings for our experiments, a PerkinElmer 3700 optical emission plasma spectrometer at SIO was used to measure Ca, Mg, and Sr in seawater in the sardine-rearing tanks. Seawater was first diluted with MQ-H_2O. Analysis of each of the tanks on 11 monthly dates during growth experiment 4 revealed no significant variations in the concentrations and ratios of the three elements (data not shown). No further seawater analyses were conducted for the other experiments.

Data analysis

Relationships between otolith weight and trace element ratios were primarily determined by correlation analysis and linear regressions either as individual fish or as the averages of pooled fish as described in Results. For growth experiments 2 and 3, theoretical dilution curves of trace element ratios were calculated based on the molar concentrations of the trace elements and Ca in otoliths of known weight in time-0 samples, assuming the increase in otolith weight with growth was due to the accretion of $CaCO_3$ only (H3, fig. 1). We compared empirical data with the H3 curves for each element ratio using nonlinear models. Our criteria for testing the H4 hypothesis to explain the results after the growth

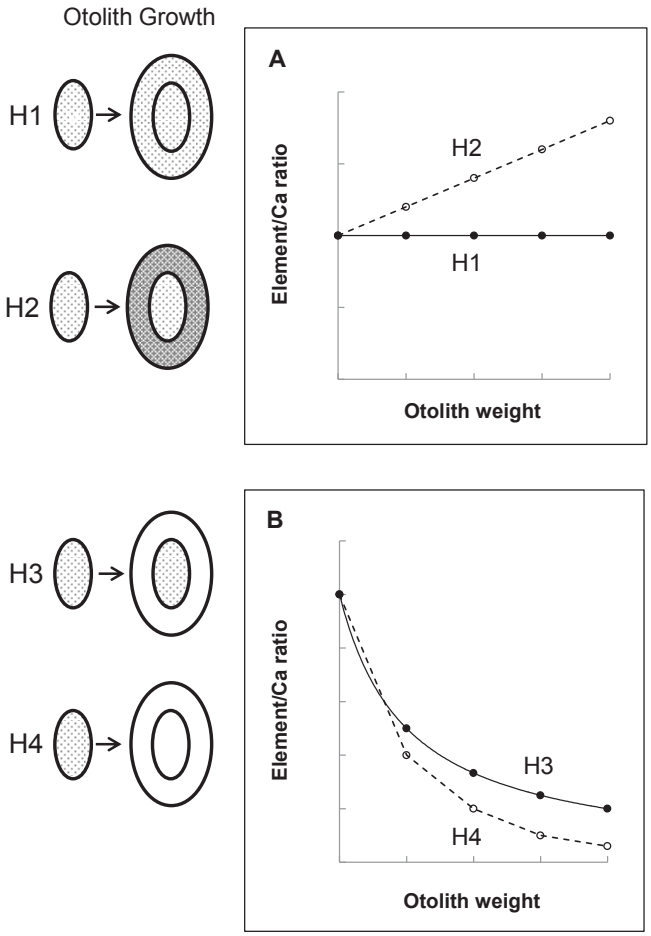

Figure 1. Four hypotheses (H1-H4) explaining possible outcomes of trace element ratios vs. otolith weight in the growth experiments. See explanation in the text.

period were based on determining whether the theoretical dilution curve described by H3 fell within the 95% confidence intervals (CI) of the predicted TE/Ca curve derived from experimental data.

Nonlinear models. Nonlinear models were developed for relating trace element ratios to otolith weight in growth experiment 2. A 3-parameter, negative exponential model was fitted to the data for Mg/Ca, P/Ca, Sr/Ca, and Ba/Ca ratios (Eq. 1), whereas a 2-parameter exponential model was used for Mn/Ca ratios (Eq. 2). The Marquardt optimization method was used to estimate parameters for all models using SAS software (version 9.2; Cary, North Carolina). The 95% confidence intervals were calculated for the expected value of element ratio-at-weight predicted from each model. These confidence intervals allowed comparison between the trajectory of element ratio-at-weight from the theoretical dilution curve to the expected value (H3) and associated uncertainties predicted from the empirically-derived models. The percentage of the variability explained from the data by each model is

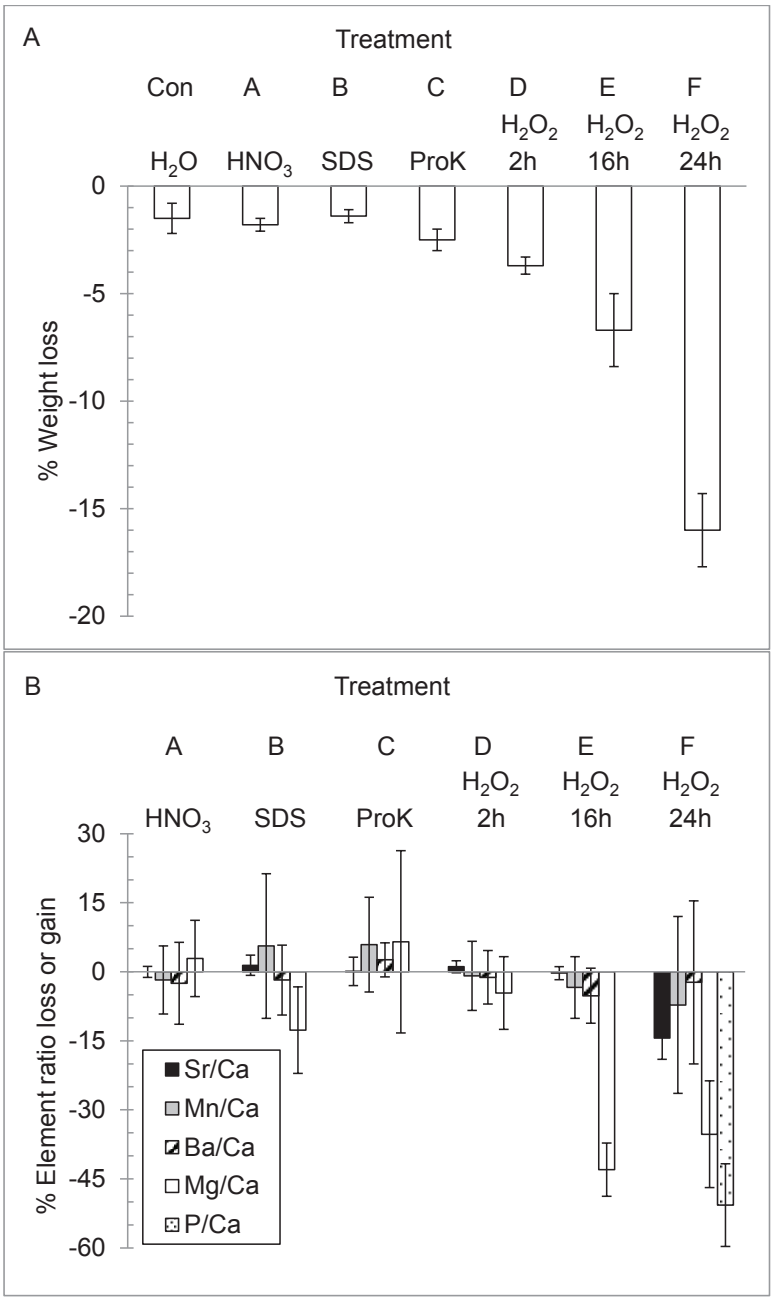

Figure 2. Experiment 1: Effects of treatments (Table 1) on juvenile *S. sagax* otoliths. The loss of otolith weight and changes in trace element composition are compared to otoliths treated with MQ-H_2O. A: Weight loss ± S.D., n = 6-8. B: Element loss (based on molar ratio to Ca) ± S.D., n = 5-8. Details are in the text.

reported using the R^2 value after adjustment for the degree of freedom:

$$(1) \quad y = y_0 + a \times e^{(-b \times w)}$$

$$(2) \quad y = a \times e^{(-b \times w)}$$

where y is the element ratio measured for each otolith, y_0 is the intercept of the model, a and b are the regression coefficients, and w is the otolith weight (mg) from each individual fish.

RESULTS

Otolith treatment, experiment 1

Weight losses of <3% after brief exposure to weak acid and protocols to dissolve proteins (treatments A–C) were similar to the control treatment in experiment 1 (fig. 2A). Overnight immersion in H_2O_2 caused more substantial weight loss (7%–16%) and a change of the sheen of the otoliths from shiny to dull (treatments E and F). The percent change of each element (calculated from molar ratios

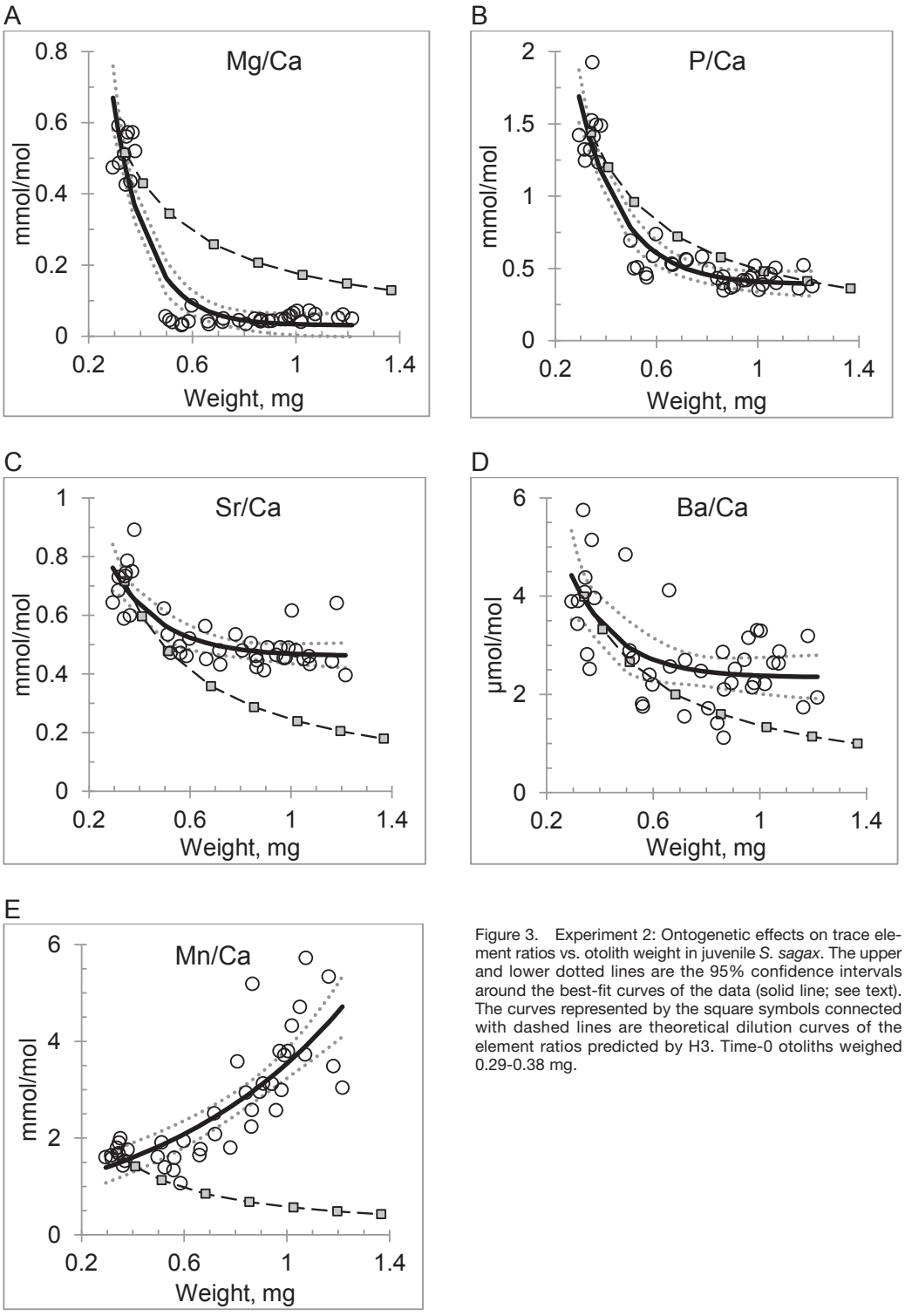

Figure 3. Experiment 2: Ontogenetic effects on trace element ratios vs. otolith weight in juvenile *S. sagax*. The upper and lower dotted lines are the 95% confidence intervals around the best-fit curves of the data (solid line; see text). The curves represented by the square symbols connected with dashed lines are theoretical dilution curves of the element ratios predicted by H3. Time-0 otoliths weighed 0.29-0.38 mg.

to Ca) in the treated otolith relative to the control otolith from the same fish indicated Sr/Ca, Mn/Ca, and Ba/Ca ratios were generally unaffected by the treatments, gaining or losing an average of ≤6% of the untreated value (fig. 2B). Mg/Ca ratios decreased by 13% after SDS treatment, and by 35%–43% after overnight treatment in 30% H_2O_2. Overnight immersion in 30% H_2O_2 from a freshly opened bottle also resulted in the loss of 51% of the P/Ca ratios in the otoliths in treatment F. Although the average weights of the otoliths were different in treatments A–E (0.720 mg) and F (0.339 mg), overnight immersion in H_2O_2 resulted in similar percent losses of Mg.

TABLE 3
Trace element ratios in otoliths of *S. sagax* in growth experiment 3. Average molar ratios (± S.E.) for Time-0, after growth in duplicate tanks (Time-End), and theoretical ratios if no further trace elements were incorporated after Time-0 based on H3 predictions. Mg/Ca, P/Ca, and Sr/Ca are mmol mol^{-1}; Mn/Ca and Ba/Ca are µmol mol^{-1}.

Sample	Mg/Ca	P/Ca	Mn/Ca	Sr/Ca	Ba/Ca
Time-0	0.267 ± 0.029	1.239 ± 0.132	2.563 ± 0.431	0.522 ± 0.024	3.108 ± 0.527
Time-End	0.063 ± 0.007	0.681 ± 0.078	3.276 ± 0.279	0.436 ± 0.018	1.937 ± 0.480
H3 Prediction	0.198	0.920	1.903	0.388	2.308

Growth experiments 2 and 3 to test ontogenetic effects

In experiment 2 in which juveniles from a single school grew in one tank, growth after eight months was very heterogeneous (table 2). Otolith weight correlated with standard length (correlation coefficient = 0.965). Trace element ratios plotted against otolith weights revealed different trends (fig. 3). We evaluated whether decreases in trace element ratios with growth indicated conservation or loss of each trace element as postulated by hypotheses H3 and H4. Each element's H3 curve was constructed based on the average trace element mass and average weight of the otoliths at time-0, e.g., Mg/Ca at time-0 was 0.515 mmol mol^{-1} in 0.342 mg otoliths (n = 10). The best-fit curves for measured element ratios and their predicted 95% CIs varied for each element. The equations describing the best-fit curves (± standard error, S.E.) for element ratios calculated against otolith weight and adjusted R^2 values were:

(3) $Mg/Ca\ (mmol\ mol^{-1}) = 0.031\ (\pm 0.02) + 5.95\ (\pm 2.46) \times e^{(-7.59\ (\pm 1.28) \times w)}$, $R^2 = 0.87$.

(4) $P/Ca\ (mmol\ mol^{-1}) = 0.39\ (\pm 0.05) + 7.29\ (\pm 2.56) \times e^{(-7.59\ (\pm\ 1.11) \times w)}$, $R^2 = 0.86$.

(5) $Sr/Ca\ (mmol\ mol^{-1}) = 0.46\ (\pm 0.02) + 1.36\ (\pm 0.83) \times e^{(-5.13\ (\pm 1.95) \times w)}$, $R^2 = 0.60$.

(6) $Ba/Ca\ (\mu mol\ mol^{-1}) = 2.35\ (\pm 0.24) + 11.09\ (\pm 11.88) \times e^{(-5.69\ (\pm 3.39) \times w)}$, $R^2 = 0.37$.

(7) $Mn/Ca\ (\mu mol\ mol^{-1}) = 0.94\ (\pm 0.14) \times e^{(-1.33\ (\pm 0.17) \times w)}$, $R^2 = 0.64$.

The calculated total mass of Mg and P in the otoliths decreased with growth, i.e., the measured Mg/Ca and P/Ca ratios (±95% CI) were below the H3 dilution curves and thus resembled H4 curves (Eq. 3 and 4, and figs. 3A and 3B, respectively). Best-fit curves in Eq. 3 and 4 had the greatest adjusted R^2 values, indicating these models can explain most of the variability in Mg/Ca and P/Ca ratios in response to growth.

Sr/Ca ratios also decreased with growth, following or exceeding the H3 dilution curve (fig. 3C) which indicated the time-0 mass of Sr was conserved in the otoliths. The values of Ba/Ca ratios generally decreased with growth, but the results were scattered with some values below the H3 dilution curve (fig. 3D). Correspondingly, Eq. 6 explained only 37% of the variability of the Ba/Ca data. Mn/Ca ratios increased with growth, and the predicted values from Eq. 7 were clearly greater than minimum expected values computed from the H3 curve and more closely resembled the H2 response (fig. 3E).

We repeated the protocol in experiment 3 using juveniles maintained in duplicate tanks. Although the time-0 juveniles were approximately four months older and larger than those used in experiment 2 (table 2), and experiment 3 ran for five months rather than eight, the overall trends in trace element composition were comparable (table 3). The results of the duplicate tanks in experiment 3 showed little variability, as indicated by the low standard errors when the data were combined. Mg/Ca and P/Ca ratios decreased with growth, and Mn/Ca ratios increased in a manner predicted by H2. Mg/Ca and P/Ca ratios calculated from H3 trace element dilutions were significantly greater than the ratios (±S.E.) measured at the end of the experiment. The results indicate Mg and P were not conserved, and their behavior resembled the ratios predicted by H4. Measured values for Sr/Ca exceeded the H3 dilution values, indicating conservation. The Ba/Ca ratios from the two tanks were inconsistent, with some measured values exceeding the H3 dilution prediction and others below it.

Comparison of growth experiments 2 and 3 showed that Mg/Ca and P/Ca ratios were highly correlated in both trials, 0.95 and 0.98, respectively. Further, the experimental data (tables 4A and 4B) demonstrated strong correlation between Mn/Ca and sardine growth assessed as otolith weight in the two experiments, 0.75 and 0.79, respectively.

Temperature effects on trace element composition (experiment 4)

In experiment 4, growth was similar at 13° and 21°C, and greatest at 17°C (table 2). Using LA-ICPMS to sample the posterior edge of the otoliths, element ratios of the time-0 otoliths were compared with ratios in new aragonite in the otoliths at the end of the experiment.

Differentiating the effects of growth and temperature on trace element incorporation was complex as was

TABLE 4
Correlation coefficients between trace element ratios and otolith weight (mg) in *S. sagax* juveniles in growth experiments 2 and 3. Ratios are mmol mol^{-1} for Mg/Ca, P/Ca, and Sr/Ca; and µmol mol^{-1} for Mn/Ca and Ba/Ca. ICPMS analyses were conducted in a single run for experiment 2 at ODU, and in a single run for experiment 3 at SIO.

A. Growth experiment 2. Data are shown in Figure 3.

	Mg/Ca	P/Ca	Mn/Ca	Sr/Ca	Ba/Ca
P/Ca	0.949				
Mn/Ca	–0.417	–0.514			
Sr/Ca	0.845	0.840	–0.442		
Ba/Ca	0.635	0.624	–0.354	0.671	
Weight	–0.744	–0.801	0.792	–0.683	–0.526

B. Growth experiment 3. Data are summarized in Table 3.

	Mg/Ca	P/Ca	Mn/Ca	Sr/Ca	Ba/Ca
P/Ca	0.983				
Mn/Ca	–0.157	–0.098			
Sr/Ca	0.648	0.688	–0.308		
Ba/Ca	0.177	0.187	–0.050	0.629	
Weight	–0.751	–0.707	0.745	–0.602	–0.021

evaluating the outcomes according to the four hypotheses. Temperature rather than growth rate or otolith size influenced the incorporation of trace elements in new otolith aragonite. Ratios of Mg/Ca and P/Ca were the highest and most variable (over 10-fold range in values) in sardine maintained at 21°C (figs. 4A and 4B). In fish cultured at 13° and 17°C, ratios of Mg/Ca and P/Ca were similar for each trace element at the two temperatures and time-0, indicating growth rate and temperature were not coupled to the composition of new otolith growth across all temperatures. Because the behavior of Mg and P had similarities, we compared them to each other. P/Mg ratios showed a linear negative correlation with temperature (fig. 4C).

Mn/Ca and Sr/Ca ratios corresponded positively and linearly with respect to temperature, but each temperature resulted in a different trend when compared to the time-0 otoliths (figs. 4D and 4E). In addition to responding positively to temperature, all Mn/Ca ratios increased with growth from time-0 values similarly to the results of growth experiments 2 and 3. Although Sr/Ca ratios showed a positive temperature effect, the ratio of Sr/Ca relative to the time-0 otoliths confounded interpretation of thermal influence. At 13°C growth temperature, otoliths accreted less Sr than that measured in the time-0 otoliths. At 17°C they accreted approximately the same amount of Sr as the time-0 otoliths, and at 21°C they incorporated greater concentrations of Sr.

Ba/Ca ratios responded differently to temperature than the other trace elements (fig. 4F). Ba/Ca ratios had a broader range of values at 13°C (over 40-fold range) than at the other temperatures, with a similar decrease in ratios at 17° and 21°C from time-0 otoliths. No trace element besides Ba demonstrated such variability at 13°C or a lack of thermal effects between 17° and 21°C.

DISCUSSION

Trace elements in treatment experiment 1

Mg and P demonstrated instability with H_2O_2 treatment which likely oxidized matrix organic matter and solubilized weakly bound trace elements in the otoliths. While weight loss indicated dissolution of aragonite under the moderately acidic conditions of unbuffered 30% H_2O_2, the selective removal of these two elements suggests their association was largely outside the carbonate crystal lattice. The percent decreases in Mg/Ca ratios after 16 and 24 h were similar although the two treatments were analyzed on different ICPMS instruments. These results validated the analyses in different instruments.

Trace elements in growth experiments 2 and 3

Growth rate heterogeneity of fish is well known in aquaculture (Kelly and Heikes 2013). Such variability occurred in experiment 2 which included sardine that hardly grew and others that doubled in size. These results allowed us to evaluate both size and age effects on trace element incorporation. The results for Mg and P indicate age was a factor in their composition because all the fish, regardless of size, had similar low concentrations at the end of the experiment. The results for Mn and Sr suggest that overall growth was a significant factor in their incorporation because there were gradients in composition that corresponded to otolith weight. The scatter in the values of Ba/Ca ratios made it difficult to interpret the relative roles of size and age in the incorporation of Ba.

The decrease or increase in trace element/Ca ratios with growth and the magnitude of change varied for each element. Among the trace elements assayed, there was at least one example for each of the outcomes predicted by the four hypotheses, H1–H4. The greatest decreases as postulated by H4 were in Mg/Ca and P/Ca ratios which also highly correlated with each other. Increases as postulated by H2 were noted in Mn/Ca ratios. The trends in thermal responses of Sr/Ca ratios in experiment 4 followed the outcomes postulated by H1, H2, and H3.

The analyses of otolith samples for experiment 2 were conducted on a different ICPMS instrument than experiment 3, yet the correlations of trace element ratios were consistent for the two experiments for Mg/Ca vs. P/Ca, Sr/Ca vs. Ba/Ca, and for all trace element ratios vs. otolith weight except Ba/Ca. Like the treatment assays in experiment 1, the results of experiments

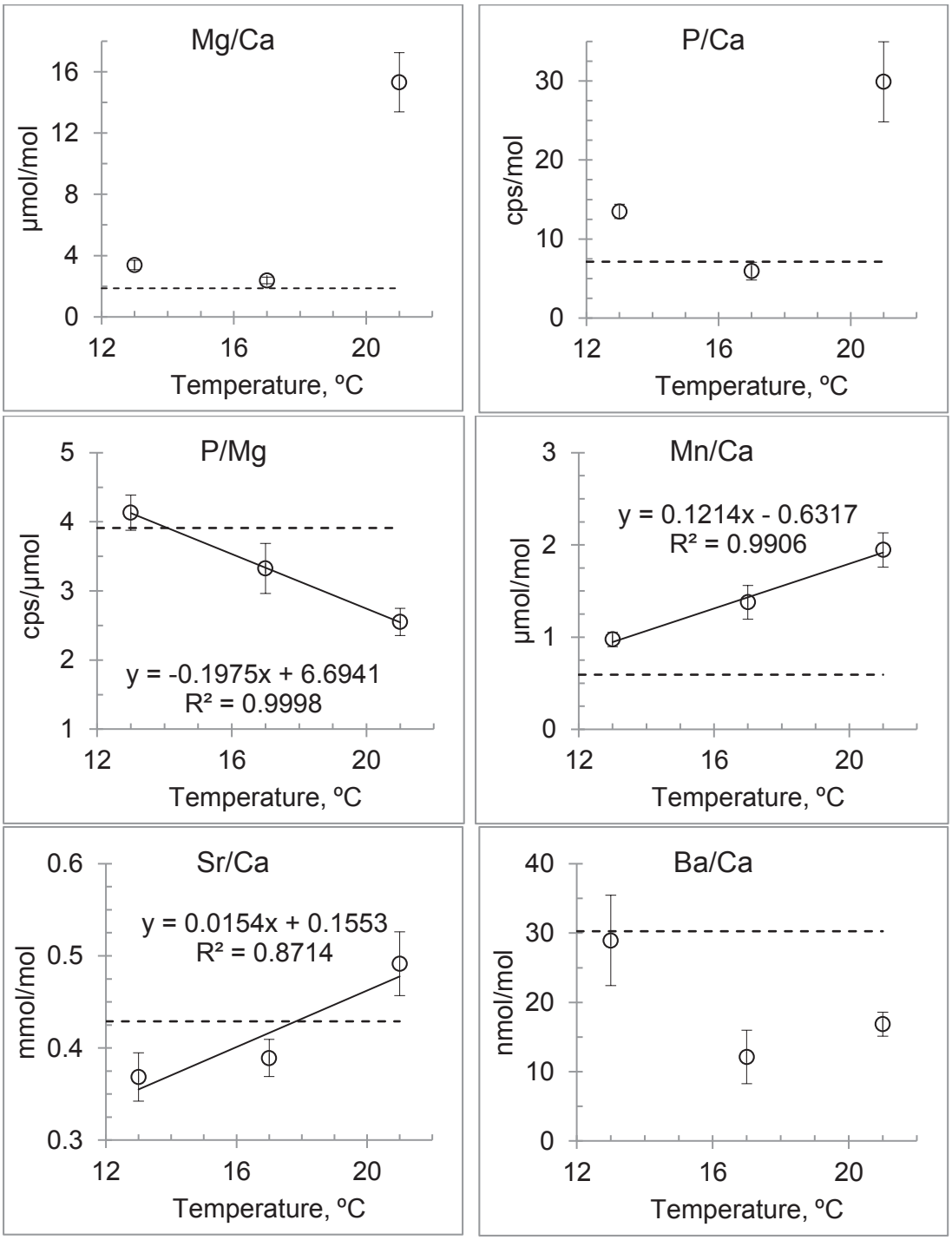

Figure 4. Experiment 4: Temperature effects on element ratios in the distal edges of *S. sagax* otoliths, averages ± S.E. Due to lack of a P standard for the LA-ICPMS analyses, P/Ca concentrations are presented as ratios of counts per second (cps) after subtraction of blank values. The average time-0 ratios are shown as a dashed line for comparison. Growth data and sample sizes are noted in Table 2. Linear regressions were drawn through the mean values of P/Mg, Mn/Ca, and Sr/Ca ratios.

2 and 3 validated the analyses conducted by different ICPMS instruments.

The elemental concentrations in our study were similar to those reported in otoliths of a number of other fish (Campana 1999), including *Sardinops sagax* from Australia (Edmonds et al. 1995). Edmonds et al. found P exceeded Sr concentrations, which agrees with our data. Some of their otoliths might have been from late age-0 sardine (0.8–1.0 mg), but most of their otoliths were larger and probably were from age-1 and older fish. Their Mg and

P concentrations overlapped with the lowest concentrations measured in our study of juvenile *S. sagax*.

Temperature effects on trace element composition (experiment 4)

Temperature positively correlated with Sr/Ca and Mn/Ca ratios, but the results for Mg, P, and Ba were mixed. Taken in conjunction with demonstrated ontogenetic influence on trace element ratios, it may be difficult to differentiate growth and thermal effects in otoliths of wild sardine of differing sizes when assigning fish to stocks and natal regions. Among the published investigations that have addressed the effects of temperature on element ratios in fish otoliths, there is little agreement across species (Campana 1999). We postulate some of the disparities may have been due to the confounding effects of growth and age.

For example, juvenile Atlantic croaker *Micropogonias undulatus* otoliths showed an inverse relationship between temperature and Mg concentration (Fowler et al. 1995). However, the authors did not account for the disparate sizes of the otoliths between the treatments. A reevaluation of their data shows clear relationships for Mg and P with respect to otolith weight when the results are compared by weight without regard to salinity and temperature. These relationships are similar to the results in our investigation in which size (and therefore growth or ontogeny) was a factor for Mg and P concentrations in juvenile sardine otoliths.

In another example, a study measuring Mg in juvenile black bream *Acanthopagrus butcheri* otoliths reported highly variable concentrations between individual fish and replicate tanks, and higher Mg/Ca ratios after growth at 24°C than at 16°C and 20°C (Elsdon and Gillanders 2002). The variability could have reflected the inherent instability of Mg in otoliths. At the end of their experiments, otoliths from fish maintained at 24°C were twice as heavy as otoliths from fish maintained at 16°C, indicating growth rather than temperature may have influenced Mg incorporation. The behavior of Mg was opposite of that noted in Pacific sardine (our study) and Atlantic croaker (Fowler et al. 1995) otoliths, i.e., Mg/Ca ratios increased with growth.

The results of our unpublished survey of otolith composition in juvenile Pacific sardine captured between the USA and Mexico concur with the findings of the present study. Investigations of other fish species have also noted an inverse relationship between Mg concentrations and otolith size (Begg et al. 1998; Rooker et al. 2001; Brophy et al. 2003; Ruttenberg et al. 2005). Begg et al. (1998) also demonstrated an inverse relationship between Mg and P concentrations in two species of mackerel (*Scomberomorus cavalla* and *S. commerson*). This trend was opposite the relationship between the two elements in sardine otoliths, suggesting the causative factors driving the disparate trace element partitions in different species are complex.

The behavior of Mg and P in juvenile sardine otoliths in our experiments was not predicted based on the generally accepted premise that trace elements are permanent chemical tags in otoliths (Campana 1999). Based on mass calculations, the results indicate Mg and P underwent in viv*o* losses that can likely be attributed to physicochemical factors of otolith structure and trace element stability.

Otolith structure and stability

Otoliths grow in sacculus endolymph fluid that exhibits diurnal changes and gradients in dissolved ions, proteins, pH, and pCO_2 (Edeyer et al. 2000; Payan et al. 2002, 2004; Borelli et al. 2001, 2003; Takagi et al. 2005; Guibbolini et al. 2006). Due to their porous structure and permeability (Gauldie et al. 1998; Gauldie 1999), otoliths are sensitive to contamination as a result of extraction, storing, and cleaning methods (Proctor and Thresher 1998; Milton and Chenery 1998; Rooker et al. 2001; Brophy et al. 2003; Swan et al. 2006). Instability noted as possible in vivo loss of Mg from otoliths in *Salmo trutta* juveniles has been described (Veinott et al. 2014). Interpretations of our findings on element stability in sardine otoliths are supported by research on non-biogenic aragonite and biogenic aragonite in other phyla.

The calcium carbonate "host" in non-biogenic and biogenic aragonite

Aragonite is an orthorhombic calcium carbonate mineral that can host small amounts of foreign ions within or between layers of the crystal lattice (e.g., at dislocations), or associated with the proteinaceous organic components in otoliths (Campana 1999; Miller et al. 2006). Foreign ions can associate with aragonite with ionic bonds, chelation, or weak attraction (e.g., adsorption). The strength of the attractions and stability of the associations between the host crystal, organic matrix, and foreign ions are dictated by charge, ionic radii, steric criteria, competing ions, concentration, temperature, crystal imperfections, and rate of crystal growth.

The incorporation of foreign ions into aragonite may not be in equilibrium with the surrounding fluid. Rapid crystal growth promotes the entrapment of ions in disequilibrium with bulk fluid concentrations, and the degree of entrapment depends on the competition between growth rate and crystal lattice diffusivity (Watson 2004). Mg, Sr, and Ba ions were enriched in non-biogenic aragonite grains relative to the concentrations predicted from equilibrium concentrations, indicating kinetic processes and entrapment controlled their distribution (Gaetani and Cohen 2006; Gabitov et al. 2006,

2008). Entrapment and growth rate effects could explain the 100-fold differences in Mg concentrations detected within individual otoliths (Milton and Chenery 1998), and some of our results.

Once trace elements are entrapped in calcium carbonate, they may retain a degree of mobility at ambient temperatures, moving in or out of crystals by solid-state diffusion along planar crystal defects (Stipp 1998; Stipp et al. 1998). Using fluorescent labeling, Beier et al. (2004) showed calcium can translocate in vivo in fish otoliths. Because otoliths have a relatively porous architecture, these lines of evidence suggest they may contain high-diffusivity pathways that could promote open-system behavior (Bruce Watson, pers. comm.).

Stable and metastable trace elements in biogenic aragonite

Many studies of trace elements in bivalves, corals, and foraminifera have been conducted because of their potential utility to reconstruct paleotemperatures of the oceans based on element ratios in skeletal carbonates. It is important to differentiate stable associations (e.g., lattice-bound within $CaCO_3$ crystals) from metastable associations (e.g., non-lattice-bound by absorption to extra-crystalline matrices) to calculate element partition coefficients in carbonates based on temperature and salinity. Various treatment protocols have been tested and compared to analyze the stability of trace elements in bivalves and corals (Watanabe et al. 2001; Schöne et al. 2010; Krause-Nehring et al. 2011; and Holcomb et al. 2015). No single method is ideal to resolve the composition of stable and metastable trace elements. In general, most investigators agree Sr and Ba are lattice-bound, and other trace elements are partly or largely non-lattice-bound. Sr has been shown to substitute well for Ca in aragonite (Plummer and Busenberg 1987; Finch and Allison 2007).

As biogenic aragonite structures, otoliths should share basic physicochemical features with bivalve shells and corals, i.e., crystalline microstructures interlayered with organic matrices, and inclusion of stable and metastable trace elements. One potentially significant difference is that otoliths remain sealed from direct contact with seawater and microorganisms in the fish sacculus while mollusk shells and corals may be subject to relatively unregulated interactions with environmental agents after initial formation.

Strontium and barium. Sr/Ca ratios are generally unaffected by treatments in bivalves (Takesue et al. 2008) and corals (Holcomb et al. 2015). Sr/Ca ratios have been shown to be relatively immune to various methods of otolith storage and cleaning (Milton and Chenery 1998; Proctor and Thresher 1998; Rooker et al. 2001; this study). We showed the effects of ontogeny and growth temperature on Sr/Ca ratios in juvenile sardine otoliths were predictable as well.

Ba/Ca ratios are also generally unaffected by treatments in bivalves (Takesue et al. 2008), corals (Holcomb et al. 2015), and otoliths (our study). Ba has been shown to be both relatively stable (Rooker et al. 2001) and relatively unstable (Swan et al. 2006) in studies addressing post-mortem artifacts in otolith preparation. The variability of Ba/Ca ratios in our experiments with sardine otoliths suggests Ba binding is controlled by a complex of factors.

Manganese. Hydrogen peroxide treatment greatly reduces Mn/Ca ratios in bivalves (Takesue et al. 2008; Krause-Nehring et al. 2011), indicating Mn is metastable and not bound to the aragonite lattice. In our otolith study, overnight exposure to 30% H_2O_2 did not affect Mn/Ca ratios. Protein binding of transition metals may largely explain the presence of these ions in otoliths (Asano and Mugiya 1993; Miller et al. 2006). As in some bivalves (Schöne et al. 2010), it is possible Mn in sardine otoliths may associate with organic matter that would not completely dissolve except under extremely acidic conditions that we did not test.

Mn concentration in otoliths has been shown to reflect ontogeny. Mn was enriched by up to a hundred-fold or more in otolith cores of diverse fish, while Mg and Ba were enriched up to about two- or three-fold in cores, and Sr was not enriched at all (Ruttenberg et al. 2005). Those results indicate larval and juvenile otolith composition changes with age in a variety of fish. In Pacific sardine, the increase in Mn/Ca ratios with both growth and temperature could make it difficult to differentiate ontogeny from environmental parameters affecting Mn incorporation.

Magnesium. Treatment experiments with bivalve and coral aragonite (Watanabe et al. 2001; Takesue et al. 2008; Schöne et al. 2010; Krause-Nehring et al. 2011; and Holcomb et al. 2015), molecular dynamics simulations (Ruiz-Hernandez et al. 2012), and X-ray analytical methods (Yoshimura et al. 2014) have confirmed Mg is largely non-lattice-bound and is associated with organic matter or extra-crystalline matrix in nanodomains of unknown nature (Finch and Allison 2007; Foster et al. 2008). In bivalves, significant amounts of Mg were enriched in the insoluble organic material that did not dissolve in dilute nitric acid commonly used to solubilize aragonite for ICPMS (e.g., 2%), but rather required stronger acidic conditions (Schöne et al. 2010).

Mg appears to be metastable in corals, bivalves, and fish otoliths (Milton and Chenery 1998; Rooker et al. 2001; this study). In H_2O_2 treatment experiments, about 40% of the Mg in the coral skeleton was removed (Watanabe et al. 2001), and about 33% of the Mg in bivalve shells was removed (Takesue et al. 2008). In our otolith

treatment experiments, overnight immersion in H_2O_2 resulted in similar losses of Mg. Instability of Mg was also detected in otoliths of living sardine. A rearing experiment with juvenile sardine using multiple sampling times would better detail the decreases of Mg with age or growth. Tracking Mg in otoliths of wild juvenile sardine to detect regional differences might lead to incorrect conclusions if element loss and otolith size and age are not considered.

Phosphorus. Evidence indicates phosphate is metastable in biogenic carbonates. Various analytical and imaging technologies have detected conformations of phosphate in bivalves and corals (Zhang et al. 2011; Mason et al. 2011). In bivalves, newly formed shell consists of nanospheres of amorphous carbonated Ca-Mg phosphate with high molar ratios of Mg/Ca (0.625 mol mol^{-1}) and P/Ca (0.714 mol mol^{-1}) (Xu and Zhang 2014). Ontogenetic effects recorded as variability in P/Ca ratios in new growth relative to bulk shell composition have been shown at the growing edge of bivalves (Takesue et al. 2008) and early in life close to the umbo (Strasser et al. 2008). If phosphate is largely adsorbed in biogenic aragonite in amorphous forms, extra-crystalline domains of hydroxylapatite, or phosphoproteins, concentrations could change due to temperature or growth. Adsorption and desorption of phosphate on non-biogenic calcium carbonate are temperature-dependent, multistep processes in seawater (Millero et al. 2001). It is likely that phosphate interactions with biogenic aragonite are similarly complex.

The covariance of Mg and P in juvenile sardine otoliths did not reflect a stoichiometry associated with magnesium phosphate minerals. Correlation between Mg and P should be analyzed in invertebrate biogenic aragonites as well to establish whether Mg-P associations are common. Like Mg, the metastability of P may result in uncertainty when evaluating regional attributes of juvenile sardine otoliths unless ontogenetic effects and possible in vivo loss are factored.

Conclusions

A major determinant of trace element composition in juvenile Pacific sardine otoliths was weight or age. Except for Mg and P, growth temperature affected each element differently. H_2O_2 treatment showed Mg and P were largely metastable while growth experiments demonstrated the apparent in vivo loss of Mg and P from juvenile sardine otoliths. The results of this study challenge the assumption that all trace elements in otoliths are permanently bound in living fish. Some trace elements may be inherently metastable due to otolith architecture, the physicochemical properties of aragonite and the associated organic matrix, and the effects of growth that might modify composition. Further studies with time-course sampling of cultured juvenile fish and mollusks might clarify some of the early processes during biogenic aragonite formation.

ACKNOWLEDGMENTS

We thank Larry Robertson for overseeing the collection of live sardine and maintaining their culture at SWFSC. We thank Russ Vetter, John Hyde, Brian Wells, and anonymous reviewers for suggestions to improve the manuscript. This study was supported by NOAA, the NOAA Fisheries and the Environment (FATE) Program, and a NRC postdoctoral fellowship to E. Dorval.

LITERATURE CITED

Asano, M., and Y. Mugiya. 1993. Biochemical and calcium-binding properties of water-soluble proteins isolated from otoliths of the tilapia, *Orechromis niloticus*. Comp. Biochem. Physiol. B: Biochem. Molec. Biol. 104:201–205.

Bath Martin, G., and M. J. Wuenschel. 2006. Effect of temperature and salinity on otolith element incorporation in juvenile gray snapper *Lutjanus griseus*. Mar. Ecol. Prog. Ser. 324:229–239.

Begg, G. A., M. Cappo, D. S. Cameron, S. Boyle, and M. Sellin. 1998. Stock discrimination of school mackerel, *Scomberomorus queenslandicus*, and spotted mackerel, *Scomberomorus munroi*, in coastal waters of eastern Australia by analysis of minor and trace elements in whole otoliths. Fish. Bull., 96:653–666.

Beier, M., R. H. Anken, and H. Rahmann. 2004. Calcium-tracers disclose the site of biomineralization in inner ear otoliths of fish. Adv. Space Res. 33:1401–1405.

Borelli, G., N. Mayer-Gostan, H. De Pontual, G. Bœuf, and P. Payan. 2001. Biochemical relationships between endolymph and otolith matrix in the trout (*Oncorhynchus mykiss*) and turbot (*Psetta maxima*). Calcified Tissue International. 69:356–364.

Borelli, G., M. E. Guibbohni, N. Mayer-Gostan, F. Priouzeau, H. De Pontual, D. Allemande, S. Puverel, E. Tambutte, and P. Payan. 2003. Daily variations of endolymph composition: relationship with the otolith calcification process in trout. J. Exper. Biol. 206:2685–2692.

Brophy, D., B. S. Danilowicz, and T. E. Jeffries. 2003. The detection of elements in larval otoliths from Atlantic herring using laser ablation ICP-MS. J. Fish Biol. 63:990–1007.

Campana, S. E. 1983. Calcium deposition and otolith check formation during periods of stress in coho salmon, *Oncorhynchus kisutch*. Comp. Biochem. Physiol. 75A:215–220.

Campana, S. E. 1999. Chemistry and composition of fish otoliths: pathways, mechanisms and applications. Mar. Ecol. Prog. Ser. 188:263–297.

Campana, S. E., S. R. Thorrold, C. M. Jones, D. Günther, M. Tubrett, H. Longerich, S. Jackson, N. M. Halden, J. M. Kalish, P. Piccoli, H. de Pontual, H. Troadec, J. Panfili, D. H. Secor, K. P. Severin, S. H. Sie, R. Thresher, W. J. Teesdale, and J. L. Campbell. 1997. Comparison of accuracy, precision, and sensitivity in elemental assays of fish otoliths using the electron microprobe, proton-induced X-ray emission, and laser ablation inductively coupled plasma mass spectrometry. Can. J. Fish. Aquat. Sci. 54:2068–2079.

Dauphin, Y., and E. Dufour. 2003. Composition and properties of the soluble organic matrix of the otolith of a marine fish: *Gadus morhua* Linne, 1758 (Teleostei, Gadidae). Comp. Biochem. Physiol. Part A. 134:551–561.

Demer, D. A., J. P. Zwolinski, K. Byers, G. R. Cutter, Jr., J. S. Renfree, S. T. Sessions, and B. J. Macewicz. 2012. Seasonal migration of Pacific sardine (*Sardinops sagax*) in the California Current ecosystem: prediction and empirical confirmation. Fish. Bull. 110:52–70.

Dorval, E., K. Piner, L. Robertson, C. S. Reiss, B. Javor, and R. Vetter. 2011. Temperature record in the oxygen stables of Pacific sardine otoliths: experimental vs. wild stocks from the Southern California Bight. J. Exper. Mar. Biol. Ecol. 397:136–143.

Edeyer, A., H. De Pontual, P. Payan, H. Troadec, A. Severe, and N. Mayer-Gostan. 2000. Daily variations of the saccular endolymph and plasma compositions in the turbot *Psetta maxima*: relationship with the diurnal rhythm in otolith formation. Mar. Ecol. Prog. Ser. 192:287–294.

Edmonds, J. S., N. Caputi, M. J. Moran, W. J. Fletcher, and M. Morita. 1995. Population discrimination by variation in concentrations of minor and trace elements in sagittae of two Western Australian teleosts. *In* Recent developments in fish otolith research, D. H. Secor, J. M. Dean, and S. E. Campana, ed. The Belle W Baruch Library in Marine Science 19. Belle W Baruch Institute for Marine Biology and Coastal Research. Columbia: University of South Carolina Press, pp. 655–670.

Elsdon, T. S., and B. M. Gillanders. 2002. Interactive effects of temperature and salinity on otolith chemistry: challenges for determining environmental histories of fish. Can. J. Fish. Aquat. Sci. 59:1796–1808.

Emmett, R. L., R. D. Brodeur, T. W. Miller, S. S. Pool, P. J. Bentley, G. K. Krutzikowsky, and J. McCrae. 2005. Pacific sardine (*Sardinops sagax*) abundance, distribution, and ecological relationships in the Pacific Northwest. Calif. Coop. Oceanic Fish. Invest. Rep. 46:122–143.

Félix-Uraga, R., V. M. Gómez-Muñoz, C. Quiñónez-Velázquez, F. N. Melo-Barrera, and W. García-Franco. 2004. On the existence of Pacific sardine groups off the west coast of the Baja California Peninsula and southern California. Calif. Coop. Oceanic Fish. Invest. Rep. 45:146–151.

Félix-Uraga, R., C. Quiñónez-Velázquez, K. T. Hill, V. M. Gómez-Muñoz, F. N. Melo-Barrera, and W. García-Franco. 2005. Pacific sardine (*Sardinops sagax*) stock discrimination off the west coast of Baja California and southern California using otolith morphometry. Calif. Coop. Oceanic Fish. Invest. Rep. 46:113–121.

Finch, A. A., and N. Allison. 2007. Coordination of Sr and Mg in calcite and aragonite. Mineral Magazine, 71:539–552.

Foster, L. C., A. A. Finch, N. Allison, C. Andersson, and L. J. Clarke. 2008. Mg in aragonitic bivalve shells: Seasonal variations and mode of incorporation in *Arctica islandica*. Chem. Geol. 254:113–119.

Fowler, A. J., S. E. Campana, C. M. Jones, and S. R. Thorrold. 1995. Experimental assessment of the effect of temperature and salinity on elemental composition of otoliths using solution-based ICPMS. Can. J. Fish. Aquat. Sci. 52:1421–1430.

Gabitov, R. I., A. L. Cohen, G. A. Gaetani, M. Holcomb, and E. B. Watson. 2006. The impact of crystal growth rate on element ratios in aragonite: An experimental approach to understanding vital effects. Geochim. Cosmochim. Acta 70:A187–A220.

Gabitov, R. I., G. A. Gaetani, E. B. Watson, A. L. Cohen, and H. L. Ehrlich. 2008. Experimental determination of growth rate effect on U^{6+} and Mg^{2+} partitioning between aragonite and fluid at elevated U^{6+} concentration. Geochim. Cosmochim. Acta 72:4058–4068.

Gaetani, G. A., and A. L. Cohen. 2006. Element partitioning during precipitation of aragonite from seawater: A framework for understanding paleoproxies. Geochim. Cosmochim. Acta 70:4617–4634.

García-Rodríguez, F. J., S. A. García-Gasca, J. De La Cruz-Agüero, and V. M. Cota-Gómez. 2011. A study of the population structure of the Pacific sardine *Sardinops sagax* (Jenyns, 1842) in Mexico based on morphometric and genetic analyses. Fish. Res. 107:169–176.

Gauldie, R. W. 1999. Ultrastructure of lamellae, mineral and matrix components of fish otolith twinned aragonite crystals: implications for estimating age in fish. Tissue & Cell 31:138–153.

Gauldie, R. W., C. E. Thacker, I. F. West, and L. Wang. 1998. Movement of water in fish otoliths. Comp. Biochem. Physiol. Part A 120:551–556.

Grant, W. S., and B. W. Bowen. 1998. Shallow population histories in deep evolutionary lineages of marine fishes: Insights from sardines and anchovies and lessons for conservation. J. Hered. 89:415–426.

Guibbolini, M., G. Borelli, N. Mayer-Gostan, F. Priouzeau, H. De Pontual, D. Allemande, and P. Payan. 2006. Characterization and variations of organic parameters in teleost fish endolymph during day-night cycle, starvation and stress conditions. Comp. Biochem. Physiol. Part A: Molec. Integrat. Physiol. 145:99–107.

Hedgecock, D., E. S. Hutchinson, G. Li, F. L. Sly, and K. Nelson. 1989. Genetic and morphometric variations in the Pacific sardine *Sardinops sagax caerulea*: comparisons and contrasts with historical data and with variability in northern anchovy *Engraulis mordax*. Fish. Bull. U.S. 87:653–671.

Hoff, G. R., and L. A. Fuiman. 1993. Morphology and composition of red drum otoliths: changes associated with temperature, somatic growth rate, and age. Comp. Biochem. Physiol. 106A:209–219.

Holcomb, M., T. M. DeCarlo, V. Schoepf, D. Dissard, K. Tanaka, and M. McCulloch. 2015. Cleaning and pre-treatment procedures for biogenic and synthetic calcium carbonate powders for determination of elemental and boron isotopic compositions. Chem. Geol. 398:11–21.

Jacob, D. E., A. L. Soldati, R. Wirth, J. Huth, U. Wehrmeister, and W. Hofmeister. 2008. Nanostructure, chemical composition and mechanisms of bivalve shell growth. Geochim. Cosmochim. Acta, 72:5401–5415.

Javor, B. J. 2013. Do shifts in otolith morphology of young Pacific sardine (*Sardinops sagax*) reflect changing recruitment contributions from northern and southern stocks? Calif. Coop. Oceanic Fish. Invest. Rep. 54:85–96.

Javor, B., N. Lo, and R. Vetter. 2011. Otolith morphometrics and population structure of Pacific sardine (*Sardinops sagax*) along the west coast of North America. Fish. Bull. 109:402–415.

Javor, B., and E. Dorval, E. 2014. Geography and ontogeny influence the oxygen and carbon stable isotopes of otoliths of Pacific sardine in the California Current. Fish. Res. 154:1–10.

Kelly, A. M., and D. Heikes. 2013. Sorting and grading warmwater fish. South. Reg. Aquaculture Center Pub. No. 391, 8 p.

Krause-Nehring, J., A. Kluegel, G. Nehrke, B. Brellochs, and T. Brey. 2011. Impact of sample pretreatment on the measured element concentrations in the bivalve *Arctica islandica*. Geochem. Geophys. Geosys. 12: art. no. Q07015.

Lo, N. C. H., B. J. Macewicz, and D. A. Griffith. 2005. Spawning biomass of Pacific sardine (*Sardinops sagax*), from 1994–2004 off California. Calif. Coop. Oceanic Fish. Invest. Rep. 46:93–112.

Lo, N. C. H., B. J. Macewicz, and D. A. Griffith. 2010. Biomass and reproduction of Pacific sardine (*Sardinops sagax*) off the Pacific northwestern United States, 2003–2005. Fish. Bull. 108:174–192.

Lo, N. C. H., B. J. Macewicz, and D. A. Griffith. 2011. Migration of Pacific sardine (*Sardinops sagax*) off the west coast of the United States. Bull. Mar. Sci. 87:395–412.

Mason, H. E., P. Montagna, L. Kubista, M. Taviani, M. McCulloch, and B. L. Phillips. 2011. Phosphate defects and apatite inclusions in coral skeletal aragonite revealed by solid-state NMR spectroscopy. Geochim Cosmochim. Acta, 75:7446–7457.

Miller, M. B., A. M. Clough, J. N. Batson, and R. W. Vachet. 2006. Transition metal binding to cod otolith proteins. J. Exper. Mar. Biol. Ecol. 329:135–143.

Millero, F., F. Huang, X. R. Zhu, X. W. Liu, and J. Z. Zhang. 2001. Adsorption and desorption of phosphate on calcite and aragonite in seawater. Aquat. Geochem. 7:33–56.

Milton, D. A., and S. R. Chenery. 1998. The effect of otolith storage methods on the concentrations of elements detected by laser-ablation ICPMS. J. Fish Biol. 53:785–794.

Mitchell, D. L., D. Ivanova, R. Rabin, T. J. Brown, and K. Redmond. 2002. Gulf of California sea surface temperatures and the North American Monsoon: mechanistic implications from observations. J. Climate 15:2261–2291.

Payan, P., G. Borelli, F. Priouzeau, H. De Pontual, G. Bœuf, and N. Mayer-Gostan. 2002. Otolith growth in trout *Oncorhynchus mykiss*: supply of Ca^{2+} and Sr^{2+} to the saccular endolymph. J. Exper. Biol. 205:2687–2695.

Payan, P., H. De Pontual, A. Edeyer, G. Borelli, G. Boeuf, and N. Mayer-Gostan. 2004. Effects of stress on plasma homeostasis, endolymph chemistry, and check formation during otolith growth in rainbow trout (*Onchorhynchus mykiss*). Can. J. Fish. Aquat. Sci. 61:1247–1255.

Pereyra, R. T., E. Saillant, C. L. Pruett, C. E. Rexroad, A. Rocha-Olivares, and A. R. Gold. 2004. Characterization of polymorphic microsatellites in the Pacific sardine *Sardinops sagax* (Clupeidae). Molec. Ecol. Notes 4:739–741.

Plummer, L. N., and E. Busenberg. 1987. Thermodynamics of aragonite-strontianite solid solutions: Results from stoichiometric solubility at 25 and 76°C. Geochim. Cosmochim. Acta 51:1393–1411.

Poulain, C., D. P. Gillikin, J. Thebault, J. M. Munaron, M. Bohn, R. Robert, Y-M. Paulet, and A. Lorrain. 2015. An evaluation of Mg/Ca, Sr/Ca, and Ba/Ca ratios as environmental proxies in aragonite bivalve shells. Chem. Geol. 396:42–50.

Proctor, C. H., and R. E. Thresher. 1998. Effects of specimen handling and otolith preparation on concentration of elements in fish otoliths. Mar. Biol. 131:681–694.

Reiss, C., D. M. Checkley, Jr., and S. J. Bograd. 2008. Remotely sensed spawning habitat of Pacific sardine (*Sardinops sagax*) and Northern anchovy (*Engraulis mordax*) within the California Current. Fish. Oceanogr. 17:126–136.

Rooker, J. R., V. S. Zdanowicz, and D. H. Secor. 2001. Chemistry of tuna otoliths: assessment of base composition and postmortem handling effects. Mar. Biol. 139:35–43.

Ruiz-Hernandez, S. E., R. Grau-Crespo, N. Almora-Barrios, M. Wolthers, A. R. Ruiz-Salvador, N. Fernandez, and N. H. de Leeuw. 2012. Mg/Ca partitioning between aqueous solution and aragonite mineral: a molecular dynamics study. Chemistry-A Europ. J. 18:9828–9833.

Ruttenberg, B. I., S. L. Hamilton, M. J. H. Hickford, G. L. Paradis, M. S. Sheehy, J. D. Standish, O. Ben-Tzvi, and R. R. Warner. 2005. Elevated levels of trace elements in cores of otoliths and their potential for use as natural tags. Mar. Ecol. Prog. Ser. 297:273–281.

Schöne, B. R., Z. Zhang, D. Jacob, D. P. Gillikin, T. Tütken, D. Garbe-Schönberg, T. McConnaughey, and A. Soldati. 2010. Effect of organic matrices on the determination of the trace element chemistry (Mg, Sr, Mg/Ca, Sr/Ca) of aragonitic bivalve shells (*Arctica islandica*)—comparison of ICP-OES and LA-ICP-MS data. Geochem. J. 44:23–37.

Smith, P. E. 2005. A history of proposals for subpopulation structure in the Pacific sardine (*Sardinops sagax*) population off western North America. Calif. Coop. Oceanic Fish. Invest. Rep. 46:75–82.

Stipp, S. L. S. 1998. Surface analytical techniques applied to calcite: evidence of solid-state diffusion and implications for isotope methods. Paleogeog. Paleoclimatol. Paleoecol. 140:441–457.

Stipp, S. L. S., J. Konnerup-Madsen, K. Franzreb, A. Kulik, and H. J. Mathieu. 1998. Spontaneous movement of ions through calcite at standard temperature and pressure. Nature, 396: 356–359.

Strasser, C. A., L. S. Mullineaux, and B. D. Walther. 2008. Growth rate and age effects on *Mya arenaria* shell chemistry: implications for biogeochemical studies. J. Exper. Mar. Biol. Ecol. 355:153–163.

Swan, S. C., A. J. Geffen, B. Morales-Nin, J. D. M. Gordon, T. Shimmield, T. Sawyer, and E. Massuti. 2006. Otolith chemistry: an aid to stock separation of *Helicolenus dactylopterus* (bluemouth) and *Merluccius merluccius* (European hake) in the Northeast Atlantic Mediterranean. ICES J. Mar. Sci. 63:504–513.

Takagi, Y., H. Tohse, E. Murayama, T. Ohira, and H. Nagasawa. 2005. Diel changes in endolymph aragonite saturation rate and mRNA expression of otolith matrix proteins in the trout otolith organ. Mar. Ecol. Prog. Ser. 294:249–256.

Takahashi, M., and D. M. Checkley, Jr. 2008. Growth and survival of Pacific sardine (*Sardinops sagax*) in the California Current region. J. Northwest Atlantic Fish. Sci. 49:129–136.

Takesue, R. K., C. R. Bacon, and J. K. Thompson. 2008. Influences of organic matter and calcification rate on trace elements in aragonitic estuarine bivalve shells. Geochim. Cosmochim. Acta 72:5431–5445.

Valle, R. S., and S. Z. Herzka. 2008. Natural variability in $\delta^{18}O$ values of otoliths of young Pacific sardine captured in Mexican waters indicates subpopulation mixing within the first year of life. ICES J. Mar. Sci. 65:174–190.

Veinott, G., P. A. H. Westley, C. F. Purchase, and L. Warner. 2014. Experimental evidence simultaneously confirms and contests assumptions implicit to otolith microchemistry research. Can. J. Fish. Aquat. Sci. 71:356–365.

Vergara-Solana, F. J., F. J. García-Rodríguez, and J. De La Cruz-Agüero. 2013. Comparing body and otolith shape for stock discrimination of Pacific sardine *Sardinops sagax* Jenyns, 1842. J. Appl. Ichthyol. 29:1241–1246.

Watanabe, T., M. Minagawa, T. Oba, and A. Winter. 2001. Pretreatment of coral aragonite for Mg and Sr analysis: Implications for coral thermometers. Geochem. J. 35:265–269.

Watson, E. B. 2004. A conceptual model for near-surface kinetic controls on the trace-element and stable isotope composition of abiogenic calcite crystals. Geochim. Cosmochim. Acta 68:1473–1488.

Xu, J., and G. Zhang. 2014. Biogenic nanospheres of amorphous carbonated Ca-Mg phosphate within the periostracum of the green mussel *Perna viridis*. J. Struct. Biol. 188:205–212.

Yoshimura, T., Y. Tamenori, H. Kawahata, and A. Suzuki. 2014. Fluctuations of sulfate, S-bearing amino acids and magnesium in a giant clam shell. Biogeosciences, 11:3881–3886.

Yoshinaga, J., A. Nakama, M. Morita, and J. S. Edmonds. 2000. Fish otolith reference material for quality assurance of chemical analyses. Mar. Chem. 69:91–97.

Zhang, F., W. Cai, J. Zhu, Z. Sun, and J. Zhang. 2011. In situ Raman spectral mapping study on the microscale fibers in blue coral (*Heliopora coerulea*) skeletons. Anal. Chem. 83:7870–7875.

BIO-ECONOMIC ASSESSMENT OF A GREEN CRAB FISHERY IN BAJA CALIFORNIA SOUTH, MEXICO

ERNESTO A. CHÁVEZ
Centro Interdisciplinario de Ciencias Marinas
Instituto Politécnico Nacional
Av. Instituto Politécnico Nacional s/n Col. Playa Palo de Santa Rita
Apdo. Postal 592
C.P. 23096, La Paz, B.C.S. México
echavez@ipn.mx

ABSTRACT

Optimum bio-economic harvesting strategies of the green crab *Callinectes bellicosus* (Stimpson) fishery of Magdalena Bay Mexico, were evaluated. The short life span implies high variability of the catch. The stock and its exploitation scenarios were evaluated with a simulation model. The stock biomass displays a slight decreasing trend over the second half of the 13 years of analysis, with a maximum of nearly 6,000 t. The fishing mortality and exploitation rate suggest that the stock was underexploited through all the period of analysis, except for two years (2009 and 2012). The profits have been over USD $200,000 for each of the last four years, whilst before then they were lower, and the efficiency of the fishery indicated by the benefit/cost ratio has been between 2 and 3. Three exploitation scenarios were evaluated, and compared to the current condition of the fishery, the maximum sustainable yield (MSY), the maximum economic yield (MEY), and the maximum economic benefit per fisher (MEBF). In order to do that, it was necessary to impose some constrains, like setting a maximum number of boats, to maintain the same number of fishers when the income per fisher was maximized, and setting a maximum age of first catch. The results with the scenarios MSY and MEY are the same with almost twice the current yield and profits. Those of the current scenario and that of MEBF also provided the same output values, meaning that the current condition almost provides the maximum benefit per fisher.

INTRODUCTION

Sixteen portunid crab species known as *jaiba* in Mexico and several Latin American countries, are distributed in the eastern tropical Pacific, and thirteen occur in western Mexico. Among these, the green crab *Callinectes bellicosus* (Stimpson 1853) is subject to exploitation in Bahía Magdalena on the west coast of Baja California South, whose catch amounts to 7.5 percent of total crab landings in northwestern Mexico (fig. 1), where the highest yields attained 17 thousand metric tons (t) in the year 2013; of which a little less than 400 t were caught in the study area. Other crabs from the same family with secondary importance as fishery resources in the region are *C. arcuatus* (Ordway 1893), and *C. toxotes* (Ordway 1983; SAGARPA 2013).

The fishery of *jaiba* (*Callinectes* spp.) in the Mexican Pacific began in 1980; its exploitation occurs mostly in the states surrounding the Gulf of California. *Jaiba* dwells in soft bottoms and sea grasses (Paul 1981; González-Ramírez 1996; Arreola-Lizárraga et al. 2003). The authorized gear in B. Magdalena is a Chesapeake type trap; there is a maximum of 8,000 authorized traps and the minimum legal size is 11.5 cm width. In the four states around the Gulf of California, total landings amounted to 17,046 t in 2013, of which 66% were caught in the state of Sinaloa at the eastern gulf (SAGARPA 2013).

Catch records display high variability, suggesting a strong influence of climate, often associated with short-lived species. In addition, the growing number of fishers creates a need for regulations, despite the scarce information on the life cycle and other aspects of the fishery, to control effort and ensure an equitable participation of the stakeholders under the stock conservation framework. The goal of this paper is to conduct a bio-economic assessment of the fishery by evaluating some exploitation scenarios intended to optimize yield, fishing effort, profits, and numbers of jobs. Maximum catch and maximum profit are different under the same level of fishing effort and in some cases a maximum value may conflict with another target of the fishery, such that some trade-offs must be critically examined in order to choose the most convenient option to consider in the decision-making process, where ideally fishers and authorities should be involved. Therefore, the purpose of the present paper is to carry-on a stock assessment involving its socio-economic aspects, in order to diagnose the condition of the fishery of Magdalena Bay, in the state of Baja California Sur, Mexico. The evaluation has the intention to provide pertinent recommendations addressed to choose the best scenarios of exploitation pursuing the maximum catch, the maximum profits, or the best social benefits under the framework of the conservation of the stock.

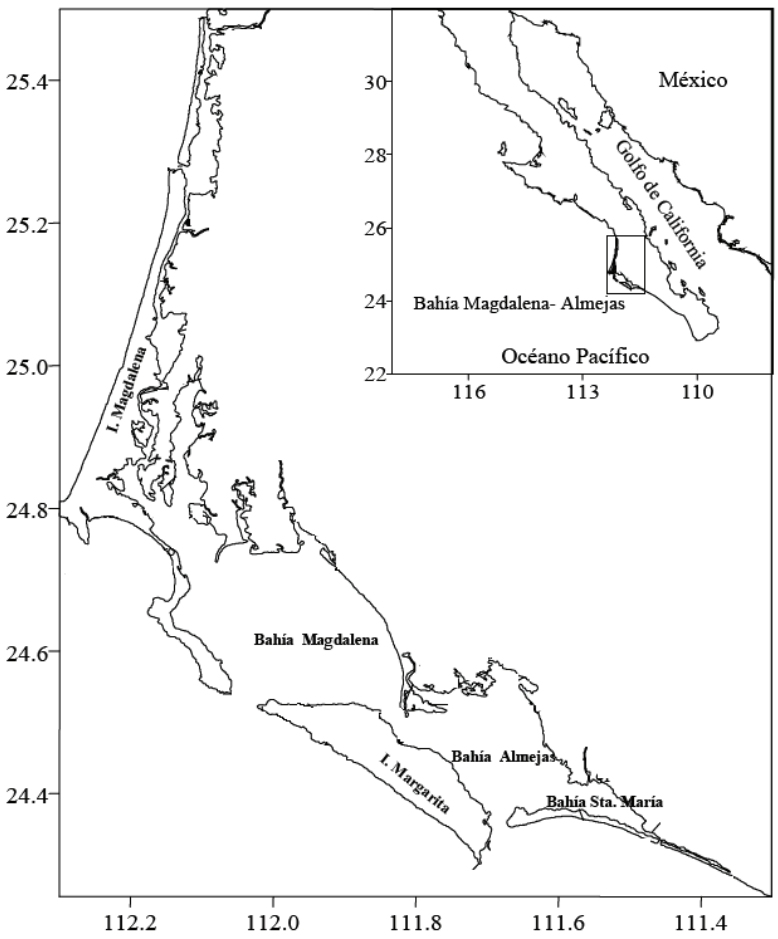

Figure 1. Magdalena Bay, Baja California South, México. Study site, where the green crab fishery takes place.

METHODS

Statistical data proceed from official catch records for the period 2001–13 (SAGARPA 2013). Population parameter values were obtained from published sources (see table 1). Some additional information, like costs and benefits of the activity, fishing days per season, number of boats, and number of fishers was obtained directly in Magdalena Bay. Some data were obtained directly by doing surveys in the study area.

Few papers provide biological data and population parameter values for *C. bellicosus* in northwestern Mexico (González-Ramírez et al. 1996; Escamilla-Montes 1998; Estrada-Valencia 1999; Molina-Ocampo et al. 2006; Huato-Soberanis et al. 2007; Hernández and Arreola-Lizárraga 2007; Rodríguez-Domínguez 2012; López-Martínez et al. 2014). A few other papers have also been produced, but they are mostly internal reports of restricted distribution.

The assessment of the stock was carried on by transforming the last thirteen years of catch data into the age structure of the population in numbers and weights per age class, with the use of the population parameter

TABLE 1

Parameter and other initial values of the *jaiba verde* (green crab), *Callinectes bellicosus* (Stimpson) of the Magdalena Bay fishery in west southern Baja California, used to feed the FISMO simulation model.

	Value	Source
Bertalanffy		
K	0.8/year	Escamilla-Montes 1998
L	16.9 cm	Hernández y Arreola-Lizárra 2007
W	465 g	This paper
to	–0.23 Years	Escamilla-Montes 1998
Length-Weight		
a	0.0706	Condition factor
b	3.11	Coefficient of allometry
Age of 1st catch	1 Years	Field samplings
Maturity age	2 Years	Field samplings
Longevity	4 Years	As 3/*K*
M	1.2	As 1.5**K*
Phi'	2.3589	Log *K* + 2 Log *L*
Value/Kg	1.6 US Dlls.	Landing site
Cost/Day	18 US Dlls.	Interviews
Num. of Boats	70	Interviews
Days/boat/season	141	Interviews
Num. of Trips	9,860	Interviews
Profits	112,873 US Dlls.	Subtracted from the costs
Benefit/Cost	1.64	Catch value/Total costs
Fishers/Boat	2	Interviews

values (table 1) and the FISMO simulation model (Chávez 2005, 2014). The model also has the capability to evaluate the economic performance of the fishing activity in the sea, before adding value to the landed catch. The socioeconomic values are part of the input and are linked into the model associating catch volume to catch value and fishing effort inferred from the fishing mortality to the cost of fishing and to the number of boats and fishers. All of these values are linked in the simulations and depend upon the biological output, so in some trials, a potentially high catch may be not profitable, or may require a high number of boats, which may be unreal for practical reasons; in these cases it was necessary to set three times the current number of boats (70), as the maximum number acceptable.

For the estimation of the numbers and weights of animals caught, the Baranov catch equation (Sparre and Venema 1992) is used. Here, the numbers in the exploited stock transformed into their weight are multiplied by the *F* estimated for that year; then, through an iterative procedure, an *F* value is found such that makes it equal to the catch each year of the series. Cohorts are followed over time with the aid of the Beverton & Holt (1957) stock-recruitment model, where the number of adults one year is the stock and the one-year-old juveniles next year are considered as recruits; this way it was possible to follow each cohort over time values year by year (Chávez 2005, 2014). Once changing *F*, until simulated catch attains the same value as the real data fits the model to real data, the user can explore fishing scenarios by just changing the fishing mortality (*F*), which is assumed directly proportional to the fishing effort, which is not known, and the age of first catch (*tc*). Here, all the variability of the fishery assumed caused by the *F*, such that in the process of fitting the model, recorded catch and simulated catch have essentially the same values. The model runs 30 years after the last one of real data, and a final tune up must be done for the simulation of exploitation scenarios, so that this fine tune-up reproduces the biological and socioeconomic variables of the last year of catch records. At this point, any fishing strategy as conceived by the user can be simulated on the basis that the only variables allowed to change are *F* and *tc*.

Socioeconomic variables as well as the status of the stock are linked in the spreadsheet, so that a change in *F*, in *tc* or both, cause changes in the catch and in the socioeconomic variables. The outputs are numerical and graphical, so it is possible to perceive any changes of the fishery and its internal biological and socioeconomic variables. For this part of the analysis, it is necessary to feed the model with the number of fishing days of an average season, the number of boats, and the number of fishers per boat. Total costs of the fishery are determined multiplying the costs/boat/day by the total number of boats. These values were obtained in the landing sites by interviewing the boat owners. Ideally, economic estimations are made after the examination of the logbooks. The catch value and the number of fishermen during the last fishing season are used to reconstruct the economic performance of the fishery. Economic benefits are determined by subtracting total costs from the catch value. All these values allow reconstruction of the fishery over time and on reconstructing the conditions of the last year is how the model simulates exploitation scenarios defined by the user.

RESULTS

The fisheries biology of the green crab

Catch and Stock Biomass. The first output of the model is the estimation of biomass over time. In Figure 2, the trend of the stock biomass, catch data, and simulated catch are displayed. The biomass is quite stable, ranging around 6,000 t, with a slight tendency to decline in the second half of the period. In contrast, the catch displays a tendency to increase almost from the first year, with a maximum of 379 t in the year 2009, and a drop to 234 t in 2013.

Fishing mortality (*F*) and exploitation rate (*E*). As a part of the assessment of the green crab fishery, values of these variables were estimated for the time series of the analysis (fig. 3). The variables display covariation, as expected. In this figure, two horizontal lines indicate the *F* at the maximum yield level (F_{MSY}) and the *E* at the same MSY level, allowing seeing at a glance, in which years the fishery was underexploited or overexploited. From here, it is evident that the fishery was underexploited through all the period of analysis, excepting the 2009 fishing season, when the stock was overexploited. This explains the reduction of the biomass estimated the following years, because the excess of fishing intensity began to have effect in the turnover capacity of the stock.

Economic variables, profits, and benefit/cost ratio

The performance of these variables indicates that the fishery has produced profits ranging from USD $58,930 in 2003 to USD $244,462 in 2006 being maintained in high levels (>$200,000) for the last six out of seven years, probably as a consequence of a high demand (fig. 4). The B/C ratio suggests that the economic efficiency of the green crab fishery has been high (above 2.0) throughout all the years, except in the years 2007 through 2010, when it ranged from B/C = 1.55 to 1.98; in this case, the relatively low efficiency of the activity was caused by an overexploitation of the stock, causing a decline in the biomass and therefore the high fishing effort led it to be less efficient.

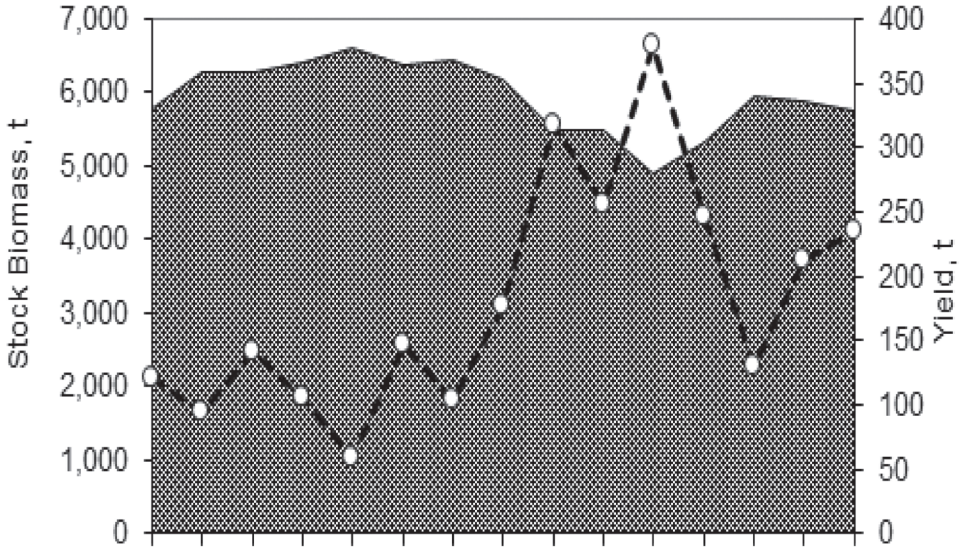

Figure 2. Stock biomass (shaded area), recorded yield (dots) and simulated yield (dotted line), fitted to catch records.

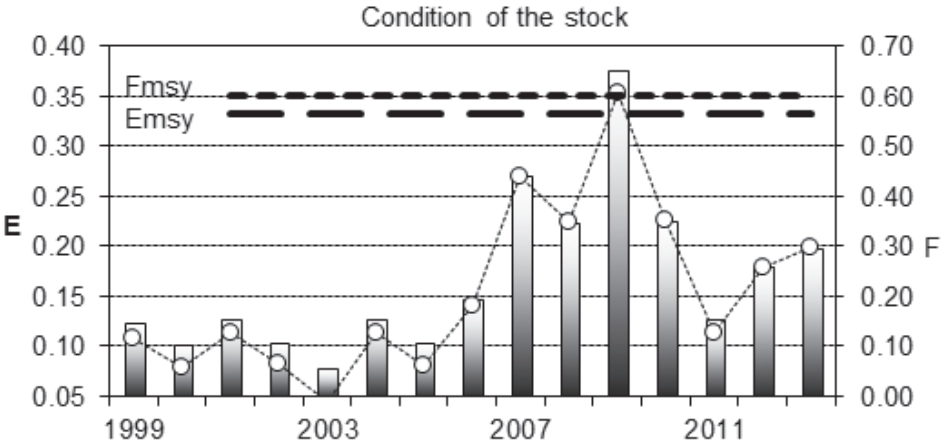

Figure 3. Fishing mortality (F), bars and exploitation rate (E), dotted line. F_{MSY} and E_{MSY} are the levels of these variables at the maximum sustainable yield and are represented as horizontal lines, as a reference to identify the fishing seasons where the fishery was under or overexploited.

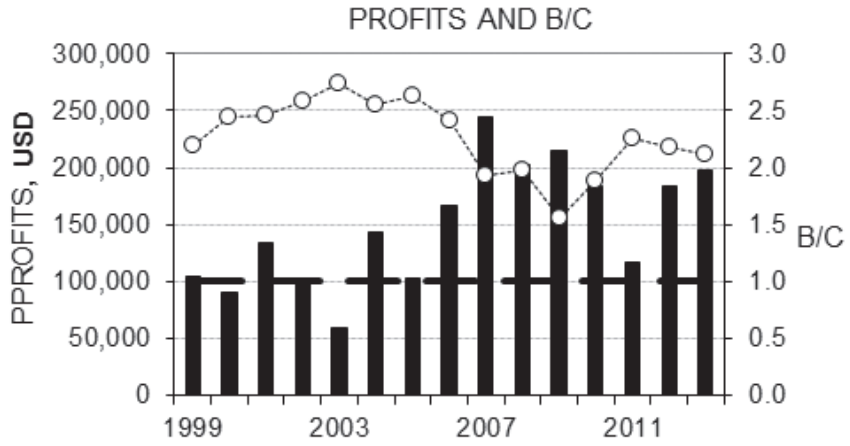

Figure 4. Economic performance of the fishery evidenced through the profits (bars, left side scale) and the benefit/cost ratio (dotted line, right side scale). The horizontal line corresponds to the economic equilibrium level = 1, when benefits and costs have the same value.

TABLE 2
Exploitation scenarios of the *jaiba verde* (*C. bellicosus*) of Magdalena Bay, Mexico. MSY: maximum sustainable yield, MEY: maximum economic yield, and MEBF: maximum economic benefit per fisher. Despite the model can find higher catch and higher profits than shown here, there were limits imposed to a maximum of 210 boats.

Management Scenarios				
Current Indicators	2012	MSY*	MEY*	MEBF*
Stock biomass t	6,769	6,663	6,663	5,769
F (/yr)	0.30	0.48	0.48	0.30
Exploitation Rate	0.20	0.29	0.29	0.20
Catch	234	405	405	234
CV	38.83	38.83	38.83	38.83
Value	374,400	648,480	648,479	374,400
Days/Boat/Season	9,864	16,031	16,031	9,864
Direct Jobs	145	425	425	145
Boats	70	210	210	70
Capacity	16,439	26,719	26,719	16,439
Days/Boat/Season	141	141	141	141
Costs/Boat/Day	18	18	18	18
Total Costs/Boat	2,535	2,525	2,535	2,535
Total Costs	177,544	288,562	288,561	177,544
Costs/Catch	759	712	712	759
B/C	2.1	2.2	2.2	2.1
Profits	196,856	359,918	359,918	196,856
Profits/Boat	2,812	1,714	1,714	2,812
Profits/Fisher	1,358	847	847	1,358
Age 1st Catch	1	3	3	2
Carapace width cm	10.6	15.6	15.6	14.1

*Selected by limiting the maximum number of boats as three times the initial number.
The model found higher values, but it was necessary to reduce the number of jobs, which was not acceptable.

Exploitation scenarios

Many exploitation scenarios can be selected; however, three options were chosen, because from the author's viewpoint, are the most evident for the stakeholders and are likely to be compared using the current condition of the fishery as reference; they are the MSY, the maximum economic yield (MEY), and the maximum economic benefit per fisher (MEBF). These targets of the simulation were evaluated in a process of dynamic optimization provided as the results of the simulation model. Numerical results of these exploitation scenarios are shown in Table 2, but in Figure 5, trends of these variables as function of F and tc are displayed.

By examining these results in Table 2, it is evident that there are many options derived from the combination of F and tc; however, numerical outputs do not discriminate social considerations to bear in mind. Therefore, it was necessary to set up some limits to the F in order to produce logical results, for instance, the maximum number of boats fixed a priori as a maximum socially acceptable of 210, was found at $F = 0.48$ (the F_{MSY} value). Another constraint imposed to the simulation was to not reduce the number of current jobs, because on the maximization search of the model, looking for the maximum total profits and per fisher, the simulation tended to reduce the number of fishers and this is considered not acceptable from the viewpoint of preservation the social value of the fishery.

By looking at results, it is remarkable to find out that within the framework of imposed constrains, the option MEBF has the same values as the current exploitation regime. In the two others (MSY and MEY), the results are coincident because of the same reason; however, without constraining the maximum number of boats, results would be quite different to each other, but not real. In conclusion, the current exploitation regime suggests that the fishermen display their activity intuitively such that they get the highest profits per fisher that the fishery can provide. As long as more fishers participate in the activity, the fishery would have to adapt to produce lower income per fisher, or they may be forced to change the fishing effort trying to maintain the current economic conditions as long as they can.

In the case of the MSY scenario, its adoption without any constrain implies a significant increase of the catch, from the current 234 t to 405 t. However, the size of first catch must be increased from 10.6 to 15.6 cm of carapace width; the profits would increase respecting to the current option, going from $196,856 to $359,918. In addition, it implies the benefit of three times more boats and the number of jobs would increase from 145 to 425. The MEY scenario shows the same values as the MSY (table 2), also by constraining the number of boats to a maximum of 210.

Data on Table 2 show specific results of the lines displayed in Figure 5a, c, corresponding to the current tc

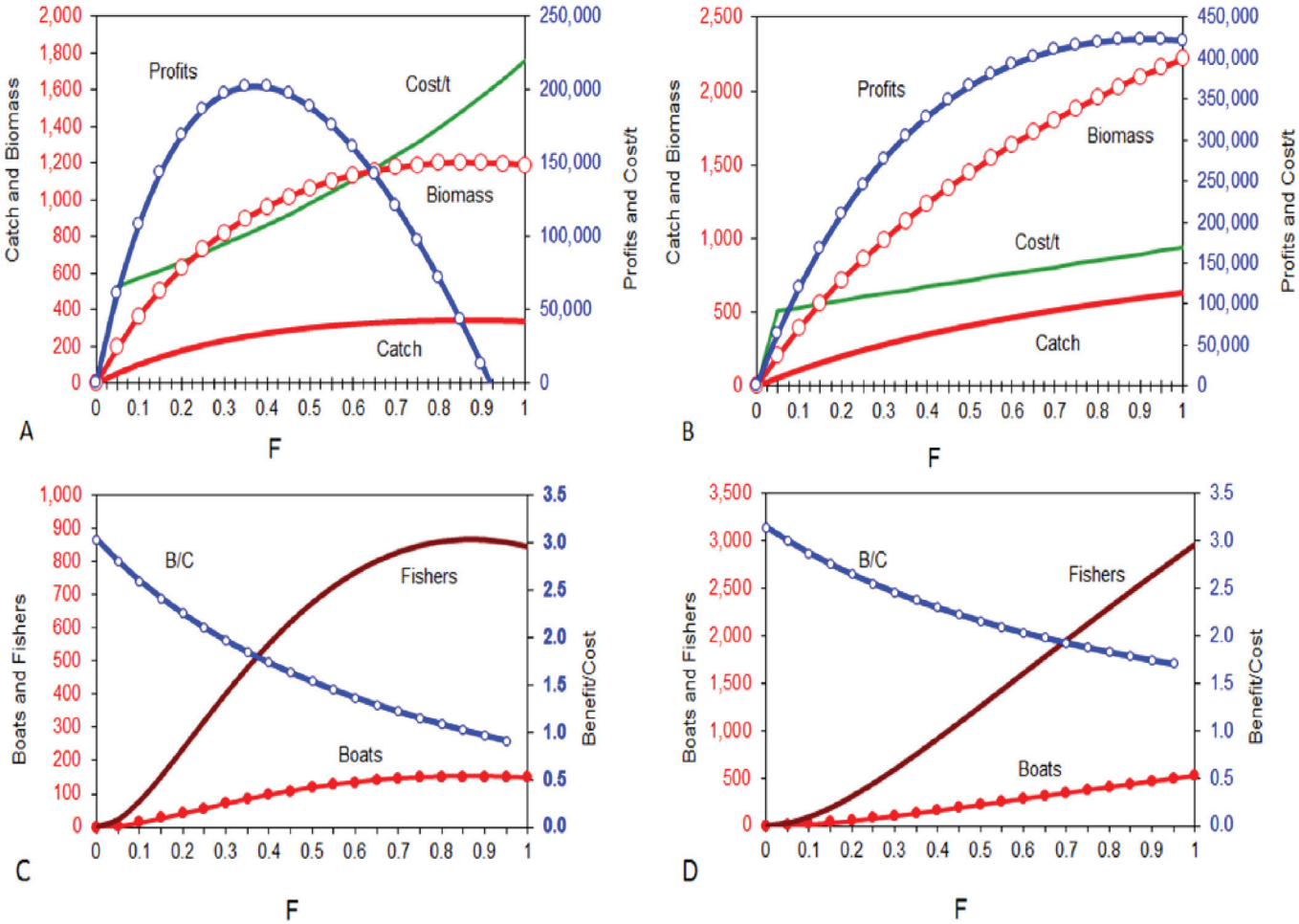

Figure 5. Display of exploitation scenarios showing the socioeconomic response of the fishery expressed as the variables catch, biomass, profits, benefit/cost, cost per t, number of boats and number of fishers under *tc* = 1 (10.6 cm, A, C left side) and *tc* = 3 (15.6 cm, B, D right side). Horizontal scale is *F*.

and they can be found by applying the value $F = 0.48$; however, in Figure 5 b, d, figures show different trend because *tc* = 3: A) trend of simulation with *tc* = 1 (carapace width = 10.6 cm); B) Same with *tc* = 3 (carapace width = 15.6 cm). The explanation of this is because when *tc* = 1 the potential production of the stock is constrained because a smaller number of crabs reaches the age of maturity, caused by the exploitation of juveniles. If *tc* = 3, a larger number of crabs is able to attain maturity age and for this reason their contribution to supply the population with more recruits may be much larger. In addition, the stock biomass is much higher than in the case when *tc* = 1 and the catch will be larger by applying the same *F*.

There are other important considerations pertinent to make by comparing these two scenarios. In reference to the economic variables, at *tc* = 1, the fishery would stop being profitable at $F = 1$. This is because the maximum stock biomass would be 1,200 *t* and the MSY = 345 t, and the cost to catch this volume is at $F = 0.9$ is $1,561. By contrast, with *tc* = 3, the stock biomass would be much higher, and at the maximum simulated $F = 1.0$, the stock biomass would be 2,221 t, but it would be not the highest one. This biomass would allow exploiting higher volumes with a lower effort at a lower cost, making the fishery more profitable with less risk of overexploiting the stock.

DISCUSSION

The model output provides estimates of the catch and other socioeconomic characteristics of the fishery, reconstructing the current conditions of the activity; afterwards the fishing mortality (*F*) and the age of first catch (*tc*) can be changed by the user to estimate the maximum yield, the maximum profits, the highest number of fishers under a profitable activity, the maximum economic benefit per fisher, and many other variables, just by changing *F* and *tc*. In addition to these, some options are able to maximize certain variables, but under non-profitable range, and the user is able to reject them; in other cases, it has been necessary to set up some limits, e.g. the maximum number of boats, as constrain for the estimation of

the F_{MSY}, F_{MEY} or the F_{MEBF}, otherwise the output values would provide unrealistic numerical options.

The development of the green crab fishery in the Mexican Pacific is quite recent and apparently its exploitation was stimulated by the crisis of the blue crab fishery in Chesapeake Bay, and provides opportunity to shrimp fishermen in June and July when the shrimp season is closed. In west Mexico, most details of the life cycle of this crab are ignored. By contrast, it is known that in the Chesapeake Bay blue crabs move upstream and downstream separately, with marked seasonal cycles of abundance (Hines et al. 1987); recruits enter the estuary in late fall and spring, growing up to 100 mm the first summer, and by the second year they reach maturity. In the study area, adults mate from July to September whilst in the eastern coast of the Gulf of California, they mate from March through September (González-Ramírez et al. 1996).

Blue crabs are segregated by the habitat by size, sex, and molt stage (Hines et al. 1987). Nursery value of habitats is largely determined by the position of crabs in the landscape (Etherington and Eggleston 2003), and fecundity is significantly related to carapace width, with a mean ranging between 2.6 to 4 million eggs (Prager et al. 1990); fecundity and age of first maturity, and the potential for fisheries-induced sperm limitation (Jivoff 2003). In west Mexico, fecundity of *C. bellicosus* ranges from 1.3 to 2.7 million eggs per female (Cisneros-Mata et al. 2014).

Due to the marine nature of the habitat in Magdalena Bay, there may be some differences in the *C. bellicosus* stock respecting to *C. sapidus* (Rathbun 1896). Female blue crab in low salinity of estuarine regions move to high salinity areas near the sea to release larvae (Carr et al. 2004), feeding intensely and acquiring energy before migrating (Jivoff 2003). The lack of rivers in the Baja California peninsula determine that waters of the Magdalena Bay to be euhaline, and the life cycle of *C. bellicosus* occurs completely in this habitat. Population persistence depends upon various combinations of threats and management must recognize and address responses to these threats (Mizerek et al. 2011).

In the Magdalena Bay fishery, the green crab displays higher reproductive activity in April–May, and mainly in August–September, although males with mature spermatophore have been seen all year round (Cisneros-Mata et al. 2014), mating on several occasions, although it is known that in the blue crab, females mate only once in their lifetime, spawning several times during the year. Topics like a decrease of males causing a reduction in egg production and a decline in recruitment (Sharov et al. 2003) must be confirmed in the green crab fishery of Magdalena Bay, which is likely to occur.

A higher abundance of males to females should be the result of an adaptive process, rather than a factor induced by exploitation; in the case of *C. bellicosus*, there is a sex ratio of about one male to 2.4 females (López-Martínez et al. 2014). In addition, males reach larger sizes than females. If this is seen as a result of natural selection, it seems logical to expect that males, which mate several times in their lifetime, should reach greater sizes enabling them to produce large amounts of sperm, enough to fertilize as many females as possible. On the other side, females are able to spawn several million eggs, despite mating only once in their lifetime. These differences in sex proportion, size, and breeding behavior may be necessary to keep balance in a steady state population.

When more details are known like spatial dynamics and dispersal of the stock biology (Etherington and Eggleston 2003), preference of male capture (Costa and Negreiros-Fransozo 1998; Sharov et al. 2003); parasite prevalence (Messik and Shields 2000), etc., a more accurate knowledge will be available for an informed decision-making process. In this regard, the application of the stock-per-recruit approach may be a convenient option for assessing the stock (Bunnell and Miller 2005); however, the use of FISMO has other advantages, being able to simulate many more exploitation scenarios. It is pertinent to mention that the development of hatcheries for replenishment of a depleted stock may offer a convenient management option for stock enhancement of the green crab fishery (Davies et al. 2003; Zmora et al. 2005; Zohar et al. 2008).

AKNOWLEDGEMENTS

The comments and suggestions by three anonymous reviewers are highly acknowledged. The author holds a research fellowship from COFAA and EDI, IPN.

REFERENCES

Arreola-Lizárraga, J. A., L. G. Hernández-Moreno, S. Hernández-Vázquez, F. J. Flores-Verdugo, C. Lechuga-Devezé, and A. Ortega-Rubio. 2003. Ecology of *Callinectes arcuatus* and *Callinectes bellicosus* (Decapoda: Portunidae) in a costal lagoon of North west Mexico. Crustaceana. 76:651–664.

Beverton, R. J., and S. S. Holt. 1957. On the dynamics of exploited fish populations. UK Ministry of Agriculture Fisheries Investigations Series 2 19:533 p.

Bunnell, D. B., and T. J. Miller. 2005. An individual-based modeling approach to spawning-potential per-recruit models: an application to blue crab (*Callinectes sapidus*) in Chesapeake Bay. Canadian Journal of Fisheries and Aquatic Sciences. 62:2560–2572.

Carr, S. D., R. A. Tankersley, J. L. Hench, R. B. Forward, and R. A. Luetich, Jr.. 2004. Movement patterns and trajectories of ovigerous blue crabs *Callinectes sapidus* during the spawning migration. Estuarine, Coastal and Shelf Science. 60:567–579.

Chávez, E. A. 2005. FISMO: A Generalized Fisheries Simulation Model. pp: 659–681. *In*: Kruse, G. H., V. F. Gallucci, D. E. Hay, R. I. Perry, R. M. Peterman, T. C. Shirley, P. D. Spencer, B. Wilson, and D. Woodby (eds.), Fisheries assessment and management in data-limited situations. Alaska Sea Grant College Program, University of Alaska, Fairbanks.

Chávez, E. A. 2014. Un modelo numérico para la administración sustentable de las pesquerías. CICIMAR Oceánides 29(2):45–56.

Cisneros-Mata, M., E. Ramírez-Félix, J. A. García-Borbón, A. Labastida-Che, C. Gómez-Rojo, and J. Madrid-Vera. 2014. Pesca de jaiba en el litoral del Pacífico Mexicano. Instituto Nacional de Pesca. 88 pp.

Costa, T. M., and M. L. Negreiros-Fransozo. 1998. The reproductive cycle of *Callinectes danae* Smith, 1869 (Decapoda Portunidae) in the Ubatuba region, Brazil. Crustaceana. 71(6):615–627.

Davis, J. L. D., A. C. Young-Williams, A. H. Hines, and J. Zohar. 2003. Assessing the potential for stock enhancement in the case of the Chesapeake Bay blue crab (*Callinectes sapidus*). Canadian Journal of Fisheries and Aquatic Sciences. 62:109–122.

Escamilla-Montes, R. 1998. Aspectos de la biología de las jaibas del género *Callinectes* en el Estero el Conchalito, Ensenada de La Paz, B.C.S. M Sc Thesis. IPN-CICIMAR. 105 p.

Estrada-Valencia, A. 1999. Aspectos Poblacionales de la Jaiba *Callinectes arcuatus* Ordway 1863, en la Laguna de Cuyutlán, Colima, México. M Sc Thesis. Faculty of Veterinarian Medicine, University of Colima. 67 p.

Etherington, L., and D. Eggleston. 2003. Spatial dynamics of large-scale multistage crab (*Callinectes sapidus*) dispersal: determinants and consequences for recruitment. Canadian Journal of Fisheries and Aquatic Sciences. 60:873–887.

González-Ramírez, P. G., J. A. García-Borbón, and P. A. Loreto-Campos. 1996. Pesquería de Jaiba. Pp: 207–226. In: Casas Valdez M, G Ponce Díaz (eds). Estudio del Potencial Pesquero y Acuícola de Baja California Sur. SEMARNAP Mexico. 365 p.

Hernández, L., and J. A. Arreola-Lizárraga. 2007. Estructura de tallas y crecimiento de los cangrejos *Callinectes arcuatus* y *C. bellicosus* (Decapoda Portunidae) en la laguna costera Las Guásimas, México Rev. Biol. Trop. 55(1):225–233.

Hines, A. H., R. N. Lipcius, and M. Haddon. 1987. Population dynamics and habitat partitioning by size, sex, and molt stage of blue crabs *Callinectes sapidus* in a subestuary of central Chesapeake Bay. Marine Ecology Progress Series. 36:55–64.

Huato-Soberanis, L., M. J. Haro-Gardy, E. Ramírez-Félix, and L. C. López-González. 2007. Estudio Socio-Económico de la Pesquería de Jaiba en Sinaloa y Sonora. CIBNOR. 92 p.

Jivoff, P. 2003. A review of male mating success in the blue crab, *Callinectes sapidus*, in reference to the potential for fisheries-induced sperm limitation. Bulletin of Marine Science. 72(2):273–286.

López-Martínez, J., L. López-Herrera, J. E. Valdez-Holguín, and C. H. Rábago-Quiroz. 2014. Population dynamics of the swimming crabs *Callinectes* (Portunidae) components of shrimp bycatch in the eastern coast of the Gulf of California. Revista de Biología Marina y Oceanografía. 49(1):17–29.

Messik, G. A., and J. D. Shields. 2000. Epizootiology of the parasitic dinoflagellate *Hematodinium* sp. in the American blue crab *Callinectes sapidus*. Diseases of Aquatic Organisms. 43:139–152.

Mizerek, T., H. M. Regan, and K. A. Hovel. 2011. Seagrass habitat loss and fragmentation influence management strategies for a blue crab *Callinectes sapidus* fishery. Marine Ecology Progress Series. 427:2477–257.

Molina-Ocampo, R. E., J. F. Márquez-Farías, and E. Ramírez-Félix. 2006. Jaiba del Golfo de California. Pp: 131–155. In: Arreguín-Sánchez F, Beléndez Moreno L, Méndez I, Gómez-Humarán I, Solana Sansores R, Rangel-Dávalos C (ed.). 2006. Sustentabilidad y Pesca Responsable en México: Evaluación y Manejo. Secretaria de Agricultura, Ganadería, Desarrollo Rural, Pesca y Alimentación. Instituto Nacional de la Pesca. México. 544 p.

Prager, M., J. R. McConaugh, C. M. Jones, and P. J. Gerr. 1990. Fecundity of blue crab, *Callinectes sapidus* in Chesapeake Bay: Biological, statistical and management considerations. Bulletin of Marine Science. 46(1):170–179.

Paul, R. 1981. Natural diet, feeding and predatory activity of the crabs *Callinectes arcuatus* and *C. toxotes* (Decapoda, Brachyura, Portunidae). Marine Ecology Progress Series. 6:91–99.

Rodríguez-Domínguez, G., S. G. Castillo-Vargasmachuca, R. Pérez-González, and A. E. Aragón-Noriega. 2012. Estimation of the individual growth parameters of the brown crab *Callinectes bellicosus* (Brachyura, Portunidae) using a multi-model approach. Crustaceana 85(1):55–69.

SAGARPA. 2013. Carta Nacional Pesquera. Secretaría de Agricultura, Ganadería, Desarrollo Rural, Pesca y Alimentación. México. 236 pp.

Sharov, A. F., J. H. Volstad, G. R. Davis, B. K. Davis, R. N. Lipcius, and M. M. Montane. 2003. Abundance and exploitation of the blue crab (*Callinectes sapidus*) in Chesapeake bay. Bulletin of Marine Science. 72(2):543–565.

Sparre, P., and S. C. Venema. 1992. Introduction to tropical fish stock assessment. Part I. Manual FAO Fisheries Technical Paper, No. 306. Rome. 376 p.

Zmora, O., A. Findiesen, J. Stubblefield, V. Frenkel, and Y. Zohar. 2005. Large-scale juvenile production of the blue crab *Callinectes sapidus*. Aquaculture. 244:129–139.

Zohar, Y. Z., A. H. Hines, O. Zmora, E. G. Johnson, R. N. Lipcius, R. D. Seitz, D. B. Eggleston, A. R. Place, E. J. Schott, J. D. Stubblefield, and J. S. Chung. 2008. The Chesapeake Bay blue crab (*Callinectes sapidus*): A multidisciplinary approach to responsible stock replenishment. Reviews in Fisheries Science. 16(1):24–34.

SEASONAL VARIABILITY OF PELAGIC AMPHIPODS OFF BAJA CALIFORNIA DURING LA NIÑA 2011 AND COMPARISON WITH A "NEUTRAL YEAR" (2005)

LADY LILIANA ESPINOSA-LEAL
BERTHA E. LAVANIEGOS
Departamento de Oceanografía Biológica
CICESE
Carretera Ensenada-Tijuana No. 3918
Zona Playitas. Apdo. Postal 360
22860 Ensenada, Baja California, México

LADY LILIANA ESPINOSA-LEAL
Departamento de Oceanografía Facultad de
Ciencias Naturales y Oceanográficas
Universidad de Concepción
Barrio Universitario s/n, Concepción
Casilla 160-C, Concepción, Chile

ABSTRACT

We describe the seasonal variation of hyperiid amphipods in oceanic waters between Punta Eugenia and Punta Abreojos, Baja California, during 2011, a cool year due to the influence of La Niña. Mean sea surface temperature in the study area was similar from January to July (16°–17°C) but cooler than usual, with anomalies of –1 to –3°C in the context of 1997–2013. Further, SST increased 3°C in October, restoring the typical temperature during this month (21°C). Vertical salinity profiles were also similar during January, April, and July, showing the influence of subarctic water in the upper layer (33.3–33.7 psu), while in October a range of higher values (33.5–33.8 psu) was observed due to the influence of subtropical water. We recorded 63 hyperiid amphipod species in 2011, the lowest number in January and the highest in October (17 and 54, respectively). Despite seasonal changes in diversity, few species (*Eupronoe minuta*, *Primno brevidens*, *Lestrigonus schizogeneios*, and *Simorhynchotus antennarius*) were the most abundant throughout the year. The exception was the warm-water species *Lestrigonus bengalensis*, which was the second most abundant in October, indicating the influence of subtropical oceanic water. Similarity analysis showed similar communities for spring and summer, while winter and autumn were very dissimilar from each other and differed from the spring–summer cluster. However, the species with highest contribution to similarity were the same (*E. minuta*, *L. schizogeneios*, and *P. brevidens*) but with different proportions. A matrix of environmental variables was correlated with the amphipod similarity matrix through a BIOENV analysis. The best combination of environmental variables (ρS = 0.644) was the 10 m depth temperature, 10 m depth salinity, mixed layer depth, stratification in the upper 100 m, and zooplankton volume (this last used as a proxy for host availability). Finally, when the community structure was compared with data from a previous amphipod study (2005), we found that species composition was very similar, but seasonal differences in the abundance of 30 of the 52 common species persist possibly due to the effects of La Niña.

INTRODUCTION

Hyperiid amphipods are marine pelagic crustaceans. The ecology of hyperiids is better known in temperate and polar regions due to their importance in food webs (Dalpadado et al. 2001; Armstrong et al. 2005; Collins et al. 2008). They have been found in stomach contents of fishes and vertebrates from tropical and subtropical regions (Repelin 1978; Satoh 2004; Mostarda et al. 2007). Amphipods exhibit symbiotic or parasitoid relationships with gelatinous organisms such as salps, ctenophores, siphonophores, and medusae (Laval 1980). Amphipod species have been used as indicator organisms because they are diverse and respond rapidly to climate events like El Niño and La Niña (Gasca et al. 2012), to decadal changes (Lavaniegos and Ohman 1999), and to the influence of mesoscale circulation (Gasca 2004; Gasca and Suarez-Morales 2004; Lavaniegos and Hereu 2009).

Few studies describing species composition in tropical regions have addressed the effects of climate variability. Gasca et al. (2012) analyzed the seasonal and interannual variability of hyperiids off the Jalisco coast during 1995–98. They observed a seasonal pattern, with one period influenced by cool water from the California Current (February–June) and another period influenced by warm water from the North Equatorial Countercurrent (July–December). Species richness and evenness were higher in the first, whereas *Hyperioides sibaginis* and *Lestrigonus bengalensis* dominated in the second. These species were particularly abundant during El Niño 1997–98. Further, Valencia et al. (2013) compared amphipod assemblages in Panama Bay during the wet and dry seasons of 2007–08. The most abundant species were also *H. sibaginis* and *L. bengalensis*, with less diversity in the neritic zone during the rainy season.

Another eastern Pacific region analyzed for seasonal variability in hyperiid abundance is the California Current (CC). Studies have been conducted in the Santa Barbara Channel (Brusca 1967a,b), off the Oregon coast (Lorz and Pearcy 1975), and off Baja California (Lavaniegos and Hereu 2009). These studies showed a mainly oceanic distribution and increasing abundance during the course of the year. Brusca (1967a) performed stratified sampling between summer 1962 and spring

1963 that suggested vertical migration for *Streetsia challengeri*, *Lestrigonus schizogeneios*, and *Primno brevidens* (the latter two reported as *Hyperia bengalensis* and *Primno macropa*). Lorz and Pearcy (1975) did not find evidence of vertical migration off Oregon over a longer period (1963–67) though only two strata were sampled (0–150 y 150–450 m). They observed some interannual variability, which was associated with a warm year in 1963, some species (*Hyperia medusarum*, *Hyperoche medusarum*, *Paraphronima gracilis*, *S. challengeri*, and *Tryphana malmi*) presenting higher abundances in the offshore region.

The most recent study on seasonal variation in the CC covered an extended area off north and central Baja California in 2005, and found minimum abundance of total amphipods in January and maximum in October (Lavaniegos and Hereu 2009). Similarity analysis showed a group associated with the main flow of the CC (*Vibilia armata*, *Lestrigonus schizogeneios*, *Eupronoe minuta*, and *Primno brevidens*), and faunistic identity for some mesoscale structures. Based on that study, the objective of the present research is to characterize the seasonal variation in hyperiid amphipod abundance during 2011 and elucidate the influence of La Niña 2010–12. The selected study area, between Punta Eugenia and Punta Abreojos (fig. 1), has high presence of tropical species and is more vulnerable to cooling.

The 2010–12 La Niña event was intense and prolonged in the Pacific Ocean. It started in July 2010, enhanced at the end of 2010 (Nam et al. 2011; Boening et al. 2012; Feng et al. 2013), and subsequently decreased in June–July 2011, though a second pulse occurred from late 2011 to mid-2012 (Hu et al. 2014). In the California Current System (CCS), intense upwelling was recorded in summer 2010, with negative temperature anomalies (1°–2°C) and low oxygen levels at some locations (Nam et al. 2011). SST anomalies off Baja California reached more negative values during La Niña 2010–12 than during La Niña 1999–2000, particularly in October 2010 and January 2011 (Bjorkstedt et al. 2011). Chlorophyll concentration presented positive anomalies and the zooplankton contained abundant medusae year round (Bjorkstedt et al. 2012; Lavaniegos et al. 2015).

METHODS

Study Area

The CCS is one of the large marine eastern boundary upwelling ecosystems, and presents high variability at different time scales. The strength of the current and mixing of the water masses vary seasonally. In spring, intense northwestern winds induce coastal upwelling and the strength of the CC is maximal, transporting a higher volume of subarctic water. As the current advances to the equator the wind field weakens, and the water is modified as a result of solar warming and mixing with subtropical water (Lynn and Simpson 1987). There is high mesoscale activity such as fronts, eddies, and squirts (Soto-Mardones et al. 2004; Jerónimo and Gómez-Valdés 2007).

The study area is located in the subtropical sector of the CCS between Punta Eugenia and Punta Abreojos (fig. 1). Punta Eugenia is considered the highest coastal prominence of the CCS and a zone of oceanographic transition (Durazo and Baumgartner 2002; Jerónimo and Gómez-Valdés 2006), with upwelling occurring year round (Zaytsev et al. 2003; Torres and Gómez-Valdés 2015). The equatorward flow prevails to the south of Punta Eugenia though the influence of the equatorial current system is perceived, mainly the North Equatorial Countercurrent, which flows eastward to the coasts of Central America and gains strength from August to January (Kessler 2006). This promotes the entrance of subtropical water off southern Baja California, slightly increasing surface salinity.

Sampling and Taxonomic Analysis

Zooplankton samples were taken during four IMECOCAL cruises performed in 2011 (fig. 1). The sampling dates for the selected study were January 1–2, April 22–25, July 14–17, and October 17–19. Oblique tows were performed at 0–200 m depth using a bongo net of 500 μm mesh width and 71 cm mouth diameter. Filtered water volume was recorded with a flowmeter in front of the net. The zooplankton samples were preserved with 4% formaldehyde buffered with sodium borate (Smith and Richardson 1977). Hydrocasts were made with a Seabird CTD in the upper 1000 m to obtain temperature and salinity data.

Thirty-five samples were analyzed for hyperiid amphipods. Two coastal shelf stations (bottom <200 m depth) where amphipods were scarce were excluded (fig. 1). All amphipods in the sample were counted and identified to species using the taxonomic keys given by Bowman (1973), Brusca (1981), and Vinogradov et al. (1996).

Data Analysis

Similarity of amphipod communities was analyzed using the Bray-Curtis index for the complete abundance database (35 samples x 63 species). We prepared a dendrogram based on the similarity matrix using the group average. Statistical significance of clusters was established with the SIMPROF test (PRIMER v.6; Clarke and Warwick 2001). Additionally, we performed a nonmetric multidimensional scaling (NMDS) analysis to supplement the ordination obtained in the dendrogram. The contribution to similarity by species in each cluster was estimated with SIMPER (Clarke and Warwick 2001).

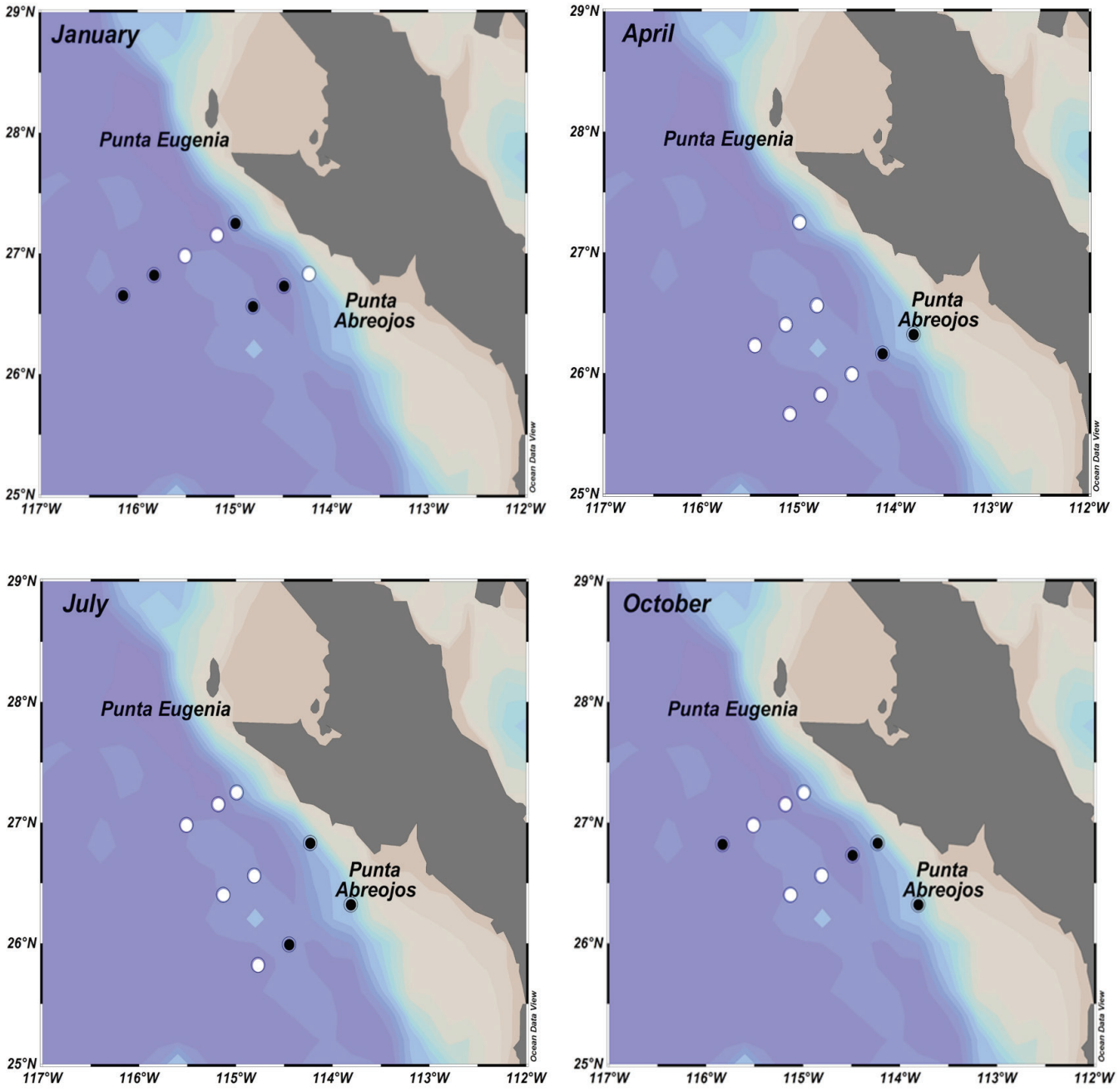

Figure 1. Sampling stations during 2011. White (black) symbols indicate occupancy during daytime (nighttime). Gray area is the coastal shelf (<200 m depth).

Evaluation of biophysical coupling was done with the BIO-ENV procedure found in Primer (Clarke and Warwick 2001). This analysis performs Spearman correlation between two similarity matrices, one is the amphipod species matrix and the other is the explanatory matrix based on Euclidian distances among environmental variables (table 1). The community matrix is fixed and for the environmental matrix, all subsets of possible combinations of variables are examined to select the best combination, that is, the one that maximizes the Spearman correlation coefficient. The depth of the mixed layer was defined as the depth where temperature changed 0.5°C relative to SST. The stratification index, based on density, was calculated following Simpson et al. (1978) for layers of 0–50, 0–100, and 0–200 m depth.

The hyperiid community of 2011 was compared with previous data from 2005 using similarity analysis. The abundances of dominant amphipod species were compared by a two-factor analysis of variance between year and month, previous transformation of data to log-

TABLE 1
Environmental variables used in correlation analysis with the similarity matrix of amphipod species through the BIOENV analysis.

Variable	Abbreviation
Temperature at 10, 30, 50, and 200 m depth	T10, T30, T50, T200
Salinity at 10, 30, 50, and 200 m depth	S10, S30, S50, S200
Dissolved Oxygen at 10, 30, 50, and 200 m depth	DO10, DO30, DO50, DO200
Mixed Layer Depth	MLD
Stratification Index from surface to 50, 100, and 200 m	SI50, SI100, SI200
Integrated Chlorophyll *a*	Ch-*a*
Zooplankton Biomass	ZB

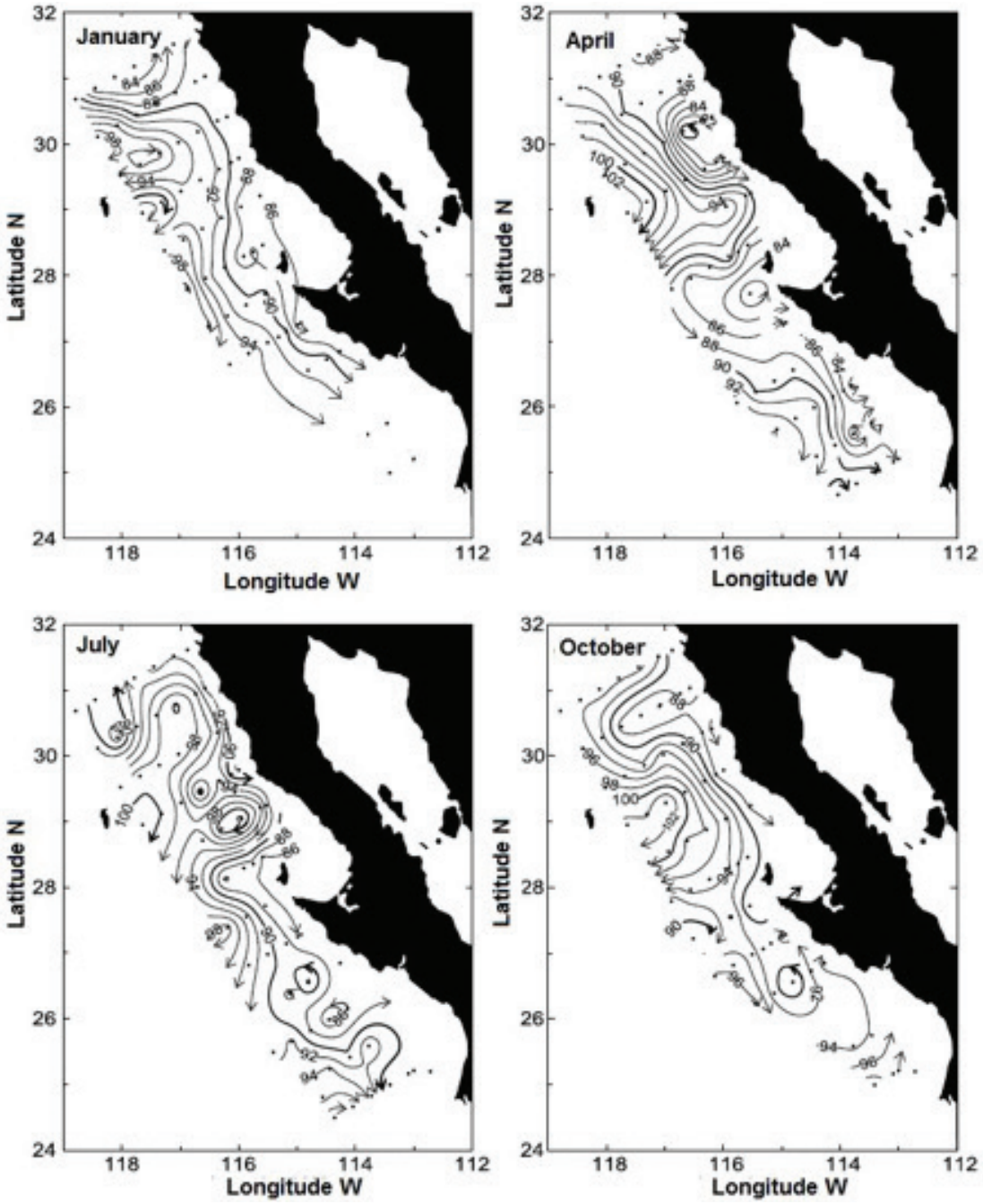

Figure 2. Geostrophic flow during 2011 estimated from 0/500 dbar dynamic height anomalies. Contour interval is 2 dynamic cm. Current direction is indicated by arrows.

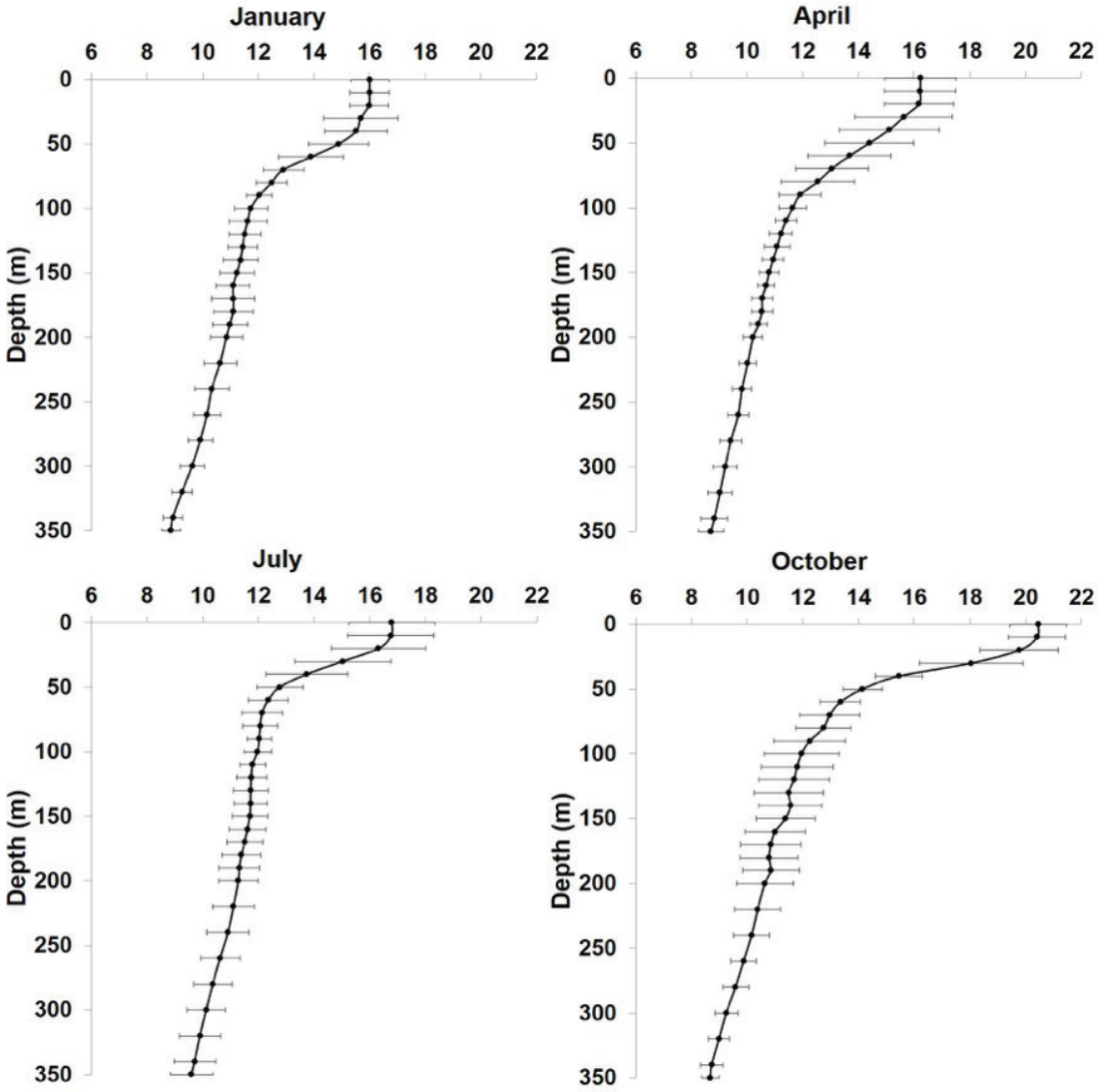

Figure 3. Vertical profiles of mean temperature (°C) and standard deviation during the four seasons in 2011.

arithms. Since the 2005 data were obtained exclusively at nighttime stations but the 2011 data combined both day and night stations, we first compared the 2011 day and night data in order to evaluate any possible influence of diel vertical migration of the organisms. Since most of the species did not present differences all samples were included for interannual comparisons.

RESULTS

Environmental Conditions

Surface circulation derived from dynamic height showed equatorward flow during the four seasons in 2011 (fig. 2). During spring and summer the flow was more intense to the north of Punta Eugenia, but there were no notable differences to the south. Mesoscale structures were minimal in January though deficient sampling in the southern part of the study area did not allow resolving the geostrophic flow. A cyclonic eddy was observed off Punta Eugenia during April but further south the flow normalized and enhanced in the study area. Small eddies were observed in July, with the main flow toward the equator. Finally, in October, a return flow from the south was observed introducing subtropical water into the study region (fig. 2).

Surface temperature (10 m) showed similar values from January to July, with mean temperature of 16°–17°C, and increased 3°C in October (fig. 3). However, below 50 m depth the temperature decreased to 14°C; therefore, in October, the thermocline was strong. Vertical salinity profiles were also similar from January to July, presenting two layers separated by a halocline (fig. 4). The upper low-salinity layer (33.3–33.7 psu) corresponding to subarctic water had variable thickness, reaching 60 m in January

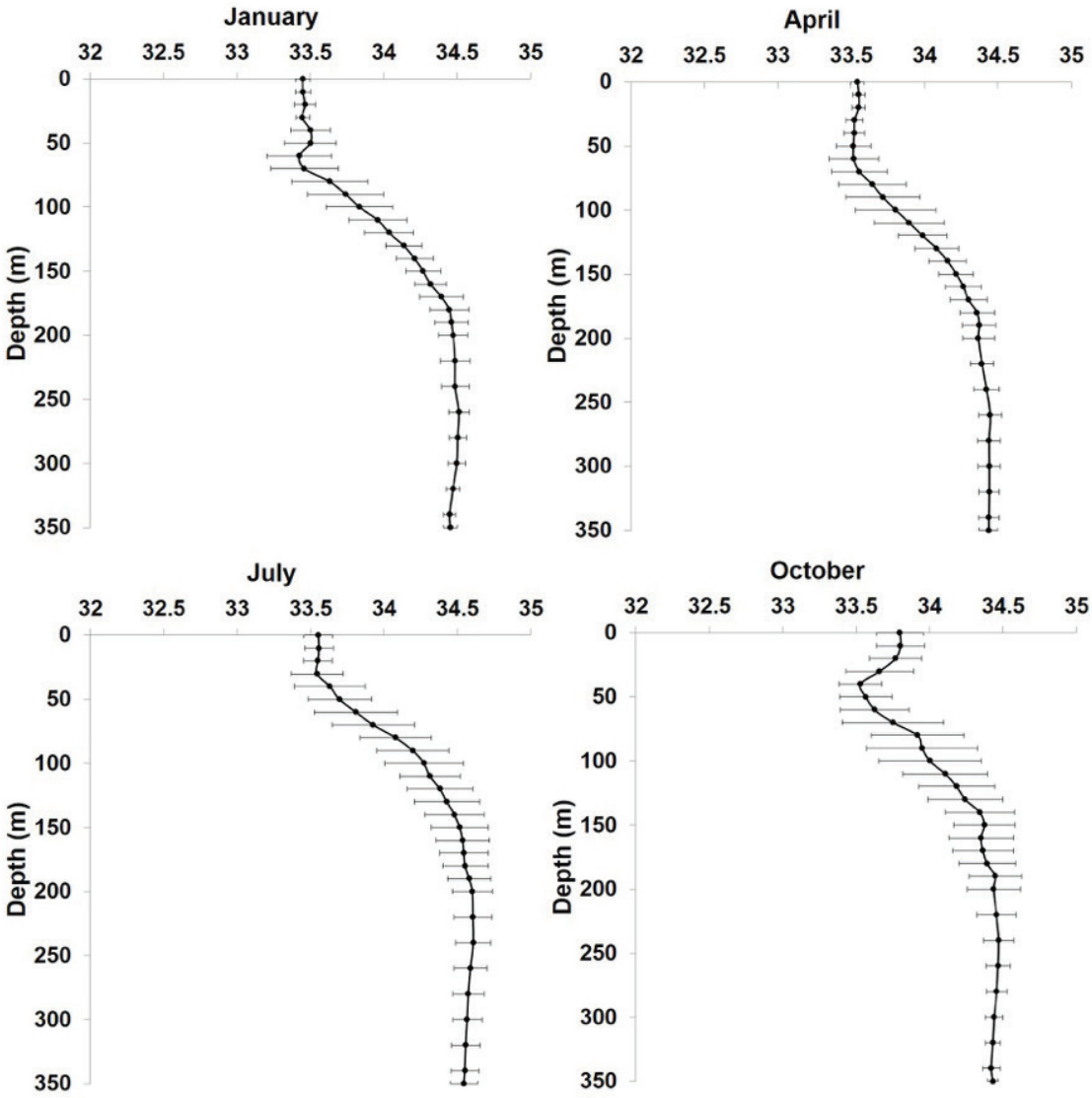

Figure 4. Vertical profiles of mean salinity (psu) and standard deviation during the four seasons in 2011.

and April, and 40 m in July. The halocline presented a progressive salinity increase by mixing with subsurface equatorial water, reaching 34.5 psu around 170 m depth.

In contrast, October presented a three-layer structure due to the presence of more saline subtropical water (33.8–34.0 psu) in the upper 30 m. Beneath this layer, the nucleus of low-salinity subarctic water was evident at 40–70 m depth, and below, salinity increased again, with maximum salinity around 200 m depth. Note that in October there was higher subsurface variability with higher standard deviation values (fig. 4), possibly linked to the cyclonic eddy affecting the study area (fig. 2).

Amphipod Community

A total of 63 species were found over the entire study period, but their presence varied seasonally (appendix 1). The most common species throughout the year were *E. minuta*, *L. schizogeneios*, and *P. brevidens*. *S. antennarius* was also common except in January 2011, when it was present in only two samples. In contrast, some species such as *Eupronoe maculata*, *Hyperietta vosseleri*, and *Scina similis*, among others, occurred at only one station during the entire period and were therefore considered rare.

The number of species as well as cumulative abundance increased during the course of the year (fig. 5). In January, 17 species were recorded with a cumulative geometric mean (GM) of 31 ind/1000 m^3. By April the number of species was twice as high and the cumulative GM increased fourfold (133 ind/1000 m^3). The number of species decreased slightly in July (from 32 to 28) but the cumulative GM increased (245 ind/1000 m^3), indicating higher dominance of certain species. Finally, the highest number of species (54) and cumulative GM (327 ind/1000 m^3) occurred in October.

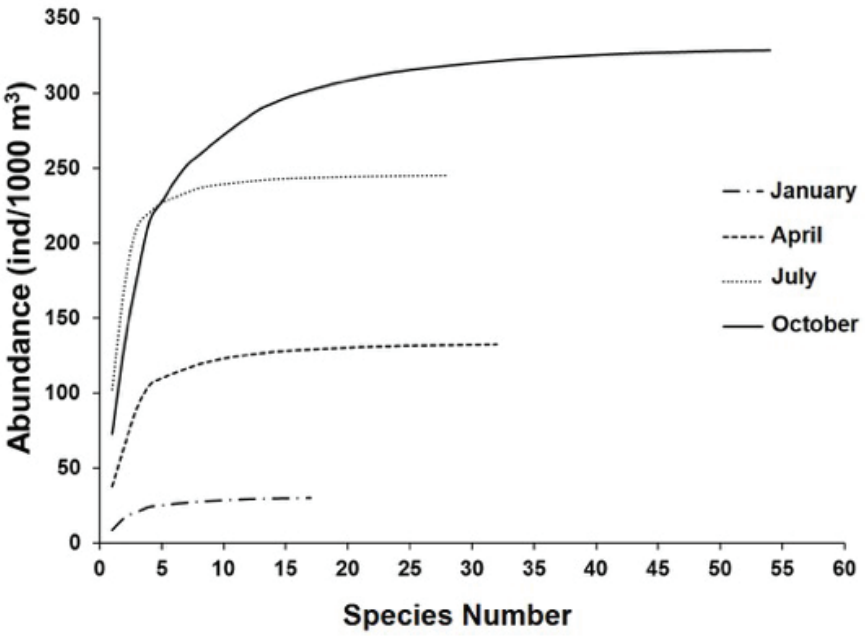

Figure 5. Cumulative abundances of amphipod species based on geometric means in decreasing order during the four seasons in 2011.

The dominant hyperiids during winter were *E. minuta*, *L. schizogeneios*, *P. brevidens*, and *V. armata*. They presented a GM ranging from 3.5 to 8.7 ind/1000 m^3, whereas the rest of species were below 2 ind/1000 m^3 (appendix 1). Other small juvenile organisms could not be identified to species but most of them belonged to the genera *Lestrigonus* and *Scina* (GM of 1.1 and 1.0 ind/1000 m^3, respectively).

In April, three dominant species (*E. minuta*, *L. schizogeneios*, and *P. brevidens*) presented GM = 38, 25, and 27 ind/1000 m^3 respectively, increasing between 240 and 525% in relation to January (appendix 1). In contrast, the abundance of *V. armata* increased moderately (32%) and it was displaced from fourth place by *S. antennarius*. Of the remaining species, one third ranged from 1 to 4.7 ind/1000 m^3 and the rest were below 0.6 ind/1000 m^3. A large number of juvenile *Lestrigonus* were found, probably pertaining to the dominant species (*L. schizogeneios*), with a GM = 36 ind/1000 m^3.

During summer, the three most abundant species continued to be *E. minuta*, *L. schizogeneios*, and *P. brevidens* but the abundance of only the last two increased (GM = 103 and 69 ind/1000 m^3, respectively), while that of *E. minuta* was similar to spring (appendix 1). Five other species showed abundances of 3 to 9.8 ind/1000 m^3, and the rest were below 2 ind/1000 m^3. As in spring, abundant juvenile *Lestrigonus* were recorded (GM = 47 ind/1000 m^3).

The most remarkable changes in composition occurred in October. The four most abundant species were *L. bengalensis*, *L. schizogenios*, *P. brevidens*, and *S. antennarius* (GM = 60, 73, 44, and 38 ind/1000 m^3, respectively). The abundances of *E. minuta* and *L. schizogeneios* decreased 65% and 29%, respectively, from July to October, whereas the population of *S. antennarius* increased 280%. Many common species observed in previous months increased in abundance during October, and other species not previously observed were recorded (*Anchylomera blossevillei*, *Tetrathyrus arafurae*, *T. forcipatus*, among others).

Cluster Analysis

Similarity analysis among stations produced four clusters (Simprof $p < 0.05$) that evidenced structural seasonal differences in the amphipod community during 2011 (fig. 6A). Most of the stations sampled in winter and autumn fell into separate clusters (2 and 1, respectively), while spring and summer presented a strong similarity and shared cluster 4. The NMDS analysis confirmed the separation of the clusters (fig. 6B).

The amphipod assemblage from the autumn cluster (1) had the maximal mean similarity (68.9%) of all clusters. The main species contributing to similarity were *L. schizogeneios* and *P. brevidens* with 8.5% each (fig. 7). However, three other species (*L. bengalensis*, *Platyscelus ovoides/serratulus*, and *S. antennarius*) had equally high percentages (7.2%–8.1%). This, in addition to the higher contribution of species in the "others" category, denoted a more diverse community compared to the rest of the clusters, with greater equitability in abundances per species.

The winter cluster (2) presented the minimal mean similarity (53.7%). *E. minuta*, *L. schizogeneios*, and *P. brevi-*

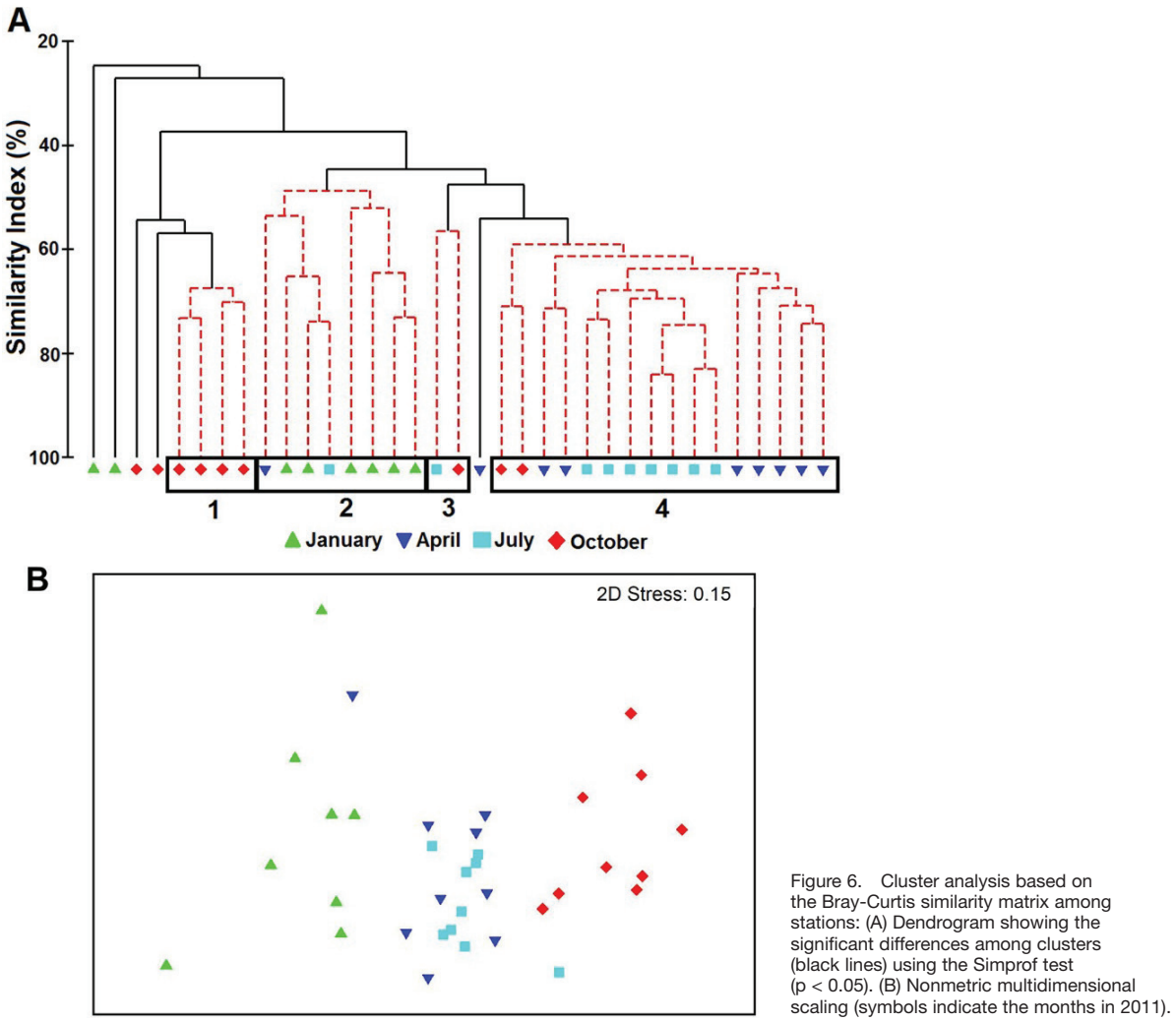

Figure 6. Cluster analysis based on the Bray-Curtis similarity matrix among stations: (A) Dendrogram showing the significant differences among clusters (black lines) using the Simprof test ($p < 0.05$). (B) Nonmetric multidimensional scaling (symbols indicate the months in 2011).

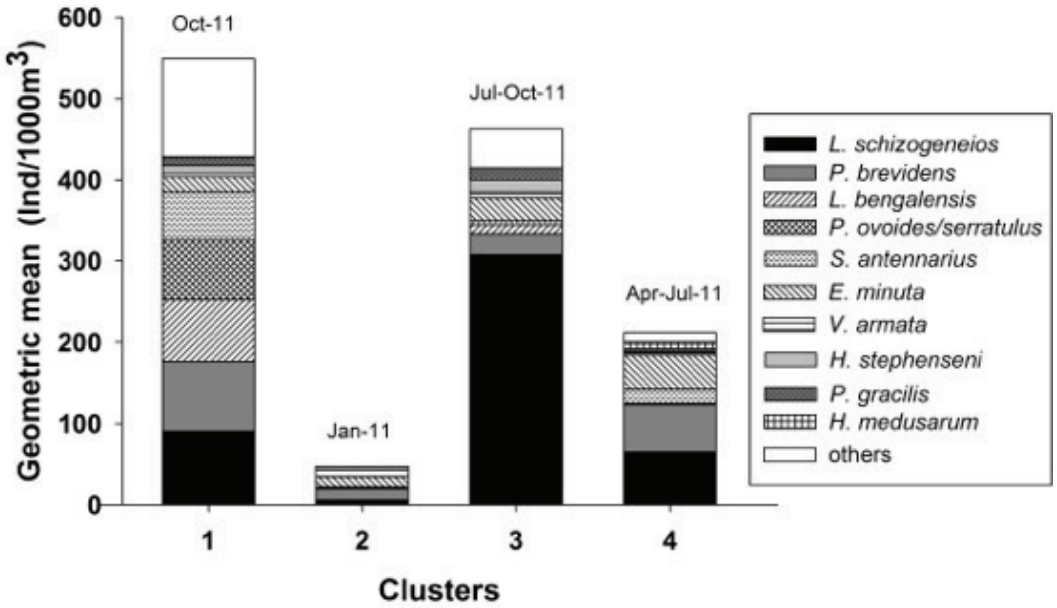

Figure 7. Stacked geometric means for the main species contributing to similarity in the clusters shown in Figure 6. The selected species are a combination of the five species with the highest contribution in each cluster obtained by SIMPER analysis. The "others" category indicates the sum of the remaining species.

TABLE 2
The best variable combinations obtained with BIOENV correlation analysis between the hyperiid amphipod community and environmental variables. Number of variables (k), Spearman rank correlation (ρS), Temperature (T10), Salinity (S10), and Dissolved Oxygen at 10 m depth (DO10), Mixed Layer Depth (MLD), Stratification Index 0–50 m (SI50), Stratification Index 0–100 m (SI100), and Zooplankton Biomass (ZB).

k	Best Variable Combinations	ρS
4	ZB, MLD, S10, T10	0.644
	ZB, MLD, S10, SI100	0.643
	ZB, MLD, S10, DO10	0.628
	ZB, MLD, T10, SI100	0.620
5	ZB, MLD, S10, T10, SI100	0.644
	ZB, MLD, S10, SI100, DO10	0.637
	ZB, MLD, S10, T10, SI50	0.623
	ZB, MLD, S10, T10, DO10	0.621
6	ZB, MLD, S10, T10, SI100, DO10	0.620
	ZB, MLD, S10, T10, SI100, SI50	0.620

dens made the highest contribution with a pooled similarity of 74% (fig. 7). However, the absolute abundance of amphipods was very low, with GM of 6, 14, and 13 ind/1000 m^3 for each one of these three species.

A pair of stations, one from July and another from October formed cluster 3, with a pooled similarity of 56.5%. The main contribution came from *L. schizogeneios* (21%), which was strongly dominant (GM of 308 ind/1000 m^3).

The highest number of stations joined in cluster 4, mainly from spring and summer, with global similarity of 63.9%. *E. minuta*, *L. schizogeneios*, and *P. brevidens* contributed the most to similarity (57.6%). These species were the same as in cluster 2, but in cluster 4 the cumulative percentage was lower. However, absolute abundance of them was considerably higher, with GMs of 42, 65, and 58 ind/1000 m^3, respectively (fig. 7).

Relation between the amphipod community and hydrography

Correlation analysis between the similarity matrix (amphipod community) and environmental conditions matrix (table 1) produced several combinations with four to six more influential variables (table 2). Spearman correlation (ρS) had similar values in all the selected combinations, and a global coefficient of 0.644, with a significance of 1% in 99 permutations. The suite of variables that best explained the community structure was a combination of temperature and salinity at 10 m depth, mixed layer depth, and the zooplankton biomass. The addition of a fifth variable (0–100 m stratification index) did not add more value to ρS, which means that increased stratification and a narrower mixed layer depth are strongly correlated.

If the environmental variables are shown with the coordinates of the NMDS plot (fig. 6B), a characteristic pattern emerges (fig. 8). Temperature at 10 m depth was similar in January and April, and the stations are positioned on the left side of the NMDS plot. It increased slightly in July and strongly in October and the stations are on the right side of the NMDS plot (fig. 8A). Salinity at 10 m depth showed a similar trend (fig. 8B). This incrementing pattern illustrates the influence of subtropical oceanic water in autumn. Furthermore, the mixed layer depth was wider during January–April but became shallower during July–October (fig. 8C). In concordance, stratification increased during the year, reaching maximal values in October (fig. 8D) as denoted by a strong thermocline (fig. 4).

Zooplankton biomass was low in winter but high from April to October, and there was high variability among stations (fig. 8E). Considering zooplankton biomass as indicator of gelatinous organisms, which contributed strongly to the volume, it is clear why amphipod abundance was so poor in January. The increase in amphipod abundance in subsequent months is consistent with greater availability of gelatinous substrate that is used by hyperiids for reproduction and feeding.

Comparison of the 2011 and 2005 amphipod communities

Before comparing amphipod communities between years, we compared abundances between sampling hours (day and night) for the year 2011 in order to discard the possible influence of diel vertical migration. Significant differences were found only for two species: *E. minuta* ($U = 80$, $p = 0.031$) and *V. armata* ($U = 74$, $p = 0.017$). The first presented higher abundance in daylight samples and the inverse occurred with the second. Due to the low number of nighttime samples for 2011 ($n = 13$), and since most of the species did not present significant day-night differences, all data from 2011 were used to compare a "cool" year (2011) with a "neutral" year (2005). However, one should keep in mind that the 2005 data based exclusively on nighttime samples may overestimate the abundance of *V. armata* and underestimate the abundance of *E. minuta* in relation to 2011, and that both are influential species due to their abundances.

Analysis of variance with year and month as factors showed significant interannual differences for several dominant species (table 3). The abundance of the preponderant species *L. schizogeneios* and *P. brevidens* was higher in 2011 than in 2005. The abundance of these species and that of *S. antennarius* tripled in 2011, and *T. malmi*, a rare species in 2005, was more common in 2011. However, the abundances of a large number of species declined during the cool year. The most notable was *V. armata* that in 2005 had a GM = 23 ind/1000 m^3 but only 20% of this amount during the cool year of 2011. A similar decrease was also observed for *P. curvi-*

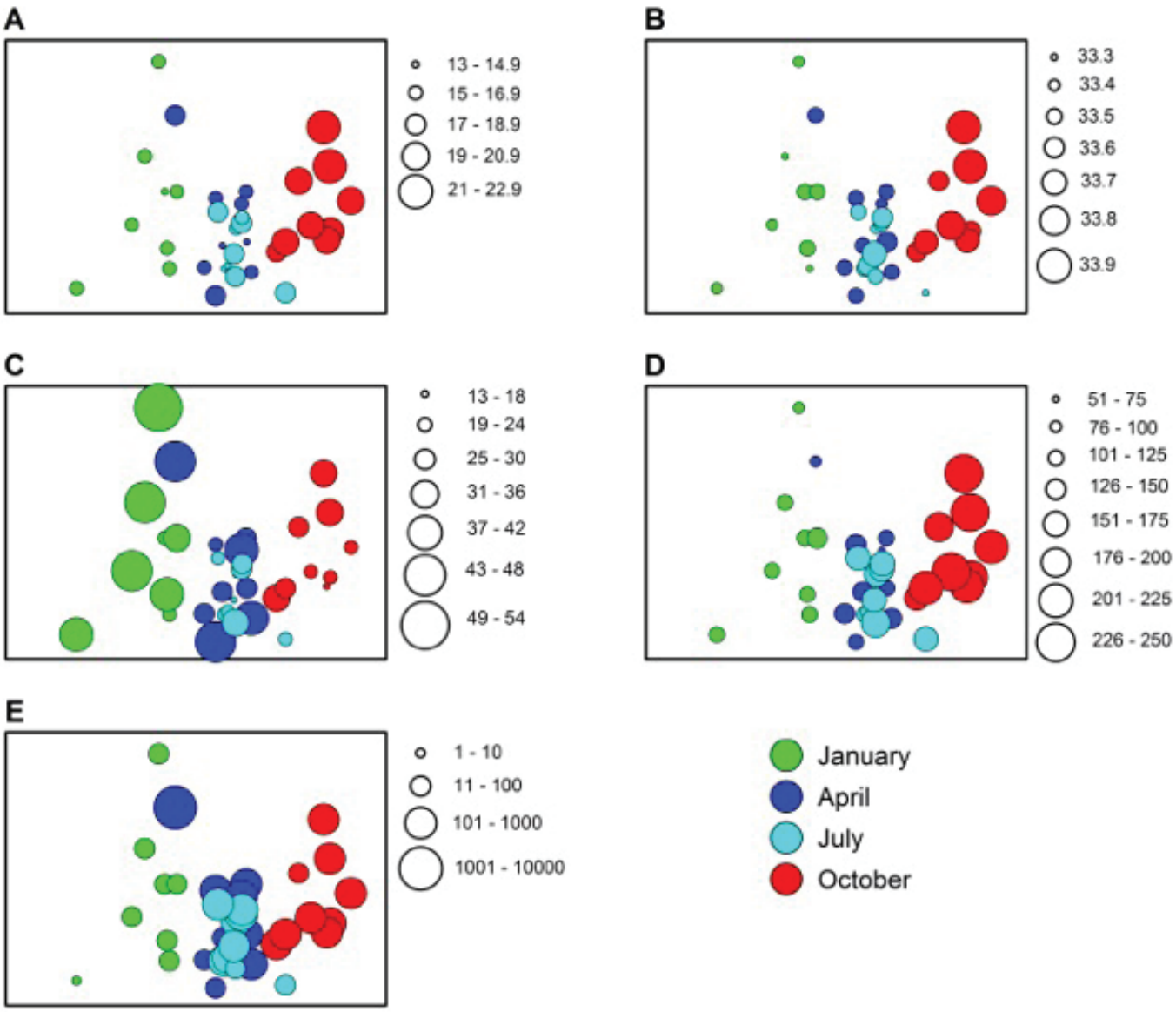

Figure 8. NMDS as in Figure 6 but varying the symbol sizes as a function of the environmental variables: (A) 10 m depth temperature, (B) 10 m depth salinity, (C) mixed layer depth (m), (D) stratification index of 0–100 m, and (E) zooplankton biomass (µl m^{-3}).

pes, *P. semilunata*, *S. borealis*, and *V. asutralis*. Other species were completely absent in the study region during 2011, such as *A. sculpturatus*, *V. gibbosa*, and *V. viatrix*, among others of certain importance in 2005. The ANOVA also indicated interaction between seasonal and interannual effects. *A. blossevillei*, *E. maculata*, *L. bengalensis*, *L. shoemakeri*, *L. pulex*, *P. atlantica*, and *R. whitei* presented interannual differences limited to some part of the year (table 3). For example, *A. blossevillei* and *L. bengalensis* were absent from January to July of 2011 but in October had similar abundances in both years. Finally, several other species did not show interannual differences but only the expected seasonal variability (table 3).

The similarity analysis combining data from 2005 and 2011 produced twelve clusters (Simprof $p < 0.05$). Four of them were identical to the clusters obtained using only 2011 data, and the numeration of clusters (1–4) was retained (fig. 9A). The rest of the conglomerates exclusively presented stations from 2005, configuring two for winter (clusters 5 and 7), two for spring (clusters 6 and 12), one for summer (cluster 11), and three for autumn (clusters 8–10). The formation of separate clusters for each year denoted interannual dissimilarity. However, the NMDS showed proximity between points of the same seasons in July and October, but not in January and April (fig. 9B). In the NMDS the stress was moderately high (0.19), indicating difficulties in establishing a two-dimensional arrangement. Therefore, we decided to maintain the arrangement obtained in the dendrogram.

TABLE 3
Dominant amphipod species from the Punta Eugenia-Punta Abreojos region. The geometric mean (GM) abundance during a "neutral year" (2005) and a cool year (2011) is shown, and the associated probability of two-way ANOVA with factors year and month. Significant values are highlighted in bold for $\alpha = 0.001$.

Species	GM (ind/1000 m^3) 2005	2011	Year	Month	Year*Month
Amphithyrus sculpturatus	1.0	—			
Anchylomera blossevillei	1.6	0.2	**<0.001**	0.115	**0.001**
Eupronoe maculata	1.0	<0.1	**0.001**	**<0.001**	**<0.001**
Eupronoe minuta	14.5	21.0	0.259	**<0.001**	0.043
Hyperoche medusarum	1.5	2.1	0.746	**<0.001**	0.567
Hyperioides longipes	0.9	0.3	0.112	0.034	0.388
H. sibaginis	1.4	0.9	0.546	**<0.001**	0.272
Hyperietta stephenseni	1.1	1.5	0.469	**<0.001**	0.344
Laxohyperia vespuliformes	1.3	0.8	0.126	**<0.001**	0.019
Lestrigonus bengalensis	7.8	1.9	**<0.001**	**<0.001**	**0.001**
L. schizogeneios	10.6	31.9	0.001	**<0.001**	0.537
L. shoemakeri	3.2	0.6	**<0.001**	0.003	**<0.001**
Lycaa pulex	2.7	0.5	**<0.001**	**<0.001**	0.001
Lycaeopsis themistoides	0.9	0.6	0.258	0.004	0.471
Oxycephalus clausi	1.8	0.7	0.017	**<0.001**	0.009
Paraphronima gracilis	2.9	2.8	0.534	**<0.001**	0.154
Phronima atlantica	1.5	0.7	0.011	0.024	**<0.001**
P. curvipes	1.2	0.1	**<0.001**	0.327	0.058
P. sedentaria	1.0	0.7	0.366	0.940	0.143
P. stebbingi	0.8	0.7	0.611	0.233	0.013
Phronimopsis spinifera	0.2	0.8	0.005	0.083	0.009
Phrosina semilunata	2.9	0.8	**<0.001**	**<0.001**	0.050
Platyscelus ovoides / P. serratulus	4.5	2.7	0.181	0.003	0.059
Primno brevidens	9.3	30.1	**<0.001**	**<0.001**	0.036
Rhabdosoma whitei	1.4	0.4	0.007	0.050	**0.001**
Scina borealis	0.8	0.1	**<0.001**	0.118	0.087
S. tullbergi	2.0	1.2	0.040	**<0.001**	0.105
Simorynchotus antennarius	2.4	9.4	**<0.001**	**<0.001**	0.002
Streetsia challengeri	0.7	0.2	0.003	0.157	0.036
Themistella fusca	0.6	0.4	0.501	**<0.001**	0.224
Tryphana malmi	0.1	1.9	**<0.001**	0.014	0.005
Vibilia armata	22.8	4.4	**<0.001**	0.103	0.097
V. australis	1.5	0.2	**<0.001**	0.053	0.289
V. gibbosa	1.0	—			
V. stebbingi	0.6	0.5	0.871	**<0.001**	0.846
V. viatrix	2.4	—			

The two clusters from January 2005 had low internal similarity, averaging 41.9% and 55.2% for clusters 5 and 7, respectively. The main species contributing to the similarity differed in each winter group (fig. 10). Group 5 included mainly nearshore stations with sparse hyperiids, *E. minuta*, *P. sedentaria*, and *Platyscelus ovoides/serratulus* being the main contributors with a pooled similarity of 51%. Hyperiid abundance was slightly higher in cluster 7 containing offshore stations (fig. 11), with *R. whitei*, *V. armata*, and *V. viatrix* as the most influential species (38% of cumulative similarity). The winter clusters from 2005 contrasted with the winter 2011 cluster 2, in which *E. minuta* and *P. brevidens* contributed 58% of the similarity (fig. 10) and did not present separation between nearshore and offshore stations (fig 11). *E. minuta* and *P. brevidens* had GMs of 13 and 14 ind/1000 m^3, respectively, compared to lower GMs in cluster 5 (8 and 2 ind/1000 m^3) and cluster 7 (3 and 1 ind/1000 m^3).

In April 2005, the two assemblages (clusters 6 and 12) contrasted strongly both in abundance and species composition (figs. 10 and 11). The cumulative sum of GMs from all species amounted to 84 ind/1000 m^3 in cluster 6 formed by offshore stations and to 337 ind/1000 m^3 in cluster 12 with nearshore stations. Mean similarity was relatively high in both (61.1% and 65.8%, respectively). The main species contributing to similarity in cluster 6 were *P. semilunata*, *P. ovoides/serratulus*, and *V. armata* (46%), while *E. minuta* and *P. brevidens*, characteristic of the CCS were absent. Cluster 12 contributed strongly to similarity due to *V. armata* (12.5%), followed by *E. minuta* (10.1%) and *V. gibbosa* (9.6%), all them with high GMs (113, 44, and 42 ind/1000 m^3, respectively). Compared to the 2011 spring–summer cluster 4, cluster 6 had high dissimilarity in dominant CCS species (*E. minuta*, *L. schizogeneios*, and *P. brevidens*). The differences between clusters 4 and 12 were due to three *Vibilia* species, with *V. gibbosa* and *V. viatrix* absent in 2011 and *V. armata* hav-

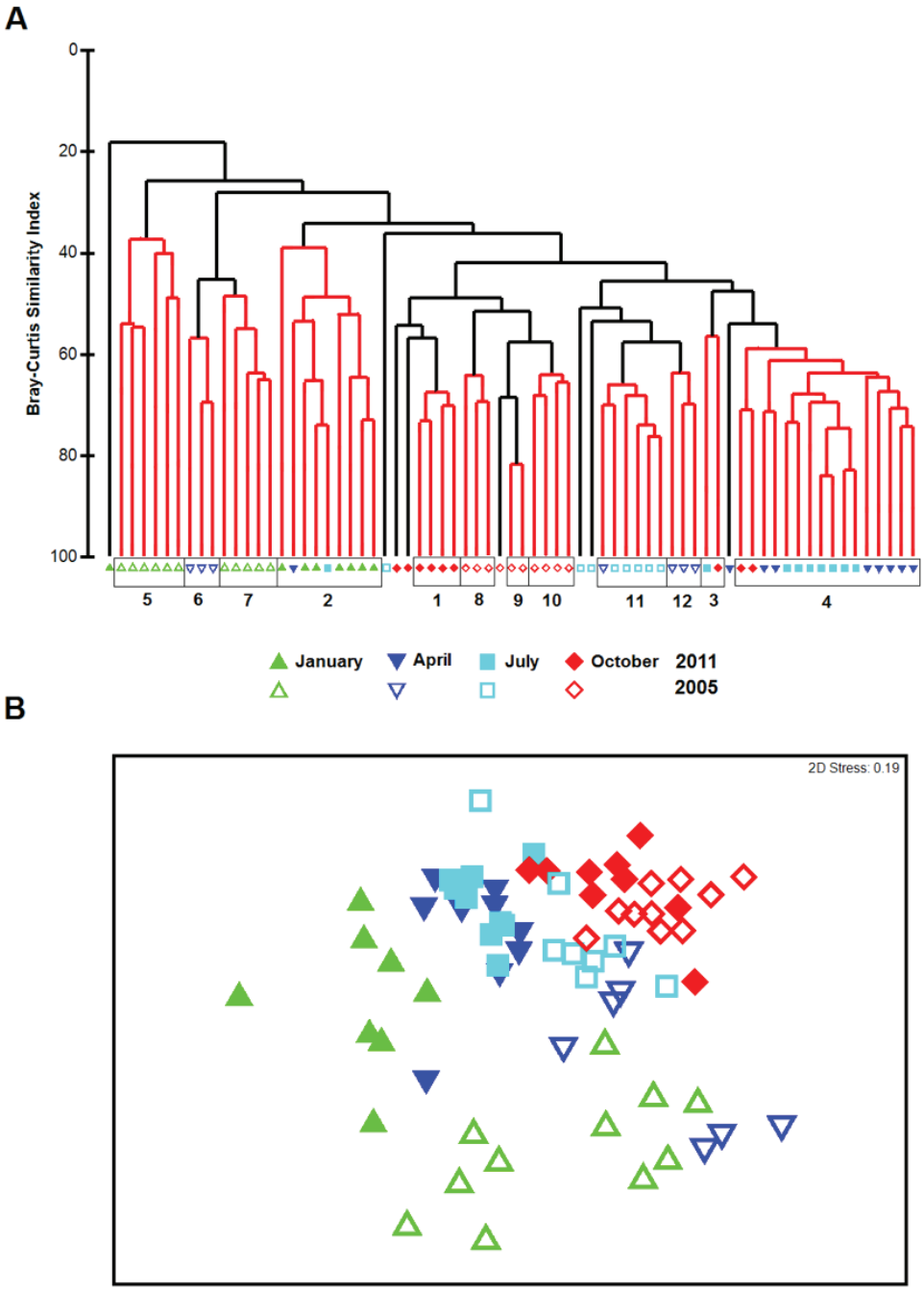

Figure 9. Cluster analysis based on the Bray-Curtis similarity combining stations from 2005 and 2011: (A) Dendrogram showing, with black lines, the significant differences among clusters using the Simprof test ($p < 0.05$). (B) Nonmetric multidimensional scaling with symbols indicating the months from 2005 (open) and 2011 (closed).

ing a GM of only 2 ind/1000 m^3, though this low estimate may not be reliable because of the inclusion of daytime samples in 2011.

The 2005 summer amphipod community only formed cluster 11, which included nearshore stations, and the only offshore station was excluded from this cluster (fig. 11). It presented strong dominance of *V. armata* (GM = 173 ind/1000 m^3) and other CC species (*E. minuta*, *L. schizogeneios*, and *P. brevidens*), which overall embraced a similarity of 37%. Cluster 11 was close to cluster 12 (from April 2005) in the dendrogram (fig. 9) and both were relatively close to cluster 4 (April–July 2011). The dissimilarity between clusters 11 and 4 is attributed mainly to *L. bengalensis* and *V. armata* (fig. 10).

October 2005 had a varied assortment of groups. The two main ones (clusters 8 and 10) show a north-

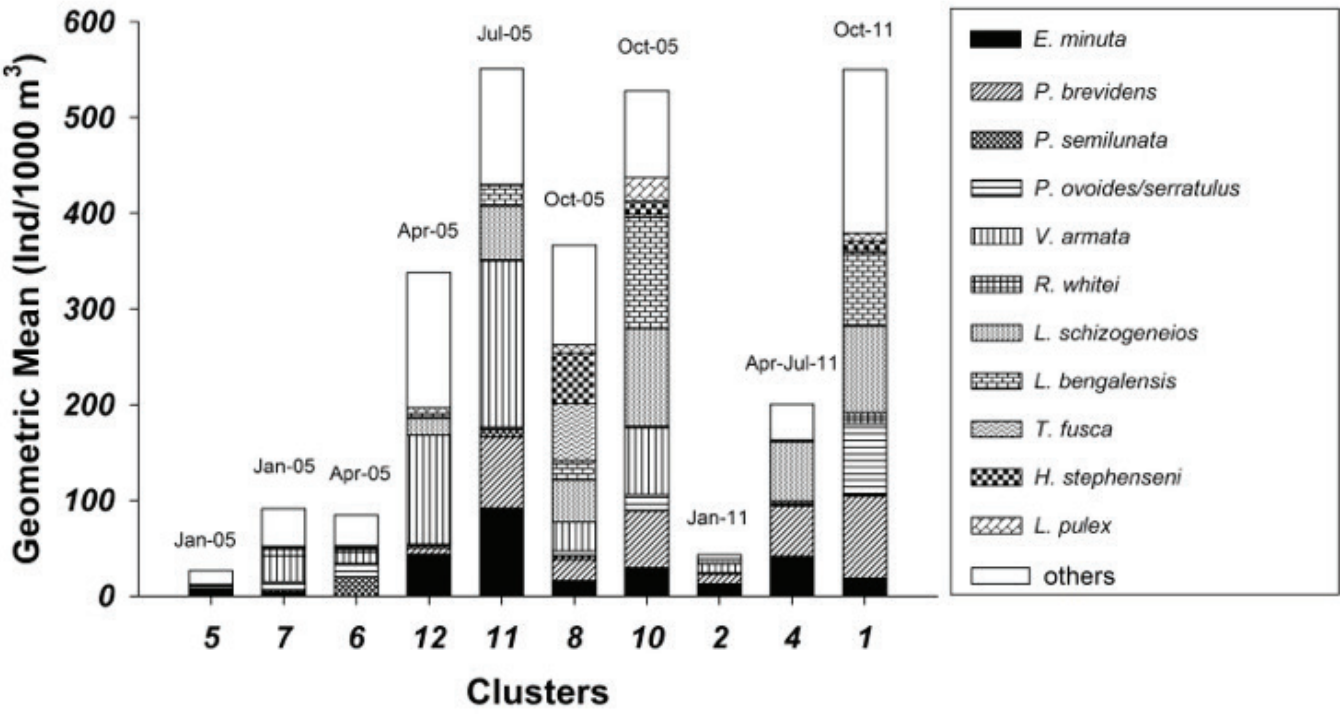

Figure 10. Stacked geometric means from species with strong contribution to similarity in the clusters shown in Figure 9A. Clusters 3 and 9 formed by a pair of stations were omitted. The selected species are a combination of the two species with the highest contribution in each cluster obtained by SIMPER analysis. The "others" category indicates the sum of the remaining species. Conglomerates are ordered as they appear in the dendrogram, excluding conglomerates 3 and 9 formed by two stations.

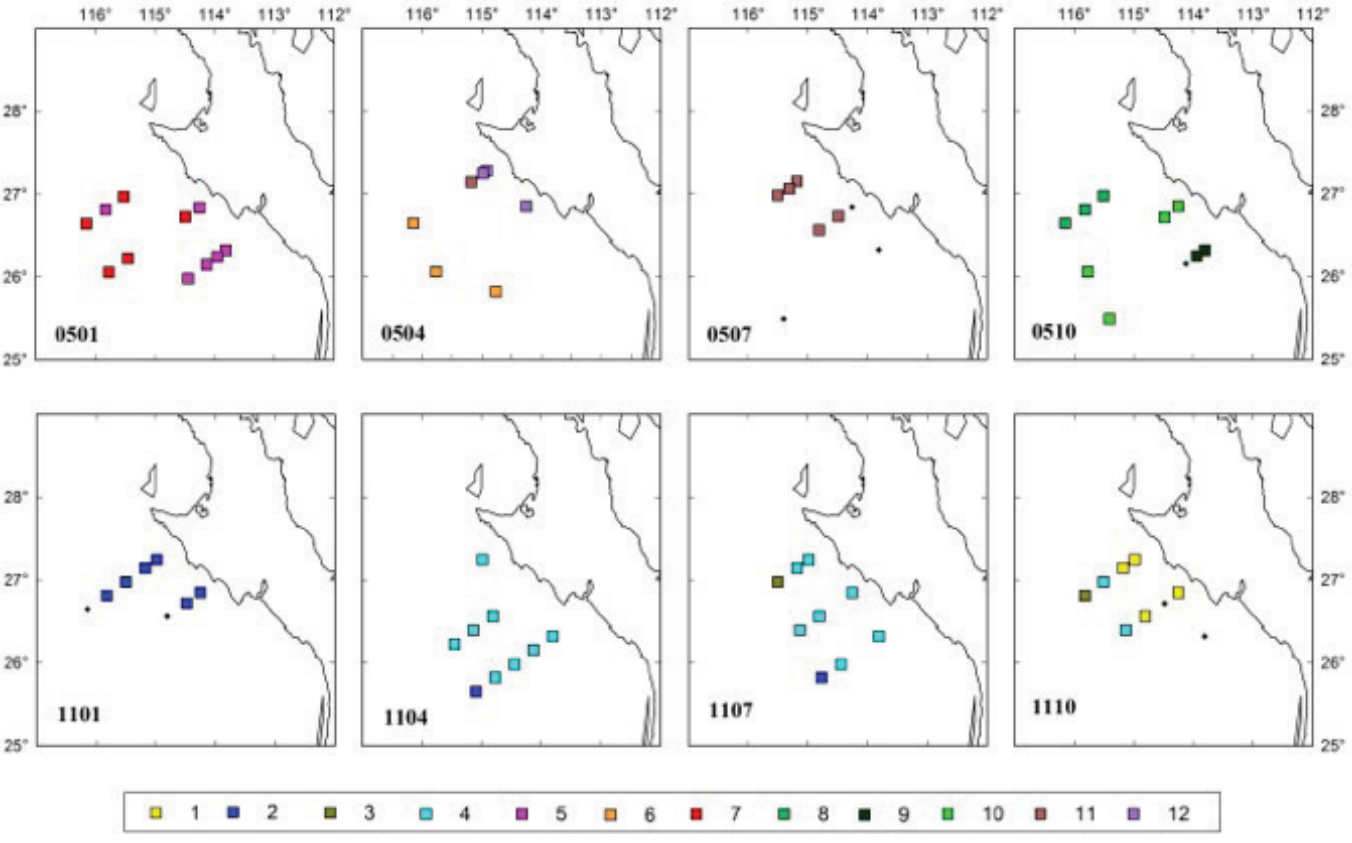

Figure 11. Geographic distribution of clusters defined in the dendrogram with combined stations from 2005 and 2011 (fig. 9A).

south arrangement and cluster 9 is formed by a pair of nearshore stations (fig. 11). These groups as well as cluster 1 from October 2011 had high hyperiid abundance and species richness (fig. 10). Though the October conglomerates appeared close to each other in the NMDS plot (fig. 9B), the most important species contributing to the similarity were different in each one of them: *H. stephenseni*, *H. vosseleri*, and *T. fusca* (summing 26%) in cluster 8; *A. sculpturatus*, *L. bengalensis*, and *L. pulex* (26%) in cluster 9; *L. bengalensis*, *L. schizogeneios*, and *V. armata* (29%) in cluster 10; and *L. schizogeneios*, *P. ovoides/serratulus*, and *P. brevidens* (25%) in cluster 1. Dissimilarity between the 2005 and 2011 October clusters was mainly due to the absence of *A. sculpturatus*, *E. maculata*, and *H. vosseleri* in cluster 1. In contrast, the GM of *P. ovoides/serratulus* was high in cluster 1 (74 ind/1000 m^3) but between 5 and 16 ind/1000 m^3 in clusters 8–10. The abundance of *S. antennarius* was also high in cluster 1 (MG = 59 ind/1000 m^3), but below 10 ind/1000 m^3 in clusters 8–10.

DISCUSSION

Climatic conditions during 2011 were associated with the cool phase of ENSO (La Niña), which lasted from summer 2010 to the beginning of 2012. This was one of the coldest events on record, characterized by a relaxation between May and July of 2011, and further resurgence of cooler conditions during autumn in the central equatorial Pacific (Thorne et al. 2012; Hu et al. 2014). In the CCS, cool SST was evident from spring 2010 until summer 2011, with enhanced upwelling activity (Bjorkstedt et al. 2011). However, in the study region, SST experienced a remarkable increase in October 2011, which affected the pelagic ecosystem. The strength of La Niña 2010–12 also affected the surface circulation. Usually, the flow of the CC is strongest from late winter (February–March) to early summer, in concordance with the seasonality of the winds (Huyer 1983; Lynn and Simpson 1987; Zaitsev 2003). However, in January 2011 the CC flow was relatively strong off Baja California (fig. 2) compared to the typical circulation for this month (see Figure 4 in Strub and James 2000). Thermohaline conditions in the study area were not entirely typical because low salinity and temperature occurred since winter instead of only at spring but the warmest water occurred in autumn as usual (Durazo 2015).

The biological consequences of La Niña included high integrated chlorophyll (>40 mg/m^2) in the Baja California region throughout most of the year, decreasing at the end of 2011, a pattern not completely consistent with observations elsewhere in the CCS (Bjorkstedt et al. 2012). Moreover, the zooplankton volume was high in 2011, above the long-term mean, with preponderance of gelatinous organisms such as hydromedusae and salps. Crustaceans responded differently. The abundance of copepods was high from January to July and decreased in October, while euphausiids had negative anomalies all year round, contrasting with the pattern observed for amphipods in the present study (Lavaniegos et al. 2015). Here we confirm the low diversity of amphipods in cold months, whether by the absence of some species or the decreased abundances of others (table 3).

Comparison of the 2011 and 2005 amphipod communities

The composition, abundance, and diversity of hyperiid amphipods off Baja California during 2011 showed a seasonal pattern as described for 2005 by Lavaniegos and Hereu (2009). In both years, both amphipod abundance and species diversity were poor in winter. The abundance of total amphipods increased from April to October but more strongly in October. Some differences in the composition and abundance of particular species reflected the cool climate during 2011 in contrast with 2005. The climate in 2005 could be considered neutral for the second part of the year but not the beginning, because El Niño conditions still prevailed in January of that year (Lyon and Barnston 2005). Therefore, it is not surprising that the winters of 2005 and 2011 had included the most dissimilar hyperiid assemblages in the cluster analysis (fig. 9).

Some species were present in 2005 but were absent in 2011, probably affected by the cooling caused by La Niña. Most notably, *A. blossevillei*, *O. clausi*, and *P. curvipes* were absent from January to July 2011, and *V. gibbosa* and *V. viatrix* were absent from January to April 2011. These species were moderately abundant in 2005 (GMs between 1 and 13 ind/1000 m^3, table 3). *A. blossevillei* in particular could be an indicator of warm conditions because it was one of the frequent species during El Niño 1997–98 in the Mexican tropical Pacific (Gasca et al. 2012). However, it is also found at subtropical latitudes as in the Canary Current (Thurston 1976), the Sargasso Sea (Gasca 2007), and the Tasman Sea (Zeidler 1992). On the other hand, *O. clausi* appears to be a species capable of tolerating wide temperature ranges because it has been recorded from subarctic (Lorz and Pearcy 1975) to tropical latitudes (Gasca et al. 2012; Valencia et al. 2013). However, it was not present during the cool months of 2011 in the present study.

The dominant species also differed between 2005 and 2011. The typical species in the CCS during 2005 were *E. minuta*, *L. schizogeneios*, *P. brevidens*, and *V. armata* (Lavaniegos and Hereu 2009). These species, except for *V. armata*, were also abundant in 2011. Our findings for *V. armata* are not those expected for the subtropical region of the CC, because though its frequency of occurrence was high during 2011, it was not abundant;

however, its abundance in 2011 may have been underestimated due to the sampling depth (0–200 m) and hour (most of the samples were collected during daylight hours). There is evidence that *V. armata* undertakes vertical migration (Brusca 1967a; Thurston 1976; Tranter 1977). According to Cornet and Gili (1993), this species presents a wide range of vertical migration, remaining between 200 and 1000 m depth during daytime. The other species with significant day-night differences was *E. minuta* but in this case, diurnal abundances were higher. Though *E. minuta* did not present interannual differences, this could be a failed result due to a possible overestimation of the 2011 abundances (excess of daytime samples). This is consistent with studies from the Gulf of California (Siegel-Causey 1982) and Canary Current (Thurston 1976), where *E. minuta* apparently exhibited reverse migration. However, in the Indian Ocean, it showed a tendency to migrate during nighttime above 200 m (Tranter 1977).

Significant interannual differences for *L. schizogeneios* and *P. brevidens* were due to substantially higher abundances in 2011, probably favored by low temperatures. According to Xu (2009), *L. schizogeneios* is able to tolerate a wide range of temperatures, but the higher abundance found during 2011 in the present study suggests a preference for temperate conditions. *P. brevidens* also shows a preference for temperate conditions defined by the 15°–18°C isotherms at 30 m depth, demarcating its southern limit of distribution in the CCS during March–July (Bowman 1978).

In the present study, *S. antennarius* was among the dominant species, but during 2005 it had low abundance. Gasca et al. (2012) recorded this species during the period influenced by the CC in the Mexican tropical Pacific, and Zeidler (1984) observed it only from March to June when temperature was decreasing and the salinity was stable off Queensland, Australia.

Comparison with other regions

The subtropical region of the CC has a high diversity of hyperiid amphipods (Lavaniegos and Ohman 1999; Lavaniegos and Hereu 2009). The influence of this current permeates even in the eastern tropical Pacific (ETP) as observed by Gasca et al. (2012) off the coast of Colima and Jalisco, where the diversity of these crustaceans showed a seasonal fluctuation despite the occurrence of El Niño 1997–98, with high diversity but low abundances during the season influenced by the CC (February–June). In contrast, during July–December the North Equatorial Countercurrent influences the region and there is low hyperiid diversity. In this region, the species *H. sibaginis* and *L. bengalensis* prevailed as the most frequent and abundant (Gasca et al. 2012). However, in the present study, these species occurred exclusively in October, and *L. bengalensis* was the second most abundant amphipod species in the study area. The tropical affinity of this species has also been confirmed in diverse tropical regions such as Banderas Bay (Gasca and Franco-Gordo 2008), Panama Bay (Valencia et al. 2013), the Australian coast (Zeidler 1984), the Caribbean Sea (Gasca and Suarez-Morales 2004), Gulf of Mexico (Gasca 2004; Gasca et al. 2009), and the Brazilian coast (Lima and Valentin 2001). Therefore, in this study *L. bengalensisis* was considered a tropical species, typical of autumn conditions when there is influence of subtropical water off Baja California. In October 2011, *H. sibaginis* was also abundant though its contribution to similarity was not as high as that of *L. bengalensis*. The latter and four other species (*L. schizogeneios*, *P. ovoides*, *P. brevidens*, and *S. antennarius*) contributed the maximal similarity percentages (fig. 7).

In the assemblage of species present in the Mexican tropical Pacific during periods influenced by the CC, one of the species that contributed strongly to similarity was *V. armata* (Gasca et al. 2012). However, the abundance of this species is low in the ETP compared with the CCS (Brusca 1981; Lorz and Pearcy 1975; Lavaniegos and Ohman 1999, 2003; Lavaniegos and Hereu 2009; Lavaniegos 2014), and with other eastern boundary upwelling ecosystems (Thurston 1976; Cornet and Gili 1993) and the Indian Ocean (Tranter 1977). In the Gulf of California, the abundance of *V. armata* was related to upwelled water derived from the mixing of subtropical surface and subsurface water (Siegel-Causey 1982). Valencia-Ramírez (2010) reported the occurrence of this species in a tongue of cool and saline water associated with the Colombia Current.

Relation between the amphipod community and environmental variables

The correlation between environmental variables and amphipod community coincided with that observed in other regions. Xu and Mei (2006) found a correlation between amphipod abundance and SST in the China Sea but exclusively in spring, explained by an oceanic tendency in amphipod distribution where SST was higher. On the contrary, off Baja California, an inverse relation between SST and amphipod abundance was found during July 2002, associated with the intrusion of subarctic water (Lavaniegos 2014). However, the correlation was stronger for *T. pacifica* compared with the subtropical species *V. armata* (Lavaniegos 2014). In 2011, the positive correlation between amphipods and temperature appeared to be related to a good reproductive season or survival during spring–summer as well as to a massive intrusion of tropical species in autumn.

Surface salinity was another variable included in the correlation analysis. In the CCS low temperature and

salinity values are indicative of subarctic water, whereas high values are associated with subtropical water (Lynn and Simpson 1987). However, in other eastern Pacific regions with high precipitation, low salinity is associated with warm tropical water, as occurs in Panama Bay, where Valencia et al. (2013) found a neritic-oceanic contrast in hyperiid assemblages explained by a plume of low salinity. In the Gulf of California, with another water mass regime, surface salinity was also the best predictor of amphipod abundance (Siegel-Causey 1982).

The tolerance of amphipods to thermohaline variability depends on the species. For example, *L. schizogeneios* is an abundant species in diverse regions, classified by Xu (2009) as eurythermal and euryhaline, supporting wide ranges of surface temperature (13.5°–28.3°C) and salinity (27.2–34.8). However, this species is not so abundant in the ETP (Gasca et al. 2012), and though persistent during all phases of ENSO 1997–98, its contribution was linked to the CC influence. Its cosmopolite tendency in warm-temperate waters and wide thermohaline tolerance may explain why *L. schizogeneios* is one of the most frequent and abundant species off Baja California.

A species with low tolerance to temperature was *T. forcipatus*, found exclusively in October 2011 with low abundance in the study area. This species could be a good indicator of alteration under local environmental conditions. It is abundant in coastal zones (Zeidler 1984; Cornet and Gili 1993) and limited to the upper 20 m (Gasca and Suarez-Morales 2004). Gasca et al. (2012) reported similar findings during ENSO 1997–98. This explains the absence of *T. forcipatus* during January–July 2011 off Baja California when SST was cool (16°–17°C), and its low abundance in October despite appropriate SST; however, its preference for the coastal shelf prevent us from finding in the present study in which only oceanic stations were analyzed.

Stratification of the water column influenced the amphipod assemblages observed in 2011 (table 2). Cornet and Gili (1993) also highlighted the influence of stratification on the amphipod community in the Benguela Current, which was compressed in the upper 40 m because of a strong thermocline and the presence of gelatinous zooplankton. Under these conditions, the organisms did not migrate vertically despite reports of migration and wide vertical distribution ranges from other regions (Brusca 1967a; Thurston 1976; Roe 1984).

Finally, with this study it was possible to establish the seasonal variability of pelagic amphipods in the CCS and that La Niña conditions had a greater effect on the surface layer during the first part of 2011. The relaxation of this event in autumn produced an extreme seasonal change, with massive intrusion of tropical species in the region off central Baja California. That extreme seasonal change could be comparable to the effect of a warming event (for example, a weak El Niño). Since different species are linked to varying environmental factors, which may not be exactly the same from event to event, it is necessary to analyze more years of rigorous analysis of species specific abundance anomalies. This will aid to a better appreciation of the scope, not just of La Nina events in general, but individual La Nina event effects. Ultimately, this will increase the robustness of year-to-year comparisons and the potential for critical comparable time series data.

ACKNOWLEDGEMENTS

Thanks to the staff participating in the IMECOCAL cruises on board the research vessel *Francisco de Ulloa*. Gilberto Gaxiola provided the chlorophyll data and Erasmo Miranda prepared the maps of dynamic heights. Thanks also to Christine Harris for English language revision of the manuscript. Financial support came from a CONACYT grant (99252) and CICESE project 625114. L. L. Espinosa-Leal received an academic scholarship from CONACYT.

LITERATURE CITED

Armstrong, J. L., J. L. Boldt, A. D. Cross, J. H. Moss, N. D. Davis, K. W. Myers, R. V. Walker, D. A. Beauchamp, and L. J. Haldorson. 2005. Distribution, size, and interannual, seasonal and diel food habits of northern Gulf of Alaska juvenile pink salmon, *Oncorhynchus gorbuscha*. Deep Sea Res. Part II 52:247–265.

Bjorkstedt, E. P., R. Goericke, S. McClatchie, E. Weber, W. Watson, N. Lo, B. Peterson, B. Emmett, R. Brodeur, J. Peterson, M. Litz, J. Gomez-Valdez, G. Gaxiola-Castro, B. Lavaniegos, F. Chavez, C. A. Collins, J. Field, K. Sakuma, P. Warzybok, R. Bradley, J. Jahncke, S. Bograd, F. Schwing, G. S. Campbell, J. Hildebrand, W. Sydeman, S.A. Thompson, J. Largier, C. Halle, S.Y. Kim, and J.Abell.2011. State of the California Current 2010–11: Regionally variable responses to a strong (but fleeting?) La Niña. Calif. Coop. Oceanic Fish. Invest. Rep. 52:36–68.

Bjorkstedt, E. P., R. Goericke, S. McClatchie, E. Weber, W. Watson, N. Lo, W. Peterson, R. Brodeur, S. Bograd, T. Auth, J. Fisher, C. Morgan, J. Peterson, R. Durazo, G. Gaxiola-Castro, B. Lavaniegos, F. Chavez, C.A. Collins, B. Hannah, J. Field, K. Sakuma, W. Satterthwaite, M.O'Farrell, S. Hayes, J. Harding, W. Sydeman, S. A. Thompson, P. Warzybok, R. Bradley, J. Jahncke, R. Golightly, S. Schneider, J. Largier, R.M. Suryan, A. J. Gladics, C.A. Horton, S.Y. Kim, S. Melin, R. De Long, and J. Abell. 2012. State of the California Current 2011–12: Ecosystems respond to local forcing as La Niña wavers and wanes. Calif. Coop. Oceanic Fish. Invest. Rep. 53:41–76.

Boening, C., J. K. Willis, F. W. Landerer, R. S. Nerem, and J. Fasullo. 2012. The 2011 La Niña: So strong, the oceans fell. Geophysical Res. Lett. 39, L19602, doi: 10.1029/2012GL053055.

Bowman, T. E. 1973. Pelagic amphipods of the genus *Hyperia* and closely related genera (Hyperiidea: Hyperiidae). Smithsonian C. Zool. 136:1–76.

Bowman, T. E. 1978. Revision of the pelagic amphipod genus *Primno* (Hyperiidea: Phrosinidae). Smithsonian C. Zoology 275:1–23.

Brusca, G. J. 1967a. The ecology of pelagic Amphipoda, I. Species accounts, vertical zonation and migration of Amphipoda from the waters off southern California. Pac. Sci. 21:382–393.

Brusca, G. J. 1967b. The ecology of pelagic Amphipoda, II: Observations on the reproductive cycles of several pelagic Amphipods from the waters off southern California. Pac. Sci. 21:449–456.

Brusca, G. J. 1981. Annotated keys to the Hyperiidea (Crustacea: Amphipoda) of North American coastal waters. Allan Hancock Found. Tech. Rep. 5:1–76.

Clarke, K. R. and R. M. Warwick. 2001. Change in marine communities: an approach to statistical analysis and interpretation. Plymouth Marine Natural Laboratory, 172 p.

Collins, M., R. Shreeve, S. Fielding, and M. Thurston. 2008. Distribution, growth, diet and foraging behaviour of the yellow-fin notothen *Patagonotothen guntheri* (Norman) on the Shag Rocks shelf (Southern Ocean). J. Fish Biol. 72:271–286.

Cornet, C., and J. M. Gili. 1993. Vertical distribution and daily migrations of hyperiid amphipods in the northern Benguela in relation to water column stratification. Deep-Sea Res. I 40:2295–2306.

Dalpadado, P., N. Borkner, B. Bogstad, and S. Mehl. 2001. Distribution of *Themisto* (Amphipoda) spp. in the Barents Sea and predator-prey interactions. ICES J. Mar. Sci. 58:876–895.

Durazo, R. 2015. Seasonality of the transitional region of the California Current System off Baja California. J. Geophys. Res., Oceans 120:1173–1196, doi: 10.1002/2014JC010405.

Durazo, R., and T. Baumgartner. 2002. Evolution of oceanographic conditions off Baja California: 1997–99. Prog. Oceanogr. 54:7–31.

Feng, M., M. J. McPhaden, S. Xie, and J. Hafner. 2013. La Niña forces unprecedented Leeuwin Current warming in 2011. Sci. Rep. 3, 1277, doi: 10.1038/srep01277.

Gasca, R. 2004. Distribution and abundance of hyperiid amphipods in relation to summer mesoscale features in the southern Gulf of Mexico. J. Plankton Res. 26:993–1003.

Gasca, R. 2007. Hyperiid amhipods of the Sargasso Sea. Bull. Mar. Sci. 81:115–125.

Gasca, R., and C. Franco-Gordo. 2008. Hyperiid amphipods (Peracarida) from Banderas Bay, Mexican Tropical Pacific. Crustaceana 81:63–575.

Gasca, R., C. Franco-Gordo, E. Godínez-Domínguez, and E. Suárez-Morales. 2012. Hyperiid amphipod community in the eastern tropical Pacific before, during, and after El Niño 1997–98. Mar. Ecol. Prog. Ser. 455:123–139.

Gasca, R., H. Manzanilla, and E. Suárez-Morales. 2009. Distribution of hyperiid amphipods (Crustacea) of the southern Gulf of Mexico, summer and winter, 1991. J. Plankton Res. 31:1493–1504.

Gasca, R. and E. Suárez-Morales. 2004. Distribution and abundance of hyperiid amphipods (Crustacea: Peracarida) of the Mexican Caribbean Sea, (August 1986). Caribb. J. Sci. 40:23–30.

Hu, Z. Z., A. Kumar, Y. Xue, and B. Jha. 2014. Why were some La Niñas followed by another La Niña? Clim. Dyn. 42:1029–1042.

Huyer, A. 1983. Coastal upwelling in the California Current system. Prog. Oceanogr. 12:259–284.

Jerónimo, G., and J. Gómez-Valdés. 2006. Mean temperature and salinity along an isopycnal surface in the upper ocean off Baja California. Cienc. Mar. 32:663–671.

Jerónimo, G., and J. Gómez-Valdés. 2007 A subsurface warm-eddy off northern Baja California in July 2004. Geophys. Res. Lett. 34, L06610, doi: 10.1029/2006GL028851.

Kessler, W. S. 2006. The circulation of the eastern tropical Pacific: A review. Prog. Oceanogr. 69:181–217.

Laval, P. 1980. Hyperiid amphipods as crustacean parasitoids associated with gelatinous zooplankton. Oceanogr. Mar. Biol. 18:11–56.

Lavaniegos, B. E. 2014. Pelagic amphipod assemblage associated with subarctic water off the West Coast of the Baja California peninsula. J. Marine Syst. 132:1–12.

Lavaniegos, B. E., and C. M. Hereu. 2009. Seasonal variation in hyperiid amphipod abundance and diversity and influence of mesoscale structures off Baja California. Mar. Ecol. Prog. Ser. 394:137–152.

Lavaniegos, B. E., L. C. Jiménez-Pérez, and G. Gaxiola-Castro. 2002. Plankton response to El Niño 1997–98 and La Niña 1999 in the southern region of the California Current. Prog. Oceanogr. 54:33–58.

Lavaniegos, B. E., O. Molina-González, and M. Murcia-Riaño. 2015. Zooplankton functional groups from the California Current and climate variability during 1997–2013. CICIMAR Oceánides 30:45–62.

Lavaniegos, B. E., and M. D. Ohman. 1999. Hyperiid amphipods as indicators of climate change in the California Current. *In* Crustaceans and the Biodiversity Crisis. Proceedings of the 4th International Crustacean Congress, Vol. 1, F. R. Schram and J. von Vaupel Klein, eds., Brill, Leiden, pp. 489–509.

Lavaniegos, B. E., and M. D. Ohman. 2003. Long-term changes in pelagic tunicates of the California Current. Deep Sea Res. II 50:2473–2498.

Lima, M., and J. Valentin. 2001. Preliminary results to the holistic knowledge of the Amphipoda Hyperiidea faunal composition off the Brazilian coast. J. Plankton Res. 23:469–480.

Lorz, H., and W. Pearcy. 1975. Distribution of hyperiid amphipods off the Oregon coast. J. Fish. Res. Board Can. 32:1442–1447.

Lynn, R., and J. Simpson. 1987. The California Current System: The seasonal variability of its physical characteristics. J. Geophys. Res. 92(C12):12947–12966, doi: 10.1029/JC092iC12p12947.

Lyon, B., and A. G. Barnston. 2005. The evolution of the weak El Niño of 2004–05. US CLIVAR Variations 3(2):1–4.

Mostarda E., D. Campo, L. Castriota, V. Esposito, M. P. Scarabello, and F. Andaloro. 2007. Feeding habits of the bullet tuna *Auxisrochei* in the southern Tyrrhenian Sea. J. Mar. Biol. Assoc. UK 87:1007–1012.

Nam, S., H. J. Kim, and U. Send. 2011. Amplification of hypoxic and acidic events by La Niña conditions on the continental shelf off California. Geophys. Res. Lett. 38, L22602, doi: 10.1029/2011GL049549.

Repelin, R. 1978. Les amphipodes pélagiques du Pacifique occidental et central: Biologie, écologie et relations trophiques avec la faune ichthyologique. Travaux et documents de l'ORSTOM, Paris 86:1–381.

Roe, H. S. J. 1974. Observations on the diurnal vertical migrations of an oceanic animal community. Mar. Biol. 28:99–113.

Satoh, K. 2004. Occurrence of *Phronima sedentaria* (Forskål, 1775) (Amphipoda, Hyperiidea) in the stomach of the longnose lancet fish, *Alepisaurus ferox* (Lowe, 1833) (Aulopiformes, Alepisauroidei) in the North and Tropical Atlantic Ocean. Crustaceana 77:729–739.

Siegel-Causey, D. 1982. Factors determining the distribution of hyperiid amphipoda in the Gulf of California. Ph.D. Thesis, University of Arizona, Tucson, 535 p.

Simpson J. H., C. M. Allen, and N. C. G. Morris. 1978. Fronts on the continental shelf. J. Geophys. Res. 83:4607–4614, doi: 10.1029/JC083iC09p04607.

Smith, P. and S. Richardson. 1977. Standard techniques for pelagic fish egg and larva surveys. FAO Fisheries Technical Paper, No. 175.

Soto-Mardones, L., A. Parés-Sierra, J. Garcia, R. Durazo, and S. Hormazabal. 2004. Analysis of the mesoscale structure in the IMECOCAL region (off Baja California) from hydrographic, ADCP and altimetry data. Deep-Sea Res. II 51:785–798.

Strub, P. T., and C. James. 2000. Altimeter-derived variability of surface velocities in the California Current System: 2. Seasonal circulation and eddy statistics. Deep-Sea Res. II47:831–870.

Thorne, P. W., K. M. Willett, A. J. Dolman, and B. D. Hall. 2012. [State of the Climate in 2011. Global Climate.] Overview. Bull. Amer. Meteor. Soc. Spec. Suppl. 93(7):S7–S11.

Thurston, M. H. 1976. The vertical distribution and diurnal migration of the Crustacea Amphipoda collected during the SOND cruise, 1965 II. J. Mar. Biol. Assoc. U.K. 56:383–470.

Torres, H. S., and J. Gómez-Valdés. 2015. Coastal circulation driven by short-period upwelling-favorable winds in the northern Baja California region. Deep-Sea Res. Part I 98:31–42.

Tranter, H. A. 1977. Further studies of plankton ecosystems in the Eastern Indian Ocean VII. Ecology of the Amphipoda. Mar. Freshwat. Res. 28:645–662.

Valencia, B., B. Lavaniegos, A. Giraldo, and E. Rodríguez-Rubio. 2013. Temporal and spatial variation of hyperiid amphipod assemblages in response to hydrographic processes in the Panama Bight, eastern tropical Pacific. Deep-Sea Res. I 73:46–61.

Valencia-Ramírez, B. 2010. Seasonal variation of hyperiid amphipod assemblages in the Colombian Pacific. Ms. Thesis, Centro de Investigación Científica y de Educación Superior de Ensenada, Baja California, México. 95 p. [In Spanish]

Vinogradov, M., A. Volkov, and T. Semenova. 1996. Hyperiid amphipods (Amphipoda, Hyperiidea) of the world oceans. Science Publishers, New Delhi, 632 p.

Xu, Z. 2009. Statistical analysis on ecological adaptation of pelagic Amphipoda in the East China Sea. Acta Oceanol. Sin. 28:61–69.

Xu, Z., and J. Mei. 2006. Study on relation between distribution and environment of pelagic amphipods. Acta Oceanol. Sin. 25:112–120.

Zaytsev, O., R. Cervantes-Duarte, O. Montante, and A. Gallegos-García. 2003. Coastal upwelling activity on the Pacific shelf of the Baja California Peninsula. J. Oceanogr. 59:489–502.

Zeidler, W. 1984. Distribution and abundance of some Hyperiidea (Crustacea : Amphipoda) in northern Queensland waters. Aust. J. Mar. Fresh. Res. 35:285–305.

Zeidler, W. 1992. Hyperiid amphipods (Crustacea: Amphipoda: Hyperiidae) collected recently from eastern Australian waters. Rec. Aust. Museum 44:85–133.

APPENDIX 1

Hyperiid amphipod species found during four seasons of 2011. The geometric mean (GM) of abundance (ind/1000 m³) and number of samples with presence (N) are shown by month. Small juvenile organisms difficult for identification are recorded only to genus. Total number of analyzed samples is indicated in parenthesis.

	January (8)		April (9)		July (9)		October (9)	
Species	GM	N	GM	N	GM	N	GM	N
Infraorder Physosomata								
Family Scinidae								
Scina borealis (G.O. Sars,1882)	—	0	—	0	—	0	0.22	2
Scina similis Stebbing,1895	—	0	—	0	—	0	0.10	1
Scina tullbergi (Bovallius, 1885)	—	0	1.97	5	0.97	4	2.44	8
Scina spp.	0.95	5		2	—	0	—	0
Infraorder Physocephalata								
Family Vibilidae								
Vibilia armata Bovallius, 1887	3.57	4	4.70	5	3.45	4	6.15	5
Vibilia australis Stebbing, 1888	—	0	—	0	0.14	1	0.50	3
Vibilia chuni Behning & Woltereck, 1912	—	0	0.18	1	0.11	1	0.29	2
Vibilia propinqua Stebbing, 1888	—	0	—	0	—	0	0.45	2
Vibilia stebbingi Behning & Woltereck, 1912	0.13	1	—	0	—	0	3.50	7
Vibilia spp.	—	0	0.87	4	0.27	2	1.48	5
Family Paraphronimidae								
Paraphronima crassipes Claus, 1879	—	0	—	0	—	0	0.22	2
Paraphronima gracilis Claus, 1879	0.45	2	3.02	6	3.02	7	7.10	8
Paraphronima spp.	0.13	1	—	0	0.13	1	0.17	1
Family Phronimidae								
Phronima atlantica Guérin-Méneville, 1836	—	0	1.01	5	0.16	1	2.25	6
Phronima colleti Bovallius, 1887	—	0	—	0	0.13	1	0.33	1
Phronima curvipes Vosseler, 1901	—	0	—	0	—	0	0.22	2
Phronima pacifica Streets, 1877	—	0	—	0	—	0	0.46	2
Phronima sedentaria (Forskål, 1775)	0.93	4	0.42	3	0.33	3	1.47	5
Phronima solitaria Guérin-Méneville, 1836	—	0	0.11	1	—	0	—	0
Phronima stebbingi Vosseler, 1901								
Phronima dunbari Shih, 1991	—	0	0.11	1	0.73	2	2.68	7
Phronima spp.	0.19	1	1.39	5	0.23	1	1.42	5
Phronimella elongata (Claus,1862)	—	0	—	0	—	0	0.73	2
Family Phrosinidae								
Anchylomera blossevillei Milne-Edwards, 1830	—	0	—	0	—	0	0.89	4
Phrosina semilunata Risso, 1822	0.13	1	1.45	6	0.89	3	0.77	4
Primno brevidens Bowman, 1978	8.17	7	27.35	9	69.12	9	43.70	9
Family Hyperiidae								
Hyperoche medusarum (Krøyer, 1838)	—	0	2.94	7	6.68	8	1.76	4
Laxohyperia vespuliformes Vinogradov & Volkov, 1982	—	0	0.11	1	0.11	1	6.13	8
Family Lestrigonidae								
Hyperietta luzoni (Stebbing, 1888)	—	0	—	0	—	0	0.80	3
Hyperietta parviceps Bowman, 1973	—	0	0.13	1	—	0	—	0
Hyperietta stebbingi Bowman, 1973	—	0	—	0	0.27	1	0.97	4
Hyperietta stephenseni Bowman, 1973	—	0	1.04	5	1.62	6	5.33	6
Hyperietta vosseleri (Stebbing, 1904)	0.13	1	—	0	—	0	—	0
Hyperietta spp.	—	0	0.14	1	0.19	1	—	0
Hyperioides longipes Chevreux, 1900	—	0	0.24	2	—	0	1.12	3
Hyperioides sibaginis (Stebbing, 1888)	—	0	—	0		1	10.99	7
Lestrigonus bengalensis Giles, 1887	—	0	—	0	—	0	59.77	9
Lestrigonus schizogeneios (Stebbing, 1888)	3.80	7	24.72	8	102.72	9	72.83	9
Lestrigonus shoemakeri Bowman, 1973	0.44	2	3.37	7	—	0	—	0
Lestrigonus spp.	1.08	3	35.61	9	46.74	9	42.77	9
Phronimopsis spinifera Claus, 1879	0.81	4	1.78	6	—	0	0.86	4
Themistella fusca (Dana, 1853)	—	0	—	0	0.33	2	1.59	4
Family Lycaeopsidae								
Lycaeopsis themistoides Claus, 1879	0.13	1	0.40	3	0.76	3	1.17	5
Lycaeopsis zambongae (Stebbing, 1888)	—	0	—	0	—	0	0.42	2
Lycaeopsis spp.	0.13	1	—	0	—	0	0.11	1
Family Pronoidae								
Eupronoe maculata Claus, 1879	—	0	0.11	1	—	0	—	0
Eupronoe minuta Claus, 1879	8.77	7	37.84	9	38.51	9	13.34	9
Parapronoe cambelli Stebbing, 1888	—	0	0.33	2	—	0	—	0
Parapronoe crustulum Claus, 1879	—	0	0.41	3	0.22	2	—	0
Parapronoe spp.	—	0	0.17	1	—	0	—	0
Pronoe capito Guérin-Méneville, 1836	—	0	0.56	4	0.23	2	0.55	3

(*continued*)

APPENDIX 1, continued

Hyperiid amphipod species found during four seasons of 2011. The geometric mean (GM) of abundance (ind/1000 m³) and number of samples with presence (N) are shown by month. Small juvenile organisms difficult for identification are recorded only to genus. Total number of analyzed samples is indicated in parenthesis.

	January (8)		April (9)		July (9)		October (9)	
Species	GM	N	GM	N	GM	N	GM	N
Family Lycaeidae								
Lycaea nasuta Claus, 1879	—	0	—	0	—	0	0.30	2
Lycaea pachypoda (Claus, 1879)	0.45	2	—	0	—	0	—	0
Lycaea pauli Stebbing, 1888	—	0	—	0	—	0	0.21	2
Lycaea pulex Marion, 1874	—	0	—	0	0.11	1	3.55	7
Lycaea serrata Claus, 1879	—	0	—	0	—	0	0.21	2
Lycaea spp.	—	0	—	0	—	0	0.55	3
Simorhynchotus antennarius (Claus, 1871)	0.36	2	15.36	9	9.84	9	37.92	9
Family Tryphaneidae								
Tryphana malmi Boeck, 1870	1.03	4	1.11	4	0.91	3	6.85	8
Family Brachyscelidae								
Brachyscelus crusculum Bate, 1861	—	0	0.31	2	—	0	0.42	3
Brachyscelus globiceps (Claus, 1879)	—	0	0.42	3	—	0	—	0
Brachyscelus spp.	—	0	—	0	0.10	1	—	0
Family Oxycephalidae								
Glossocephalus milneedwardsi Bovallius, 1887	—	0	—	0	—	0	0.11	1
Oxycephalus clausi Bovallius, 1887	—	0	0.11	1	—	0	6.59	6
Oxycephalus piscator Milne-Edwards, 1830	—	0	—	0	—	0	0.44	3
Oxycephalus spp.	—	0	—	0	—	0	0.43	2
Rhabdosoma minor Fage, 1954	—	0	—	0	—	0	0.22	1
Rhabdosoma whitei Bate, 1862	—	0	0.11	1	—	0	2.27	5
Rhabdosoma spp.	—	0	—	0	—	0	0.30	2
Streetsia challengeri Stebbing, 1888	0.28	2	0.26	2	—	0	0.12	1
Streetsia mindanaonis (Stebbing, 1888)	—	0	—	0	—	0	0.11	1
Family Platyscelidae								
Platyscelus ovoides (Risso, 1816)								
Platyscelus serratulus Stebbing, 1888	0.67	3	0.58	3	3.44	6	13.13	7
Tetrathyrus arafurae Stebbing, 1888	—	0	—	0	—	0	0.71	3
Tetrathyrus forcipatus Claus, 1879	—	0	—	0	—	0	1.90	7
Tetrathyrus spp.	—	0	—	0	—	0	0.28	1
Family Parascelidae								
Parascelus edwardsi Claus, 1879	—	0	—	0	0.11	1	0.92	3
Parascelus typhoides Claus, 1879	—	0	—	0	0.10	1	0.42	3
Parascelus spp.	—	0	—	0	—	0	0.19	1

JOINT LIKELIHOOD FUNCTION BASED ON MULTINOMIAL AND NORMAL DISTRIBUTIONS FOR ANALYZING THE PHENOTYPIC GROWTH VARIABILITY OF GEODUCK CLAM *PANOPEA GLOBOSA*

MARLENE ANAID LUQUIN-COVARRUBIAS
Centro de Investigaciones Biológicas del Noroeste
Instituto Politécnico Nacional 195
Col. Playa Palo de Santa Rita Sur, CP 23096
La Paz, B.C.S., México

ENRIQUE MORALES-BOJÓRQUEZ
Centro de Investigaciones Biológicas del Noroeste
Instituto Politécnico Nacional 195
Col. Playa Palo de Santa Rita Sur, CP 23096
La Paz, B.C.S., México
ph: +52 612 123 8484 ext. 3115
fax: +52 612 125-3625
emorales@cibnor.mx

SERGIO SCARRY GONZÁLEZ-PELÁEZ
Centro de Investigaciones Biológicas del Noroeste
Instituto Politécnico Nacional 195
Col. Playa Palo de Santa Rita Sur, CP 23096
La Paz, B.C.S., México

Universidad Autónoma de Baja California Sur
Carretera al Sur km 5.5, CP 23080
La Paz, B.C.S. México

DANIEL BERNARDO LLUCH-COTA
Centro de Investigaciones Biológicas del Noroeste
Instituto Politécnico Nacional 195
Col. Playa Palo de Santa Rita Sur, CP 23096
La Paz, B.C.S., México

ABSTRACT

In age and growth studies the individual variability is recognized as a source of bias, if it is not taken into account in the analyses it can lead to overestimates or subestimates of the mean length at age of a cohort. In this study, a new approach for analyzing individual shell length-at-age variability was developed for *Panopea globosa* using a joint negative log-likelihood where both shell length frequency distributions (0.105–7.04 mm) and shell length–at-age (100–187 mm) data sets were combined. Six candidate growth models were analyzed that included assumptions about the variance for each age in the population, and the best growth model was selected using a multimodel inference approach. Growth modeling including phenotypic growth variability showed that estimates of t_0 were better than those computed from conventional growth models. We found that the Johnson model was the best candidate growth model for fitting both data sets.

INTRODUCTION

A frequent assumption in stock assessment models is that individual growth in marine organisms can be described adequately through mean growth parameters. However, these parameters are usually estimated from length-at-age data, and they are highly variable (Sainsbury 1980). This means that the growth models are fit to average trajectories that ignore intrinsic biological variability about individual growth. For several marine populations is recognized that the length-at-age variability decreases with time or age (growth compensation), or the inverse pattern, where length-at-age variability increases with age (growth depensation) (Pfister and Stevens 2002). For effective fisheries management, the length structure is biologically useful; and catch-at-length analysis have been applied to Pacific cod (*Gadus macrocephalus*), longneck croaker (*Pseudotolithus typus*), and round scad (*Decapterus russellii*) (Sullivan et al. 1990); red sea urchin (*Strongylocentrotus franciscanus*) (Lai and Bradbury 1998); red king crab (*Paralithodes camtschaticus*) and tanner crab (*Chionoecetes bairdi*) (Zheng et al. 1995, 1998); jumbo squid (*Dosidicus gigas*) (Morales-Bojórquez and Nevárez-Martínez 2010); and Pacific yellowleg shrimp (*Farfantepenaeus californiesis*) (Morales-Bojórquez et al. 2013). This is associated to the facility of data collection, hence the length structure of an exploited population can be informative of biological factors useful for stock conservation (e.g. length-at-first maturity, selectivity, length-at-first capture).

Several approaches have been used to analyze the length-at-age variability based on deterministic and stochastic growth models. Sainsbury (1980) analyzed the effect of individual variability using the von Bertalanffy growth model (VB), concluding that this feature is important and can be measured from individual growth parameters; if this is not included and considered as a source of bias in the estimation of growth parameters, then the results will be overestimated, affecting the mean length at age of a cohort. Kirkwood (1983) used length increments and length-at-age data for parameterizing the VB. This study implements a proposal first suggested by Sainsbury (1980), where a joint likelihood function based on two sources of data could be more informative in comparison to simply the length-at-age data. The methodology in Kirkwood (1983) is possibly the most inclusive in following Sainsbury (1980) suggestion, however he did not analyze the individual variability in VB. Parma and Deriso (1990) also analyzed the phenotypic variability in growth assuming two hypotheses: 1) stochastic environmental effects are associated with intrinsic sources of growth variability; and 2) variability in the initial length distribution of young organisms are

caused by the individuals having intrinsically different growth potentials. This approach was applied to analyze the effects of the variability on expected yield and reproductive potential of a cohort. Specific individual variability in growth parameters for the VB were modeled based on numerical simulation, thus the phenotypic variability in growth was assessed not from empirical data but from expected parameters distribution (maximum asymptotic length and growth coefficient) (Pilling et al. 2002). Recently, Restrepo et al. (2010) analyzed length frequency and shell length-at-age data using the VB and assumed that the residuals were normally distributed with the variance increasing with the length; this approach allowed for estimating the variance for each age observed in the population.

The stochastic growth models are able to show individual-to-individual changes, their impacts on growth parameters, and provide estimates of theoretical trajectories from length-at-age data, a result which is not commonly represented by deterministic growth models. According to Troynikov et al. (1998) the mean growth rate in early stages (e.g., larvae, juveniles) increases linearly or exponentially, however when the organisms are recruits or mature the growth rate decreases, presenting a growth pattern with dual phases. The stochastic methods applied to individual variability in growth studies have been mainly based on tag-recapture data and Fabens method (von Bertalanffy growth model). Wang et al. (1995) proposed an unconditional likelihood function for analyzing the variability in growth of *Penaeus semisulcatus* from changes in asymptotic length and age-at-tagging, this procedure allows them to obtain unbiased estimation of individual growth, considering that the mean growth curve is increasing as a function of time. Troynikov and Gorfine (1998) explicitly showed a stochastic parameterization applied to Gompertz growth model assuming gamma, log normal and Weibull probability density functions for k and L_∞ parameters; an application of this approach was developed for *Heterodontus portusjacksoni* where simultaneously the length-at-age heterogeneity and random variation in growth coefficient for the von Bertalanffy growth model were analyzed, although the random variation can be included in more of its parameters (Tovar-Ávila et al. 2009). Laslett et al. (2002) proposed a modification to the von Bertalanffy growth model which included a logistic growth rate, expressing the new model with five parameters. This model was able to estimate two growth rates (juveniles and adults) representing individual changes in asymptotic length and variability in time of tagging.

Another approach to analyze phenotypic variability in growth was focused on evaluating the impact of outliers commonly observed in the length-at-age data. Thus, Francis (1988) proposed eliminating the atypical data (outliers) using average data of age; this procedure gives the same weight to all data and a better fit to the growth curves. In addition, previous studies of growth have assumed two types of residuals commonly known as additive error and multiplicative error, which show a constant variance or homocedasticity (Wang and Liu 2006). Both approaches are based on normal and log-normal probabilistic density distributions and they have not been suitable for detecting the impact on growth parameters when atypical observations are observed in the samples. Chen et al. (2003) proposed three methods where the size of the tails of the normal distribution can be fitted with respect to the proportion of outliers in the data (known as fat tail distributions): 1) the thickness of tails is determined by the degrees of freedom using a student's t distribution, 2) the size of tails is increased by adding a fixed small value ($\lambda = 0.01$) within the normal distribution function, and 3) mixtures distributions where a new parameter is added to represent a proportion of outliers. However, these statistical procedures do not estimate length-at-age variability, assuming a constant variance. It is beyond the scope of this study to analyze the effect of outliers based on fat tail distributions. Moreover, this type of statistical procedure is only valid if the variance is constant and is influenced by the proportion of data assumed as outliers, this analyses has been documented previously for *Panopea globosa* by Morales-Bojórquez et al. (2015). In contrast, the hypothesis of this study focuses on showing a statistical procedure for estimating the variance-at-age when the variance is not constant for all ages in the population.

Given this background, studies on age and growth of geoduck populations have begun focusing on analyzing average growth trajectories of *Panopea generosa* based on VB (Hoffman et al. 2000; Bureau et al. 2002; Campbell and Ming 2003). However, a new approach was recently applied using information theory (mainly multimodel inference) whereby candidate growth models were analyzed based on different individual growth properties. However, although better trajectories were fitted to the observed shell length-at-age data, these described average growth curves (Cruz-Vázquez et al. 2012; Aragón-Noriega et al. 2015; González-Peláez et al. 2015; Hidalgo-de-la-Toba et al. 2015; Zaidman and Morsan 2015). Hence, these new efforts in age and growth modeling studies were limited since they failed to estimate the intrinsic phenotypic variability in growth of *Panopea* species. For *P. generosa* it has been reported that its lifespan may even exceed 150 years (Bureau et al. 2002); while the longevity reported for several other species is close to 50 years (Gribben and Creese 2005; Zaidman and Morsan 2015). In this study, a new approach for analyzing individual shell length-at-age variability was developed for *Panopea globosa* using a joint negative log-

likelihood combining both shell length frequency distributions and shell length–at-age data sets.

MATERIAL AND METHODS

Biological data

For illustrative purposes, two sources of data were used to estimate a combined growth curve for *P. globosa* from the southwestern Baja California Peninsula. Shell length–at-age data for individuals from 3 to 47 years were obtained from González-Peláez et al. (2015). Specific details about sample preparation (shells), reading and accuracy verification, age validation, and results of ageing error were reported by González-Peláez et al. (2015). While that shell length frequency data at early growth stages (0.105–7.04 mm, n = 867) were obtained under rearing experimental conditions from fertilization (in vitro) to 68th day at 19°C. The measurements of shell length (mm) of the larval and juvenile growth stages were selected assuming a simple random sampling. Thus, from the 34th day a sample of 72 organisms were sampled weekly during the following 6 weeks. We measured the shell lengths of these individuals by taking digital images and processing them with Sigma Scan Pro, ver. 5.0 (Systat Software, Richmond, CA, USA). The larvae were cultured at 1 ind/ml and the food supply given was *Isochrysis galbana*, while the juveniles were isolated individually and fed with mixture of microalgae *Isochrysis galbana* (50%) and *Chaetoceros* sp. (50 %). For both developmental stages the fed ration was between 30,000 and 45,000 cells/ml (unpublished data). This study analyzed shell length–at-age and shell length frequency distribution data of the whole ontogenic cycle of the geoduck clam *Panopea globosa* (trocophora larvae, pediveliger larvae, dissoconch and juvenile stages, including adult stages) in order to describe its phenotypic growth variability. Consequently, both data sets were integrated to cover the widest shell length (SL) range possible, including ages and shell length for early stages less than 1 year, and individuals from 3 to 47 years, this age range represents a shell length from 0.105 to 187 mm SL. This approach was identified as more comprehensive since it provided a complete age range for estimating multiple parameters for each candidate growth model evaluated; this procedure inclusiveness was suitable for jointly analyzing two data sets.

Analysis of shell length–at-age data

The individual growth of *P. globosa* was analyzed using the following six candidate growth models: (1) von Bertalanffy which exhibits an initial fast growth phase, gradually decreasing to attain the asymptotic length, it has no inflexion point for $t > 0$ (Breen et al. 1991; Hoffman et al. 2000; Aragón-Noriega et al. 2015); (2) Gompertz assumes an exponential decrease of the growth rate with size (González-Peláez et al. 2015); (3) Johnson describes a sigmoid growth with a very strong asymmetry and inflexion point very low close to 0 (Hidalgo-de-la-Toba et al. 2015); (4) Logistic considers an alternative sigmoidal curve (Cruz-Vázquez et al. 2012); (5) the generalized von Bertalanffy growth model (GVB) has a similar interpretation to the VB, however an additional parameter provide greater flexibility for fitting the curve (González-Peláez et al. 2015); and (6) the Richards model which describes several growth forms according to different values of δ_1, the inflection point can be located in any position of the curve (Zaidman and Morsan 2015). Thus, the estimated shell length–at-age ($\hat{l}$) was computed from the following mathematical functions:

$$\hat{l} = L_\infty \left[1 - exp^{-k(t - t_0)}\right] \quad (1)$$

$$\hat{l} = L_\infty \, exp^{-exp[-k(t - t_0)]} \quad (2)$$

$$\hat{l} = L_\infty \, exp^{-\left[\frac{1}{k}(t - t_0)\right]} \quad (3)$$

$$\hat{l} = L_\infty \left[1 + exp^{-k(t - t_0)}\right]^{-1} \quad (4)$$

$$\hat{l} = L_\infty \left[1 - exp^{-k(t - t_0)}\right]^{\delta 1} \quad (5)$$

$$\hat{l} = L_\infty \left[1 + \tfrac{1}{\alpha} \, exp^{-k(t - t_0)}\right]^{-\delta 1} \quad (6)$$

The growth parameters (θ_i) for the six candidate growth models are: L_∞ is average maximum shell length reached by older individuals; for the von Bertalanffy growth model k represents the growth coefficient; in the generalized von Bertalanffy and Richards growth models, k has similar interpretation; for Gompertz growth model the parameter k is the rate of exponential decrease of the relative growth rate with age; in the Logistic growth model, k is the relative growth rate parameter; for the Johnson growth model k is the rate at which the asymptotic shell length is reached (Katsanevakis 2006; González-Peláez et al. 2015); t_0 parameter is the theoretical age of the fish at zero size under the assumption that the von Bertalanffy (1938) growth curve describes the growth accurately right down to zero length. Even if this unlikely assumption is true, fish will be born with some positive length, so t_0 will usually be negative. The definition changes according to candidate growth models, e.g., the Logistic, Johnson, and Gompertz models correspond to the inflection point for each curve; for generalized von Bertalanffy growth model t_0 has similar interpretation as in the von Bertalanffy assuming the equation to be valid at all ages; a similar assumption is applied to the Richards growth model (see Katsanevakis 2006; Magnifico 2007 for details). According to Cailliet

TABLE 1
Mathematical function of expected shell length ($\hat{\mu}_a$), and variance σ^2_a for each modal group *a* according to shell length frequency distributions for early stages.

Model	Function $\hat{\mu}_a$	Function σ^2_a	Source	Eq.
VB	$\hat{\mu}_{aVB} = \Upsilon\,[1 - exp^{-\omega(a-t_0)}]$	$\sigma^2_{aVB} = \sigma^2_{\Upsilon_{VB}}\,[1 - exp^{-\omega(a-t_0)}]^2$	1,2	(15, 16)
GM	$\hat{\mu}_{aGM} = \Upsilon\ exp^{-exp[-\omega(a-t_0)]}$	$\sigma^2_{aGM} = \sigma^2_{\Upsilon_{GM}}\,[exp^{-exp(-\omega(a-t_0))}]^2$	This study	(17, 18)
JN	$\hat{\mu}_{aJN} = \Upsilon\ exp^{-\left[\frac{1}{\omega}(a-t_0)\right]}$	$\sigma^2_{aJN} = \sigma^2_{\Upsilon_{JN}}\,[exp^{-\left[\frac{1}{\omega}(a-t_0)\right]}]^2$	This study	(19, 20)
LG	$\hat{\mu}_{aLG} = \Upsilon\,[1 + exp^{-\omega(a-t_0)}]^{-1}$	$\sigma^2_{aLG} = \sigma^2_{\Upsilon_{LG}}\,[(1 + exp^{-\omega(a-t_0)})^{-1}]^2$	This study	(21, 22)
GVB	$\hat{\mu}_{aGVB} = \Upsilon\,[1 - exp^{-\omega(a-t_0)}]^{\delta_1}$	$\sigma^2_{aGVB} = \sigma^2_{\Upsilon_{GVB}}\,[(1 - exp^{-\omega(a-t_0)})^{\delta_1}]^2$	This study	(23, 24)
RC	$\hat{\mu}_{aRC} = \Upsilon\left[1 + \frac{1}{\alpha}\ exp^{-\omega(a-t_0)}\right]^{-\delta_1}$	$\sigma^2_{aRC} = \sigma^2_{\Upsilon_{RC}}\left[\left(1 + \frac{1}{\alpha}\ exp^{-\omega(a-t_0)}\right)^{-\delta}\right]^2$	This study	(25, 26)

The subindices are defined as: VB = von Bertalanffy, GM = Gompertz, JN = Johnson, LG = Logistic, GVB = generalized von Bertalanffy, RC = Richards.1) von Bertalanffy (1938), 2) Restrepo et al. (2010).

et al. (2006) the t_0 parameter is largely artificial, in so far as it defines the age at which the organism would be of zero length if it grew throughout its life with the same pattern of growth as in the post-larval phase; α and δ_1 are dimensionless parameters, both providing greater flexibility for modeling the data.

According to Restrepo et al. (2010) the estimated variance for each age observed (σ_i^2) in the VB (σ^2_{iVB}) can be expressed as:

$$\sigma^2_{iVB} = \sigma^2_{L\infty VB}\left[1 - exp^{-k(t-t_0)}\right]^2 \tag{7}$$

Thus, different σ_i^2 were estimated for the rest of the candidate growth models based on the following mathematical implementations (Luquin-Covarrubias et al. 2016):

Gompertz

$$\sigma^2_{iGM} = \sigma^2_{L\infty GM}\left[exp^{-\,exp(-k(t-t_0)}\right]^2 \tag{8}$$

Johnson

$$\sigma^2_{iJN} = \sigma^2_{L\infty JN}\left[exp^{-\left(\frac{1}{k}(t-t_0)\right)}\right]^2 \tag{9}$$

Logistic

$$\sigma^2_{iLG} = \sigma^2_{L\infty LG}\left[(1 + exp^{-k(t-t_0)^{-1}}\right]^2 \tag{10}$$

GVB

$$\sigma^2_{iGVB} = \sigma^2_{L\infty GVB}\left[(1 - exp^{-k(t-t_0)})^{\delta_1}\right]^2 \tag{11}$$

Richards

$$\sigma^2_{iRC} = \sigma^2_{L\infty RC}\left[(1 + \frac{1}{\alpha}\ exp^{-k(t-t_0)})^{-\delta_1}\right]^2 \tag{12}$$

where $\sigma^2_{L_\infty}$ is the variance for older individuals, and the abbreviations associated with subindices *i* and L_∞ identify the candidate growth model. This statistical procedure analyzes the intrinsic variability of shell length-at-age data for different candidate growth models, assuming that the residuals are normally distributed with the variance increasing as a function of the age (Restrepo et al. 2010). The negative log-likelihood function ($\mathcal{L}_1$) describing the best fit between observed (l_i) and estimated ($\hat{l}$) shell length-at-age data is expressed as follows:

$$\mathcal{L}_1 = \Sigma_i\left[\frac{\ln(2\pi\sigma_i^2)}{2} + \frac{(l_i - \hat{l}_i)^2}{2\pi\sigma_i^2}\right] \tag{13}$$

Analysis of shell length frequency data

Shell length data for early growth stages (0.105 to 7.04 mm) of *P. globosa* were analyzed using frequency histograms. Thus, the shell length frequency distribution for each age group (*a*) was estimated using a normal probabilistic density function (Zar 1999):

$$\hat{f}(L_a) = \Sigma_{a=1}^{n}\left[\int_{-\infty}^{L_{a,a_i}} \frac{1}{\sqrt{2\pi\sigma_a^2}}\ exp\left[-\frac{1}{2\sigma_a^2}(L_a - \hat{\mu}_a)^2\right] dL_{a_i}\right]\lambda_{a_i} \tag{14}$$

where (L_a) is the observed shell length, ($\hat{\mu}_a$) is the average shell length for each age group *a*, λ_{ai} represents a parameter of fit for the observed frequency data within each age group *a*, *i* represents the sequential number of modal values estimated, and σ_a^2 is the variance for each age group *a*. The estimation of $\hat{\mu}_a$ and σ_a^2 was done for each group *a* following the statistical criteria as described in Table 1 (equations 15–26). The parameters associated to equations 15–26 are: Υ represents the larger shell length for younger individuals; ω growth coefficient for younger individuals; σ^2_Υ is the variance for larger individuals observed in the early growth stages. The differences between the observed and expected shell length frequency distributions were fitted assuming a multinomial distribution expressed as negative log-likelihood function defined as $\mathcal{L}_2$:

$$\mathcal{L}_2 = -ln\ L(f|\theta i) = \Sigma_{a=1} f(L_a|ln)\left[\frac{\hat{f}(L_a)}{\Sigma\hat{f}(L_a)}\right] - \Sigma_{i=1}^{n}(f_a - \hat{f}_a)^2 \quad (27)$$

where $f(L_a)$ is the observed shell length frequency and $\hat{f}(L_a)$ is the predicted shell length frequency within the average shell length group L_a. A penalization function (eq. 27) was included in the negative log-likelihood for estimating the frequency of individuals for each age group, (f_a) is shell length frequency distribution observed in the sample, and ($\hat{f}_a$) represents the number of predicted observations. The age groups were identified using Akaike information criterion through: $AIC = 2\mathcal{L}_2 + 2p$, where p is the parameter number for each model fitted to shell length frequency distribution (Haddon 2001). The lowest value AIC was used for determining if the statistic fit can be improved by adding a new mode (Montgomery et al. 2010). This allows for ensuring that the age groups are close to t_0 and that an accurate estimation of all growth parameters is attained.

Parameters estimation

The candidate growth models were fitted to both data sets, minimizing a joint negative log-likelihood function ($\mathcal{L}_J$) through Newton algorithm contained in the Visual Basic Applications™ (Neter et al. 1996):

$$\mathcal{L}_J = \mathcal{L}_1 + \mathcal{L}_2 \quad (28)$$

To achieve a more accurate estimate of the parameters, the minimizing was done by phases, the parameters less sensitive were simultaneously estimated in the first group considering the statistical propriety of each model (Υ, ω, σ^2_Υ, α, δ_1, λ_{a_1} and λ_{a_2}), while the rest retained the values initially assigned. Once the objective function was minimized for a particular phase, the other parameters were added and evaluated gradually (L_∞, k, t_0, $\sigma^2_{L\infty}$), thus this was carried out in order to complete the total optimization of $\mathcal{L}_J$ (Legault and Restrepo 1998).

Confidence intervals

The statistical χ^2 used in our study was applied as a non-parametric estimator for estimating confidence intervals ($\alpha = 0.05$). The rationale is based on the possibilities that the confidence regions can be asymmetric rather than symmetrical ellipses as assumed by asymptotic methods, and if this occurs the likelihood-profile or contour method is preferred because it is computationally more efficient than bootstrapping (Haddon 2001; Morales-Bojórquez and Nevárez-Martínez 2010). We estimated the confidence intervals (CI) for the θ_i parameters using a likelihood-profile method (Hilborn and Mangel 1997), the advantage of this approach is that it provides an estimate of the asymmetric confidence intervals either individually or jointly. The estimator assumes a χ^2 distribution with $n = 1$ degrees of freedom (df), when the estimation is individual, thus all values smaller or equal to 3.84 are accepted (Morales-Bojórquez and Nevárez-Martínez 2005); this approach was solved for the following parameters: Υ, ω, σ^2_Υ, α, δ_1, λ_{a_1},λ_{a_2}, t_0, $\sigma^2_{L\infty}$. When the estimation is joint and there is any type of correlation (covariance) between parameters, the CI become wider, in this case the likelihood-contour method is preferred (Cerdenares-Ladrón-de-Guevara et al. 2011), this was applied to L_∞ and k parameters. If there was no correlation between parameters then the confidence intervals would be unbiased (Zepeda-Benitez et al. 2014a). Thus, a χ^2 distribution with $n = 2$ degrees of freedom (df) was applied, such that values equal or less than 5.99 are accepted within CI (Zar 1999). The χ^2 estimator is described as follows by Haddon (2001):

$$CI = 2[\mathcal{L}_J - In\,L(\theta_i)] \leq \chi^2_{df,1-\alpha} \quad (29)$$

where $\mathcal{L}_J$ is the joint negative log-likelihood of the most likely value of θ_i; $-ln\ L(\theta_i)$ is the negative log-likelihood based on hypotheses about the value of θ_i (profile or contour), and $\chi^2{}_{1-\alpha}$ is the value of χ^2 distribution with a confidence level $1-\alpha = 0.05$ and $df = 1$ (profile), or 2 (contour) (Haddon 2001).

Growth model selection

The fit of the six candidate growth models was compared using AIC_c bias corrected for small samples, this condition is defined if $n/\theta_i < 40$ (Zepeda-Benitez et al. 2014b).

$$AIC_c = 2 \times \mathcal{L}_J + 2 \times \theta_i + \frac{2 \times \theta_i(\theta_i + 1)}{n - \theta_i - 1} \quad (30)$$

where $\mathcal{L}_J$ is the joint negative log-likelihood function (eq. 28), θ_i is the number of estimated parameters for each growth model, and n is the number of observed data (shell length-at-age and shell length frequency data). The model with the smallest AIC value is considered the best fit to the data (Burnham and Anderson 2002). Differences between the AIC_c for each growth model (i) were calculated as $\Delta_i = AIC_{c,i} - AIC_{c,min}$ according to Burnham and Anderson (2002). The candidate growth models with $\Delta_i > 10$ do not have statistical support and cannot be considered; with $4 < \Delta_i < 7$ have partial statistical support, and $\Delta_i < 2$ have high statistical support.

We estimated the plausibility of each candidate growth model defined as Akaike weight (w_i) (Katsanevakis 2006):

$$w_i = \frac{\exp(-0.5\ \Delta_i)}{\Sigma_{i=1}^{6}\exp(-0.5\ \Delta_i)} \quad (31)$$

TABLE 2
Number of modal values selected from AIC using the shell length frequency distributions for early stages.

	Parameters	Negative log-likelihood function	AIC
Mode 1	3	3628.84	7263.69
Mode 2	6	3186.15	6384.31
Mode 3	9	3163.44	6344.89
Mode 4	12	3156.55	6337.10
Mode 5	15	3184.68	6399.37

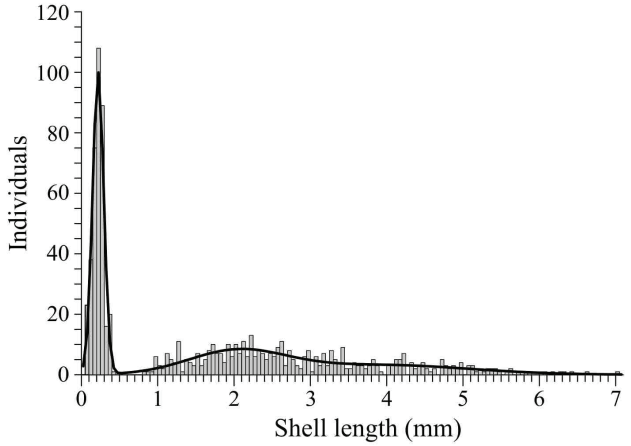

Figure 1. Shell length frequency distributions for each age group (*a*) estimated for early stages.

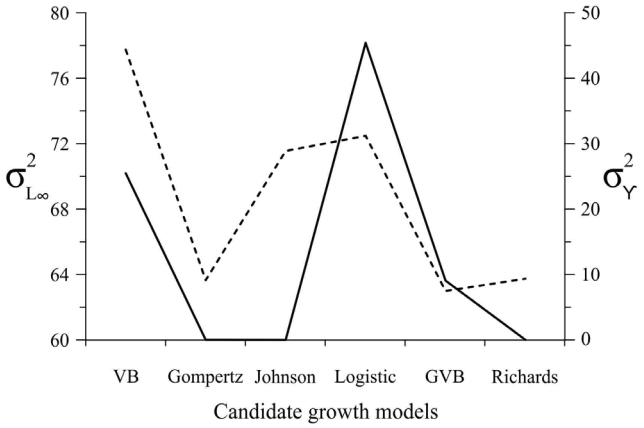

Figure 2. Comparison of the variance $\sigma^2_{L\infty}$ for older (discontinuous line) and σ^2_Y younger individuals (continuous line) estimated for each candidate growth model analyzed.

Following the multimodel inference approach, the model-averaged asymptotic length $\overline{L}_\infty$ was estimated as a weighted average using all six models, with the prediction of each model weighted by w_i. Thus, the model-averaged asymptotic shell length is:

$$\overline{L}_\infty = \Sigma_{i=1}^{6} w_i \hat{L}_\infty \quad (32)$$

The unconditional standard error of $\overline{L}_\infty$ was estimated as (Katsanevakis 2006):

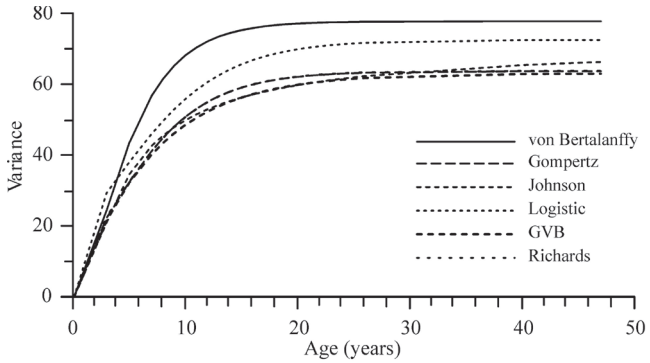

Figure 3. Trajectories of the variance for each age *i* according each candidate growth model analyzed.

$$SE(\overline{L}_\infty) = \Sigma_{i=1}^{6} w_i \left[\mathrm{var}\left(\hat{L}_\infty / g_i\right) + \left(\hat{L}_\infty - \overline{L}_\infty\right)^2\right]^{1/2} \quad (33)$$

where var $\overline{L}_i / g_i$ is the estimate variance of observed data with respect to each candidate growth model g_i.

RESULTS

The multinomial distribution fitted to shell length frequency data for early growth stages of *P. globosa* allowed for estimating four age groups. The AIC estimated from the hypotheses of one age group until five age groups are shown in Table 2. The mean value of the age group 1 was 0.22 mm, (SD = 0.07, λ_{a_1} = 18.49), this age group was very well identified for the multinomial function; the mean value for the age group 2 was 1.15 mm, (SD = 0.14, λ_{a_2} = 1.50), while the third and fourth age groups showed mean values of 3.78 mm (SD = 1.18, λ_{a_3} = 10.46), and 2.11 mm (SD = 0.51, λ_{a_4} = 9.44). Comparatively, the fifth age group showed mean value of 4.70 mm (SD = 17.27, λ_{a_5} = 2.43), however the presence of fifth age group increased the AIC value, consequently the addition of this last age group did not improve the statistical fit of the multinomial function (fig. 1).

This preliminary estimation was useful to define the initial number of age groups to be included when shell length-at-age data were added. Thus, the parameters for both datasets were jointly optimized to each candidate growth model (table 3). The parameters estimated showed that for $\sigma^2_{L\infty}$ and σ^2_Y the VB (77.73 and 25.46, respectively), and Logistic model (72.47 and 45.40, respectively) had the higher values (fig. 2). The effect of $\sigma^2_{L\infty}$ and σ^2_Y within the VB and Logistic model were influencing the estimates, where the variance for each age *i* was highest. The rest of the candidate growth models showed similar trends in σ^2_i estimates with lower values (fig. 3). The ontogenic growth trajectory from the two sources of data to geoduck clam are shown in Figure 4. Thus, the datasets were informative of the different growth parameters with respect to early or adult stages.

TABLE 3
Parameters and confidence intervals (in parenthesis) estimated from joint negative log-likelihood profile or contour ($P < 0.05$) for different growth functions. The sample size for early stages was 867 individuals, and average shell length-at-age data were 24 observations.

Parameter	von Bertalanffy	Gompertz	Johnson	Logistic	GVB	Richards
Υ	12.11 (11.40–12.80)	0.36 (0.36–0.38)	0.06 (0.06–0.07)	16.18 (15.70–16.80)	7.23 (7.04–7.46)	0.29 (0.28–0.30)
L_∞	164.69 (159.80–170.00)	167.78 (163.50–173.50)	179.48 (175.00–182.50)	168.53 (161.80–175.80)	169.82 (164.20–176.20)	167.84 (162.55–173.60)
ω	0.27 (0.26–0.28)	30.41 (29.50–31.50)	18.66 (18.19–19.09)	32.25 (32.04–32.46)	0.02 (0.02–0.03)	87.47 (86.00–89.00)
k	0.27 (0.23–0.33)	0.21 (0.18–0.25)	0.55 (0.52–0.55)	0.20 (0.15–0.26)	0.15 (0.13–0.19)	0.21 (0.18–0.26)
t_0	0.027 (0.0263–.0267)	0.067 (0.0671–0.0678)	0.069 (0.069–0.070)	0.23 (0.238–0.239)	0.0322 (0.0321–0.0322)	0.04 (0.0446–0.0449)
σ^2_Y	25.46 (24.46–26.46)	0.02 (0.022–0.024)	0.0008 (0.00076–0.00084)	45.40 (43.19–47.38)	9.06 (8.57–9.48)	0.014 (0.014–0.015)
$\sigma^2_{L\infty}$	77.73 (48.00–144.00)	63.65 (40.00–118.00)	71.55 (48.00–132.00)	72.47 (49.00–133.00)	63.00 (38.30–111.50)	63.74 (38.60–113.00)
δ_1					0.533 (0.530–0.535)	14.31 (14.15–14.46)
α						14.11 (13.90–14.32)
λ_{a_1}	1.84 (1.83–1.84)	1.84 (1.83–1.84)	1.84 (1.83–1.84)	1.84 (1.83–1.84)	1.84 (1.83–1.84)	1.84 (1.83–1.84)
λ_{a_2}	2.17 (2.17–2.18)	2.17 (2.17–2.18)	2.17 (2.17–2.18)	2.17 (2.17–2.18)	2.17 (2.1–2.18)	2.17 (2.17–2.18)

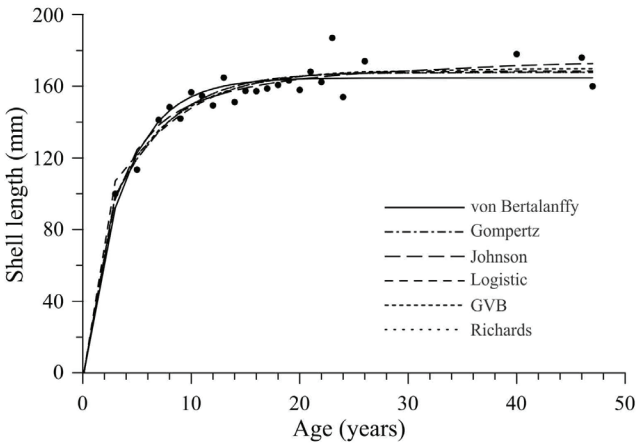

Figure 4. Candidate growth models fitted to shell length-at-age and shell length frequency data of *Panopea globosa*. Points represent shell length-at-age data observed.

The variability estimated in growth parameters showed that average maximum shell length (L_∞) varied from 164.69 mm (VB) to 179.48 mm (Johnson model), for the rest of the growth models this parameter was less than 169.82 mm. The k parameter changed between $k = 0.15$ and $k = 0.55$ for GVB and Johnson model, respectively. The general pattern of variability in this parameter shows that it was commonly estimated as a value less than $k = 0.27$. The parameter associated with t_0 presented the minimum value for VB ($t_0 = 0.027$), and the maximum value for the Logistic growth model ($t_0 = 0.23$) (table 3). The variation of ω for younger individuals varied from 0.02 (GVB) to 87.47 (Richards growth model), and the larger shell length estimated for younger individuals (Υ)ranged between 0.06 and 16.18 for the Johnson and the Logistic growth models, respectively (table 3).

The final parameterization including shell length frequency distributions and shell length-at-age data showed convergence in the objective function when only two age groups were assessed, the addition of the third and fourth age group caused lack in convergence. This means that the interactions between both datasets statistically discriminated the useful of the third and fourth age group, which were used as seed values in the joint negative log-likelihood function. Thus, new age groups in the shell length frequency distributions were restimated to each candidate growth model, the first age group was 0.20 mm ($\sigma^2_a = 7.6x10\text{-}4$), and the second was 2.91 mm

TABLE 4
Ranking of the six growth models based on the Akaike information criterion (AIC_c) according to the number of parameters for each candidate growth model (θ_i), Akaike difference (Δ_i), and the Akaike weight (w_i).

Model	θ_i	AIC_c	Δ_i	w_i
Johnson	9	6612.02	0.00	0.47
Gompertz	9	6612.44	0.41	0.38
Logistic	9	6615.35	3.32	0.08
GVB	10	6617.67	5.64	0.02
von Bertalanffy	9	6618.11	6.08	0.02
Richards	11	6625.62	13.59	0.00

($\sigma_a^2 = 0.14$). Specific details on the λ_{a_i} estimates and confidence intervals are shown in Table 3.

Model selection

According to AIC_c estimates, the best fit to the shell length frequency and shell length-at-age data of *P. globosa* was described by Johnson growth model ($AIC_c = 6612.02$, $\Delta_i = 0.00$, $w_i = 0.47$). A second function that showed statistical support was the Gompertz growth model ($AIC_c = 6612.44$, $\Delta_i = 0.41$, $w_i = 0.38$). Despite the Logistic, GVB, and von Bertalanffy models varying within $4 < \Delta_i < 7$ showing partial statistical support, these functions had Akaike weight less than 0.08. Finally, the Richards growth model had no statistical support fitting both data sets (table 4). In this study, the best candidate growth models were the sigmoid functions (also known as curve S-shaped). Comparatively, the asymptotic curves crossing the *t*-axis (age) and without inflection point, as well as generalized growth models showed less statistical performance expressed in the AIC_c estimates. Given that five candidate growth models had $\Delta_i < 7$, the model-averaged asymptotic length was estimated as 173.38 mm (CI = 154.71-192.05 mm $P < 0.05$; $SE(\overline{L}_\infty) = 9.52$ mm.

DISCUSSION

This study was based on the hypothesis of depensatory growth applied to *Panopea globosa*, previous studies ignored the effect of the individual variability commonly observed in age-at-shell length data for geoduck in the Mexican Pacific. Given that the asymptotic growth pattern in geoduck is very well known, we incorporated the individual variability in several deterministic asymptotic growth models. The new integrated shell length-at-age and shell length frequency distribution growth model has improved assumptions about geoduck clam individual growth compared to conventional growth models. In this study, individual variability in geoduck growth was explicitly included; this allows a better parameterization of the candidate growth models. Sainsbury (1980) explained that many mollusks have high variability in their individual growth parameters due to changing age composition, and this is commonly observed in the variability of increments of length-at-age. We found that the age composition of the *Panopea globosa* is informative about L_∞ and k parameters; however, t_0 parameter estimated from average shell length-at-age growth curves may be over- or underestimated. Thus, the estimation of L_∞ and k for each candidate growth model using this joint negative log-likelihood function showed similar values to those reported by González-Peláez et al. (2015), where they found values between $L_\infty = 164.6$ mm SL (Richards) and $L_\infty = 181.1$ mm SL (Johnson), and the growth coefficient estimates varied between $k = 0.14$ (GVB) and $k = 0.49$ (Johnson). In general terms, the k parameter in the models used is a measure of the time required for specified growth increments to take place, however its comparison is not possible because the path or trajectory taken by the growth process in each model (Brisbin et al. 1987). Different studies have shown high variations for estimates of t_0; this lack in accuracy about t_0 has commonly been reported in different species of the genus *Panopea*. For *P. abbreviata* (Argentina), *P. generosa* (Canada), and *P. zelandica* (New Zealand) negative values were observed when VB was used (Breen et al. 1991; Campbell and Ming 2003; Morsan and Ciocco 2004; Gribben and Creese 2005; Morsan et al. 2010). In contrast, for *P. generosa* distributed in United States waters, estimates for t_0 parameter had positive values (Hoffman et al. 2000) (table 5).

For *Panopea* species the formation of the shell begins approximately 48 hours after fertilization, and from 1.5 mm SL they are juveniles (Goodwin and Pease 1989), therefore negative and extremely high values of t_0 do not provide useful information about this parameter in its early growth stages. Recently, the multimodel inference approach has been applied to age and growth modeling of *Panopea* spp.; however, this statistical procedure did not yield better estimates of t_0, either values highly skewed were also computed for several stocks (table 6). Our study described successfully estimates of t_0 for six growth models improved the growth curves at the origin (age 0); this was supported by the inclusion of shell length frequency distribution of early stages associated with the joint negative log-likelihood function. These new features must be adopted in growth modeling, since these allow for increasing the accuracy for t_0 estimates, thus improving its biological interpretation. For the t_0 parameter, if a lack of convergence is observed during the optimization process to estimate this parameter, then the final estimation of t_0 can vary its order of magnitude such as was reported for *P. abbreviata* (–46.96, –35.76, –31.87; 133.06, 57.76); and *P. globosa* (–2.99, –1.85, –1.31) (table 6). Pardo et al. (2013) suggested several alternatives for better estimates of t_0; the first is to modify VB using a fixed value of average length-at-age zero

TABLE 5
Estimates of the age when shell length theoretically is zero for *Panopea* spp. using the von Bertalanffy growth model.

Species	Country	Location	t_0	Source
P. globosa	Mexico	Bahía del Sol	–0.200	Cortez-Lucero et al. (2011)
P. generosa	Mexico	San Quintín	–3.190	Calderon-Aguilera et al. (2010)
		Islas Coronado	–2.040	
	United States	Hunter Point	0.719	Hoffman et al. (2000)
		Agate Passage	0.183	
		Fishermans Point	0.552	
		Dallas Bank	0.334	
	Canada	Yellow Bank	–1.420	Campbell and Ming (2003)
		Gabriola Island	–1.020	
P. abbreviata	Argentina	Puerto Lobos	–1.500	Morsan and Ciocco (2004)
		Puerto Lobos	–0.487	Morsan et al. (2010)
		El Sótano	–2.397	Morsan et al. (2010)
P. zelandica	New Zealeand	Golden Bay	–3.800	Breen et al. (1991)
		Shelly Bay	–1.690	Gribben and Creese (2005)
		Kennedy Bay	–1.670	Gribben and Creese (2005)

defined as L_0 parameter, which is empirical or a known value of length for organisms at their early growth stages. Consequently, L_0 can be fixed, estimating only L_∞ and k parameters. However, L_0 parameter can be iteratively sampled from a normal distribution of possible values of length at an early growth stage; or it can be constrained over the range from known values of L_0 thus assessing the effect in convergence thereby fixing this range.

In this study, estimates for t_0 parameter ranged from 0.027 to 0.23, negative values for this parameter were not computed. The best candidate growth model showed $t_0 = 0.069$ (Johnson) and $t_0 = 0.067$ (Gompertz), where both estimates were very close. In previous studies of age and growth of *P. globosa*, the results estimated for t_0 were highly variable; González-Peláez et al. (2015) showed values from –1.85 (VB) to 28.91 (Schnute), and the best candidate growth model selected by AIC_c was $t_0 = 0.003$ (Gompertz). Aragón-Noriega et al. (2015) analyzed shell length-at-age data for two populations of *P. globosa* in the upper Gulf of California, they reported negative values ranging from $t_0 = –2.99$ (VB) to $t_0 = –0.005$ (Logistic) to Puerto Peñasco, Sonora, and an interval of variation from $t_0 = –1.20$ (VB) and $t_0 = 6.86$ (Gompertz) to San Felipe, Baja California. In the central Gulf of California the estimates of t_0 for *P. globosa* ranged within positive values from 0.24 (VB) to 2.26 (Logistic) (Cruz-Vázquez et al. 2012). For *P. generosa*, Hidalgo-de-la-Toba et al. (2015) analyzed five growth models, among them, three computed $t_0 = 0$ (VB, Gompertz, and Johnson), while that the Logistic growth model estimated $t_0 = 1.34$, and $t_0 = 1.78$ for the Schnute growth model. This last model was also used by Cruz-Vázquez et al. (2012) and Aragón-Noriega et al. (2015), however they did not report results associated with t_0, assuming that $t_0 = 0$ (table 6).

We found that the combined growth curves using shell length frequency distributions and shell length-at-age data provided more information about t_0 parameter for different growth models. A similar approach was discussed by Sainsbury (1980) and Kirkwood (1983), and they concluded that a joint likelihood function applied to both data sets provided a better description of growth over the range of lengths to which VB was fitted. According to Restrepo et al. (2010), they used a penalty term for each year analyzed (1970–76), using only length frequency observations. A penalty term represents a weight governing the amount of influence of each data set (shell length-at-age and shell length frequency distribution), and this should be implemented in the joint log-likelihood function. However, according to Quinn and Deriso (1999), each penalty term is the inverse of the estimated variance of each data set, assuming that the variance is constant. In this study, we had data from early stages obtained from rearing conditions during 2013. Our analysis estimated an individual variability-at-age observed in shell length-at-age and shell length frequency distribution data, thus the variance was not constant; and consequently the inverse of the estimated variance that could represent the penalty term for each negative log-likelihood was not applicable, because we estimated variance-at-age. For any penalty term estimated, the main problem was to select the variance representing the best amount of influence of each data set, given that we estimated 26 variance-at-age values, potentially to choose arbitrarily a variance-at-age (or average value) could represent bias in the joint negative log-likelihood function affecting the optimization of parameters in the candidate growth models selected.

TABLE 6
Estimates of the age when shell length theoretically is zero for *Panopea* spp. using the multimodel inference approach.

Species	Country	Location	Model	t_0	Source
P. globosa	Mexico	Bahía Magdalena	VB	–1.857	González-Peláez et al. (2015)
			GM	0.003	
			JN	–0.301	
			GVB	0.713	
			RC	5.583	
			SC	28.911	
		Puerto Peñasco	VB	–2.990	Aragón-Noriega et al. (2015)
			GM	–1.310	
			LG	–0.005	
			SC	–	
			SC-RC	–	
		San Felipe	VB	–1.200	Aragón-Noriega et al. (2015)
			GM	6.860	
			LG	2.970	
			SC	–	
			SC-RC	–	
		Empalme	VB	0.247	Cruz-Vázquez et al. (2012)
			GM	1.401	
			LG	2.260	
			SC-RC	–	
P. generosa	Mexico	Punta Canoas	VB	0.000	Hidalgo-de-la-Toba et al. (2015)
			GM	0.000	
			JN	0.000	
			LG	1.340	
			SC	1.780	
P. abbreviata	Argentina	El Sótano	VB	–3.830	Zaidman and Morsan (2015)
			GM	0.120	
			LG	–1.770	
			RC	–31.870	
			SC-RC	–	
		Punta Colorada	VB	–1.560	Zaidman and Morsan (2015)
			GM	0.290	
			LG	0.780	
			RC	1.400	
			SC-RC	–	
		Puerto Lobos	VB	–1.750	Zaidman and Morsan (2015)
			GM	0.230	
			LG	0.370	
			RC	–3.760	
			SC-RC	–	
		La Tapera	VB	–2.670	Zaidman and Morsan (2015)
			GM	0.200	
			LG	0.200	
P. abbreviata	Argentina	La Tapera	RC	–1.980	Zaidman and Morsan (2015)
			SC-RC	–	
		Playa Fracasso	VB	–46.960	Zaidman and Morsan (2015)
			GM	0.020	
			LG	133.060	
			RC	57.760	
			SC-RC	–	
		Punta Conos	VB	–8,720	Zaidman and Morsan (2015)
			GM	0,070	
			LG	–1,400	
			RC	–35,760	
			SC-RC	–	

The candidate growth models used in different studies are defined as:VB = von Bertalanffy, GM = Gompertz, JN = Johnson, LG = Logistic, GVB = generalized von Bertalanffy, RC = Richards, SC = Schnute, SC-RC = Schnute-Richards.

We used a new approach based on phenotypic variability in growth observed in *P. globosa*; it allowed that the variance for each age was also computed, and this feature has not been previously modeled for *Panopea* species. Finally, our findings showed that the VB had higher variance for each age, and it was not suitable for *Panopea globosa*. We believe that if more data sources are included in this joint log-likelihood function (e.g., mark-recapture observation) then the ontogenic life cycle can be represented, and improved parameters could be used in the stock assessment models (e.g., maximum yield per recruit), which would be useful in setting management quantity guidelines for *Panopea* species in the Mexican Pacific (Aragón-Noriega et al. 2012). This analysis and methodological approach based on phenotypic variability in growth of *Panopea globosa* was found to be useful and probably its use can have wider applicability, thus allowing its use with other mollusks and marine organisms for more accurate modeling of growth.

ACKNOWLEDGMENTS

The authors thank to Consejo Nacional de Ciencia y Tecnología México (CONACYT) for the financial support received throughout the project contract number 241603. Marlene Anaid Luquin Covarrubias was a recipient of the CONACYT postgraduate fellowship (contract number 636852). We appreciate the comments of the reviewers and we wish to extend our sincere thanks to them for their insightful comments which undoubtedly has improved the quality of our manuscript.

LITERATURE CITED

Aragón-Noriega, E. A., E. Alcántara-Razo, L. E. Calderon-Aguilera, and R. Sánchez-Fourcade. 2012. Status of geoduck clam fisheries in Mexico. J. Shellfish Res. 31:733–738.

Aragón-Noriega, E. A., L. E. Calderon-Aguilera, and S. A. Perez-Valencia. 2015. Modeling growth of the cortes geoduck *Panopea globosa* from unexploited and exploited beds in the northern gulf of California. J. Shellfish Res. 34:119–127.

Bertalanffy, L. von. 1938. A quantitative theory of organic growth (Inquiries on growth laws. II). Human Biol. 10:181–213.

Breen, P. A., C. Gabriel, and T. Tyson. 1991. Preliminary estimates of age, mortality, growth, and reproduction in the hiatellid clam *Panopea zelandica* in New Zealand. N. Z. J. Mar. Freshwater. 25:231–237.

Brisbin, I., C. Collins, G. White, and D. McCallum. 1987. A new paradigm for the analysis and interpretation of growth data: The shape of things to come. The Auk. 104:552–554.

Bureau, D., W. Hajas, N. W. Scurry, C. M. Hand, G. Dovey, and A. Campbell. 2002. Age, size structure and growth parameters of geoducks (*Panopea abrupta*, Conrad 1849) from 34 locations in British Columbia sampled between 1993 and 2000. Can. Tech. Rep. Fish. Aquat. Sci. 2413:84 pp.

Burnham, K. P., and D. R. Anderson. 2002. Model selection and multimodel inference: a practical information theoretic approach. 2nd ed. New York: Springer. 488 pp.

Cailliet, G.M., W. D. Smith, H. F. Mollet, and K. J. Goldman. 2006. Age and growth studies of chondrichthyan fishes: the need for consistency in terminology, verification, validation, and growth function fitting. Environ. Biol. Fish. 77:211–228.

Campbell, A., and M. D. Ming. 2003. Maturity and growth of the Pacific geoduck clam, *Panopea abrupta*, in southern British Columbia, Canada. J. Shellfish Res. 22:85–90.

Cerdenares-Ladrón-de-Guevara, G., E. Morales-Bojórquez, and R. Rodríguez-Sánchez. 2011. Age and growth of the sailfish *Istiophorus platypterus* (Istiophoridae) in the Gulf of Tehuantepec, Mexico. Mar. Biol. Res. 7:488–499.

Chen, Y., Y. Jiao, and L. Chen. 2003. Developing robust frequentist and Bayesian fish stock assessment methods. Fish Fish. 4:105–120.

Cruz-Vázquez, R., G. Rodríguez-Domínguez, E. Alcántara-Razo, and E. A. Aragón-Noriega. 2012. Estimation of individual growth parameters of the Cortes geoduck *Panopea globosa* from the central Gulf of California using a multimodel approach. J. Shellfish Res. 31:725–732.

Francis, R. I. C. C. 1988. Maximum likelihood estimation of growth and growth variability from tagging data. N. Z. J. Mar. Freshwater. 22:43–51.

González-Peláez, S. S., E. Morales-Bojórquez, D. B. Lluch-Cota, S. E. Lluch-Cota, and J. J. Bautista-Romero. 2015. Modeling geoduck growth: multimodel inference in *Panopea globosa* from the southwestern Baja California Peninsula, Mexico. J. Shellfish Res. 34:101–112.

Goodwin, C.L., and B. Pease. 1989. Species profiles: life histories and environmental requirements of coastal fishes and invertebrates (Pacific northwest). Pacific geoduck clam. U.S. Fish. Wildl. Serv. Biol Rep. 82(11.120). U.S. Army Corps of Engineers, TR EL82-4. 14 pp.

Gribben, P. E., and R. G. Creese. 2005. Age, growth, and mortality of the New Zealand geoduck clam, *Panopea zelandica* (Bivalvia: Hiatellidae) in two North Island populations. Bull. Mar. Sci. 77:119–135.

Haddon, M. 2001. Modelling and quantitative methods in fisheries. 2nd ed. Florida: Chapman and Hall. 406 pp.

Hidalgo-de-la-Toba, J. A., S. S. González-Peláez, E. Morales-Bojórquez, J. J. Bautista-Romero, and D. B. Lluch-Cota. 2015. Geoduck *Panopea generosa* growth at its southern distribution limit in North America using a multimodel inference approach. J. Shellfish Res. 34:91–99.

Hilborn, R., and M. Mangel. 1997. The ecological detective: confronting models with data. 1st ed. New Jersey: Princeton University Press. 315 pp.

Hoffman, A., A. Bradbury, and C. L. Goodwin. 2000. Modeling geoduck, *Panopea abrupta* (Conrad, 1849) population dynamics: I. Growth. J. Shellfish Res. 19:57–62.

Katsanevakis, S. 2006. Modelling fish growth: model selection, multimodel inference and model selection uncertainty. Fish. Res. 81:229–235.

Kirkwood, P. 1983. Estimation of von Bertalanffy growth curve parameters using both length increment and age-length data. Can. J. Fish. Aquat. Sci. 40:1405–1411.

Lai, H. L., and A. Bradbury. 1998. A modified catch-at-size analysis model for a red sea urchin (*Strongylocentrotus franciscanus*) population. *In* Proceedings of the North Pacific Symposium on Invertebrate Stock Assessment and Management, G. S. Jamieson, and A. Campbell, ed. Can. Spec. Publ. Fish. Aquat. Sci. 125:85–96.

Laslett, G. M., J. P. Eveson, and T. Polacheck. 2002. A flexible maximum likelihood approach for fitting growth curves to tag-recapture data. Can. J. Fish. Aquat. Sci. 59:976–986.

Legault, C. M., and V. R. Restrepo. 1998. A flexible forward age-structured assessment program. ICCAT Working Document. 15 pp.

Luquin-Covarrubias, M. A., E. Morales-Bojórquez, S. S. González-Peláez, and D. B. Lluch-Cota. 2016. Modeling of growth depensation of the geoduck clam *Panopea globosa* based on a multimodel inference approach. J. Shellfish Res. 35(2):379-387.

Magnifico, G. 2007. New insights into fish growth parameters estimation by means of length-based methods. Ph.D. Thesis in Evolutionary Biology and Ecology. University of Rome Tor Vergata. 202 pp.

Montgomery, S. S., C. T. Wash, M. Haddon, C. L. Kesby, and D. D. Johnson. 2010. Using length data in the Schnute model to describe growth in a metapenaeid from waters off Australia. Mar. Freshwater Res. 61:1435–1445.

Morales-Bojórquez, E., and M. O. Nevárez-Martínez. 2005. Spawner-recruit patterns and investigation of Allee effect in Pacific sardine *Sardinops sagax caeruleus* in the Gulf of California, Mexico. Calif. Coop. Oceanic Fish. Invest. Rep. 46:161–174.

Morales-Bojórquez, E., and M. O. Nevárez-Martínez. 2010. Catch-at-size analysis for *Dosidicus gigas* in the central Gulf of California, Mexico. Fish. Res. 106:214–221.

Morales-Bojórquez, E., J. López-Martínez, and L. F. J. Beléndez-Moreno. 2013. Estimating biomass, recruitment, and harvest rate for the Pacific yellowleg shrimp *Farfantepenaeus californiensis* from a size-based model. J. Shellfish Res. 32:815–823.

Morales-Bojórquez, E., E. A. Aragón-Noriega, H. Aguirre-Villaseñor, L. E. Calderón-Aguilera, and V. Y. Zepeda-Benitez. 2015. Selection of models

to predict *Panopea globosa* growth: application of a mixture probability distribution function. J. Shellfish Res. 34: 129–136.

Morsan, E., and N. F. Ciocco. 2004. Age and growth model for the southern geoduck, *Panopea abbreviata*, off Puerto Lobos (Patagonia, Argentina). Fish. Res. 69:343–348.

Morsan, E., P. Zaidman, M. R. Ocampo, and N. Ciocco. 2010. Population structure, distribution and harvesting of southern geoduck, *Panopea abbreviata*, in San Matías Gulf (Patagonia, Argentina). Sci. Mar. 74:763–772.

Neter, J., M. H. Kutner, J. Nachtschien, and W. Wasserman. 1996. Applied linear statistical models. 4th ed. Chicago: McGraw-Hill/Irwin. 1408 pp.

Pardo, S. A., A. B. Cooper, and N. K. Dulvy. 2013. Avoiding fishy growth curves. Methods Ecol. Evol. 4:353−360.

Parma, A. M., and R. B. Deriso. 1990. Dynamics of age and size composition in a population subject to size- selective mortality: effects of phenotypic variability in growth. Can. Fish. Aquat. Sci. 47:274–289.

Pfister, C. A., and F. R. Stevens. 2002. The genesis of size variability in plants and animals. Ecology. 83:59–72.

Pilling, G. M., G. P. Kirkwood, and S. G. Walker. 2002. An improved method for estimating individual growth variability in fish, and the correlation between von Bertalanffy growth parameters. Can. J. Fish. Aquat. Sci. 59:424–432.

Quinn T., and R. Deriso. 1999. Quantitative fish dynamics. Oxford: Oxford University Press. 560 pp.

Restrepo, V. R., G. A. Diaz, J. F. Walter, J. D. Neilson, S. E. Campana, D. Secor, and R. L. Wingate. 2010. Updated estimate of the growth curve of Western Atlantic bluefin tuna. Aquat. Living Resour. 23:335–342.

Sainsbury, J. 1980. Effect of individual variability on the von Bertalanffy growth equation. Can. J. Fish. Aquat. Sci. 37:241–247.

Sullivan, P. J., H. L. Lai, and V. F. Gallucci. 1990. A catch-at-size analysis that incorporates a stochastic model of growth. Can. J. Fish. Aquat. Sci. 47:184–198.

Tovar-Ávila, J., V. S. Troynikov, T. I. Walker, and R. W. Day. 2009. Use of stochastic models to estimate the growth of the Port Jackson shark, *Heterodontus portusjacksoni*, off Eastern Victoria, Australia. Fish. Res. 95:230–235.

Troynikov, V. S., R. W. Day, and A. M. Leorke. 1998. Estimation of seasonal growth parameters using a stochastic Gompertz model for tagging data. J. Shellfish. Res. 17:833–838.

Troynikov, V. S., and H. K. Gorfine. 1998. Alternative approach for establishing legal minimum length for abalone based on stochastic growth models for length increment data. J. Shellfish. Res. 17:827–831.

Wang, Y. G., M. R. Thomas, and I. Somers. 1995. A maximum likelihood approach for estimating growth from tag-recapture data. Can. J. Fish. Aquat. Sci. 52:252–259.

Wang, Y., and Q. Liu. 2006. Comparison of Akaike information criterion (AIC) and Bayesian information criterion (BIC) in selection of stock-recruitment relationships. Fish. Res. 77:220–225.

Zaidman, P. C., and E. Morsan. 2015. Growth variability in a metapopulation: The case of the southern geoduck (*Panopea abbreviata*). Fish. Res. 172:423–431.

Zar, J. H. 1999. Biostatistical analysis. Englewood Cliffs, NJ: Prentice-Hall. 633 pp.

Zepeda-Benitez, V. Y., E. Morales-Bojórquez, J. López-Martínez, and A. Hernández-Herrera. 2014a. Growth model selection for the jumbo squid *Dosidicus gigas* from the Gulf of California, Mexico. Aquat. Biol. 21:231–247.

Zepeda-Benítez, V. Y., E. Morales-Bojórquez, C. Quiñonez-Velázquez, and C. A. Salinas-Zavala. 2014b. Age and growth modelling for early stages of the jumbo squid *Dosidicus gigas* using multi-model inference. Calif. Coop. Oceanic Fish. Invest. Rep. 55:197–204.

Zheng, J., M. C. Murphy, and G. H. Kruse. 1995. A length-based population model and stock–recruitment relationship for the red king crab, *Paralithodes camtschaticus*, in Bristol Bay, Alaska. Can. J. Fish. Aquat. Sci. 52:1229–1246.

Zheng, J., G. H. Kruse, and M. C. Murphy. 1998. A length-based approach to estimate population abundance of Tanner crab, *Chionoecetes bairdi*. *In* Proceedings of the North Pacific Symposium on Invertebrate Stock Assessment and Management, G. S. Jamieson, and A. Campbell, ed. Can. Spec. Publ. Fish. Aquat. Sci. 125:97–105.

ANOMALOUS EPIPELAGIC MICRONEKTON ASSEMBLAGE PATTERNS IN THE NERITIC WATERS OF THE CALIFORNIA CURRENT IN SPRING 2015 DURING A PERIOD OF EXTREME OCEAN CONDITIONS

KEITH M. SAKUMA, JOHN C. FIELD,
NATHAN J. MANTUA, STEPHEN RALSTON
Fisheries Ecology Division
Southwest Fisheries Science Center
National Marine Fisheries Service
National Oceanic and Atmospheric Administration
110 McAllister Way
Santa Cruz, California 95060
ph: (831) 420-3945
Keith.Sakuma@noaa.gov

BALDO B. MARINOVIC, CYNTHIA N. CARRION
Institute for Marine Sciences
University of California Santa Cruz
Santa Cruz, CA 95060

ABSTRACT

We report on the anomalous distribution, abundance, and community structure patterns of epipelagic micronekton from a midwater trawl survey in May–June 2015 that has a 26-year time series within a core region off central California (36°35'–38°10'N) and a 12-year time series with expanded spatial coverage (extending from 32°42.5'–39°50'N). The 2015 survey took place during an extended period of record-breaking warm surface temperatures in much of the northeast Pacific Ocean. In the neritic waters off central and northern California, this broad-scale extended marine heat wave was combined with more localized, above average coastal upwelling in spring 2015 that led to slightly cooler than normal surface temperatures over the continental shelf and shelf break. The unusual micronekton assemblages in our 2015 trawl survey featured anomalously high catches of warm water species such as pelagic red crabs (*Pleuroncodes planipes*), coincident with high catches of colder water species such as YOY rockfish (*Sebastes* spp.), and also large catches of pelagic tunicates such as *Pyrosoma atlanticum*. Principal component analysis (PCA) on a subset of the most frequently occurring species for both the shorter time series (expanded survey area) and the longer time series (core region) yielded similar results to previous studies off central California, with a suggested alternation between micronekton communities dominated by coastal pelagic species and those dominated by YOY groundfish (rockfish, Pacific hake [*Merluccius productus*], and sanddabs [*Citharichthys* spp.]), krill, and cephalopods. In addition, the leading principal components for the different regions of the expanded survey area were highly correlated, suggesting similar micronekton community responses to forcing mechanisms over a broad spatial scale. As the PCA analysis was limited to a relatively small subset of species and the time series for some frequently encountered species are not continuous throughout the history of the survey, we also report on species that reflect additional aspects of the unusual nature of the 2015 survey catches. Together, these results indicate that the micronekton community structure in the late spring of 2015 was highly anomalous in that species characteristic of what might generally be considered three different nominal states (YOY groundfish/market squid and krill, warm-water subtropical species, and pelagic tunicates) were all encountered in high abundance.

INTRODUCTION

Oceanographic conditions within the California Current were highly variable from 2013–15. The region experienced extremely strong coastal upwelling and anomalously cold sea surface temperatures (SSTs) in 2013, near average coastal upwelling and record warm temperatures in 2014 (with mesoscale differences in upwelling patterns after June of 2014), and continued warm temperatures offshore with localized above average coastal upwelling in 2015 for areas north of 33°N (Wells et al. 2013; Leising et al. 2014, 2015). These conditions took place during an unprecedented marine heat wave for the broader northeast Pacific that developed in multiple stages, starting with rapid warming in the Gulf of Alaska in fall 2013 (Bond et al. 2015), warming in coastal Baja and southern California in spring 2014 (Zaba and Rudnick 2016), rapid warming of the neritic waters of central California in July 2014 (National Marine Fisheries Service 2014), and then a broad coast-wide warming from Alaska to Mexico in fall–winter 2014–15 (Di Lorenzo and Mantua 2016). In winter 2015, oceanographic conditions off California included anomalously low chlorophyll and an anomalously deep thermocline (Jacox et al. 2016), while in spring 2015 conditions included localized above average coastal upwelling and cooler than normal SSTs over the continental shelf and shelf break (fig. 1, Leising et al. 2015).

The anomalous oceanographic conditions over the 2013–15 period had dramatic impacts on the marine ecosystems of the northeast Pacific, including unprecedented toxic algal blooms and massive fisheries closures, and unusual mortality events for several populations of

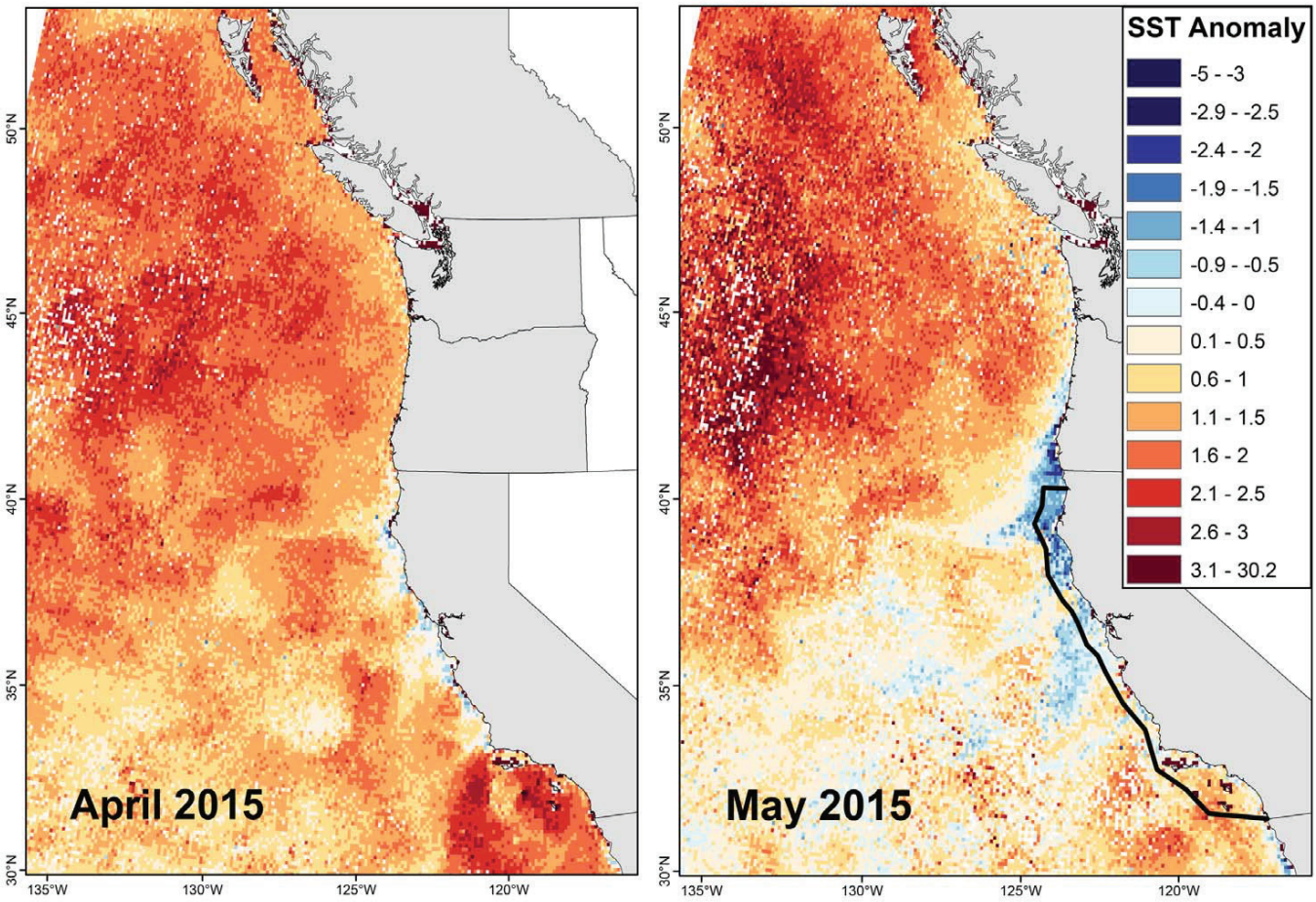

Figure 1. SST anomalies for months preceding and during the 2015 survey, with the spatial coverage of the survey overlaid (data from NOAA CoastWatch Program, 1985–95 climatology).

seabirds and marine mammals (reviewed in Di Lorenzo and Mantua 2016; Jacox et al. 2016). The cascading impacts to marine fisheries and coastal communities, particularly as a consequence of the toxic algal blooms, were also considered to be substantial (Peterson et al. 2015; Welch 2016).

Historically, during warm periods in the California Current, temperate upwelling associated species such as young-of-the-year (YOY) rockfish (*Sebastes* spp.), market squid (*Doryteuthis opalescens*), and krill (Euphausiacea) have been observed to be at low to very low abundance levels (Lenarz et al. 1995; Brodeur et al. 2006; Ralston et al. 2013, 2015). In such years, more southerly distributed warm water species such as the pelagic red crab (*Pleuroncodes planipes*) and California lizardfish (*Synodus lucioceps*) tend to increase in abundance and extend their distribution northward (Longhurst 1967; Aurioles-Gamboa et al. 1994). In order to examine the effects of the recent oceanographic conditions on the marine ecosystem, we analyzed data from a midwater trawl survey that has sampled the shelf and shelf-break waters off the central California coast for an extended period (1990–2015), with spatial coverage expanded to the majority of the California coast over a shorter time period (2004–15).

The Fisheries Ecology Division (FED) of the Southwest Fisheries Science Center (SWFSC) has conducted a midwater trawl survey off central California since 1983 with the primary goal of developing pre-recruit indices for YOY rockfish (Ralston et al. 2013). However, the survey also samples numerous other components of the epipelagic micronekton (free swimming organisms generally <200 mm), including many of the most frequently encountered forage species in a recently developed database of predator food habits in the California Current (Szoboszlai et al. 2015; see also Ainley et al. 2015). Ralston et al. (2015) analyzed these data to evaluate the species assemblage over a 23-year time span (1990–2012) and observed a contrast between the abundance of YOY groundfish (rockfish, Pacific hake and sanddabs, *Citharichthys* spp.), market squid, and krill with the abundance of adult clupeoids (Pacific sardine, *Sardinops sagax*, and northern anchovy, *Engraulis mordax*) and myctophids (Myctophidae). YOY groundfish, mar-

ket squid, and krill were more abundant during years with depressed sea level anomalies (indicative of equatorward transport anomalies) and cooler conditions in the California Current, while clupeoids and myctophids were more abundant during years with elevated sea level anomalies (poleward transport anomalies) and warmer conditions. For our study, we expand upon the analysis of Ralston et al. (2015) using data from a shorter time series, but greater spatial coverage. In addition, we examined the observed impacts of the recent northeastern Pacific marine heat wave (Bond et al. 2015; Leising et al. 2015; Di Lorenzo and Mantua 2016) on the late spring micronekton and forage community over the shelf and shelf-break waters of the southern part of the California Current (Southern California Bight to Cape Mendocino).

METHODS

Midwater Trawl Survey

The FED SWFSC has conducted annual surveys in May through mid-June from 1983–2015 (and ongoing) using a modified Cobb midwater trawl with a 26 m headrope, 9.5 mm stretched mesh codend liner, and theoretical mouth opening of 12 m x 12 m (Wyllie Echeverria et al. 1990; Ralston et al. 2013). Trawl duration was 15 minutes at a target headrope depth of 30 m except for a few nearshore stations where bottom depths were shallower than 55 m, in which case the target headrope depth was adjustesd to 10 m to avoid contact with the bottom. Ship's speed through the water was ~3.7 km/hr (2.0 knots) and all trawls were conducted at night due to net avoidance during the day (FED SWFSC unpublished data). Trawls were conducted at fixed stations, although the number and location of these stations has changed over the years as new stations were added and others discontinued (fig. 2). For example, starting in 1997 select nearshore stations were discontinued due to reoccurring large catches of jellyfish (*Chrysaora fuscescens* and *Aurelia* spp.), which frequently damaged the gear, thus reducing sampling efficiency. A small percentage of trawls were also made of shorter duration (5 vs. 15 minutes) when jellyfish or pelagic tunicates were present in high abundance. Catches were then standardized to an expected 15 minute haul using a correction factor derived from comparing catch rates of 5 and 15 minute trawls conducted at the same time and place. Furthermore, some stations were dropped to add new stations in order to extend the spatial coverage farther offshore (e.g., two new stations were added off Monterey Bay in 2015; see inset of fig. 2). Despite these changes, most of the Central California core region stations have been sampled continuously since 1983. Additional survey details are provided in Ralston et al. (2013, 2015).

In 2004, in recognition of the need to sample a broader geographical range of a suite of YOY rockfish species, the survey area was expanded from San Diego to Point Delgada just south of Cape Mendocino (Sakuma et al. 2006) and in 2013 from Cape Mendocino north to survey the entire coast of California from the Mexican to Oregon borders. For the years with expanded spatial coverage (2004–15), the survey area can be separated into five regions: south, south central, core, north central, and north, which are shown in fig. 2. As the north region has only a limited amount of data (just three years), this region was excluded from the analyses in this study. No sampling was done in the south region in 2011 due to vessel and logistic constraints, nor in the north central region in 2012 due to inclement weather. From 1983–2008 the survey was conducted aboard the NOAA ship *David Starr Jordan*. After 2008, the survey was conducted aboard a mixture of charter vessels and NOAA ships including the NOAA ship *Miller Freeman* in 2009, the charter vessel *Frosti* in 2010, the charter vessel *Excalibur* in 2011, the NOAA ship *Bell M. Shimada* in 2012, and the charter vessel *Ocean Starr* (actually the repurposed *David Starr Jordan*) in 2013–15.

All fish and select invertebrates were sorted and enumerated at sea with the YOY rockfish frozen and returned to the laboratory for further analysis. While YOY rockfish and other groundfish (e.g., Pacific hake) have been consistently enumerated at sea since 1983, subsampling of many other forage species, such as krill and mesopelagic fishes, was not standardized until 1990. In addition, in collaboration with University of California Santa Cruz (UCSC), krill were identified to species beginning in 2002. Note that for 2013–15 all krill numbers are preliminary (based on a small subsample of species assignments at sea) with the final numbers by species awaiting ongoing laboratory confirmation. Additionally, there was a hiatus in the identification of large jellyfish (*Chrysaora* spp. and *Aurelia* spp.) and gelatinous micronekton such as *Thetys vagina*, other salps (Salpidae), *Pyrosoma atlanticum*, and pelagic mollusks (Pterotracheoidea) that began in 2002, in response to time demands at sea. However, enumeration of large jellyfish resumed in 2005 in collaboration with UCSC, and enumeration of gelatinous micronekton was resumed in 2012 due to their prominence in the trawl catches that year.

Hydrographic Data

Conductivity, temperature, and depth (CTD) casts were done at each nighttime trawl station starting in 1987. Additional CTD casts were made during the daytime in the area around the trawl stations, although the locations were not standardized until 1991. As the survey area expanded, new daytime CTD stations were added (fig. 2). CTD casts were typically conducted to the lesser

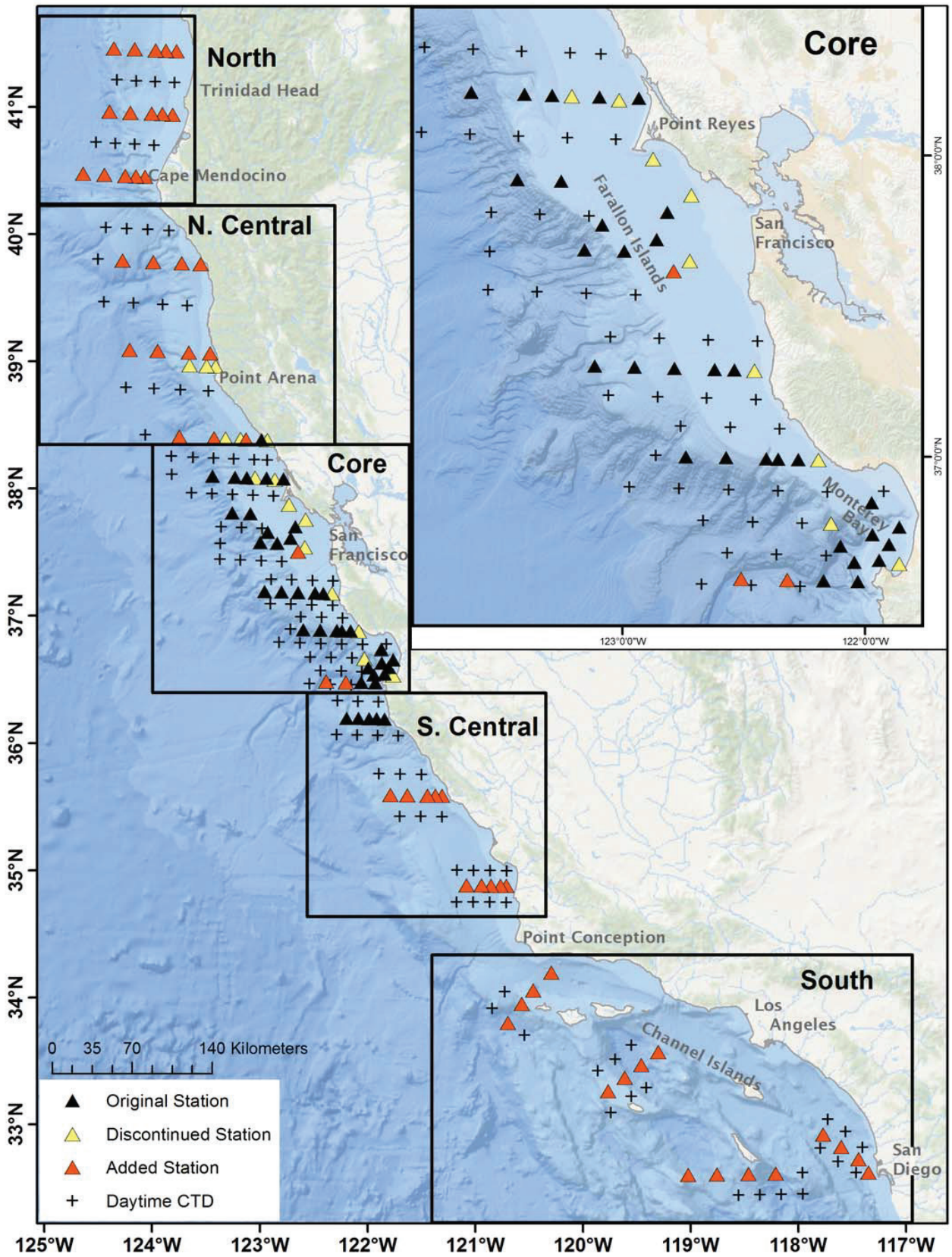

Figure 2. Midwater trawl and CTD station locations off California. Inset map shows the locations of the core region stations historically sampled since 1983. Stations that were added in later years and historic stations that are no longer currently sampled (discontinued) are also shown. In 2004, the survey area was expanded to include the south, south central, and north central regions. The north region was added in 2013.

TABLE 1

Species/taxa occurring in 10% or more of trawls in the expanded survey area (All Areas) from 2004–15 listed in decreasing order of occurrence. The percent occurrence within each of the four survey regions is also shown. The region with the highest percent occurrence is in bold. For Ontogeny, Y = young-of-the-year, A = age 1+, and U = undetermined. With the exception of krill, all species/taxa were also enumerated in the core region since 1990 (data not shown). Species specific enumeration of krill began in 2002 with only total krill numbers available from 1990–2001 (data not shown).

Common Name	Scientific Name	Ontogeny	South	South Central	Core	North Central	All Areas
Krill	*Euphausia pacifica*	U	**89.3**	79.7	81.4	86.5	83.2
Sanddab	*Citharichthys* spp.	Y	**81.6**	79.1	79.3	72.5	78.7
Rockfish	*Sebastes* spp.	Y	**81.6**	73.8	73.9	68.4	74.5
Krill	*Thysanoessa spinifera*	U	61.1	55.6	**70.9**	35.2	62.4
Market Squid	*Doryteuthis opalescens*	U	**84.4**	65.2	51.2	17.1	54.1
Myctophid	Myctophidae	U	**82.8**	52.9	40.0	63.7	52.2
Pacific Hake	*Merluccius productus*	Y	50.0	42.8	53.8	**57.0**	52.1
Sergestid	Sergestidae	U	**57.0**	38.0	32.3	54.4	40.3
Octopus	Octopoda	U	38.9	**44.9**	30.7	28.5	33.7
Krill	*Nematoscelis difficilis*	U	**71.7**	35.3	19.6	39.9	33.3
Squid	Teuthoidea	U	**47.5**	28.9	22.4	42.0	30.2
California Headlightfish	*Diaphus theta*	U	34.0	29.4	22.6	**52.9**	29.5
California Smoothtongue	*Leuroglossus stilbius*	U	**50.0**	31.0	24.5	15.5	28.5
Blue Lanternfish	*Tarletonbeania crenularis*	U	15.2	36.4	23.1	**57.5**	28.1
Deep-Sea Smelt	Bathylagidae	U	37.3	19.3	17.7	**48.7**	25.5
Goby	Gobiidae	U	**55.3**	30.5	15.5	4.7	22.8
Rex Sole	*Glyptocephalus zachirus*	Y	5.3	12.8	25.1	**28.0**	20.5
Northern Anchovy	*Engraulis mordax*	A	17.2	**28.9**	20.6	2.6	18.7
Northern Anchovy	*Engraulis mordax*	Y	**50.4**	29.4	7.9	6.2	17.8
Pacific Sardine	*Sardinops sagax*	A	9.4	**17.7**	16.7	16.1	15.5
Slender Sole	*Lyopsetta exilis*	Y	7.0	12.3	**19.2**	12.4	15.3
Pacific Sanddab	*Citharichthys sordidus*	A	1.2	12.8	**20.4**	8.8	14.5
Barracudina	Paralepididae	U	23.4	8.6	8.1	**33.7**	14.3
Flatfish, Right Eye	Pleuronectidae	Y	1.6	5.4	16.9	**23.3**	13.6
King-Of-The-Salmon	*Trachipterus altivelis*	U	16.0	**22.5**	11.0	6.2	12.7
Pacific Hake	*Merluccius productus*	A	4.1	5.4	14.6	**15.0**	11.7
Lingcod	*Ophiodon elongatus*	Y	2.5	4.8	**16.9**	8.3	11.7

of 10 m off the observed bottom depth or 500 m (some 1000 m casts have been conducted over time), with fluorometry data collection initiated in 1997 and oxygen data collection initiated in 2007. In 2011 no daytime CTD stations were sampled due to vessel and logistic constraints and no casts were done in the south region. In addition, in 2012 no CTDs were done in the north central region due to inclement weather. Similar to the trawl data, the north region CTDs are not included in our current study due to the limited temporal coverage.

Analysis

The mean CTD temperature, salinity, and density at 30 m depth (between 25 and 35 m, i.e., the target depth sampled by the midwater trawl) for each year were estimated for the four regions (south = 2004–10 and 2012–15, south central = 2004–10 and 2012–15, core = 1991–2015, and north central = 2004–11 and 2013–15) as well as the mean depth of the 26.1 isopycnal. Only CTD stations that were consistently sampled every year within each region were used (see appendix 1 for the number of CTD casts by year and region).

Catch data from currently active trawl stations from the four survey regions (south, south central, and north central from 2004–15 and core from 1990–2015) were transformed by ln (trawl catch + 1) and the mean catch for each year was then plotted for select species/species groups (see appendix 1 for the number of trawls completed by year and region). The species or taxa that occurred in at least 10% of trawls conducted in the expanded survey area from 2004–15 are also provided, with the percent occurrence within each of the four survey regions during this time period (table 1). With the exception of krill (identified to species starting in 2002), the species/taxa listed in Table 1 were also consistently enumerated within the core region from 1990–2015. The species/taxa from this shorter time series (2004–15) in the expanded survey area are comparable to the longer time series (1990–2012) reported by Ralston et al. (2015) for the core region. A complete list of all the species collected from the expanded survey area, and their percent occurrence by region, is also provided (appendix 2), and the original catch data are available online.[1]

[1]Data are served by the ERDDAP, website https://coastwatch.pfeg.noaa.gov/erddap/index.html. Data set is entitled "Rockfish Recruitment and Ecosystem Assessment Survey," metadata are also provided.

Similar to the analyses of Ralston et al. (2015) we conducted a community analysis using principal components analysis (PCA), a frequently used method of examining patterns of covariance within time series data in order to concentrate the variance in the dataset into a smaller number of more easily interpretable indices (see also Hare and Mantua 2002; Koslow et al. 2011 for comparable analyses). As we expanded the spatial coverage to include the regions outside of the core region (i.e., south, south central, and north central), the shorter time series necessitated a reduction in the number of taxa that could be included (the number of variables must typically be smaller than the number of years in a PCA) relative to the analyses in Ralston et al. (2015). Nine taxa were chosen based on a combination of the relative frequency of occurrence (as in Ralston et al. 2015) and their relative importance in the food web. Specifically, we selected taxa that were present in at least 10% of trawls in three of the four regions (and overall), as well as were included in the 20 most frequently encountered forage taxa described in a meta-analysis of food habits studies in the California Current (Szoboszlai et al. 2015). As in Ralston et al. (2015) we pooled all YOY rockfish into one taxon due to the previously described strong temporal co-variability. However, unlike Ralston et al. (2015) we did the same with the two commonly observed species of YOY sanddab, Pacific and speckled (*Citharichthys sordidus* and *C. stigmaeus*) as well as all species of myctophids (including the California headlightfish, *Diaphus theta*, and the blue lanternfish, *Tarletonbeania crenularis*) as they too tended to co-vary over the longer time period in the core region (Ralston et al. 2015, although see Koslow et al. 2011). Although krill were identified to species from 2002–15, we pooled all adult stages of krill into a common group, as in Ralston et al. (2015). The remaining taxa in this analysis were also represented in the Ralston et al. (2015) analysis and include market squid, YOY Pacific hake, adult northern anchovy, adult Pacific sardine, and octopus (*Octopoda*). This level of taxonomic resolution is also consistent with that reported by Szoboszlai et al. (2015).

We developed year-specific abundance estimates based on an analysis of variance (ANOVA) model applied to haul-specific log-transformed catch data, where year and station were estimated as the main effects, and the year effects were calculated from parameter estimates by averaging over station effects using a least-squares means approach (the R package lsmeans [R Core Team 2012]). This model-based approach accommodates unbalanced sampling, but is less than ideal if abundance patterns are strongly influenced by interactions between years and stations. However, as in Ralston et al. (2015), the two factor ANOVA models performed well for virtually all taxa, and the resulting trends were consistent with those developed by using the mean of the log catch rate alone. The results of the ANOVA were subsequently converted into standardized anomalies based on the mean and standard deviation of the year effects for each taxa and region, and the matrix of standardized values over time was analyzed using PCA (the R package princomp [R Core Team 2012]). The PCA subsequently provides a set of scores (or, principal components) that reflect descending fractions of the temporal variability of the original data set. The analysis also produces loadings (or eigenvectors) that reflect the weightings of each of the scores on any given input component (e.g., the input taxa), such that positive loadings reflect a positive correlation with a given score (or PC) and negative loadings reflect a negative correlation, and eigenvalues, which indicate the amount of variance explained by each score.

RESULTS

Hydrographic Data

Data collected from CTD casts between 1991–2015 in the core region showed warm, low salinity, low density water with a deep 26.1 isopycnal layer in 1992 and 1998 and cold, saline, dense water with a shallow 26.1 isopycnal layer in 1991, 1999, 2008, and 2012 (fig. 3). Data from the other regions starting in 2004 generally follow the same trend observed in the core region. However, after 2012, there was a general warming trend with decreased salinity and density and a deeper 26.1 isopycnal layer, with the exception of the north central region, which saw cooler, higher salinity, higher density water and the shallowest 26.1 isopycnal layer in that region's time series in 2015. Our data for 2015 is consistent with the observation that despite anomalously warm surface waters offshore, the above average upwelling indices recorded in the spring of 2015 led to near average temperature, salinity, and density at 30 m in the south central and core survey regions during May–June (see Leising et al. 2015). An anomalously deep 26.1 isopycnal was observed in the south, south central, and core regions from May–June 2015.

Species Catch Trends

In general, the annual mean catches of YOY groundfish and market squid showed similar patterns across years (fig. 4). YOY rockfish, YOY Pacific hake, YOY sanddabs, and market squid abundances were low in most regions in 1998 and 2005–07, while catches were very high in 2013 and 2015. In the core region both YOY rockfish and YOY sanddabs had the highest catches observed in the 26-year time series in 2013 and 2015. However, while YOY rockfish and YOY Pacific hake abundances were low in 1992, 1995, and 2012, market squid catches were relatively high in those years, with the highest

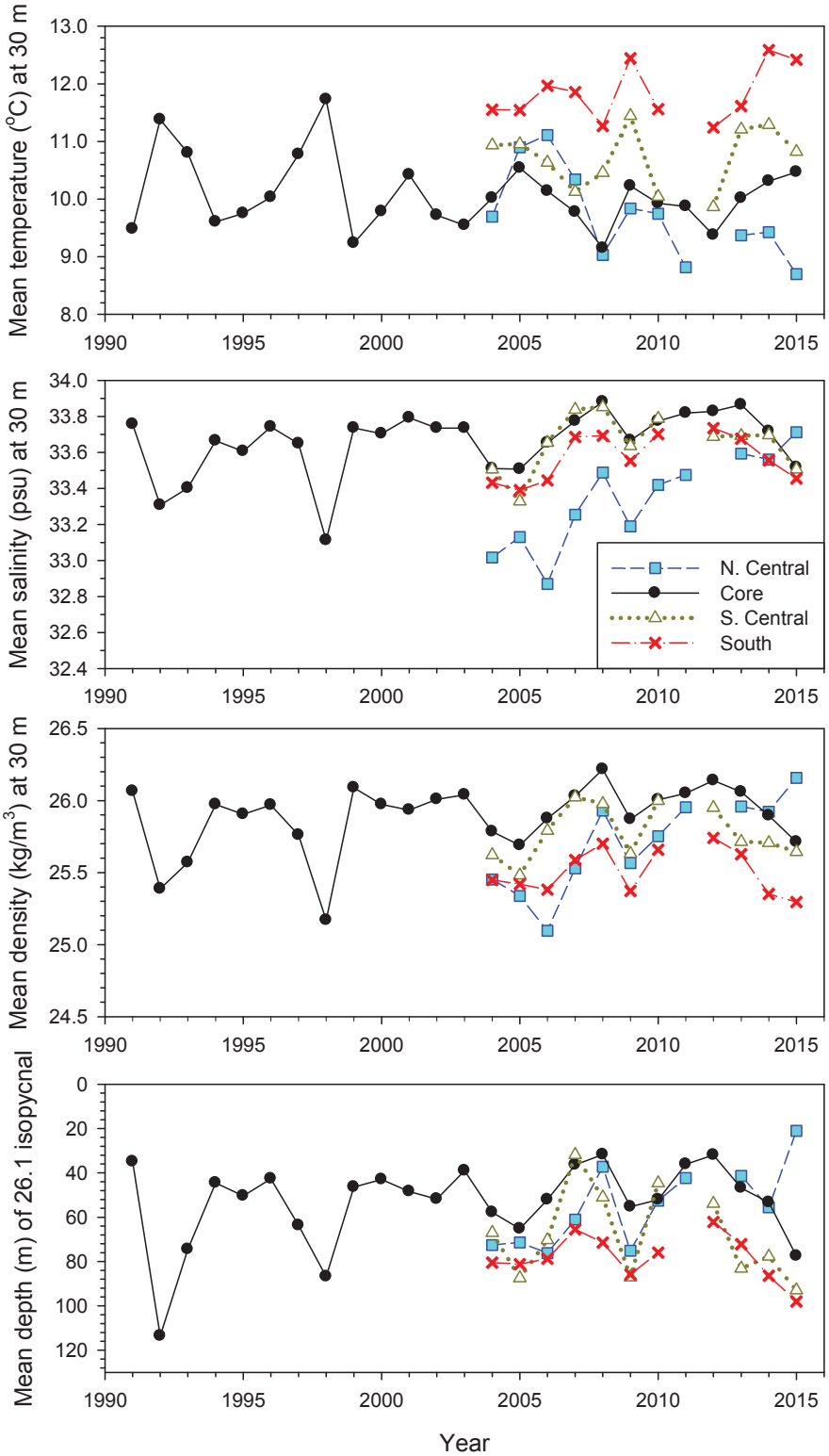

Figure 3. Annual mean temperature (°C), salinity (psu), and density (kg/m³) at 30 m depth and the mean depth of the 26.1 isopycnal from CTD data.

catch for market squid occurring in the south region in 2012. In addition, market squid were more abundant in 2014 than in 2013 and 2015 (although abundance was still relatively high in those years) and the highest catches of YOY sanddabs were observed in the south and south central regions in 2014. Patterns across regions generally showed similar trends although some region-specific differences were apparent for any given year. For

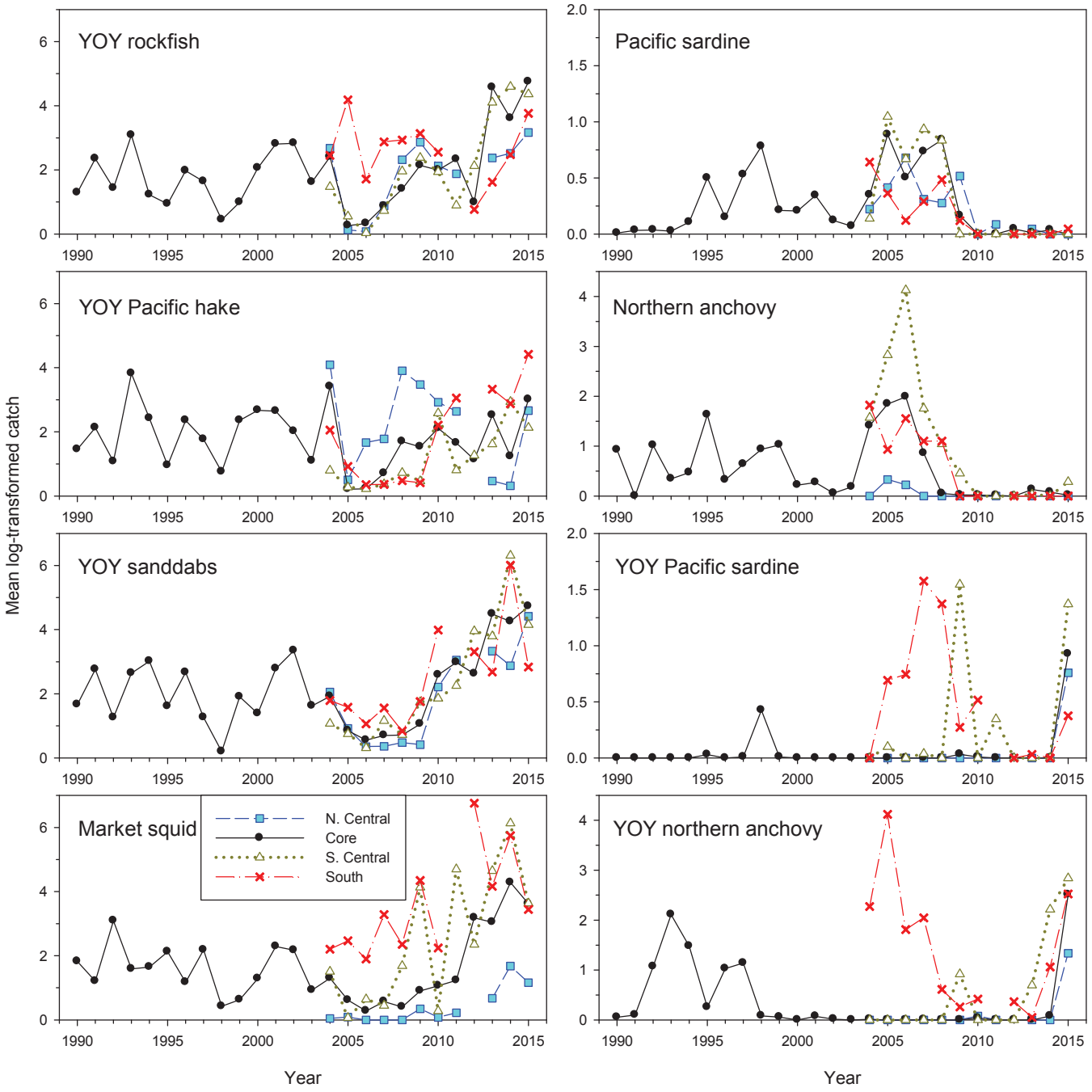

Figure 4. Annual means of log-transformed catches of YOY rockfish, YOY Pacific hake, YOY sanddabs, market squid, adult and YOY Pacific sardine, and adult and YOY northern anchovy from the south, south central, core, and north central regions.

example, YOY Pacific hake tended to have inverse catch trends between the southern (both south and south central) and north central regions in many years (with the core region catches typically falling between the two extremes), and YOY rockfish had very high catches in the core and south central regions in 2013, but relatively low catches in the south.

In contrast to the YOY groundfish, adult Pacific sardine and northern anchovy were abundant in 1995 and 2005–07, with catches declining dramatically beginning in 2010 and extending through 2015 (fig. 4). While the annual trends for YOY Pacific sardine and anchovy track those of the adults for most years, there was an increase in YOY northern anchovy in 2014 and record high catches of the YOY of both species in 2015 for the south central, core, and north central regions.

Myctophid catches in all regions were high in 2004–05 and 2009–10 (fig. 5). A dramatic drop in catches

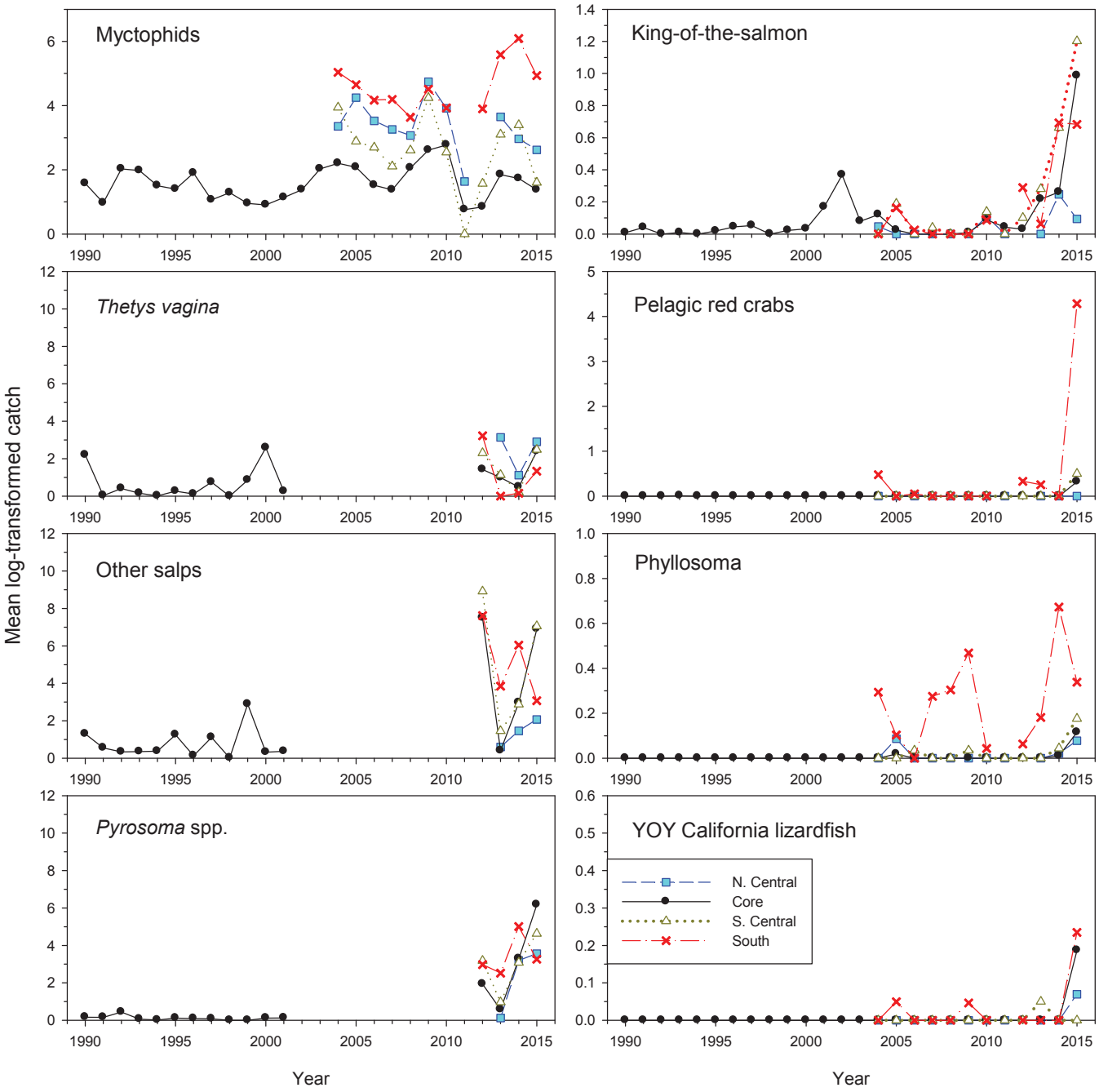

Figure 5. Annual means of log-transformed catches of myctophids, *Thetys vagina*, other salps, *Pyrosoma atlanticum*, king-of-the-salmon, pelagic red crabs, phyllosoma, and YOY California lizardfish from the south, south central, core, and north central regions.

occurred in 2011–12 with catches increasing somewhat in 2013. The highest catches were observed in the south region in 2014. Catches in all regions declined in 2015.

Catches of pelagic tunicates (salps and *Pyrosoma atlanticum*) were extraordinarily large in 2012 (which, as previously mentioned, led to damaged gear and the decision to resume counting them that year) (fig. 5, see also Wells et al. 2013). The unusually high salp biomass was also observed in both pelagic plankton samples and sediment trap collections in the offshore region of the Monterey Canyon (Smith et al. 2014). While in 2013 other salps and *Pyrosoma atlanticum* declined substantially from the 2012 levels, by 2015 their numbers were back up with the highest catches of *Pyrosoma* ever observed within the core region. Trends for the salp *Thetys vagina* were slightly different as large catches were observed in 1990 and 2000 within the core region. In addition, they were relatively abundant in the north central region in 2013 with decreased abundances in all regions in 2014. However, similar

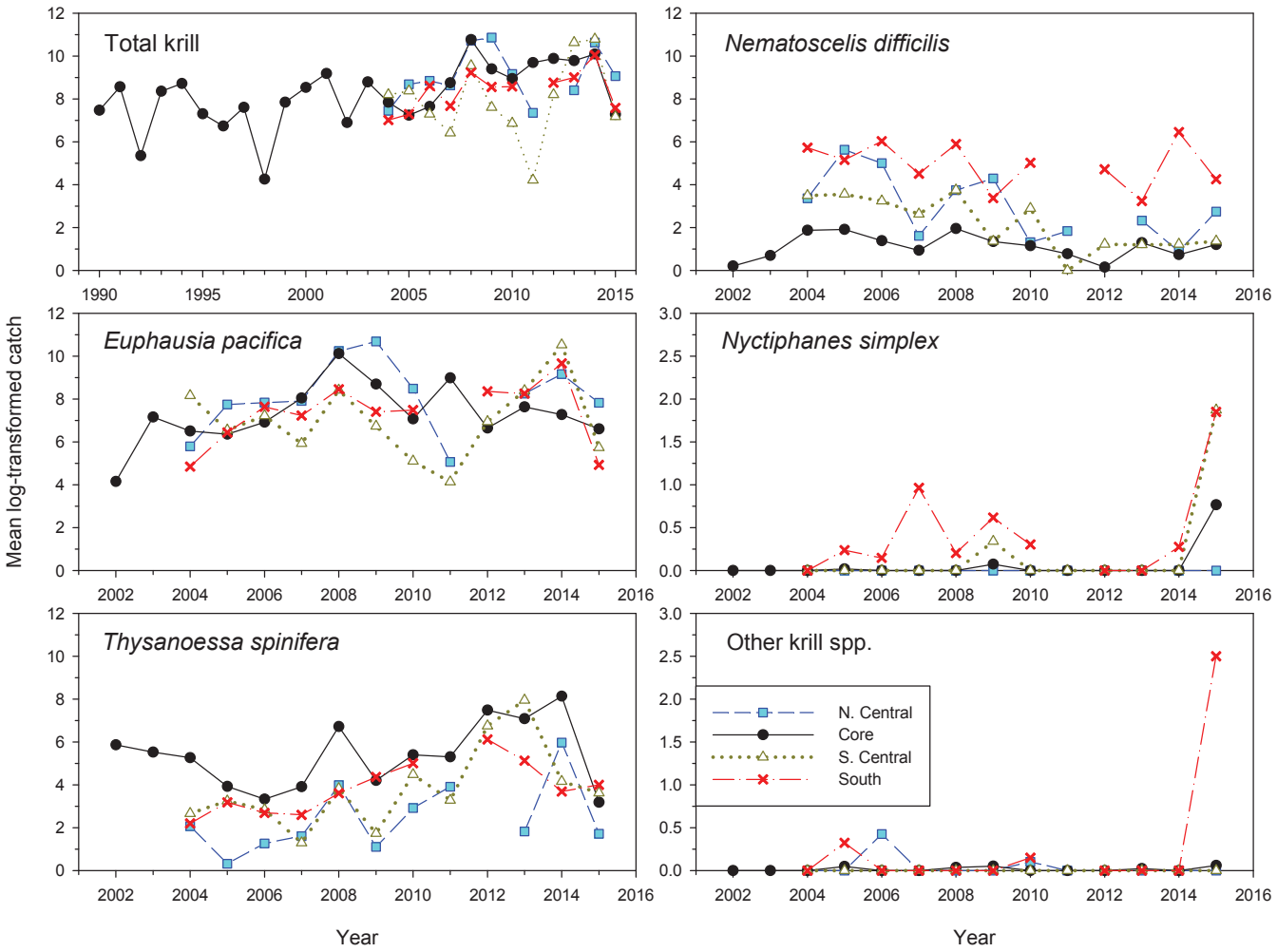

Figure 6. Annual means of log-transformed catches of total krill, *Euphausia pacifica*, *Thysanoessa spinifera*, *Nyctiphanes simplex*, *Nematoscelis difficilis*, and other krill species (species other than the previous four species) from the south, south central, core, and north central regions.

to the other gelatinous micronekton, catches of *Thetys vagina* increased in 2015.

Southerly distributed or offshore species with notable catches in 2015 in most (if not all) of the regions sampled in this survey included king-of-the-salmon (*Trachipterus altivelis*), pelagic red crabs, phyllosoma stage of California spiny lobster (*Panulirus interruptus*), and YOY California lizardfish (fig. 5). Also, the smalleye squaretail (*Tetragonurus cuvieri*) was collected for only the third time (prior occurrences were in 1985 and 1988) with raw catches in 2015 being 2.7 times greater than all prior years combined (2015 n = 19, while 1985 and 1988 combined n = 7). In addition, the following species were collected for the first time ever in the survey: the greater argonaut (*Argonauta argo*, n = 4), the pelagic stingray (*Dasyatis violacea*, n = 1), the slender snipefish (*Macroramphosus gracilis*, n = 6), and YOY Pacific bonito (*Sarda chiliensis*, n = 3). However, all of these latter species were encountered in the southern stations sampled only since 2004, so the presence of these and other southerly distributed species may not be hugely anomalous relative to past warm events in this region.

Total krill abundance in the core region was highest in 2008 while the lowest catches were observed in 1992 and 1998 (fig. 6). Catches were also quite low in the north central and south central regions in 2011. While catches in all regions increased in 2014 there was a dramatic decrease in abundance in all regions in 2015. This decrease in total krill catch in 2015 is due to the decrease in catches of the two numerically dominant species *Euphausia pacifica* and *Thysanoessa spinifera*. In contrast, there was an increase in catches of the more southern species *Nyctiphanes simplex* in 2015 with the highest catches ever observed in the south, south central, and core regions. There was also a large increase in other (typically rare) krill catches in the south region comprised mostly of the warm water species *Euphausia eximia*, which had not previously been collected by this survey, but are widely acknowledged to be a subtropical species based on historical plankton sampling (Brinton

TABLE 2
Principal component scores and variance explained by region.

	South		South Central		Core		North Central	
	PC1	PC2	PC1	PC2	PC1	PC2	PC1	PC2
2004	3.06	–0.19	1.13	–0.37	0.38	–1.98	0.26	1.91
2005	2.94	–1.76	3.03	–0.99	3.7	–0.71	2.66	–1.32
2006	1.96	1.77	3.01	–0.74	3.28	–0.5	2.88	–1.08
2007	1.02	0.03	2.35	–0.03	2.27	0.66	1.46	0.04
2008	0.97	1.37	0.41	–0.83	1.08	1.29	0.53	0.83
2009	–0.87	0.04	–0.75	–1.01	0	–0.11	0.47	–0.67
2010	–0.71	0.14	–0.02	1.1	–0.86	–0.56	–0.57	–0.1
2011	n/a	n/a	0.65	2.33	–0.6	1.39	–0.15	2.06
2012	–1.79	1.5	–0.46	1.26	–0.59	1.79	n/a	n/a
2013	–2.21	0.12	–2.94	–0.93	–2.93	–0.42	–1.68	–0.66
2014	–3.65	–0.69	–4.27	–1.02	–2.75	0.52	–3.42	–2.69
2015	–0.66	–2.29	–2.06	1.29	–2.91	–1.3	–2.38	1.72
Variance explained	52%	18%	58%	15%	58%	15%	43%	25%

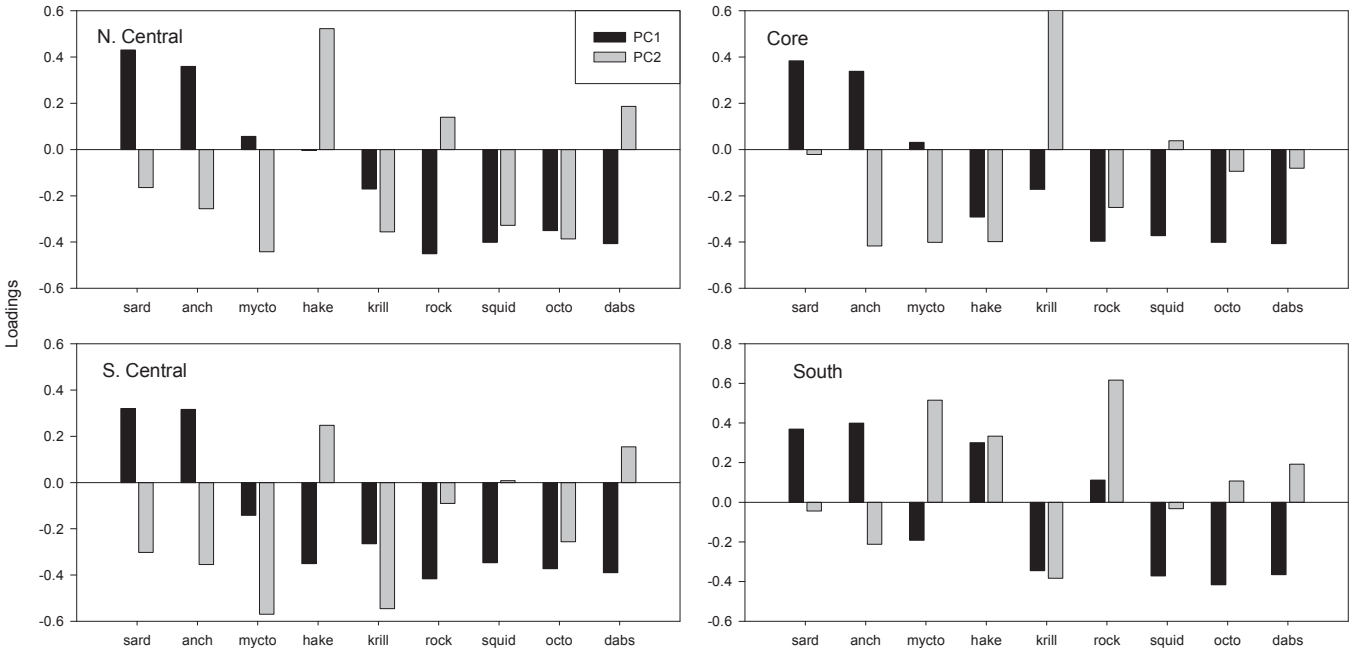

Figure 7. Loadings on PC1 and PC2 by taxa and region for the short (2004–15) time series. The order (from left to right) is determined by the average loading value across all four regions for each species or taxonomic group. Taxa abbreviations: Pacific sardine = sard, northern anchovy = anch, myctophid = mycto, YOY Pacific hake = hake, YOY rockfish = rock, market squid = squid, octopus = octo, and YOY sanddabs = dabs.

and Townsend 2003).

Principal Components Analysis

The results of the PCA were comparable to those originally reported by Ralston et al. (2015), with the first principal component (PC1) explaining between 43% and 58% of the variability for any given region, and the second principal component (PC2) explaining between 15% and 25% (table 2). The patterns in the loadings were generally comparable to the Ralston et al. (2015) analysis (where the species included overlapped), and these patterns are shown by region (fig. 7). In general, coastal pelagic species (Pacific sardine and northern anchovy) loaded on the opposite signs as YOY rockfish, YOY sanddabs, market squid, octopus, and krill. Myctophids and Pacific hake did not consistently load with either of these groups, often loading weakly with the first PC (e.g., Pacific hake in the north central region, myctophids in the north central and core region) or alternating between strong positive or negative loading. Interestingly, YOY rockfish and YOY Pacific hake in the southern region loaded with the coastal pelagic species, while myctophids loaded with krill, market squid, octopus, and sanddabs. In the core and south central regions all of the YOY groundfish loaded strongly with the cephalopods and krill.

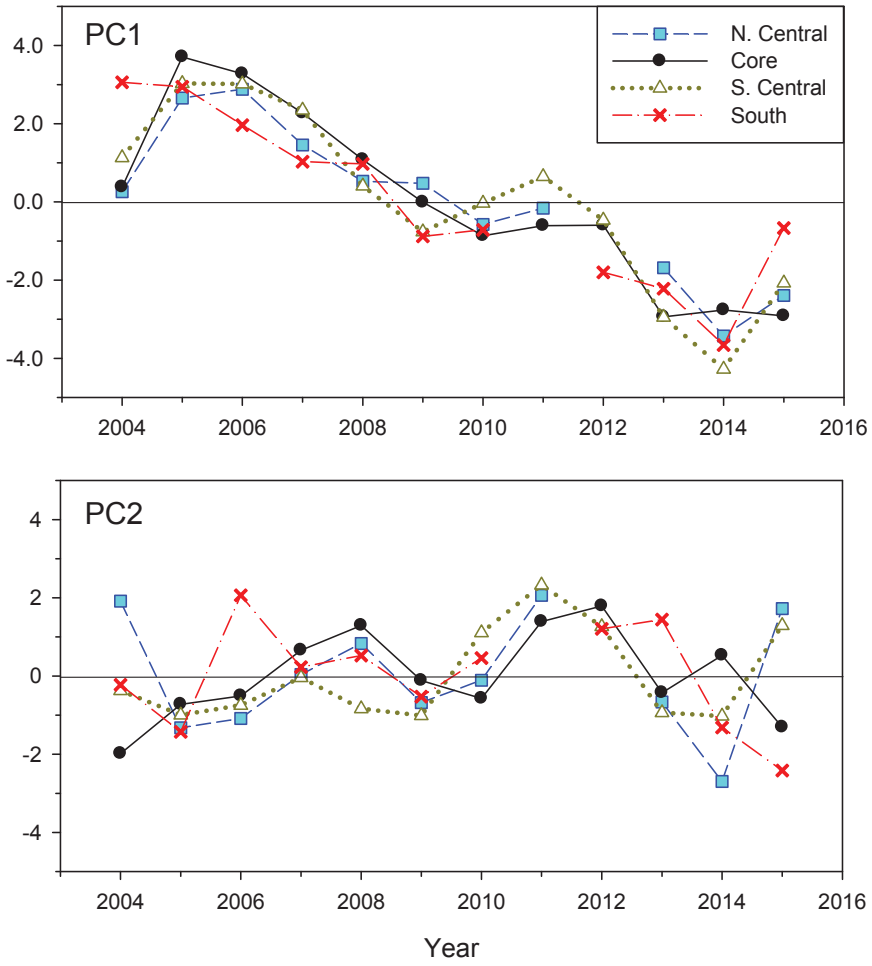

Figure 8. Time series of PCs 1 and 2 by region for the short (2004–15) time series.

This suggests little or no consistency in the relative abundance of YOY Pacific hake or myctophids across space, in contrast to the abundance of most of the other groups in this analysis. Unlike the loadings of PC1, loadings on PC2 did not follow a consistent pattern across space, and loadings tended to be greater for those species that did not load heavily on PC1, such as myctophids, YOY Pacific hake, and krill, and these tended to not show covariation in the loading patterns across space. For example, YOY Pacific hake did not load significantly on PC1 in the north central region, but had the highest loadings of all taxa on PC2 in that region, while similar patterns were seen for krill in the core region and myctophids in the south central region.

Despite some differences in the trends of various species across space, and some modest, but nontrivial differences in the loadings across space, PC1s in all four regions were highly correlated and followed a strongly consistent pattern (fig. 8). There was an increase in values between 2004 and 2005, a declining trend through 2014, and then a small uptick in most regions in 2015. The 2013–15 period varied substantially from the previous (2004–12) period for all regions in PC1, although these years all had mixed trends for PC2. Moreover, all four of the PC1s were strongly and significantly correlated with one another (correlation coefficients ranged from 0.81 to 0.96, table 3), indicating that the micronekton communities in all of these regions were generally responding to similar forcing mechanisms, although the effects may be realized in slightly different manifestations (e.g., different loadings, reflecting differences in regional abundances) depending on the region. PC2s

TABLE 3
Correlation Coefficients for PCs 1 and 2 by region

PC1	South	South Central	Core	North Central
South	1			
South Central	0.889	1		
Core	0.815	0.935	1	
North Central	0.831	0.950	0.965	1
PC2	**South**	**South Central**	**Core**	**North Central**
South	1			
South Central	–0.079	1		
Core	0.338	0.262	1	
North Central	–0.106	0.668	–0.100	1

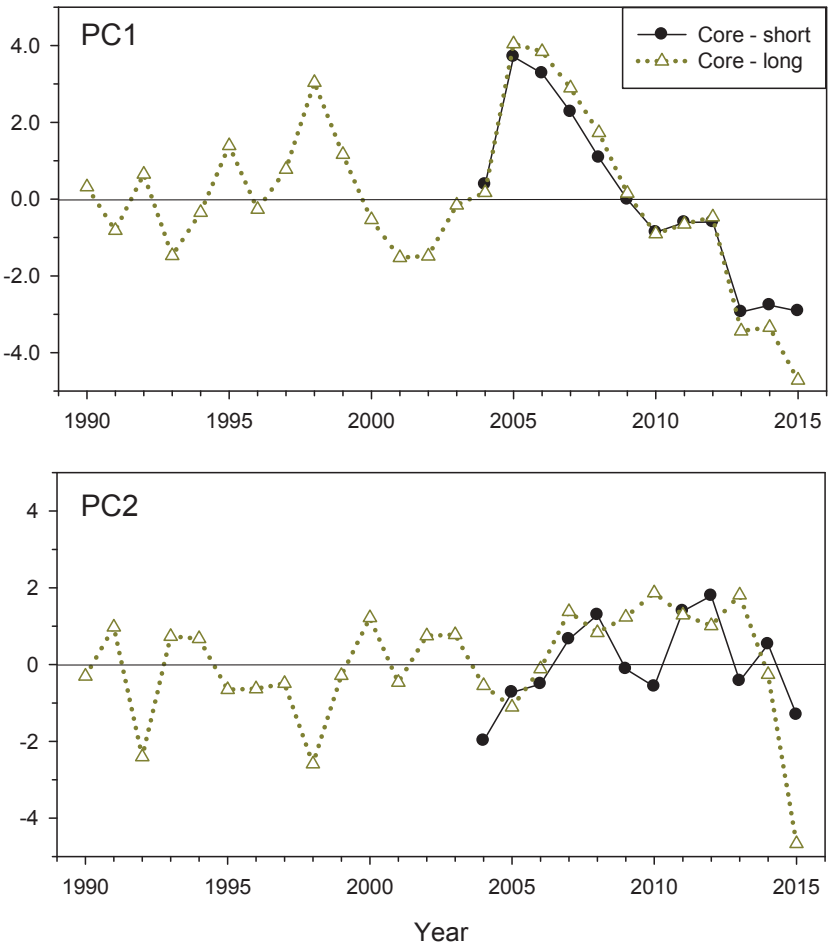

Figure 9. Comparison of short (2004–15) to long (1990–2015) time series in the consistently sampled core (central California) region.

for each region did not appear to track each other consistently over time, although the core and south central PC2s were well correlated, suggesting either that different processes are driving the patterns reflected in the south and north central time series, or that collectively the time series are too short to interpret the patterns in the second PCs in a comprehensive manner.

Extending the analysis for the core region over the entire duration of the time series (1990–2015), as an extension of the Ralston et al. (2015) analysis provided a result consistent with the shorter-term trend for this region. This indicates that the relationships among the different groups are coherent over longer time scales (fig. 9). More importantly, the extended time series in the core region reveals the extent to which 2015 is highly anomalous relative to the preceding 25 years. Specifically, the lowest score in the 26-year time series occurs in 2015 for both PC1 and PC2, demonstrating that even when considering only a small subset of the epipelagic micronekton community, the community structure in 2015 is highly anomalous.

Phase plots of the first and second PCs by region (fig. 10) illustrate that the trends in the second PCs are less consistent across space than those of the first PCs, and the unusual nature of the past three years as strongly separated from past "low productivity" periods (2005–06). Note that the core region plot includes the longer (1990–2015) time period, which emphasizes the unusual community structure observed in recent years. Due to autocorrelation in both these results and in most climate indices, a meaningful evaluation of the relationship to climate forcing is beyond the scope of this analysis.

DISCUSSION

A number of analyses have reported on the unusual atmospheric and oceanographic conditions within the northeast Pacific and the California Current in the 2013–15 time period (Bond et al. 2015; Leising et al. 2015; Zaba and Rudnick 2016; Di Lorenzo and Mantua 2016; Jacox et al. 2016). Our results are consistent in documenting the unusual nature of this event from the perspective of the epipelagic micronekton community off of California, for which the survey catches were unusual, even in the context of past warm periods. As described

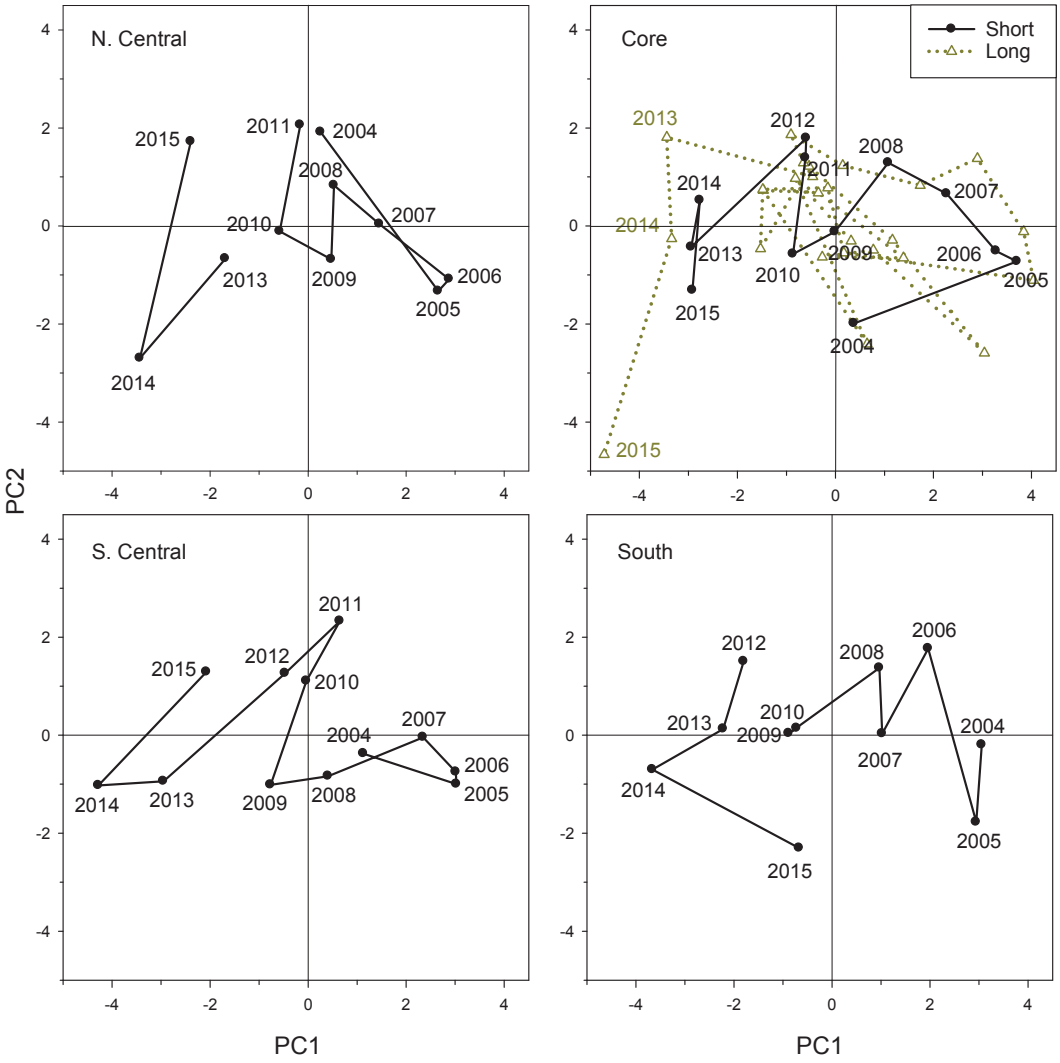

Figure 10. Phase plots of PC1 (horizontal axis) against PC2 (vertical axis) by region of the short (2004–15) time series. For the core region, the long (1990–2015) time series is also shown.

in the introduction, offshore SSTs in the northeastern Pacific were considerably warmer than average during the spring and summer of 2015, despite the fact that above average upwelling winds kept coastal SSTs closer to long-term mean levels above 33°N during the time period of our survey (fig. 1). Our concurrent CTD sampling showed cool temperatures and a shallow 26.1 isopycnal in the north central region indicative of ongoing coastal upwelling (fig. 3). In contrast, in the other regions of the survey, temperatures were fairly warm with a deep 26.1 isopycnal. These time series from the expanded survey area are relatively short (12 years) and other evaluations of long-term subsurface conditions could be better made with longer term oceanographic data sets (such as CalCOFI). Of particular interest to this analysis is that the abundance of many forage species (YOY groundfish, krill, market squid, and mesopelagic fishes) ranged from average to record high levels during this warm event, unusual relative to the response from past warm events (figs. 4–6). In contrast, adult coastal pelagic species (Pacific sardine and northern anchovy) remained at very low levels (similar to those observed over the past 5–6 years), although high catches of the YOY of both species were widely observed throughout the survey area (fig. 4). These trends are consistent with those observed in the stock assessment for Pacific sardine (Hill et al. 2015) as well as analyses of relative abundance trends of northern anchovy based on CalCOFI data (Fissel et al. 2011; MacCall et al. 2016).

The PCA results showed that trends in relative abundance of the most frequently encountered micronekton species were very consistent over the spatial scale of this survey, indicating that the ocean forcing was acting over a fairly broad scale of 500–1000 km. However, north of Cape Mendocino, catches of YOY rockfish and other groundfish were at very low levels in both 2014 and 2015 (Leising et al. 2015), suggesting that the biologi-

cal impacts of these anomalous conditions are heterogeneous over still broader spatial scales. This is likely a function of the major promontories that represent different oceanographic and biogeographic regions, such as Point Conception and Cape Mendocino (Checkley and Barth 2009; Gottscho 2016). While all of the PCAs indicated that the 2013–15 period was anomalous relative to the years that preceded, the PCA for the core region for the longer time series (1990–2015) clearly demonstrated just how unusual the community structure was in 2015 relative to historical patterns. For both PCs the scores were essentially unprecedented in the history of the survey, even before considering the multitude of taxa that were not included in this relatively narrow representation of the epipelagic micronekton community.

The abundance of numerous southern, warm water species is typically considered to be an indicator of strong El Niño-driven warm events off the West Coast of the United States. In 2015, we observed record high numbers of pelagic red crabs, California spiny lobster phyllosoma, California lizardfish, and the largely subtropical krill *Nyctiphanes simplex* (figs. 5–6). Pelagic red crabs are widely recognized to be a classic El Niño signature species, typically confined to upwelling regions and coastal areas off Baja California (Longhurst 1967). Similarly, California spiny lobster phyllosoma have been described as associated with all varieties of warm events, from El Niño to positive phases of the Pacific Decadal Oscillation (PDO) (Koslow et al. 2012). California lizardfish are considered relatively common throughout the Southern California Bight and rare north of Point Conception, but were found throughout the West Coast during the 1982–83 El Niño (Pearcy et al. 1985; Lea and Rosenblatt 2000), and in 2015 they were observed at very high abundances (relative to this time series) throughout the survey area. *Nyctiphanes simplex* also normally occur south of Point Conception, but its distribution can extend much further northward with increased abundances observed during El Niño years (Marinovic et al. 2002; Brinton and Townsend 2003). Additionally, subtropical and tropical species such as the greater argonaut, slender snipefish, YOY Pacific bonito, and the krill *Euphausia eximia* were recorded for the first time in the survey in 2015, although all of these were encountered only in the southern survey region.

The particularly unusual aspect about 2015 is that these warm, El Niño indicator species have historically been present when most other micronekton species (YOY groundfish, market squid, the coastal krill *Thysanoessa spinifera*) are at low abundance levels. For example 1983, 1992, 1998, and 2005–06 were anomalously warm, low productivity years throughout the northern California Current associated with low numbers of YOY groundfish, market squid, and krill (Lenarz et al. 1995; Brodeur et al. 2006; Ralston et al. 2013, 2015). By contrast, YOY rockfish numbers in 2015 were the highest ever observed in the 33-year history of this time series (fig. 4), and numbers of other forage species typically associated with high-transport, high productivity conditions (such as YOY sanddabs, YOY Pacific hake, and market squid) were also at above average to very high levels. Simultaneously, the abundance of gelatinous zooplankton (primarily pelagic tunicates, such as salps and *Pyromosa atlanticum*, but also including pelagic mollusks) (fig. 5) continued to be sustained at high numbers (albeit from an interrupted time series). This gelatinous zooplankton assemblage is widely acknowledged to have the potential for substantial impacts on the productivity and energy flow of pelagic ecosystems by virtue of their extraordinarily high growth potential (Silver 1975) and the intense grazing pressure exhibited during periods of high abundance (Lavaniegos and Ohman 2007). The high abundance of pelagic tunicates could have also been a contributing factor to the ongoing record numbers of king-of-the-salmon (fig. 5), which are known to prey on the salp-associated hyperiid amphipod *Phronima* (Shenker 1983) that was also observed at high abundance in 2015. Although *Phronima* abundance data only exist from an interrupted time series (1990–2001 and 2015), the 2015 abundance was nearly an order of magnitude greater than in any previous year. The smalleye squaretail is also considered to be a salp-associated species (Janssen and Harbison 1981) and in 2015 we observed the highest catches in the 33-year history of the survey. While there were indications in 2012 that the high abundance of salps in the California Current were in part seeded from northern regions (Wells et al. 2013), the species composition and sources of the high abundances of salps in the California Current in 2015 is unclear.

The micronekton community structure in the late spring of 2015 was highly unusual in that species characteristic of all three of what might very generally be considered nominal states (YOY groundfish/market squid and krill dominated catches, subtropical species dominated catches, and pelagic tunicate dominated catches) were encountered in high abundance throughout the survey area. Ongoing efforts to develop diversity indices (such as species richness and evenness) are consistent with the observations that 2015 included extraordinarily high levels of taxonomic diversity.[2] The extent to which this event is truly unprecedented with respect to long-term variability is unclear. The relative "normality" of ocean conditions during the time of the survey was clearly indicative of only localized conditions (strong upwelling during a period of otherwise warm ocean

[2]Biodiversity of pelagic fish reflects unprecedented climate variability in the California Current. Unpublished manuscript (in preparation). J. A. Santora, E. L. Hazen, I. D. Schroeder, S. J. Bograd, K. Sakuma, and J. C. Field.

conditions) during a year in which large scale climate and ocean conditions were highly anomalous (Bond et al. 2015; Leising et al. 2015; Di Lorenzo and Mantua 2016; Jacox et al. 2016). The future of upwelling under climate change scenarios has been extensively evaluated, but most projections are considered to be highly uncertain due to a number of factors, which includes the expectation of high spatial heterogeneity in mesoscale physical characteristics and processes (Bakun et al. 2015; Garcia-Reyes et al. 2015). Given this consideration, the observation that the micronekton community seems to be responding to a highly consistent signal over the scale of approximately eight degrees of latitude (albeit over a relatively short time frame) is also of some interest. One global climate model prediction that may be somewhat more robust is the expectation for a northward shift in the distribution of upwelling centers (Rykaczewski et al. 2015), and in this scenario, the unusual abundance patterns observed in 2015 could be indicative of the expected types of response in the micronekton community, in which unusual transport patterns and mixing of water masses lead to a more heterogeneous mix in the micronekton assemblage.

Although it is too early to fully assess the potential impacts on a broad suite of higher trophic level predators, levels of seabird productivity (breeding success) at the Southeast Farallon Islands (shown in Santora et al. 2014 and references therein) link closely to the pelagic forage assemblage sampled by our survey and indicate average to above average levels of productivity for most seabird species in spring 2015 (Leising et al. 2015). However, this observation is limited to fledging chicks rather than the longer-term productivity of the populations. Given that the summer and fall of 2015 continued to demonstrate considerably warm and unusual ocean conditions, the longer term impacts may take considerable time to fully understand.

We recognize that our data and analysis on the expanded survey area off California are not necessarily representative of the entire extent of the California Current. Comparable surveys to ours (initially focused on sampling YOY Pacific hake) have also been conducted off Oregon and Washington by a collaborative effort between the Northwest Fisheries Science Center (NWFSC) and the Pacific Whiting Conservation Cooperative (PWCC) from 2001–09 (described in Sakuma et al. 2006), and in 2011, 2013–15 by the NWFSC (R. Brodeur, pers. com.). While differences in time period and taxonomic resolution of catches exist, incorporating the data of all of these surveys (likely on a limited set of species) could better resolve mesoscale abundance, distribution, and species assemblage patterns and how these communities respond to both local and large-scale forcing within the California Current off the entire West Coast.

The assemblage of epipelagic micronekton in our study represents some of the most important prey species for a broad suite of higher trophic level predators in the California Current ecosystem (Ainley and Boekelheide 1990; Wells et al. 2012; Thayer et al. 2014; Fleming et al. 2015; McClatchie et al. 2016; Szoboszlai et al. 2015; Ainley et al. 2015). Consequently, tracking the relative abundance, distribution, and forcing factors related to the productivity of this assemblage represents a key step towards quantifying prey availability and predator responses in a manner that would improve both resource management decisions and our understanding of the longer term impacts of climate variability and climate change on the California Current ecosystem.

ACKNOWLEDGMENTS

We would like to thank the officers and crew of the NOAA ships *David Starr Jordan*, *Miller Freeman*, and *Bell M. Shimada* as well as the captain and crew of the charter vessels *Frosti*, *Excalibur*, and *Ocean Starr*. Thanks to the scientists from FED SWFSC, UCSC, and numerous additional research institutions who participated in data collections over the many decades of this survey. Thanks to Rebecca Miller for preparing Figures 1 and 2. Thank you to Andrew Leising and two anonymous reviewers for their thoughtful comments and suggestions on earlier versions of this manuscript.

LITERATURE CITED

Ainley, D. G., and R. J. Boekelheide. 1990. Seabirds of the Farallon Islands; structure and dynamics of an upwelling system community. Stanford University Press, Stanford, California.

Ainley, D. G., P. B. Adams, and J. Jahncke. 2015. California current system-Predators and the preyscape. Journal of Marine Systems 146:1–2.

Aurioles-Gamboa, D., M. I. Castro-Gonzalez, and R. Perez-Flores. 1994. Annual mass strandings of pelagic red crabs, *Pleuroncodes planipes* (Crustacea: Anomura: Galatheidae), in Bahia Magdalena, Baja California Sur Mexico. Fishery Bulletin 92:464–470.

Bakun, A., B. A. Black, S. J. Bograd, M. Garcia-Reyes, A. J. Miller, R. R. Rykaczewski, and W.J. Sydeman. 2015. Anticipated effects of climate change on coastal upwelling ecosystems. Current Climate Change Reports 1(2):85–93.

Bond, N. A., M. F. Cronin, H. Freeland, and N. Mantua. 2015. Causes and impacts of the 2014 warm anomaly in the NE Pacific. Geophysical Research Letters 42(9):3414–3420.

Brinton, E., and A. Townsend. 2003. Decadal variability in abundances of the dominant euphausiid species in the southern sectors of the California Current. Deep Sea Research II 50: 2449–2472.

Brodeur, R. D., S. Ralston, R. L. Emmett, M. Trudel, T. D. Auth, and A. J. Phillips. 2006. Anomalous pelagic nekton abundance, distribution, and apparent recruitment in the northern California Current in 2004 and 2005. Geophysical Research Letters 33, L22S08. doi:10.1029/2006GL026614.

Checkley, D. M., and J. A. Barth. 2009. Patterns and processes in the California Current System. Progress in Oceanography 83:49–64.

Di Lorenzo, E., and N. Mantua. 2016. Multi-year persistence of the 2014/15 North Pacific marine heatwave. Nature Climate Change. doi:10.1038/nclimate3082.

Fissel, B. E., N. C. Lo, and S. Herrick Jr. 2011. Daily egg production, spawning biomass and recruitment for the central subpopulation of Northern anchovy 1981–2009. California Cooperative Oceanic and Fisheries Investigation Reports 52:116–135.

Fleming, A. H., C. T. Clark, J. Calambokidis, and J. Barlow. 2015. Humpback whale diets respond to variance in ocean climate and ecosystem conditions in the California Current. Global Change Biology 22(3):1214–24.

Garcia-Reyes, M., W. J. Sydeman, D. S. Schoeman, R. R. Rykaczewski, B. A. Black, A. J.Smit, and S. J. Bograd. 2015. Under Pressure: Climate Change, Upwelling, and Eastern Boundary Upwelling Ecosystems. Frontiers in Marine Science 2:109.

Gottscho, A. D. 2016. Zoogeography of the San Andreas Fault system: Great Pacific Fracture Zones correspond with spatially concordant phylogeographic boundaries in western North America. Biological Reviews 91: 235–254.

Hare, S. R., and N. J. Mantua. 2000. Empirical evidence for North Pacific regime shifts in 1977 and 1989. Progress in Oceanography 47(2):103–145.

Hill, K. T., P. R. Crone, E. Dorval, and B. J. Macewicz. 2015. Assessment of the Pacific Sardine Resource in 2015 for USA Management in 2015–16. Pacific Fishery Management Council. http://www.pcouncil.org/coastal-pelagic-species/stock-assessment-and-fishery-evaluation-safe-documents/.

Jacox, M. G., E. L. Hazen, K. D. Zaba, D. L. Rudnick, C. A. Edwards, A. M. Moore, and S.J. Bograd. 2016. Impacts of the 2015–2016 El Niño on the California Current System: Early assessment and comparison to past events. Geophysical Research Letters 43(13):7072–7080.

Janssen, J., and G. R. Harbison. 1981. Fish in salps: the association of square-tails (*Tetragonurus* spp.) with pelagic tunicates. Journal of the Marine Biological Association of the United Kingdom 61(04):917–927.

Koslow, J. A., R. Goericke, A. Lara-Lopez, and W. Watson. 2011. Impact of declining intermediate-water oxygen on deepwater fishes in the California Current. Marine Ecology Progress Series 436:207–218.

Koslow, J. A., L. Rogers-Bennett, and D. J. Neilson. 2012. A time series of California spiny lobster (*Panulirus interruptus*) phyllosoma from 1951 to 2008 links abundance to warm oceanographic conditions in southern California. California Cooperative Oceanic Fisheries Investigations Reports 53:132–139.

Lavaniegos, B. E., and M. D. Ohman. 2007. Coherence of long-term variations of zooplankton in two sectors of the California Current System. Progress in Oceanography, 75(1): 42–69.

Lea, R. N., and R. H. Rosenblatt. 2000. Observations on fishes associated with the 1997–98 El Niño off California. California Cooperative Oceanic Fisheries Investigations Reports 41:117–129.

Leising, A. W., I. D. Schroeder, S. J. Bograd, E. P. Bjorkstedt, J. Field, K. Sakuma, J. Abell, R. R. Robertson, J. Tyburczy, W. T. Peterson, R. Brodeur, C. Barcelo, T. B. Auth, E. A. Daly, G. S. Campbell, J. A. Hildebrand, R. M. Suryan, A. J. Gladics, C. A. Horton, M. Kahru, M. Manzano-Sarabia, S. McClatchie, E. D. Weber, W. Watson, J. A. Santora, W. J. Sydeman, S. R. Melin, R. L. DeLong, J. Largier, S. Kim, F. P. Chavez, R. T. Golightly, S. R. Schneider, P. Warzybok, R. Bradley, J. Jahncke, J. Fisher, and J. Peterson. 2014. State of the California Current 2013-14: El Niño looming. California Cooperative Oceanic Fisheries Investigations Reports 55:51–87.

Leising, A. W., I. D. Schroeder, S. J. Bograd, J. Abell, R. Durazo, G. Gaxiola-Castro, E. P. Bjorkstedt, J. Field, K. Sakuma, R. R. Robertson, R. Goericke, W. T. Peterson, R. Brodeur, C. Barceló, T. D. Auth, E. A. Daly, R. M. Suryan, A. J. Gladics, J. M. Porquez, S. McClatchie, E. D. Weber, W. Watson, J. A. Santora, W. J. Sydeman, S. R. Melin, F. P. Chavez, R. T. Golightly, S. R. Schneider, J. Fisher, C. Morgan, R. Bradley, and P. Warybok. 2015. State of the California Current 2014–15: Impacts of the Warm-Water "Blob." California Cooperative Oceanic Fisheries Investigations Reports 56:31–68.

Lenarz, W. H., D. A. Ventresca, W. M. Graham, F. B. Schwing, and F. Chavez. 1995. Explorations of El Niño events and associated biological population dynamics off central California. California Cooperative Oceanic Fisheries Investigations Reports 36:106–119.

Longhurst, A. R. 1967. The pelagic phase of *Pleuroncodes planipes* Stimpson (Crustacea, Galatheidae) in the California Current. California Cooperative Oceanic Fisheries Investigations Reports 11:142–154.

MacCall, A. D., W. J. Sydeman, P. C. Davison, and J. A. Thayer. 2016. Recent collapse of northern anchovy biomass off California. Fisheries Research 175:87–94.

Marinovic, B. B., D. A. Croll, N. Gong, S. R. Benson, and F. P. Chavez. 2002. Effects of the 1997–99 El Niño and La Niña events on zooplankton abundance and euphausiid community composition within the Monterey Bay coastal upwelling system. Progress in Oceanography 54:265–277.

McClatchie, S., J. Field, A. R. Thompson, T. Gerrodette, M. Lowry, P. C. Fiedler, W. Watson, K. M. Nieto, and R. D. Vetter. 2016. Food limitation of sea lion pups and the decline of forage off central and southern California. Royal Society Open Science 3(3), p.150628. DOI: 10.1098/rsos.150628.

National Marine Fisheries Service. 2014 (July 30). A remarkable warming of central California's coastal ocean. Retrieved September 23, 2016 from https://swfsc.noaa.gov/news.aspx?Division=FED&ParentMenuId=54&id=19435.

Pearcy, W., J. Fisher, R. Brodeur, and S. Johnson. 1985. Effect of 1983 El Niño on coastal nekton off Oregon and Washington. In Wooster, W. S. and D. L. Fluharty (Editors) "El Nino north-Nino effects in the eastern subarctic Pacific ocean." Cambridge University Press: Cambridge. 312 pp.

Peterson, W. T., M. Robert, and N. Bond. 2015. The warm Blob continues to dominate the ecosystem of the northern California Current. 2016. PICES Press 23 (2):44–46. http://meetings.pices.int/publications/pices-press.

R Core Team. 2012. R: A language and environment for statistical computing. R Foundation for Statistical Computing, Vienna, Austria. ISBN 3-900051-07-0. http://www.R-project.org/.

Ralston, S., K. M. Sakuma, and J. C. Field. 2013. Interannual variation in pelagic juvenile rockfish abundance—going with the flow. Fisheries Oceanography 22:288–308. doi:10.1111/fog.12022.

Ralston, S., J. C. Field, and K. S. Sakuma. 2015. Longterm variation in a central California pelagic forage assemblage. Journal of Marine Systems 146: 26–37. http://dx.doi.org/10.1016/j.jmarsys.2014.06.013.

Rykaczewski, R. R., J. P. Dunne, W. J. Sydeman, M. García-Reyes, B. A. Black, and S. J. Bograd. 2015. Poleward displacement of coastal upwelling-favorable winds in the ocean's eastern boundary currents through the 21st century. Geophysical Research Letters 42(15):6424–6431.

Sakuma, K. M., S. Ralston, and V. G. Wespestad. 2006. Interannual and spatial variation in the distribution of young-of-the-year rockfish (*Sebastes* spp.): expanding and coordinating a survey sampling frame. California Cooperative Oceanic Fisheries Investigations Reports 47:127–139.

Santora, J. A., I. D. Schroeder, J. C. Field, B. K. Wells, and W. J. Sydeman. 2014. Spatio-temporal dynamics of ocean conditions and forage taxa reveals regional structuring of seabird-prey relationships. Ecological Applications 24(7):1730–1747.

Shenker, J. M., 1983. Distribution, size relationships, and food habits of juvenile king-of-the-salmon, *Trachipterus altivelis*, caught off the Oregon coast. Fishery Bulletin 81:161–164.

Silver, M. W. 1975. The habitat of *Salpa fusiformis* in the California Current as defined by indicator assemblages. Limnology and Oceanography 20(2):230–237.

Smith Jr., K. L., A. D. Sherman, C. L. Huffard, P. R. McGill, R. Henthorn, S. Von Thun, H. A. Ruhl, M. Kahru, and M. D. Ohman. 2014. Large salp bloom export from the upper ocean and benthic community response in the abyssal northeast Pacific: Day to week resolution. Limnology and Oceanography 59(3):745–757.

Szoboszlai, A. I., J. A. Thayer, S. A. Wood, W. J. Sydeman, and L. E. Koehn. 2015. Forage species in predator diets: Synthesis of data from the California Current. Ecological Informatics 29:45–56.

Thayer, J. A., J. C. Field and W. J. Sydeman. 2014. Changes in California chinook salmon diet over the past 50 years: relevance to the recent population crash. Marine Ecology Progress Series 498:249–261.

Wells, B. K., J. A. Santora, J. C. Field, R. MacFarlane, B. B. Marinovic, and W. J. Sydeman. 2012. Population dynamics of Chinook salmon *Oncorhynchus tshawytscha* relative to prey availability in the central California coastal region. Marine Ecology Progress Series 457:125–137.

Wells, B. K., I. D. Schroeder, J. A. Santora, E. L. Hazen, S. J. Bograd, E. P. Bjorkstedt, V. J. Loeb, S. McClatchie, E. D. Weber, W. Watson, A. R. Thompson, W. T. Peterson, R. D. Brodeur, J. Harding, J. Field, K. Sakuma, S. Hayes, N. Mantua, W. J. Sydeman, M. Losekoot, S. A. Thompson, J. Largier, S. Y. Kim, F. P. Chavez, C. Barcelo, P. Warzybok, R. Bradley, J. Jahncke, R. Goericke, G. S. Campbell, J. A. Hildebrand, S. R. Melin, R. L. DeLong, J. Gomez-Valdes, B. Lavaniegos, G. Gaxiola-Castro, R. T. Golightly, S. R. Schneider, N. Lo, R. M. Suryan, A. J. Gladics, C. A. Horton, J. Fisher, C. Morgan, J. Peterson, E. A. Daly, T. D. Auth, and J. Abell. 2013. State of the California Current 2012–13: No Such Thing as an "Average" Year. California Cooperative Oceanic Fisheries Investigations Reports 54:37–71.

Welch, C. 2016. The blob that cooked the Pacific. National Geographic. September, 2016. http://www.nationalgeographic.com/magazine/2016/09/warm-water-pacific-coast-algae-nino/.

Wyllie-Echeverria, T., W. H. Lenarz, and C.A. Reilly. 1990. Survey of the abundance and distribution of pelagic young-of-the-year rockfish, *Sebastes*, off central California. U.S. Dep. Commer., NOAA Tech. Memo., NOAA-TM-NMFS-SWFSC-147, 125 pp.

Zaba, K. D., and D. L. Rudnick. 2016. The 2014–2015 warming anomaly in the Southern California Current System observed by underwater gliders. Geophysical Research Letters 43. doi:10.1002/2015GL067550.

APPENDIX 1

Number of standard station trawls and CTDs by year and region used in the current study. Note that additional nonstandard trawls and CTDs were conducted in most years, but these were not used in the analyses and therefore not listed. No trawls or CTDs were conducted in the south region in 2011 due to vessel/logistic constraints and none were conducted in the north central region in 2012 due to inclement weather. In addition, due to vessel/logistic constraints, no daytime CTD stations were sampled in 2011 thereby reducing the number of CTD stations consistently sampled across years to only those conducted at nighttime trawls stations.

	Trawls				CTDs			
Year	South	South Central	Core	North Central	South	South Central	Core	North Central
1990			80					
1991			93				66	
1992			73				56	
1993			75				51	
1994			75				45	
1995			74				47	
1996			76				48	
1997			74				47	
1998			79				50	
1999			77				53	
2000			84				54	
2001			78				52	
2002			65				41	
2003			86				48	
2004	19	5	76	15	13	2	47	2
2005	28	11	73	16	17	4	46	2
2006	28	20	63	27	16	4	36	3
2007	26	18	82	24	15	4	44	3
2008	30	22	31	10	15	6	30	2
2009	15	20	72	12	9	4	48	2
2010	16	5	74	23	10	2	46	4
2011		2	48	8			33	2
2012	11	11	58		11	2	50	
2013	22	22	60	16	14	4	37	3
2014	14	25	66	22	9	6	41	4
2015	35	26	64	20	20	5	36	3

APPENDIX 2

Species/taxa occurring in the expanded survey area (All Areas) from 2004–15 listed in decreasing order of occurrence. The percent occurrence within each of the four survey regions is also shown. For Ontogeny, Y = young-of-the-year, A = age 1 +, and U = undetermined. With the exception of krill, Years = ALL, denotes species/taxa that were also consistently enumerated in the core region since 1990 (data not shown). Krill have an * as species specific enumeration began in 2002 with only total krill numbers (i.e., no species specific counts) available from 1990–2001 (data not shown). For species/taxa not consistently enumerated from 2004–15, the years in which they were enumerated are listed in the Years column. Species/taxa with a ** were also enumerated from 1990–2001 (data not shown).

Common Name	Scientific Name	Ontogeny	Years	South	South Central	Core	North Central	All Areas
Krill	*Euphausia pacifica*	U	ALL*	89.3	79.7	81.4	86.5	83.2
Sanddab	*Citharichthys* spp.	Y	ALL	81.6	79.1	79.3	72.5	78.7
Rockfish	*Sebastes* spp.	Y	ALL	81.6	73.8	73.9	68.4	74.5
Pyrosoma	*Pyrosoma* spp.	U	2012–15**	87.8	79.8	65.4	60.3	71.1
Salp	Salpidae	U	2012–15**	82.9	77.4	61.1	46.6	65.9
Krill	*Thysanoessa spinifera*	U	ALL*	61.1	55.6	70.9	35.2	62.4
Phronima	*Phronima* spp.	U	2015**	45.7	96.2	57.6	55.0	61.2
Market Squid	*Doryteuthis opalescens*	U	ALL	84.4	65.2	51.2	17.1	54.1
Myctophid	Myctophidae	U	ALL	82.8	52.9	40.0	63.7	52.2
Pacific Hake	*Merluccius productus*	Y	ALL	50.0	42.8	53.8	57.0	52.1
Thetys Salp	*Thetys vagina*	U	2012–15**	36.6	41.7	38.9	67.2	42.4
Armhook Squid	*Gonatus* spp.	U	2006–15	39.1	47.4	35.8	56.2	40.8
Sergestid	Sergestidae	U	ALL	57.0	38.0	32.3	54.4	40.3
Octopus	Octopoda	U	ALL	38.9	44.9	30.7	28.5	33.7
Krill	*Nematoscelis difficilis*	U	ALL*	71.7	35.3	19.6	39.9	33.3
Squid	Teuthoidea	U	ALL	47.5	28.9	22.4	42.0	30.2
Blacktip Squid	*Abraliopsis felis*	U	2006–15	57.4	25.7	16.7	52.5	29.8
California Headlightfish	*Diaphus theta*	U	ALL	34.0	29.4	22.6	52.9	29.5
California Smoothtongue	*Leuroglossus stilbius*	U	ALL	50.0	31.0	24.5	15.5	28.5
Blue Lanternfish	*Tarletonbeania crenularis*	U	ALL	15.2	36.4	23.1	57.5	28.1
Deep-Sea Smelt	Bathylagidae	U	ALL	37.3	19.3	17.7	48.7	25.5
Goby	Gobiidae	U	ALL	55.3	30.5	15.5	4.7	22.8
Rex Sole	*Glyptocephalus zachirus*	Y	ALL	5.3	12.8	25.1	28.0	20.5
Northern Anchovy	*Engraulis mordax*	A	ALL	17.2	28.9	20.6	2.6	18.7
Northern Anchovy	*Engraulis mordax*	Y	ALL	50.4	29.4	7.9	6.2	17.8
Sword-Tail Squid	*Chiroteuthis calyx*	U	2006–15	13.7	19.9	13.6	30.3	16.8
Heteropod	Pterotracheoidea	U	2012–15**	43.9	17.9	8.2	12.1	16.4
Pacific Sardine	*Sardinops sagax*	A	ALL	9.4	17.7	16.7	16.1	15.5
Slender Sole	*Lyopsetta exilis*	Y	ALL	7.0	12.3	19.2	12.4	15.3
Pacific Sanddab	*Citharichthys sordidus*	A	ALL	1.2	12.8	20.4	8.8	14.5
Barracudina	Paralepididae	U	ALL	23.4	8.6	8.1	33.7	14.3
Flatfish, Right Eye	Pleuronectidae	Y	ALL	1.6	5.4	16.9	23.3	13.6
King-Of-The-Salmon	*Trachipterus altivelis*	U	ALL	16.0	22.5	11.0	6.2	12.7
Boreal Clubhook Squid	*Onychoteuthis borealijaponica*	U	2013–15	8.5	12.3	12.2	19.0	12.6
Sea Nettle	*Chrysaora fuscescens*	U	2005–15**	0.0	0.8	21.5	2.7	12.5
Octopoteuthis	*Octopoteuthis deletron*	U	2015	0.0	15.4	19.7	5.0	12.2
California Lanternfish	*Symbolophorus californiensis*	U	2005–15	24.5	14.3	6.7	18.0	12.2
Pacific Hake	*Merluccius productus*	A	ALL	4.1	5.4	14.6	15.0	11.7
Lingcod	*Ophiodon elongatus*	Y	ALL	2.5	4.8	16.9	8.3	11.7
Dover Sole	*Microstomus pacificus*	Y	ALL	5.3	10.2	10.9	11.4	9.9
Pacific Sardine	*Sardinops sagax*	Y	ALL	26.2	17.1	4.4	3.6	9.7
Pacific Pompano	*Peprilus simillimus*	U	ALL	13.5	15.0	9.1	0.5	9.5
Turbot	*Pleuronichthys* spp.	Y	ALL	2.9	18.7	7.9	10.9	8.8
Moon Jelly	*Aurelia* spp.	U	2005–15**	2.1	10.5	10.6	2.7	8.2
Medusafish	*Icichthys lockingtoni*	U	ALL	6.2	13.9	6.1	11.4	7.9
Combfish	Zaniolepididae	U	ALL	6.6	8.0	9.7	1.0	7.8
Blackdragon	Idiacanthidae	U	ALL	15.6	7.5	4.0	6.7	6.8
Sand Sole	*Psettichthys melanostictus*	Y	ALL	0.0	3.2	8.7	8.3	6.5
Plainfin Midshipman	*Porichthys notatus*	U	ALL	0.4	13.9	6.5	1.6	5.8
Jack Mackerel	*Trachurus symmetricus*	Y	ALL	30.3	3.7	0.0	0.0	5.7
Fried Egg Jellyfish	*Phacellophora camtschatica*	U	2009–15	1.8	8.1	6.3	3.0	5.5
Glass Shrimp	*Pasiphaea pacifica*	U	ALL	8.2	8.0	4.9	1.0	5.3
Longfin Dragonfish	*Tactostoma macropus*	U	ALL	1.2	5.4	5.0	11.9	5.3
Painted Greenling	*Oxylebius pictus*	Y	ALL	8.2	10.7	3.8	0.5	5.0
Spiny Lobster Larvae	Palinuridae	U	ALL	20.1	3.7	1.1	2.6	4.9
Cabezon	*Scorpaenichthys marmoratus*	Y	ALL	3.3	8.0	4.6	4.7	4.8
Pacific Argentine	*Argentina sialis*	U	ALL	4.9	4.8	5.6	0.0	4.6
Blackbelly Dragonfish	*Stomias atriventer*	U	ALL	23.8	1.1	0.3	0.0	4.4
Fish	Pisces	Y	ALL	8.2	4.8	2.8	4.7	4.2

(*continued*)

APPENDIX 2, continued

Species/taxa occurring in the expanded survey area (All Areas) from 2004–15 listed in decreasing order of occurrence. The percent occurrence within each of the four survey regions is also shown. For Ontogeny, Y = young-of-the-year, A = age 1 +, and U = undetermined. With the exception of krill, Years = ALL, denotes species/taxa that were also consistently enumerated in the core region since 1990 (data not shown). Krill have an * as species specific enumeration began in 2002 with only total krill numbers (i.e., no species specific counts) available from 1990–2001 (data not shown). For species/taxa not consistently enumerated from 2004–15, the years in which they were enumerated are listed in the Years column. Species/taxa with a ** were also enumerated from 1990–2001 (data not shown).

Common Name	Scientific Name	Ontogeny	Years	South	South Central	Core	North Central	All Areas
Pelagic Red Crab	*Pleuroncodes planipes*	U	ALL	17.2	3.2	1.5	0.0	4.2
Sculpin	Cottidae	Y	ALL	0.4	2.7	5.4	5.2	4.1
Loosejaw	Malacosteidae	U	ALL	9.4	5.4	1.8	6.2	4.1
Pacific Electric Ray	*Torpedo californica*	U	ALL	1.2	2.7	6.0	0.5	4.0
Pipefish	Syngnathidae	U	ALL	8.6	10.7	1.9	0.0	3.9
Crangon Shrimp	*Crangon* spp.	U	ALL	0.0	0.5	5.0	7.3	3.9
Ronquil	Bathymasteridae	U	ALL	5.7	5.0	0.5	0.8	3.8
Krill	*Nyctiphanes simplex*	U	ALL*	11.1	6.4	1.8	0.0	3.7
Slender Sole	*Lyopsetta exilis*	A	ALL	1.6	1.6	4.5	3.1	3.4
Pandalid Shrimp	*Pandalus jordani*	U	ALL	0.8	0.0	3.8	7.8	3.3
Snailfish	Liparidae	U	ALL	0.4	0.0	3.3	9.8	3.2
Pacific Tomcod	*Microgadus proximus*	Y	ALL	0.0	0.0	3.9	3.1	2.6
Smelt	Osmeridae	A	ALL	0.0	0.0	2.9	6.2	2.5
North Pacific Spiny Dogfish	*Squalus suckleyi*	U	ALL	0.0	2.7	3.5	1.0	2.5
Wolf-Eel	*Anarrhichthys ocellatus*	Y	ALL	2.5	3.2	2.4	1.0	2.3
Highfin Dragonfish	*Bathophilus flemingi*	U	ALL	1.6	2.1	1.1	8.3	2.3
Baseball Squid	*Cranchia scabra*	U	2005–15	5.8	4.4	0.7	2.3	2.3
Lightfish	Phosichthyidae	U	ALL	9.0	2.1	0.5	0.5	2.2
Fire Squid	Pyroteuthidae	U	2008–15	11.9	0.8	0.2	0.0	2.2
Blob Octopus	Alloposidae	U	2006–15	9.6	1.2	0.6	0.0	2.1
Pallid Eelpout	*Lycodapus mandibularis*	U	ALL	1.6	0.5	3.1	0.0	2.1
Mantis Shrimp	Stomatopoda	U	2009–15	14.2	0.0	0.0	0.0	2.0
Poacher	Agonidae	U	ALL	0.4	2.7	2.5	1.0	2.0
Shrimp	Natantia	U	ALL	2.1	6.4	1.1	0.0	1.8
Leptocephalus	Elopomorpha	Y	ALL	5.7	0.5	0.5	3.1	1.8
Purple-Striped Jelly	*Chrysaora colorata*	U	2005–15**	0.7	3.0	2.0	0.0	1.7
Greenling	Hexagrammidae	Y	ALL	4.1	0.5	1.3	1.0	1.6
Humboldt Squid	*Dosidicus gigas*	U	2005–15	0.0	1.7	1.3	4.5	1.5
Pacific Mackerel	*Scomber japonicus*	A	ALL	0.4	1.1	1.8	2.1	1.5
Irish Lord	*Hemilepidotus* spp.	Y	ALL	0.0	0.0	1.8	2.6	1.3
Krill	*Euphausia eximia*	U	ALL*	7.0	0.0	0.1	0.0	1.3
King Salmon	*Oncorhynchus tshawytscha*	Y	ALL	0.0	0.0	2.1	0.0	1.2
California Lizardfish	*Synodus lucioceps*	U	ALL	2.5	0.5	1.1	0.5	1.2
Jack Mackerel	*Trachurus symmetricus*	A	ALL	0.8	3.2	0.9	0.5	1.1
Arrowtooth Flounder	*Atheresthes stomias*	Y	ALL	0.0	0.0	0.8	3.6	0.9
Pacific Herring	*Clupea pallasii*	A	ALL	0.0	0.0	1.0	2.6	0.9
Lamprey	Petromyzontidae	U	ALL	0.0	0.0	1.3	1.6	0.9
Fish	Pisces	U	ALL	2.5	0.5	0.8	0.0	0.9
Pacific Sandlance	*Ammodytes hexapterus*	U	ALL	0.0	0.0	1.1	1.6	0.8
Jacksmelt	*Atherinopsis californiensis*	U	ALL	0.0	0.0	1.5	0.0	0.8
Red Shrimp	*Bentheogennema burkenroadi*	U	ALL	2.5	1.1	0.4	0.5	0.8
Sablefish	*Anoplopoma fimbria*	Y	ALL	0.8	1.6	0.8	0.0	0.8
King Salmon	*Oncorhynchus tshawytscha*	A	ALL	0.0	0.0	1.4	0.0	0.8
Smelt	Osmeridae	Y	ALL	0.0	0.0	0.5	3.6	0.8
English Sole	*Parophrys vetulus*	A	ALL	0.0	0.0	1.1	0.5	0.7
Pacific Mackerel	*Scomber japonicus*	Y	ALL	3.7	0.0	0.0	0.0	0.6
Smalleye Squaretail	*Tetragonurus cuvieri*	U	ALL	2.1	1.1	0.3	0.0	0.6
Eelpout	Zoarcidae	U	ALL	0.8	1.1	0.4	1.0	0.6
Ragfish	*Icosteus aenigmaticus*	U	ALL	0.4	0.5	0.4	1.6	0.6
Ronquil	Bathymasteridae	U	ALL	0.4	0.0	0.4	1.6	0.5
Krill	Euphausiacea	U	ALL	0.8	1.1	0.3	0.5	0.5
Robust Clubhook Squid	*Onykia robusta*	U	2006–15	1.0	0.6	0.2	0.6	0.4
Krill	*Euphausia gibboides*	U	ALL*	2.1	0.0	0.0	0.5	0.4
Mysid	Mysidacea	U	ALL	0.0	0.0	0.8	0.0	0.4
Ghost Shrimp	*Callianassa californiensis*	U	ALL	0.0	0.0	0.5	0.5	0.4
Bigscale	Melamphaidae	U	ALL	1.2	0.5	0.0	0.5	0.4
Common Mola	*Mola mola*	U	ALL	0.0	1.6	0.3	0.0	0.4
Spookfish	Opisthoproctidae	U	ALL	0.0	0.5	0.3	1.0	0.4
Starry Flounder	*Platichthys stellatus*	Y	ALL	0.4	0.0	0.5	0.0	0.4

(*continued*)

APPENDIX 2, continued

Species/taxa occurring in the expanded survey area (All Areas) from 2004–15 listed in decreasing order of occurrence. The percent occurrence within each of the four survey regions is also shown. For Ontogeny, Y = young-of-the-year, A = age 1 +, and U = undetermined. With the exception of krill, Years = ALL, denotes species/taxa that were also consistently enumerated in the core region since 1990 (data not shown). Krill have an * as species specific enumeration began in 2002 with only total krill numbers (i.e., no species specific counts) available from 1990–2001 (data not shown). For species/taxa not consistently enumerated from 2004–15, the years in which they were enumerated are listed in the Years column. Species/taxa with a ** were also enumerated from 1990–2001 (data not shown).

Common Name	Scientific Name	Ontogeny	Years	South	South Central	Core	North Central	All Areas
Starry Flounder	*Platichthys stellatus*	A	ALL	0.0	0.0	0.1	2.1	0.4
Topsmelt	*Atherinops affinis*	U	ALL	0.0	0.0	0.5	0.0	0.3
Krill	*Euphausia mutica*	U	ALL*	1.2	0.0	0.1	0.0	0.3
Krill	*Euphausia recurva*	U	ALL*	0.0	0.0	0.3	1.0	0.3
Curlfin Sole	*Pleuronichthys decurrens*	A	ALL	0.0	1.6	0.1	0.0	0.3
Krill	*Thysanoessa gregaria*	U	ALL*	0.8	0.0	0.3	0.0	0.3
Slender Snipefish	*Macroramphosus gracilis*	U	ALL	1.2	0.0	0.0	0.0	0.2
Grunt Sculpin	*Rhamphocottus richardsonii*	Y	ALL	0.0	0.0	0.1	1.0	0.2
Argonaut	*Argonauta argo*	U	ALL	0.8	0.0	0.0	0.0	0.1
Clupeiform	Clupeiformes	Y	ALL	0.4	0.0	0.1	0.0	0.1
Threespine Stickleback	*Gasterosteus aculeatus*	U	ALL	0.0	0.0	0.3	0.0	0.1
Sunbeam Lampfish	*Lampadena urophaos*	U	ALL	0.8	0.0	0.0	0.0	0.1
Snipe Eel	Nemichthyidae	U	ALL	0.4	0.0	0.1	0.0	0.1
Armhook Squid	*Berryteuthis* spp.	U	2009–15	0.0	0.0	0.2	0.0	0.1
Wolf-Eel	*Anarrhichthys ocellatus*	A	ALL	0.0	0.5	0.0	0.0	0.1
Arrowtooth Flounder	*Atheresthes stomias*	A	ALL	0.0	0.0	0.0	0.5	0.1
Pacific Saury	*Cololabis saira*	U	ALL	0.0	0.0	0.0	0.5	0.1
Pelagic Stingray	*Dasyatis violacea*	U	ALL	0.4	0.0	0.0	0.0	0.1
Rex Sole	*Glyptocephalus zachirus*	A	ALL	0.0	0.0	0.1	0.0	0.1
Dover Sole	*Microstomus pacificus*	A	ALL	0.0	0.0	0.1	0.0	0.1
Silver Salmon	*Oncorhynchus kisutch*	Y	ALL	0.0	0.0	0.1	0.0	0.1
Salmon	*Oncorhynchus* spp.	U	ALL	0.0	0.0	0.1	0.0	0.1
Lingcod	*Ophiodon elongatus*	A	ALL	0.0	0.0	0.1	0.0	0.1
Sand Sole	*Psettichthys melanostictus*	A	ALL	0.0	0.0	0.1	0.0	0.1
Big Skate	*Raja binoculata*	U	ALL	0.0	0.0	0.1	0.0	0.1
Pacific Bonito	*Sarda chiliensis*	Y	ALL	0.4	0.0	0.0	0.0	0.1
Scombrid	Scombridae	Y	ALL	0.4	0.0	0.0	0.0	0.1
Hatchetfish	Sternoptychidae	U	ALL	0.4	0.0	0.0	0.0	0.1
California Tonguefish	*Symphurus atricauda*	A	ALL	0.0	0.0	0.1	0.0	0.1

INSTRUCTIONS TO AUTHORS

CalCOFI Reports is a peer-reviewed journal. Papers submitted for publication in the "Scientific Contributions" section are read by two or more referees and by arbiters when necessary; "Symposium" papers are invited by the convener of the annual symposium and are reviewed and edited at the convener's discretion. The "Reports, Review, and Publications" section contains newsworthy information on the status of stocks and environmental conditions; the papers in this section are not peer reviewed; the CalCOFI Editorial Board will not consider unsolicited review papers.

The CalCOFI Editorial Board will consider for publication in the "Scientific Contributions" section manuscripts not previously published elsewhere that address the following in relation to the North Pacific, the California Current, and the Gulf of California: marine organisms; marine chemistry, fertility, and food chains; marine fishery modeling, prediction, policy, and management; marine climatology, paleoclimatology, ecology, and paleoecology; marine pollution; physical, chemical, and biological oceanography; and new marine instrumentation and methods.

Submission Guidelines

Submissions are open year-round. Please submit manuscripts as MS word documents in electronic format via email to: calcofi_coordinator@coast.ucsd.edu. (use Word; see "Manuscript Guidelines" below for more details on preparing tables and figures). Include one complete file with all tables and figures for reviewers.

The manuscript should contain the following parts:

1. A title page containing the manuscript's title, your name, your institutional affiliation and contact information (address, telephone and fax numbers, e-mail address), and a word count
2. An abstract of no more than 150 words that succinctly expresses only the manuscript's most central points, using the active voice
3. Body of the text, including any footnotes
4. Literature cited, in alphabetical order
5. Acknowledgments, if any
6. Tables
7. Figures and captions

Manuscript Guidelines

Length. Unless previously approved by the Scientific Editor, manuscripts should not exceed 6,000 words, including title page, abstract, text body, footnotes, acknowledgments, and literature cited but excluding figures and tables.

Text. Double-space all elements of the text, allow margins of at least 1 inch on all sides, and use a standard font (such as Times or Times New Roman) no smaller than 12 points. Number the pages consecutively. Eliminate all nonessential formatting. Indicate subordination of heads consistently; for example, use all caps for the main heads, boldface for the next level, and italics for the third level. To indent paragraphs, use the tab key, not the space bar or a "style" feature of any sort. Never use letters for numbers or vice versa; in other words, do not type the lowercase "el" for the number "one" or the capital letter "oh" for zero. Use your word-processor's automatic footnoting feature to insert footnotes. Acknowledgments, if included, should be placed at the end of the text and may include funding sources. Place the entire text (title page, abstract, text body, footnotes, acknowledgments, and literature cited) in one document file, and label it with your name—for example, "Smith text.doc."

Tables. Use your word-processor's *Table* feature, rather than spaces or tabs, to create the columns and rows. Use *minimal* formatting, and do not insert vertical or horizontal rules. Double-space the tables and use a standard font, such as Times or Times New Roman. Number the tables consecutively, and provide a brief title for each. Place explanatory material and sources in a note beneath the table. Be sure each table is specifically referred to in the text.

Figures. Figures should be in black and white or color, Submit figures—whether drawings, graphs, or photographs—as separate, high-resolution electronic files (preferably 300 ppi for better printing purposes). Label the files, for example, "Smith fig 1" and "Smith fig 2." If you are submitting as a PDF, please embed all fonts. If your figures are embedded in your Word docs, please create separate high-resolution PDF files of each figure from the original art file. Please review your files after saving them as PDFs, to make sure all your figures translated correctly. Contributors are advised to make a trial reduction of complex figures to ensure that patterns, shading, and letters will remain distinct when reduced. Include a north arrow and latitude and longitude lines on maps. Use consistent labels and abbreviations and the same style of lettering for all figures if possible. Number figures consecutively, and specifically refer to each in the text. Provide a caption for each figure. Gather the captions together, and place them at the end of the electronic text file, following the "Literature Cited" section.

Editorial Style

For matters of editorial style, contributors should consult recent editions of *CalCOFI Reports.* Contributors may also refer to *The Chicago Manual of Style*, 15th ed. Whenever possible, write in the first person, and use active verbs. Use the full name of a person, organization, program, or agency when mentioning it for the first time in your manuscript. Double-check the spelling of non-English words, and include special characters such as accents and umlauts. Use correct SI symbols for *units of measure* in figures, tables, and text (other units may be given in parentheses). Prepare *equations* in accordance with similar expressions in the printed literature.

Cite *sources* in the text as Smith (1999) or Smith and Jones (2000) or (Gabriel et al. 1998; Smith and Jones 2000) (the latter when there are three or more authors). There should be no comma between author and date. References should be cited in chronological order from the oldest to the most recent.

In the "Literature Cited" section, show sources alphabetically by the first author's surname, and secondarily in chronological order with earliest dates first. Provide surnames and first initials of all authors; do not use "et al." for multi-authored works. No source should appear in the "Literature Cited" section unless it is specifically cited in the text, tables, or figure captions. *Personal communications* and *unpublished documents* should not be included in the "Literature Cited" section but may be cited in the text in parentheses; use footnotes only when parentheses will not suffice. Abbreviate journal titles to match BIOSYS usage. Each source must be complete according to the following guidelines. Please note that initials follow the primary author's surname, but for secondary authors initials come before the surnames:

ARTICLE IN A JOURNAL:

Barnes, J. T., L. D. Jacobson, A. D. MacCall, and P. Wolf. 1992. Recent population trends and abundance estimates for the Pacific sardine (*Sardinops sagax*). Calif. Coop. Oceanic Fish. Invest. Rep. 33:60–75.

BOOK:

Odum, E. P. 1959. Fundamentals of ecology. 2nd ed. Philadelphia: Saunders. 546 pp.

CHAPTER IN A BOOK:

Wooster, W. S., and J. L. Reid Jr. 1963. Eastern boundary currents. *In* The sea, M. N. Hill, ed. New York: Interscience Pub., pp. 253–280.

If your manuscript is accepted for publication, we will provide further guidance regarding preparing it for editing.

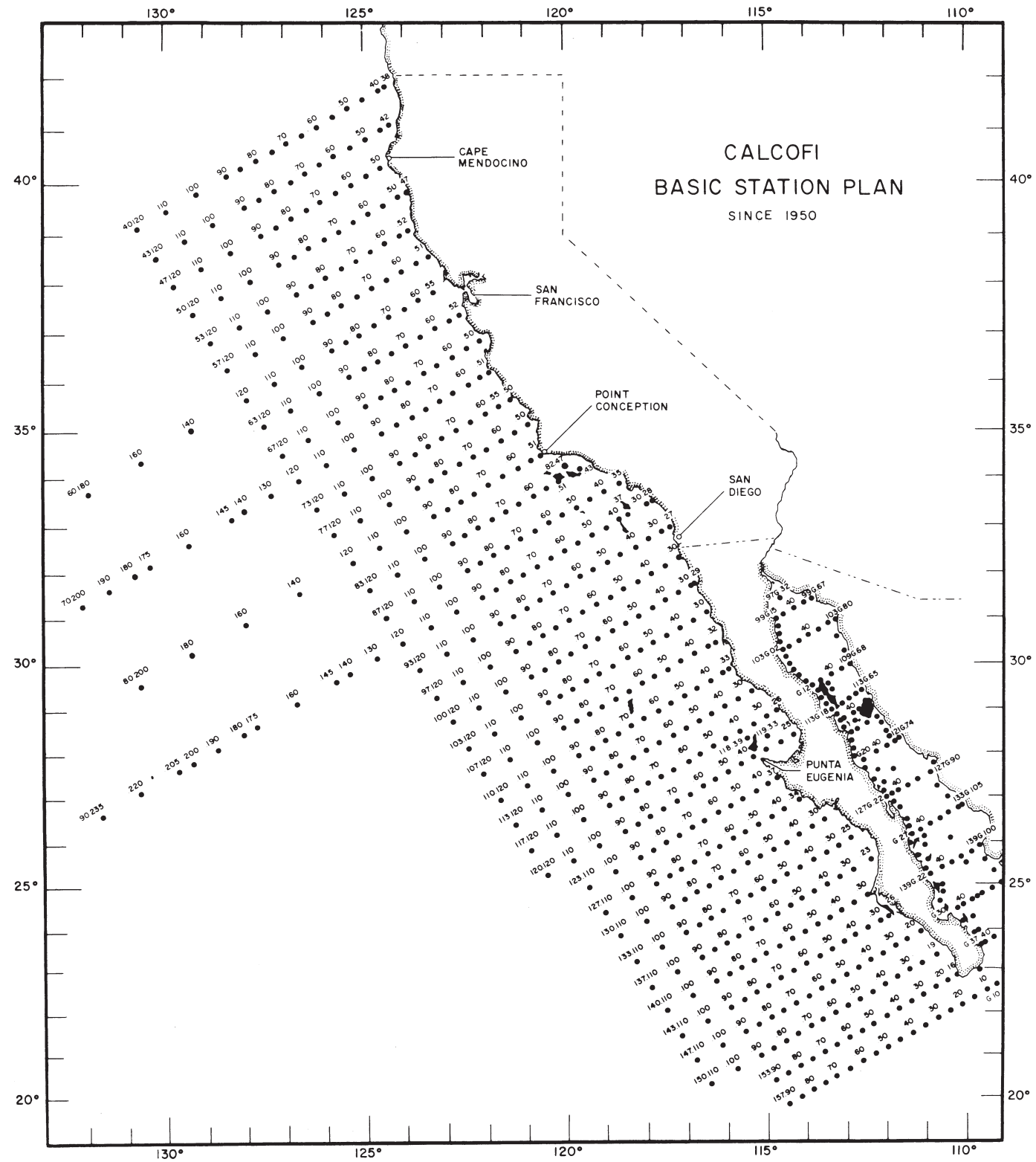

CALCOFI

BASIC STATION PLAN
SINCE 1950